# INTEGRATION OF SURFACE SEISMIC WAVES, LABORATORY MEASUREMENTS, AND DOWNHOLE ACOUSTIC TELEVIEWER IMAGING, IN GEOTECHNICAL CHARACTERIZATION: OGDEN, KS

by

AMELIA ERIN FADER

B.S., Kansas State University, 2010

A THESIS

submitted in partial fulfillment of the requirements for the degree

MASTER OF SCIENCE

Department of Geology
College of Arts and Sciences

KANSAS STATE UNIVERSITY
Manhattan, Kansas

2012

Approved by:

Major Professor
Abdelmoneam Raef

# Abstract

Geotechnical site characteristics are a function of the subsurface elastic moduli and the geologic structures. This study integrates borehole, surface and laboratory measurements for a geotechnical investigation that is focused on investigating shear-wave velocity (Vs) variation and its implication to geotechnical aspects of the Ogden test site in eastern Kansas. The area has a potential of seismicity due to the seismic zone associated with the Nemaha formation where earthquakes pose a moderate hazard. This study is in response to recent design standards for bridge structures require integrating comprehensive geotechnical site characterization. Furthermore, evaluation of dynamic soil properties is important for proper seismic response analysis and soil modeling programs. In this study, near surface geophysical site characterization in the form of 2D shear-wave velocity (Vs) structure that is compared with laboratory measurements of elastic moduli and earth properties at simulated in situ overburden pressure conditions and synergy with downhole Acoustic Televiewer time and amplitude logs, proved very robust "validated" workflow in site characterization for geotechnical purposes. An important component of a geotechnical site characterization is the evaluation of in-situ shear modulus, Poisson's ratio and reliable and accurate elastic modulus ($\lambda$) and shear modulus ($\mu$) estimates are important in a good geotechnical site characterization. The geophysical site characterization, undertaken in this study, will complement and help in extrapolating drilling and core-based properties deduced by the geotechnical engineers interested at the test site.

# Table of Contents

# List of Figures

# List of Tables

# List of Equations

# Acknowledgements

I would like to thank the Kansas Department of Transportation for funding this research project, in particular Neal Croxton for project coordinator, Robert Henthorne for project approval, and the KDOT Drilling team. My major professor Abdelmoneam Raef, as well as my thesis committee members Asad Esameily and Matthew Brueseke. The people from the University of Kansas and Kansas Geological Survey whom hosted the MASW short course: Julian Ivanov, Tyler Schwenk and Brian Miller. The professors whom were the reason I joined the geology department for the advice and help they gave: Matt and Iris Totten. I would also like to thank Derek Ohl and Randi Isham for their help during acquisition and laboratory measurements

# Chapter 1 - Introduction

Key factors to a geotechnical site characterization are S-wave velocities and several quality parameters. Soil mechanics play an important role in environmental, engineering, earthquake zonation and hydrocarbon exploration applications and research. Site characterization analysis can be greatly improved by the combination of non-invasive surface seismic, laboratory measurements, and invasive borehole methods. Earth properties and characterization of near surface soil and rock materials can be defined by the combined interpretation of core analysis, acoustic imaging of the borehole wall, and near surface shear-wave velocity profile (Hunze et al., 2007). Surface seismic methods can provide parameters relevant to the dynamic behavior of a large volume of shallow soil, laboratory core analysis provides earth properties and the acoustic borehole method provides high quality dip and azimuth measurements for the investigation of fractures, changes in lithology and other sedimentary features (Hunze et al., 2007).

In the past decade, a sizeable volume of research has been published concerning the use of seismic methods for geotechnical evaluations and earthquake seismicity surveys. There are two divisions within seismic methodology; borehole methods and surface methods. Borehole methods are often viewed as more reliable and accurate, but require an extensive drilling program that would exponentially increase the cost of most surveys. Surface methods such as reflection/refraction focus on the propagation of body-waves, but do not satisfactorily image the near surface layers. In fact, these near surface layers inhibit the imaging of deeper formations. The surface-wave method is cost effective and better at imaging the near surface because of the wavelength of the Rayleigh (and/or Love) waves generated by the source (Park et al., 2002; Xia et al., 2003). Usually Rayleigh waves (ground roll) are the focus of surface seismic surveys, but there are a few instances where Love waves could be used (Socco et al., 2010). The background principle of how and why surface-waves are used is based on the dispersive nature of surface-waves, the fact that different wavelengths propagate/penetrate to different depths and the corresponding phase velocities represent the elastic properties of the layers which they penetrate into.

Surface-wave surveys are noninvasive and cost effective, so the additional cost of laboratory measurements and a limited number of invasive boreholes can improve the processed results (Xia et al., 1999). Data collected from these auxiliary methods can be used as constraining parameters for the inversion step; the constrained and unconstrained results can be compared to see what contrasts exist. Constraints, in theory, improve the reliability of the final model and make site characterization more comprehensive. Drilling boreholes is an additional expense but if used sparingly the data will improve results without much of an increase to cost. An acoustic televiewer can be used to record detailed, oriented caliper and structural information based on high resolution, ultrasonic travel-time and amplitude images. Borehole measurements are often the source of constraining parameters in the inversion of MASW data, but laboratory measurements can also be used for parameterization of the initial model for data inversion. By analyzing cores in a lab we are able to calculate density ($\rho$), Poisson's ratio ($\sigma$), Young's modulus, Bulk modulus, and P-and S-wave velocities. Data sets acquired through multiple methods can be compared and parameters can be taken from one and used during the processing of another. There are a growing number of publications exploring integration and/or joint processing of various method datasets to improve non-uniqueness, resolution, and accuracy (Xia et al., 1999; Xia et al., 2003; Song, 2007; Lou et al., 2007; Lou et al., 2011). An example, beyond the scope of this project, is the joint use of fundamental and higher modes, multi-modal use can greatly improve results (Lou et al., 2011).

When public safety is concerned improved understanding of the near surface geology for stability and longevity can be evaluated for large structures such as building or bridges. Geotechnical evaluations are often done in areas of varying degrees of earthquake zonation and known areas of faulting or karst formations. When one thinks of earthquake hazards, Kansas is not the first place to come to mind, but eastern Kansas is considered a zone of moderate hazard (Kansas Geological Survey, 2000). This moderate zone of seismic activity is associated with the Nemaha Ridge (Figure 2). The information acquired from geotechnical site characterizations can be used to design higher quality large-scale structures such as bridges, dams, power plants and buildings.

Our test site was located close to Ogden as seen in Figure 1. We integrated results from data sets of three geophysical methods: Multi-Channel Analysis of Surface Waves (MASW),

downhole Acoustic Televiewer, and ultrasonic laboratory measurements of compressional- and shear-waves velocities and elastic moduli. Surface-wave data was acquired using the Multi-Channel Analysis of Surface Waves (MASW) method, borehole data was acquired using an Acoustic Televiewer Imaging system and laboratory measurements were acquired using an ultrasonic velocity measuring device (ULT 100 system manufactured by GCTS). The data sets were compared and information from one was used to constrain and improve results from another.

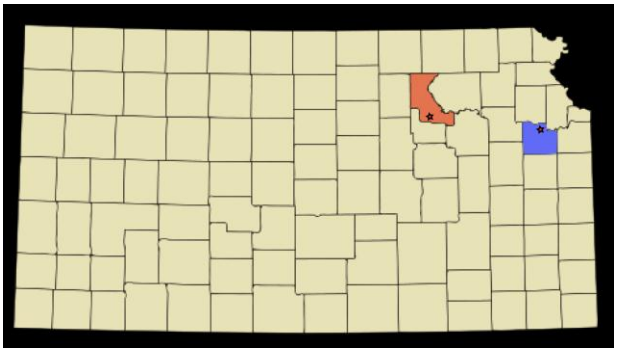

Figure 1 - site locations Douglas (blue) Riley (red) counties
From KGS

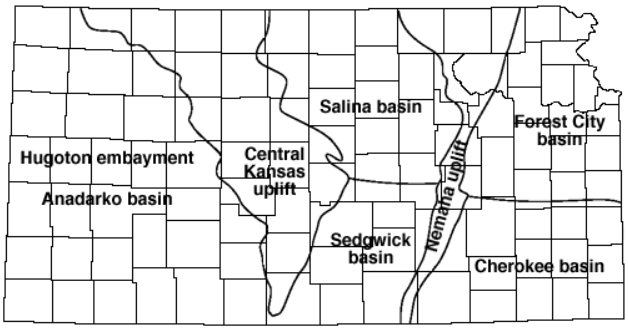


Figure 2 - Kansas Basin and Uplift Boundaries
From KGS

# Chapter 2 - Background

There are a variety of different methods that can be employed during a near surface geotechnical site characterization, limiting factors such as geologic composition, accessibility, and budget influence the use and application of a method. This project used Multi-channel Analysis of Surface-Waves (MASW), ultrasonic laboratory measurements, and Acoustic Televiewer (ATV) imaging. Though the methods differ from one another, the data acquired from each can be integrated to improve the final analysis.

## Acoustic Televiewer

There are two types of televiewers: acoustic televiewers (ATV) and optical televiewers (OTV). Acoustic televiewers (ATV) were first developed in the late 1960's by the petroleum industry, though a limited number of researchers used the device earlier (Williams and Johnson, 2004). Widespread use occurred in the mid to late 1990's, mainly for ground-water studies. The first standalone optical televiewer system (OTV) was created in 1987 but its use was limited to groundwater studies because they were not compatible with common and widely used logging systems at first (Williams and Johnson, 2004). Most ATV tools have a length of 1.7 – 3.7 m with a diameter of 40-50 mm and the systems use an ultrasonic pulse echo setup with a 0.5 – 1.5 MHz transducer (Williams and Johnson, 2004). The ATV system could have one of two types of transducers, the more common rotating transducer in which the beam is moves or a fixed transducer in which the acoustic beam is fixed but a rotating convex reflector (Figure 3) bounces the beam 360° as the device is pulled up hole (Williams and Johnson, 2004).

In certain situation either ATV or OTV is optimal for imaging. ATV is better at recording fractures in darker rocks and recording in less than ideal conditions such as water or light mud-filled boreholes and can image through plastic casing when borehole wall stability is a concern (Williams and Johnson, 2004). But when wall stability is not a problem, such as imaging in solid granite/rock, OTV would record images with higher detail. As well as clearly imaging walls with iron staining, chemical precipitations or bacterial growths (which can indicate flow of ground water and/or contamination). In near surface investigations ATV has a distinctive advantage over OTV. ATV can image through plastic PVC casing while OTV

cannot, with OTV casing is only used in unstable soil areas to keep the borehole open. The cased soil areas usually are disturbed at the borehole wall so fractures cannot be resolved but soil transitions can be detected by an ATV (GeoVision; Schepers et al., 2001). In situations where both ATV and OTV can be used, images can be integrated and when the images from both are compared discrepancies of fracture location and orientation can be seen though some discrepancies can be expected because of how the tools respond differently, this can be resolved during integration (Williams and Johnson, 2004).

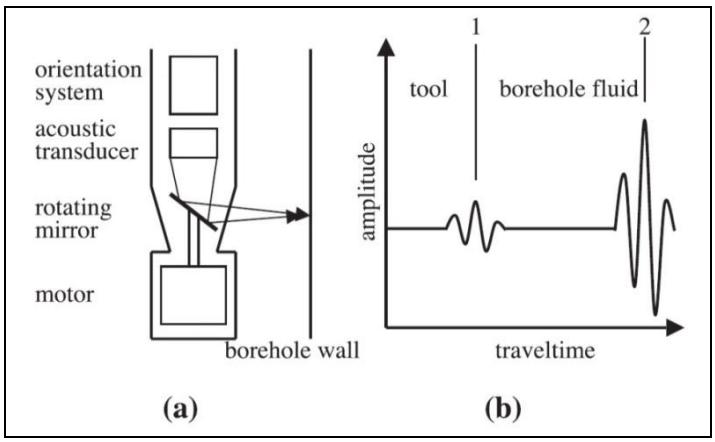

Figure 3 - ATV Multi Echo (Deltombe and Schepers, 2004)

Neither kind of televiewer records seismic velocity data. An acoustic televeiwer with a multi echo system emits a signal and records what reflects off the casing and then the borehole wall, resulting in imaging of both casing and borehole wall. The imaging is created from the amplitude and the time data of the reflected signal. While an OTV collects actual photos of the borehole hall, requiring a lighting system and no casing. The ATV creates photographic-like images from the transit time and amplitude of the reflected signal and high-resolution caliper logs can be generated from the transit time data (Williams and Johnson, 2004). For an ATV the contrast between the acoustic impedance of the borehole fluid and the borehole wall can provide the relative hardness of the borehole wall. Fluctuations in the borehole wall, or borehole deviation, can inhibit the detection of changes in lithology, foliation, bedding and sealed fractures if the acoustic contrast is not sufficient (Williams and Johnson, 2004). Image orientation and tool centralization are critical for high quality data and accurate structure orientation. A three-axis fluxgate magnetometer and three accelerometers are used for the orientation of a televiewer, the magnetometer and accelerometers allows for an oriented borehole wall image and the true three-dimensional location of the measurement. Centralization of

boreholes is accomplished by the use of steel, brass, plastic or rubber sliding end bowsprings, depending on the size of the borehole. With an ATV if the tool and resulting images are decentralized there will be a vertical striping/stripping of transit-time and amplitude images, and a decentralized OTV log would display similar light and dark bands (Williams and Johnson, 2004).

## Laboratory Measurements at Ultrasonic Velocities

Laboratory measurements are meant to independently measure or calculate elastic properties of rock samples. Generally there is an attempt to simulate the in-situ conditions of each sample; pressure or fluid (Ohsaki and Iwasaki, 1973; Han, 1986; Zhang and Bentley, 2005). For near surface sedimentary units it is risky to incorporate fluid and pressure, the result could be highly destructive if pressure is not applied equally over all surfaces of the sample. There are two categories laboratory tests fall under, static and dynamic. Static tests cause permanent deformation in the sample. Dynamic tests apply a small stress and strain; any resulting deformation is not permanent and allows the specimen to go through the sampling process multiple times (Zhang and Bentley, 2005).

### *Elastic Moduli and Earth Properties*

The elastic properties can be split into two categories for simplification: the elastic moduli and earth properties. The elastic moduli ($\lambda$) group is composed chiefly of Young's modulus (E), Shear modulus ($\mu$) sometimes called Rigidity modulus and Bulk modulus (K). The more easily measured and more commonly used earth property group consist of P- and S-wave velocities ($V_p$ & $V_s$), density ($\rho$) and Poisson's ratio ($\sigma$). In engineering application, sometimes the elastic modulus is used when referring to Young's modulus. As long as two elastic properties are known (eg. E, G or K) the others can be calculated. Young's modulus is the ratio of stress to strain, the Shear modulus describes the response to shearing strains and the Bulk modulus is a measure of resistance to uniform compression. The $V_p$ and $V_s$ values are derived from the elastic moduli and density.

The elastic moduli can be affected by cracks, pores or the presence of fluids. The behavior of pore fluids effect stiffness. Dynamic tests using high frequencies give little time for

the pressure of the pore fluids to redistribute and reach equilibrium, resulting in the sample to appear stiffer (Zhang and Bentley, 2005). For wet rocks, the moisture in pore spaces will cause an increase in the elastic moduli, the increase is generally greater for the bulk modulus than in the shear modulus, also Poisson's ratio increases with increasing water saturation. The elastic moduli are important variables for site characterization but are values primarily used by engineers. Geologists focus more on physical properties such as $V_s$, $V_p$, density ($\rho$) or Poisson's ratio ($\sigma$).

### *Poisson's Ratio: Background and Sensitivity*

Poisson's ratio can be described as either, the measure of the compressibility of a material perpendicular to the stress applied, or the ratio of latitudinal to longitudinal strain. Poisson's ratio in geological publications typically uses the symbol ($\sigma$), while engineering publications almost always the symbol ($\nu$), in very rare cases $V_s/V_p$ has been used but should not be confused with the $V_p/V_s$ ratio. Poisson's ratio typically ranges between 0.0-0.5, the value range for most geologic material is typically between 0.05-0.45 (Gercek, 2007). There are two methods for calculating Poisson's ratio, static and dynamic, which will be discussed shortly. Poisson's ratio is influenced by several factors; rock composition, water saturation, depth/effective pressure and cracks/pore space.

The dynamic Poisson's ratio ($\nu_d$ or $\sigma_d$) is calculated from the measurements of compressional ($V_p$) and shear velocities ($V_s$) from seismic data, sonic well logs, or laboratory measurements (Equation 1 and Equation 2). The static Poisson's ratio ($\nu_s$ or $\sigma_s$) method involves a uniaxial loading test used to calculate the ratio of radial strain and axial strain ($\varepsilon_r/\varepsilon_z$), often used for engineering applications. The difference between static and dynamic comes/arises from the strain amplitude and frequency applied (Zhang and Bentley, 2005). The static method applies large stress that yields large strain, causing the sample to have irrecoverable deformation. The dynamic method involves tests (sonic, laboratory, etc.) focused on the propagation of the signal through the site/sample at small stress and strain, causing small elastic deformation. These factors make dynamic less destructive, more cost effective, and more time efficient. Even with the advantages to dynamic Poisson's ratio it is considerably different from static Poisson's ratio (Zhang and Bentley, 2005). In our project dynamic Poisson's ratio was calculated from

ultrasonic laboratory measurements. The calculated Poisson's ratios along with the calculated densities of core samples were used as confining parameters for the surface-wave inversion.

$$\nu_d = \frac{(V_p/V_s)^2 - 2}{2\,(V_p/V_s)^2 - 2}$$

Equation 1 - Poisson's Ratio

or

$$(V_p/V_s) = [(1 - \nu_d)/(\tfrac{1}{2} - \nu_d)]^{1/2}$$

Equation 2 - Poisson's Ratio

Factors that influence Poisson's ratio include the propagation of $V_p$ and $V_s$ which depends on rock composition, depth/effective pressure and cracks/pore space. Each propagate differently through different rock types because of the; cementation, crystal size and shape, pore space, water content, etc., (Zhang and Bentley, 2005). Also, depending on the effective pressure cracks may or may not be influential to Poisson's ratio, but moisture content will always be influential.

The rock composition influences Poisson's ratio because the composition effects how the wave (seismic, ultrasonic, etc.,) propagates. A method for clastic rocks focuses on clay content for a rough estimation (Zhang and Bentley, 2005; Han, 1986). There is an (AVO) assumption that the Poisson's ratio of a dry rock is approximately equal to the Poisson's ratio of the composing minerals (Mavko et al., 1998). This method is debatable, especially in our instance when our samples were only ambient dry (not oven dried). Few geologic publications describe or discuss acceptable near surface Poisson's ratio ranges for elements, minerals, or rock types. One publication that does discuss reported/acceptable ranges is (Gercek 2007), but the moisture content is not specified, even though in the paper it is noted "[…] values of Poisson's ratio of [saturated] rocks are larger than the drained values" (Gercek, 2007). The state of saturation of a sample is important, moisture will cause the P-wave velocity ($V_p$) to increase, resulting in a larger Poisson's ratio. Cracks and pore spaces effect/affect the amount of moisture a sample can hold when saturated and with increased moisture results in increased Poisson's ratio.

In-situ and simulated laboratory overburden (burial depth) or effective pressure has an effect on Poisson's ratio, with sufficient pressure most thin cracks will close and not influence

the ratio. There is evidence that at shallow depths Poisson's ratio is not consistent and can vary for a variety of reasons (eg. lithology etc.,) (Nicholson and Simpson, 1985; Boore and Joyner 1997). Just below the water table Poisson's ratio generally is close to 0.5, from this point down to at around 3~4 km (1.86~2.48 mi.) the ratios gradually reaches a value near 0.25 (Nicholson and Simpson 1985; Boore and Joyner 1997; Boore et al., 2007).

Cracks can be defined as pores with low aspect ratios, the influence cracks have over Poisson's ratio is dependent upon the saturation state of the sample as well as the amount and orientation of the cracks (Zhang and Bentley, 2005). If we were to analyzes the difference between static and dynamic elastic properties we would see that, when cracks occur in a small amount of the total volume, the ratio of static versus dynamic Poisson's ratio will approach one (Zhang and Bentley, 2005). At high effective pressure cracks and pore spaces have little influence on the value of Poisson's ratio, the opposite is true when at low effective pressures. A sample with a substantial amount of cracks will have a significant decrease in Poisson's ratio, but if there are few or very thin cracks the rock or mineral composition will be the primary influence (Zhang and Bentley, 2005). Pore spaces do not respond the same as cracks when exposed to laboratory induced effective pressure; their presence remains. Dry pores will inhibit Vp and moisture in the pores (saturated) will speed up $V_p$. $V_p$ in a dry porous medium like limestone would be slower than it would be in a saturated limestone. Rock types characterized as having little or few pore spaces will show little variation.

Our samples do not exhibit substantial pore space, but are near surface sedimentary units. The main points we will focus on will be rock composition and saturation. During the inversion process we will use the laboratory measurements of Poisson's ratio and density to constrain the inversion process.

### *Poisson's Ratio: The Debate*

The debate behind Poisson's ratio could fill a book (if anyone bothered to write it)( Ohsaki and Iwasaki, 1973; Nicholson and Simpson, 1985; Han, 1986; Boore and Joyner, 1997; Brown et al., 2002; Gretener, 2003; Boore et al., 2007; Gercek, 2007). For our project the value of dynamic Poisson's ratio was calculated from $V_s$ and $V_p$. Since $V_p$ is affected by the degree of water saturation while $V_s$ is not, the result will vary depending on water saturation. Therefore,

laboratory measurements and in-situ measurements of Poisson's ratio will differ from one another. The same can be said about the Poisson's ratio taken above and below the water table (loosely regarded at top of saturation zone). The location of the water table is something that seems to fall between the 'cracks' in the debate and is at the root of the discussion Boore had with Ozdogan (Oz) Yilmaz (Boore et al., 2007). This was an important concept/element that we had to take into account during the final processing steps. When constraining the final inversion the dry laboratory measurements were used. I must note that our cores were not dried in an oven and were not kept in sealed containers, so they were affected by ambient humidity. Also, it must be kept in mind that our samples were measured at ultrasonic frequencies/velocities, regardless the Poisson's ratio and density will be the same (Han, 1986). We could not compare the ultrasonic $V_s$ and $V_p$ velocities to the seismic velocities often reported by scientists (did not have a conversion from ultrasonic to seismic).

For a brief historical account of the birth/development and maturation of Poisson's ratio, Gercek (2007) is a good source. Primarily the debate centers on what is an acceptable assumption for Poisson's ratio. There are scientist/scholars who argue Poisson's ratio does not fit naturally into seismic equations, but that argument is from the engineering perspective, that geology should be uniform and fit neatly, geology will never fit neatly anywhere. The debate over assumed values of Poisson's ratio is complicated by the fact variables that affect it are not taken into account (water table, depth, etc.,). The most common values of Poisson's ratio that are often assumed during processing (inversion) are 1/4 (0.25), 2/3 (0.33), and a value approaching, but not exceeding 9/20 (0.45). The proper application of each assumption are not well defined, and often assumed with little investigation. Often the same value is applied to all depths, above and below the water table. Poisson's ratio is effected/affected by water saturation and should not be disregarded.

Often assumptions regarding associations, not observations are made. So the distribution of Poisson's ratio is often assumed to be one of three things; 1. It is constant, 2. it is a function of depth, or 3. it is a function of Vs. For the constant the most commonly used values are either 0.25 or 0.33, but for near-surface materials Poisson's ratio is not predictable and can vary greatly (Figure 4 and Figure 5). At depths greater than 3km Poisson's has a general trend of approaching 0.25 (Nicholson and Simpson, 1985). A value of 0.33 is sometimes assumed to be

the value of material above the water table (Brown et al., 2002). But depth is not the overriding factor, as mentioned previously saturation state is a factor along with rock composition.

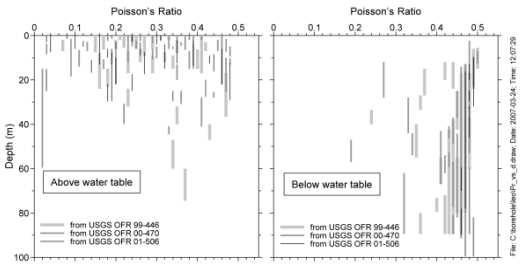


*Figure 3. Poisson's ratio versus depth for material above and below the water table, using values from recent measurements of velocities in southern California (Gibbs et al., 1999, 2000, 2001). The length of each vertical line spans the depth range for each particular constant-velocity layer from which Poisson's ratio was determined.*

Figure 4 - Poisson's ratio above (left) and below (right) the water table (Brown et al.,2002)

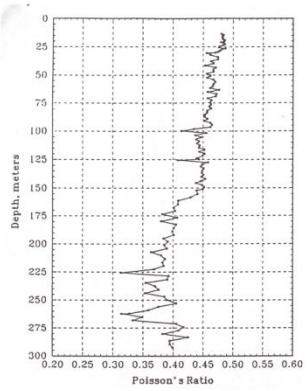


*Figure 2. The reference is "(Nigbor and Imai, 1994)". Given Bob Nigbor's close association with P-S suspension logging, I assume that the results in this figure are based on P-S suspension logging.*

Figure 5 - Poisson's ratio, expect water table is not labeled. Most likely where the line starts is the top of the water table. (Boore et al., 2007)

## MASW Acquisition

### *Multi-Channel Analysis of Surface Waves*

There are two widely used surface-wave acquisition set-ups; Spectral Analysis of Surface Waves (SASW) and Multi-Channel Analysis of Surface Waves (MASW). Either can be utilized for near surface site characterization but differ in acquisition and data handling. SASW was introduced in the early 1980's and utilizes spectral analysis of ground roll (Park et al., 1997). The components include 2 receivers with a seismic source; the receivers do not have a specific offset because during acquisition the receivers are moved to cover the desired area and depth. Constant rearrangement of the receivers caused the process to take several hours and covering a large area is difficult. SASW was introduced by Stokoe and others at the University of Texas Austin but over time has been replaced by the faster MASW method (Park et al., 1997).

The MASW method, a field layout is shown in Figure 6, also focuses on Rayleigh-waves, but the setup is different than SASW. Researchers at the Kansas Geologic Survey (KGS) developed this acquisition technique approximately 15 years ago. There can be 12 or more receivers with consistent spacing; this set receiver configuration makes acquisition fast. In the MASW method there are two divisions based on the source used, if an impulsive source is used it is called MASWI but if a vibroseis is used it is MASWV. The distinction is important because

when an impulsive source such as a hammer is used, the frequency-domain (CCSAS) approach is used but when a swept source like a vibroseis is used a time-domain approach is used (Park et al., 1997). A hammer is cheaper, easier and faster, but it is difficult to control the spectral contents of the generated surface waves (Park et al., 1997). The bandwidth of the recorded surface-waves tends to be narrower, which limits investigation depth and resolution.

### *Surface-Waves*

Surface-waves do not penetrate as deeply as body-waves; instead they travel near the earth's surface (Figure 6) along a boundary between two differing mediums, such as earth-air or earth-water boundaries. The dispersive nature of these waves means velocity changes as a function of frequency, which is then exploited to create a near-surface shear-wave velocity ($V_s$) profile. Rayleigh-waves are generated by P- and S-waves interfering with one another. Rayleigh-wave particle motion is in the vertical direction while Love-wave particle motion is in the horizontal direction (Figure 7). We are not concerned with Love waves in our study because when both vertical receivers and a vertical source are used Love waves are often not recorded. Ground roll, a component of Rayleigh wave, accounts for more than two thirds of generated seismic energy and is often recorded well by the multi-channel method. As mentioned earlier, Rayleigh waves are almost always dispersive, except when a solid homogeneous half-space is encountered (Xia and Miller, 2010). Rayleigh waves penetrate approximately as deep as the length of one wavelength. Longer wavelengths penetrate to greater depths, usually having greater phase velocities, and are more sensitive to the elastic properties of deeper layers. Shorter wavelengths are sensitive to physical properties of the shallower layers. The contrast between short and long wavelengths is the reasons each individual mode will exhibit a unique phase velocity for each unique wavelength, causing the dispersive nature of the wave in layered material (Xia and Miller, 2010).

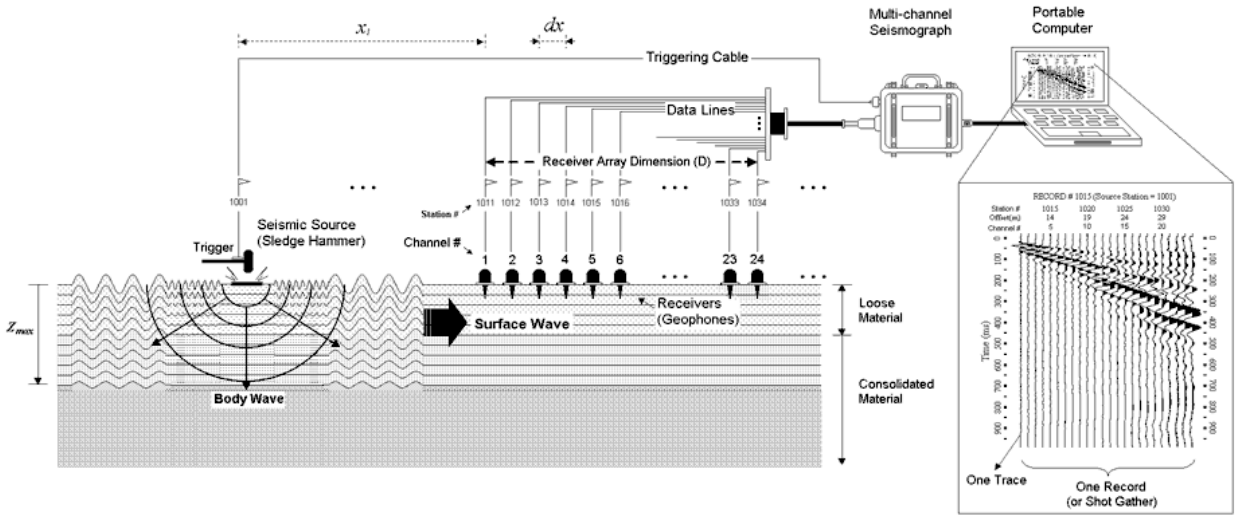


Figure 6 - Surface and Body wave propagation, MASW general setup (KGS: http://www.kgs.ku.edu/software/surfseis/active.html)

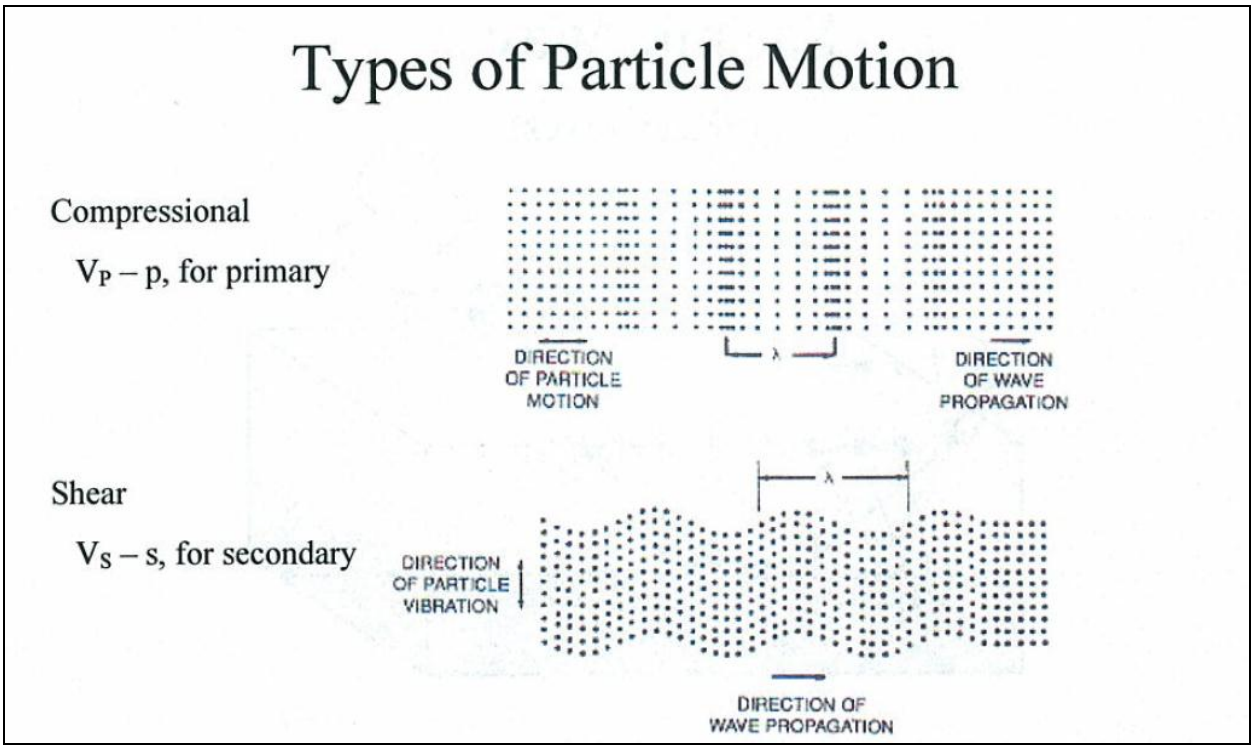


Figure 7 - Types of partial motion: Compressional and Shear (P and S) (From KSGS short course)

# MASW Data Inversion and Integration

## *Inversion and Integration*

The shear-wave velocity ($V_s$) of near surface materials and its effects on seismic-wave propagation are the fundamental interest in many groundwater, engineering and environmental studies. A $V_s$ profile can be extracted from the inversion of MASW data. The inversion results can be improved by additional data; addition of higher modes, earth properties, etc., (Xia et al., 1999; Xia et al., 2008). In this project the surface-wave data does not exhibit applicable higher mode characteristics so we focus on the addition of earth properties and elastic moduli as confining parameters (density, thickness, and Poisson's ratio). These additional confining parameters are measured independently of the MASW method. Commonly, independent data is measured using a borehole method but is expensive. For this project our independent measurements were taken from rock cores in a laboratory at ultrasonic frequencies, a less expensive method.

Before confining our data it is important to understand how sensitive surface-wave data might be to a confining parameter. The data may be more sensitive to one parameter than another; this can be determined by observing the change in the Rayleigh-wave phase velocity. In Xia's 1999 publication the effect of four earth properties and their influence on phase-velocity were examined; $V_s$, $V_p$, density and layer thickness. As expected, Vs was the most influential, this is why the inversion of Rayleigh-wave dispersive data is asserted as an accurate method to calculate a Vs profile, but Vp is the least influential (Xia et al., 1999). Layer thickness is the second most influential parameter but is dependent on the number of layers at the investigation site. Third is density, its influence is consistently the same across different rock types and is stronger influence than Vp.

When the thickness of a layer model is increased by 25% there will be a change of 16% in the Rayleigh-wave phase velocities (Xia et al., 1999). Layer thickness has a noticeable effect on Rayleigh-wave phase velocity, but is often eliminated from the inversion process because the subsurface can be subdivided into many thin layers with constant and distinct $V_s$. Xia et al. (1999) concluded that since the phase velocity was most sensitive to changes in Vs, the inversion of Rayleigh-wave dispersive data adequately calculates $V_s$. The final two parameters are density

($\rho$) and $V_p$, both of which can be accurately measured. A 25% increase in density results in approximately a 10% change to the phase-velocity. It is easy to obtain real world density with accuracy greater than 25%. $V_p$ is much less influential than density. If $V_p$ is increased by 25% the phase velocity is only subtly effected an average change of 3% is observed (Xia et al., 1999). Even though it has a weak influence, the accuracy like density only varies within 25% of actual. According to Xia 1999, from the order of most influential to least are $V_s$ (39%), thickness (16%), density (10%) and $V_p$ (3%).

In additional to these 4 previously mentioned earth properties Poisson's ratio can also be employed as a confining parameter. The ratio is calculated from $V_p$ and $V_s$, it is a unitless value, therefore when calculated from seismic and ultrasonic data each should be relatively similar or close to one another (Han, 1986; Grochau and Gurevich, 2009). Since our laboratory measurements are at ultrasonic frequencies/velocities we cannot directly input these values as constraints, but we can use them to determine Poisson's ratio. How the parameters can be integrated will be discussed later in the paper.

# Chapter 3 - Geologic Setting

## Tectonic Setting and Seismicity

The majority of Kansas is classified as an area of minor earthquake risk except for the two known areas of anomalously high seismicity, the Nemaha Ridge and the Midcontinent Rift (Figure 2 and Figure 8). The Nemaha Ridge is classified as a zone of moderate hazard that extends across the state from Omaha, Nebraska to Oklahoma City, Oklahoma. The Ridge is associated with a structural high in the underlying granitic/crystalline Precambrian basement; it is approximately 415 mi. (670 km) long and 13 mi. (30 km) wide. The Nemaha Ridge formed ~300 Ma and has active faults on the east (Humboldt fault zone) and west boundaries (Burchett et al., 1985; Kansas Geological Survey, 2000). Another item of tectonic interest is the proximity of the Midcontinent Rift, approximately 50 mi. (80 km) west of the Nemaha Ridge. The Midcontinent Rift formed approximately 1100 Ma and is considered a failed rift that in Kansas, cuts through older Precambrian basement and is filled with gabbro, basalt and metasediments (Merriam, 2010). The rift spans from the Lake Superior Region through Minnesota into Iowa and through southeast Nebraska and into central Kansas. It is only 30 - 50 mi (50 - 80 km) wide in Kansas. The Humboldt fault zone (Figure 8) is located to the eastern side of the Nemaha Ridge, shown in Figure 8. This feature passes near Wamego, east of Manhattan, and strikes to the south, just east of Wichita. There is a definite correlation between earthquakes and the tectonic structures in the Humboldt Fault zone (Burchett et al., 1985). Several moderate earthquakes of magnitude 5 or greater have occurred along the west side of the Nemaha Ridge, but the areas of highest seismic activity are along the eastern side of the Humboldt Fault zone. Any earthquakes near Manhattan, Kansas (Ogden site) are most likely associated with the Humboldt Fault zone (Burchett et al., 1985). Micro-earthquakes in northeastern Kansas are also likely associated with continued glacial isostatic adjustment or rebound; the area is in close proximity to the southern limits of Kansas glaciation. Burchett et al., 1985 concluded that eastern Kansas earthquakes were related to the know structural features of the area and the most likely region of future earthquake activity would be along the eastern boundary of the Nemaha Rift (Uplift), the Midcontinent Rift and basin boundaries associated with the two.

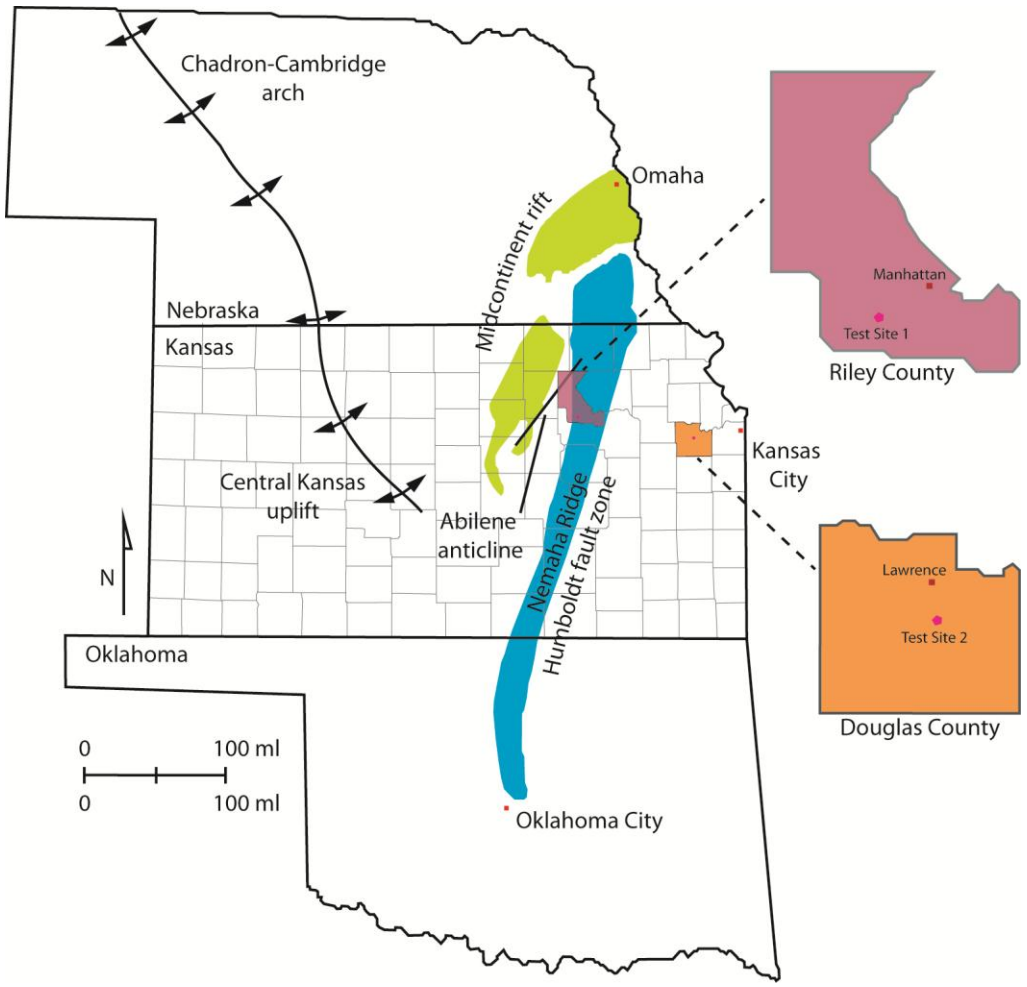


Figure 8 - Regional tectonic features From KGS http://www.kgs.ku.edu/Publications/pic3/pic3_4.html

## Surface Stratigraphy and KDOT Borehole Records

The Ogden site is in Riley County, KS and is located within the Nemaha. The Nemaha Ridge separates the Salina and Sedgwick basins from the Forest City and Cherokee basins as displayed in Figure 2. Figure 9 depicts the age of geologic materials exposed at the surface and a simplified cross section our site; has Permian units over Pennsylvanian units. Of the three boreholes, the Sevenmile borehole has Permian and Pennsylvanian material but the cores from the Ogden North and Ogden South boreholes only exhibit Pennsylvanian. In the cross sectional view of Figure 9 you can see faulting between Geary and Wabaunsee counties, this faulting is unlabeled but appears to most likely be related to the Nemaha Uplift Figure 2.

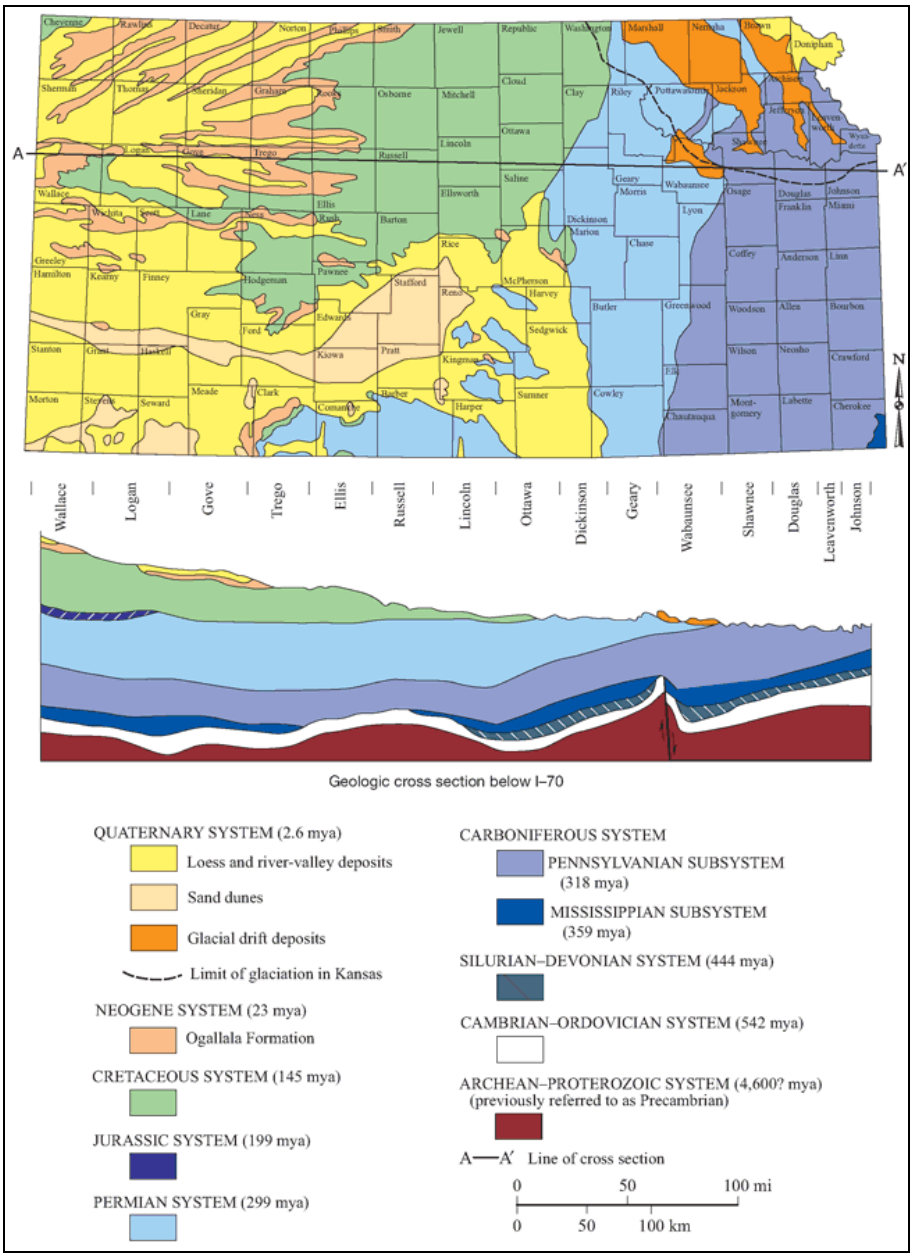


Figure 9 - Generalized Geologic Map of Kansas. Roughly follows Interstate 70 From KGS

All units observed in the borehole records, excluding alluvium, are part of the Council Grove group (Figure 10) and most from Sevenmile, fall within the Permian (299.0 to 251.0 Ma) and the remaining units are part of the Pennsylvanian (318.1 – 299.0 Ma) (Smith, 2011). In March of 2010, the Kansas stratigraphic nomenclature was updated and the separation between the Permian and the Pennsylvanian falls between the Bennett shale and the Glenrock limestone. Both are part of the Red Eagle limestone and the boundary is only seen in the Sevenmile borehole. The Ogden site is within the Nemaha Ridge area and is in the Kansas River floodplain

resulting in a very thick layer of alluvium that is 51 ft thick in the Sevenmile borehole and 61 to 62 ft. thick in the Ogden North and South boreholes (Figure 29).

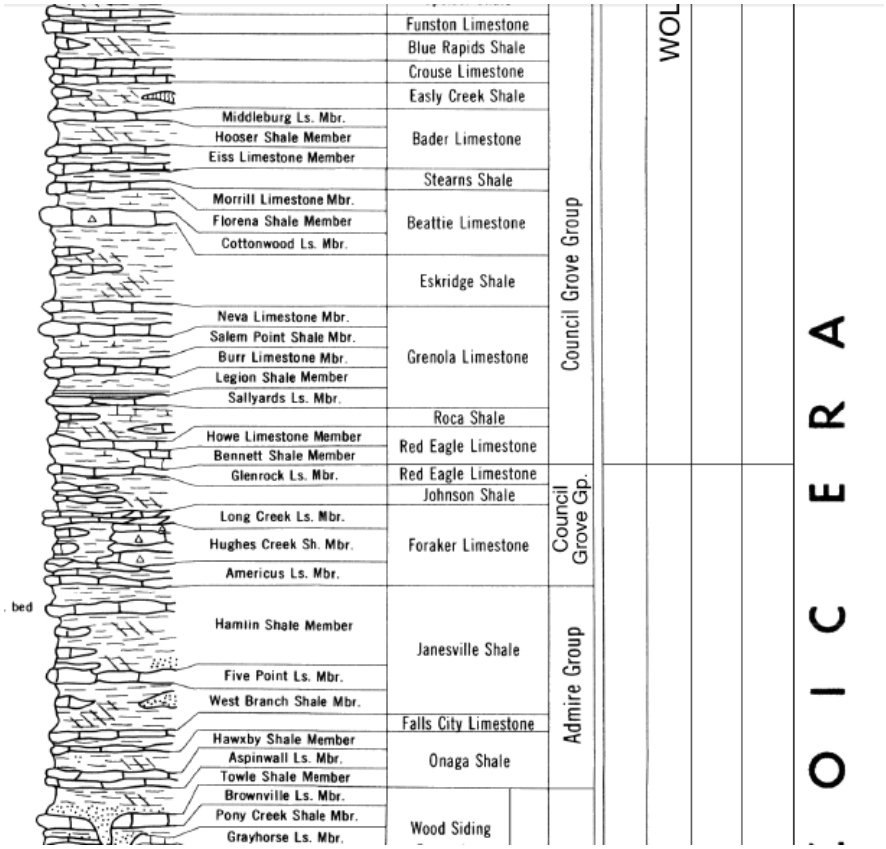

Figure 10 - 2010 Geologic Column From KGS

The Ogden test site is close to the edge of the Nemaha Uplift and has thick unconsolidated or poorly consolidated alluvium and sedimentary deposits. These thick deposits of unconsolidated sediment/alluvium at the surface intensify the potential seismic hazard because of the increased risk of liquefaction. This alluvium consist of silty clay and sands with some gravel at depths, it ranges between 51 – 62 ft. thick. The bedrock formations are consolidated sedimentary rocks, some of which crumble when exposed to water and pressure. The Johnson Shale Formation is present in all three borehole records, but the Permian units are missing from the North and South boreholes. In the Sevenmile borehole, the Roca Shale, Howe Limestone and Bennett Shale all exhibit signs of weathering and uncharacteristic qualities, presence of silty limestone and absence of distinctive coloring. Possibly the units were eroded away in the locations of the North and South boreholes or the units thinned and were heavily weathered to the point the units did not survive the coring process. The Glenrock Limestone Member (1.2 ft.)

showed little sign of weathering but was still absent from the North and South boreholes; either the units were very heavily weathered and did not survive the coring process or possibly the unit was completely eroded away between the Sevenmile borehole and the North and South boreholes (KDOT, 2009; KDOT, 2011). The Sevenmile data will be dropped form further discussions since it was considerably farther from the MASW acquisition then the North and South boreholes. Due to correlation issues, further analysis of the lithology will be discussed later in the paper.

# Chapter 4 - Methodology

There are a variety of different methods that can be employed during a near surface geotechnical site characterization, limiting factors such as geologic composition, accessibility, and budget influence the use and application of a method. This project used Multi-channel Analysis of Surface-Waves (MASW), ultrasonic laboratory measurements, and Acoustic Televiewer (ATV) imaging. Though the methods differ from one another, the data acquired from each can be integrated to improve the final analysis.

## Acoustic Televiewer

In this near surface project, since OTV cannot image through casing, only ATV imaging was used. The ATV used was a downhole-digital, fixed high-frequency transducer and multi-echo system, along with a diameter of 40mm, required a PVC casing with a minimum 2.5 in. inner diameter. During acquisition the fixed transducer emitted an acoustic beam and a rotating convex reflector bounced the beam 360° as the device recorded while pulled up-hole (Williams and Johnson, 2004). The only problem was the provided centralizers were to large for the PVC pipe, we had to construct our own centralizers out of paint rollers, rubber grommets, zip ties and tape (Figure 11 and Figure 12). The casing used was schedule 40 with flush threading (aka acme threading), an inner diameter of 2.445 in., and outer diameter of 2.875 in. and an inner pressure rating of 250 lb.. Multi-echo systems can image the borehole walls through the plastic pipe/casing that is used when there is a chance the walls are unstable and might collapse. Each PVC casing segment was 10ft. long, with threading making them slightly shorter (~2 - 3inch).

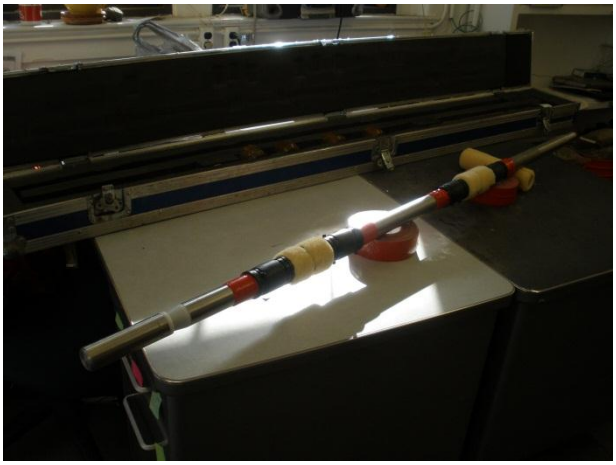

Figure 11 - ATV Stabilization System

Figure 12 - ATV Stabilization System close up

## Ultrasonic Velocity Measurements

For laboratory measurements samples were prepared using a wet/dry rock saw, the use of water was avoided as much as possible for consistency because some samples were near surface moderately consolidated sedimentary rocks. Portions of the cores provided by the Kansas Department of Transportation (Figure 13 and Figure 14) were fragmented, resulting in the length of the cut samples to range from 2 in. to 4 in. long. In sections with less fragmentation the longer samples were prepared (RS3 11.219 in.). Physical properties include density (ρ) of samples are listed in Table 1. Figure 15 shows a prepared core; preparation required the ends to be cut smooth and parallel in order for proper wave propagation.

| North (Ogden, Riley CTY) Physical Properties of Cores | | | | | | | | | | | | | | |
|---|---|---|---|---|---|---|---|---|---|---|---|---|---|---|
| ID | Density (g/cm^3) | Lt. (in.) | Dia. (in.) | Top dpt. (ft.) | Bot. dpt. (ft.) | Avg. dpt. (ft) | Core Set | CSet dpt. | C | R | RQD | Lt. (mm) | Dia. (mm) | Mass (g) |
| RN1 | 2.22 | 5.450 | 2.00 | 64.875 | 65.329 | 65.102 | Core 2 | 63.5 - 66.5 | 3 | 2.7 | 2.1/ 3.0 | 139 | 51 | 629.8 |
| RN3-S | 2.24 | 5.670 | 2.00 | 67.042 | 67.514 | 67.278 | Core 3 | 66.5 - 68.5 | 2 | 2 | 1.6/ 2.0 | 144.5 | 51 | 660.4 |
| RN3-R | 2.24 | 5.670 | 2.00 | 67.042 | 67.514 | 67.278 | Core 3 | 66.5 - 68.5 | 2 | 2 | 1.6/ 2.0 | 144.5 | 51 | 661.5 |
| RN5 | 2.4 | 6.4375 | 2.00 | 70.792 | 71.328 | 71.060 | Core 4 | 68.5- 73.5 | 5 | 5 | 100 | 162.5 | 51 | 796.1 |
| RN6 | 2.16 | 7.625 | 2.00 | 72.427 | 73.063 | 72.745 | Core 4 | 68.5 - 73.5 | 5 | 5 | 100 | 192 | 51 | 849.0 |
| RN7 | 2.16 | 9.875 | 2.00 | 74.333 | 75.156 | 74.745 | Core 5 | 73.5 - 78.5 | 5 | 5 | 100 | 250 | 51 | 1101.2 |
| RN8 | 2.25 | 7.625 | 2.00 | 75.198 | 75.833 | 75.516 | Core 5 | 73.5 - 78.5 | 5 | 5 | 100 | 194 | 51 | 893.5 |
| RN9 | 2.26 | 9.250 | 2.00 | 75.833 | 76.604 | 76.219 | Core 5 | 73.5 - 78.5 | 5 | 5 | 100 | 233.5 | 51 | 1076.3 |
| RN10 | 2.27 | 8.688 | 2.00 | 77.609 | 78.333 | 77.971 | Core 5 | 73.5 - 78.5 | 5 | 5 | 100 | 220 | 51 | 1019.5 |

Table 1 - Physical properties of South borehole (KDOT North)

Figure 13 - North core set (KDOT South)

Figure 14 - South core set (KDOT North)


Figure 15 - A prepared core sample

The ULT 100 testing system transmitted P- and S-waves through the sample allowing estimation of P- and S-wave velocities to calculate Poisson's ratio (σ), Bulk modules (K), Young's modulus (E) and Shear (Rigidity) modulus (μ). The ULT 100 testing system was combined with a manually operated hydraulic press; this set up can be seen in Figure 16. The cores were originally tested at 250 lbf (pound per foot) pressure increments starting at 0 lbf and going up to 1000 lbf. After these initial tests, it was determined that pressure increments of 30lbf, half in-situ lbf and in-situ lbf would be efficient. The value of density (ρ) did not change with variation of pressure so only one value is given. No acoustic coupling (e.g., honey, petroleum jelly) was used; it would have contaminated the sample and required washing/rinsing, which for some samples would have destroyed them.


Figure 16 - ULT system and hydraulic press setup

The simulated in-situ overburden was calculated using the assumption that 1 ft. of overburden was equal to 1 Psi and the unit conversion of 1 Psi is equal to 1 $lbf/in^2$. For each core sample the average depth (middle) of each sample was taken from the KDOT borehole reports

and was calculated using the equations below (Equation 4 and Equation 5). Figure 17 shows a core sample placed in the press and simulated overburden being set.

$$1\ ft \approx 1\ Psi \approx 1\ \frac{lbf}{in^2}$$

Equation 3 - Units for overburden calculation

$$Pressure\ (Psi) = \frac{Force\ (lbf)}{Surface\ Area\ (in^2)}$$

Equation 4 - Calculating Psi

$$\left(Avg.insitu\ depth\ in\ ft\ [\frac{lbf}{in^2}]\right)(Surface\ area\ of\ core\ [in^2]) = Calc.\ Insitu\ [lbf]$$

Equation 5 - Calculate in-situ lbf for middle depth of core sample

Figure 17 - Close up of core sample in hydraulic press while applying calculated overburden

The samples were run in batches based on their length due to the cumbersome limitations of adjusting the hydraulic press. On the screen captures of ULT program (Figure 18, Figure 19, Figure 20 and Figure 21) the P- and S-wave waveforms can be seen, the waveforms displays amplitude maximums and minimums, along with the change of wavelength over time at the initial test overburden of 0 lbf and 1000 lbf applied to the Douglas county sample. The different increments showed the behavior and visibility of the waveform is dependent on the simulated overburden applied. Graphs of the P- and S-wave waveforms at the three simulated overburdens at the three different increments of pound per foot applied to the sample can be seen in Figure 23 and Figure 24. Waveforms for all samples suitable for picking can be found in the appendix. Methodology behind picking will be discussed in the next section and further analysis of samples will be presented in the results section.

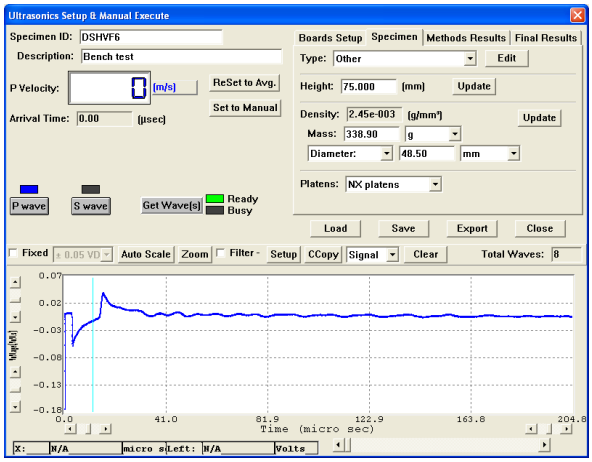

Figure 18 - P-wave of sample DSHVF6 bench test (0 lbf)

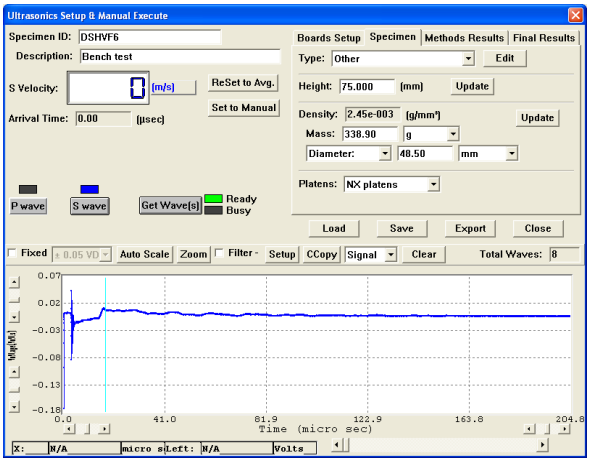

Figure 19 - S-wave of sample DSHVF6 bench test (0 lbf)

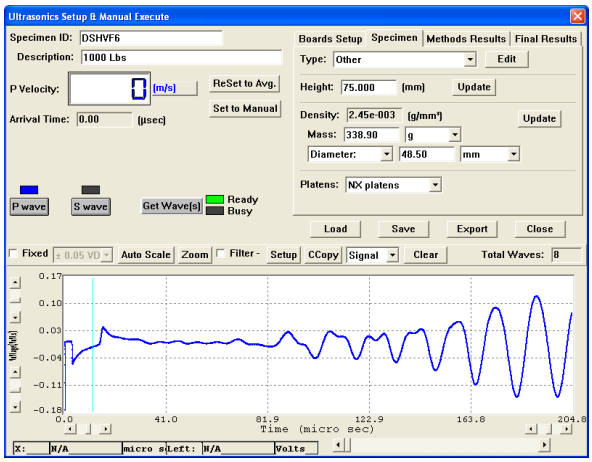

Figure 20 - P-wave sample of DSHVF6 at 1000 lbf

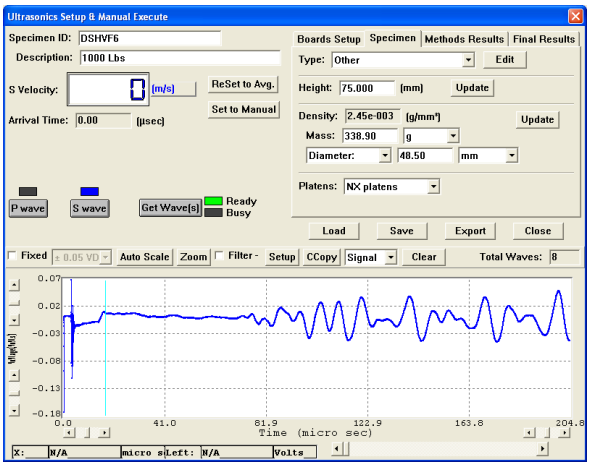

Figure 21 - S-wave of sample DSHCF6 at 1000 lbf

## *Methodology Behind Picking of Waveforms*

As mentioned in the previous paragraph, picking of the waveform was an important aspect of the laboratory measurements. Picking for the P- and S-wave were initially approached differently. The S-waves, the waveforms from the three chosen effective pressures were compared and the point at which the waveforms consistently oscillated but started diverging from one another was designated as the optimal picking point. The P-waves proved more difficult, initially the picking point (blue arrow in Figure 22) was where the middle point between where waveform initially peaked then tapered down before the signal started to oscillate. This zone was where the signal first started to oscillate and did so inconstantly due to background noise. There was a problem with the initial picking point, from this picking point the calculated value of Poisson's ratio (σ) (~0.45) was to high and not suitable for an ambient dry

core sample (Brown et al., 2002; Boore et al, 2007; Gercek, 2007). The P-waves were re-evaluated and it was determined the most repeatable point of picking was when the three waveforms diverged from one another (Figure 24). This yielded a Poisson's ratio lower than expected but within the acceptable range set forth by Gercek (2007). This complication is the reason for the extensive research into Poisson's ratio.

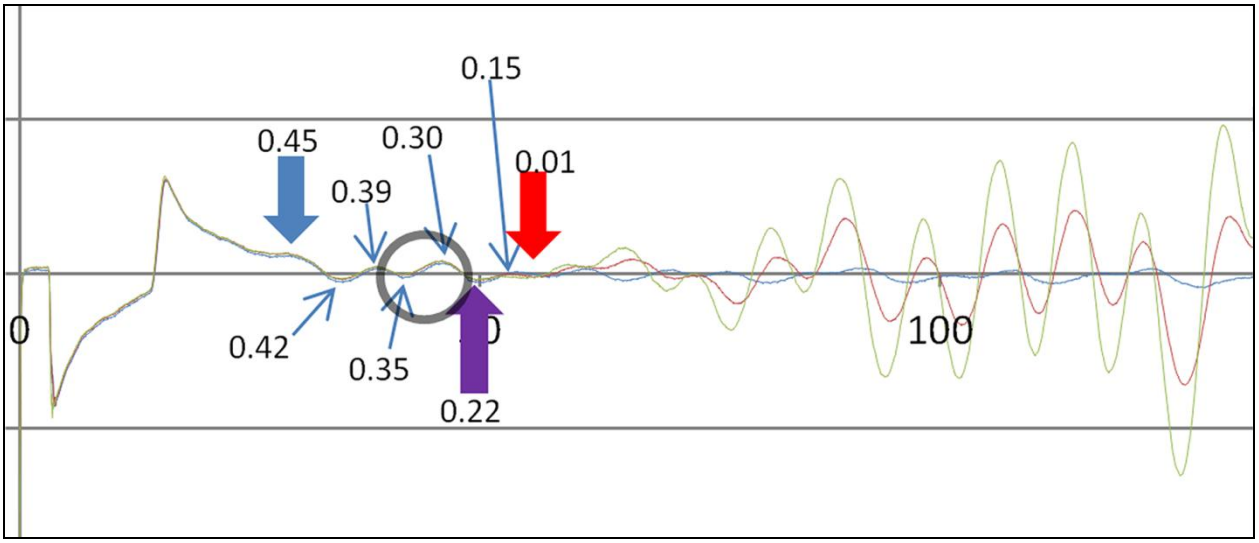


Figure 22 - RN5 P-wave Picking evaluation (Poisson's Ratio Value). Blue Arrow Standard picking. Purple arrow Altered picking. Red arrow is to close to zero.

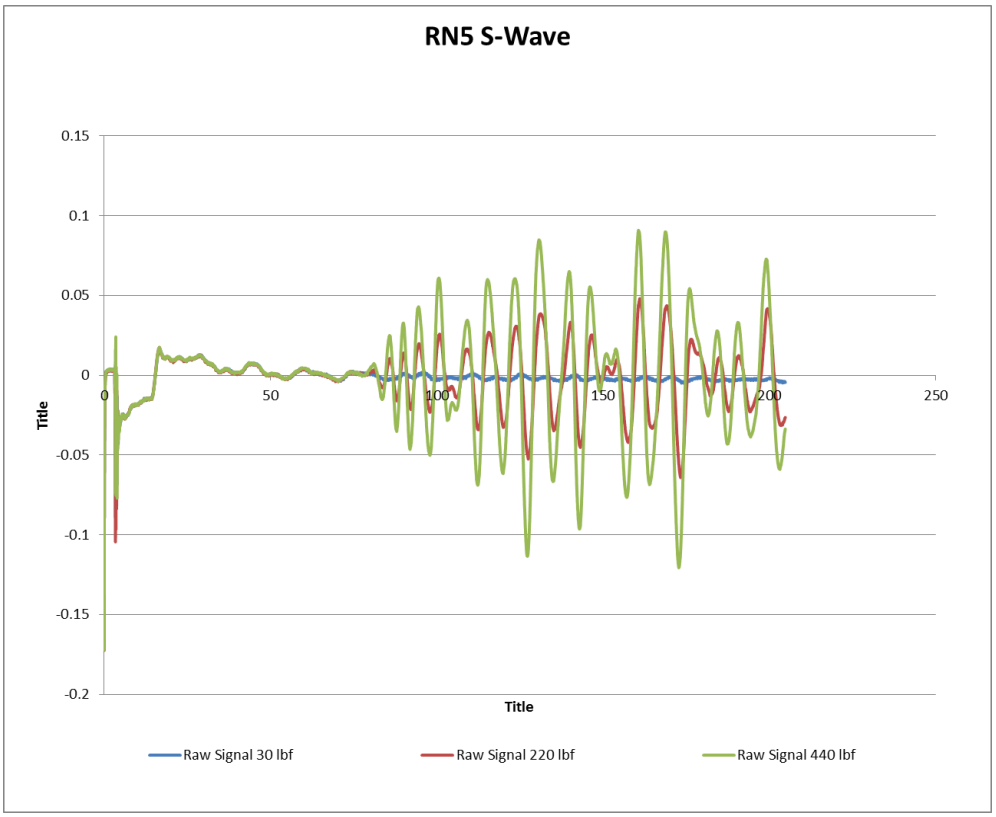


Figure 23 - S-wave waveforms at 3 pressure increments

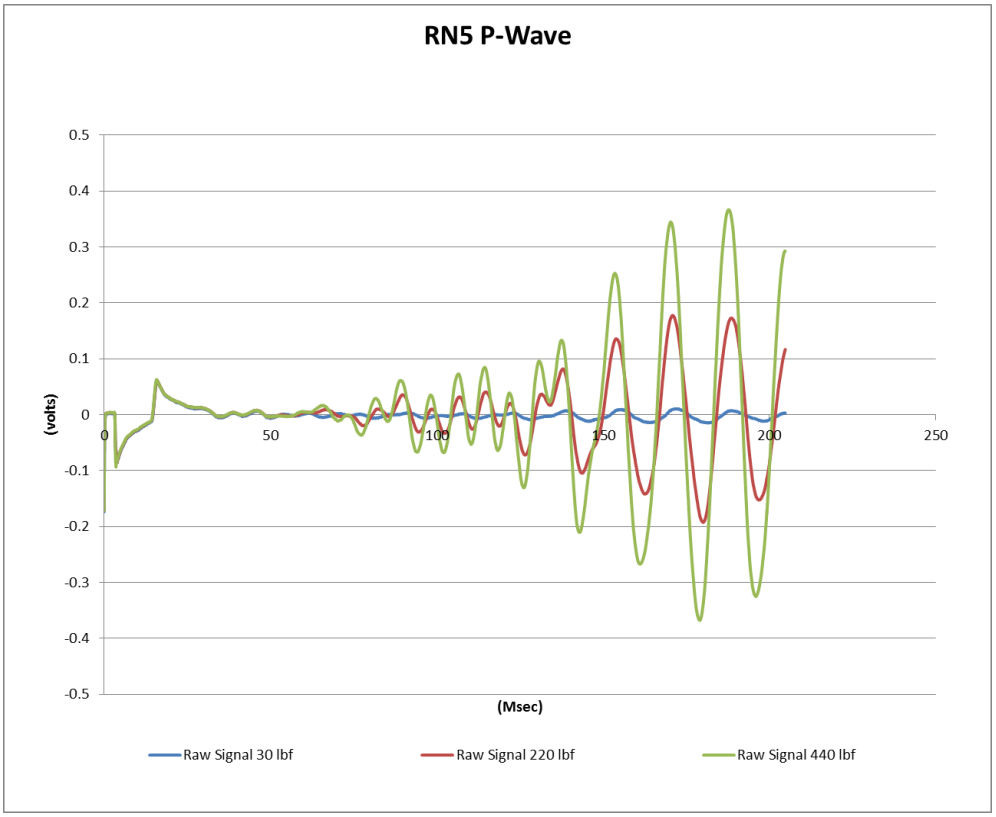


Figure 24 - P-wave waveforms at 3 pressure increments


Figure 25 - S-wave picking

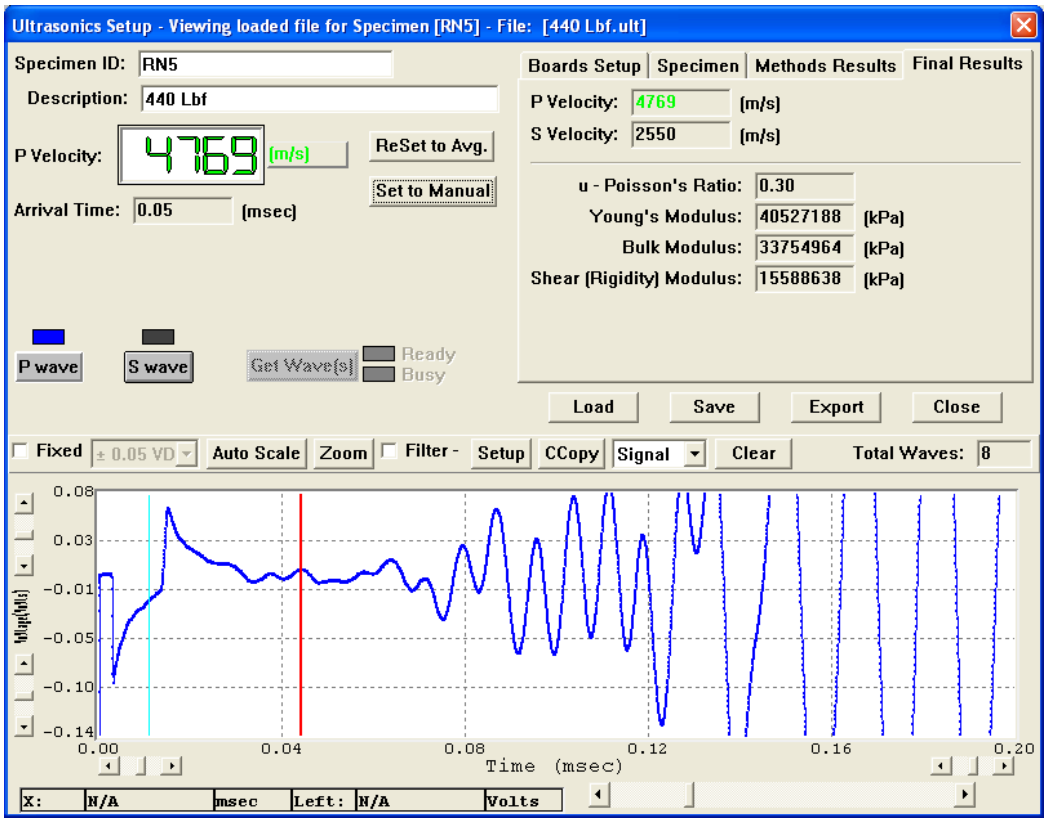


Figure 26 - P-wave alternate picking style

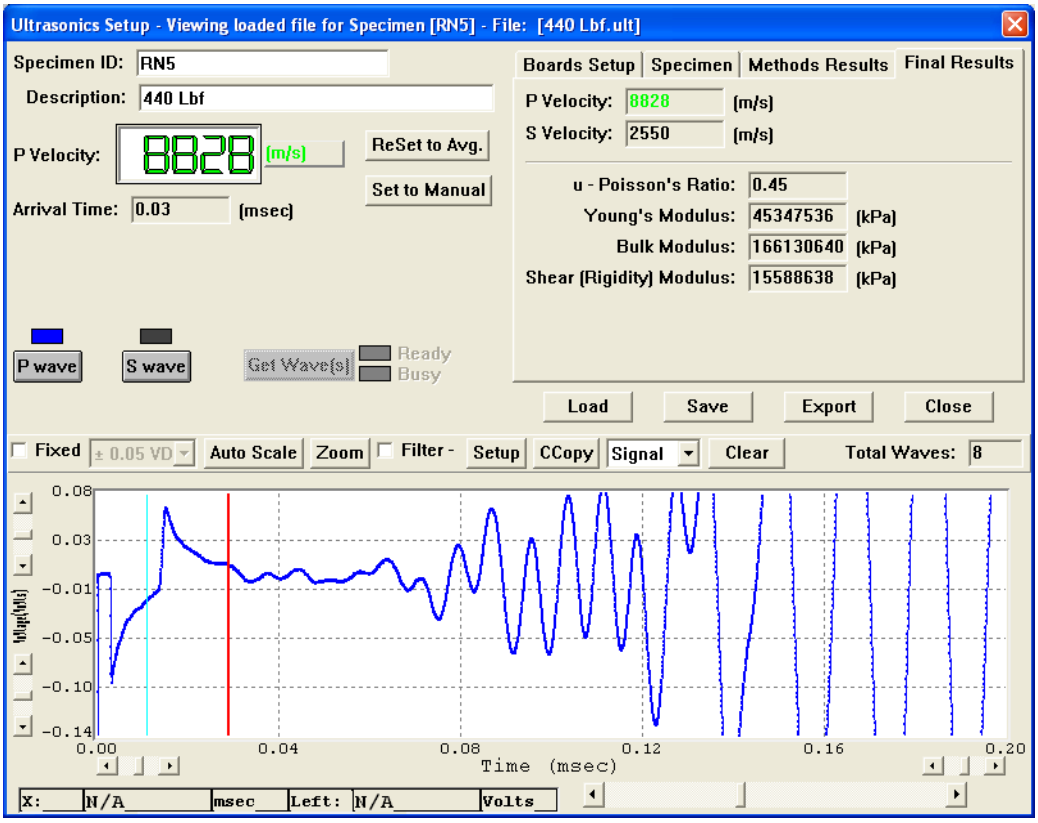


Figure 27 - P-wave standard picking style

The change in picking methodology resulted in the P- and S-waves both being picked in the same way at the point when the waveforms started to diverge from one another. The P-wave picking was difficult since the background noise interfered with the main signal so the peaks and troughs of the waveform were evaluated first and then the divergent picking point was determined. In the above case Figure 22 shows a close up analysis of the waveforms and a perplexing thing was found, that picking at the divergent point in this case resulted in a Poisson's ratio of 0.01, this did not correlate well with the values of the RN6 samples that was within the same lithologic unit (siltstone) (**Error! Reference source not found.**). So picking was done at he first repeatable trough, the purple arrow on Figure 22.

## MASW Method

MASW-data acquisition components were ordered and the Kansas State University Geology land-streamer was built, shown in Figure 28. A vertical-force source (sledge hammer) was used to generate Rayleigh-waves and recorded by a 24 channel of 4-Hz natural-frequency

receivers spaced 3 ft. apart with a source offset of 15 ft.  An aerial image of the MASW acquisition and the boreholes can be seen in Figure 29.

Figure 28 - KSU land-streamer

Figure 29 - Ogden Test Site: MASW Acquisition and Boreholes (Red-Sevenmile)(Yellow-North&South) from Google Earth

Our acquisition parameters used during MASW acquisition was: 24 channel cable, 3 feet distance between each receiver, and an offset of 15 feet between the source and the first receiver. This set up shifted 36 feet between each shot (Figure 30). In each shot there are 24 traces, when geometry is assigned each trace is titled with a numerical value that is saved in the header fields of the project dataset/database.

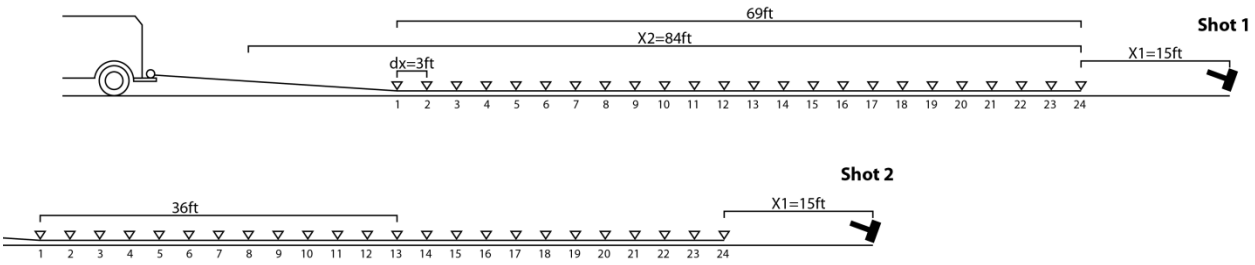


Figure 30 - MASW setup from shot 1 to shot 2

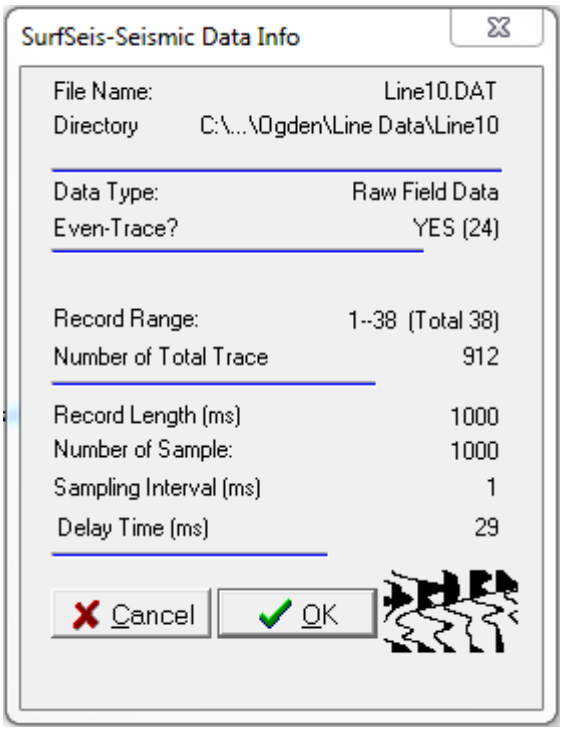


Figure 31 - Acquisition sampling information

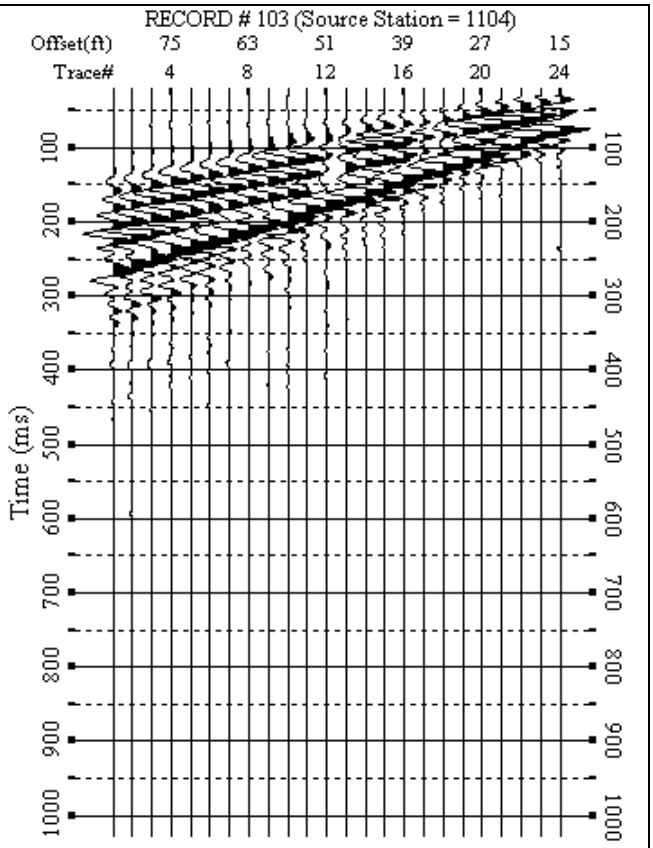


Figure 32 - Raw shot record from Line 15 station number 1104

During our acquisition the seismic software used numbered the receivers in reverse, the first receiver was numbered 24 and the second 23 and so on, this required special attention when importing data sets. The position of the source and receiver are assumed to be in a straight line, along the x-axis, relative to one another, so the value of SOU_Y and REC_Y remain zero. Further discussion of the MASW data will be covered in the following section.

## MASW Data Processing and Inversion

Previously discussed was the sensitivity and influence of confining parameters can have on the inversion of surface-wave data. In this section it will be discussed how we extracted and integrated our chosen confining parameters. Since we are using SurfSeis we can input $V_s$, $V_p$, density ($\rho$) and Poisson's ratio ($\sigma$) into the layer model within the program. Density ($\rho$) was the most readily and easily inputted value with an approximate influence of 10% (Xia et al., 1999). The laboratory measured Poisson's ratio ($\sigma$) can easily be used but we have to keep in mind that this value is for core samples which were abidingly dehydrated and will have a $\sigma$ lower than the saturated value encountered in-situ. Since laboratory measurements were taken at ultrasonic velocities those measurements of $V_s$ and $V_p$ cannot be directly inputted and since a simple conversion from ultrasonic to seismic velocities does not exist they cannot be used as confining parameters. The intent is to use density and possibly Poisson's ratio to constrain the layers imaged by the MASW method, this will be discussed further in the data and results section.

The entire procedure of analyzing MASW data consists of three steps; acquiring dispersive Rayleigh-wave data, building dispersion curves and the inversion of picked dispersion curves to create the S-wave velocity profile ($V_s$). The accuracy of the Vs profile depends solely on the accuracy of the dispersion curves, making it a critical step (Park et al., 1997). One of the most important parameters in the geotechnical estimation of near-surface soil or rock shaking response is the shear-wave velocity profile ($V_s$) (Hunter et al., 2010). "Shear-wave velocity techniques constitute the most versatile approaches to earthquake hazard mapping and site investigations" (Hunter et al., 2010).

### *Processing and Inversion*

We can take the recorded surface-wave data and analyses the Rayleigh wave dispersive nature to construct the S-wave velocity profile ($V_s$) and shear moduli ($\mu$), the shear moduli can be calculated because of the relationship between $V_s$ and $\mu$, illustrated by Equation 6.

$$V_S = \sqrt{\frac{\mu}{\gamma}}$$

Equation 6 - Relation between S-wave velocity and shear moduli

Our surface-wave data was originally processed using the RadexPro software, later a different program, SurfSeis, was purchased because the program made it easier to enter, manipulate and conduct final inversion of the surface-wave data. SurfSeis had a visual or 'graphical' geometry assignment, making this step much simpler and reduced the chance for human error that could have arisen from entering equations incorrectly.

To improve the overall signal the bottom mute applied to all data sets was 'loose' enough that the seismic-wave, specifically the surface-wave signal was not reduced. No top muting was done because after several experiments not improvement was seen in the later phases or inversion results. As you can see on the figure below (Figure 33) the surface-wave is recorded with a later arriver then the other components.

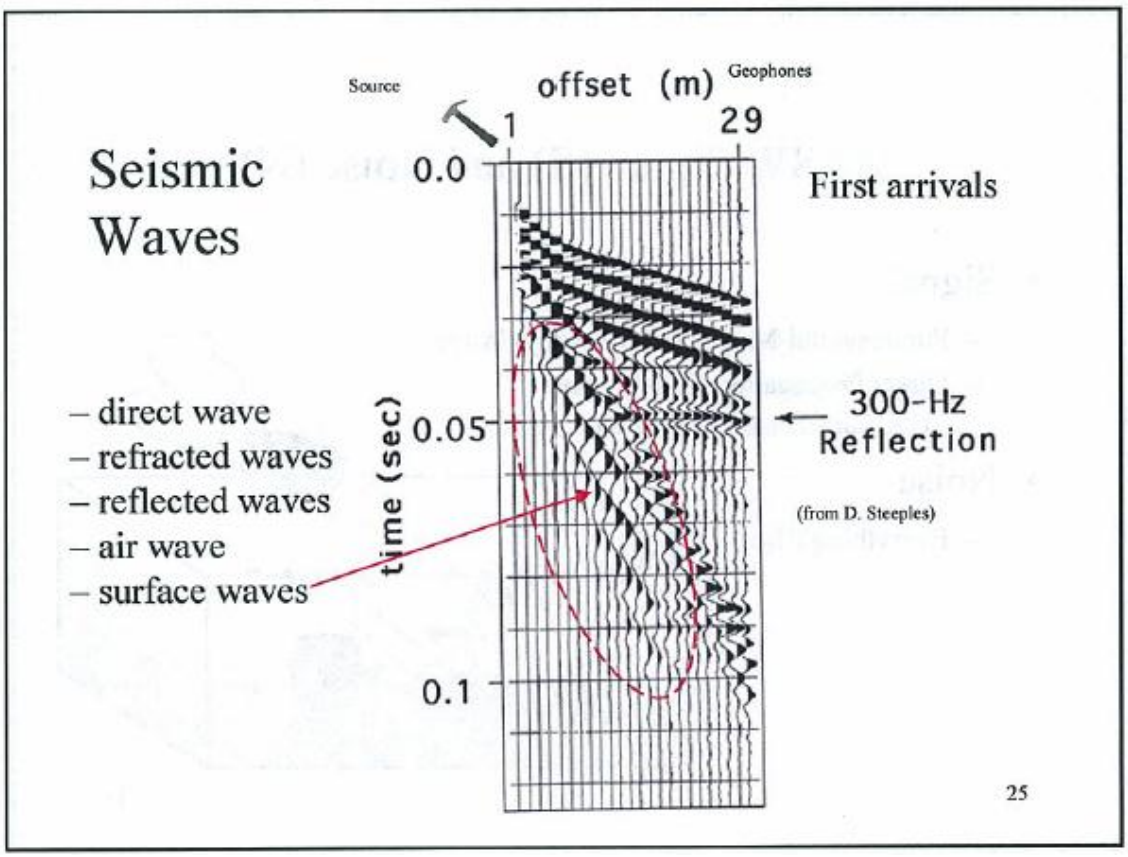


Figure 33 - Components of a Seismic-Wave From KSGS short course

In the case out our data from Line 11 and Line 10 it is difficult to clearly distinguish trends in the signal (Figure 35 and Figure 38). In the case of Line 11, in Figure 36 everything below the red line (travel time ~50-150) are surface-waves and everything above the blue line are refraction first-arrivals and head-waves. The trend between the red and blue lines could be

guided-waves/ head-wave train or it might be the high-velocity trend of the surface-waves (Kansas Geological Survey, 2012).

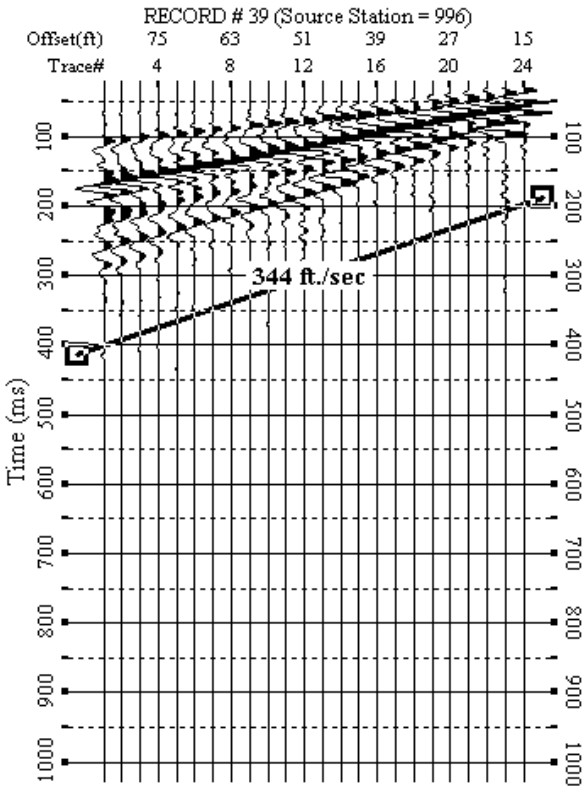


Figure 34 - Bottom Muting on Seismic Record Line 11

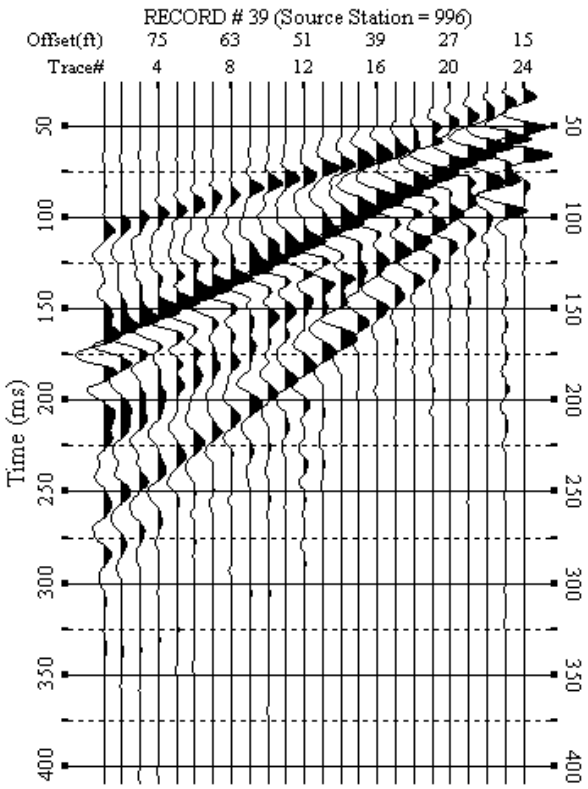


Figure 35 - Seismic Record from Line 11 enlarged

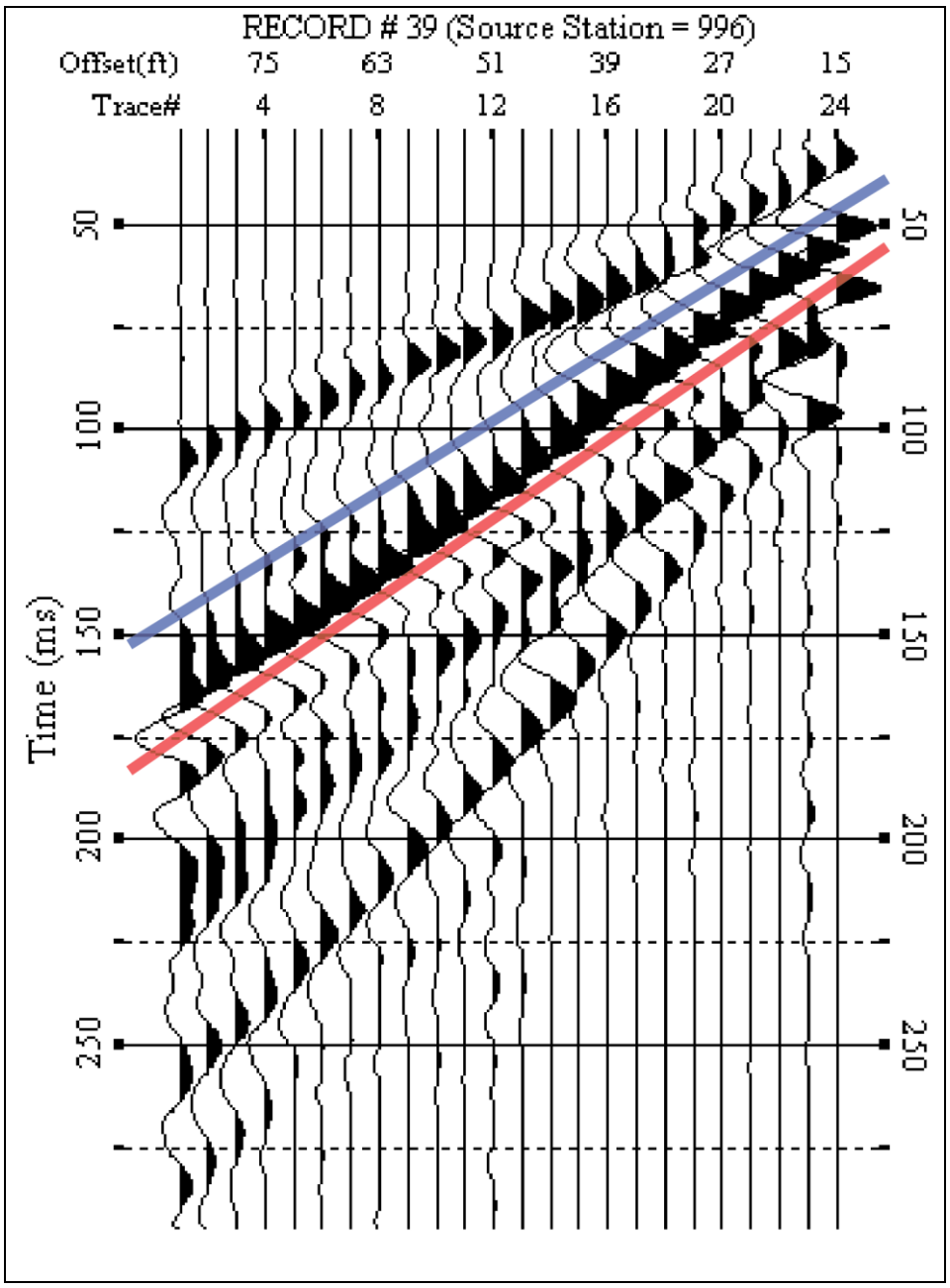


Figure 36 - Wave components marked on enlarged record from Line 11

All other records from the other lines look similar to Figure 35 except records from Line 10. Figure 38 is a record from Line 10 in which the seismic signal forms a thin linear trend, very different than the other lines. Line 10 was acquired on top of a dirt road created by KDOT as a heavy machinery access road during the earthworks phase of construction. The dirt road was far more compact then the locations of the other remaining seismic lines. Most likely the highly

compacted dirt was the cause of the seismic signal components to arrive at the same time, causing a signal collapse (component overlap) on the record and created a thin linear trend.

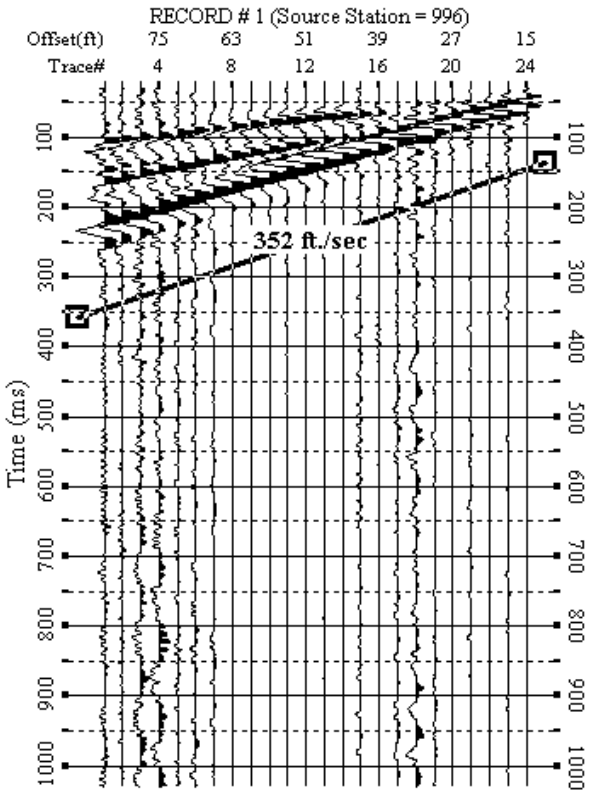


Figure 37 - Line 10 first seismic shot record, less collapse seen here.

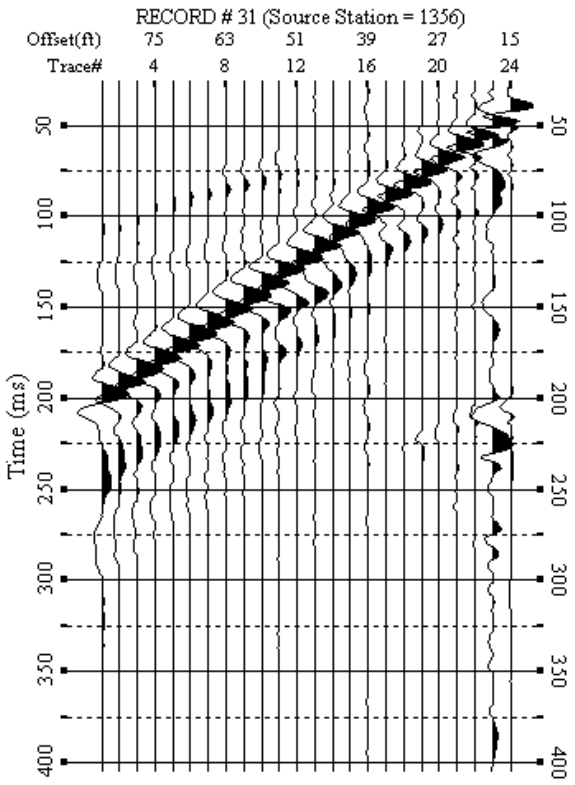


Figure 38 - Signal collapsed and components overlapping. This seismic record from Line 10, taken on top of a dirt road used by heavy machinery. This is the last shot record for Line 10.

The early processing phase when surface-wave data was imported into SurfSeis was relatively simple; the 'graphical' geometry assignment and easy to manipulate muting was very helpful. After the analysis of the seismic records was completed the next step was to create the dispersion curves. These dispersion curves (DCs) were then picked; the picking of the DC's should not be confused with the picking done for the laboratory measurements. Once picking was completed initial inversion without constraining parameters were conducted and the resulting Shear wave (S-wave) velocity models calculate. Both the dispersion curves and initial inversion results can be found in the appendix. In the next section I will discuss the creation of dispersion curves, how picking was done, after that I will describe the inversion process and results and the integration inversion results will be discussed in the Data and Results section.

### *Array Setup*

Surface-wave array setups depend on the underlying geology and the physical state of the area (eg. moisture, urban traffic). An array setup used in one area may efficiently record data with multi modal separation while in another area the data may suffer from higher mode

contamination. The quality of the fundamental mode can be influenced by several field parameters: receiver spacing (dx), the source offset ($X_1$), the number of receivers (N) and the length of the receiver spread (D or $X_T$). The most influential field parameters are the receiver spread length and the source offset ($X_1$) (Park, 2005).

Field parameters and processing method can influence the accuracy of the surface-wave data. The most influential are the receiver spread (D or $X_T$) and the source offset ($X_1$). Long and short of each field parameter have benefits and drawbacks. An increased receiver spread (D) improves mode separation and allows for deeper maximum depth of investigation ($Z_{max}$). The downside to a large receiver spread (D) is poor horizontal resolution because of the special averaging effect, so the length of the spread (D) should be decided based on balancing these 3 factors. The source offset ($X_1$) can be either long or short, the shorter offset allows for improved shallow imaging because of higher frequencies and the long allows for deeper imaging due to lower frequencies. But both suffer from either the near field or the far field effect respectively. The near-field effect can be seen on a seismic record/shot gather in the 1m closest to the source as a weakening in the amplitudes and a reduction in the coherency. The far-field effect occurs when higher mode and body-wave domination are present and appears on a seismic record/shot gather as far out at 100m.

From the Kansas Geological Survey short course (2012) it was learned that several rules of thumb are used for calculating offset ($X_1$), maximum depth of investigation ($Z_{max}$) and receiver spread size (D). It is generally assumed that the spread size is equivalent to the maximum depth of investigation in an ideal situation (Equation 7). The source offset is generally assumed to be 50% of the spread size (D) but can range between 16% to 100%, it depends on what the operator is trying to optimize and the geology of the area. In our project we used a linear land streamer array to acquire multiple records with the same source-receiver configuration and moved the array a fixed distance (dSR) of 36ft or 12 stations along linear lines for each shot. A diagram of the setup used in this project can be seen in Figure 39. The receiver spread size was 69ft, theoretically we should have been able to the depth of 69ft using SurfSeis but the data was not theoretical, it was real world data with real sources of noise and attenuation which impeded our project.

$$D = Zmax$$

Equation 7 - General assumption that receiver spread is equivalent to maximum investigation depth

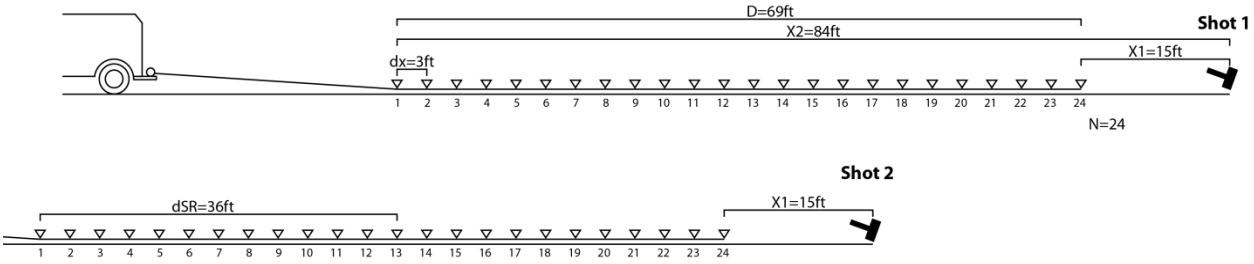


Figure 39 - Array setup

### *Example of Processing and Inversion Prior to Integration*

After the surface-wave data set was imported and geometry assigned the dispersion curves were created. Dispersion curves (DCs) and the picking done on each is important to the final inversion result. DCs are 1-d profiles representations of the data set that will be strung together to create a 2-D profile during the inversion process. The DCs are representations of frequency verses phase velocity. In other studies the primary focus was the fundamental mode (M0), but more recent studies have focused on the inclusion of higher modes (M1, M2, etc.) during the inversion process to improve (Xia et al., 2003; Lou et al., 2007; Song and Gu, 2007; Luo et al., 2011). Unfortunately, the combination of the near surface geology and our MASW array setup was unable to create/record higher modes suitable for the inversion process. In Figure 41 you can see that only the fundamental mode (M0) is visible and no suitable higher mode is present, the same is true for all the seismic lines. On Figure 41 a few green anomalies at about 2000 m/sec, 20 Hz but there is hardly anything there and it is heavily deteriorated by noise. Since no suitable higher modes were present, a tighter viewing window focusing on the fundamental mode was created to make the DC picking phase easier and can be seen in Figure 43. At this point anything besides the fundamental mode is considered noise even if they are artifacts of higher modes, if they interfere with the fundamental mode it is called higher mode contamination.

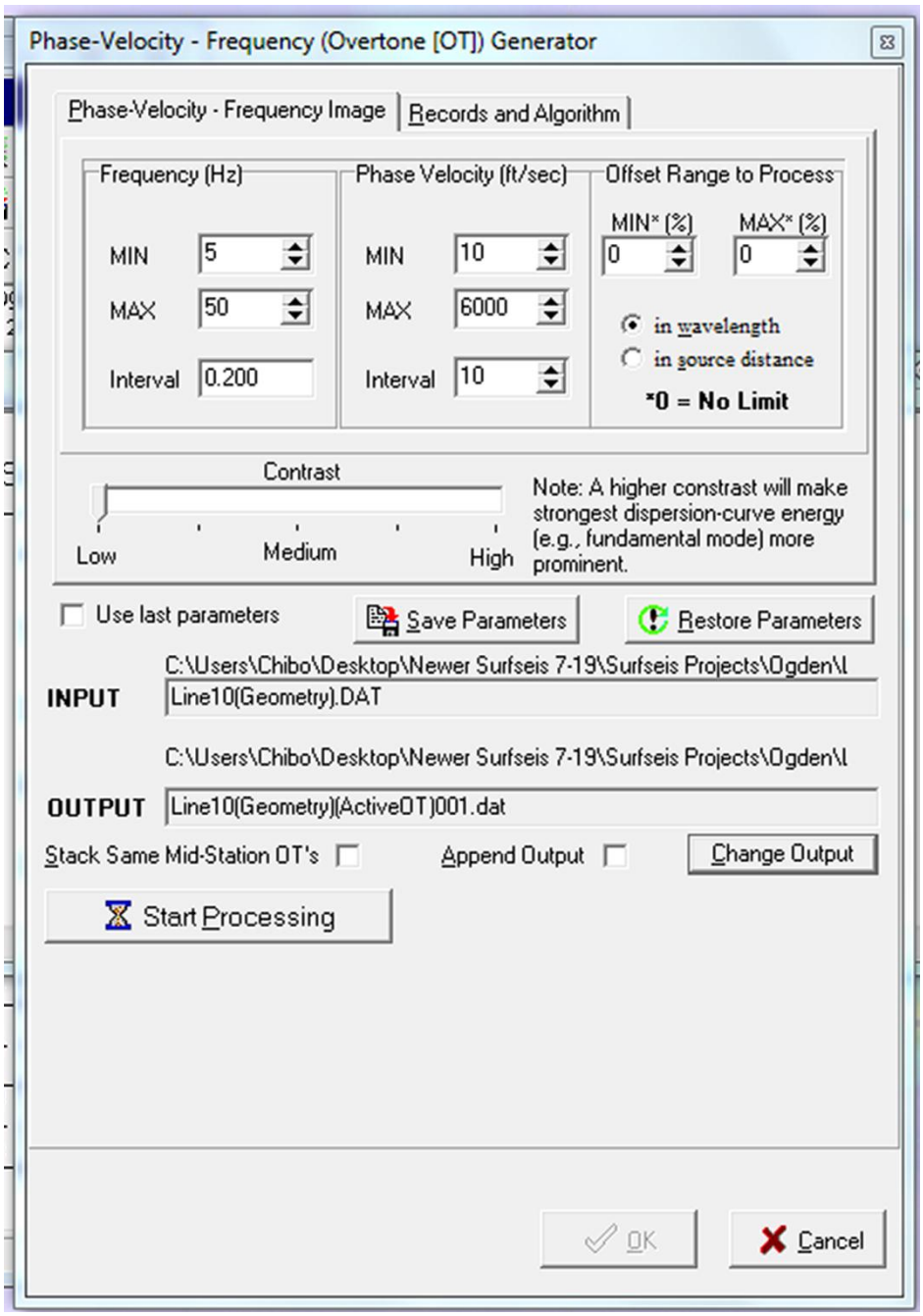


Figure 40 - Parameters for large window view in figure below

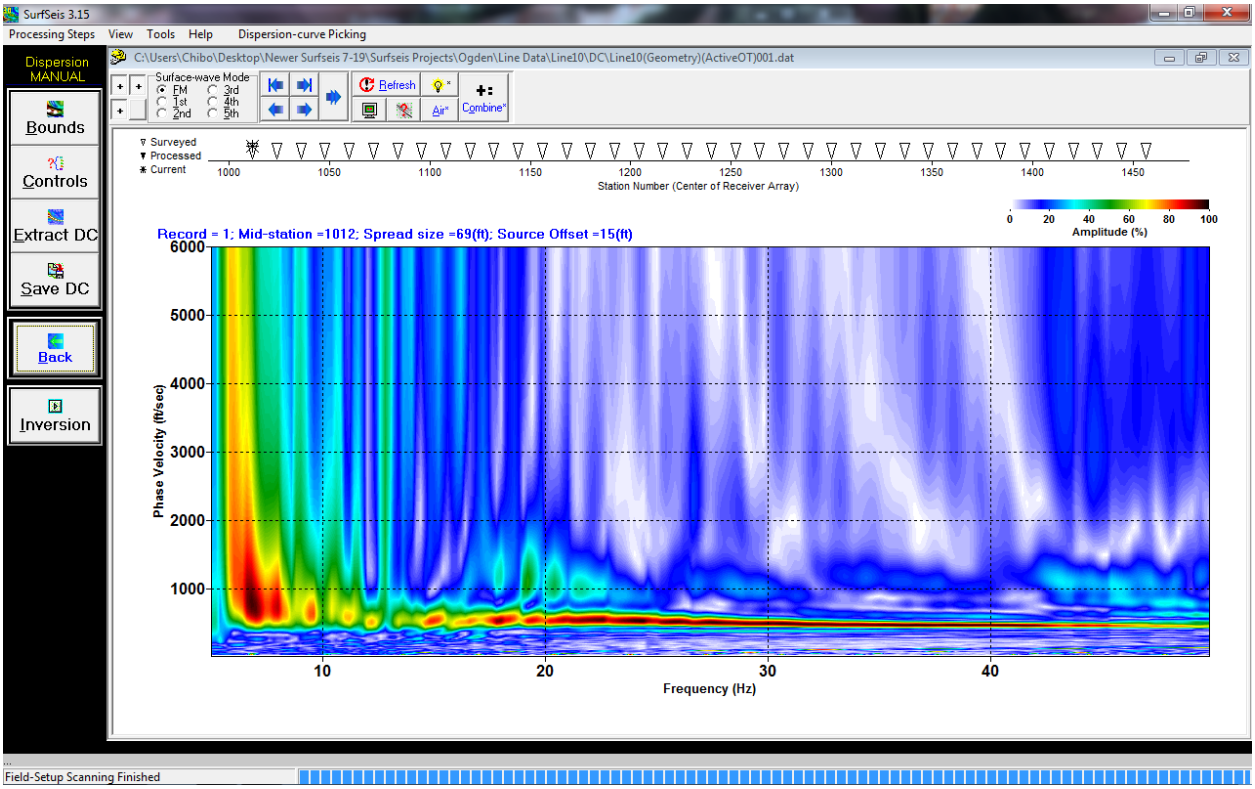


Figure 41 - Example of no higher modes, Line 10.

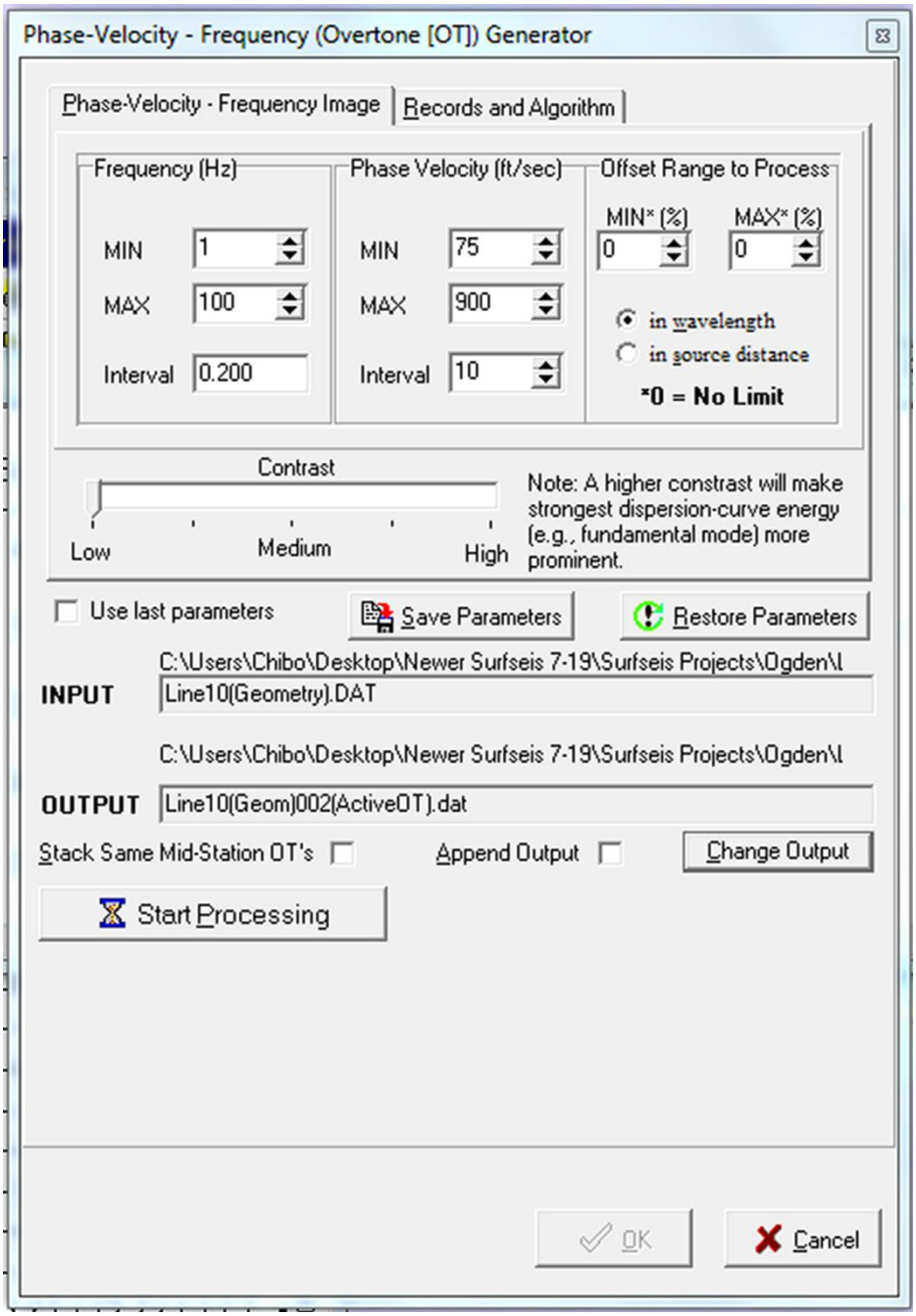

Figure 42 - Parameters for tighter window

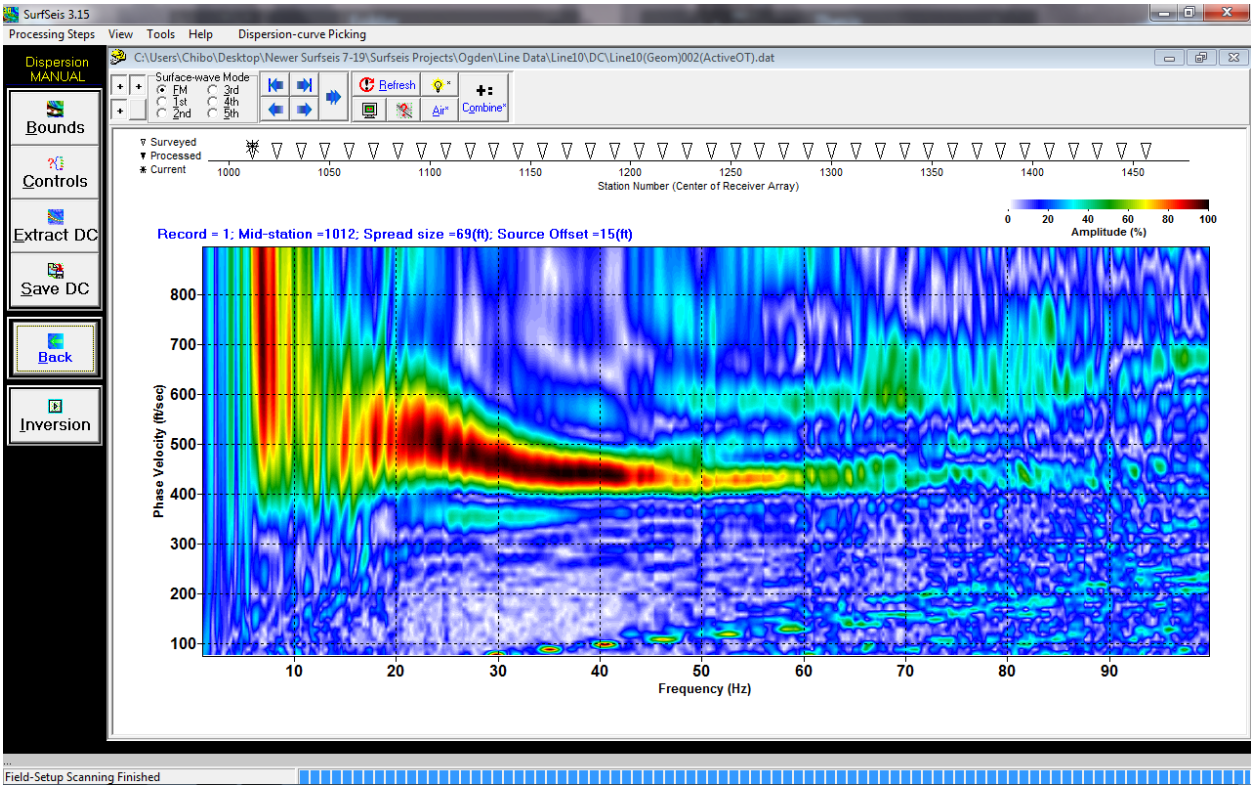

Figure 43 - Dispersion curve with smaller viewing window, Line 10

The basic principle behind picking dispersion curves (DCs) is picking along the highest amplitudes (red-black). The finer details of the picking of DCs is subjective and varies from person to person. There is no clear method that results in identical picking results between two people. If a person is conservative while another is aggressive, the final inversion results will differ greatly. The difference between aggressive and conservative picking has to do with how far left on the DC a person picks. Picking to the far left is risky and will often results in anomalous/inconsistent results. Picking to the far left is what constitutes the difference between aggressive and conservative picking, but picking to the far right is generally done in both picking approaches. Aggressive picking to the far left is generally discouraged unless certain circumstances can be established (geophone frequency, and bounds). Aggressive picking on either side of the DC is generally confirmed using the 'Bounds' tool and can be seen in Figure 44, it can be used to scan through all the DC's of a line to see the trend between each. By observing the trend you can easily pick to the far right with high confidence. Using this tool for picking to the far left is not as helpful and does not raise confidence in aggressive far left picking.

Picking to the far left is risky due to the basic principles of the data and is influenced by how the data was acquired. Lower frequencies are less stable and the frequency of geophones used influence how far left into these lower frequencies picking can theoretically be done (Kansas Geological Survey, 2012). Higher frequency geophones have a limited max investigation depth (40Hz ~ < 10 m) (Kansas Geological Survey, 2012). The rule of thumb learned from the 2012 Kansas Geological Survey MASW short-course was picking into the lower frequencies to the far left is limited by the frequency of the geophones used and that: 4 Hz geophones allow for picking as far left as 2.25 Hz, 10 Hz geophones allow for picking as far left as 5 Hz, and 40 Hz geophones allow for picking as far left as 15 Hz. Geophones with a frequency of 2 Hz can be purchased but they are expensive and difficult to operate (Kansas Geologic Survey, 2012). A in depth evaluation of the array setup can be found in the previous section.

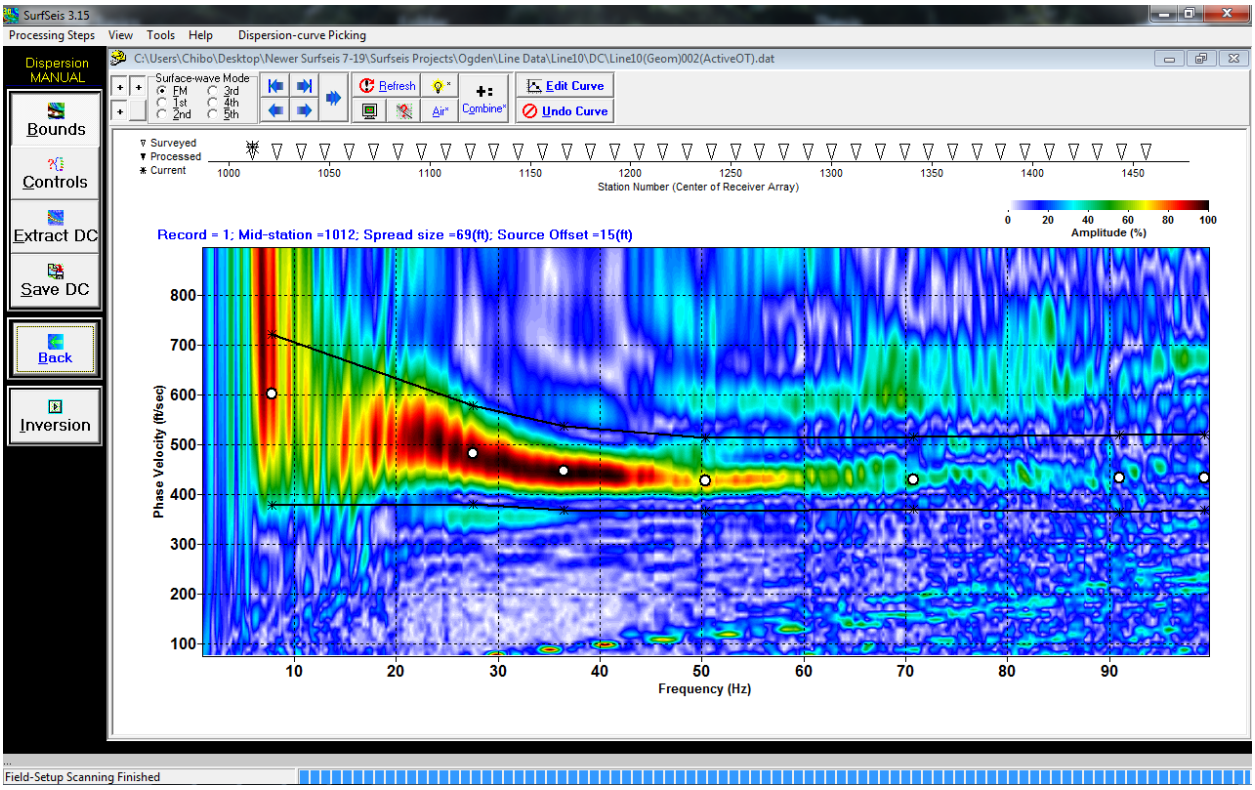

Figure 44 - Dispersion curve picking boundaries, Line 10

Regardless of the frequency of the geophones and the setup of the array used picking to the far left can be difficult due to the typical hyperbole appearance of the dispersion curve on the left side. The upturn at the left hand side should not follow the steep upturn but instead be a

slight curve reminiscent of the upturn (Kansas Geological Survey, 2012). An example of the slight curved upturn in the lower frequencies can be seen in the picked dispersion curve in Figure 45.

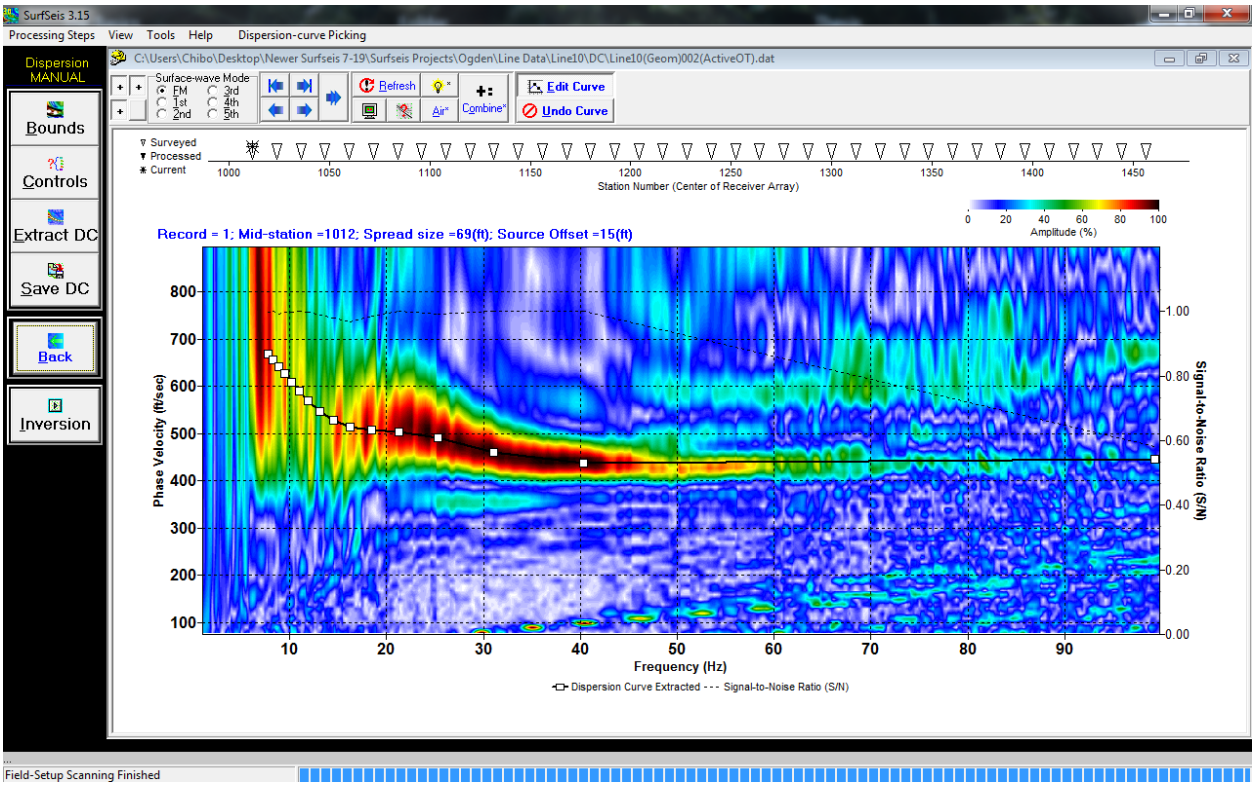

Figure 45 - Dispersion curve picked, Line 10

## *Inversion Without Integration*

Once picking of all the dispersion curves (DCs) in a line were finished the data was moved into the inversion phase. For this section all examples will come from the Line_12 (LossBot)MUTE dataset, basic information about the dataset can be found in Figure 46. First the data files created from picking of DCs were saved were imported into the inversion option in SurfSeis called 'Invert Dispersion Curves'. The dispersion files were loaded and sorted by surface location and displayed in the 'Initial Layer Model for Dispersion Curve' (Figure 47).

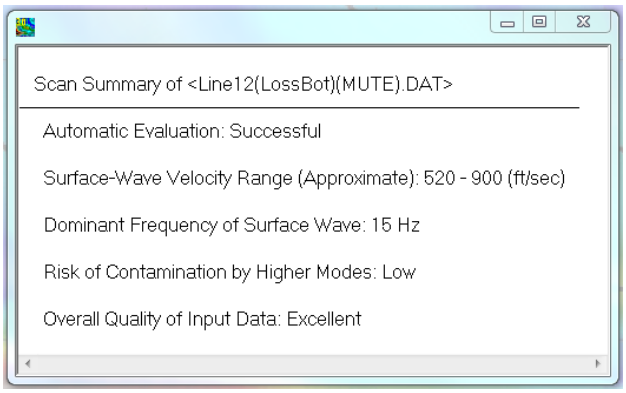


Figure 46 - Scan Summary of Line12(LossBot)(MUTE) dataset

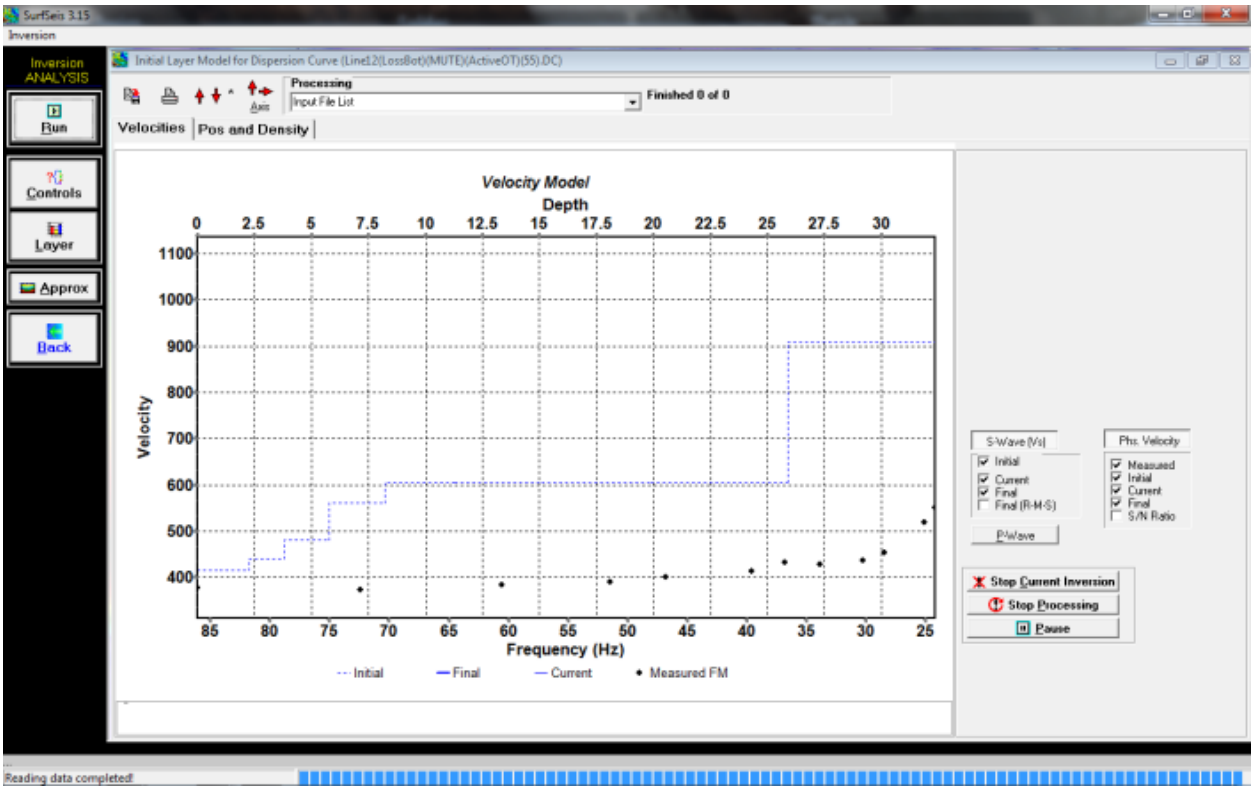


Figure 47 - Initial Layer Model for Dispersion Curve: Default 10 Layer

Once the DCs were loaded, parameters needed to be defined before the inversion can be run. Within SurfSeis there are a lot of parameters and setting that were evaluated before preceding the inversion calculation. The majority of these parameters and settings can be found within the 'Inversion Controls' that can be found under the 'Control' button on the left side of Figure 47. The 'Input Files' tab (Figure 48) lists the selected DCs, here specific DCs can be added or removed.

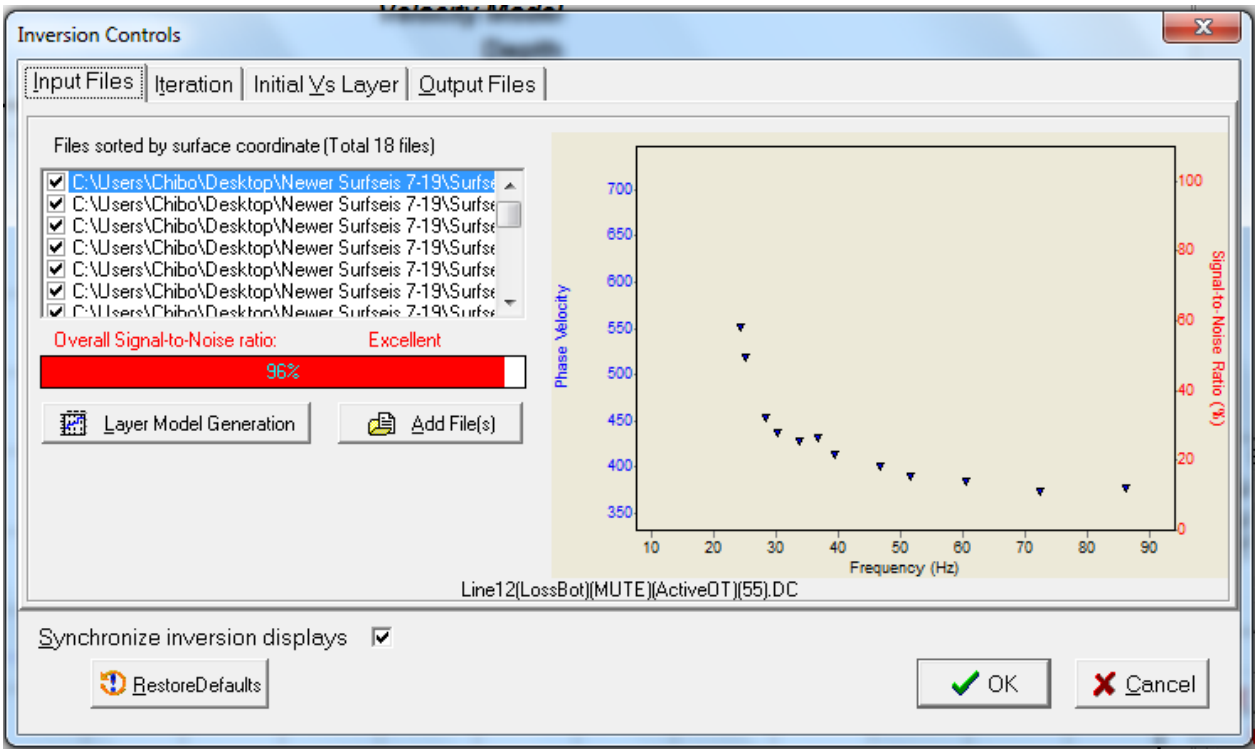


Figure 48 - Inversion Controls : Input Files Tab

Next the layer properties needed to be adjusted. Clicking on the 'Layer Model Generation' button to edit the layer properties. Here the default number of layers was 10 (Figure 49), but was changed to 4 layers and will be discussed later in this section, or the 'Depth conversion ratio' can be changed. The 'Depth conversion ratio' is the ratio between the depth of penetration and the apparent wave length (velocity/frequency). The 'Depth to half space (Zmax)' was calculated by the software and kept since SurfSeis did so well with the geometry. The 'Thickness model' can be changed here or after clicking the 'View/Edit Layer Model' button. 'Equal' would make all layers equal to one another, 'Variable' has thicknesses calculated from the inputted data and 'User Defined' is just that, user defined. Variable thickness was used for this inversion. The 'View/Edit' button pulls up a window (Figure 50) displaying the variables for the layers, it is possible to edit these variables and I will discuss this later.

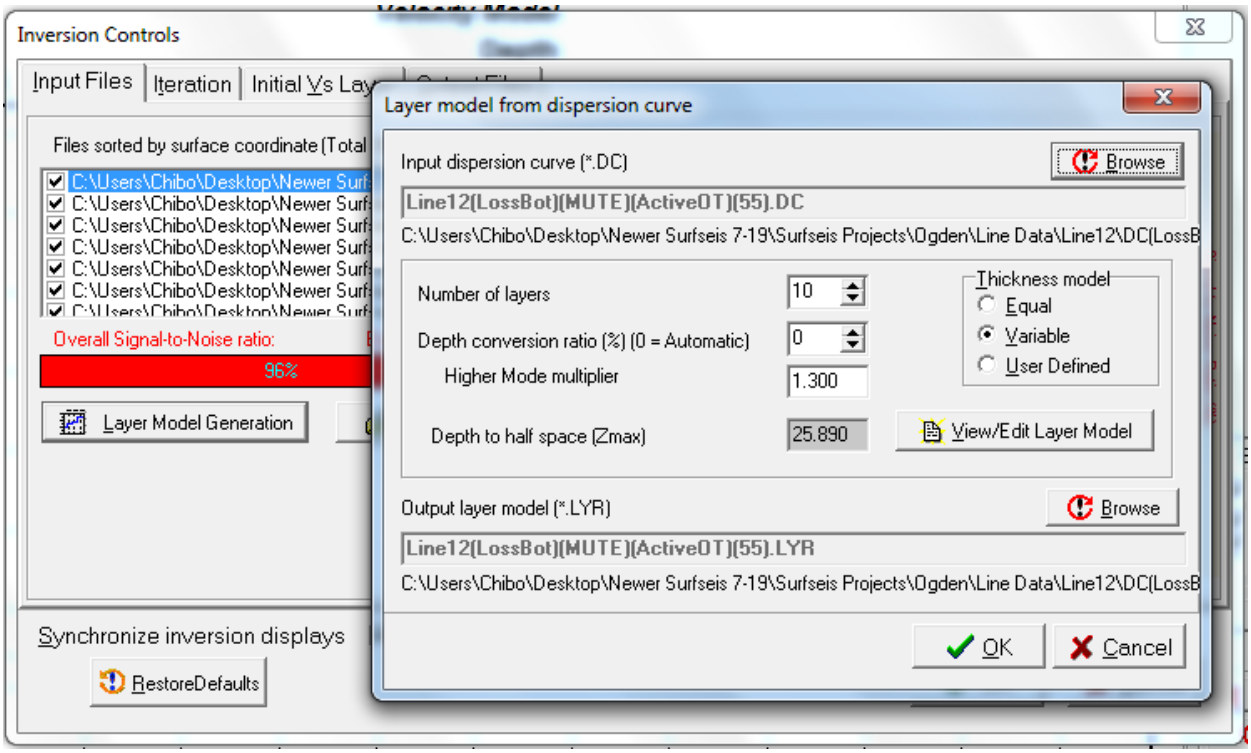


Figure 49 - Inversion Controls : Input Files : Layer Model Generation Window (Default 10 Layers)

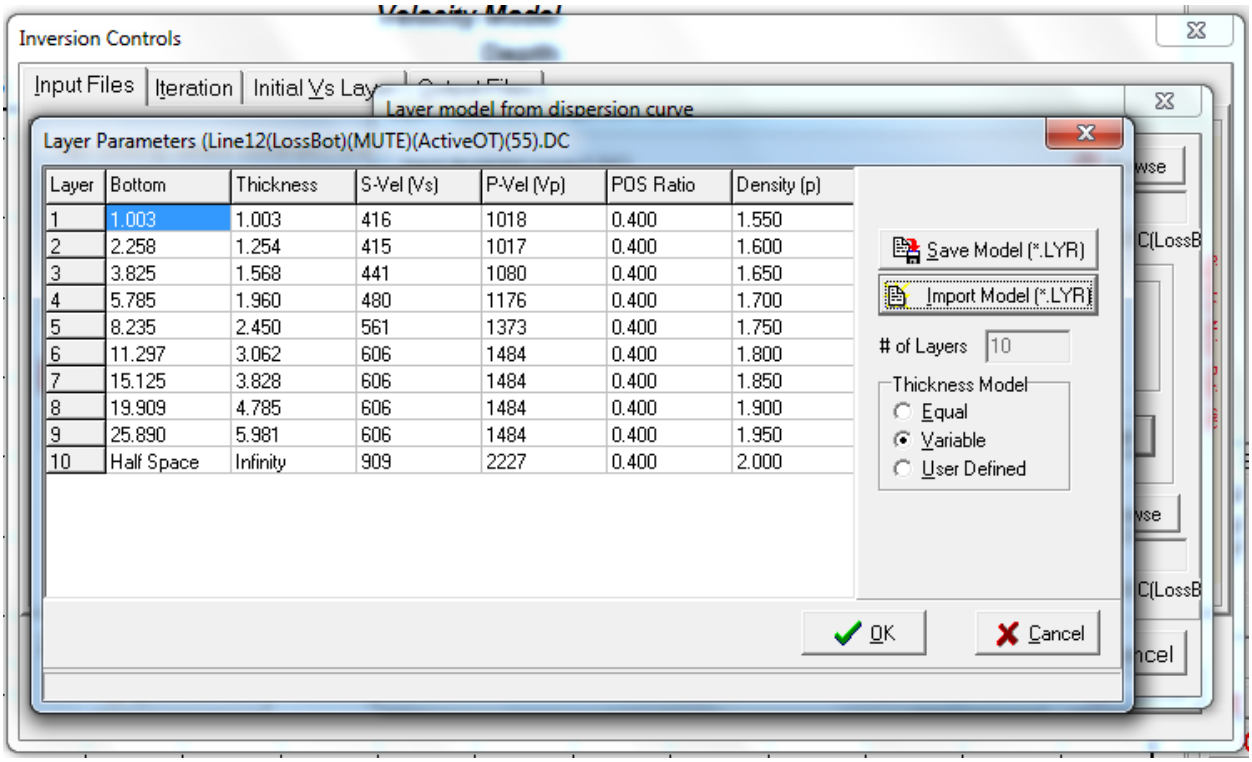


Figure 50 - View/Edit Layer Model Window (Default 10 layer model)

Going back to the ‘Inversion Controls’ window, the ‘Iteration’ tab (Figure 51) has a number of important variables that can be adjusted, most of the labels are self-explanatory. The

'Stopping Criteria' quadrant I kept the default 'RMS Error' of 5.00 and the 'Max Iteration' of 7. RMS(E) is the abbreviation for root-mean-square error and is a measurement of the difference between values a predicted by the inversion modeling. Iterations are the repetition of creating models, the results of one iteration is used as a starting point for the next iteration. Multiple iterations of a single dispersion curve yield an averaged result, but to many iterations can negatively affect the data by over averaging it. The A-Priori Assumption quadrant only affects the layer model and is only used if you intend to input variables from outside sources such as well logs or laboratory measurements. When I discus entering my laboratory measurements I will continue to have the fixed Poisson's ratio bubble checked. The 'Weighting of Individual Points' quadrant gives you the option of weighting the measured values for each black dot seen in the inversion window (Figure 47) also seen in the 'Input Files' tab (Figure 48). As long as the signal-to-noise ratios of the DCs are fairly good, equal weighting should be used. The final quadrant, the 'Inversion-velocity Range' section, has a default scale of 0.45 and 1.80 for the max and min velocities. I used the default scale values of 0.45 and 1.80 for all lines for consistency.

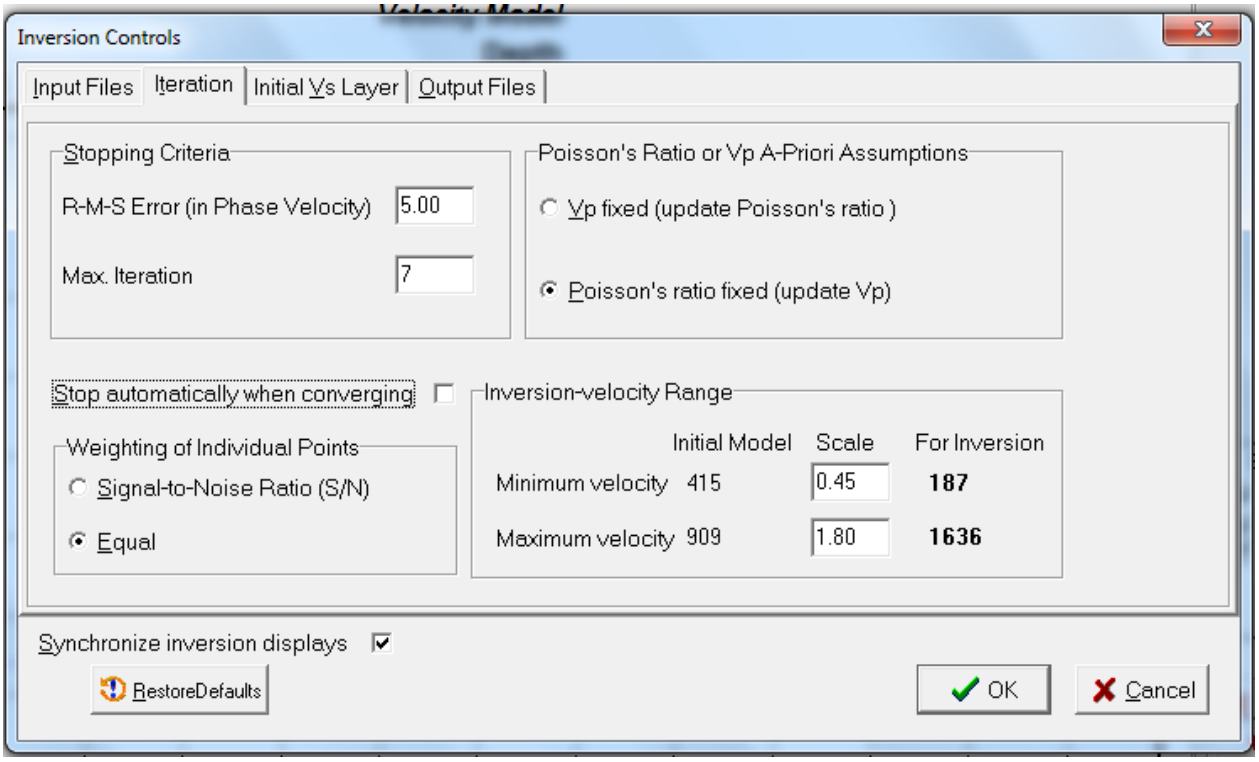


Figure 51 - Iteration Tab

The 'Initial $V_s$ Layer' tab gives the user control over whether or not a model from a different DC or from a different line is used to influence the current inversion/integration. The

'Each Dispersion Curve' option allows for each DC to be created individually with no influence form other DCs. The 'Previous Vs model inverted' option allows for the results from the previous line inverted influencing the current inversion. The 'Fixed $V_s$ model' option is used when adjustments, other than the number of layers, are made to the layered model. I will discuss the use of the 'Fixed $V_s$ model' later in this section.

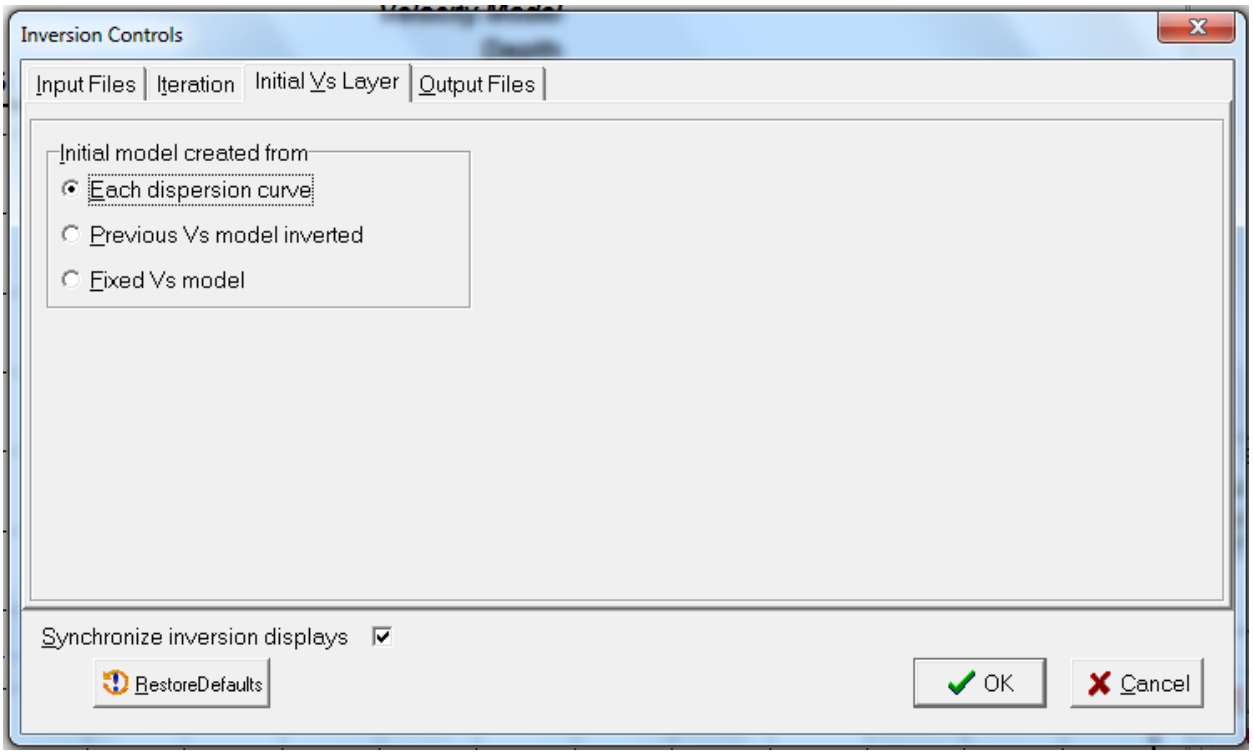


Figure 52 - Initial Vs Layer Tab

The 'Output Files' tab (Figure 53) deals with the outputted files, the location and name of the $V_s$ and RMSE files and the option of creating an excel file. The excel file can only be created when a fixed depth model is employed.

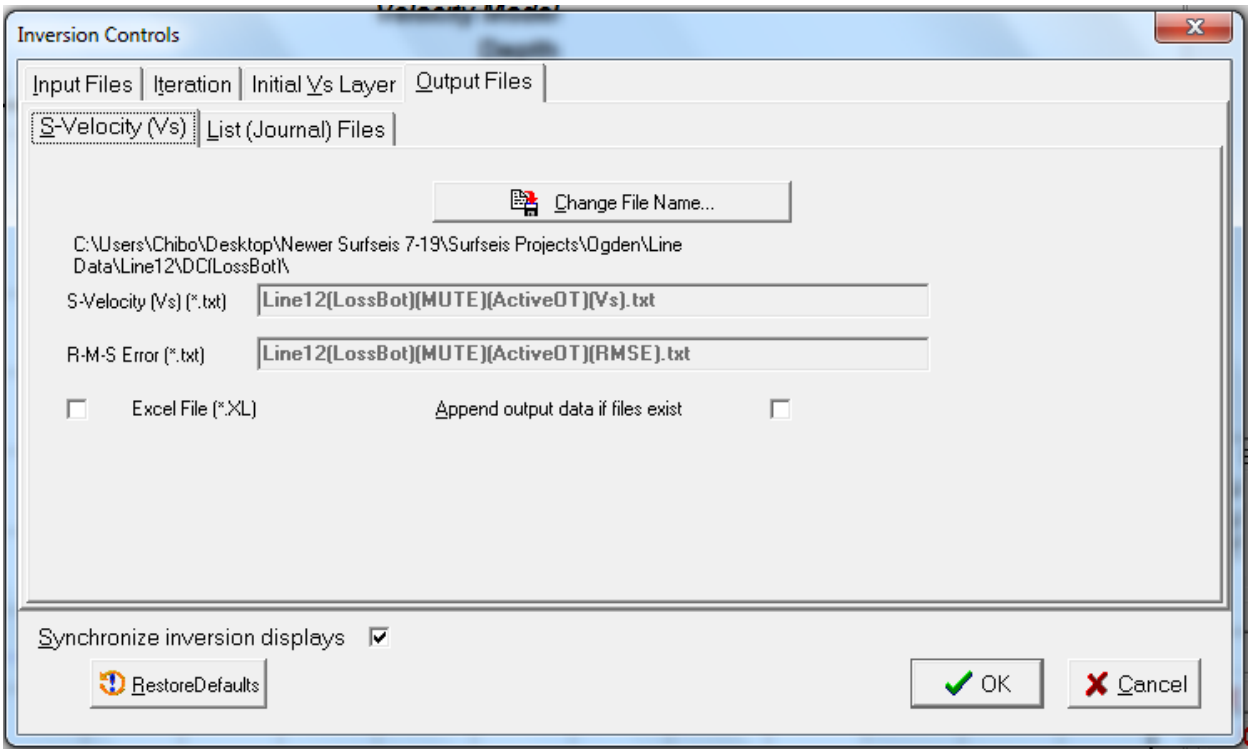


Figure 53 - Output Files Tab

The parameters used for initial inversions, no integration, were mentioned in the above paragraphs with the exception of changing the number of layers from 10 to 4 (Figure 54). A 4-layer model was chosen because the ATV image indicates several locations of distinct transitions in the upper 50 – 60 ft. Even if the inverted surface-wave data cannot reach a depth greater than 30 ft, it is likely at there could be 4 distinct locations with differing velocities. From Figure 47 at least two major steps in the velocity model can be seen at 74 Hz and 37 Hz, these two major steps are still be present in the 4-layer model seen in Figure 55 and Figure 56. By changing to the 'Pos and Density' tab a graph displaying the change in Poisson's ratio and Density can be found (Figure 58). Here you see that Poisson's ratio is considered constant at 0.4 and density increases slightly with depth. The 'Approx' button on the left allows us to see a simplistic example of what the $V_s$ 2D model might look like (Figure 57).

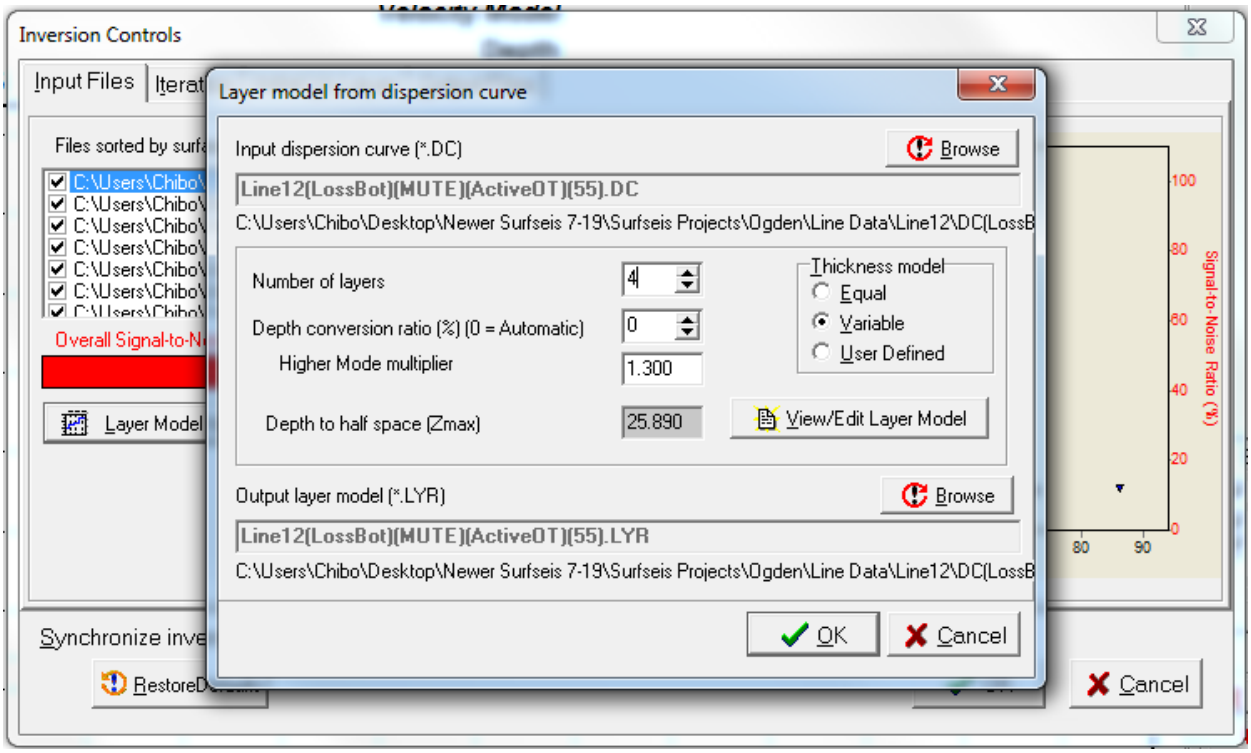


Figure 54 - Change to 4 Layer Model

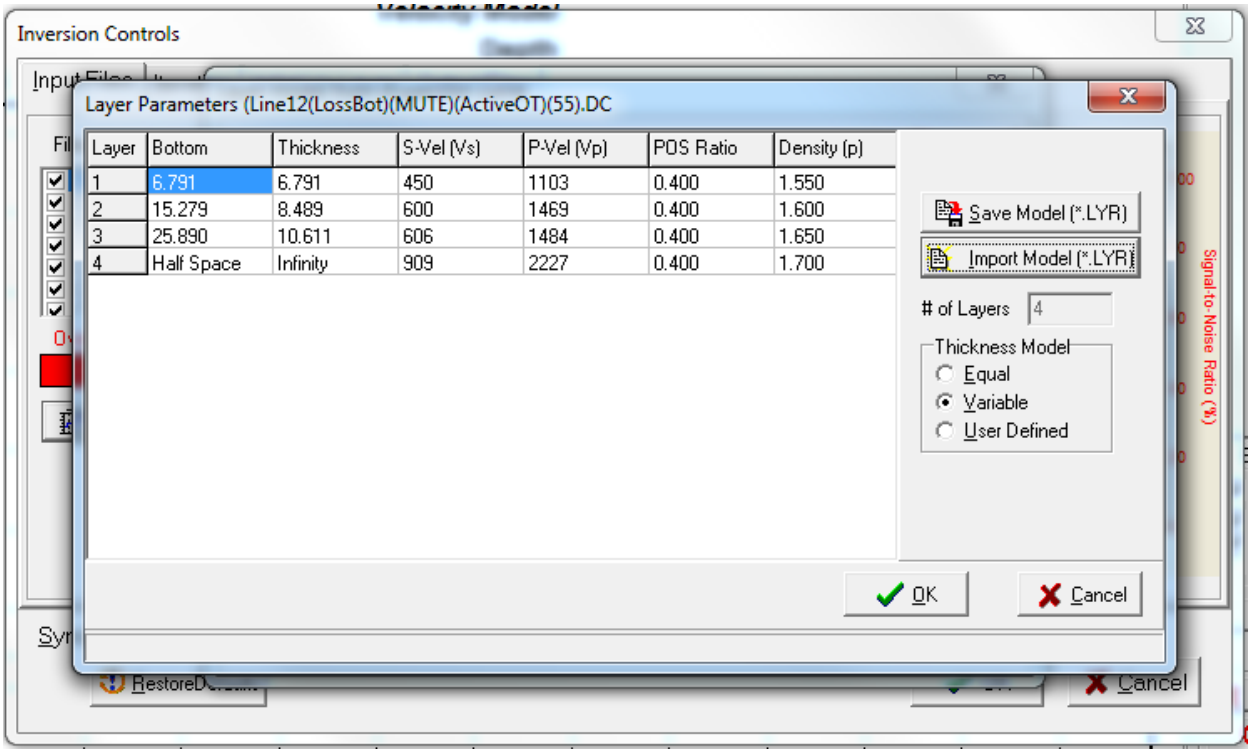


Figure 55 - View/Edit Layer Model : Layer Parameters

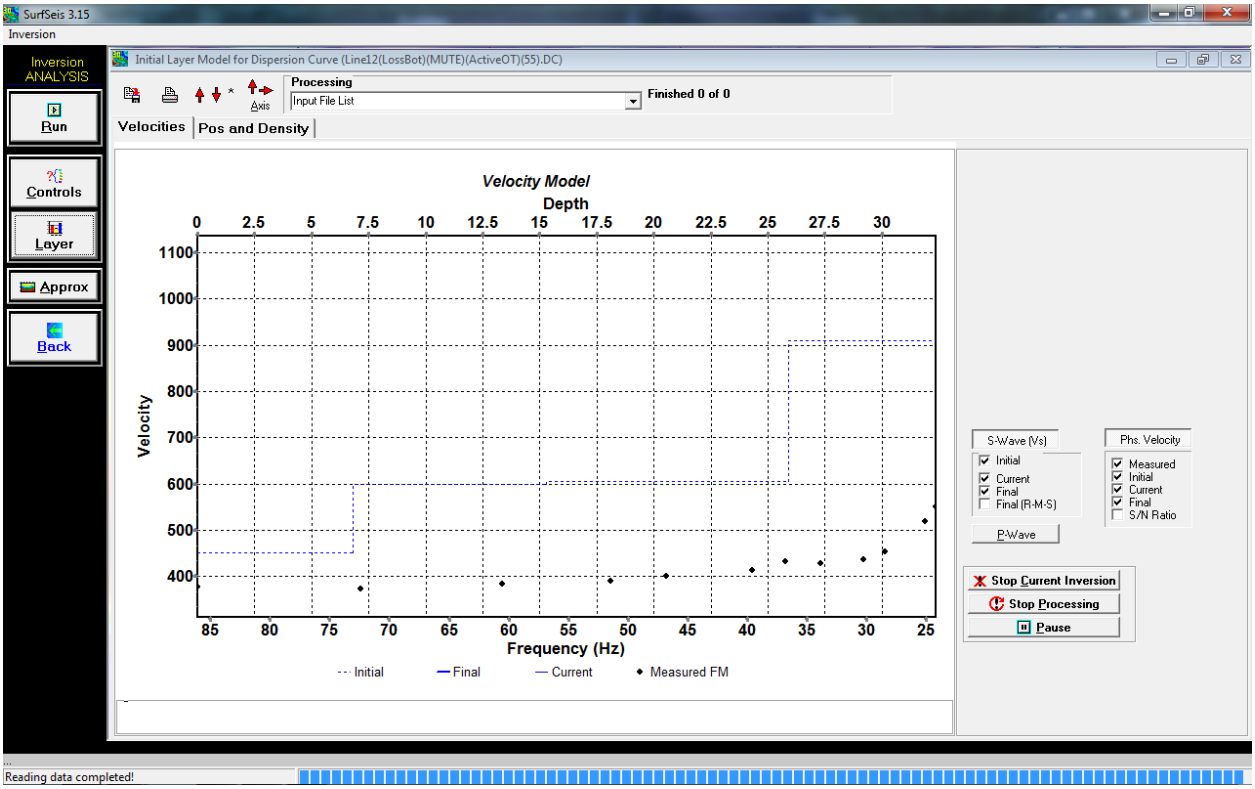


Figure 56 - Initial Layer Model for Dispersion Curve (4 Layer Model)

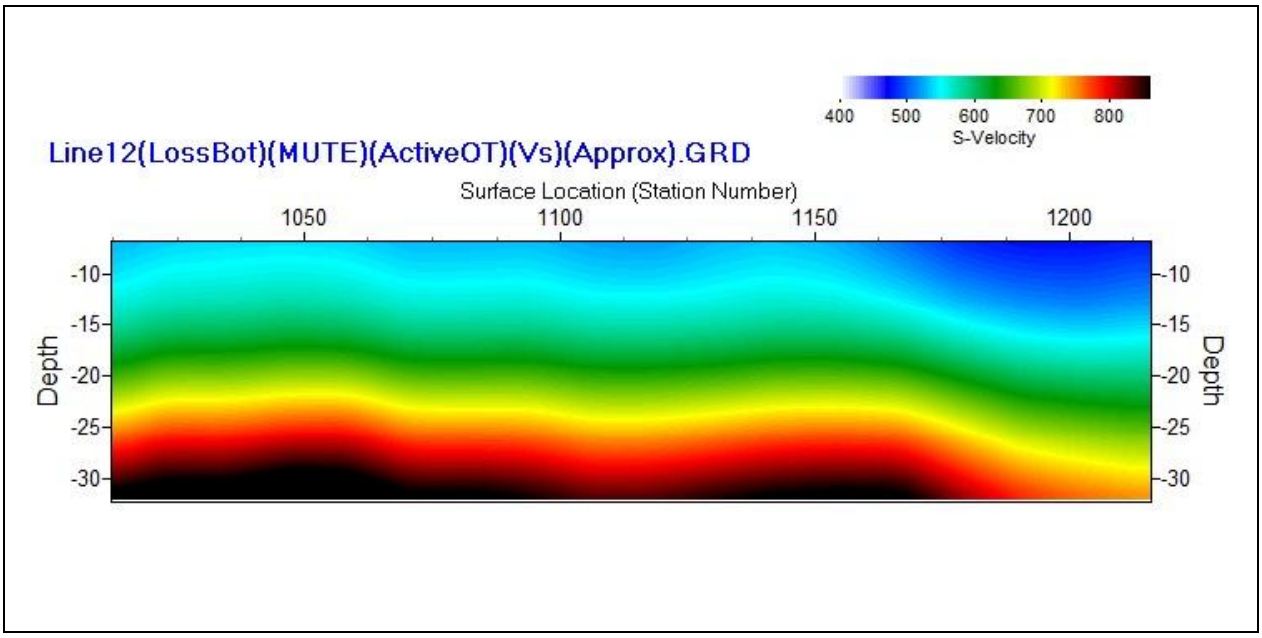


Figure 57 - 'Approx' 2D Vs Map/Model

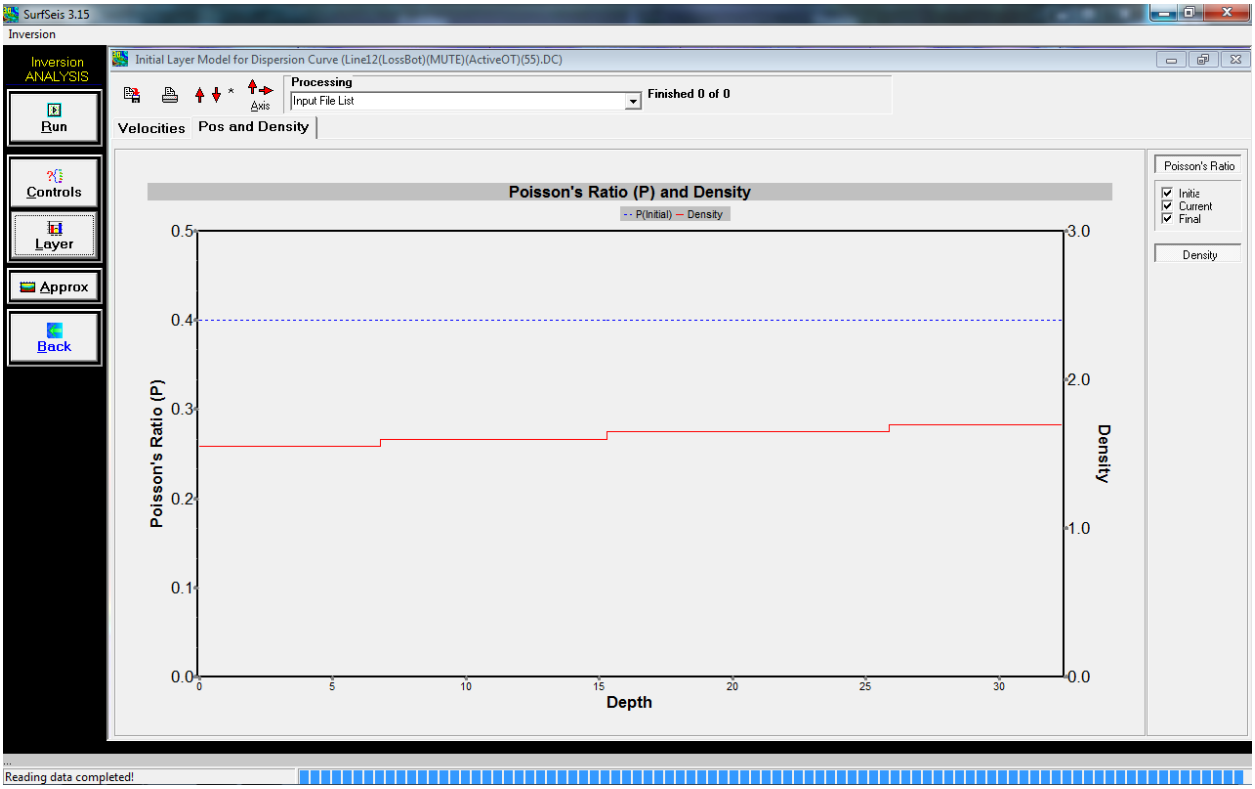


Figure 58 - Poisson's Ratio and Density Graph

Once all the parameters and variables are acceptable the next step is to run the inversion. While the inversion is running the screen with display the progress (Figure 59 and Figure 60) calculation for each iteration and from the previous DC model (Figure 60, Figure 61, Figure 62 and Figure 63). The dashed blue line is the initial generated layer model before the iterations started. The thick blue line is the final model generated from the iterations done on the previous DC. The thin solid blue line displays the current model, and changes with each iteration. The curved bold blue line is the DC from the previous modeled DC. The curved green line is the currently modeled DC. The curved dashed green line is the initial model DC; it is linked with the blue dashed line. The black dots are labeled as the 'Measured FM'; they are measured from the current DC being inverted/iterated.

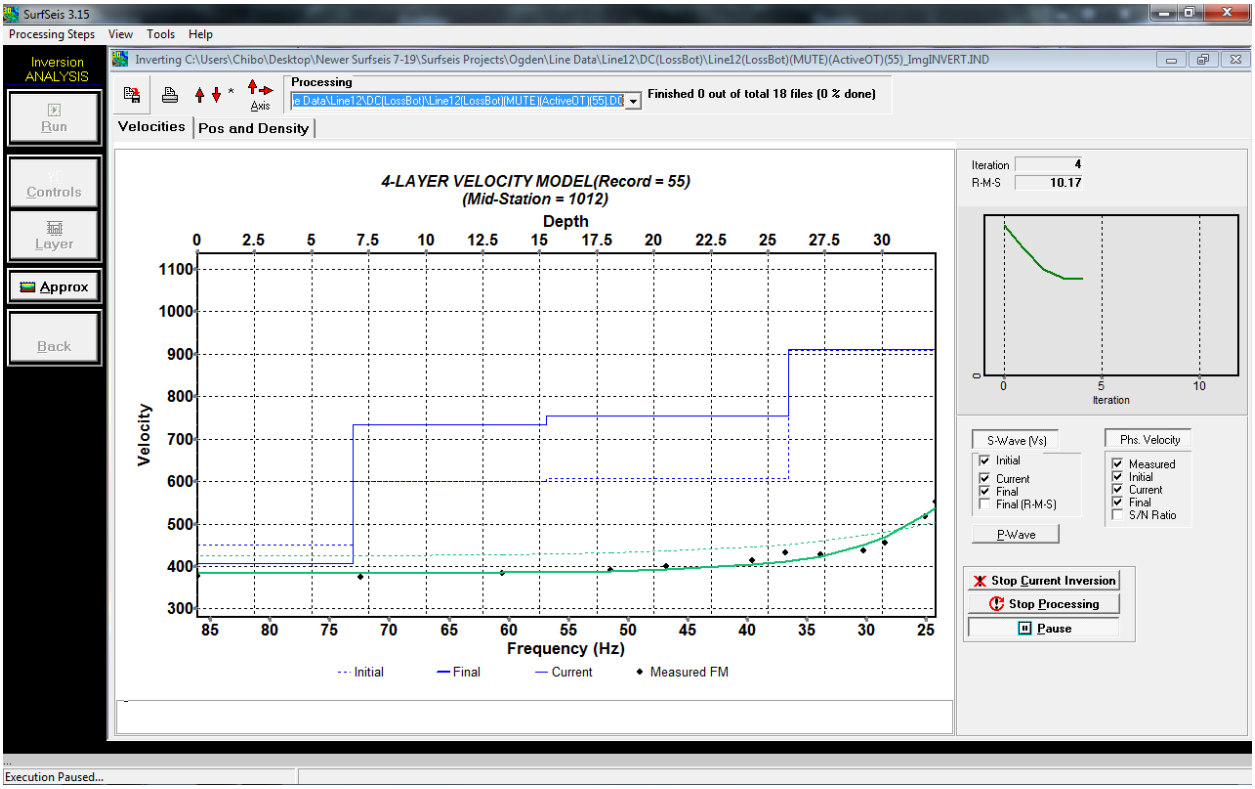


Figure 59 - Before first DC inversion has finished (0 of 18)

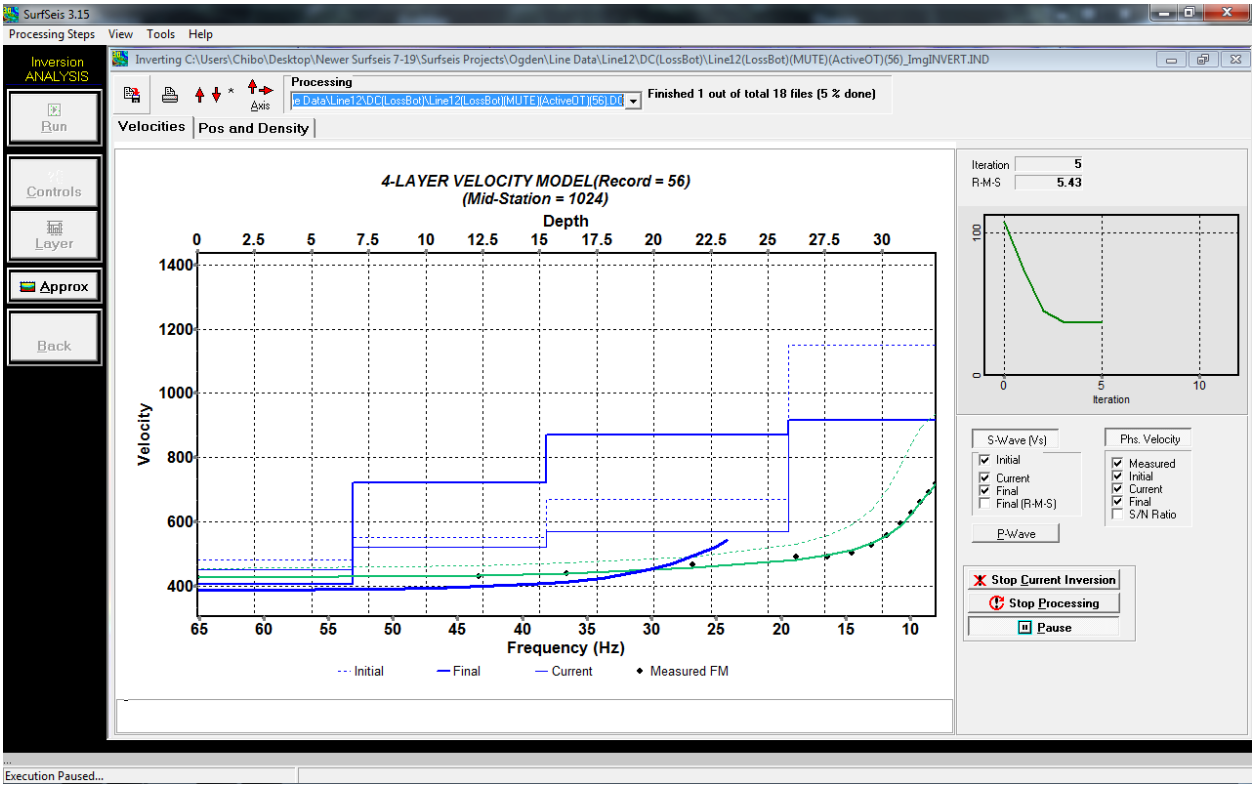


Figure 60 - After first DC inversion finished, notice more lines (1 of 18)

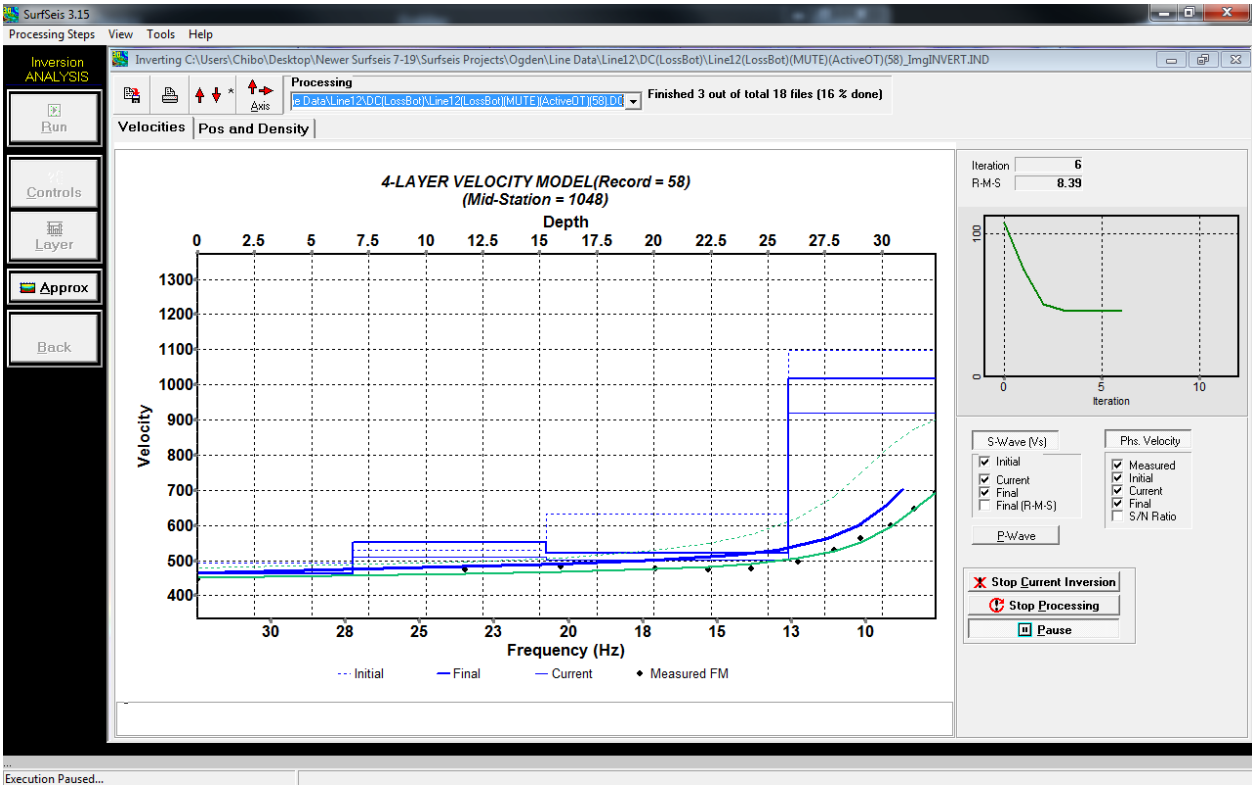


Figure 61 - DC inversion (3 of 18)

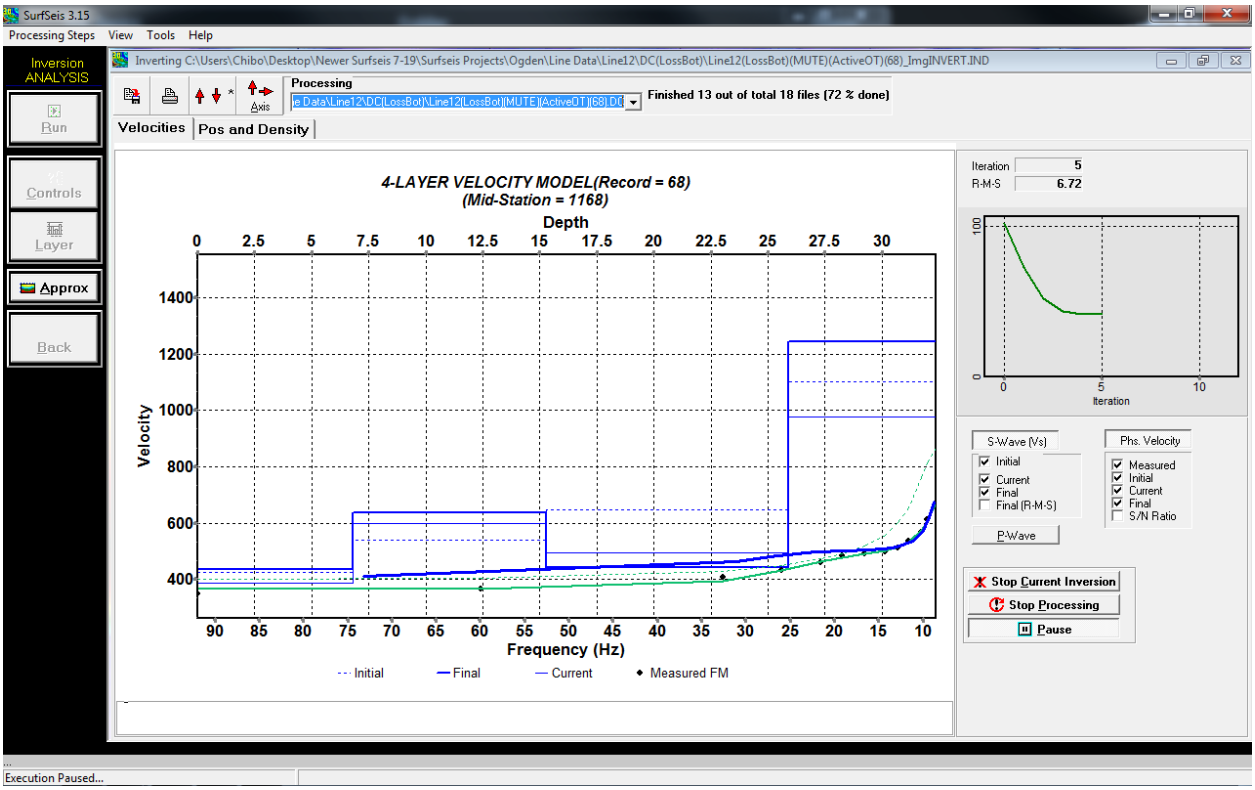


Figure 62 - Dc inversion (13 of 18)

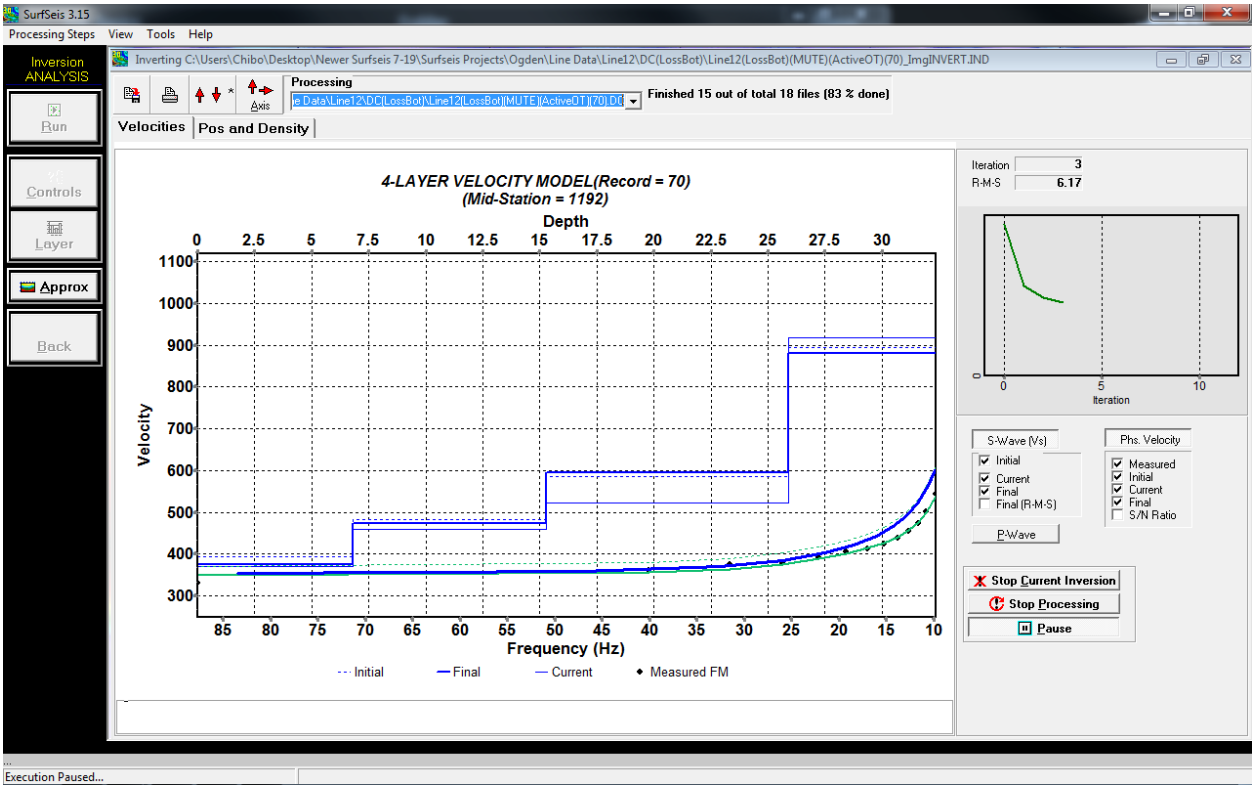


Figure 63 - DC inversion (15 of 18)

Once the software has finished the inversion results, 2D $V_s$ and RMSE models, will automatically be displayed. The 'Approx' model (Figure 64) can be compared with the $V_s$ result (Figure 65), it tends to be less detailed and often does not match well with the $V_s$ result. The range of the color bar tends to vary depending on the data inputted; from line to line the color bar range varies and hampers comparison/linking. All inversions were additionally saved with a range of 200 – 1000 (Figure 66). The 2D model of the RMSE can be found below (Figure 67).

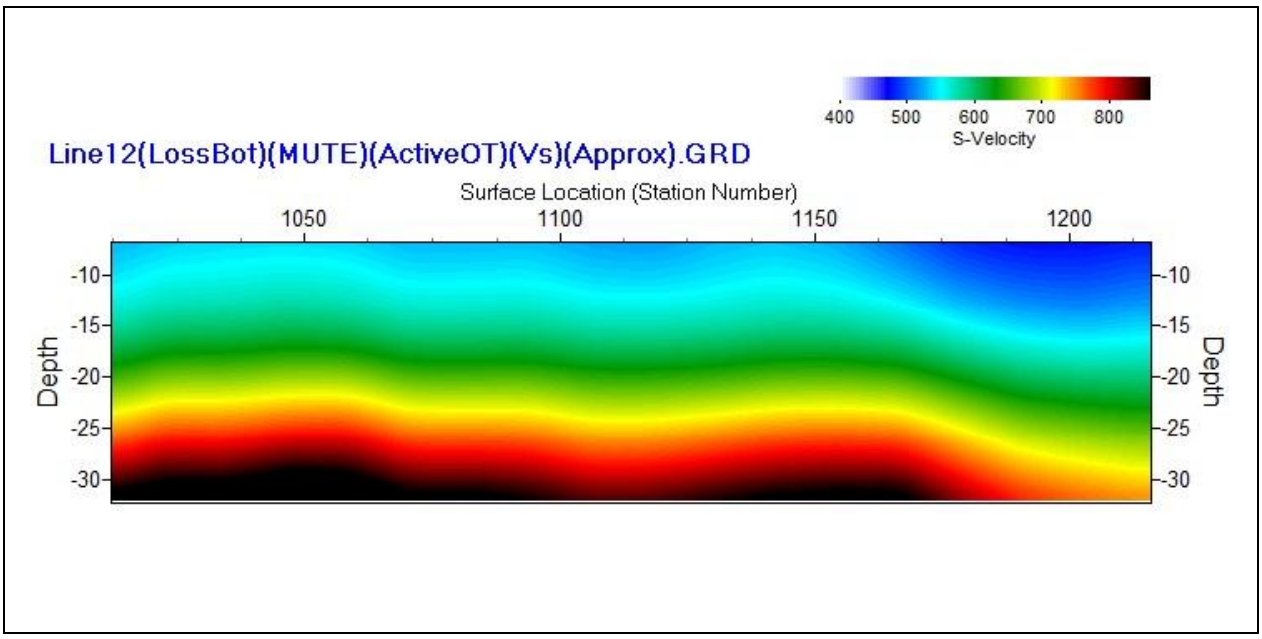


Figure 64 - Approx (again)

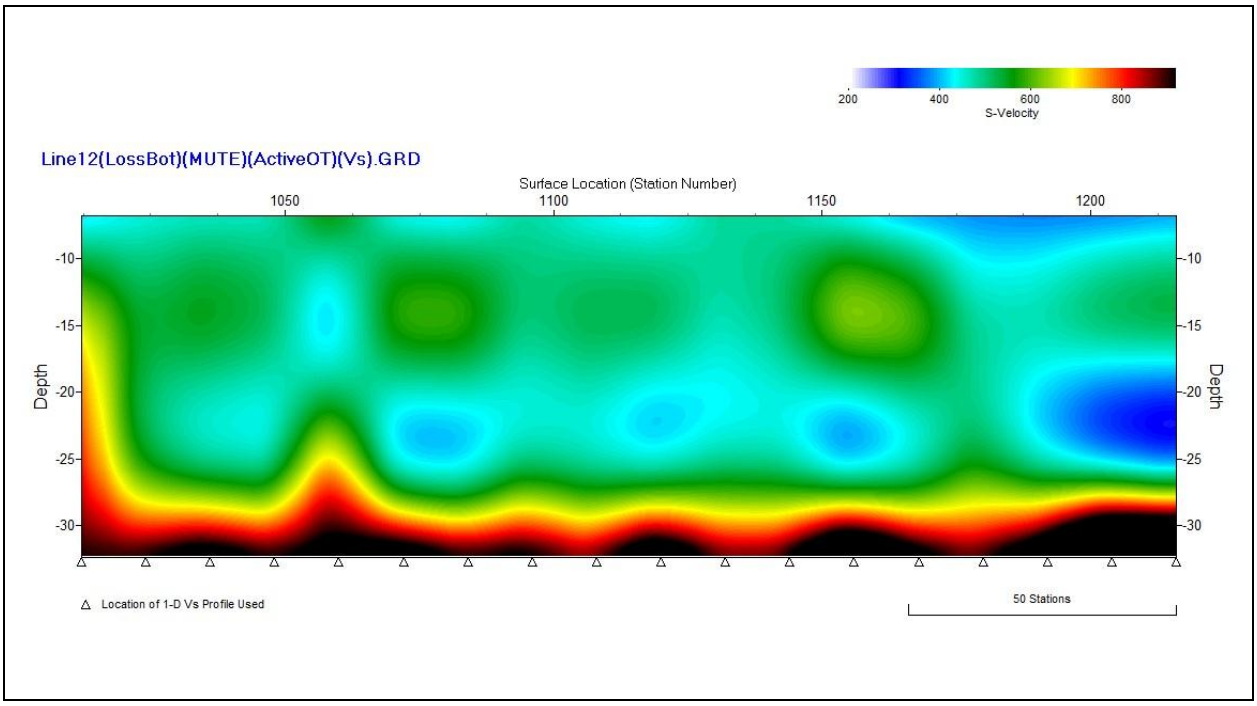


Figure 65 - Vs Model (Default Range)

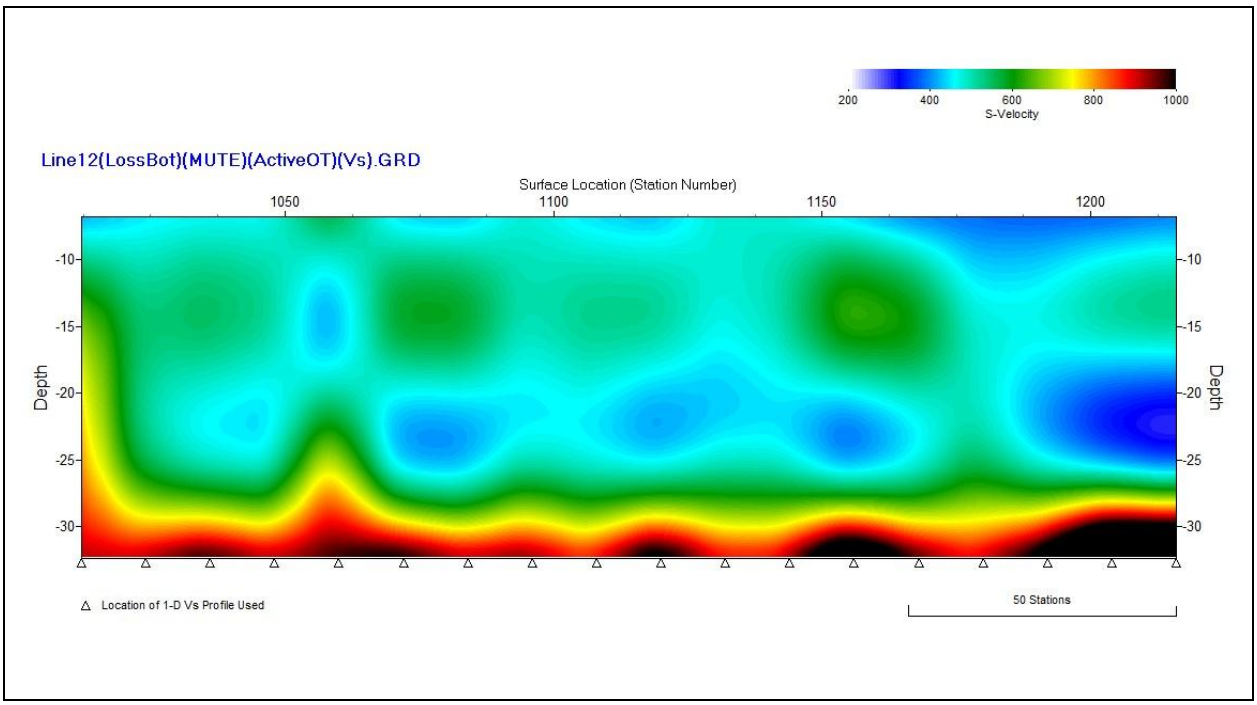


Figure 66 - Vs Model (Range 200 - 1000)

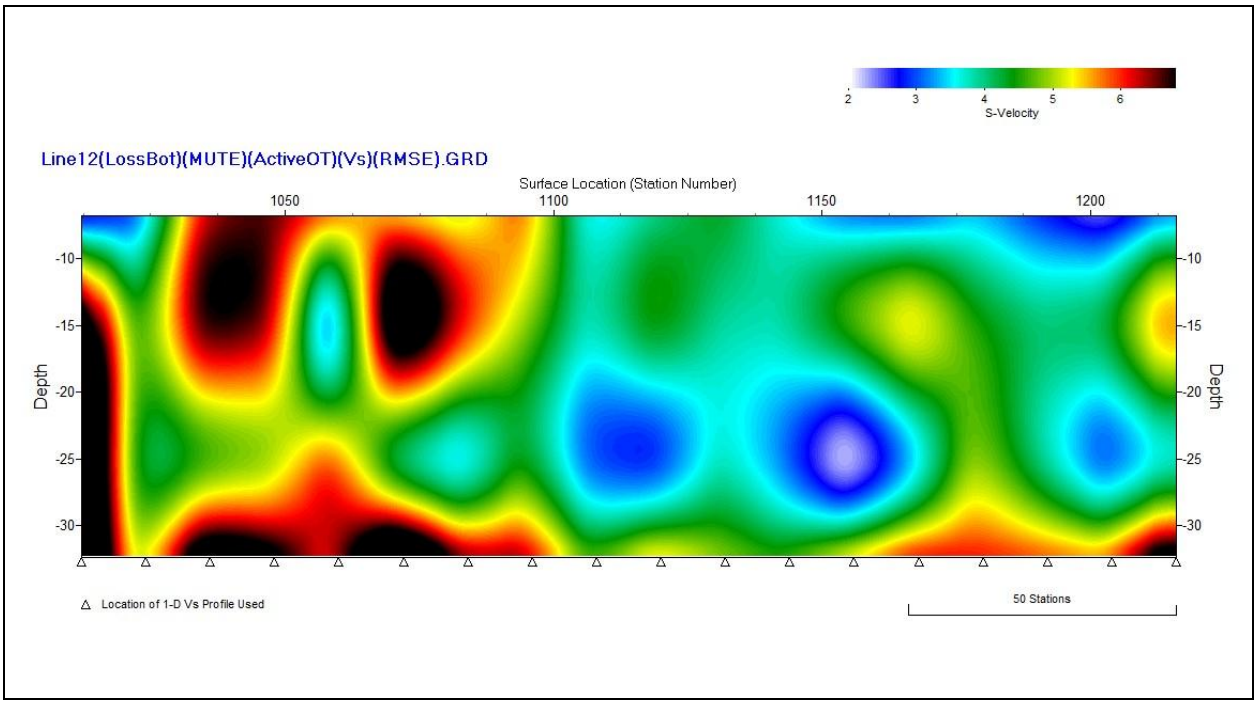


Figure 67 - RMSE Model

## *All inversion results from Ogden without integration*

The mute line, scan summaries and inversion results from all 6 lines from the Ogden site can be found below. The dispersion curves and additional data can be found in the appendix.

***Line 10***

1. Mute

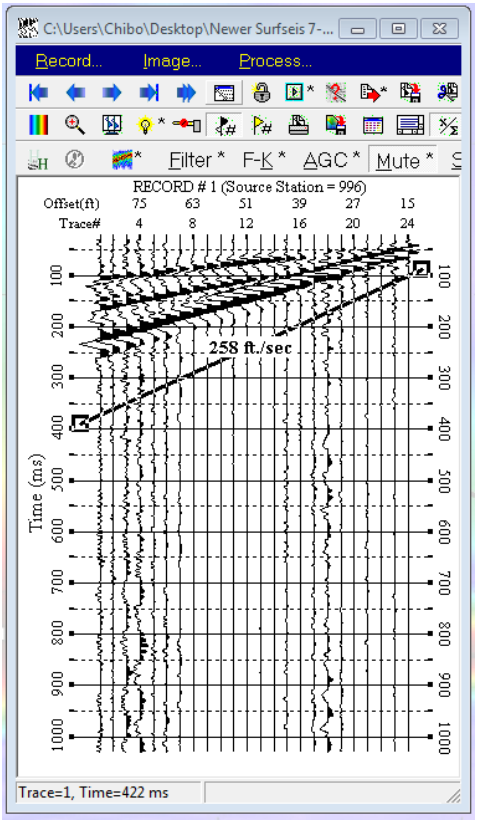


Figure 68 - Line 10 Mute Line displayed on a Raw record, this is the mute used for LossBot

2. Scan Summary

    a. Raw

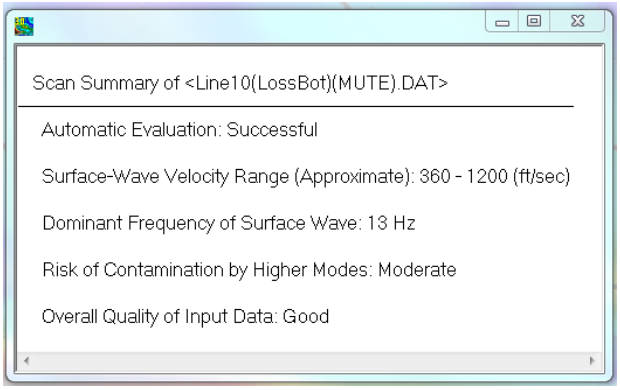


    b. LossBot

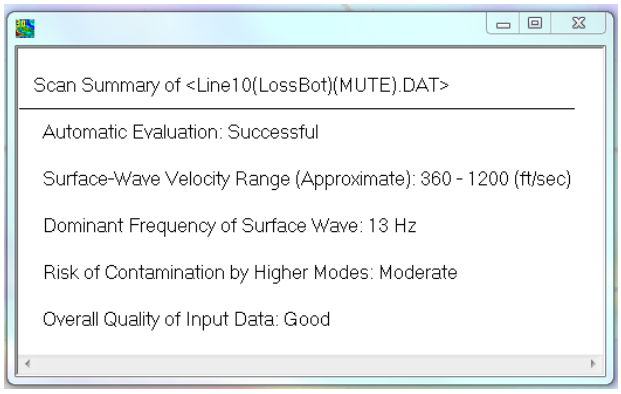


3. Vs

a. Raw

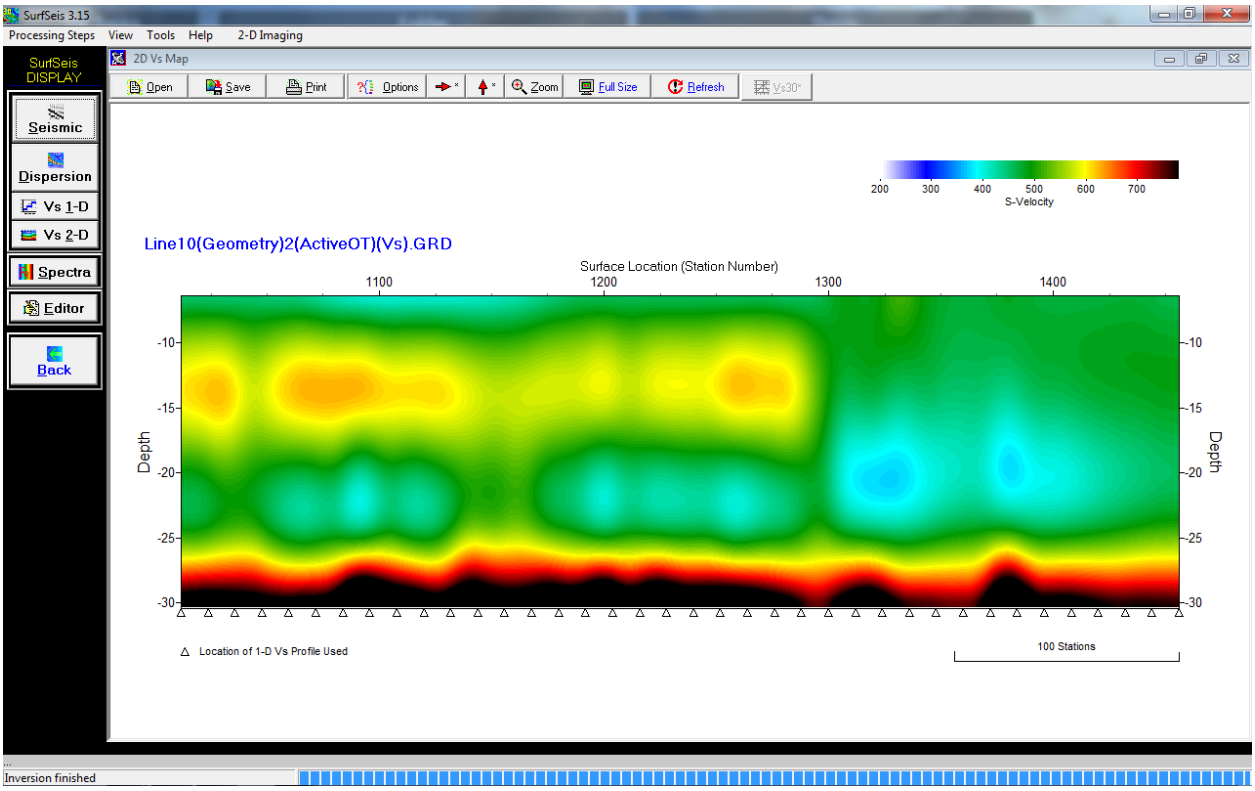


Figure 69 - Line 10 Vs Raw

b. LossBot

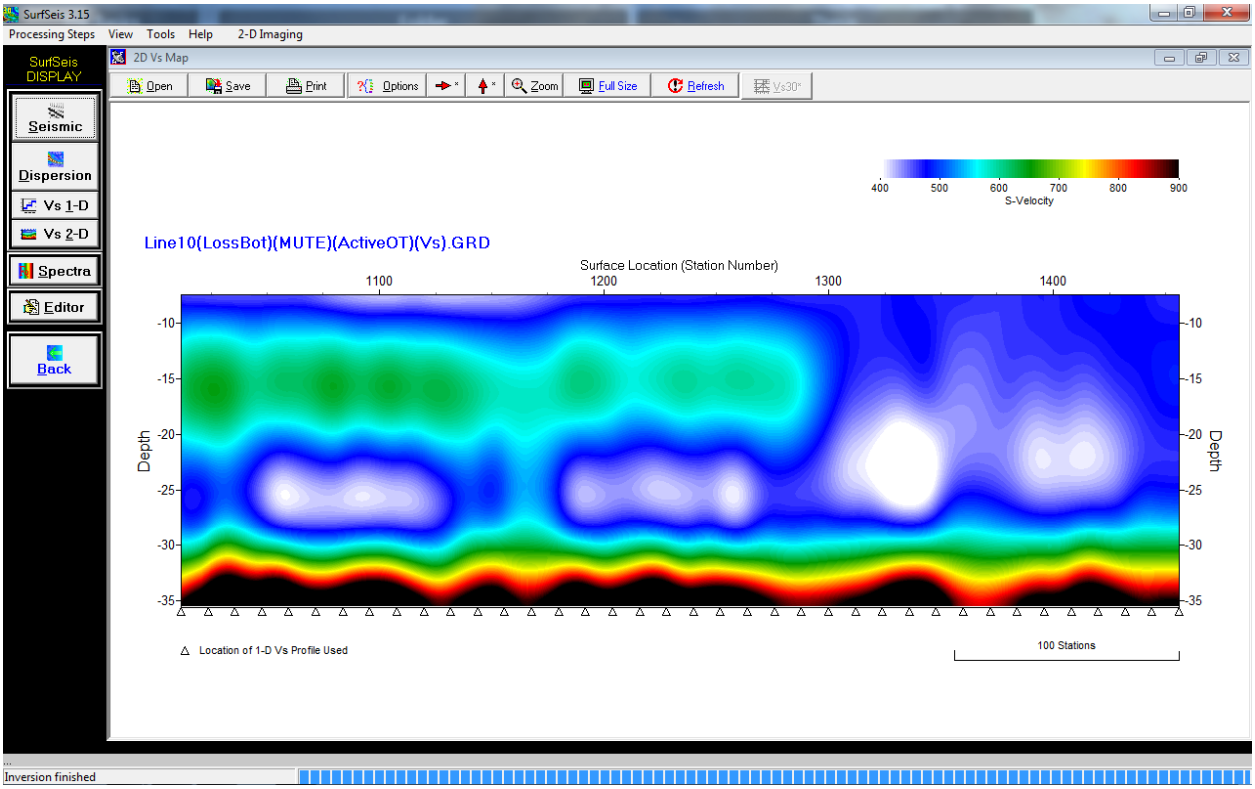


Figure 70 - Line 10 Vs LossBot

4. RMSE
    a. Raw

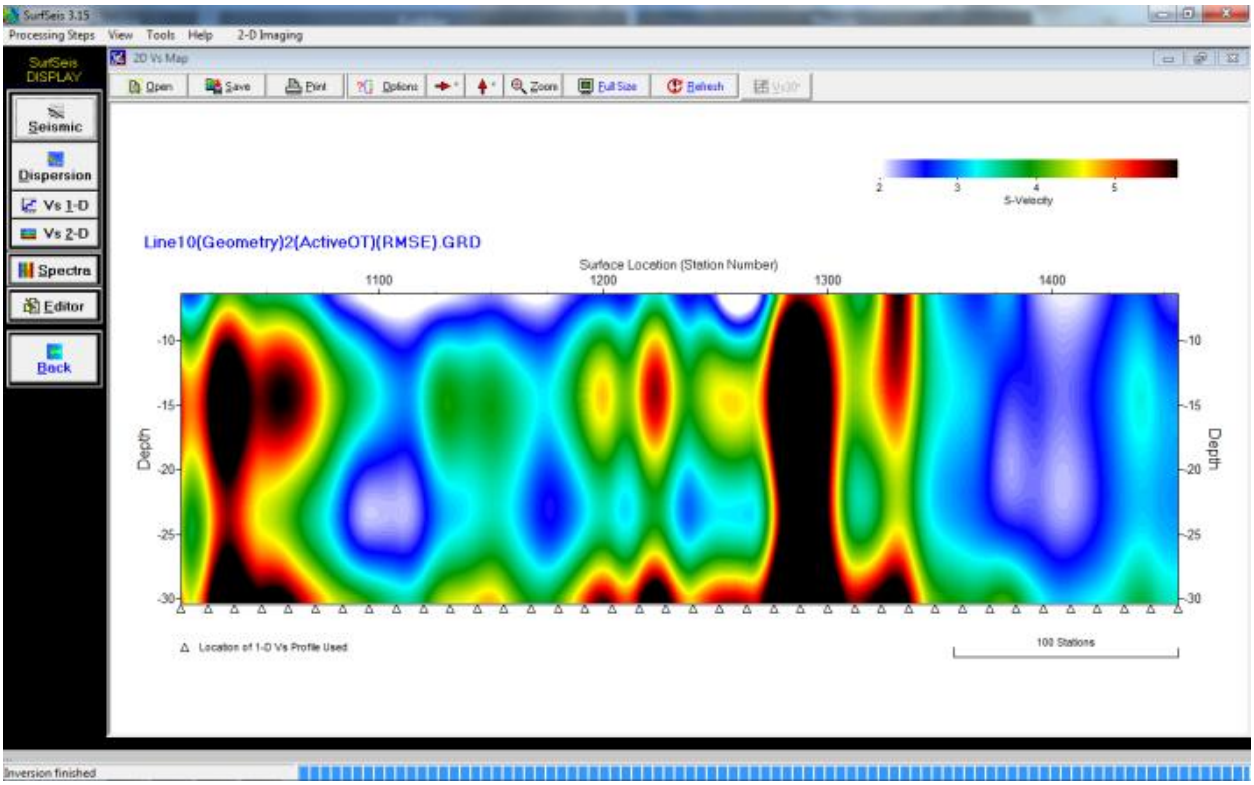


Figure 71 - Line 10 RMSE Raw

b. LossBot

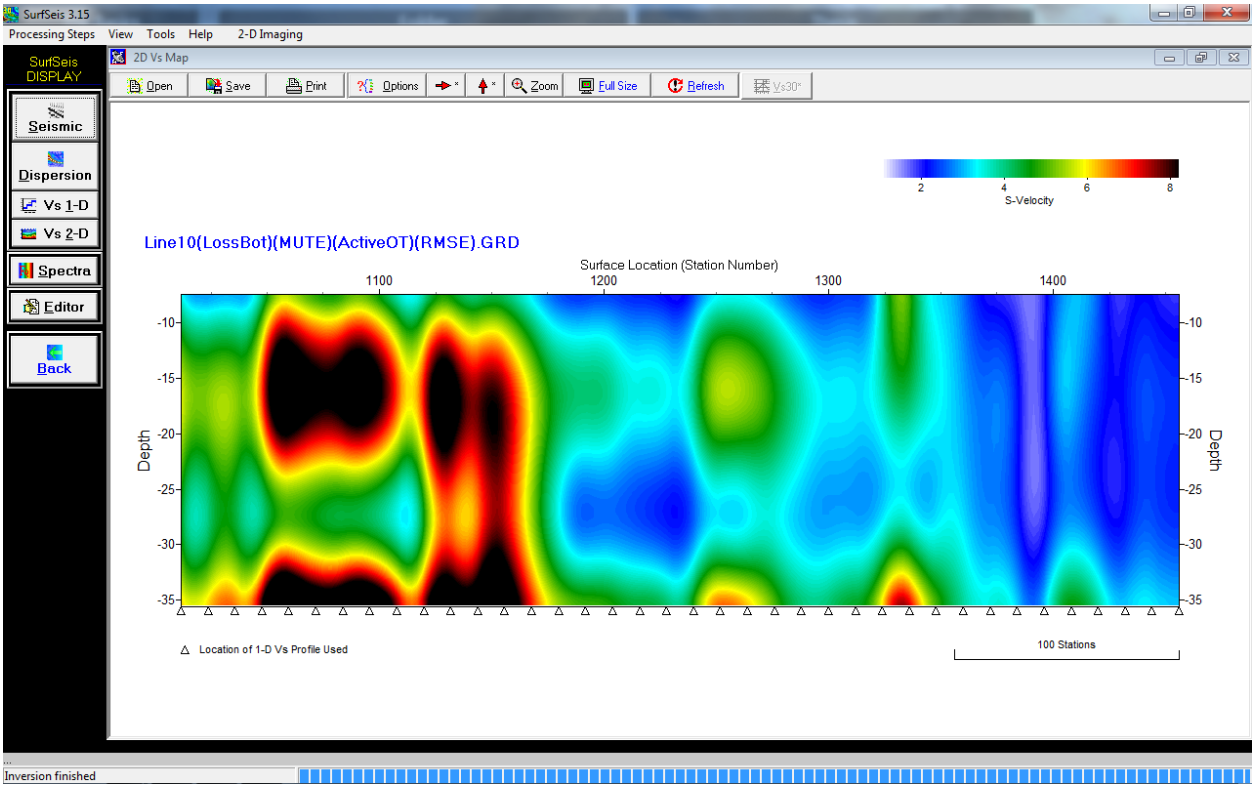


Figure 72 - Line 10 RMSE LossBot

***Line 11***

1. Mute

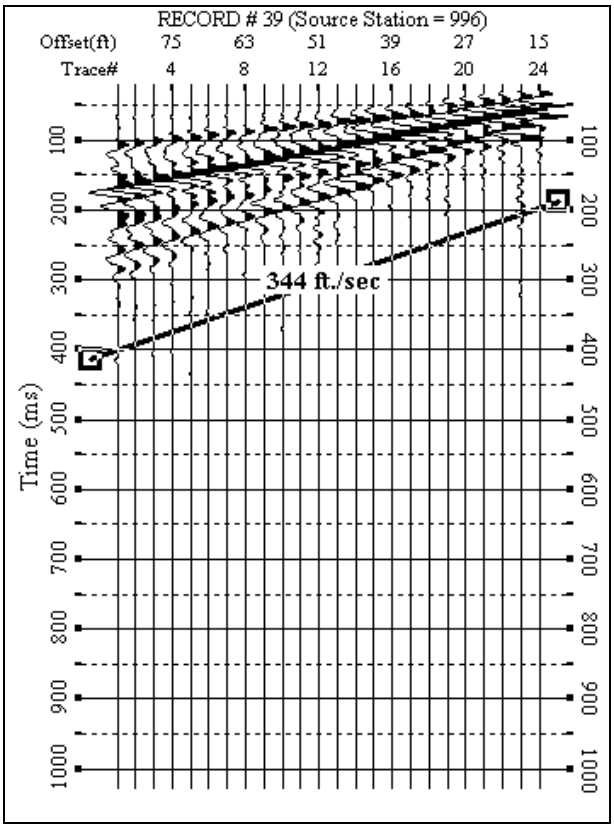


Figure 73 - Line 11 Mute line for LossBot

2. Scan Summary
    a. Raw

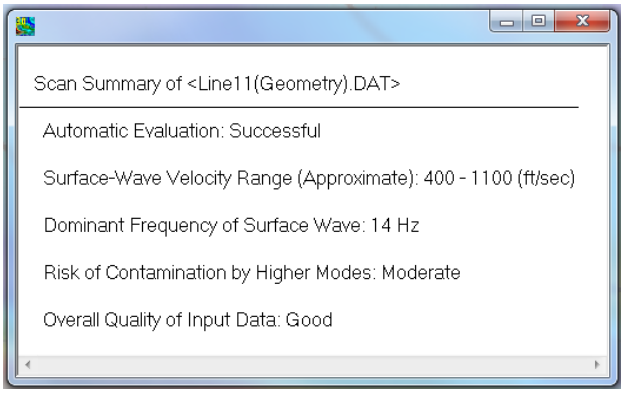


    b. LossBot

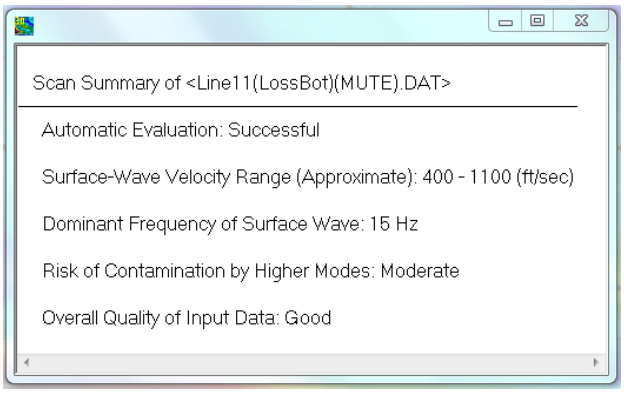


3. Vs

   a. Raw

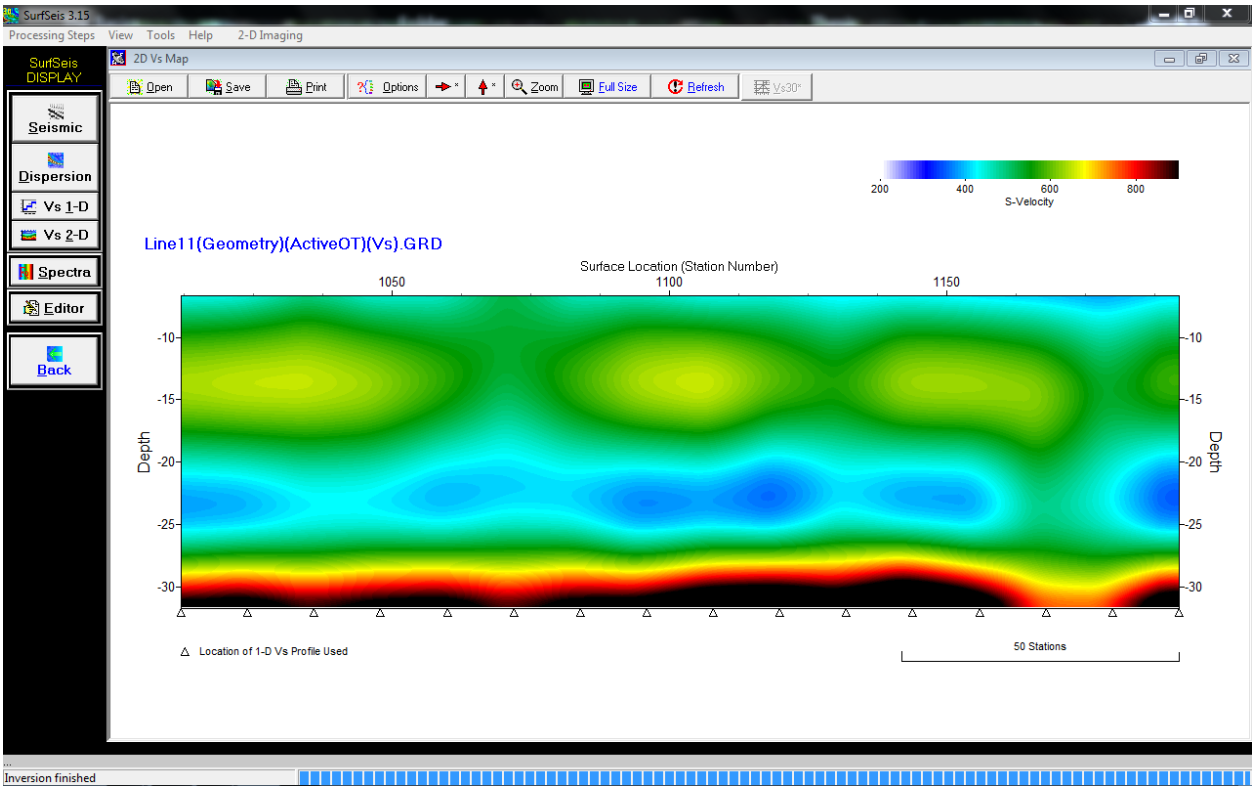


Figure 74 - Line 11 Vs Raw

   b. LossBot

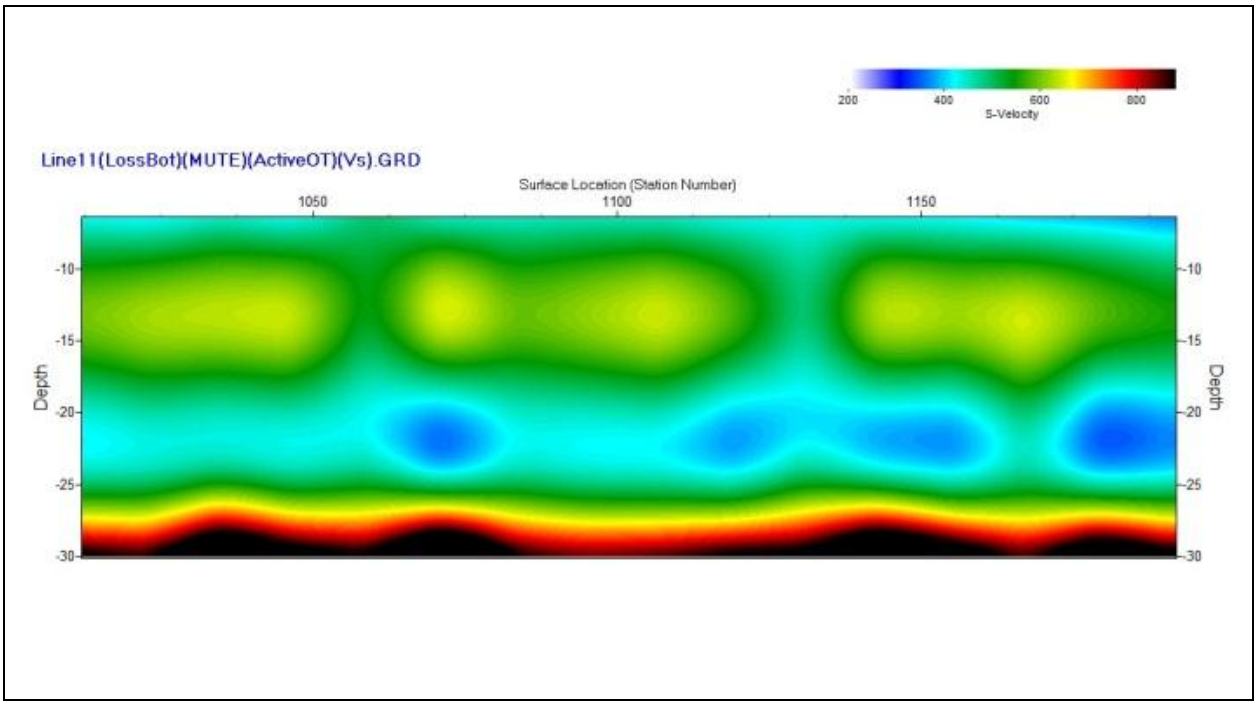


Figure 75 - Line 11 Vs LossBot

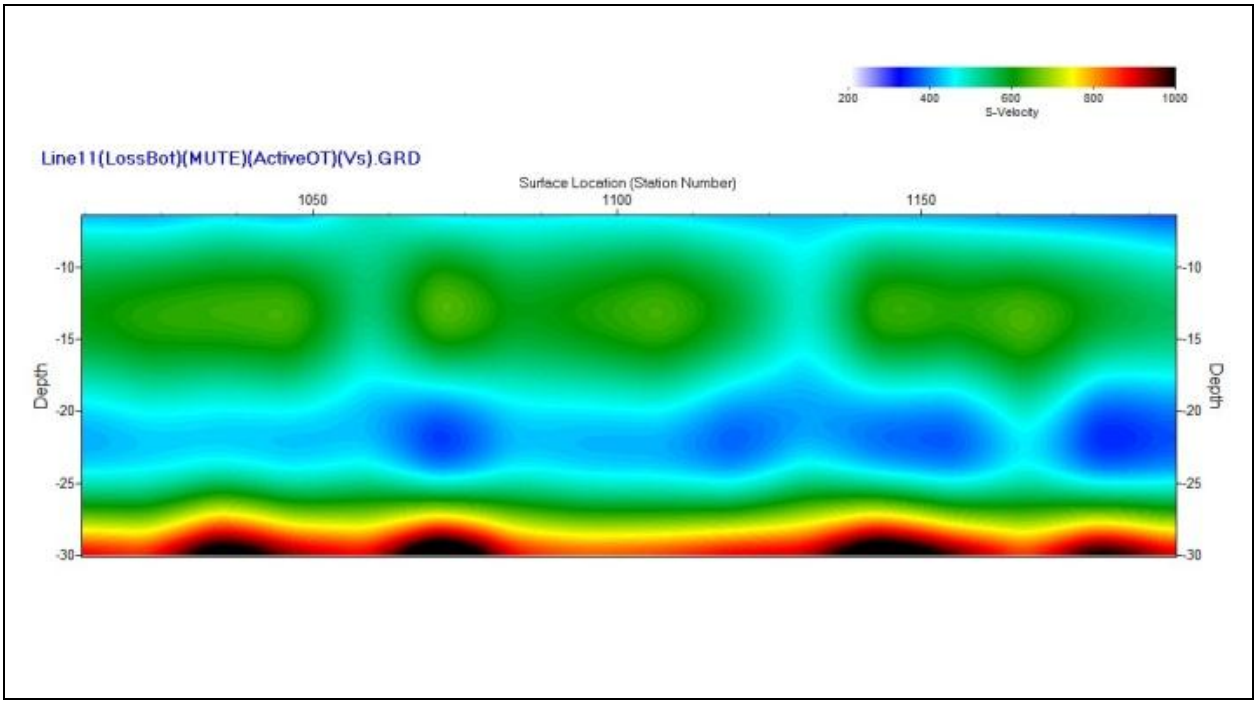


Figure 76 - Line 11 Vs LossBot (200-1000 range)

4. RMSE
    a. Raw

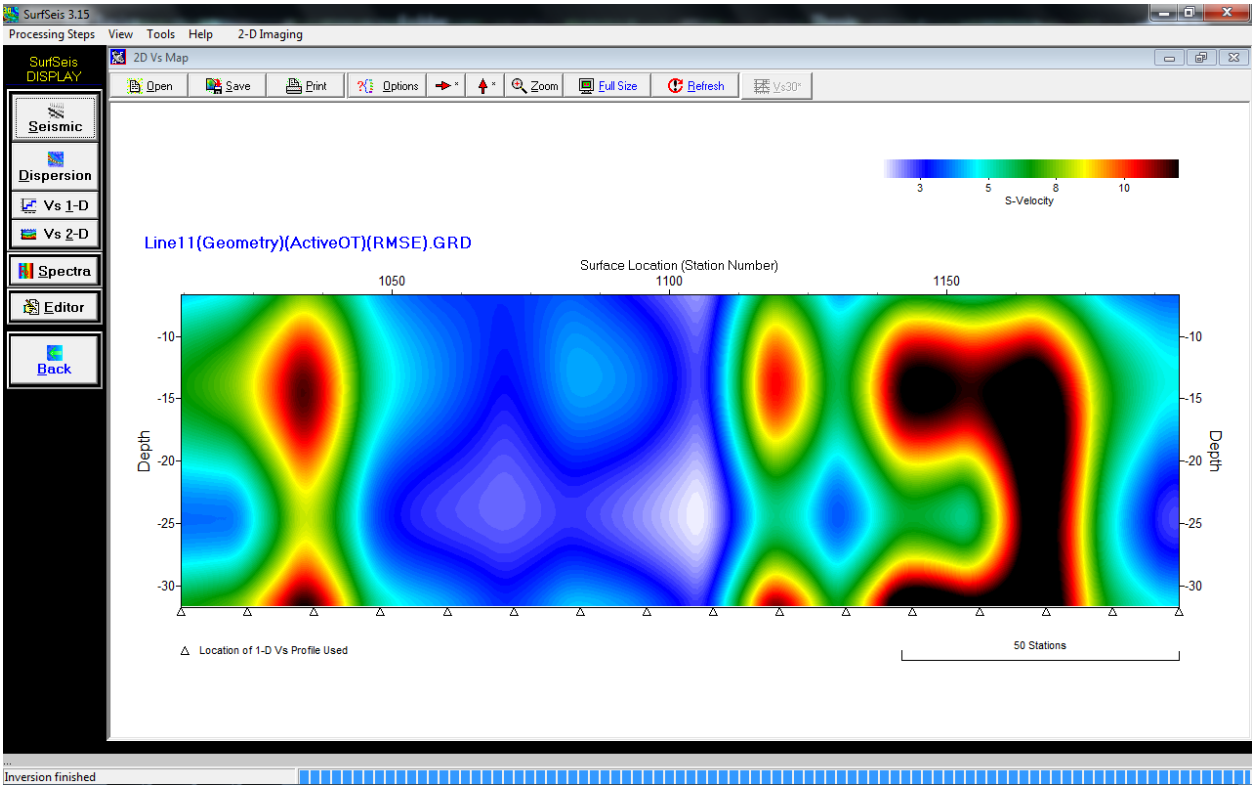


Figure 77 - Line 11 RMSE Raw

b. LossBot

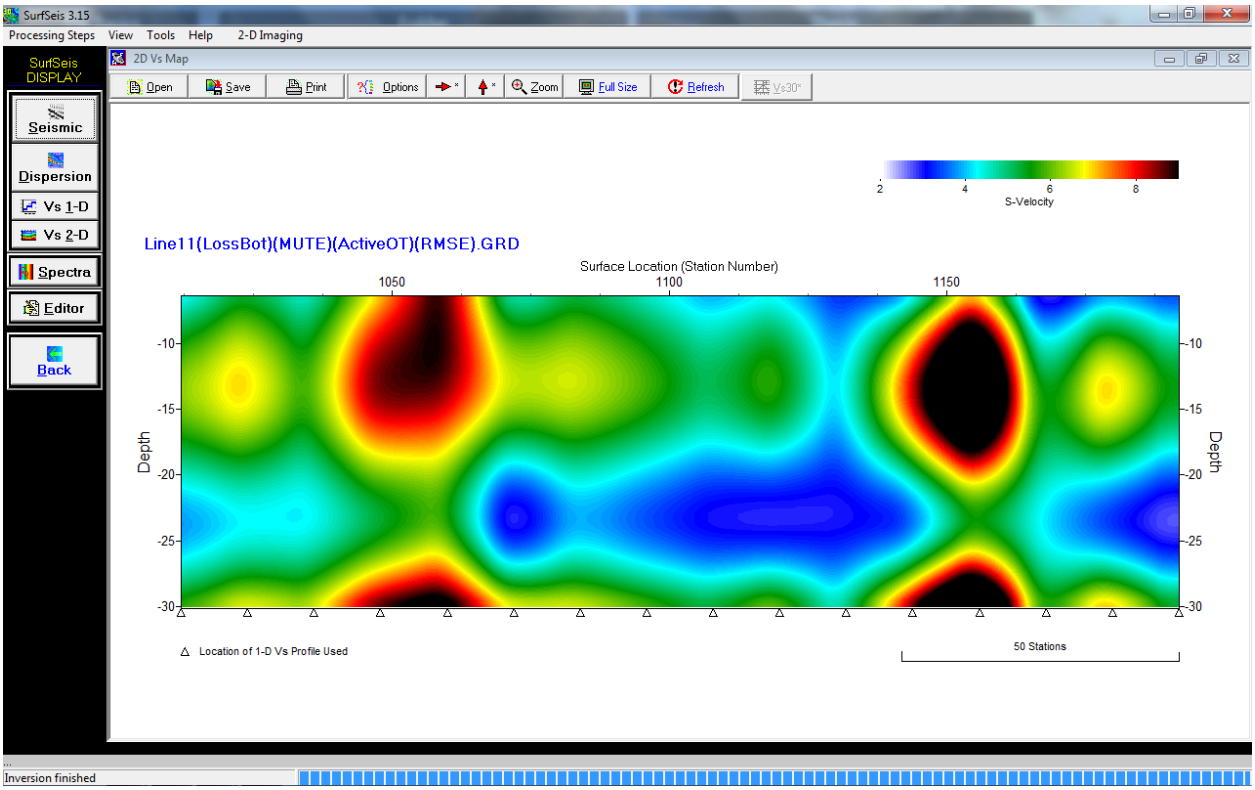


Figure 78 - Line 11 RMSE LossBot

***Line 12***

1. Mute

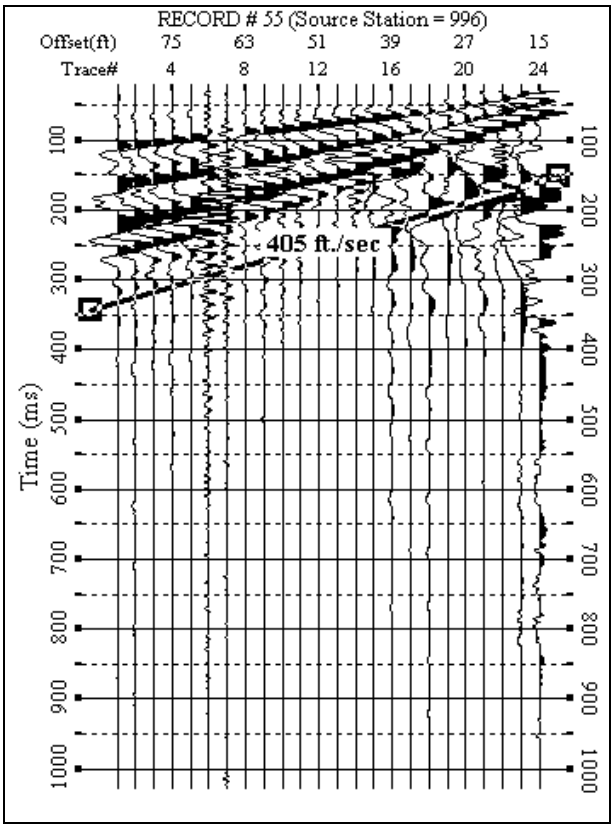


Figure 79 - Line 12 Mute line for LossBot

2. Scan Summary
    a. Raw

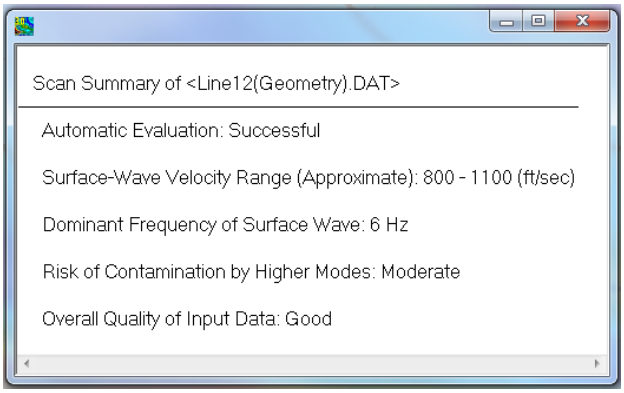


    b. LossBot

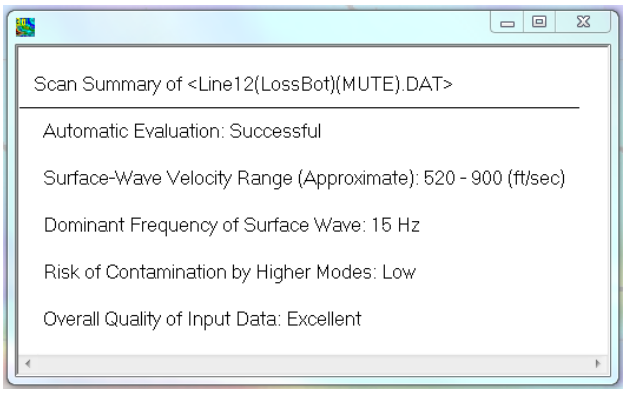


3. Vs

a. Raw

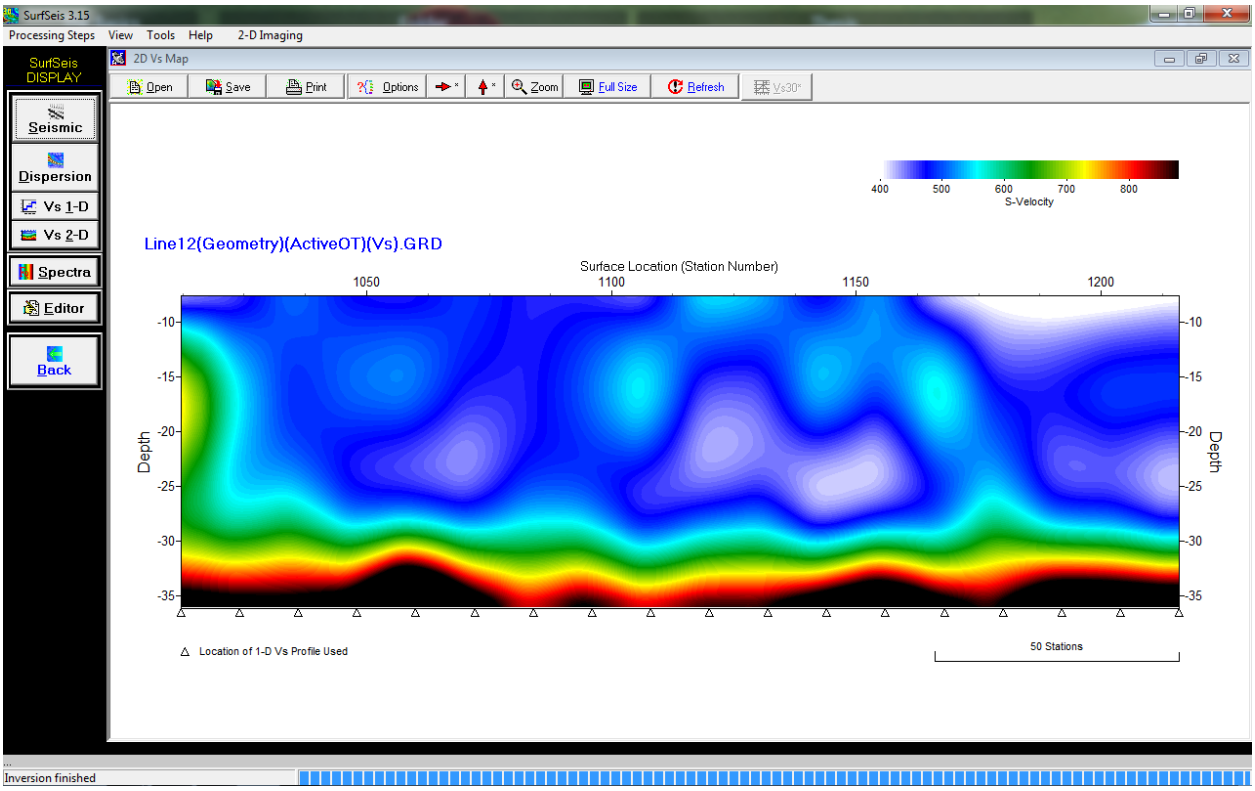


Figure 80 - Line 12 Vs Raw

b. LossBot

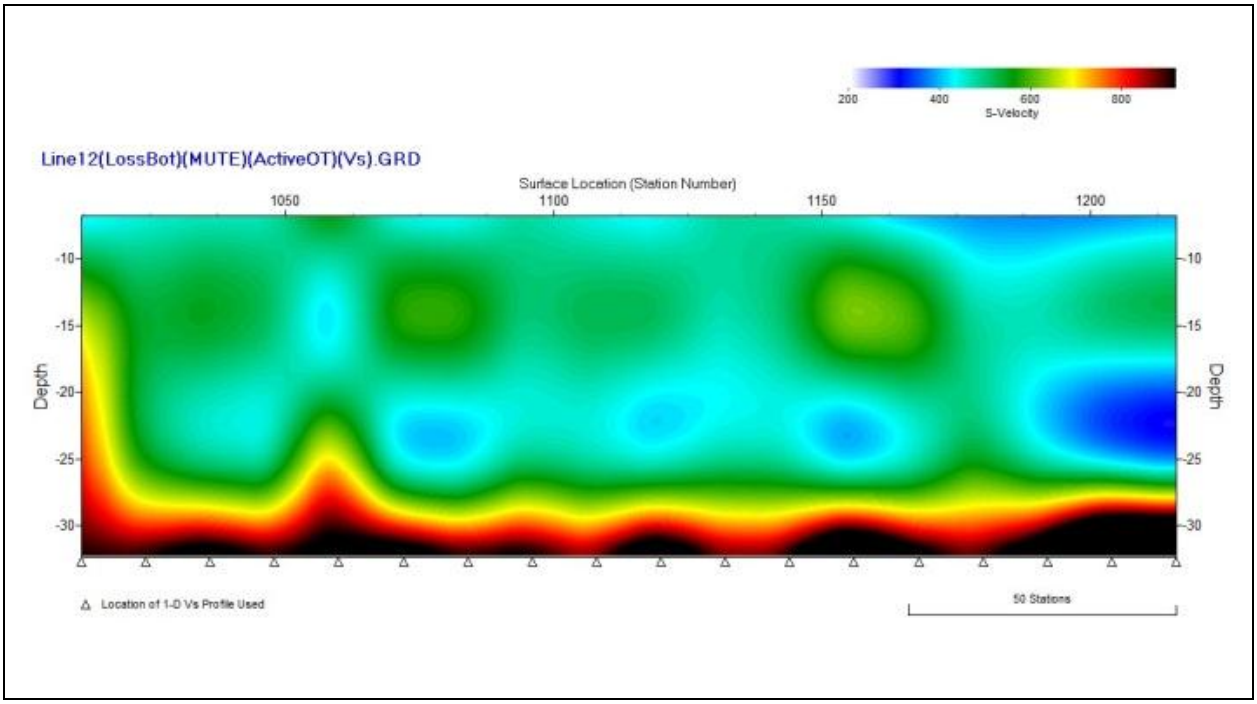


Figure 81 - Line 12 Vs LossBot

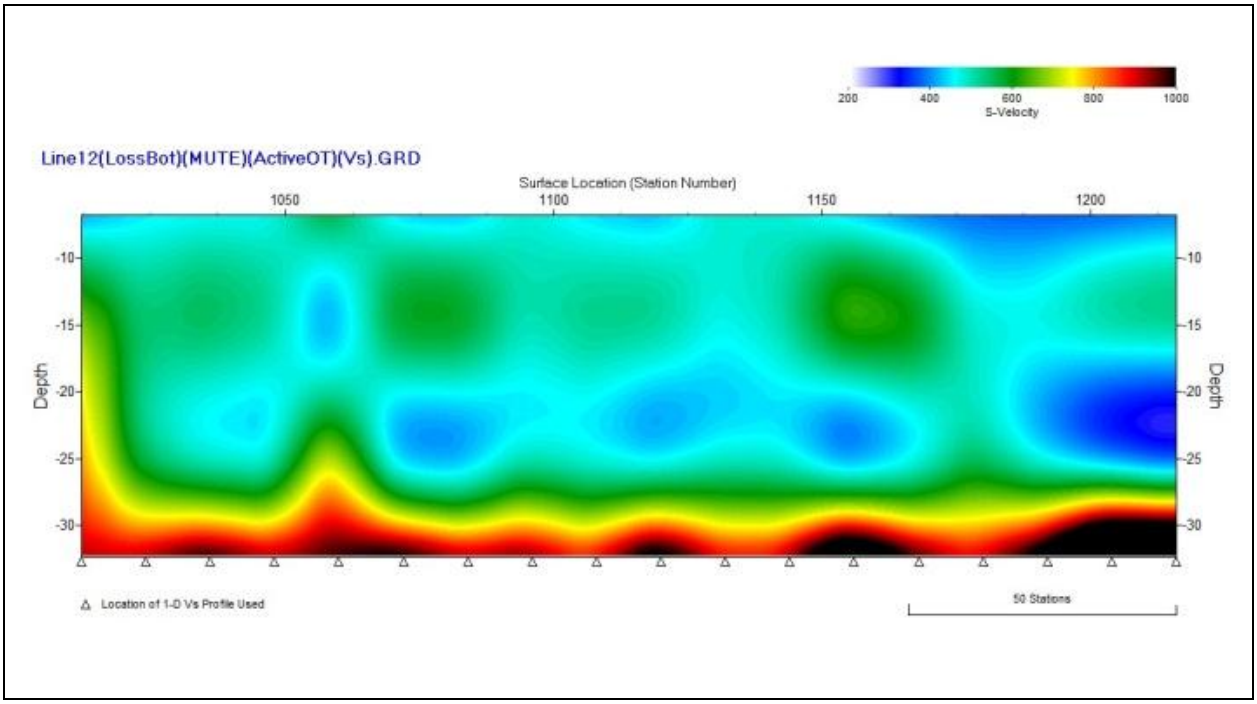


Figure 82 - Line 12 Vs LossBot (200-1000 range)

4. RMSE
    a. Raw

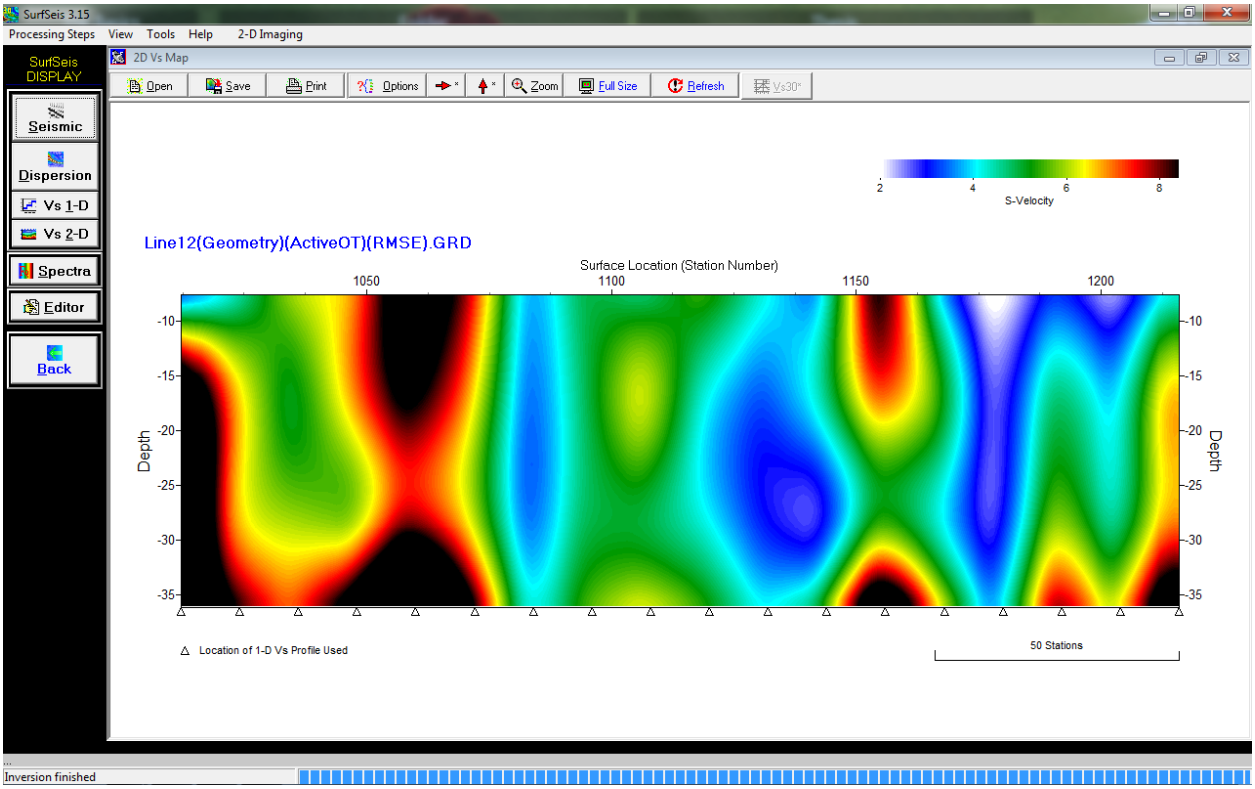


Figure 83 - Line 12 RMSE LossBot

b. LossBot

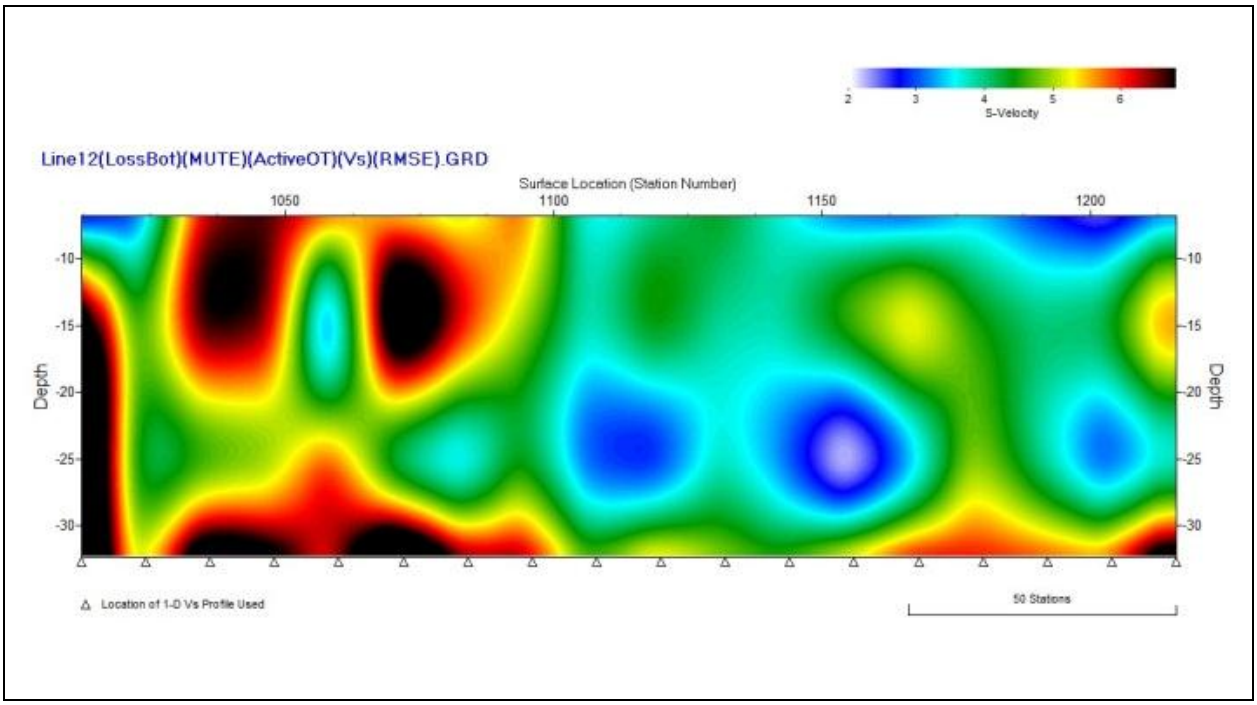


Figure 84 - Line 12 RMSE LossBot

***Line 13***

1. Mute

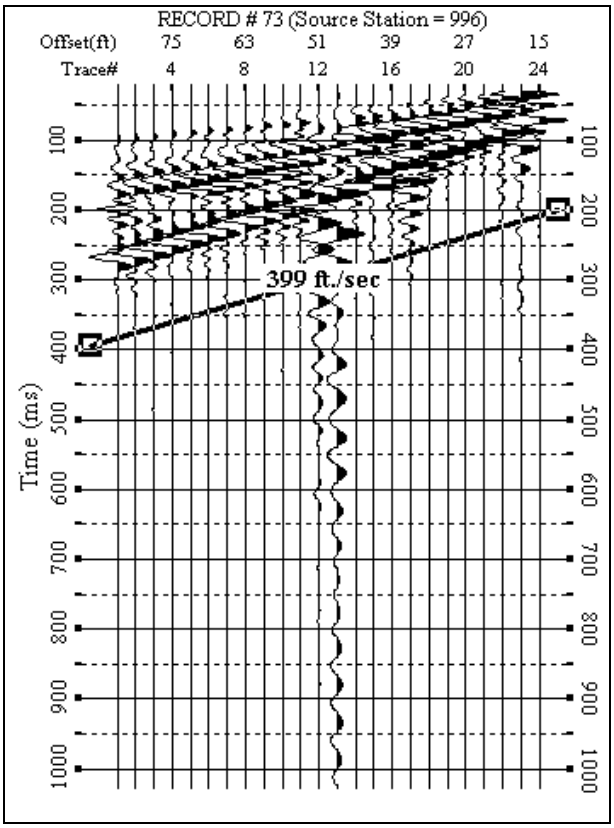


Figure 85 - Line 13 Mute line for LossBot

2. Scan Summary
    a. Raw

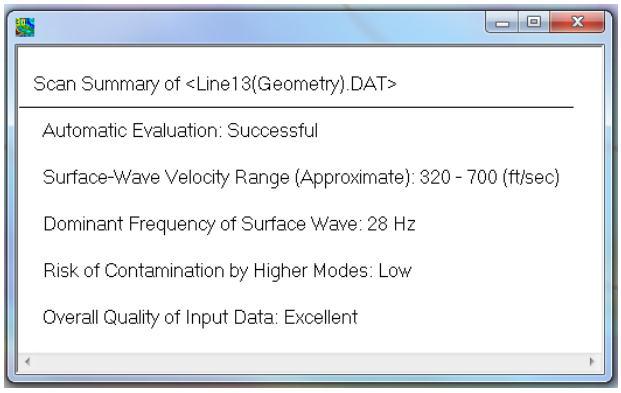


    b. LossBot

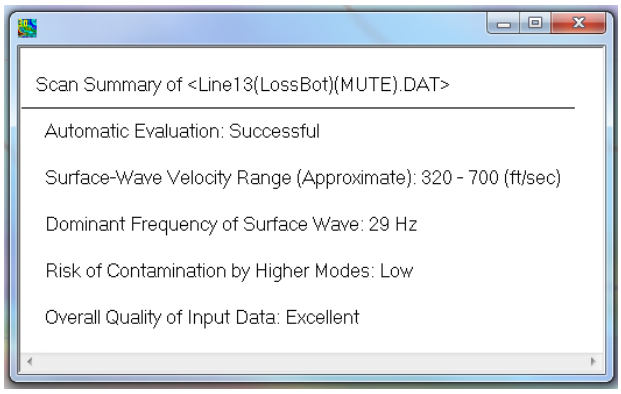


3. Vs

   a. Raw

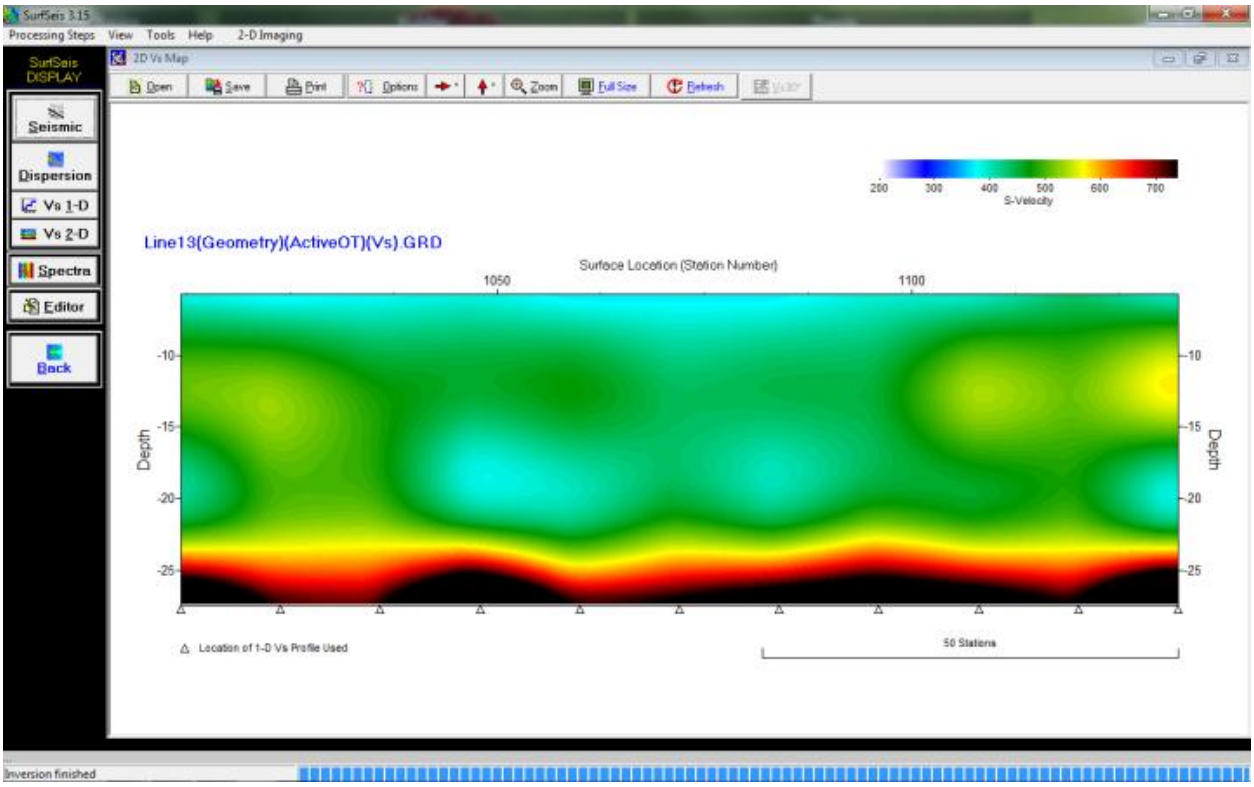


Figure 86 - Line 13 Vs Raw

   b. LossBot

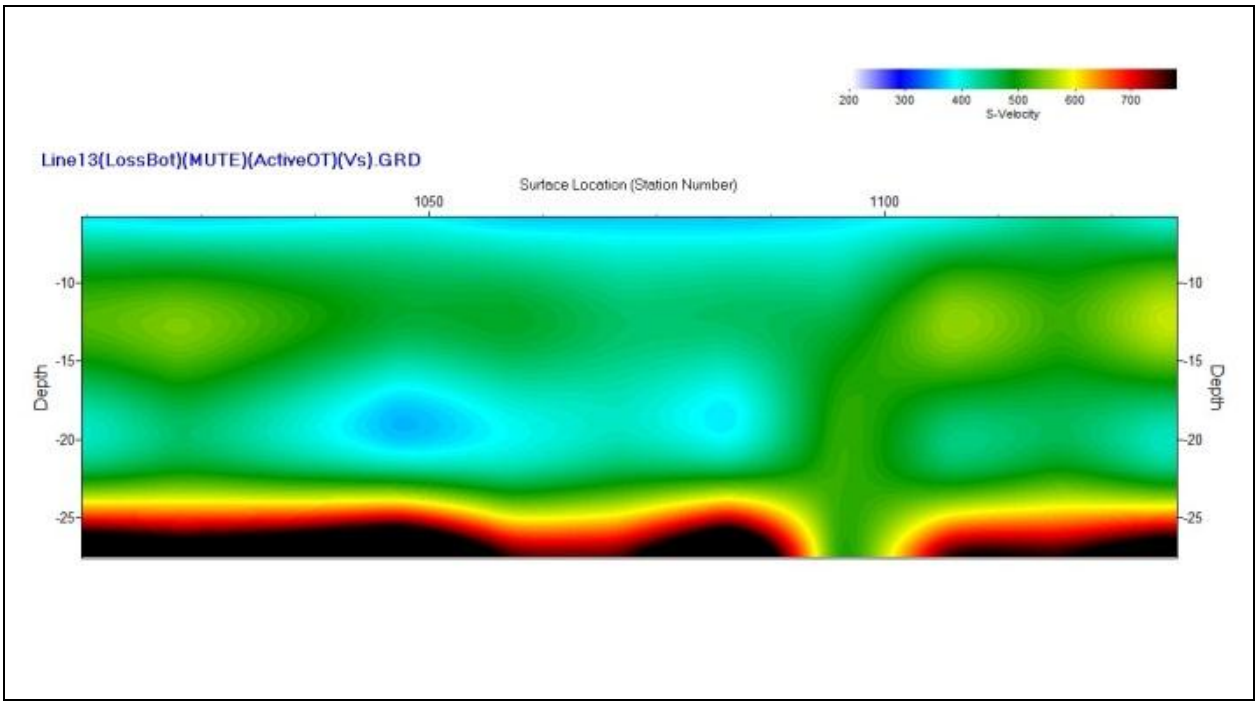


Figure 87 - Line 13 Vs LossBot

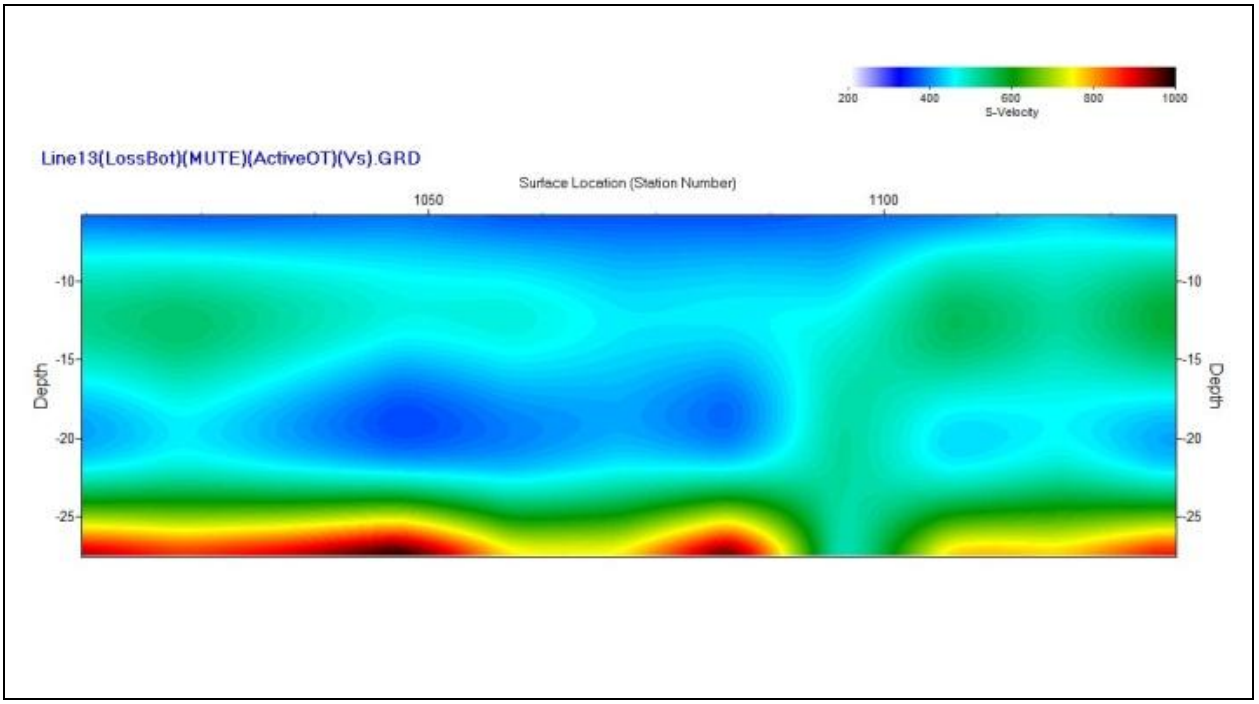


Figure 88 - Line 13 Vs LossBot (200-1000 range)

4. RMSE
    a. Raw

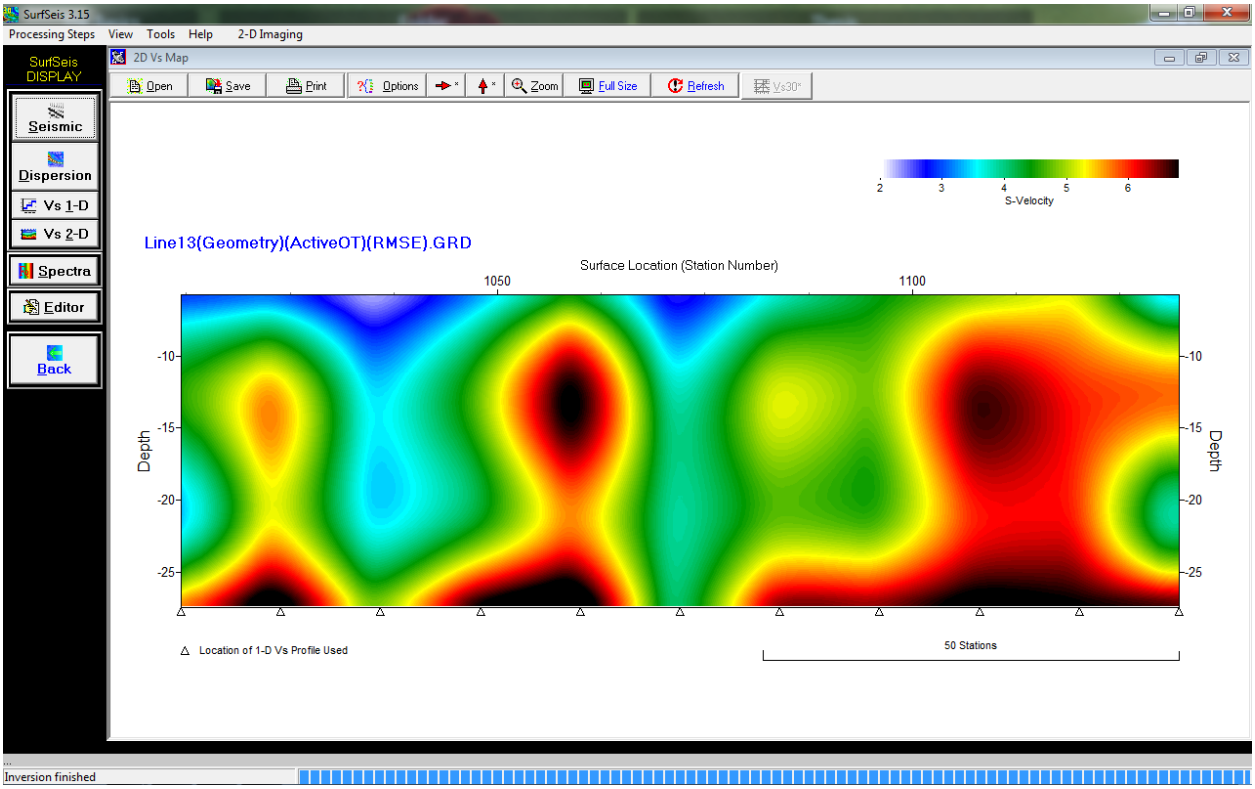


Figure 89 - Line 13 RMSE Raw

b. LossBot

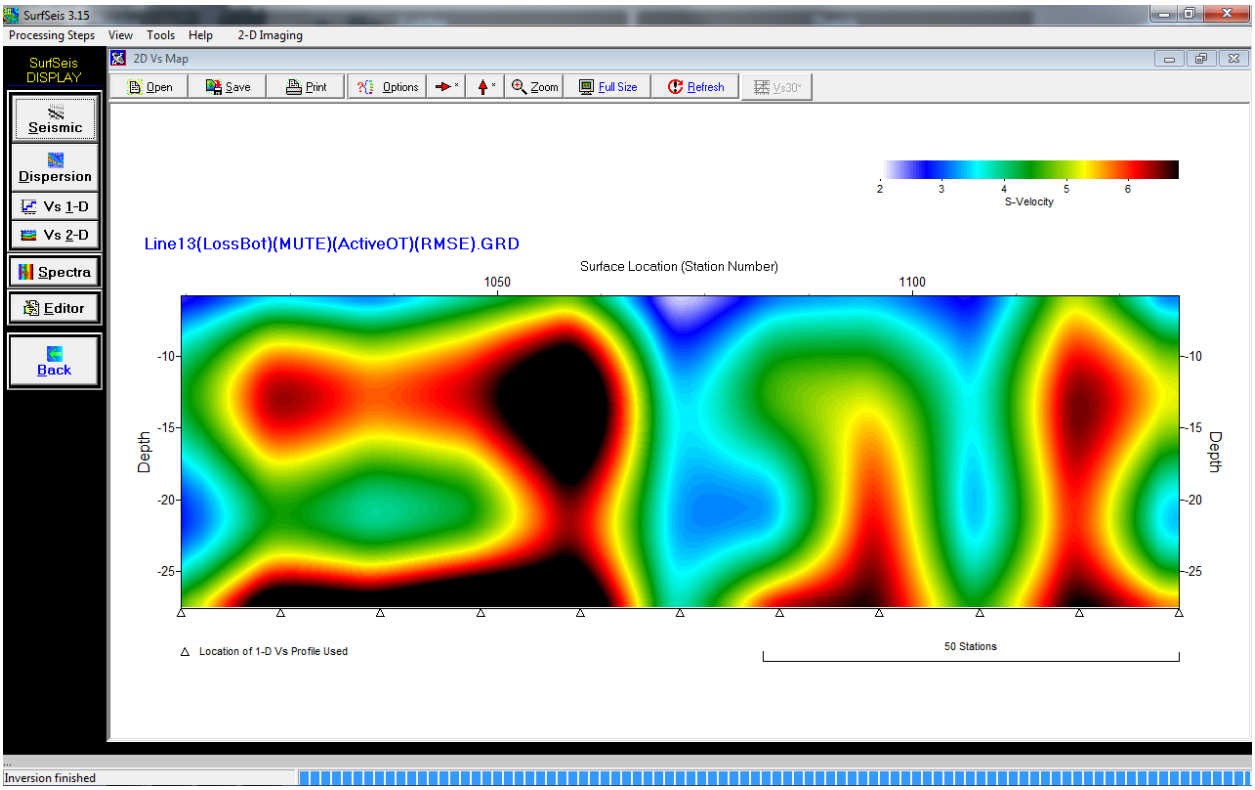


Figure 90 - Line 13 RMSE LossBot

***Line 14***

1. Mute

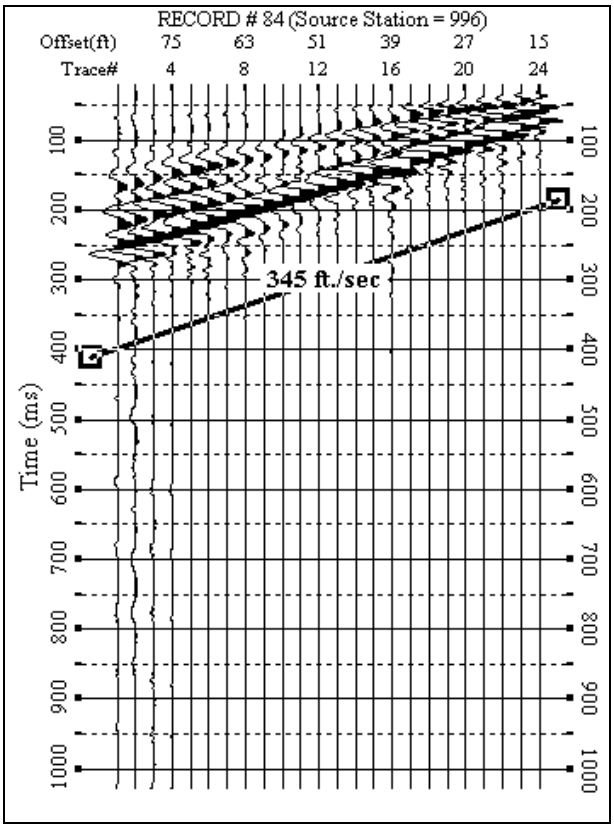


Figure 91 - Line 14 Mute line for LossBot

2. Scan Summary

   a. Raw

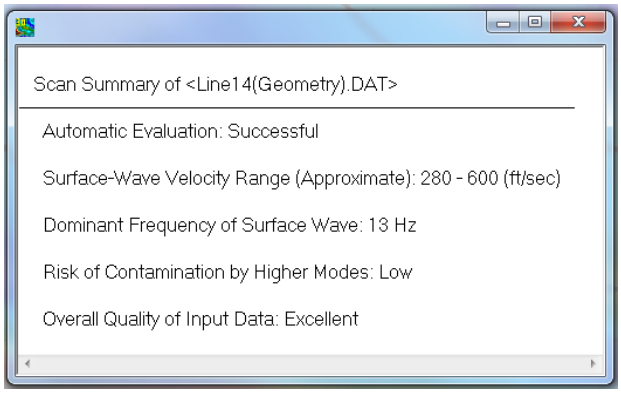


   b. LossBot

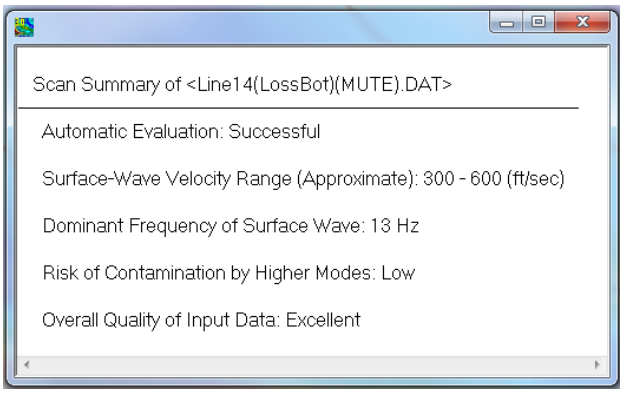


3. Vs

a. Raw

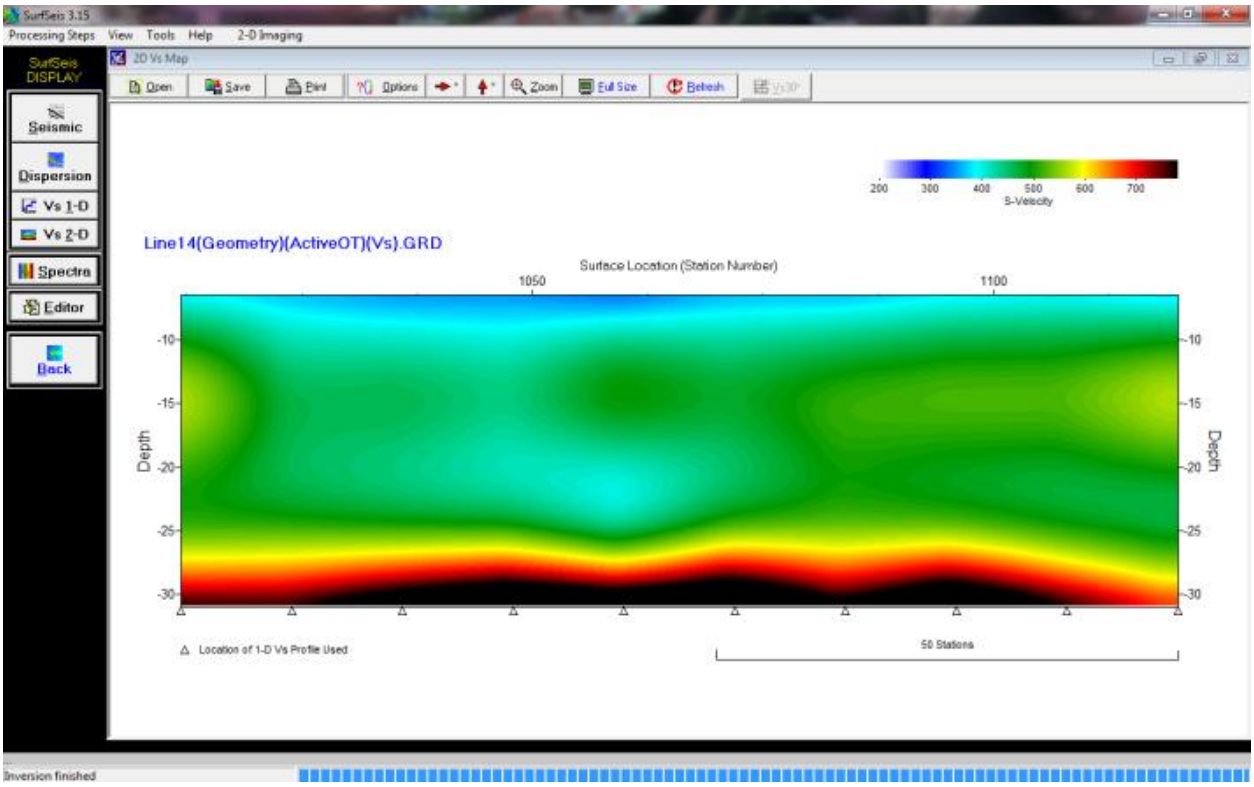


Figure 92 - Line 14 Vs Raw

b. LossBot

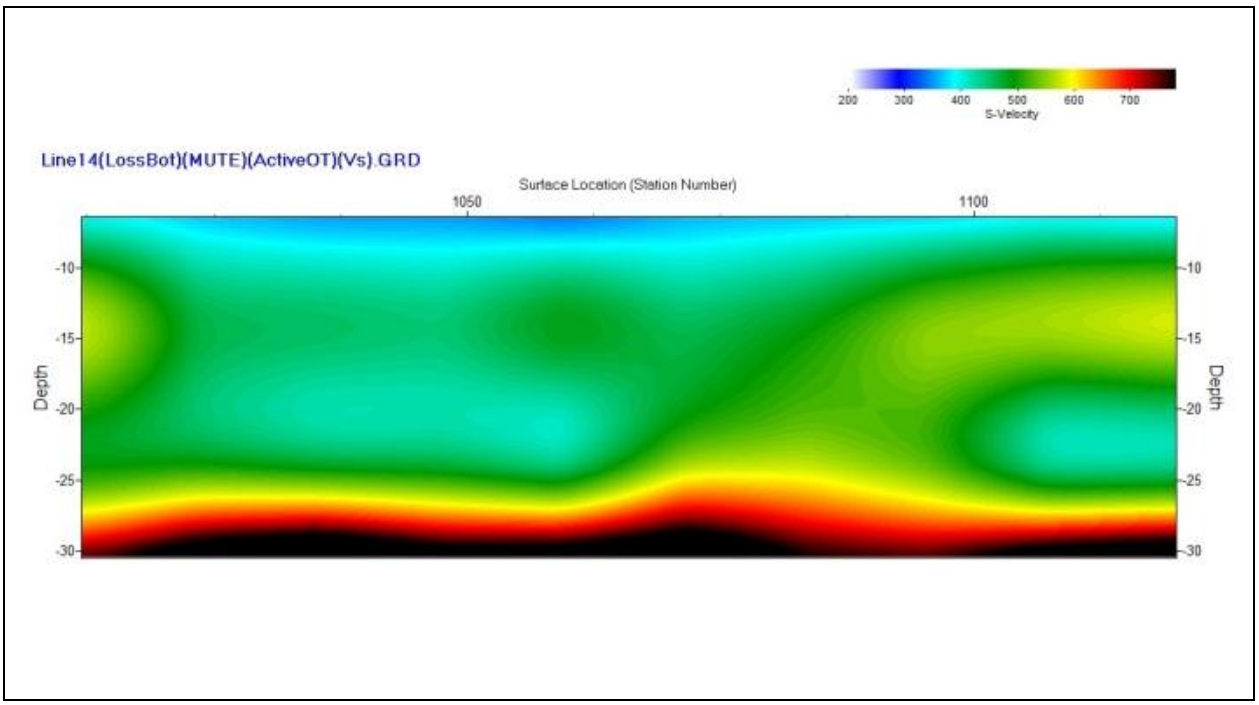


Figure 93 - Line 14 Vs LossBot

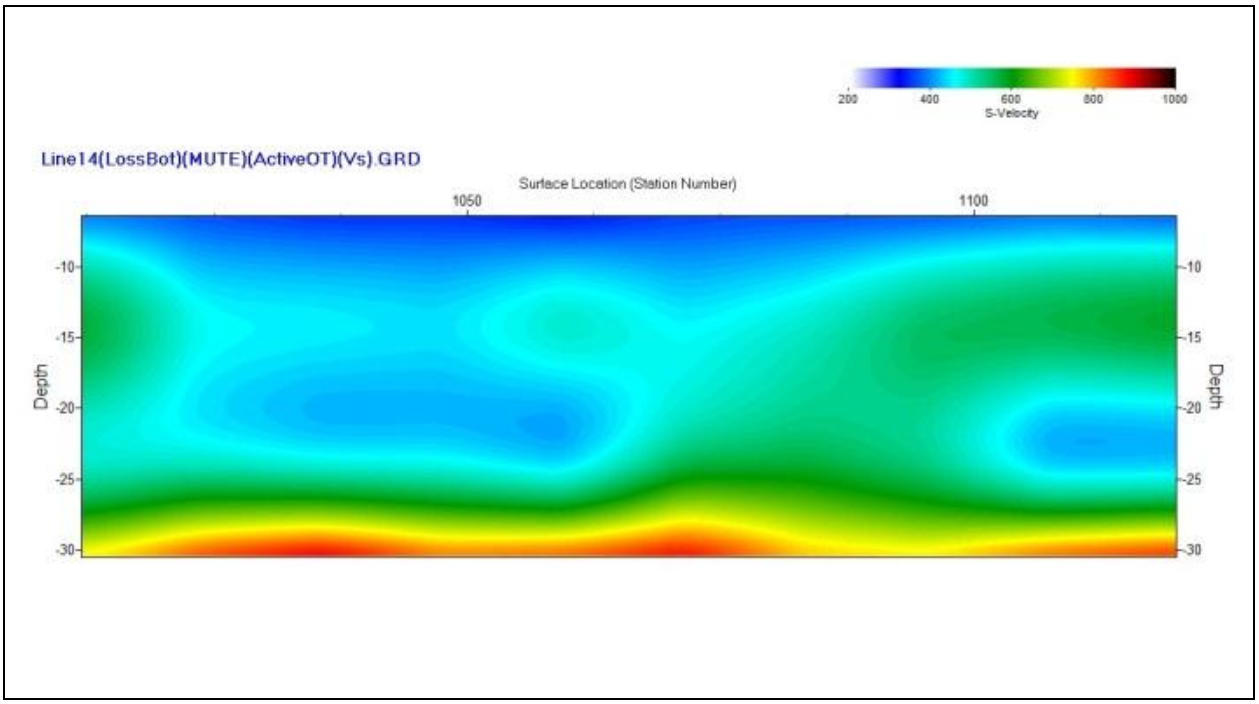


Figure 94 - Line 14 Vs LossBot (200-1000 range)

4. RMSE
    a. Raw

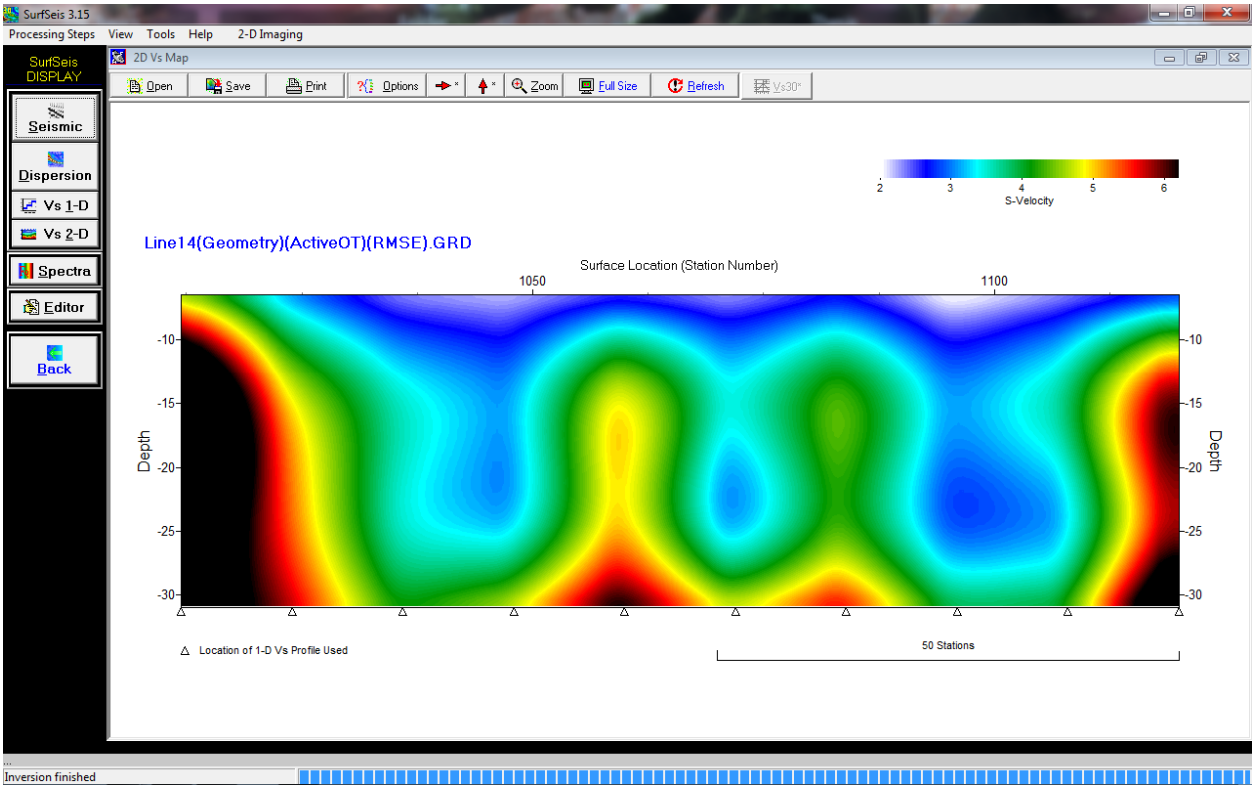


Figure 95 - Line 14 RMSE Raw

b. LossBot

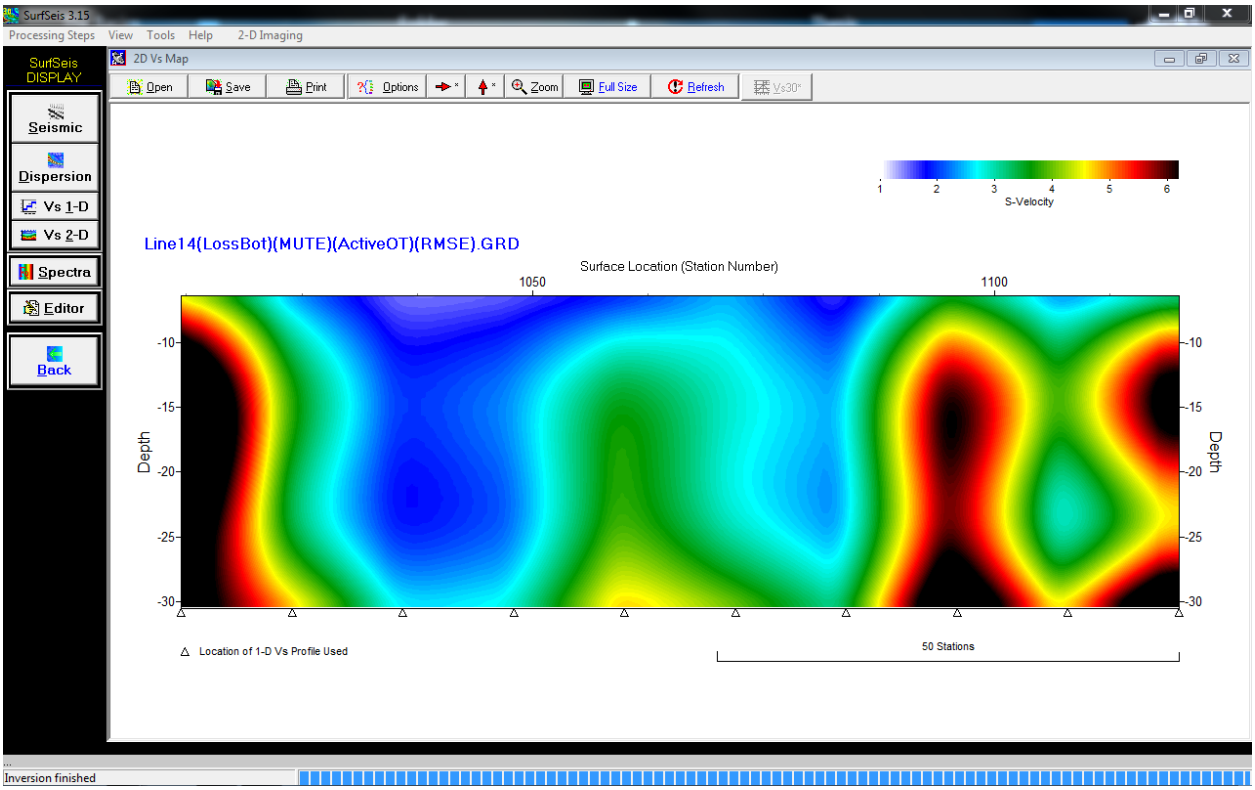


Figure 96 - Line 14 RMSE LossBot

***Line 15***

1. Mute

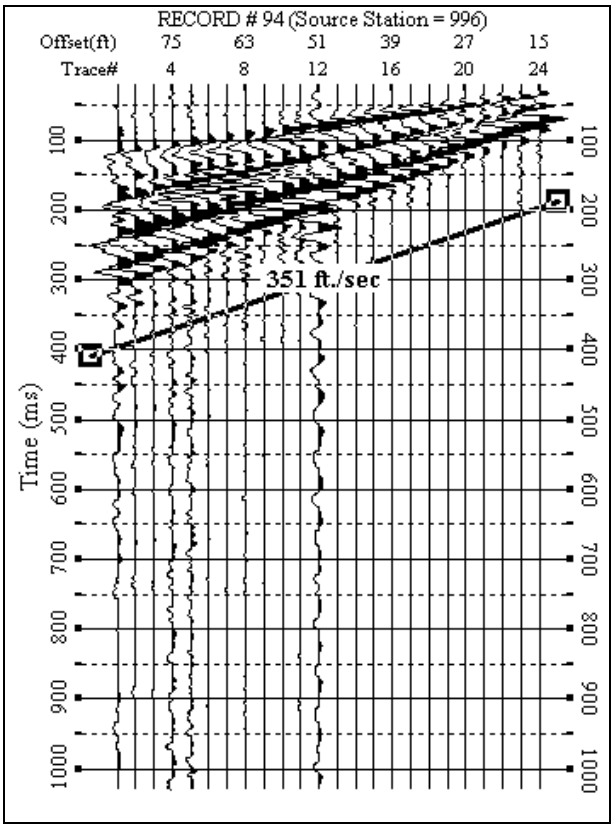


Figure 97 - Line 15 Mute line for LossBot

2. Scan Summary

    a. Raw

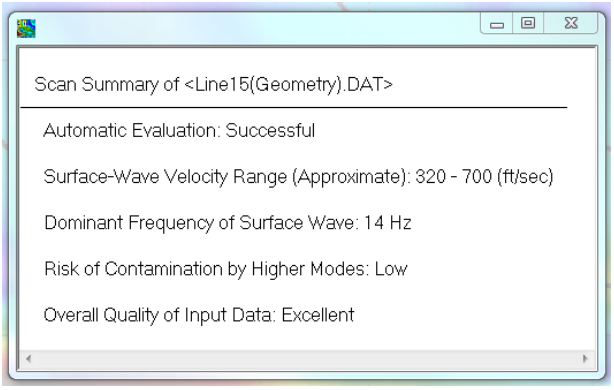


    b. LossBot

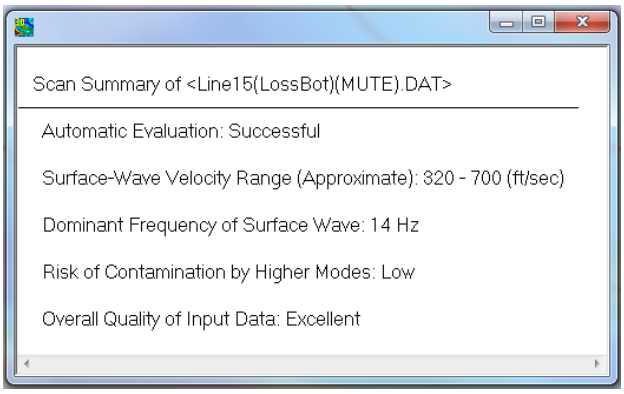


3. Vs

   a. Raw

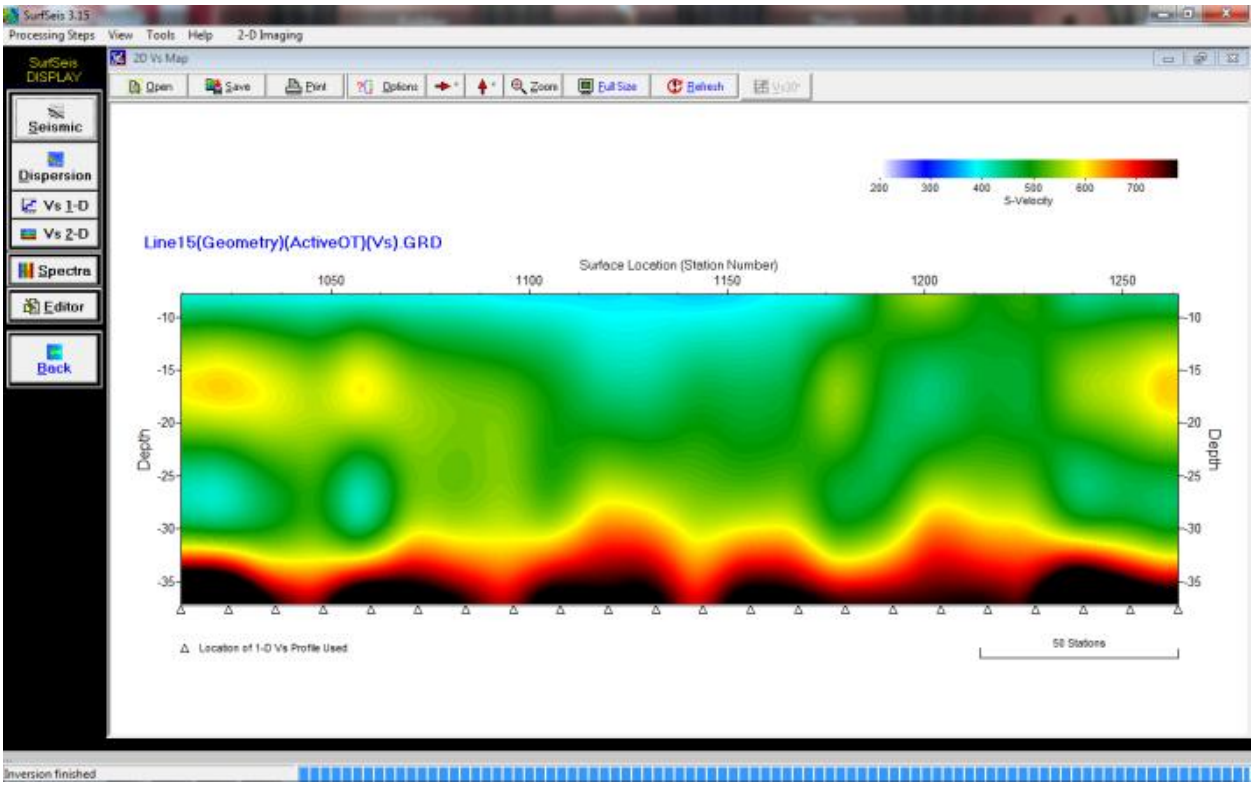


Figure 98 - Line 15 Vs Raw

   b. LossBot

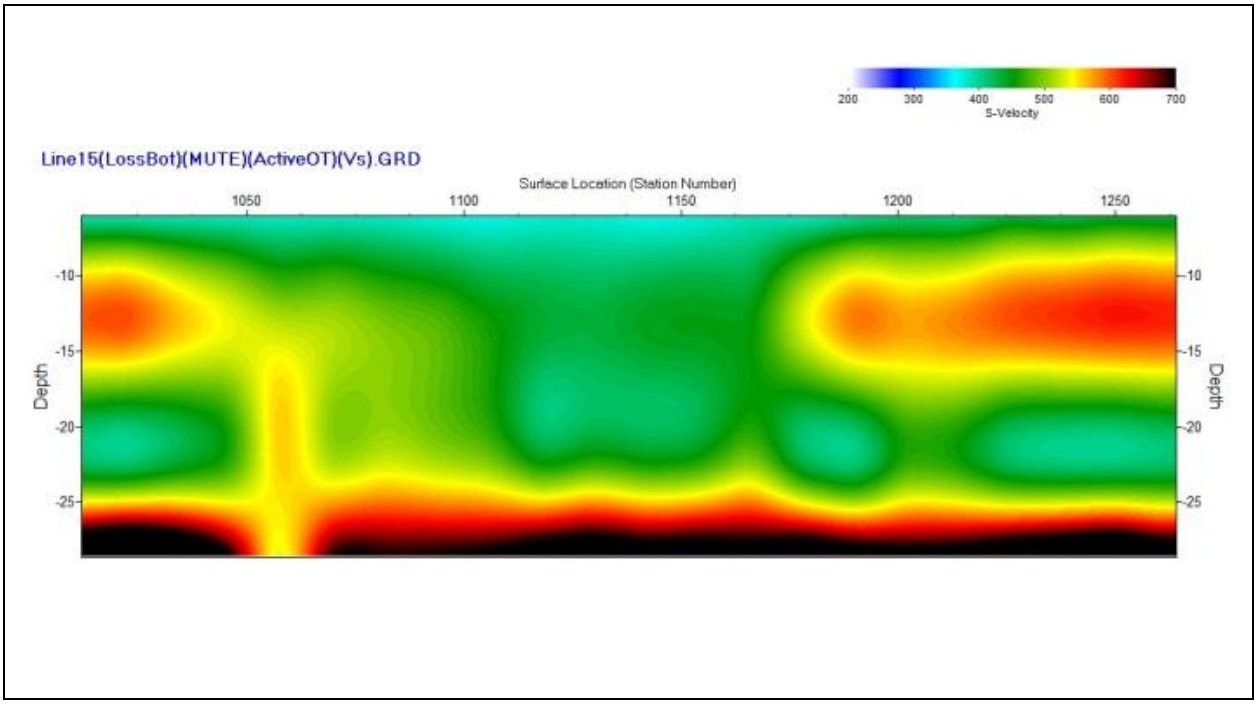


Figure 99 - Line 15 Vs LossBot

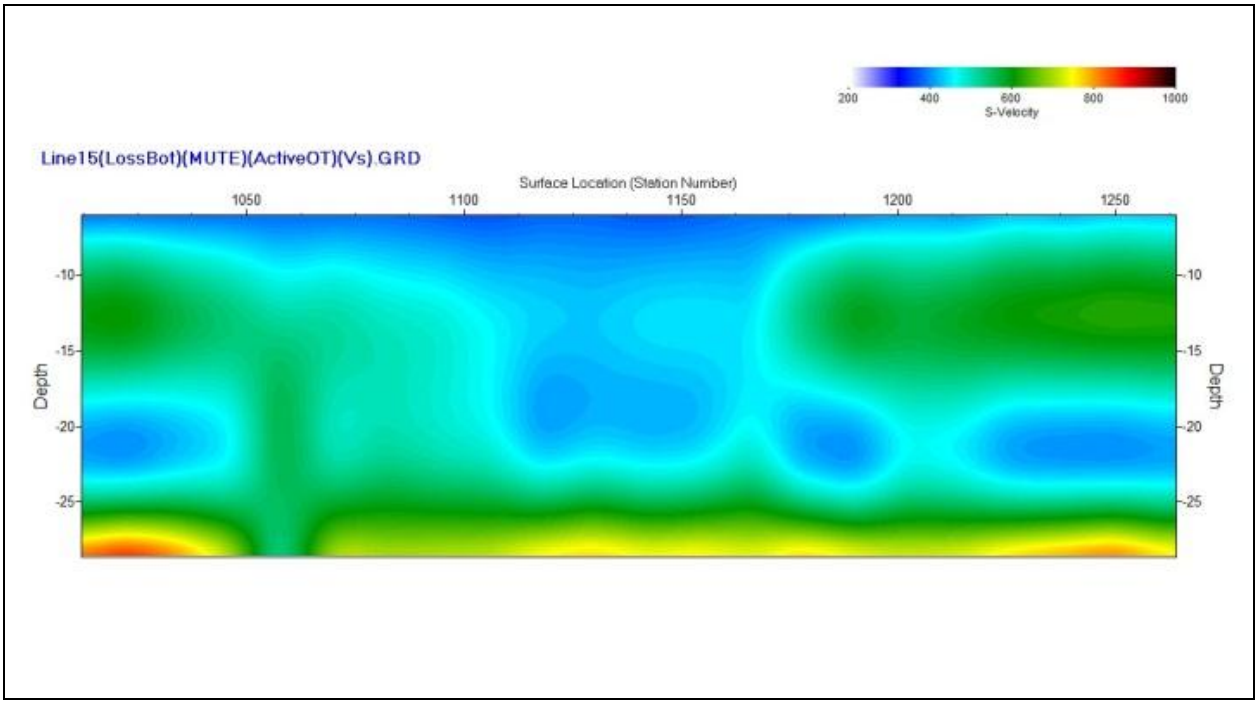


Figure 100 - Line 15 Vs LossBot (200-1000 range)

4. RMSE
    a. Raw

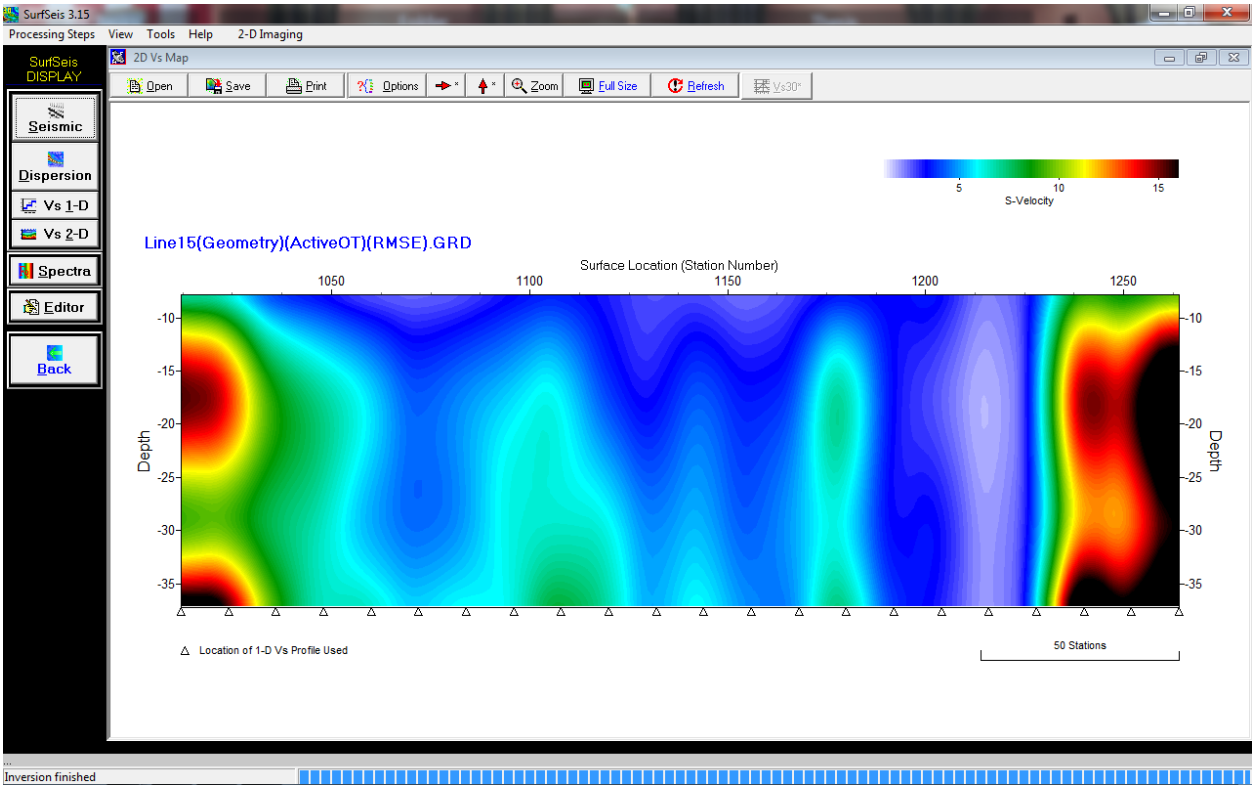

Figure 101 - Line 15 RMSE Raw

b. LossBot

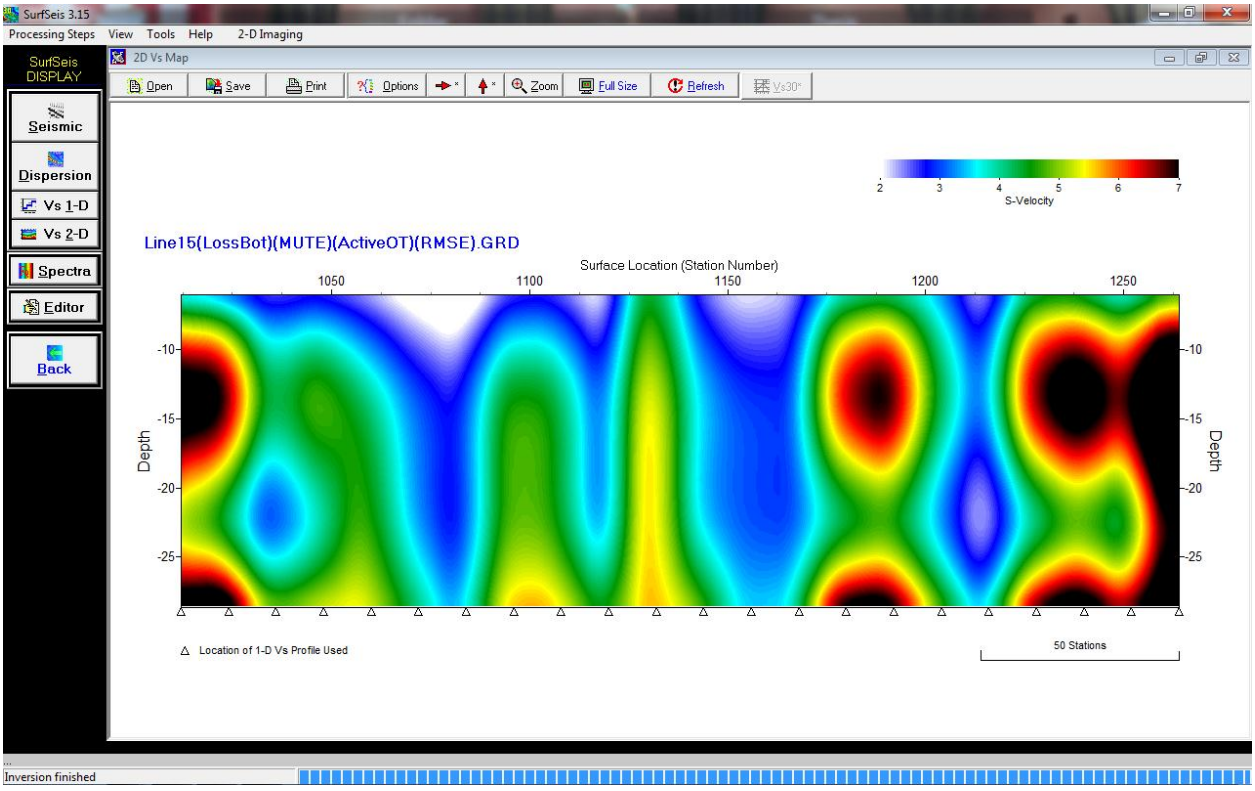

Figure 102 - Line 15 RMSE LossBot

After all 6 lines from the Ogden site had been inverted and documented the next step was to integrate the MASW surface-wave data with the ultrasonic laboratory measurements. Issues arose during this phase some mentioned previously but all will be discussed later in MASW SurfSeis Integration Inversion Results subsection the data and results section.

# Chapter 5 - Data and Results

We conducted the MASW acquisition, completed processing and interpretation of surface-wave datasets and completed laboratory testing on suitable core samples. The combination of the surface-wave datasets and the laboratory measurements was difficult because of the debate over the accuracy of data and the expected/accepted value of Poisson's ratio.

## Acoustic Televiewer

Below is the image of the borehole wall of Ogden North and Ogden South. According to the borehole records, discussed earlier, approximately 60 ft. of unconsolidated/poorly consolidated sediments (alluvium) and the remanding 20 ft. of bedrock with the Johnson Shale and Foraker Limestone Formations. But that is not what we see in the ATV image. The PVC casting was placed on in the unconsolidated sediment and it is possible that the yellow we see is not the true indicator of the bedrock. This would also mean any features that do exist are blurred and possibly poorly represented in the ATV image. Unfortunately the ATV data processing program (WellCAD) is unavailable to us currently. Further work that could be done on this project is reexamining the data and trying a different processing workflow.

### *Introduction*

Linking the lithology with the ATV image was difficult because of issues surrounding the cores from the North and South boreholes at the Ogden test site. It was very difficult to link the KDOT lithology with the corresponding ATV image because of inconsistencies in the lithology reports and in the total length of cores. After careful review a more accurate lithology was created, the variation in length was resolved and the lithology was correlated with the ATV images.

### *Initial Problem*

The issues first arose when the KDOT lithologies were compared with the ATV images. I noticed that the start or top of the bedrock in the KDOT South lithology fit better with the North ATV image and the same was true for the North lithology and the South ATV image (Figure 103). From this point on the title of KDOT North and South lithologies were switched,

North became South and South became North. I believe this was justified because we were certain that the north ATV was from the North borehole (etc.,), also we had to assume the KDOT coring start depths were correct because there was no evidence to say otherwise without making them dependent on the ATV image. We swapped the boreholes but kept the recorded start depth, next we compared the lithologies to one another and noticed that even though the ATV images were in agreement with one another, the upper portion of the KDOT lithologies were not. The variation in the upper KDOT lithologies was due to the fact the South core set was heavily fragmented and the first 3 feet were almost exclusively rubble. As mentioned before, this prompted the necessity of a closer examination of both core set lithologies.

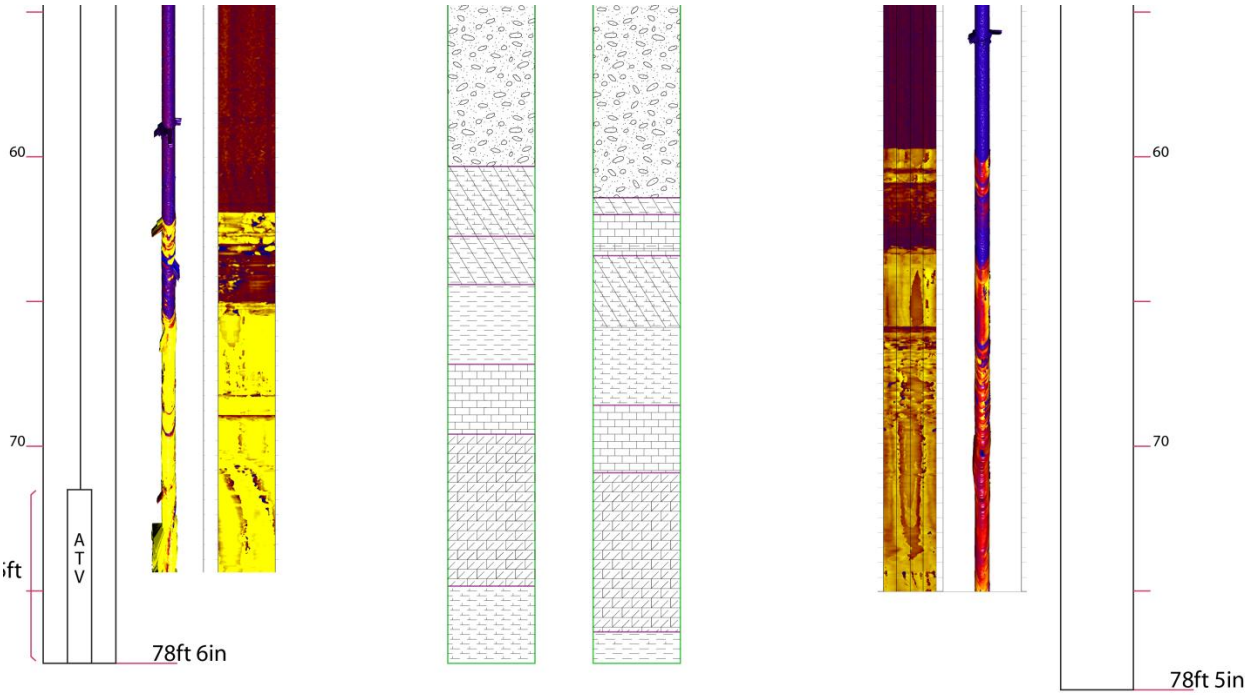


Figure 103 - Difficulty with top of bedrock in KDOT lithology reports

## *ATV Accuracy*

Before examining the lithology we checked the accuracy of the ATV image. To determine the accuracy of the ATV image we checked the scale and orientation of it in the diagram comparing them with the lithology and the borehole. The vertical scale of the borehole diagram was correct and the scale on the sides of the ATV images had small tick marks every 6inches and two is equivalent to the 1ft scale. So the ATV image is not stretched, the vertical scale of it is accurate/equivalent. Next I evaluated the elevation of the ground surface and the depth to the water table. The ATV device can only record images when the transducer is in

water, the top of the water table was easy to find (Figure 104). In both boreholes KDOT recorded 6ft 2in from the surface to the top of the water table, very close to my measurement of 6ft 6in for both boreholes. Concerning ground level, the site was very flat so I assumed the equal elevation at both boreholes and the KDOT report supported this assumption. The scale, water table and ground surface were accurate meaning the ATV images were correct, the issue then fell onto the lithology provided by KDOT.

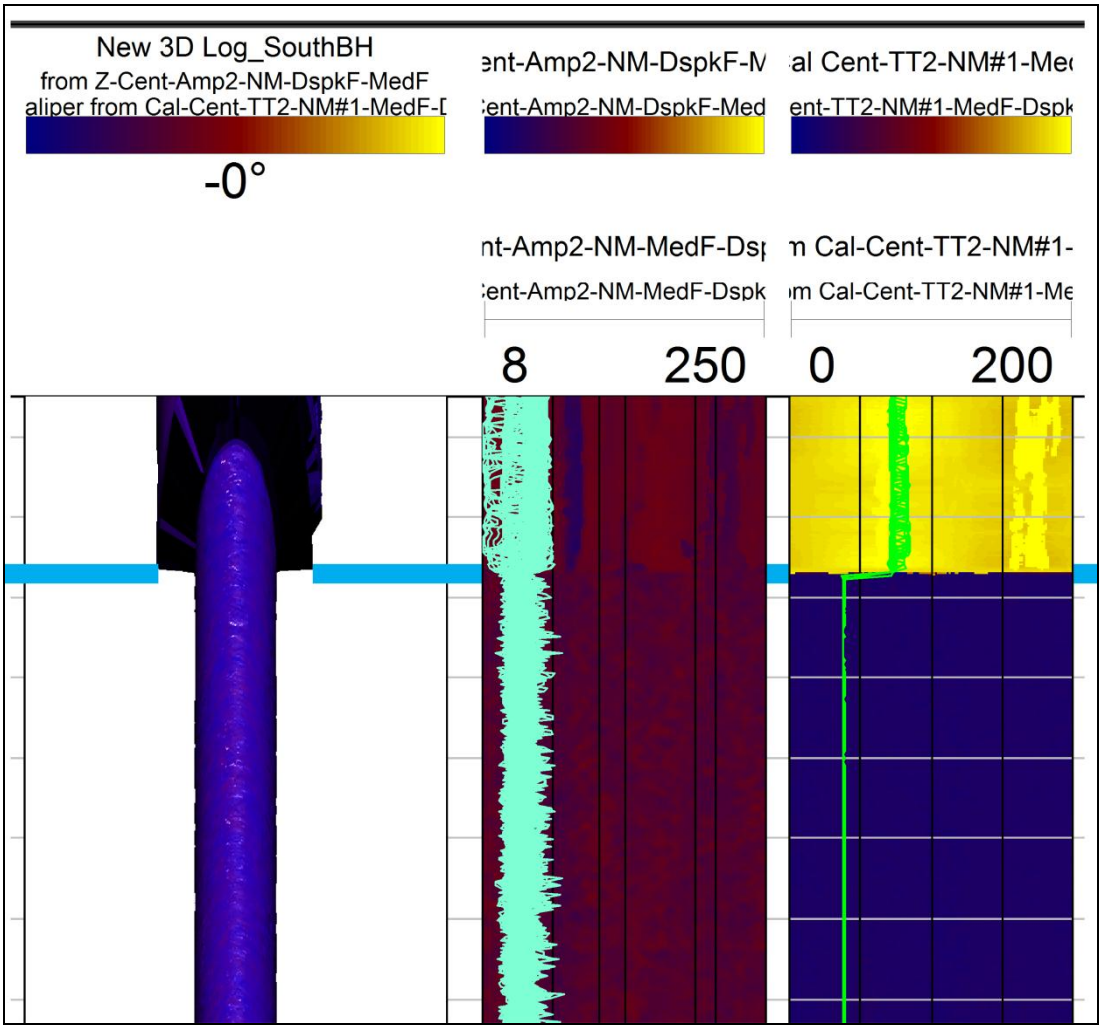


Figure 104 - Image showing how easily the water table can be seen on the 3D log, the borehole wall Amplitude log and the borehole Travel Time log

## *Necessary to Redo Lithology*

### *Total Core Length*

We determined that the ATV image, water table and ground elevation were accurate, also we assumed the bedrock start depth was accurate since we had nothing to contradict it. Since these variables had the correct vertical scale and were accurately placed, the next step was to examine the core sets (core boxes). First we determined the total length of each set of cores, then created a map of the core boxes and record observations used to determine changes in lithology and aid in linking the lithology with the ATV images. The total length, according to the KDOT reports was 17ft and 17.1ft for the North and South boreholes with only a difference of 1.2in. Initially, after examining the core boxes my rough estimates yielded a difference of 10in between North and South. The North had 18ft 2in of cores, was 1ft 2in longer than what KDOT reported. The South had 17ft 4.5in and was 3.3in shorter than what KDOT reported. Next I attempted a more accurate measurement by pushing the contents of each column to the top of the box and measuring the 'gap' at the bottom and subtracting the value from the 2ft length of the box. This resulted in a North core length of 17ft 4in and a South core length of 16ft 0in. Finally I measured the length of each 'individual' piece (small segments were lumped together) resulting in a North core length of 16ft 6¼in and a South core length of 16ft 7¼in. The 'individual' piece measurements were helpful and allowed me to make a core box map to keep track of where a segment came from and correctly record my observations (yellow squares in **Error! Reference ource not found.** and **Error! Reference source not found.**). The true total length measurement could have been somewhere between the 'gap' and 'individual' values but I think the 'individual' measurement was the most accurate, from this point on it is the measurement used.

| Total Core Length | | | |
|---|---|---|---|
| | North | South | Difference |
| KDOT | 17.0 ft | 17.1 ft | 0.1 ft |
| BOX Length | 18 ft 2.5 in (218.5 in) | 17 ft 4.5 in (208.5 in) | 10 in |
| *Difference from KDOT* | + 1ft 2in EXTRA | - 3.3 in LESS | |
| *Amount of gap* | 10.50 in | 16.25 | |
| Gap measurement | 208.00 in (17ft 4in) | 192.00 in (16ft 0in) | 16 in (1ft 4in) |
| Individual measurement | 198.25 in (16ft 6.25in) | 199.25 in (16ft 7.25in) | 1 in |

Table 2 - Total core length, multiple methods/sources

| KDOT info | | |
|---|---|---|
| | North (ft) | South (ft) |
| Depth of borehole | 78.4 | 78.5 |
| Alluvium | 60.3 | 61.4 |
| Bedrock | 17 | 17.1 |

Table 3 - Basic KDOT information

### *Lithology Introduction*

Once the total and segment lengths were determined a detailed analysis of the stratigraphic names and changes in lithology was carried out. The KDOT stratigraphic formation names were correct but the boundaries were shifted and formation members were identified and can been seen in **Error! Reference source not found.** and **Error! Reference source not und.**. The lithologic description depends on the person doing the description. The initial description was done by a geologist employed by KDOT and is technically accurate but not detailed enough; shale was used as a catchall term and this is not uncommon practice (Holland, 2012). When evaluated the core lithology I examined the texture/grain size, hardness, color, calcareousness, visible bedding and small-scale structures.

### *Identification Parameters*

Hardness was rudimentary determined by striking the core with the blunt side of a pocketknife as well as picking up the cores to determine how heavy they felt and how soft they felt when compressed in my hand. The calcareousness was determined using hydrochloric acid and a pocketknife to create a fresh surface free of dust and debris. When the hydrochloric acid was applied to the fresh surface it was observed for a length of time to assess if there was delayed effervescence, this helped to determine the existence of a dolomitic limestone layer in the upper half of the Foraker limestone formation. In the Core Box Charts below (**Error! eference source not found.** and **Error! Reference source not found.**) the vertical lines on the left side of each column contain 3 lines the right column lines are blue and green line is for density, the middle red line represents significant calcareousness and the left side represent the formations or members I assigned to the cores. The visible bedding and small-scale structures labeled, 'Top of Gray/Green Sh.,' 'Brown Line,' two black bands 'Bl 1' and 'Bl 2' (**Error! eference source not found.** and **Error! Reference source not found.**), can be seen in both core sets and showed a correlation between the two boreholes.

### *Use of Core Box Chart as Map*

As mentioned previously the core segment map was very helpful for correctly recording observations and interpreting the changes in lithology. I used the map to resolve the issue with the variation in upper KDOT lithologies. After closer examination the South rubble exhibited similar characteristics to the upper lithology of the North core set, texture, hardness and calcareousness. After applying limited assumptions (without adding length) the upper South adequately agreed with the upper North. This upper section will be discussed further later in this section. Below in **Error! Reference source not found.** and **Error! Reference source not und.** my interpretation of the core set lithology can be seen and a comparison between the KDOT lithology and my lithology can be seen in Figure 107. Also the thickness and bottom depth of each unit can be found in Table 4 and Table 5.

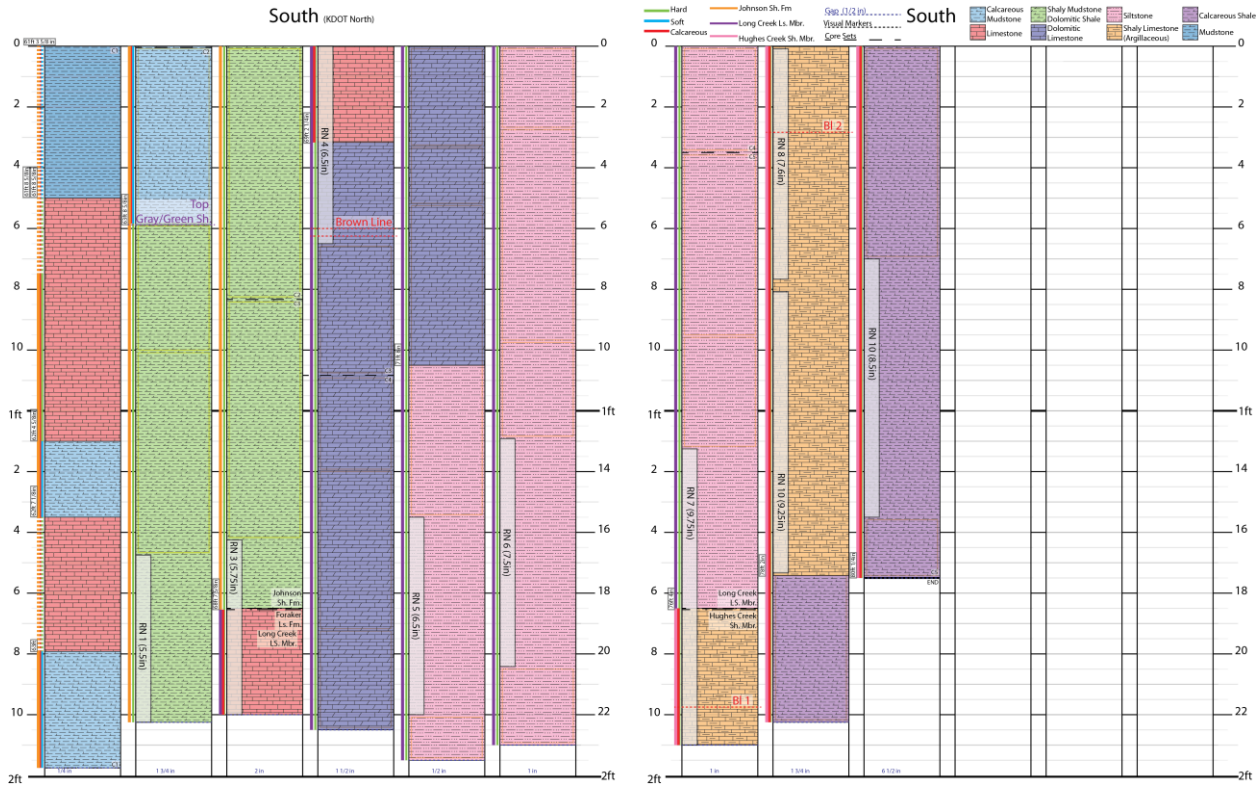


Figure 105 - Core Box Chart: KDOT North (Switched to SOUTH)

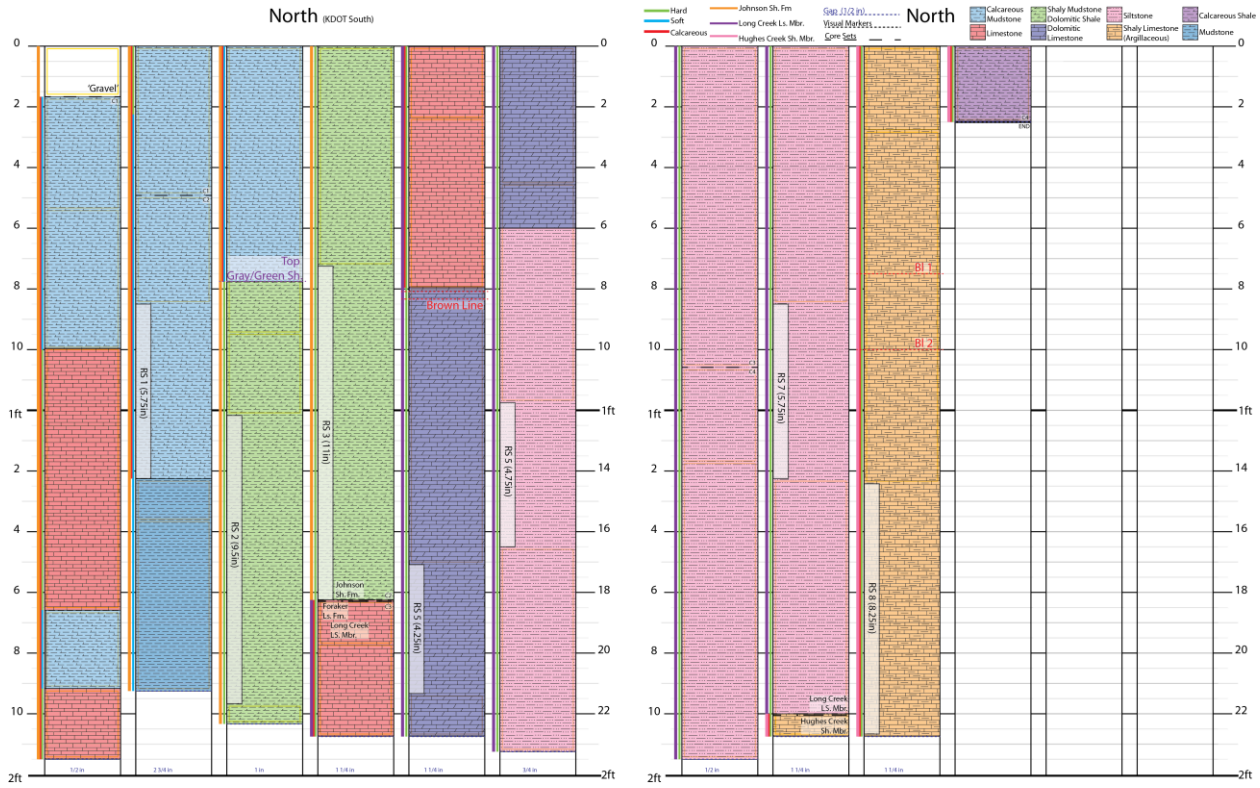


Figure 106 - Core Box Chart: KDOT South (Switched to NORTH)

| **North (Start depth: 737in, 61’ 5’’ ) (KDOT South)** | | | | | |
|---|---|---|---|---|---|
| | | ***Thickness*** | | ***Depth*** | |
| Lyr. | Litho. Type | Inches | Feet & Inch | Inches | Feet & Inch |
| 0 | | 0 | 0'-0" | 737 | 61'-5" |
| 1 | Calc. MudSt. | 8.25 | 0'-8.25" | 745.25 | 62'-1.25" |
| 2 | Limestone | 8.5 | 0'-8.5" | 753.75 | 62'-9.75" |
| 3 | Calc. MudSt. | 2.75 | 0'-2.75" | 756.5 | 63'-0.5" |
| 4 | Limestone | 2.25 | 0'-2.25" | 758.75 | 63'-2.75" |
| 5 | Calc. MudSt. | 8.5 | 0'-8.5" | 767.25 | 63'-11.25" |
| 6 | MudSt. | 7 | 0'-7" | 774.25 | 64'-6.25" |
| 7 | Calc. MudSt. | 7.75 | 0'-7.75" | 782 | 65'-2" |
| 8 | Sh. MudSt. | 31.75 | 2'-7.75" | 813.75 | 67'-9.75" |
| 9 | Limestone | 12.25 | 1'-0.25" | 826 | 68'-10" |
| 10 | Dolo. Ls. | 20.75 | 1'-8.75" | 846.75 | 70'-6.75" |
| 11 | Siltstone | 62.75 | 5'-2.75" | 909.5 | 75'-9.5" |
| 12 | Sh. Ls. | 23.25 | 1'-11.25" | 932.75 | 77'-8.75" |
| 13 | Limey Sh. | 2.5 | 0'-2.5" | 935.25 | 77'-11.25" |

Table 4 - North thickness and bottom depths (KDOT South)

| **South (Start depth: 735.625in, 61’ 3.6’’) (KDOT North)** | | | | | |
|---|---|---|---|---|---|
| | | ***Thickness*** | | ***Depth*** | |
| Lyr. | Litho. Type | Inches | Feet & Inch | Inches | Feet & Inch |
| 0 | | 0 | 0'-0" | 735.625 | 61'-3.625" |
| 1 | Calc. MudSt. | 5 | 0'-5" | 740.625 | 61'-8.625" |
| 2 | Limestone | 8 | 0'-8" | 748.625 | 62'-4.625" |
| 3 | Calc. MudSt. | 2.5 | 0'-2.5" | 751.125 | 62'-7.125" |
| 4 | Limestone | 4.875 | 0'-4.875" | 756 | 63'-0" |
| 5 | Calc. MudSt. | 8.625 | 0'-8.625" | 764.625 | 63'-8.625" |
| 6 | Sh. MudSt. | 35 | 2'-11" | 799.625 | 66'-7.625" |
| 7 | Limestone | 6.75 | 0'-6.75" | 806.375 | 67'-2.375" |
| 8 | Dolo. Ls. | 29.75 | 2'-5.75" | 836.125 | 69'-8.125" |
| 9 | Siltstone | 54.5 | 4'-6.5" | 890.625 | 74'-2.625" |
| 10 | Sh. Ls. | 22 | 1'-10" | 912.625 | 76'-0.625" |
| 11 | Limey Sh. | 22.25 | 1'-10.25" | 934.875 | 77'-10.875" |

Table 5 - South thicknesses and bottom depths (KDOT North)

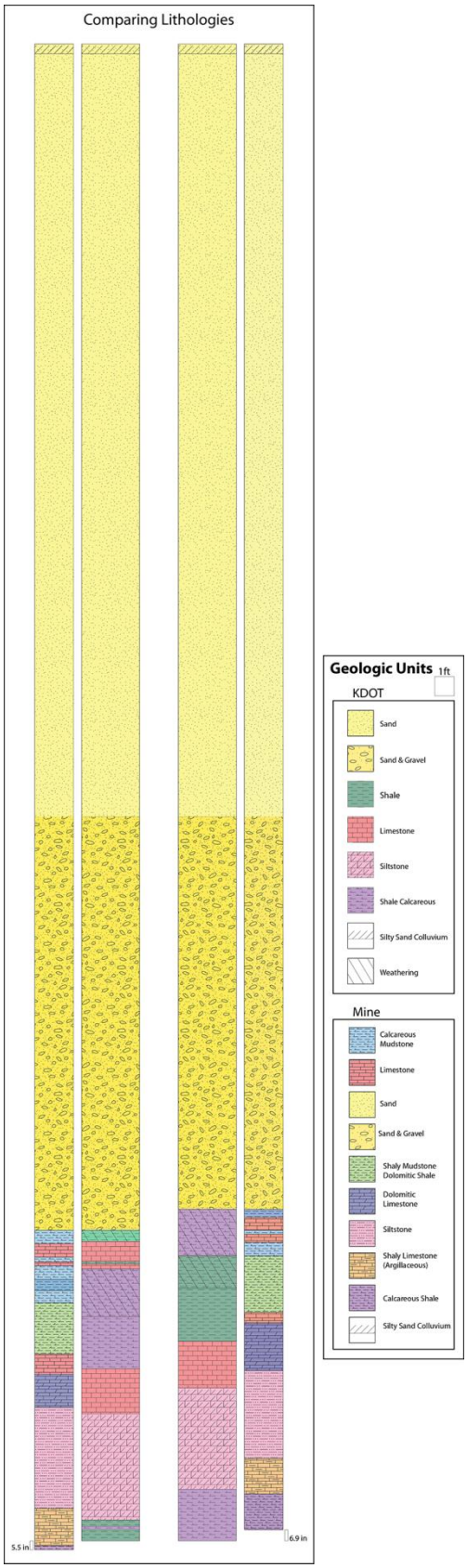


Figure 107 - Comparing KDOT (center) and my initial lithologies (outer)

***Issue with Upper Lithology***

After completing my interpretation of the lithology I compared it with the ATV image (Figure 108), a close up of the bedrock with lithology transitions can be seen in Figure 109. After the initial compression a discrepancy arose between the South ATV and lithology within the mudstone below the second limestone layer. This discrepancy is probably due to the fact that in the South core set a lot of the upper material was reduced to rubble forcing me to infer lithology but I did not add length in these areas. The ATV images density and fractures; but the fractures in the present cores are attributed to the coring process itself. There is no evidence of fracturing in the area and assume no structure fractures are present or were imaged. It is possible for units exhibiting fissile layering would show up as fractures, but units with fissile layers such as black shales have a low density and would show up as dark no matter what. But the cores do not contain a true shale. In the ATV image the yellow portions correlate to dense units and the purple portions correlate to soft units, the lower mudstone correlates to the thick purple bands at 63ft:North and 61ft:South, but the South lithology does not support this. From the rubbly state and the ATV image we can safely assume that a significant portion of the lower mudstone was lost and length needs to be added back in to improve the correlations across the board.

I suspected that due to the rubbly state of the upper portion of the South core set that length within the lowest mudstone unit was lost during the coring process possibly because of the process or because of the poor condition of the unit. It is important to note that the mudstone units in the South borehole are in significantly worse condition than the counter parts in the North borehole. In the South borehole a significant amount of pink sand grains were present, so much that the top 3-5 inches of of the green/gray dolomitic shale unit was ground down into a cone shape. While I inferred the lithology of the upper South borehole from the rubble I did not add any length to it, it is very likely that length was lost here. It appears no significant amount of length was lost in the second mudstone unit or in the two limestone units it is sandwiched between. From my observations the majority of the missing length was probably from the lower mudstone layer, it is also possible that a portion of length is missing from the top mudstone layer. I chose to focus on the lower mudstone layer, compared it to the counterpart in the North borehole, there was a 14 inch difference between the two. Adding in 14 inches to the South lower mudstone was difficult to justify, there was a 6.9in difference in length between my lithology interpretation and the one provided by KDOT, an additional 7in to the lower mudstone

was not unreasonable and since it improves the correlation between lithologies and the ATV images I believed it justified. A close up comparison of my original lithology (Figure 109) and my inferred lithology (Figure 110) can be seen below and a full image of my original lithology (Figure 108) and my inferred lithology (Figure 111) can also be seen.

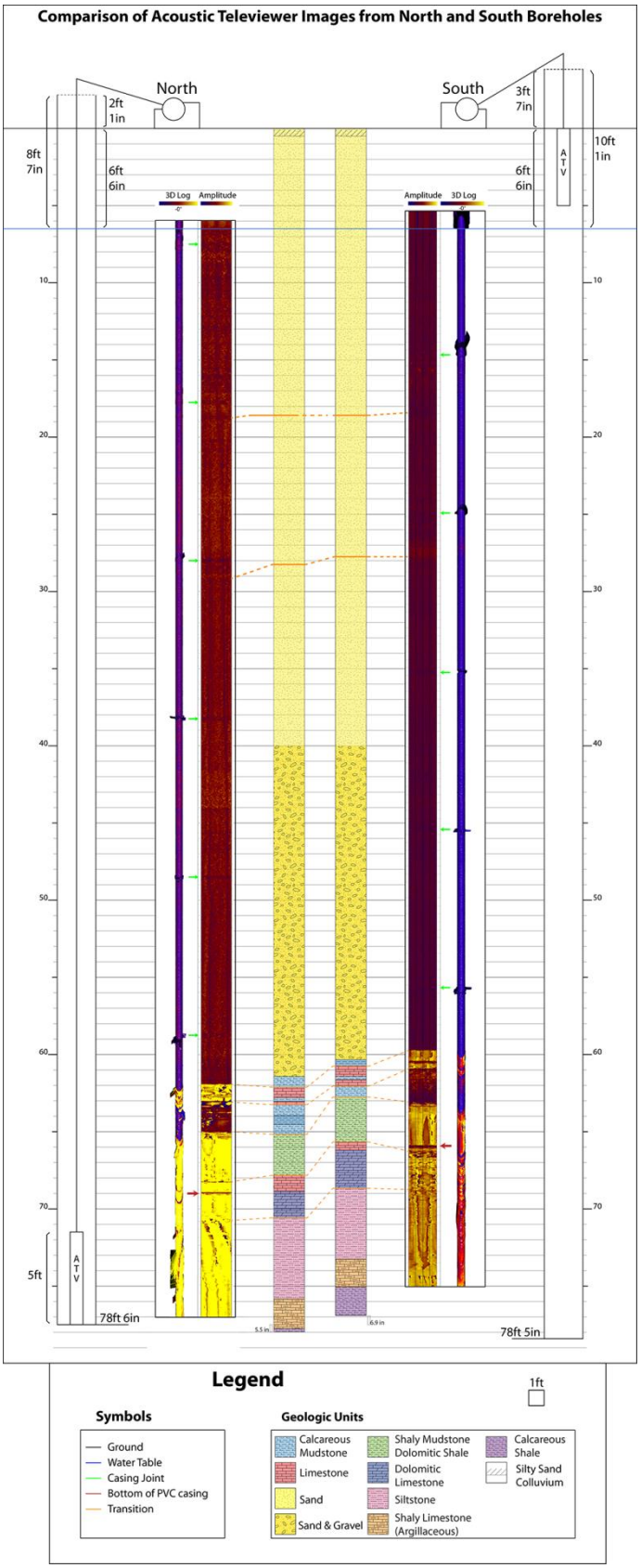


Figure 108 - Comparison of ATV image with my initial lithology

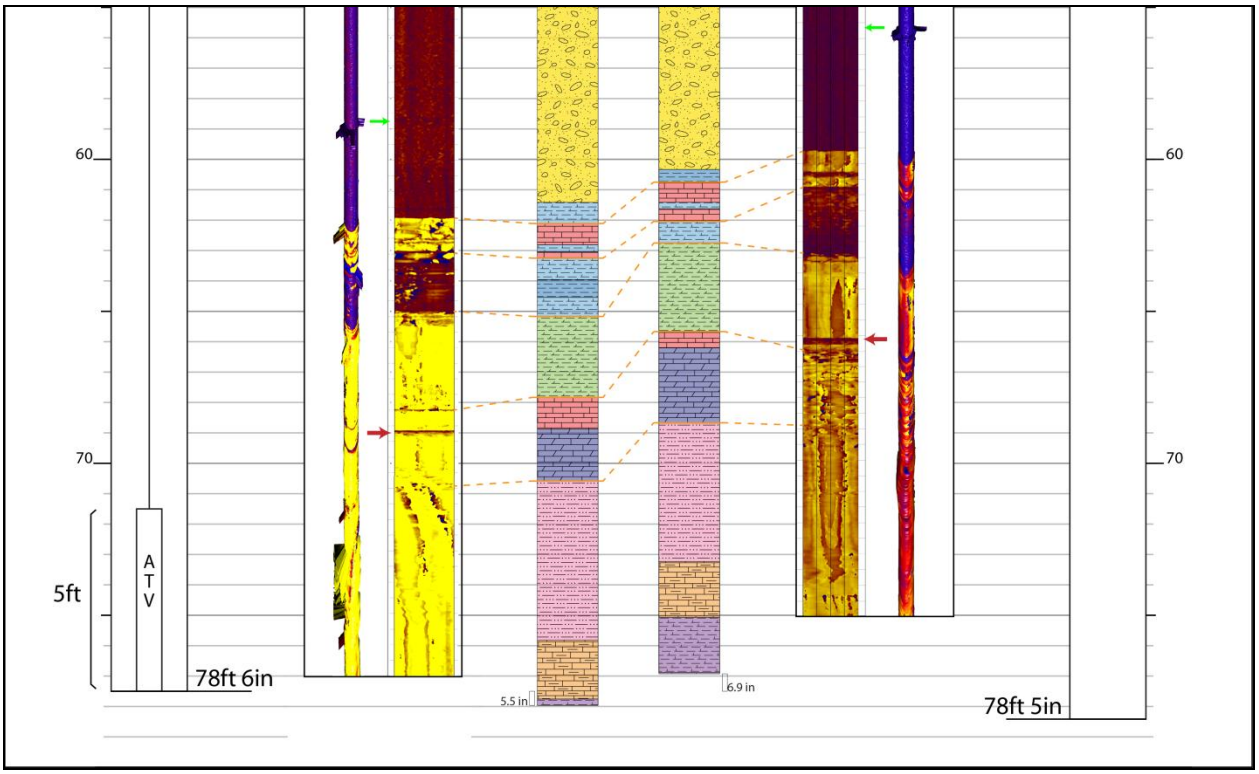


Figure 109 - Close up of ATV images and original lithology with transitions

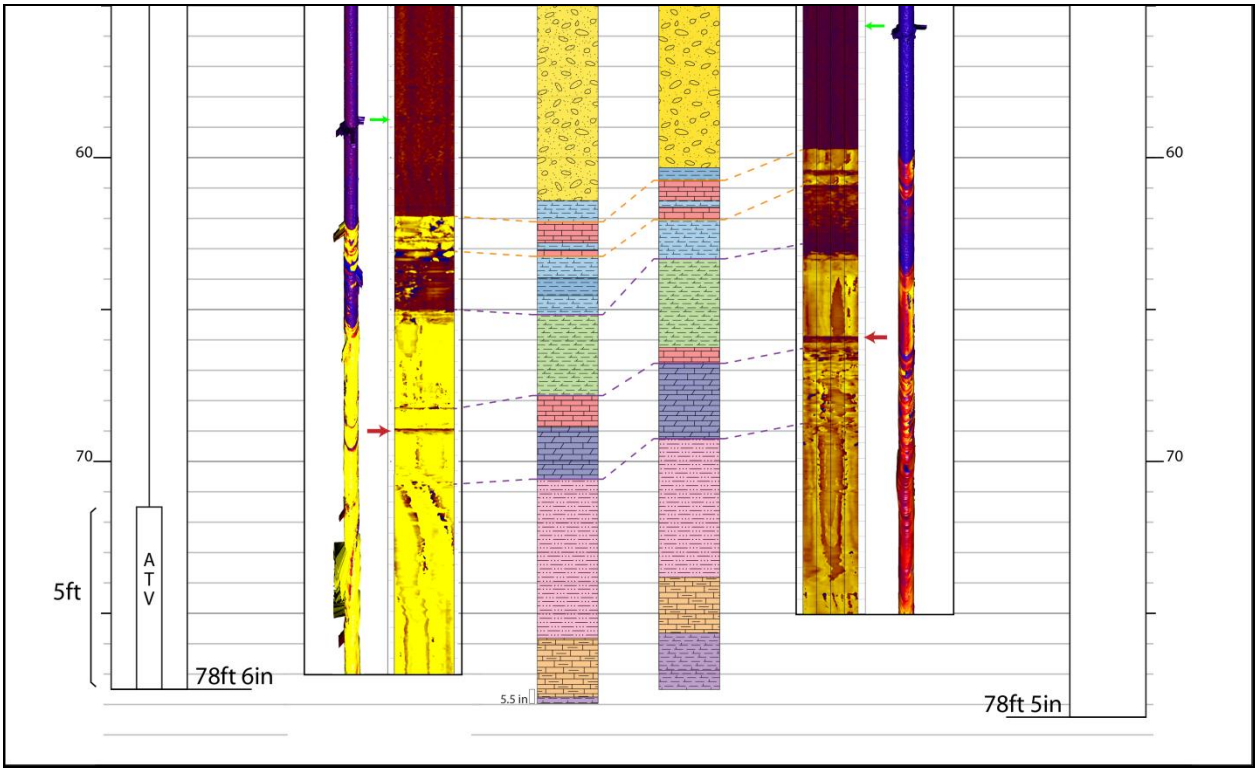


Figure 110 - Close up of ATV images and my inferred lithology with transitions (new inferred transitions in purple)

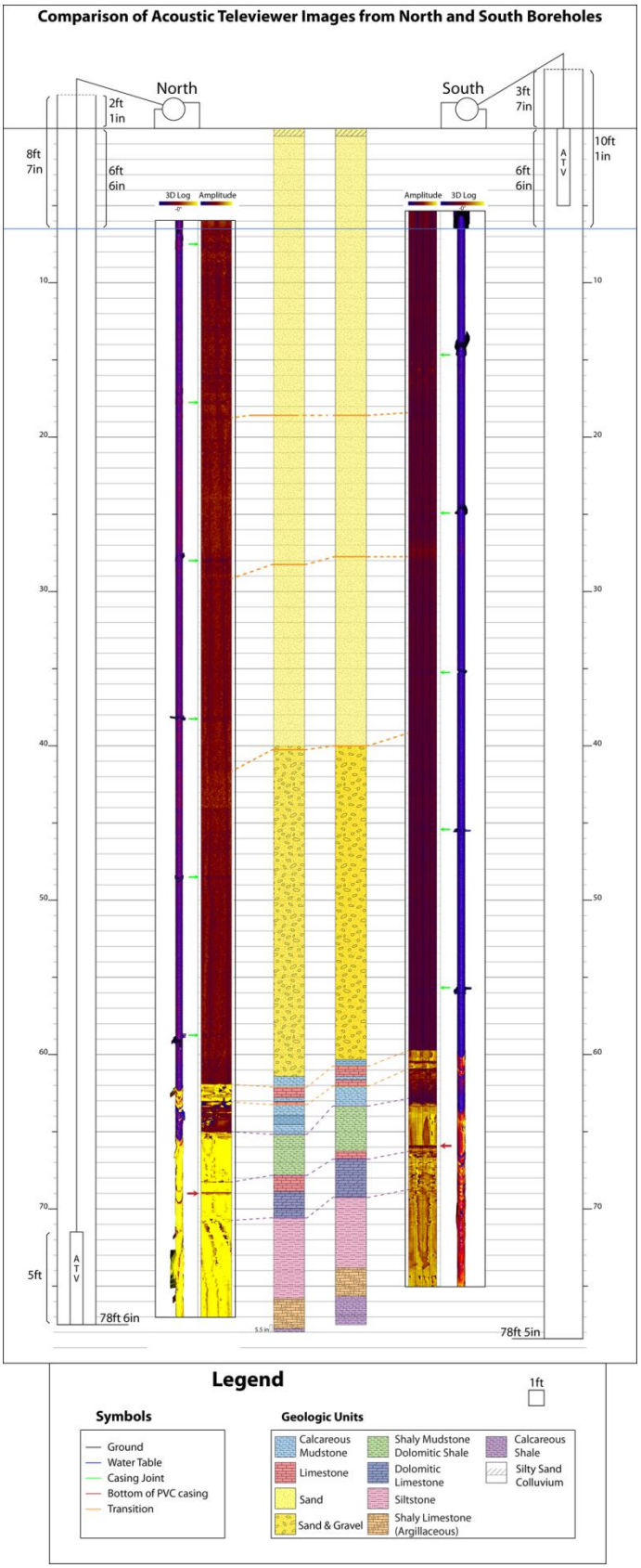


Figure 111 - Comparison of ATV image with my inferred lithology

### *ATV Conclusion*

After double-checking the ATV data, the inconsistencies were due to the simplistic lithology provided by KDOT. After closer examination and repeated comparison to the ATV image a detailed and precise lithology was created and the correlations between the lithologies and the ATV images were improved and help us to understand the underlying geology of the area. And remaining discrepancies could be attributed to the destructive coring process or possible human error, but overall the data and correlations appear accurate.

After close analysis, I believe there is possible human error contaminating the ATV image. The ATV image is not in agreement with the borehole reports, I believe the top of the bedrock maybe false positive or an error in depth measurement occurred. The suspicion arises from the fact that, between boreholes, a distance almost identical to the offset of the PVC casing jointing offsets the top of the bedrock. Now, the PVC casting did not extend all the way to the bottom of the hole but the top of the imaged bedrock (yellow) does not correspond to the end of the PVC casting. Taking into account each PVC segment is approximately 10 ft long, I believe the end of the PVC occurs and can be seen at just above the 75ft on the North log and just below the 70ft marker on the South log.

## Laboratory Ultrasonic Velocity Measurements

The ULT100 system was used to measure and calculate several earth and elastic properties including: density, compressional-waves, shear-waves, Poisson's ratio, Young's modulus, bulk modulus and shear modulus. Physical properties of cores can be seen below Table 6.

| North (Ogden, Riley CTY) Physical Properties of Cores | | | | | | | | | | | | |
|---|---|---|---|---|---|---|---|---|---|---|---|---|
| ID | Density (g/cm^3) | Lt. (in.) | Dia. (in.) | Top dpt. (ft.) | Bot. dpt. (ft.) | Avg. dpt. (ft) | C | R | RQD | Lt. (mm) | Dia. (mm) | Mass (g) |
| RN1 | 2.22 | 5.450 | 2.00 | 64.875 | 65.329 | 65.102 | 3 | 2.7 | 2.1/3.0 | 139 | 51 | 629.8 |
| RN3-S | 2.24 | 5.670 | 2.00 | 67.042 | 67.514 | 67.278 | 2 | 2 | 1.6/2.0 | 144.5 | 51 | 660.4 |
| RN3-R | 2.24 | 5.670 | 2.00 | 67.042 | 67.514 | 67.278 | 2 | 2 | 1.6/2.0 | 144.5 | 51 | 661.5 |
| RN5 | 2.4 | 6.4375 | 2.00 | 70.792 | 71.328 | 71.060 | 5 | 5 | 100 | 162.5 | 51 | 796.1 |
| RN6 | 2.16 | 7.625 | 2.00 | 72.427 | 73.063 | 72.745 | 5 | 5 | 100 | 192 | 51 | 849.0 |
| RN7 | 2.16 | 9.875 | 2.00 | 74.333 | 75.156 | 74.745 | 5 | 5 | 100 | 250 | 51 | 1101.2 |
| RN8 | 2.25 | 7.625 | 2.00 | 75.198 | 75.833 | 75.516 | 5 | 5 | 100 | 194 | 51 | 893.5 |
| RN9 | 2.26 | 9.250 | 2.00 | 75.833 | 76.604 | 76.219 | 5 | 5 | 100 | 233.5 | 51 | 1076.3 |
| RN10 | 2.27 | 8.688 | 2.00 | 77.609 | 78.333 | 77.971 | 5 | 5 | 100 | 220 | 51 | 1019.5 |

Table 6 - Example of physical properties

The ‘picking’ done to determine the values for ultrasonic (P) compressional- and (S) shear-wave velocities were additionally used to calculate earth properties and elastic moduli; density, Poisson’s ratio, Young’s modulus, bulk modulus and shear modulus. These properties, seen in the tables below, were intended to be used for cross validation. But since there is not conversion between ultrasonic and seismic velocities (without addition of data eg. sonic log) only density and elastic moduli such as Poisson’s ratio could be considered to be used during the inversion process. Further discussion of the ‘picking’ process can be found in the methodology section.

After extracting the data through the picking process we noticed the Poisson’s ratio was much higher than expected. Our samples were dried at room condition, not in an oven, but this possible source of moisture could not account for the high Poisson’s ratio values. So it was determined that background noise was over riding the main signal at the initial P-wave picking point. So P-wave picking was redone at the point where the waveforms start to diverge. For a close to dry sample I believe these values are truer to the real world. You will notice from the below tables that Young’s and bulk moduli are effected by the change in picking, while shear modulus is not. After pointing this out it must be mentioned that our MASW data is from an area with a high water table and thorough water saturation. So these values of Poisson’s ratio are not identical.

**North Standard Picking:** First Arrivals & Elastic Prop.

| | Avg. Dpt. (ft.) | lbf | P-Vel (m/s) | S-Vel (m/s) | Poisson's Ratio | Youngs (MPa) | Bulk (MPa) | Shear (Mpa) |
|---|---|---|---|---|---|---|---|---|
| RN1 | 65.102 | RN1-30 | 7593 | 1663 | 0.47 | 18102 | 119680 | 6137 |
| | | RN1-205 | 7627 | 1643 | 0.48 | 17665 | 121034 | 5985 |
| | | RN1-410 | 7869 | 1636 | 0.48 | 17540 | 129437 | 5936 |
| RN5 | 71.060 | RN5-30 | 8759 | 2349 | 0.46 | 38685 | 166329 | 13237 |
| | | RN5-220 | 8945 | 2546 | 0.46 | 45275 | 171152 | 15549 |
| | | RN5-440 | 8828 | 2550 | 0.45 | 45348 | 166131 | 15589 |
| RN6 | 72.745 | RN6-30 | 9959 | 2215 | 0.47 | 31321 | 200534 | 10625 |
| | | RN6-230 | 10488 | 2214 | 0.48 | 31336 | 223940 | 10610 |
| | | RN6-460 | 10468 | 2233 | 0.48 | 31873 | 222782 | 10796 |
| RN7 | 74.745 | RN7-30 | 13374 | 2010 | 0.49 | 25922 | 374047 | 8708 |
| | | RN7-235 | 13543 | 2070 | 0.49 | 27495 | 383181 | 9239 |
| | | RN7-470 | 13896 | 2076 | 0.49 | 27660 | 403960 | 9291 |
| RN8 | 75.516 | RN8-30 | 10199 | 1941 | 0.48 | 25164 | 223203 | 8495 |
| | | RN8-240 | 10250 | 2092 | 0.48 | 29185 | 223693 | 9871 |
| | | RN8-480 | 10563 | 2096 | 0.48 | 29299 | 238364 | 9901 |
| RN9 | 76.219 | RN9-30 | 12039 | 1786 | 0.49 | 21435 | 317431 | 7199 |
| | | RN9-240 | 12119 | 1846 | 0.49 | 22894 | 321157 | 7692 |
| | | RN9-480 | 12276 | 1903 | 0.49 | 24324 | 329133 | 8175 |

Table 7 - Example of standard picking values North Borehole

**North Altered picking**: Poisson's Point

| | Avg. Dpt. (ft.) | lbf | P-Vel (m/s) | S-Vel (m/s) | Poisson's Ratio | Young's (MPa) | Bulk (MPa) | Shear (Mpa) |
|---|---|---|---|---|---|---|---|---|
| RN1 | 65.102 | RN1-30 | 2570 | 1663 | 0.14 | 13988 | 6468 | 6137 |
| | | RN1-205 | 2573 | 1643 | 0.16 | 13837 | 6702 | 5985 |
| | | RN1-410 | 2563 | 1636 | 0.16 | 13729 | 6661 | 5936 |
| RN5 | 71.05989 | RN5-30 | 4215 | 2349 | 0.27 | 33745 | 24957 | 13237 |
| | | RN5-220 | 4252 | 2546 | 0.22 | 37955 | 22635 | 15549 |
| | | RN5-440 | 4269 | 2550 | 0.22 | 38122 | 22916 | 15589 |
| RN6 | 72.74479 | RN6-30 | 3534 | 2215 | 0.18 | 24995 | 12869 | 10625 |
| | | RN6-230 | 3514 | 2214 | 0.17 | 24844 | 12576 | 10610 |
| | | RN6-460 | 3515 | 2233 | 0.16 | 25080 | 12351 | 10796 |
| RN7 | 74.74479 | RN7-30 | 3327 | 2010 | 0.21 | 21120 | 12254 | 8708 |
| | | RN7-235 | 3352 | 2070 | 0.19 | 22021 | 11906 | 9239 |
| | | RN7-470 | 3358 | 2076 | 0.19 | 22128 | 11928 | 9291 |
| RN8 | 75.51563 | RN8-30 | 3106 | 1941 | 0.18 | 20039 | 10423 | 8495 |
| | | RN8-240 | 3135 | 2092 | 0.10 | 21686 | 9000 | 9871 |
| | | RN8-480 | 3159 | 2096 | 0.11 | 21923 | 9299 | 9901 |
| RN9 | 76.21878 | RN9-30 | 3136 | 1786 | 0.26 | 18140 | 12592 | 7199 |
| | | RN9-240 | 3113 | 1846 | 0.23 | 18902 | 11610 | 7692 |
| | | RN9-480 | 3102 | 1903 | 0.20 | 19590 | 10817 | 8175 |

Table 8 - Example of altered picking values North Borehole

Dynamic Poisson's ratio method involves measuring compressional- and shear-wave velocities ($V_p/V_s$). Compressional- and shear-wave velocities can be measured from one of several sources; seismic data, sonic well logs, or laboratory measurements; by sending signals through samples at small stress and strain, and used to calculated the dynamic Poisson's ratio ($\sigma_d$). Dynamic Poisson's ratio is most favorable for several reasons, (Zhang and Bentley, 2005), the velocity measurement is less destructive to the sample so further or additional testing could be done, it is more cost effective and more time efficient.

For laboratory measurements we have close to dry samples (ambient humidity) and when overburden is simulated the majority of cracks were sealed. So for us the main factor influencing Poisson's ratio were moisture and mineral composition. Few publications describing/discuss acceptable near surface Poisson's ratio ranges for elements, minerals, or rock types. A publication that does discuss acceptable ranges is Gercek (2007), but the moisture content is not specified, even though in the paper it is noted "[…] undrained values of Poisson's ratio of rocks are larger than the drained values" (Gercek, 2007).

For our project we are interested in the values for limestone, shale, siltstone and alluvium. At the Ogden site we have approximately 60 ft of alluvium, the upper portion starts off medium grained sand with some silt lenses near the top, with depth the grading becomes courser to coarser sand and gravel (~40-60ft) (KDOT, 2011). A breakdown of the alluvium is as follows; first the upper most foot was loose sand then silty sand for another foot then at 10 ft depth a mix of sand and gravel with increasing coarseness. So, trusting Gercek graphs (Figure 112 and Figure 113) depicting typical ranges of Poisson's ratio of several rock types, we can observe that limestone (0.1-0.33), shale (0.03-0.32), and siltstone (0.13-0.35) have a broad range. Gercek also give a table of granular soil types; loose sand (0.2-0.4), medium dense sand (0.25-0.4), dense sand (0.3-0.45), silty sand (0.2-0.4), sand and gravel (0.15-0.35), and saturated cohesive soils (~0.5).

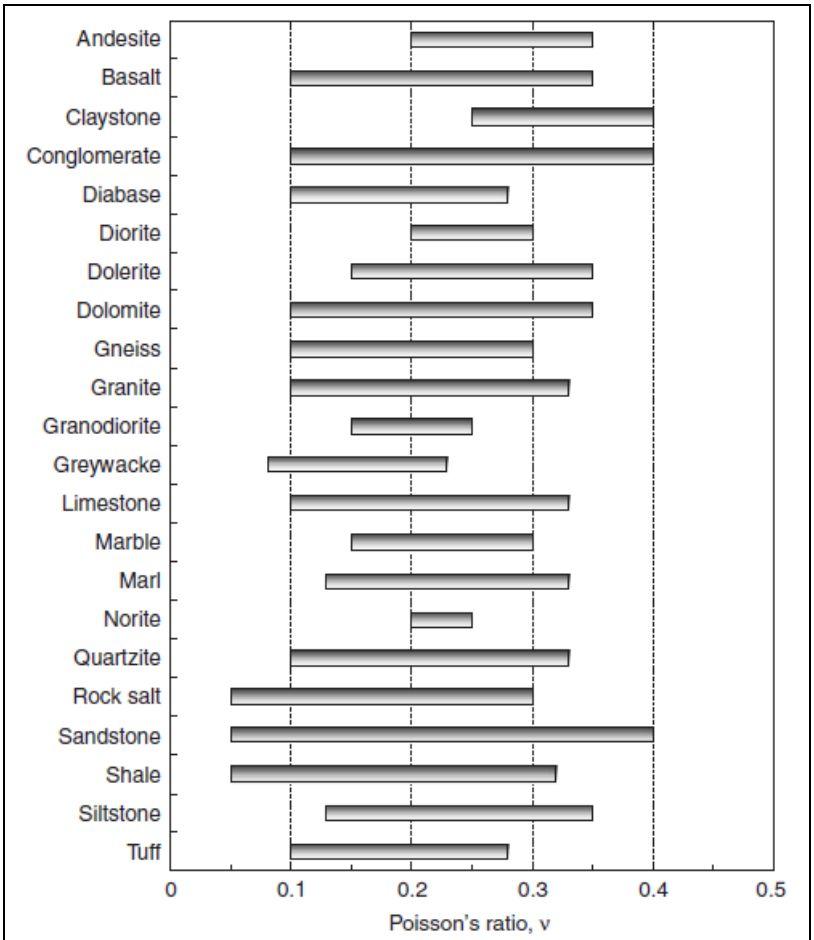


Fig. 4. Typical ranges of values for Poisson's ratio of some rock types (data after [33,34,44–46]).

Figure 112 - Typical range for Poisson's ratio reported by Gercek (2007)

Table 6
Typical ranges of values of Poisson's ratio for granular soils [81]

| Soil type | Poisson's ratio |
|---|---|
| Loose sand | 0.20–0.40 |
| Medium dense sand | 0.25–0.40 |
| Dense sand | 0.30–0.45 |
| Silty sand | 0.20–0.40 |
| Sand and gravel | 0.15–0.35 |
| Saturated cohesive soils | ~0.50 |

Figure 113 - Typical ranges of Poisson's ratio for soils (Gercek, 2007)

Since Poisson's ratio is calculated from $V_s$ and $V_p$, even though we used ultrasonic frequencies our Poisson's ratio is still valid, the main factor affecting our Poisson's ratio was where to pick for the P-wave. After evaluation it was discovered that the standard picking point for Poisson's ratio was not acceptable, the values were to high and where representative of saturated samples, but our samples were dry. This caused us to reevaluate our waveforms and determine that background noise was playing a larger role than expected. The hope was to find a repeatable point where the background noise and actual signal over lapped which would result in a leveling out. But an easily recognizable point was not found in the majority of waveforms. So picking at the point the waveforms diverged from one another was adopted for the P-wave. Picking was not simple or straight forward, we had to analyses and make a critical decision/assumption based on our observations.

Basically, Poisson's ratio for unconsolidated sediments below the water table should be around 0.4. While sediments above the water table can vary greatly (discussed previously) because of partial saturation, changes in lithology, and possible measurement error. The cores used in our laboratory measurements where not saturated, they were relatively dry but exposed to ambient humidity. So we should treat these cores like we would material above the water table, a Poisson's ratio of 0.4 or greater would not be valid. As previously saw in Figure 58 SurfSeis uses the assumption that Poisson's ratio is 0.4 and constant, since the water table is so close to the surface this assumption can be considered valid.

## MASW SurfSeis Integrated Inversion Results

After initial processing and integration was completed the next step was to integrate the laboratory measurements with the MASW surface-wave data sets. The results from initial conservative and trustworthy picking were not able to image deep enough to overlap with the core samples measured in the laboratory. My attempt to correct this was to pick the dispersion curves more aggressively and farther to the left, which resulted in deeper imaging. The aggressive picking yielded questionable inversion results, but regardless of that the aggressive picking was unable to image deep enough (max 40 – 50 ft). Only Line 10 acquired on top of a compact dirt road was capable of reaching a depth of 60ft. Even though the aggressive picking of Line 10 was capable of reach 60ft it still did not overlap with the highest core sample RS1

from 63.4 ft. From this it was concluded that the intended integration of Ogden data was prevented because the bedrock was to deep.

In this section I will document my attempt at aggressive picking and the subsequent results in this section. And I will discuss in detail alternative approaches for future research and my conclusions. The data sets with aggressive picking was labeled '(LossBot)Mob' and was pick as far left as theoretically possible. Theoretically according to the Kansas Geological Survey since our project used 4.5 Hz geophones, we should be able to observe frequencies as low as 2.25 Hz. A safe assumption was that picking as low as 3 Hz was definitely theoretically valid. For the aggressive picking (Mob) the displayed minimum frequency was set to 3 Hz (Figure 114). Even though picking as far back to 3 Hz was theoretically valid the data did not always support that.

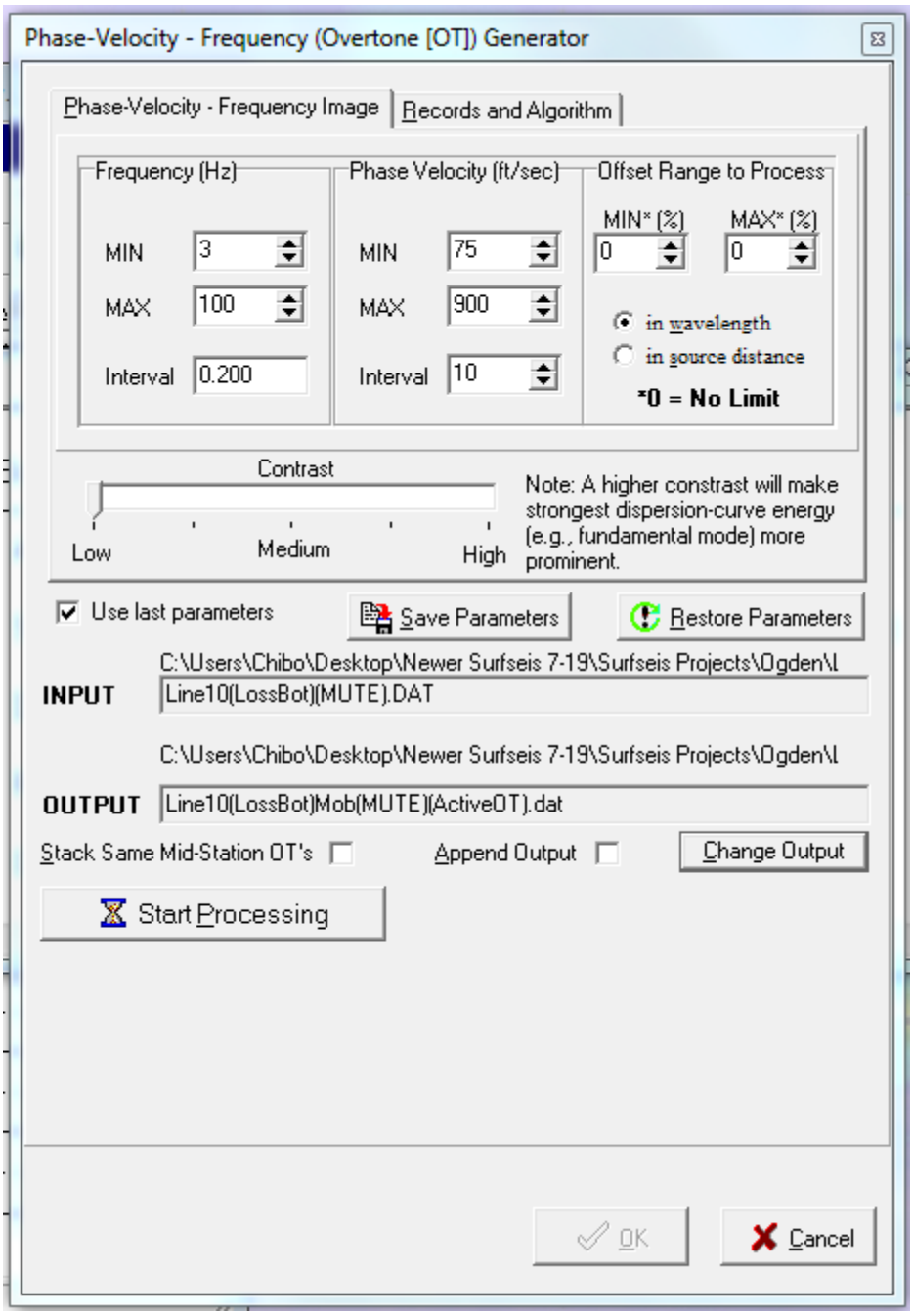


Figure 114 - Aggressive dispersion curve display window

The goal was to pick in a similar fashion as the conservatively picked LossBot data sets but as far to the left as possible for the aggressively picked data set. In most cases I was able to pick as far back at 5 Hz (Figure 115 and Figure 116), all the aggressively picked dispersion curves, from every line, can be found in the Appendix. Additionally, Figure 117 and Figure 118 exhibit some 'pull-up' distortion most likely due to higher mode contamination or an artifact in the dataset created during acquisition. 'Pull-up' distortions occur when higher modes

contaminate the fundamental causing spikes in the Phase Velocity. The 'pull-up' events at higher frequencies were subtle and in some dispersion curves caused the trailing tail to end, become less visible or to turn up a bit. In our data the higher frequency tail tended to turned up, to counter for it picking at the last reliable point (falling in red or light green) was used as a guide and no picking points after were placed higher (on the Phase Velocity axis).

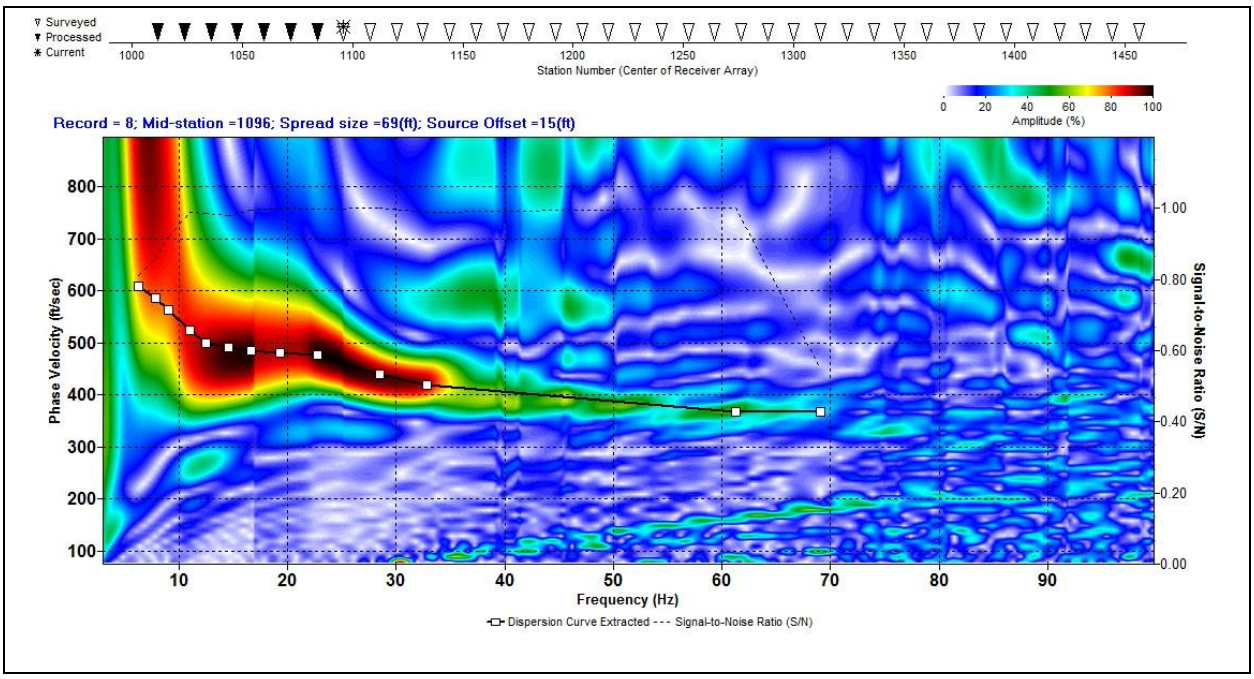


Figure 115 - Aggressive Picking of dispersion curve (8) from Line 10, back to 5 Hz

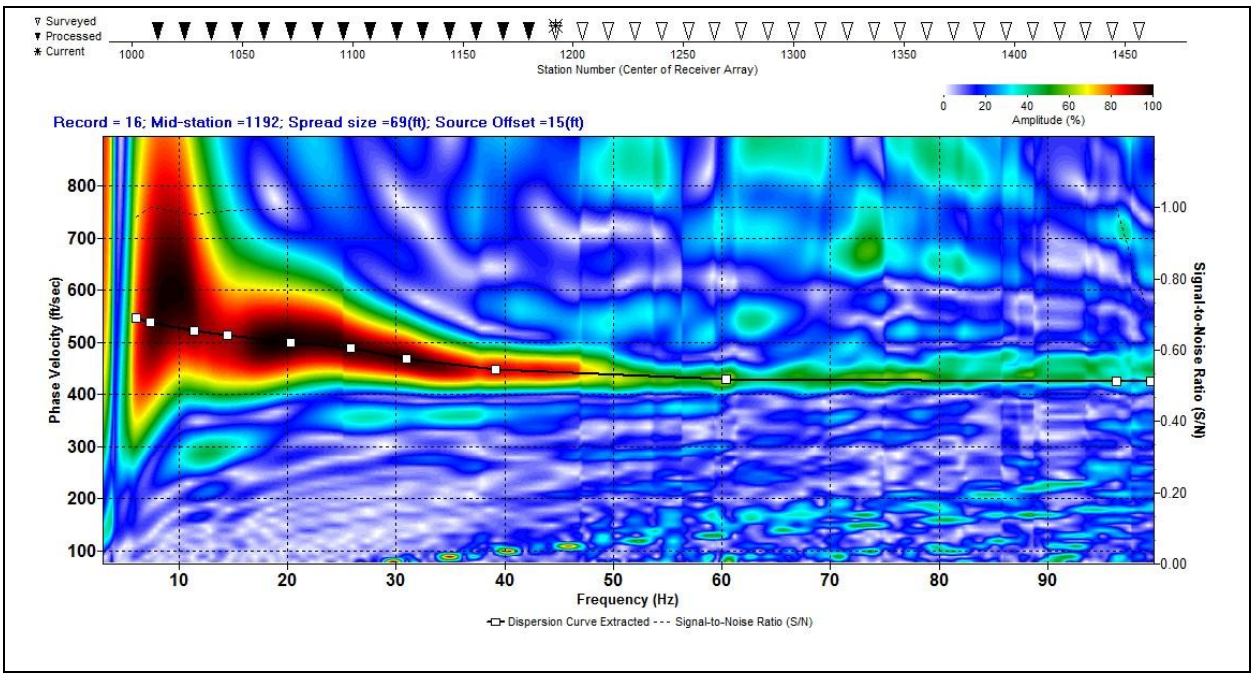


Figure 116 - Aggressive Picking of dispersion curve (16) from Line 10, back to 5 Hz

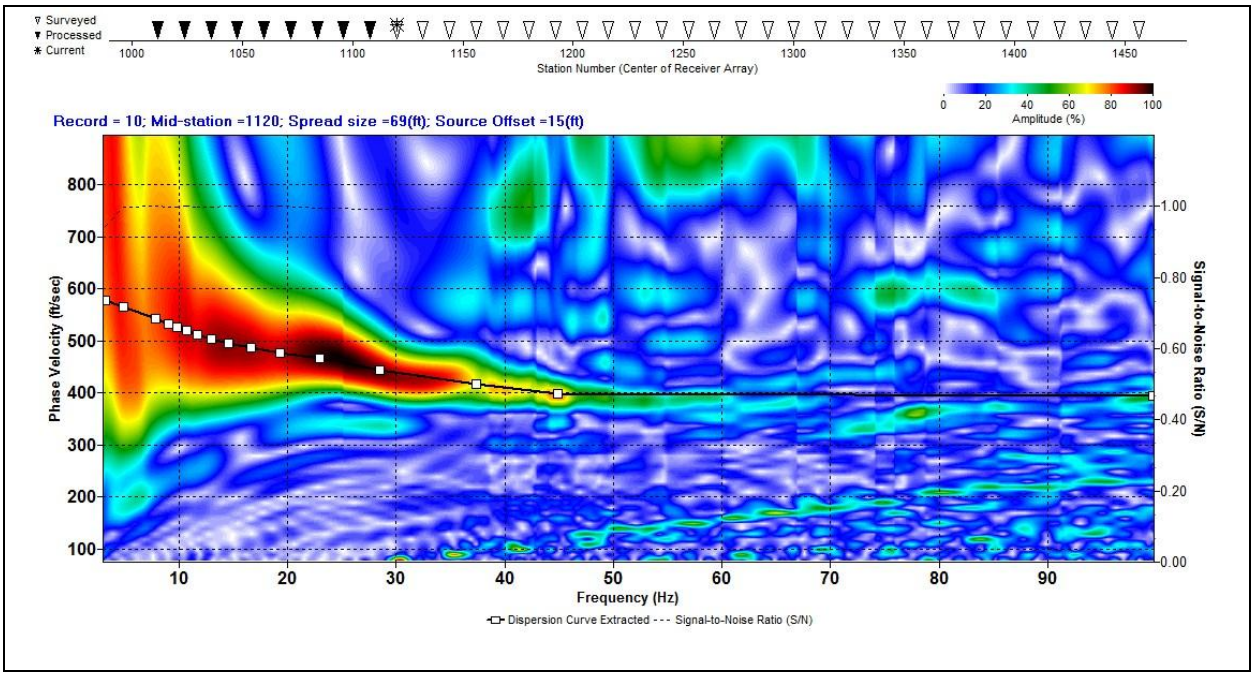


Figure 117 - Aggressive Picking of dispersion curve (10) from Line 10

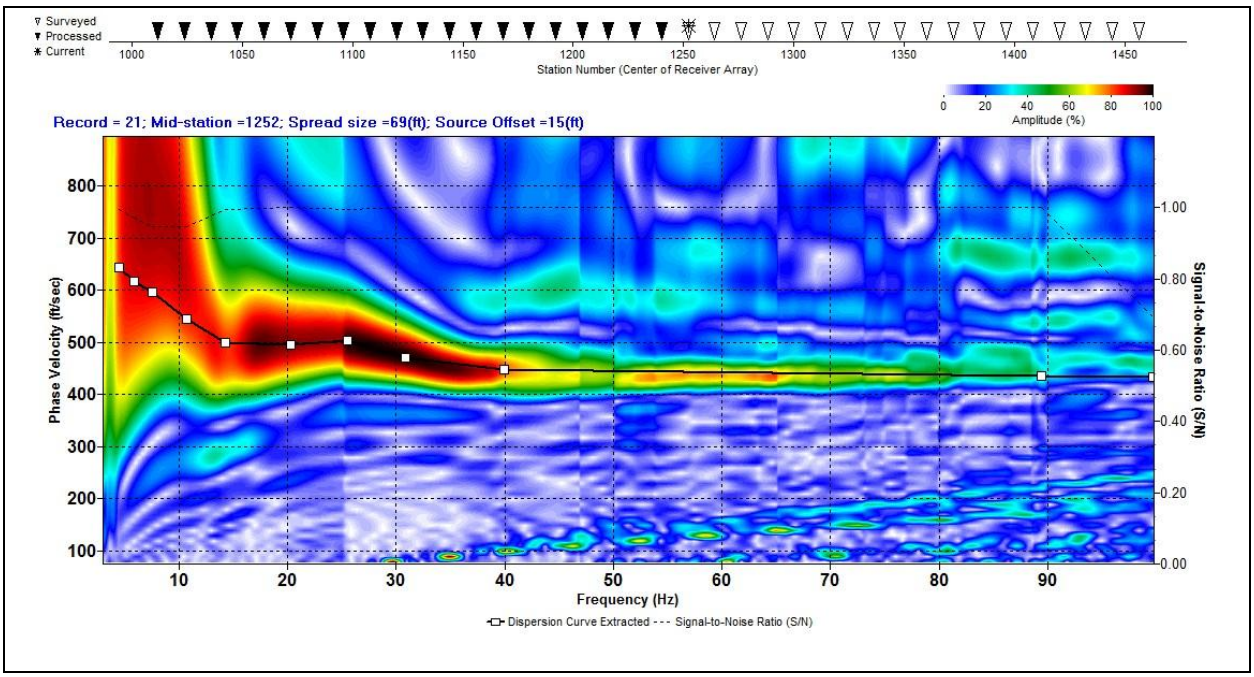


Figure 118 - Aggressive Picking of dispersion curve (21) from Line 10

Once picking was completed the parameters for inversion remained the same as pervious inversions since the aggressive results need to be compared with the conservative results. The 'Approx' 2D $V_s$ model can be seen below in Figure 119, it looked relatively good but when compared with the final $V_s$ model (Figure 120) it was not as accurate or detailed, just like we saw previously with Line 12. The aggressive 2D $V_s$ model exhibits some anomalous features that are not true representations of the geology. From the 2012 Kanas Geological Survey short course, I learned that low velocity bubbles (the blue at 45-50 ft. depth) are either artifacts created during the picking phase or there were utilities under the survey. Since we know there were not buried utilities lines and since the conservatively picked inversion results of Line 10 did not exhibit such apparent signs of low velocities bubbles, it was safe to assume that this low velocity layer was an artifact created during processing. The creation of these artifacts was caused by the aggressive picking and it was determined that the quality of the data made it unreliable in addition to the fact it did not overlap with the highest core samples (RN1 65.1ft, RS1 63,4ft). The aggressive inversion results were unreliable and were discarded.

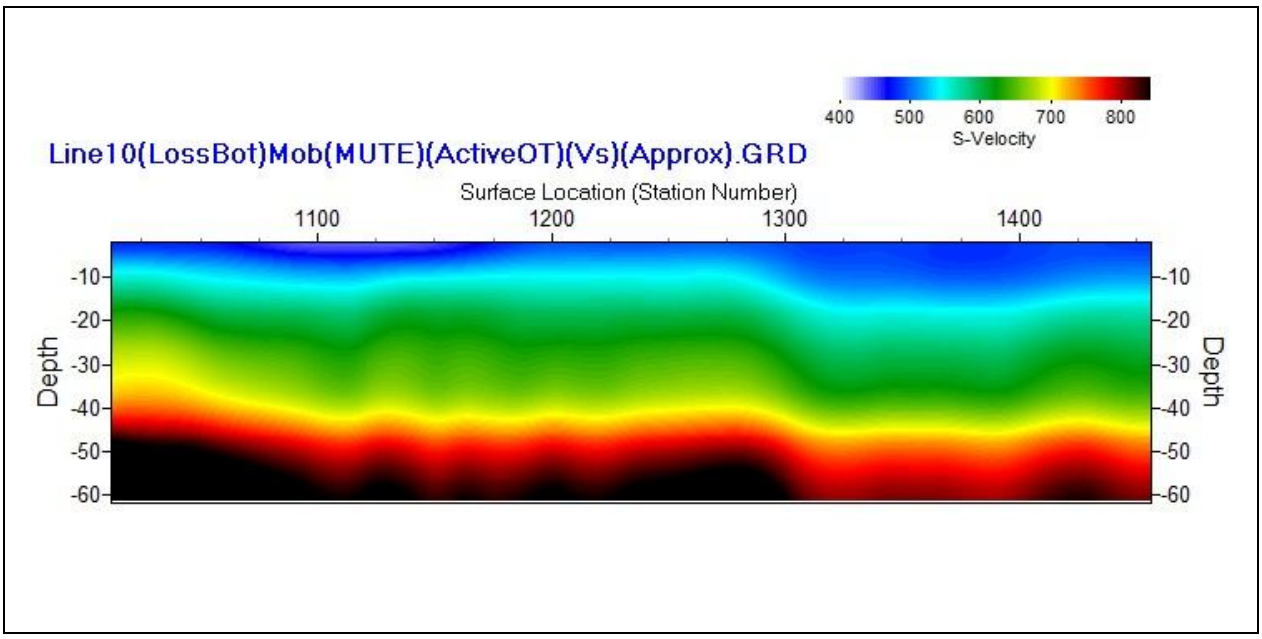


Figure 119 - 'Approx' 2D Vs Model of Aggressive picking

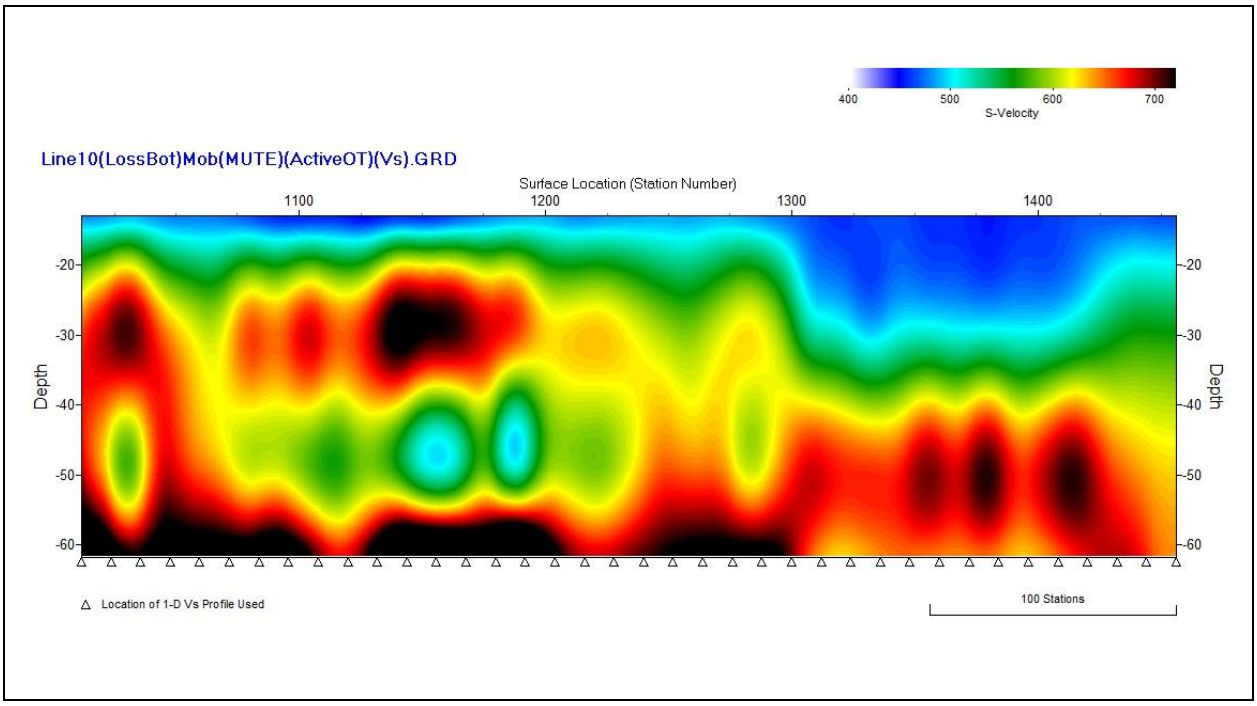


Figure 120 - Aggressive 2D Vs Model

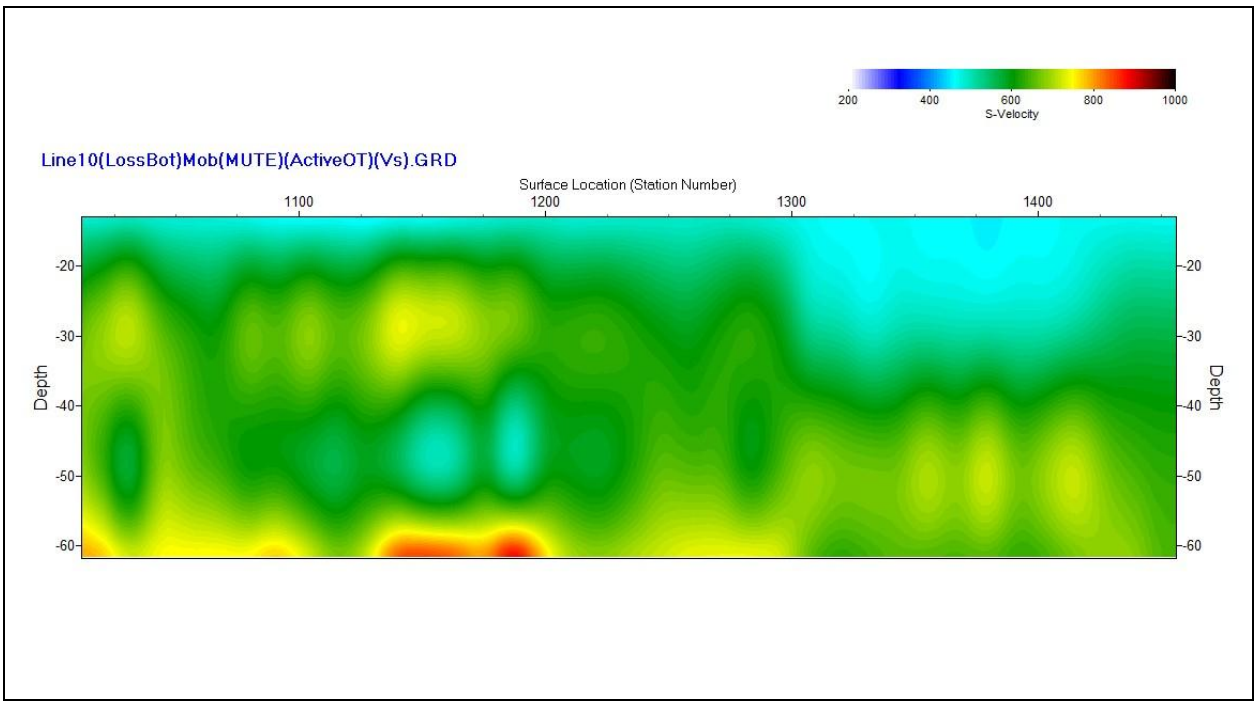


Figure 121 - Aggressive 2D Vs Model (range 200-1000)

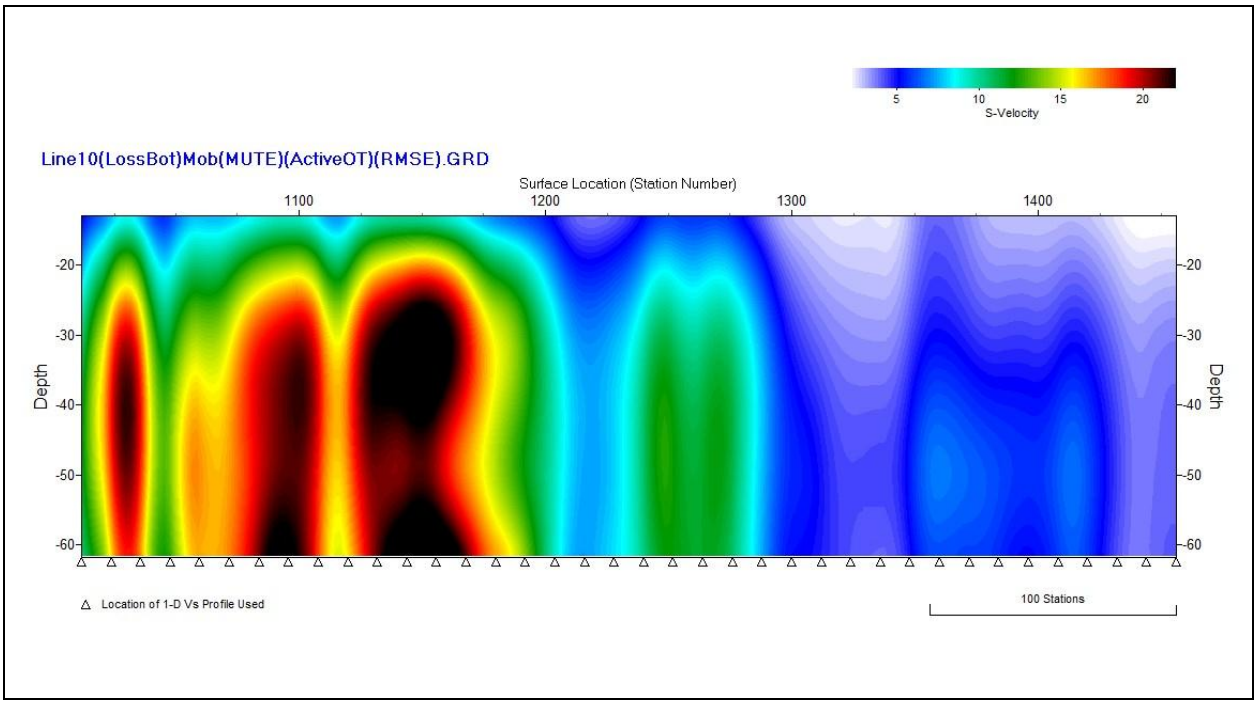


Figure 122 - Aggressive 2D RMSE Model

Neither the conservatively nor the aggressively picked dataset reach the depth of the shallowest core samples, the integration of overlapping data cannot be done with the Ogden data sets and an alternative approach would needed to make it work. There are two approaches that could be taken for future research; manipulating the data we currently have or conduct a new

acquisition. Manipulating the data we currently have would not be a true integration, it would be the stitching together of the two data sets but would requiring additional velocity and elastic modulus estimates from an external or additional source such as a sonic log from a nearby well. The additional data could be collected through an additional acquisition or possibly be found through searching the KDOT or KGS libraries. The second option, a new MASW acquisition, could be approached a few ways; a longer source to first receiver offset could possibly image greater depths, or a passive and active acquisition could be combined to increase the quality of the fundamental mode frequency range observed resulting in greater imaging depths (Kansas Geological Survey 2012). In the following section I will reiterate that the Ogden data set cannot be integrated presently, but for future research there are alternative approaches that could be executed to make the integration of surface-wave and laboratory data from the Ogden site possible.

# Chapter 6 - Conclusion

This project analyzed in detail the near surface geology of the Ogden area near a large and newly built bridge structure. This detailed information will be used by engineers to further evaluate the stability and longevity of the bridge and to determine how the near surface material would respond in the case of a seismic event. From our ATV data our understanding of the near surface lithology was improved and a 1.14 degree dip from south to north was discovered but no faults were found. Using the surface-wave data we created a reliable shear-wave velocity model with minimal introduction of error from the dispersion curve picking process. And from our laboratory experiments we were able to measure and calculate physical and elastic properties for engineers to use.

The final phase of this project was to integrate laboratory measurements with the surface-wave data but the data sets do not overlap. Without the overlap we cannot use information from one data set to constrain and refine the values from the other.

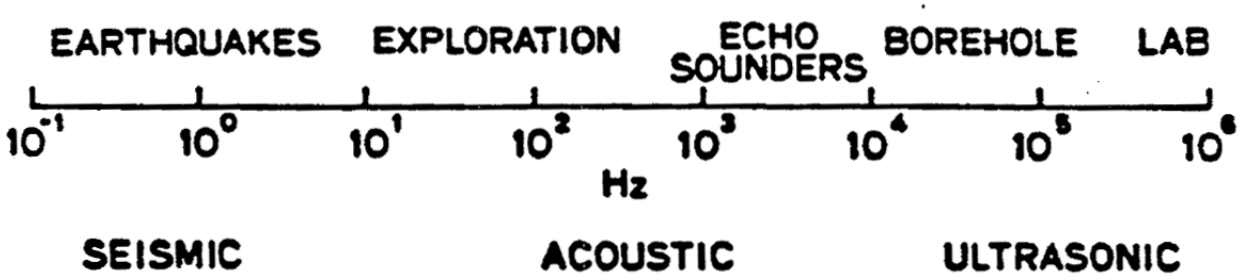


Figure 123 - Velocity Scale From Han, 1986

As mentioned in the Data and Results section the proposed integration of surface-wave data and laboratory measurements from the Ogden site was not possible because the data did not overlap. Originally the second site in Douglas County was part of this thesis but was dropped because of time constraints and a lack of acoustic televiewer data, but it would most likely suffer from a lack of overlap because the lines were acquired in similar conditions as Line 10 from Ogden and the cores were at similar depth. The surface-wave data from Douglas was acquired on top of two parallel heavily compacted dirt roads and the same array setup was used. The geology and top of bedrock was very similar to Ogden so it is reasonable to assume that the

surface-wave and laboratory data will not overlap as well. In the case of the Ogden data, with the current data sets there is no way to integrate the data using the method originally proposed. Future research would be needed before attempting stitching the data sets together or a new acquisition with different array parameters would be needed.

Even though the surface-wave data and the core samples do not overlap this project did unearth information that could be used in future studies. The information would be useful for a future study into the potential response of near-surface geologic materials, the number of layers has been determined from the acoustic televiewer images and the continuity of the geologic units have been confirmed by the acoustic televiewer images. The density, elastic properties and ultrasonic velocities provided by laboratory measurements could be used to create a shear model. In this project we collected a lot of data and information and attempted to integrate it together but do to a lack of overlap we were inhibited. The information we gathered could be used in different studies or used as a starting place for further research. Though some unexpected hiccups prevented us from integrating the data as intended, a lot can be learned from the data. From this study areas for future research have been determined, such a repeating the acquisition using different parameters for integration or the addition of a borehole log could be used to stitch together the current data sets and possibly used for integration. This project yielded a lot of information and ideas of for further research.

# Chapter 7 - Further Research

The approach to reach a more optimal results would be to conduct a second MASW surface-wave acquisition at the Ogden site. If repeated with a different MASW array setup the imaging depth could be improved but this depends on the array setup used and the specific geology of the site. A test generally called 'practical estimation of spread and source offset' test, the source offset is increased and comparison of the dispersion curves (DCs) done to determine which offset optimized data collection (Kansas Geological Survey, 2012). Additionally the spread length of the geophones can be experimented with it would be more time consuming because it would require rearranging the geophones on the land streamer. The KSU land streamer already uses 4.5 Hz geophones which are cost effective, easy to use and generally accepted as optimal equipment (Kansas Geological Survey, 2012). If a new acquisition were done the optical and practical thing to do would be to conduct an experiment examining the source offset and geophone spread effects on the quality of data recorded.

The second option, if a new acquisition were to be done, is to acquire passive and active surface-wave data sets and combine them using the SurfSeis program. The active method uses a source (sledgehammer) operated by the acquisition team while the passive method would use urban sources (traffic or train). Combined the active method would increase the lateral resolution of the shallow geology while the passive method would increase the frequency range of the observed fundamental mode resulting in improved or clearer lower frequencies and increased imaging depth (Kansas Geological Survey, 2012). During the short course offered by the Kansas Geological Survey it was recommended that the top 1 sec from the nearest active traces and the bottom 1-30 sec of the passive traces should be used when combining the active and passive methods.

Alternatively a different approach using only the information currently available would be to attempt 'stitching' the data sets together but this would not be a true integration. Research into this method would be necessary to establish validity and to fill in gaps. The main 'gap' of concern would be the space between the bottom of the 2D $V_s$ model and the top of the cores used in the laboratory measurements, but could be resolved with the addition of a borehole log such as a sonic log. The second 'gap' would be the fact that the laboratory measurements were

conducted at ultrasonic velocities and since no simple conversion between ultrasonic and seismic velocities exists (Odumosu et al., 2007; Grochau and Gurevich, 2009; Sayers and Chopra, 2009) a site specific study would be required to establish a link between the different magnitudes of velocities (Figure 123). Potentially if the acoustic televiewer data could be reevaluated it may be possible to extract a vertical velocity profile that could be used for integration because the data would overlap with both the surface-wave and laboratory data sets; but may require a conversion between different magnitudes of velocity previously mentioned.

An attempt to stitching the current data sets together without additional information would result in unreliable and likely unrealistic results. With a stretch of the imagination and a lot of additional research into accurate velocity and elastic values for the missing section between 30 ft. and 60 ft. it could be possible to create a result that could be accurate and reliable. In my attempt to stitch the data sets together the bottom unit of the MASW surface-wave data was extended down to the top of the first core sample, this can easily be considered highly inaccurate but without additional information there is not much that can be done about it. An additional inaccurate assumption made was the velocities of the laboratory measurements, it was assumed these values were slightly greater than the surface-wave values because of the general assumption that velocity increases with depth (Nicholson and Simpson, 1985). The results from the roughly stitched together data were not promising, any anomalies present were exacerbated especially in the 'gap' between 30-60 ft., this stitching attempt cannot be considered valid. Further research into velocities and elastic modulus values could increase accuracy and possibly validate future stitching attempts.

Potentially additional information could be extracted from the ATV dataset it could be used for integration as long as the variables (eg. $V_p$ or $V_s$) from the log and the surface-wave have comparable magnitudes (Figure 123). Additionally the exploration of a site specific velocity conversion would be helpful for extracting accurate values from the sonic log mentioned previously. It is possible that with the additional borehole data and integration between it and the surface-wave data and laboratory data could be done separately from one another.

Depending on the objective many different approaches could be taken; adding to current data sets or reacquiring one or more data sets. Either approach still builds on the information and results produced from this project.

# Chapter 8 - Bibliography


Boore, D. M., & Joyner, W. B. (1997). Site amplifications for generic rock sites. *Bulletin of the Seismological Society of America, 87*(2), 327-341.

Boore, D. M., Yilmaz, O., & Kayen, R. (2007). *David boore's notes on poisson's ratio (the relation between vp and vs).* Unpublished manuscript.

Brown, L. T., Boore, D. M., & Stokoe, K. H. (2002). Comparison of shear-wave slowness profiles at 10 strong-motion sites from noninvasive SASW measurements and measurements made in boreholes. *Bulletin of the Seismological Society of America, 92*(8), 3116-3133.

Burchett, R. R., Luza, K. V., Van Eck, O. J., & Willson, F. W. (1985). *Seismicity and tectonic relationships of the nemaha uplift and midcontinent geophysical anomaly: Final project summary* U.S. Nuclear Regulatory Commission. Division of Health, Siting,and Waste Management.;.

Calderon-Macias, C., & Luke, B. (2010). Sensitivity studies of fundamental- and higher-mode rayleigh-wave phase velocities in some specific near-surface scenarios. In R. D. Miller, J. H. Bradford, K. Holliger & R. B. Latimer (Eds.), *Advances in near-surface seismology and ground-penetrating radar* (pp. 185). Tulsa, Okla.; Washington, D.C.; Denver, Colo.: Society of Exploration Geophysicists ; American Geophysical Union ; Environmental and Engineering Geophysical Society.

Choon B Park. (2005). MASW horizontal resolution in 2D shear-velocity (vs) mapping *KGS Open File Report 2005-4,*

Croxton, N. M. (2009). *Seven mile borehole report*(KDOT) Kansas Department of Transportation.

DECO Geophysical SC. (2011). *Tutorial on: Multichannel analysis of surface wave (MASW) in the RadExPro software.*http://www.radexpro.com/downloads/tutorials/default.ivp#masw

Deltombe, J., & Schepers, R. (2004). New developments in real-time processing of full waveform acoustic televiewer data. *Journal of Applied Geophysics, 55*(1-2), 161-172.

Geist, J. W. (2011). *Ogden north and south borehole reports*(KDOT) Kansas Department of Transportation.

Geist, J. W., & Croxton, N. M. (2009). *Bridge foundation geology report*(KDOT) Kansas Department of Transportation.

GeoVision Geophysical Services. *Borehole televiewer logging methods.*http://www.geovision.com

Gercek, H. (2007). Poisson's ratio values for rocks. *International Journal of Rock Mechanics and Mining Sciences, 44*(1), 1-13.

Gretener, P. (2003). Summary of the poisson's ratio debate 1990-2003. *CSEG Recorder, 28*, 44.

Grochau, M., & Gurevich, B. (2009). Testing gassmann fluid substitution: Sonic logs versus ultrasonic core measurements. *Geophysical Prospecting, 57*(1), 75-79.

Han, D., & Stanford University. Dept. of Geophysics. (1986). *Effects of porosity and clay content on acoustic properties of sandstones and uncosolidated sediments*. Stanford, Calif.: Stanford University, Dept. of Geophysics, School of Earth Sciences.

Holland, S. (2012). *Lithology tip sheet* Retrieved 10/15/2012, 2012, from http://paleodb.org/public/tips/lithtips.html

Hunter, J. A., Motazedian, D., Crow, H. L., Brooks, G. R., Miller, R. D., Pugin, A. J. -., et al. (2010). Near-surface shear-wave velocity measurements for soft-soil earthquake-hazard assessment: Some canadian mapping examples. In R. D. Miller, J. H. Bradford, K. Holliger & R. B. Latimer (Eds.), *Advances in near-surface seismology and ground-penetrating radar* (pp. 339). Tulsa, Okla.; Washington, D.C.; Denver, Colo.: Society of Exploration Geophysicists ; American Geophysical Union ; Environmental and Engineering Geophysical Society.

Hunze, S., & Wonik, T. (2007). Lithological and structural characteristics of the lake bosumtwi impact crater, ghana: Interpretation of acoustic televiewer images. *Meteoritics & Planetary Science, 42*(4-5), 779-792.

Kansas Geologic Survey. (2000). *Stratigraphy of riley and geary county geology.* Retrieved 10/4/2012, 2012, from http://www.kgs.ku.edu/General/Geology/Riley/strat01.html

Kansas Geologic Survey. (2012). *Advanced surface wave (MASW) methods short-course notebook.* Unpublished manuscript.

Kansas Geologic Survey. (2012). *MASW short-course notebook.* Unpublished manuscript.

Luo, Y., Xia, J., Liu, J., Liu, Q., & Xu, S. (2007). Joint inversion of high-frequency surface waves with fundamental and higher modes. *Journal of Applied Geophysics, 62*(4), 375-384.

Luo, Y., Xia, J., Xu, Y., & Zeng, C. (2011). Analysis of group-velocity dispersion of high-frequency rayleigh waves for near-surface applications. *Journal of Applied Geophysics, 74*(2-3), 157-165.

Mavko, G., Mukerji, T., & Dvorkin, J. (1998). *The rock physics handbook: Tools for seismic analysis in porous media*. Cambridge ; New York: Cambridge University Press.

Merriam, D. F. (2010). The geology and petroleum resources of kansas: A review from alpha to omega or from the pleistocene to the precambrian. *Natural Resources Research, 19*(4), 293-316.

Miller, R. D., Bradford, J. H., Holliger, K., & Latimer, R. B. (2010). *Advances in near-surface seismology and ground-penetrating radar*. Tulsa, Okla.; Washington, D.C.; Denver, Colo.: Society of Exploration Geophysicists ; American Geophysical Union ; Environmental and Engineering Geophysical Society.

Nicholson, C., & Simpson, D. W. (1985). Changes in Vp/Vs with depth: Implications for appropriate velocity models, improved earthquake locations, and material properties of the upper crust. *Bulletin of the Seismological Society of America, 75*(4), 1105-1123.

Odumosu, T., Torres-Verdin, C., Salazar, J., Ma, J., Voss, B., & Wang, G. L. (2007). Proceedings of SPE annual technical conference and exhibition; estimation of dry-rock elastic moduli based on the simulation of mud-filtrate invasion effects on borehole acoustic logs

Park, C. B., Miller, R. D., & Xia, J. (1997). Multi-channel analysis of surface waves (MASW) "A summery report of technical aspects, experimental results, and perspective".

Park, C. B., Miller, R. D., & Ivanov, J. (2002). Filtering surface waves. *Proceedings of the SAGEEP*, Las Vegas, Nevada.

Sayers, C., & Chopra, S. (2009). Introduction to this special section—Rock physics *The Leading Edge, 28*(1), 15.

Schepers, R., Rafat, G., Gelbke, C., & Lehmann, B. (2001). Application of borehole logging, core imaging and tomography to geotechnical exploration. *International Journal of Rock Mechanics and Mining Sciences [1997], 38*(6; 6), 867-876.

Smith, D. (2011). *Geologic time scale* Retrieved 10/4/2012, 2012, from http://www.ucmp.berkeley.edu/help/timeform.php

Socco, L. V., Boiero, D., Foti, S., & Piatti, C. (2010). Advances in surface-wave and body-wave integration
. In R. D. Miller, J. H. Bradford, K. Holliger & R. B. Latimer (Eds.), *Advances in near-surface seismology and ground-penetrating radar* (pp. 55). Tulsa, Okla.; Washington, D.C.; Denver, Colo.: Society of Exploration Geophysicists ; American Geophysical Union ; Environmental and Engineering Geophysical Society.

Song, X., & Gu, H. (2007). Utilization of multimode surface wave dispersion for characterizing roadbed structure. *Journal of Applied Geophysics, 63*(2), 59-67.

Steeples, D. W., & Brosius, L. (1998). *Earthquakes.* Retrieved August/9, 2011, from http://www.kgs.ku.edu/Publications/pic3/pic3_1.html

Williams, J. H., & Johnson, C. D. (2004). Acoustic and optical borehole-wall imaging for fractured-rock aquifer studies. *Journal of Applied Geophysics, 55*(1-2), 151-159.

Xia, J., & Miller, R. D. (2010). Estimation of near-surface shear-wave velocity and quality factor by inversion of high-frequency rayleigh waves

. In R. D. Miller, J. H. Bradford, K. Holliger & R. B. Latimer (Eds.), *Advances in near-surface seismology and ground-penetrating radar* (pp. 17). Tulsa, Okla.; Washington, D.C.; Denver, Colo.: Society of Exploration Geophysicists ; American Geophysical Union ; Environmental and Engineering Geophysical Society.

Xia, J., Miller, R. D., & Park, C. B. (1999). Estimation of near-surface shear-wave velocity by inversion of rayleigh waves *Geophysics, 64*(3), 691.

Xia, J., Miller, R. D., Park, C. B., & Tian, G. (2003). Inversion of high frequency surface waves with fundamental and higher modes. *Journal of Applied Geophysics, 52*(1), 45-57.

Xia, J., Miller, R., & Xu, Y. (2008). Data-resolution matrix and model-resolution matrix for rayleigh-wave inversion using a damped least-squares method. *Pure & Applied Geophysics, 165*(7), 1227-1248.

Xu, Y., Luo, Y., Liang, Q., Wang, L., Song, X., Liu, J., et al. (2010). Investigation and use of surface-wave characteristics for near-surface applications. In R. D. Miller, J. H. Bradford, K. Holliger & R. B. Latimer (Eds.), *Advances in near-surface seismology and ground-penetrating radar* (pp. 37). Tulsa, Okla.; Washington, D.C.; Denver, Colo.: Society of Exploration Geophysicists ; American Geophysical Union ; Environmental and Engineering Geophysical Society.

YORIHIKO, O., & RYOJI, I. (1973). ON DYNAMIC SHEAR MODULI AND POISSON'S RATIOS OF SOIL DEPOSITS. *Soils and Foundations, 13*(4), 61.

Zhang, J. J., & Bentley, L. (2005). Factors determining poisson's ratio. *Crewes Research Report, 17*

# APPENDIX

# Chapter 9 - Appendix A – Cores: Physical Properties, Elastic Properties and Waveform Graphs

## Sevenmile (Ogden, Riley Country)

| **Sevenmile** (Ogden, Riley CTY) Physical Properties of Cores | | | | | | | | | | | | | | |
|---|---|---|---|---|---|---|---|---|---|---|---|---|---|---|
| ID | Density (g/cm^3) | Lt. (in.) | Dia. (in.) | Top dpt. (ft.) | Bot. dpt. (ft.) | Avg. dpt. (ft) | Core Set | Core set dpt. | C | R | RQD | Lt. (mm) | Dia. (mm) | Mass (g) |
| R0.1 | 2.27 | 2.66 | 2.05 | 57.078 | 57.300 | 57.182 | Core 1 | 54.0 - 57.3 | | 2.7 | 42 | 68 | 52.5 | 334.2 |
| R4 | 2.31 | 3.54 | 2.05 | 64.505 | 64.800 | 64.653 | Core 3 | 62.3 - 67.3 | | 4.5 | 100 | 90 | 52.5 | 449.5 |
| R5 | 2.22 | 4.56 | 20.5 | 65.400 | 65.780 | 65.590 | Core 3 | 62.3 - 67.3 | | 4.5 | 100 | 116 | 52.5 | 556.8 |
| R6 | 2.29 | 4.46 | 2.05 | 66.345 | 66.717 | 66.531 | Core 3 | 62.3 - 67.3 | | 4.5 | 100 | 113.5 | 52.5 | 551.6 |
| R7 | 2.26 | 3.16 | 2.05 | 72.600 | 72.863 | 72.732 | Core 5 | 71.8 - 77.0 | | 4.4 | | 80.5 | 52.5 | 386.3 |
| R8 | 2.34 | 10.55 | 2.05 | 74.621 | 75.500 | 75.060 | Core 5 | 71.8 - 77.0 | | 4.4 | | 266.5 | 52.5 | 1327.1 |
| R11 | 2.35 | 4.03 | 2.05 | 79.500 | 79.838 | 79.668 | Core 6 | 77.0 - 80.5 | | 3.5 | 100 | 103 | 52.5 | 513.2 |

| **Sevenmile Standard Picking** | | | | | | | | |
|---|---|---|---|---|---|---|---|---|
| First Arrivals & Elastic Prop. | | | | | | | | |
| | Avg. Dpt. (ft) | lbf | P-Vel (m/s) | S-Vel (m/s) | Poisson's Ratio | Young's (MPa) | Bulk (MPa) | Shear (Mpa) |
| R0.1 | 57.18196 | R0.1-30 | 3626 | 1795 | 0.34 | 19579 | 20097 | 7319 |
| | | R0.1-190 | 3651 | 1917 | 0.31 | 21864 | 19139 | 8348 |
| | | R0.1-380 | 3712 | 1930 | 0.31 | 22242 | 20005 | 8459 |
| R4 | 64.6525 | R4-30 | 4779 | 1686 | 0.43 | 18751 | 43937 | 6561 |
| | | R4-215 | 4794 | 1621 | 0.44 | 17404 | 44931 | 6062 |
| | | R4-430 | 4860 | 1626 | 0.44 | 17526 | 46367 | 6098 |
| R5 | 65.59 | R5-30 | 6256 | 1299 | 0.48 | 11057 | 81801 | 3742 |
| | | R5-215 | 6348 | 1296 | 0.48 | 11005 | 84403 | 3722 |
| | | R5-430 | 6394 | 1303 | 0.48 | 11136 | 85617 | 3766 |
| R6 | 66.53108 | R6-30 | 6095 | 1663 | 0.46 | 18487 | 76557 | 6332 |
| | | R6-220 | 6110 | 1712 | 0.46 | 19542 | 76490 | 6704 |
| | | R6-440 | 6212 | 1723 | 0.46 | 19818 | 79237 | 6795 |
| R7 | 72.73167 | R7-30 | 4232 | 1402 | 0.44 | 12782 | 34548 | 4443 |
| | | R7-240 | 4293 | 1534 | 0.43 | 15166 | 34556 | 5315 |
| | | R7-480 | 4358 | 1543 | 0.43 | 1543 | 35746 | 5379 |
| R11 | 79.66792 | R11-30 | 5476 | 1502 | 0.46 | 15450 | 63287 | 5294 |
| | | R11-235 | 5615 | 1529 | 0.46 | 16021 | 66665 | 5487 |
| | | R11-525 | 5740 | 1542 | 0.46 | 16310 | 69857 | 5581 |

| **Sevenmile Altered picking** | | | | | | | | |
|---|---|---|---|---|---|---|---|---|
| Poisson's Point | | | | | | | | |
| | Avg. Dpt. (ft) | lbf | P-Vel (m/s) | S-Vel (m/s) | Poisson's Ratio | Young’s (MPa) | Bulk (MPa) | Shear (Mpa) |
| R0.1 | 57.18196 | R0.1-30 | 2885 | 1795 | 0.18 | 17328 | 9133 | 7319 |
| | | R0.1-190 | 2880 | 1917 | 0.10 | 18398 | 7705 | 8348 |
| | | R0.1-380 | 2951 | 1930 | 0.13 | 19048 | 8486 | 8459 |
| R4 | 64.6525 | R4-30 | 2483 | 1686 | 0.07 | 14065 | 5475 | 6561 |
| | | R4-215 | 2465 | 1621 | 0.12 | 13565 | 5931 | 6062 |
| | | R4-430 | 2473 | 1626 | 0.12 | 13655 | 5983 | 6098 |
| R5 | 65.59 | R5-30 | 1969 | 1299 | 0.11 | 8341 | 3607 | 3742 |
| | | R5-215 | 1968 | 1296 | 0.12 | 8320 | 3626 | 3722 |
| | | R5-430 | 1969 | 1303 | 0.11 | 8362 | 3574 | 3766 |
| R6 | 66.53108 | R6-30 | 2650 | 1663 | 0.18 | 14881 | 7631 | 6332 |
| | | R6-220 | 2689 | 1712 | 0.16 | 15543 | 7602 | 6704 |
| | | R6-440 | 2682 | 1723 | 0.15 | 15607 | 7399 | 6795 |
| R7 | 72.73167 | R7-30 | 2310 | 1402 | 0.21 | 10738 | 6137 | 4443 |
| | | R7-240 | 2342 | 1534 | 0.12 | 11953 | 5306 | 5315 |
| | | R7-480 | 2320 | 1543 | 0.10 | 11869 | 4987 | 5379 |
| R11 | 79.66792 | R11-30 | 2417 | 1502 | 0.19 | 12550 | 6648 | 5294 |
| | | R11-235 | 2422 | 1529 | 0.17 | 12824 | 6451 | 5487 |
| | | R11-525 | 2438 | 1542 | 0.17 | 13022 | 6509 | 5581 |

## R0.1

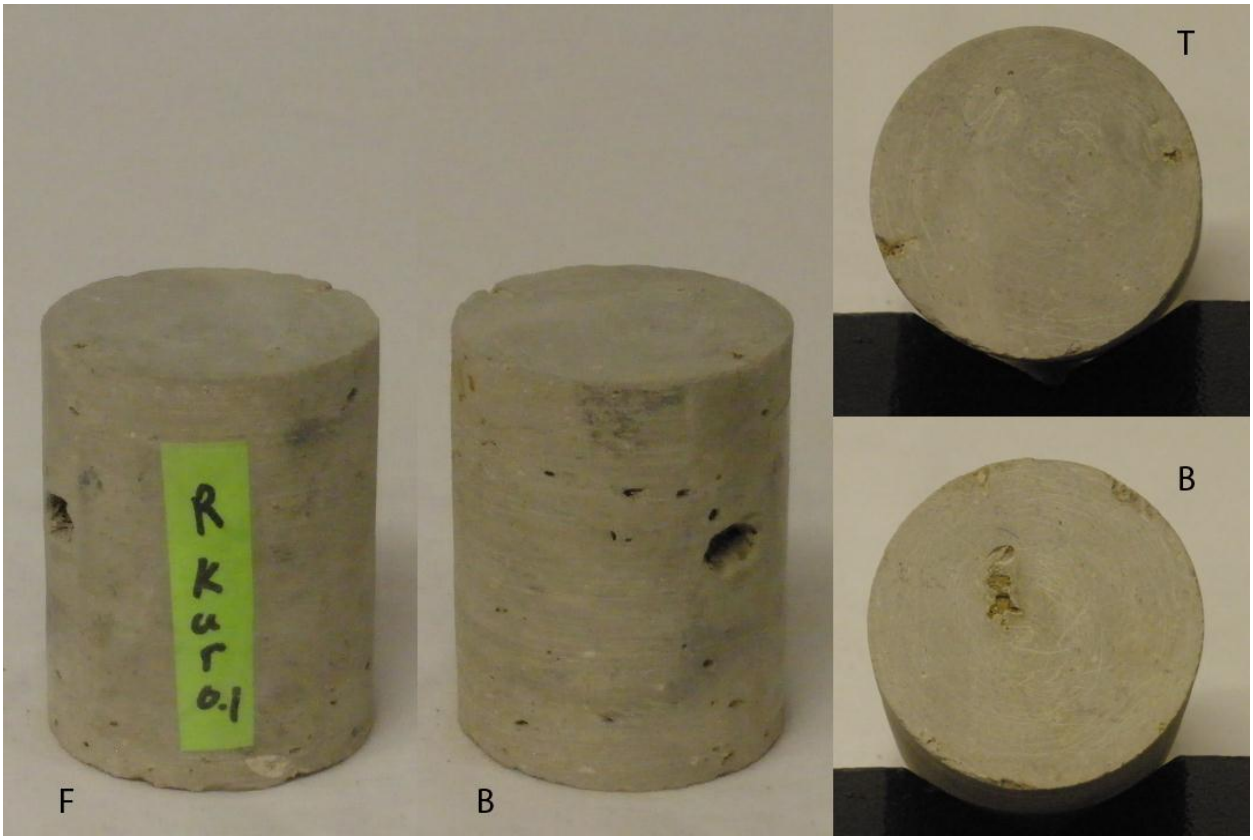


| **Sevenmile** (Ogden, Riley CTY) Physical Properties of Cores | | | | | | | | | | | | | | |
|---|---|---|---|---|---|---|---|---|---|---|---|---|---|---|
| ID | Density (g/cm^3) | Lt. (in.) | Dia. (in.) | Top dpt. (ft.) | Bot. dpt. (ft.) | Avg. dpt. (ft) | Core Set | Core set dpt. | C | R | RQD | Lt. (mm) | Dia. (mm) | Mass (g) |
| R0.1 | 2.27 | 2.66 | 2.05 | 57.078 | 57.300 | 57.182 | Core 1 | 54.0 - 57.3 | | 2.7 | 42 | 68 | 52.5 | 334.2 |

| **Sevenmile Standard Picking** | | | | | | | | |
|---|---|---|---|---|---|---|---|---|
| First Arrivals & Elastic Prop. | | | | | | | | |
| | Avg. Dpt. (ft) | lbf | P-Vel (m/s) | S-Vel (m/s) | Poisson's Ratio | Young's (MPa) | Bulk (MPa) | Shear (Mpa) |
| R0.1 | 57.18196 | R0.1-30 | 3626 | 1795 | 0.34 | 19579 | 20097 | 7319 |
| | | R0.1-190 | 3651 | 1917 | 0.31 | 21864 | 19139 | 8348 |
| | | R0.1-380 | 3712 | 1930 | 0.31 | 22242 | 20005 | 8459 |

| **Sevenmile Altered picking** | | | | | | | | |
|---|---|---|---|---|---|---|---|---|
| Poisson's Point | | | | | | | | |
| | Avg. Dpt. (ft) | lbf | P-Vel (m/s) | S-Vel (m/s) | Poisson's Ratio | Young's (MPa) | Bulk (MPa) | Shear (Mpa) |
| R0.1 | 57.18196 | R0.1-30 | 2885 | 1795 | 0.18 | 17328 | 9133 | 7319 |
| | | R0.1-190 | 2880 | 1917 | 0.10 | 18398 | 7705 | 8348 |
| | | R0.1-380 | 2951 | 1930 | 0.13 | 19048 | 8486 | 8459 |

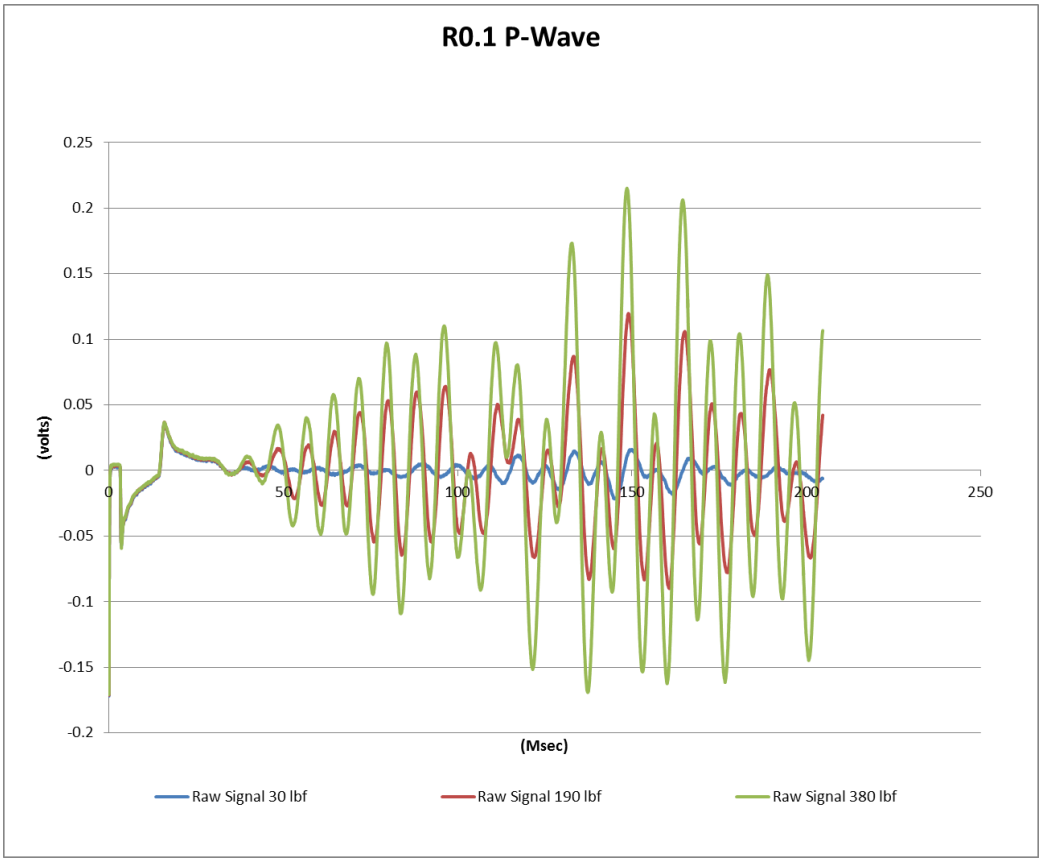
R0.1 P-Wave
0.25
0.2
0.15
0.1
0.05
0
-0.05
-0.1
-0.15
-0.2
(volts)
0
50
100
150
200
250
(Msec)
Raw Signal 30 lbf
Raw Signal 190 lbf
Raw Signal 380 lbf

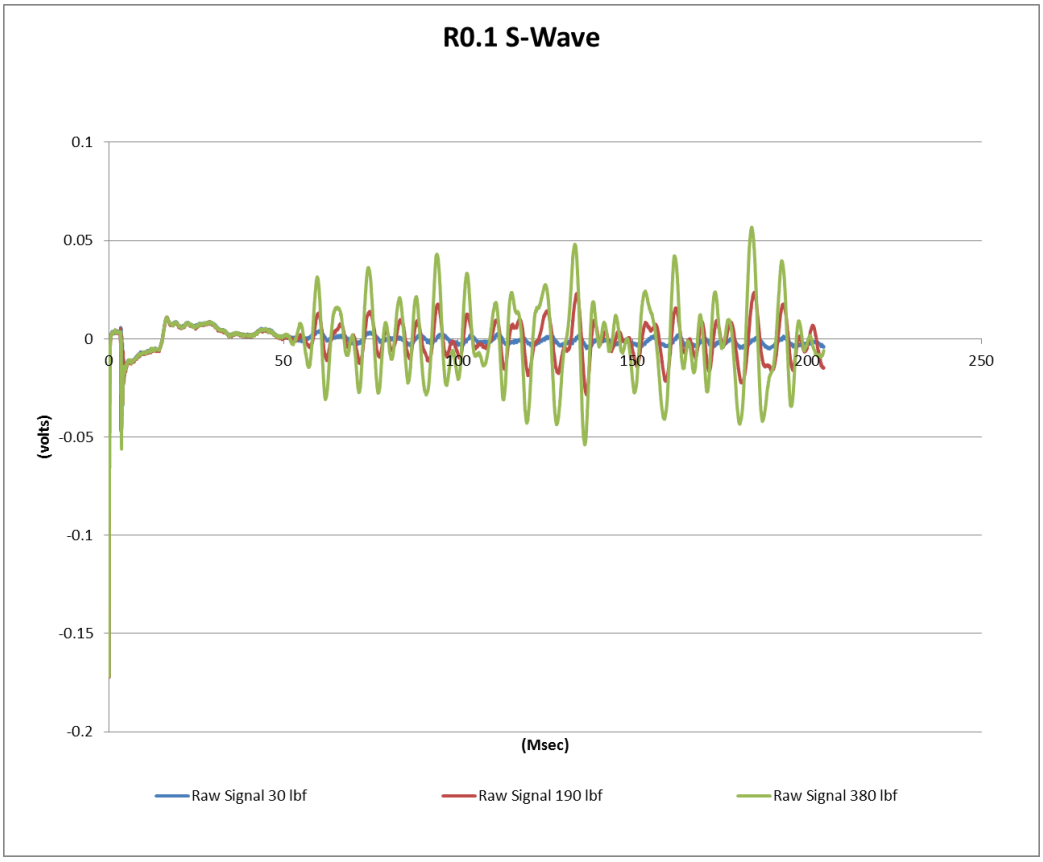
R0.1 S-Wave
0.1
0.05
0
-0.05
-0.1
-0.15
-0.2
(volts)
0
50
100
150
200
250
(Msec)
Raw Signal 30 lbf
Raw Signal 190 lbf
Raw Signal 380 lbf

**R4**

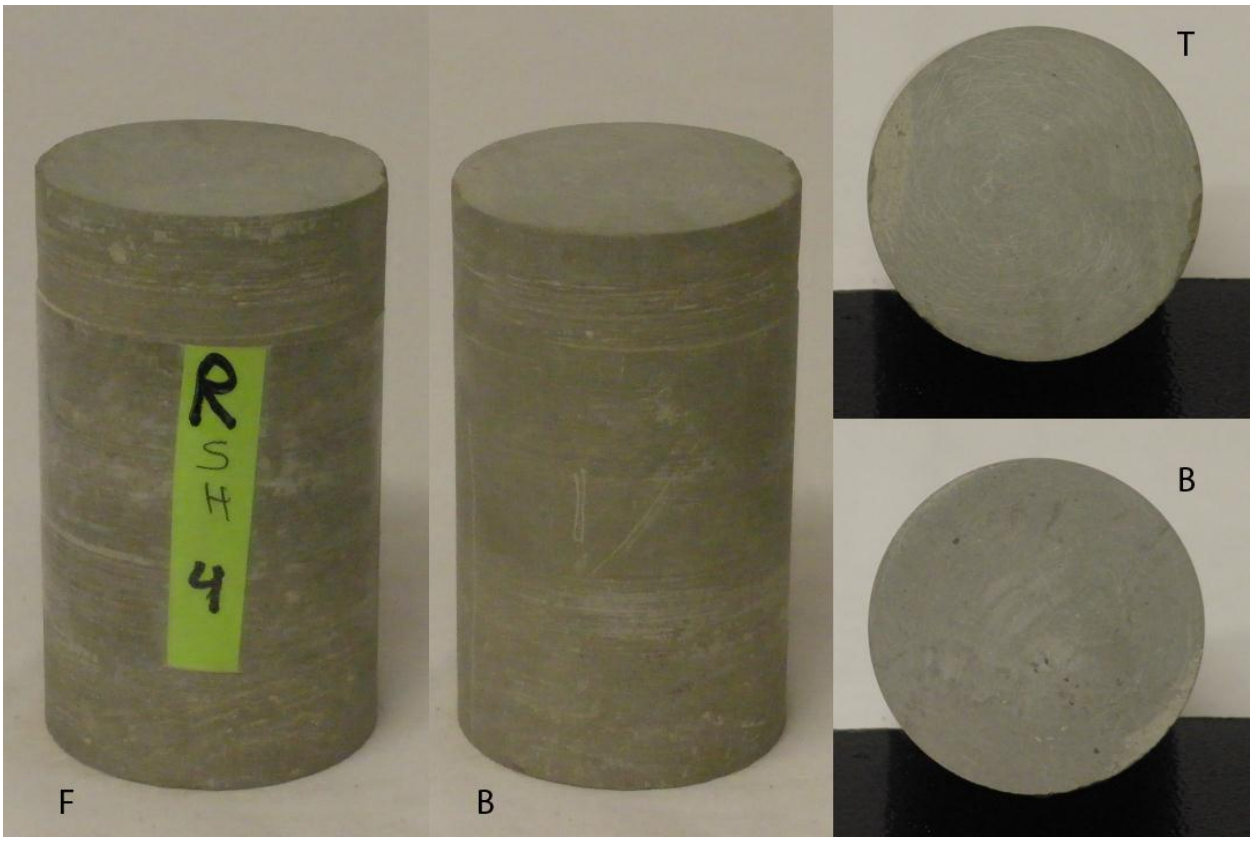


| **Sevenmile** (Ogden, Riley CTY) Physical Properties of Cores | | | | | | | | | | | | | | |
|---|---|---|---|---|---|---|---|---|---|---|---|---|---|---|
| ID | Density (g/cm^3) | Lt. (in.) | Dia. (in.) | Top dpt. (ft.) | Bot. dpt. (ft.) | Avg. dpt. (ft) | Core Set | Core set dpt. | C | R | RQD | Lt. (mm) | Dia. (mm) | Mass (g) |
| R4 | 2.31 | 3.54 | 2.05 | 64.505 | 64.800 | 64.653 | Core 3 | 62.3 - 67.3 | | 4.5 | 100 | 90 | 52.5 | 449.5 |

| **Sevenmile Standard Picking** | | | | | | | | |
|---|---|---|---|---|---|---|---|---|
| First Arrivals & Elastic Prop. | | | | | | | | |
| | Avg. Dpt. (ft) | lbf | P-Vel (m/s) | S-Vel (m/s) | Poisson's Ratio | Young's (MPa) | Bulk (MPa) | Shear (Mpa) |
| R4 | 64.6525 | R4-30 | 4779 | 1686 | 0.43 | 18751 | 43937 | 6561 |
| | | R4-215 | 4794 | 1621 | 0.44 | 17404 | 44931 | 6062 |
| | | R4-430 | 4860 | 1626 | 0.44 | 17526 | 46367 | 6098 |

| **Sevenmile Altered picking** | | | | | | | | |
|---|---|---|---|---|---|---|---|---|
| Poisson's Point | | | | | | | | |
| | Avg. Dpt. (ft) | lbf | P-Vel (m/s) | S-Vel (m/s) | Poisson's Ratio | Young's (MPa) | Bulk (MPa) | Shear (Mpa) |
| R4 | 64.6525 | R4-30 | 2483 | 1686 | 0.07 | 14065 | 5475 | 6561 |
| | | R4-215 | 2465 | 1621 | 0.12 | 13565 | 5931 | 6062 |
| | | R4-430 | 2473 | 1626 | 0.12 | 13655 | 5983 | 6098 |

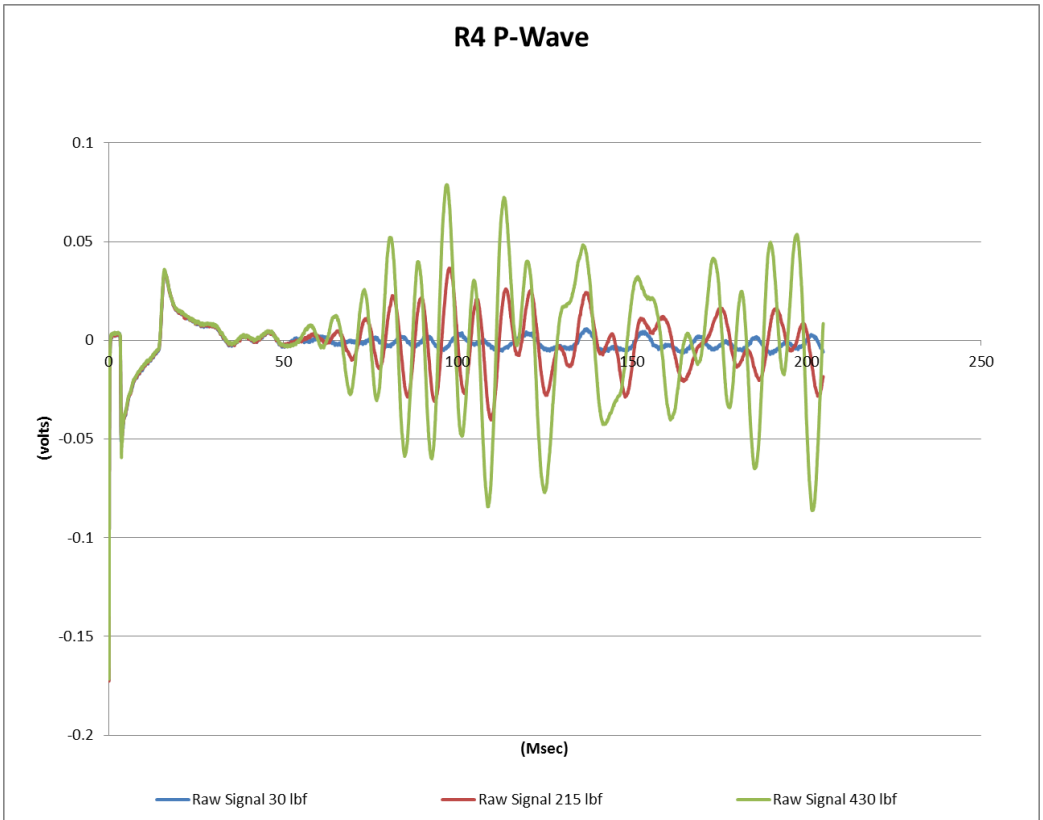
R4 P-Wave
0.1
0.05
0
-0.05
-0.1
-0.15
-0.2
0
50
100
150
200
250
(volts)
(Msec)
Raw Signal 30 lbf
Raw Signal 215 lbf
Raw Signal 430 lbf

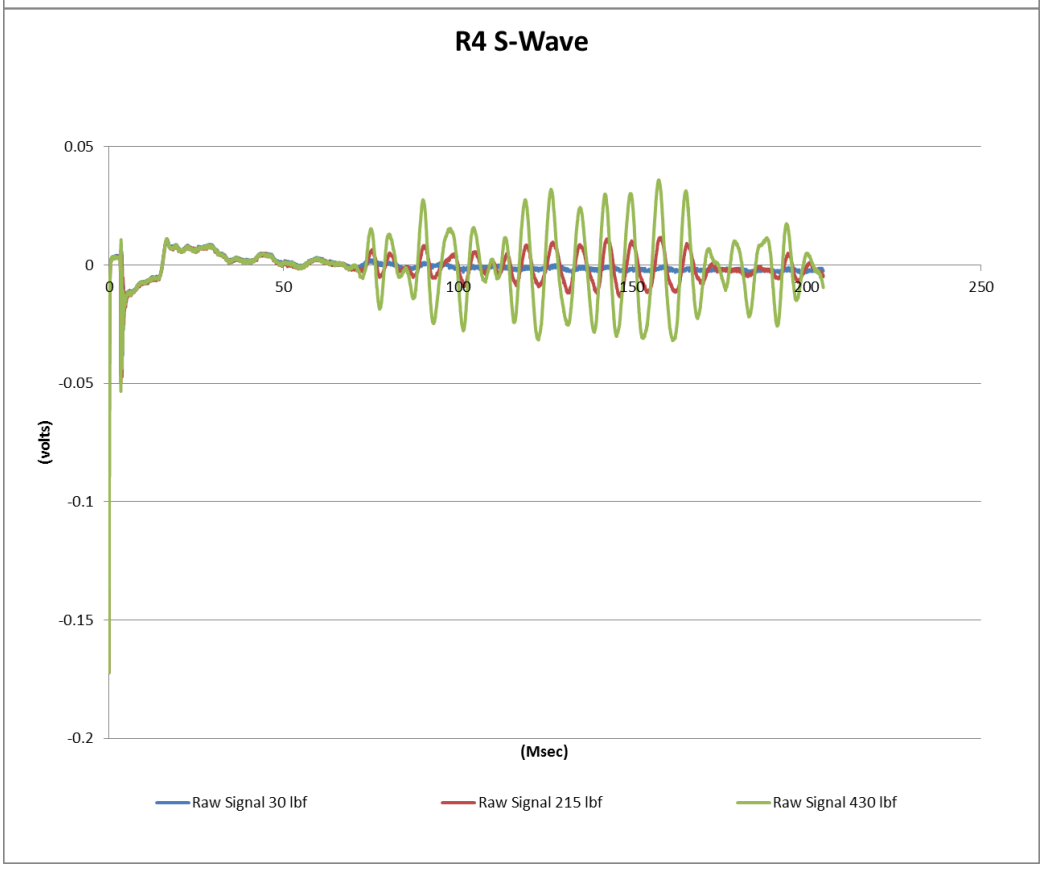
R4 S-Wave
0.05
0
-0.05
-0.1
-0.15
-0.2
0
50
100
150
200
250
(volts)
(Msec)
Raw Signal 30 lbf
Raw Signal 215 lbf
Raw Signal 430 lbf

**R5**

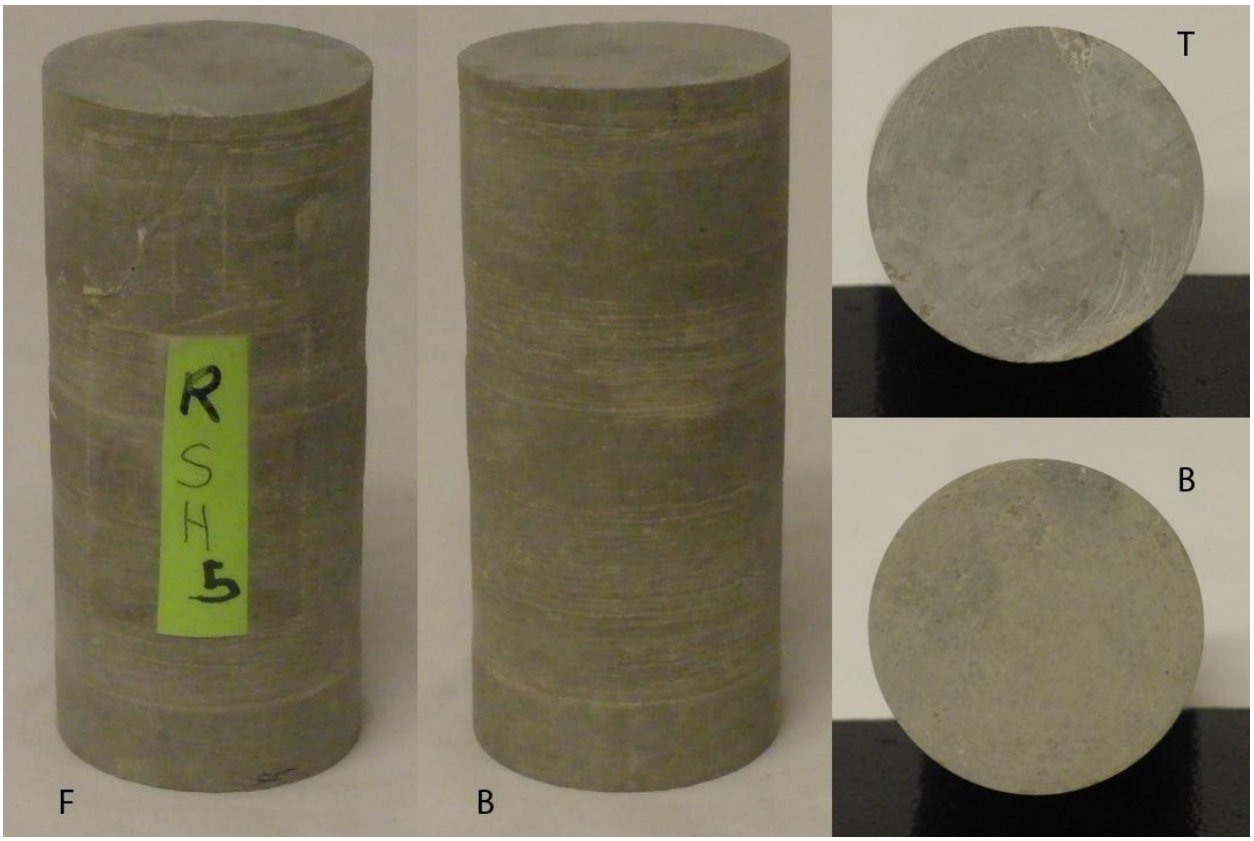


| **Sevenmile** (Ogden, Riley CTY) Physical Properties of Cores | | | | | | | | | | | | | | |
|---|---|---|---|---|---|---|---|---|---|---|---|---|---|---|
| ID | Density (g/cm^3) | Lt. (in.) | Dia. (in.) | Top dpt. (ft.) | Bot. dpt. (ft.) | Avg. dpt. (ft) | Core Set | Core set dpt. | C | R | RQD | Lt. (mm) | Dia. (mm) | Mass (g) |
| R5 | 2.22 | 4.56 | 20.5 | 65.400 | 65.780 | 65.590 | Core 3 | 62.3 - 67.3 | | 4.5 | 100 | 116 | 52.5 | 556.8 |

| **Sevenmile Standard Picking** | | | | | | | | |
|---|---|---|---|---|---|---|---|---|
| First Arrivals & Elastic Prop. | | | | | | | | |
| | Avg. Dpt. (ft) | lbf | P-Vel (m/s) | S-Vel (m/s) | Poisson's Ratio | Young's (MPa) | Bulk (MPa) | Shear (Mpa) |
| R5 | 65.59 | R5-30 | 6256 | 1299 | 0.48 | 11057 | 81801 | 3742 |
| | | R5-215 | 6348 | 1296 | 0.48 | 11005 | 84403 | 3722 |
| | | R5-430 | 6394 | 1303 | 0.48 | 11136 | 85617 | 3766 |

| **Sevenmile Altered picking** | | | | | | | | |
|---|---|---|---|---|---|---|---|---|
| Poisson's Point | | | | | | | | |
| | Avg. Dpt. (ft) | lbf | P-Vel (m/s) | S-Vel (m/s) | Poisson's Ratio | Young's (MPa) | Bulk (MPa) | Shear (Mpa) |
| R5 | 65.59 | R5-30 | 1969 | 1299 | 0.11 | 8341 | 3607 | 3742 |
| | | R5-215 | 1968 | 1296 | 0.12 | 8320 | 3626 | 3722 |
| | | R5-430 | 1969 | 1303 | 0.11 | 8362 | 3574 | 3766 |

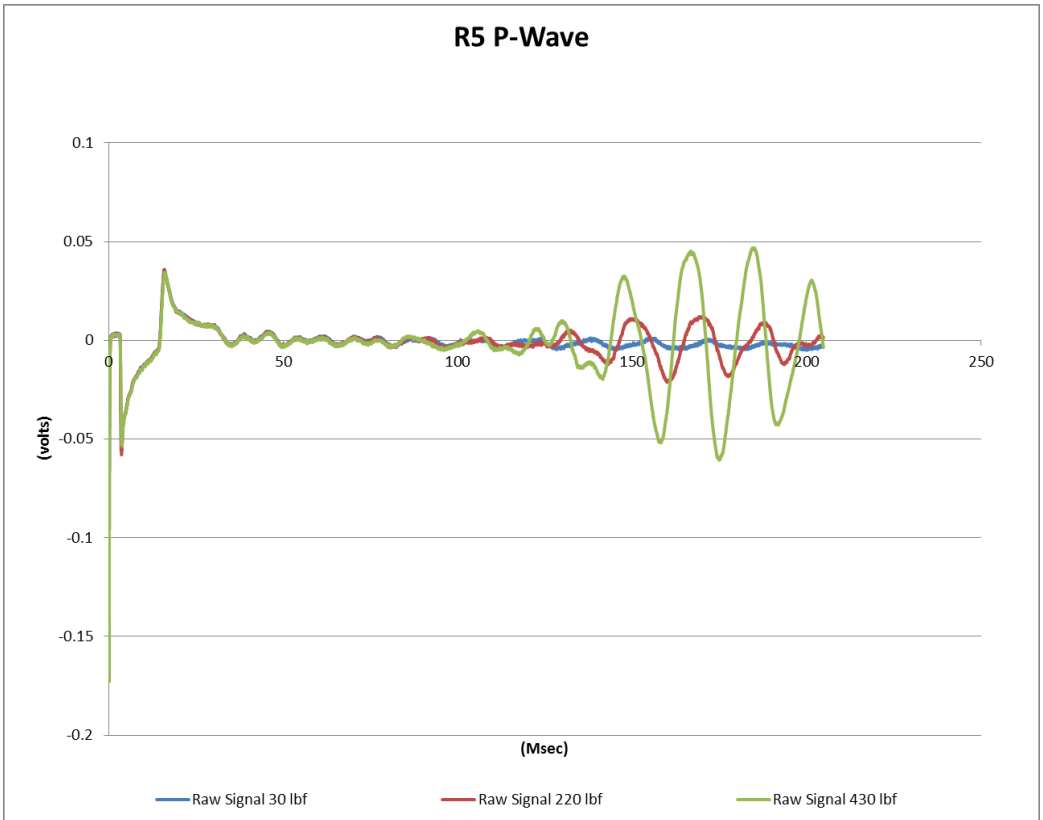
R5 P-Wave
0.1
0.05
0
-0.05
-0.1
-0.15
-0.2
(volts)
0
50
100
150
200
250
(Msec)
Raw Signal 30 lbf
Raw Signal 220 lbf
Raw Signal 430 lbf

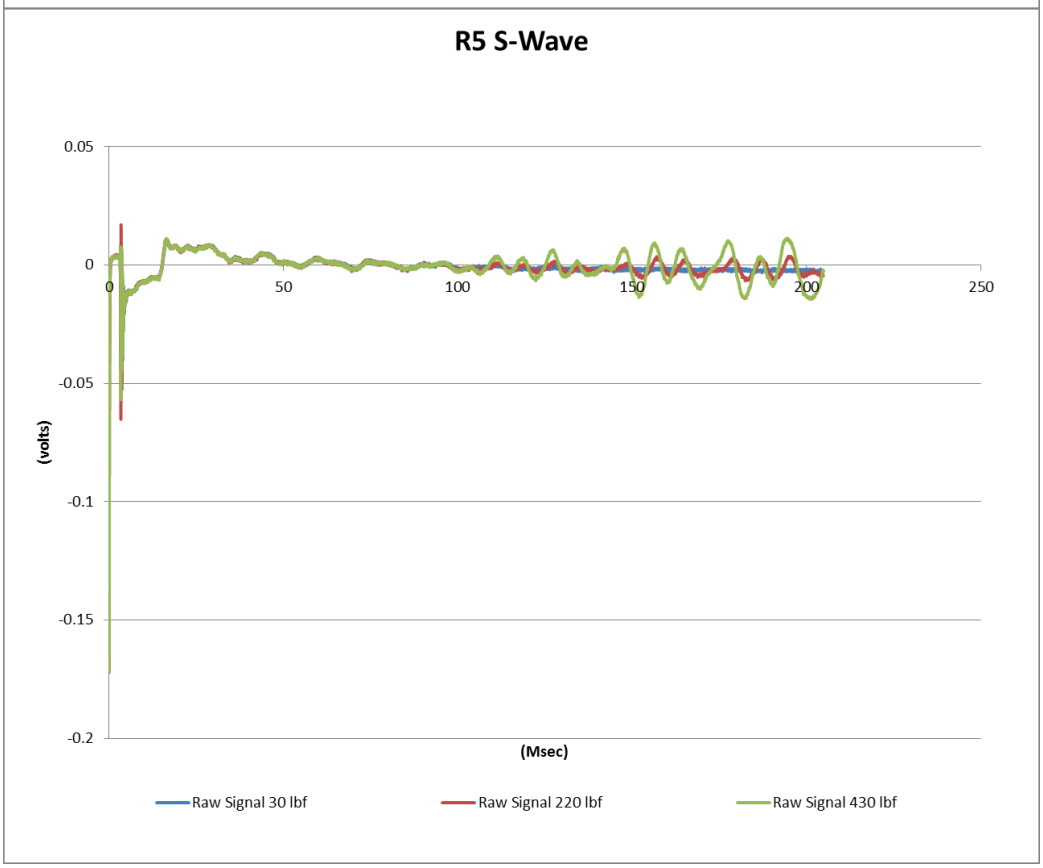
R5 S-Wave
0.05
0
-0.05
-0.1
-0.15
-0.2
(volts)
0
50
100
150
200
250
(Msec)
Raw Signal 30 lbf
Raw Signal 220 lbf
Raw Signal 430 lbf

## R6

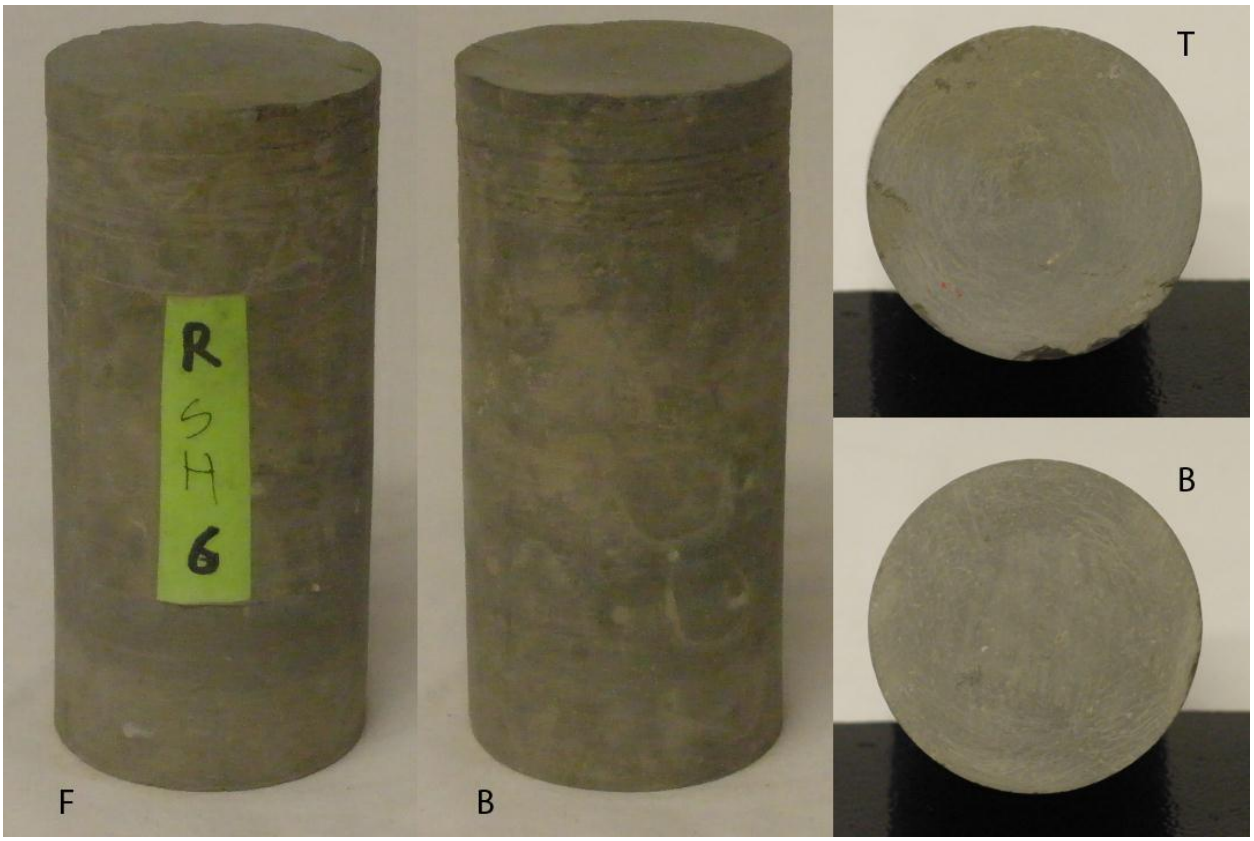


| **Sevenmile** (Ogden, Riley CTY) Physical Properties of Cores | | | | | | | | | | | | | | |
|---|---|---|---|---|---|---|---|---|---|---|---|---|---|---|
| ID | Density (g/cm^3) | Lt. (in.) | Dia. (in.) | Top dpt. (ft.) | Bot. dpt. (ft.) | Avg. dpt. (ft) | Core Set | Core set dpt. | C | R | RQD | Lt. (mm) | Dia. (mm) | Mass (g) |
| R6 | 2.29 | 4.46 | 2.05 | 66.345 | 66.717 | 66.531 | Core 3 | 62.3 - 67.3 | | 4.5 | 100 | 113.5 | 52.5 | 551.6 |

| **Sevenmile Standard Picking** | | | | | | | | |
|---|---|---|---|---|---|---|---|---|
| First Arrivals & Elastic Prop. | | | | | | | | |
| | Avg. Dpt. (ft) | lbf | P-Vel (m/s) | S-Vel (m/s) | Poisson's Ratio | Young's (MPa) | Bulk (MPa) | Shear (Mpa) |
| R6 | 66.53108 | R6-30 | 6095 | 1663 | 0.46 | 18487 | 76557 | 6332 |
| | | R6-220 | 6110 | 1712 | 0.46 | 19542 | 76490 | 6704 |
| | | R6-440 | 6212 | 1723 | 0.46 | 19818 | 79237 | 6795 |

| **Sevenmile Altered picking** | | | | | | | | |
|---|---|---|---|---|---|---|---|---|
| Poisson's Point | | | | | | | | |
| | Avg. Dpt. (ft) | lbf | P-Vel (m/s) | S-Vel (m/s) | Poisson's Ratio | Young's (MPa) | Bulk (MPa) | Shear (Mpa) |
| R6 | 66.53108 | R6-30 | 2650 | 1663 | 0.18 | 14881 | 7631 | 6332 |
| | | R6-220 | 2689 | 1712 | 0.16 | 15543 | 7602 | 6704 |
| | | R6-440 | 2682 | 1723 | 0.15 | 15607 | 7399 | 6795 |

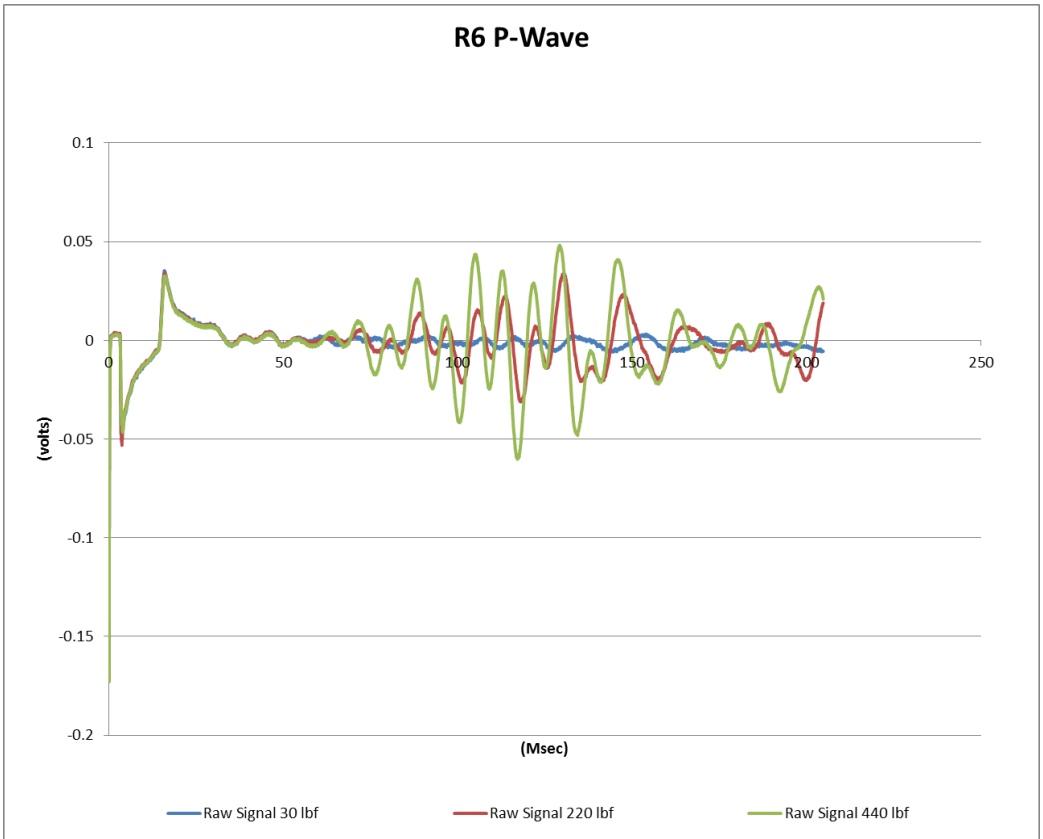
R6 P-Wave
0.1
0.05
0
-0.05
-0.1
-0.15
-0.2
(volts)
0
50
100
150
200
250
(Msec)
Raw Signal 30 lbf
Raw Signal 220 lbf
Raw Signal 440 lbf

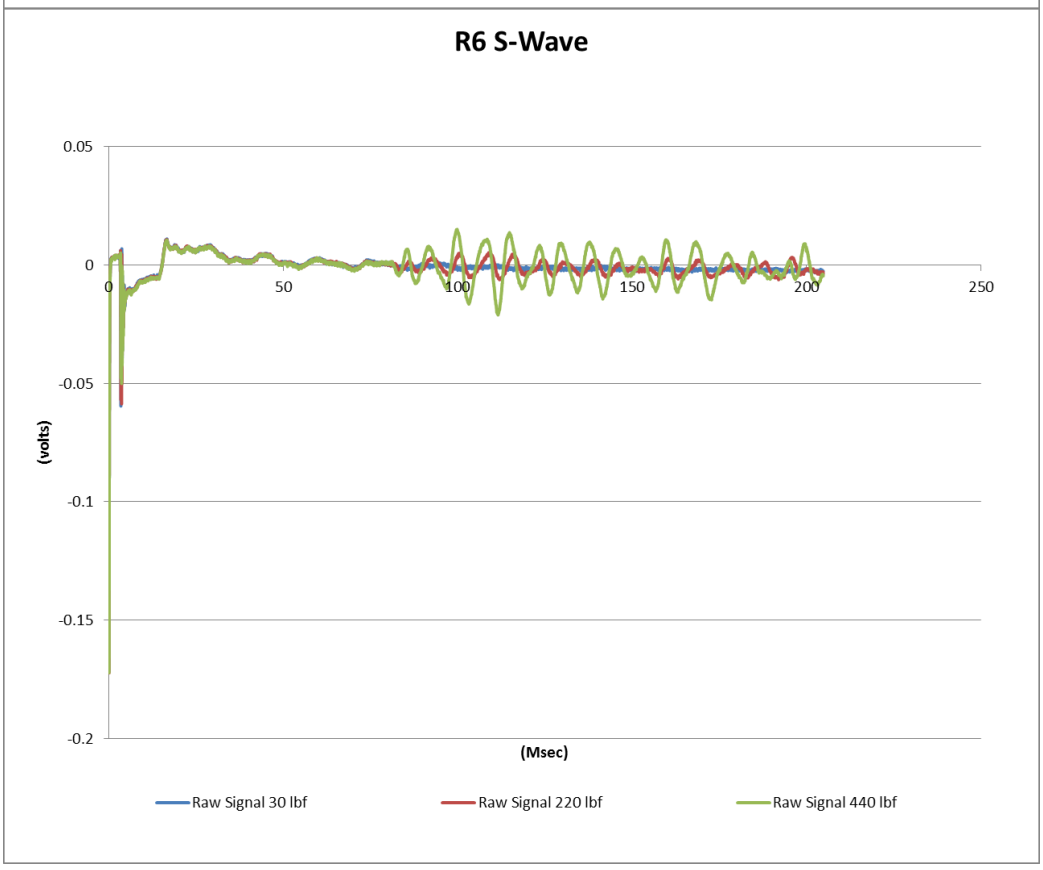
R6 S-Wave
0.05
0
-0.05
-0.1
-0.15
-0.2
(volts)
0
50
100
150
200
250
(Msec)
Raw Signal 30 lbf
Raw Signal 220 lbf
Raw Signal 440 lbf

**R7**

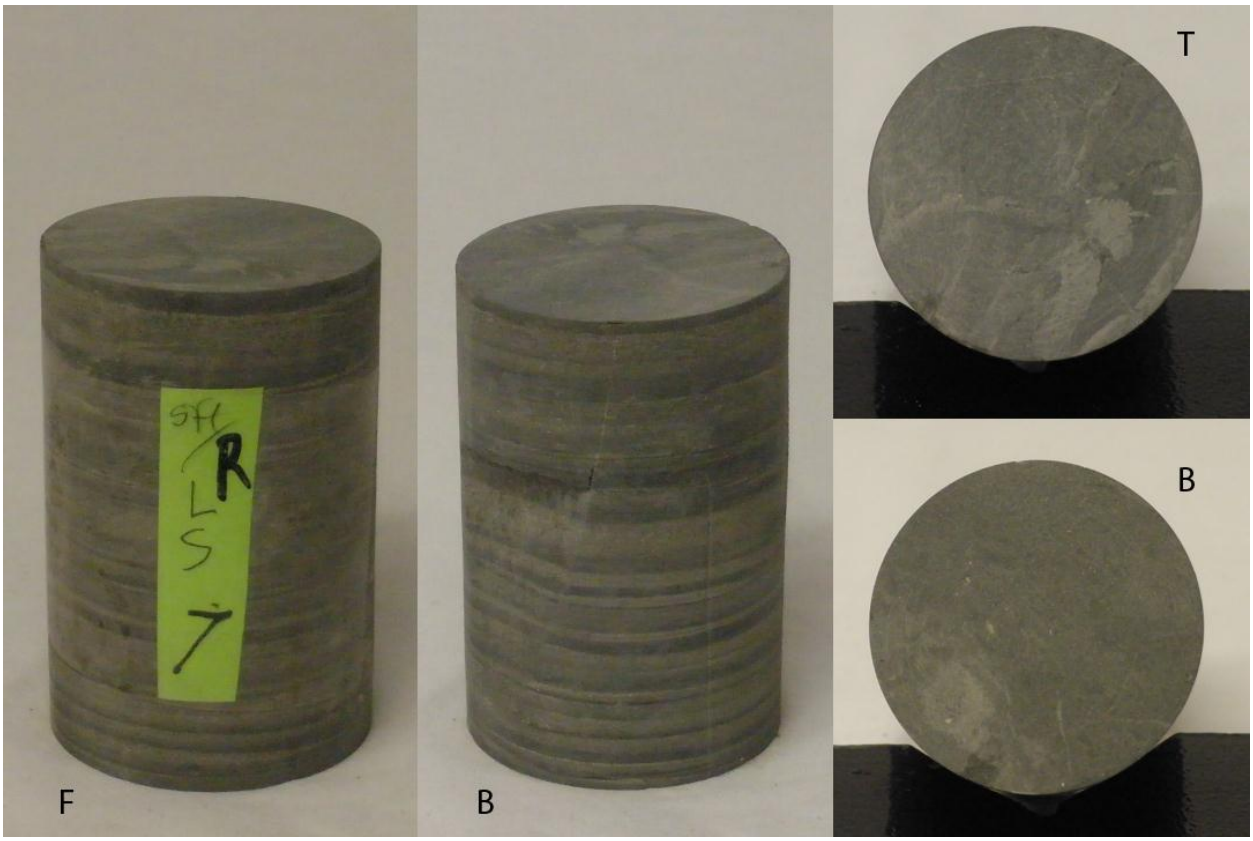


| **Sevenmile** (Ogden, Riley CTY) Physical Properties of Cores | | | | | | | | | | | | | | |
|---|---|---|---|---|---|---|---|---|---|---|---|---|---|---|
| ID | Density (g/cm^3) | Lt. (in.) | Dia. (in.) | Top dpt. (ft.) | Bot. dpt. (ft.) | Avg. dpt. (ft) | Core Set | Core set dpt. | C | R | RQD | Lt. (mm) | Dia. (mm) | Mass (g) |
| R7 | 2.26 | 3.16 | 2.05 | 72.600 | 72.863 | 72.732 | Core 5 | 71.8 - 77.0 | | 4.4 | | 80.5 | 52.5 | 386.3 |

| **Sevenmile Standard Picking** | | | | | | | | |
|---|---|---|---|---|---|---|---|---|
| First Arrivals & Elastic Prop. | | | | | | | | |
| | Avg. Dpt. (ft) | lbf | P-Vel (m/s) | S-Vel (m/s) | Poisson's Ratio | Young's (MPa) | Bulk (MPa) | Shear (Mpa) |
| R7 | 72.73167 | R7-30 | 4232 | 1402 | 0.44 | 12782 | 34548 | 4443 |
| | | R7-240 | 4293 | 1534 | 0.43 | 15166 | 34556 | 5315 |
| | | R7-480 | 4358 | 1543 | 0.43 | 1543 | 35746 | 5379 |

| **Sevenmile Altered picking** | | | | | | | | |
|---|---|---|---|---|---|---|---|---|
| Poisson's Point | | | | | | | | |
| | Avg. Dpt. (ft) | lbf | P-Vel (m/s) | S-Vel (m/s) | Poisson's Ratio | Young's (MPa) | Bulk (MPa) | Shear (Mpa) |
| R7 | 72.73167 | R7-30 | 2310 | 1402 | 0.21 | 10738 | 6137 | 4443 |
| | | R7-240 | 2342 | 1534 | 0.12 | 11953 | 5306 | 5315 |
| | | R7-480 | 2320 | 1543 | 0.10 | 11869 | 4987 | 5379 |

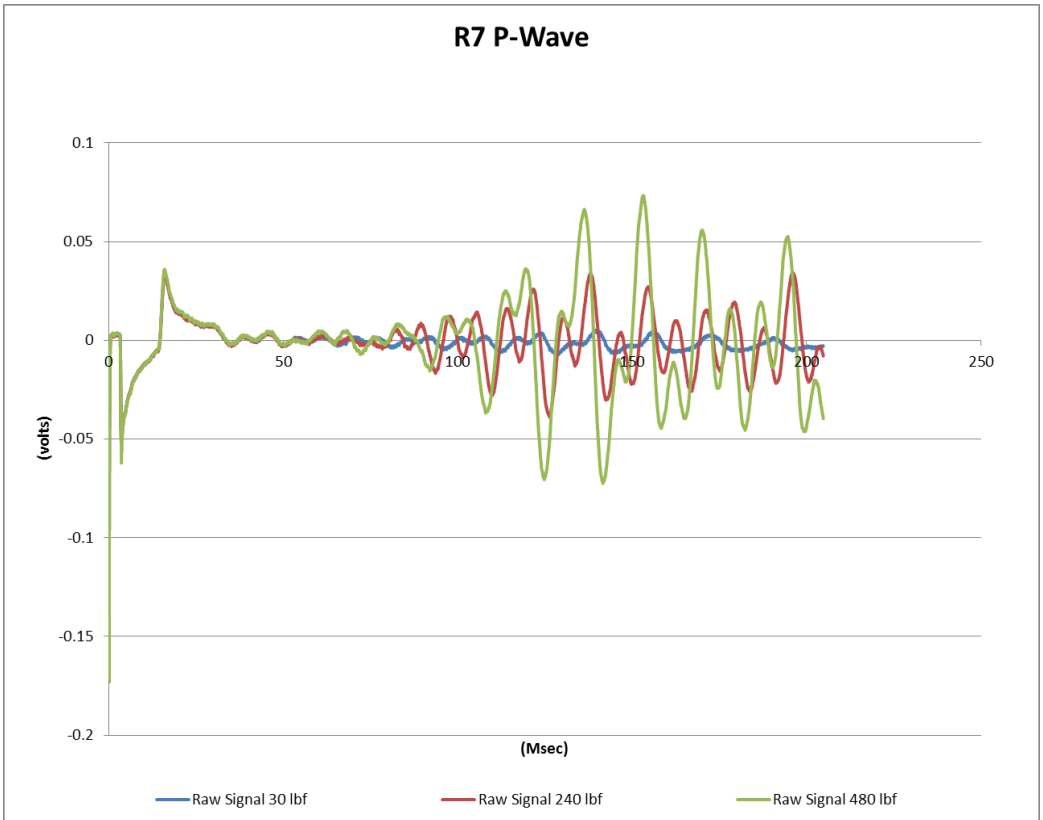
R7 P-Wave
0.1
0.05
0
-0.05
-0.1
-0.15
-0.2
0
50
100
150
200
250
(volts)
(Msec)
Raw Signal 30 lbf
Raw Signal 240 lbf
Raw Signal 480 lbf

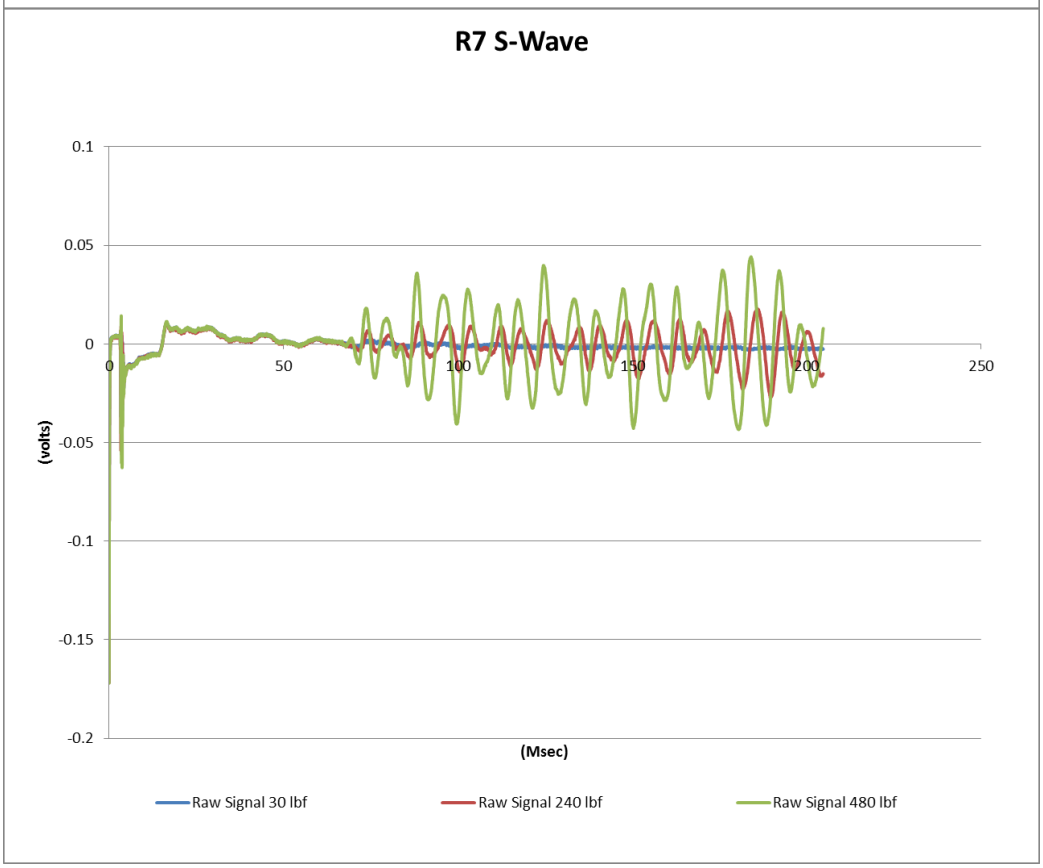
R7 S-Wave
0.1
0.05
0
-0.05
-0.1
-0.15
-0.2
0
50
100
150
200
250
(volts)
(Msec)
Raw Signal 30 lbf
Raw Signal 240 lbf
Raw Signal 480 lbf

**R8**

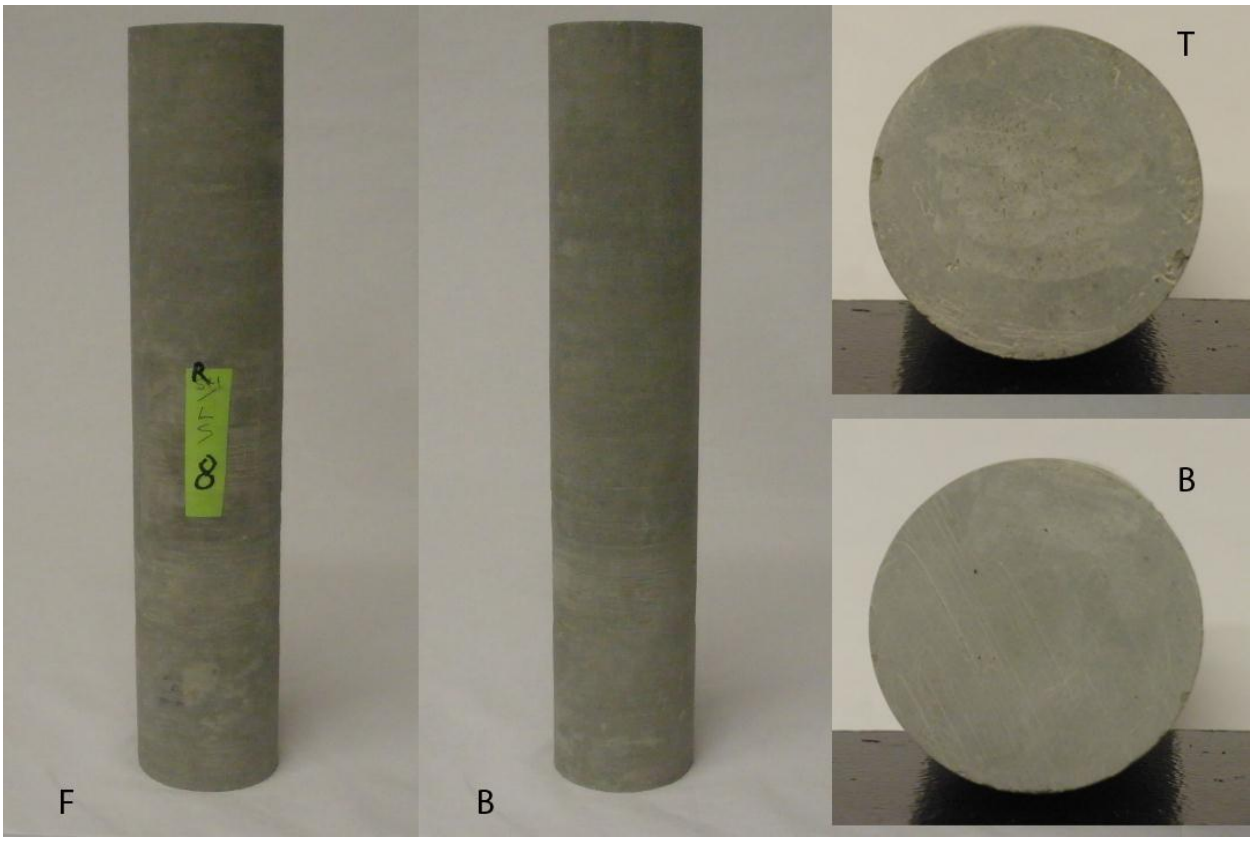


| **Sevenmile** (Ogden, Riley CTY) Physical Properties of Cores | | | | | | | | | | | | | | |
|---|---|---|---|---|---|---|---|---|---|---|---|---|---|---|
| ID | Density (g/cm^3) | Lt. (in.) | Dia. (in.) | Top dpt. (ft.) | Bot. dpt. (ft.) | Avg. dpt. (ft) | Core Set | Core set dpt. | C | R | RQD | Lt. (mm) | Dia. (mm) | Mass (g) |
| R8 | 2.34 | 10.55 | 2.05 | 74.621 | 75.500 | 75.060 | Core 5 | 71.8 - 77.0 | | 4.4 | | 266.5 | 52.5 | 1327.1 |

Waveform unsuitable for picking

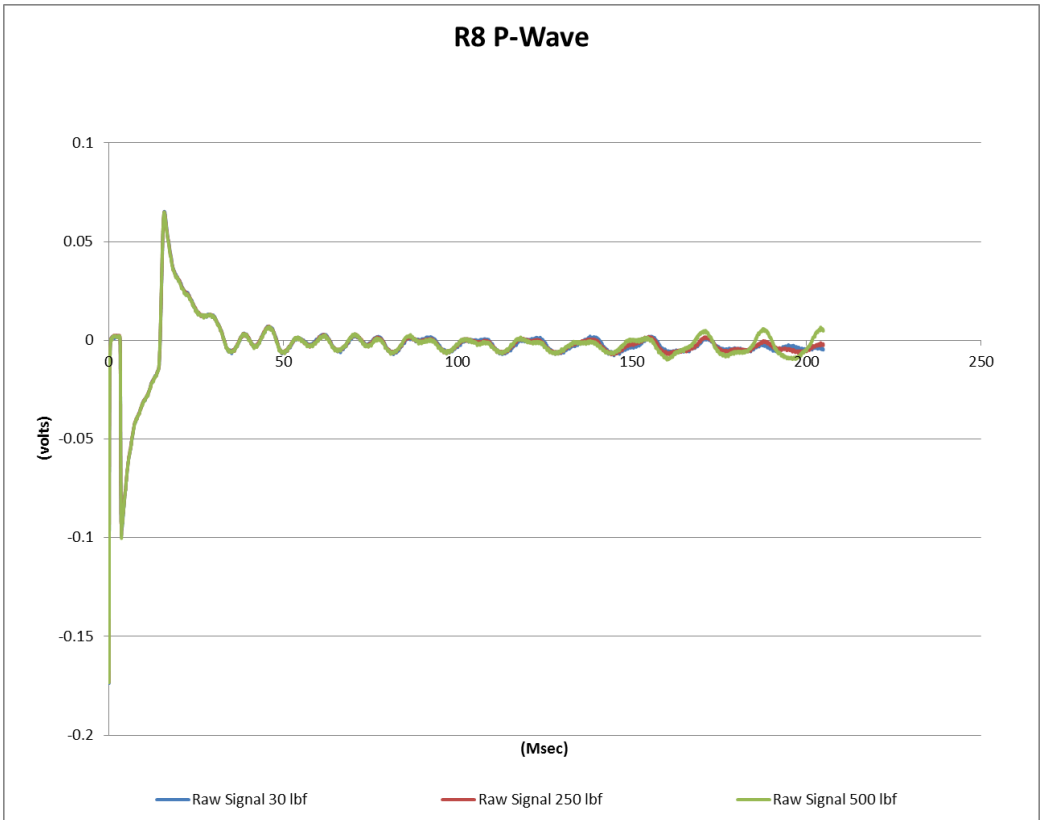
R8 P-Wave
0.1
0.05
0
-0.05
-0.1
-0.15
-0.2
(volts)
0
50
100
150
200
250
(Msec)
Raw Signal 30 lbf
Raw Signal 250 lbf
Raw Signal 500 lbf

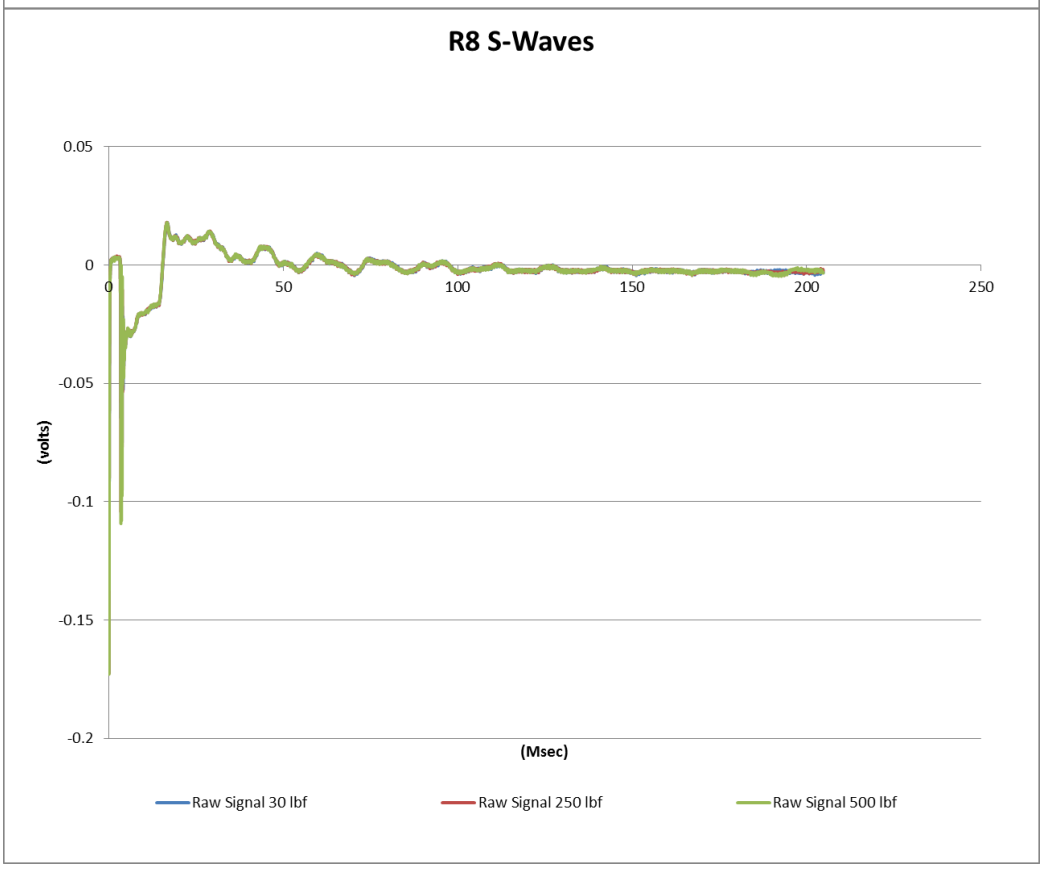
R8 S-Waves
0.05
0
-0.05
-0.1
-0.15
-0.2
(volts)
0
50
100
150
200
250
(Msec)
Raw Signal 30 lbf
Raw Signal 250 lbf
Raw Signal 500 lbf

**R11**

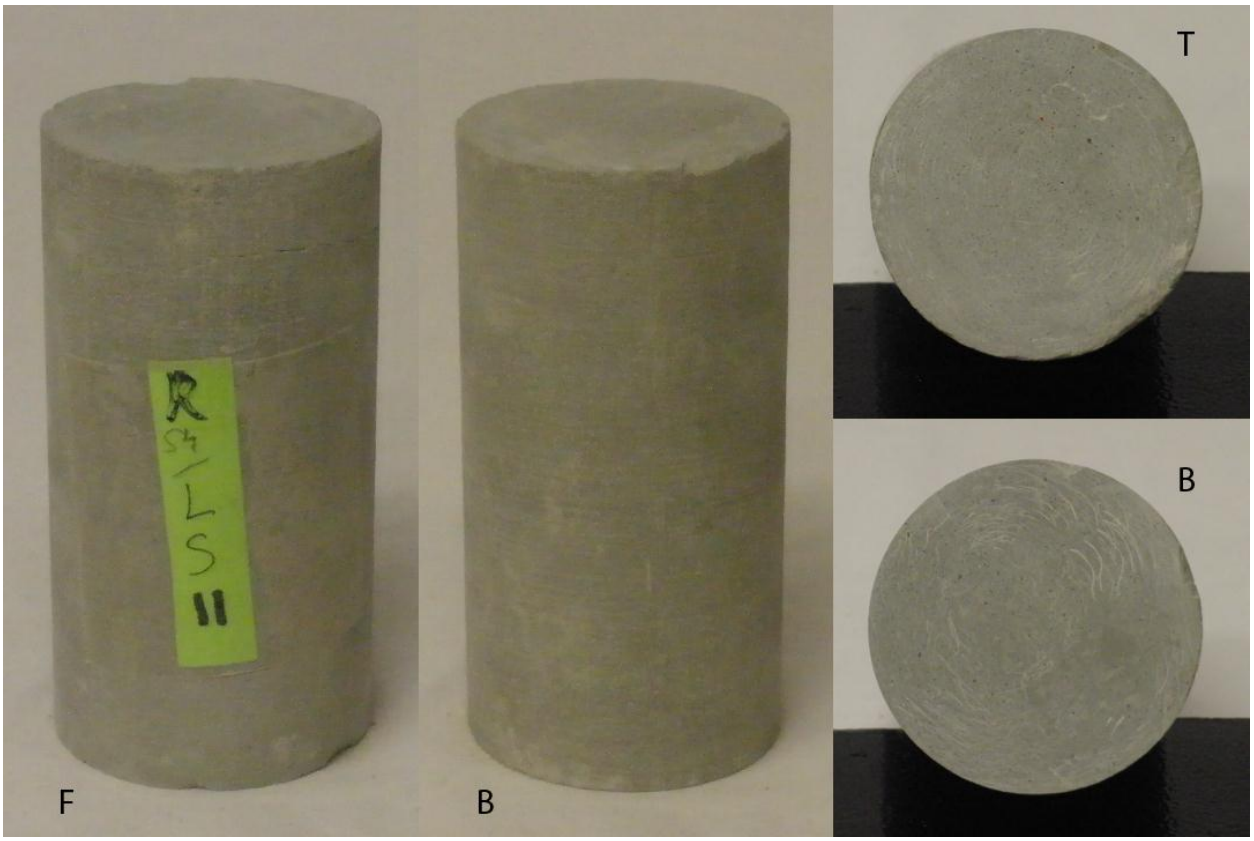


| **Sevenmile** (Ogden, Riley CTY) Physical Properties of Cores | | | | | | | | | | | | | | |
|---|---|---|---|---|---|---|---|---|---|---|---|---|---|---|
| ID | Density (g/cm^3) | Lt. (in.) | Dia. (in.) | Top dpt. (ft.) | Bot. dpt. (ft.) | Avg. dpt. (ft) | Core Set | Core set dpt. | C | R | RQD | Lt. (mm) | Dia. (mm) | Mass (g) |
| R11 | 2.35 | 4.03 | 2.05 | 79.500 | 79.838 | 79.668 | Core 6 | 77.0 - 80.5 | | 3.5 | 100 | 103 | 52.5 | 513.2 |

| **Sevenmile Standard Picking** | | | | | | | | |
|---|---|---|---|---|---|---|---|---|
| First Arrivals & Elastic Prop. | | | | | | | | |
| | Avg. Dpt. (ft) | lbf | P-Vel (m/s) | S-Vel (m/s) | Poisson's Ratio | Young's (MPa) | Bulk (MPa) | Shear (Mpa) |
| R11 | 79.66792 | R11-30 | 5476 | 1502 | 0.46 | 15450 | 63287 | 5294 |
| | | R11-235 | 5615 | 1529 | 0.46 | 16021 | 66665 | 5487 |
| | | R11-525 | 5740 | 1542 | 0.46 | 16310 | 69857 | 5581 |

| **Sevenmile Altered picking** | | | | | | | | |
|---|---|---|---|---|---|---|---|---|
| Poisson's Point | | | | | | | | |
| | Avg. Dpt. (ft) | lbf | P-Vel (m/s) | S-Vel (m/s) | Poisson's Ratio | Young's (MPa) | Bulk (MPa) | Shear (Mpa) |
| R11 | 79.66792 | R11-30 | 2417 | 1502 | 0.19 | 12550 | 6648 | 5294 |
| | | R11-235 | 2422 | 1529 | 0.17 | 12824 | 6451 | 5487 |
| | | R11-525 | 2438 | 1542 | 0.17 | 13022 | 6509 | 5581 |

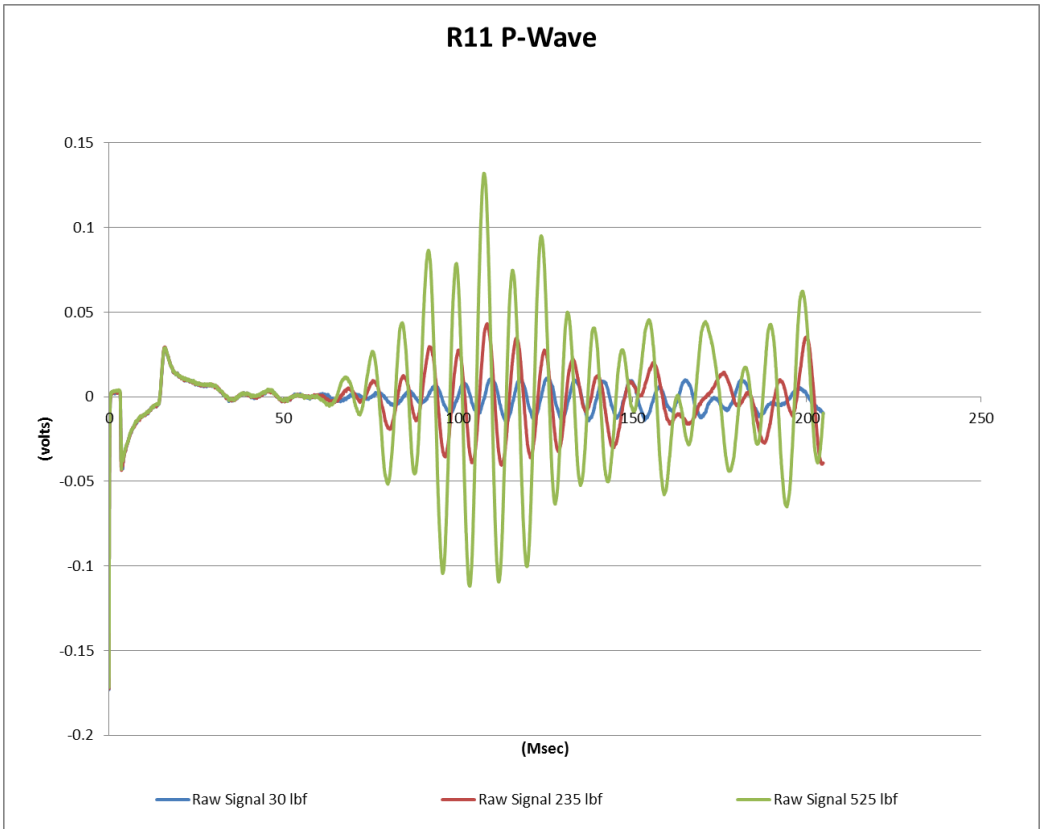
R11 P-Wave
0.15
0.1
0.05
0
-0.05
-0.1
-0.15
-0.2
(volts)
0
50
100
150
200
250
(Msec)
Raw Signal 30 lbf
Raw Signal 235 lbf
Raw Signal 525 lbf

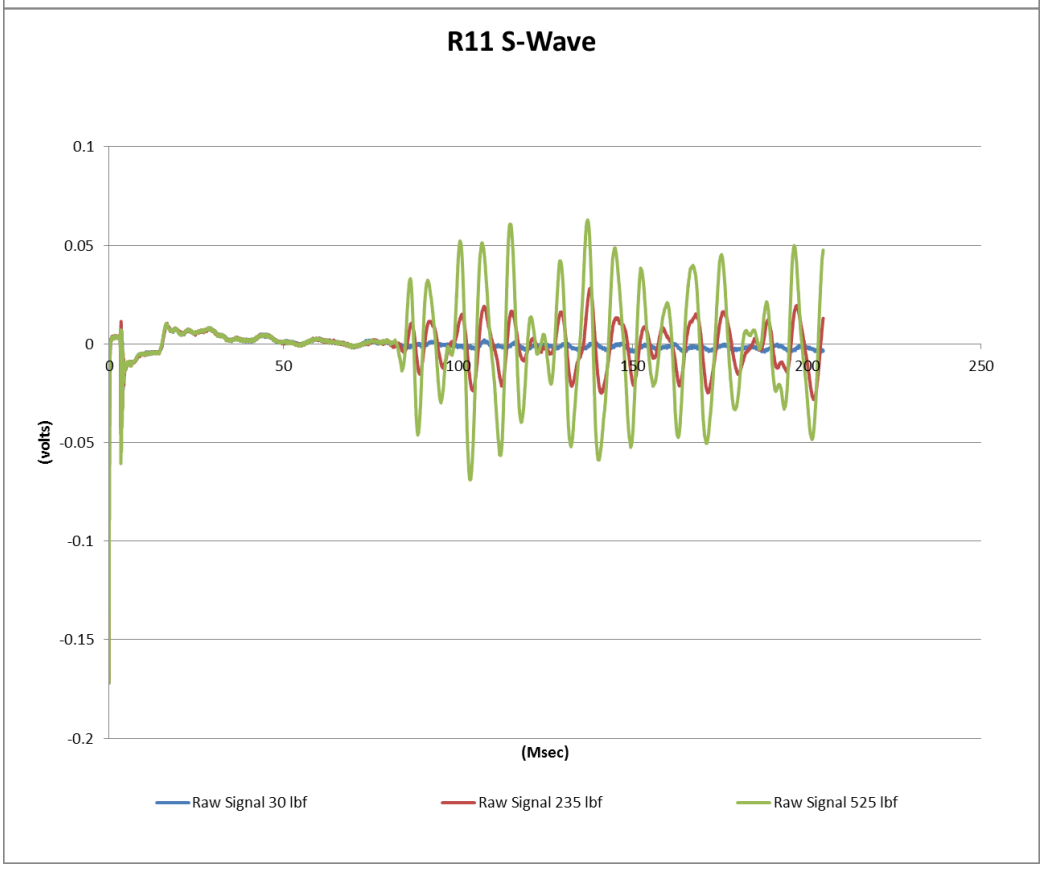
R11 S-Wave
0.1
0.05
0
-0.05
-0.1
-0.15
-0.2
(volts)
0
50
100
150
200
250
(Msec)
Raw Signal 30 lbf
Raw Signal 235 lbf
Raw Signal 525 lbf

## SOUTH {KDOT North Borehole} (Ogden, Riley County)

| **North** (Ogden, Riley CTY) Physical Properties of Cores | | | | | | | | | | | | | | |
|---|---|---|---|---|---|---|---|---|---|---|---|---|---|---|
| ID | Density (g/cm^3) | Lt. (in.) | Dia. (in.) | Top dpt. (ft.) | Bot. dpt. (ft.) | Avg. dpt. (ft) | Core Set | Core set dpt. | C | R | RQD | Lt. (mm) | Dia. (mm) | Mass (g) |
| RN1 | 2.22 | 5.450 | 2.00 | 64.875 | 65.329 | 65.102 | Core 2 | 63.5 - 66.5 | 3 | 2.7 | 2.1/3.0 | 139 | 51 | 629.8 |
| RN3-S | 2.24 | 5.670 | 2.00 | 67.042 | 67.514 | 67.278 | Core 3 | 66.5 - 68.5 | 2 | 2 | 1.6/2.0 | 144.5 | 51 | 660.4 |
| RN3-R | 2.24 | 5.670 | 2.00 | 67.042 | 67.514 | 67.278 | Core 3 | 66.5 - 68.5 | 2 | 2 | 1.6/2.0 | 144.5 | 51 | 661.5 |
| RN5 | 2.4 | 6.437 | 2.00 | 70.792 | 71.328 | 71.060 | Core 4 | 68.5 - 73.5 | 5 | 5 | 100 | 162.5 | 51 | 796.1 |
| RN6 | 2.16 | 7.625 | 2.00 | 72.427 | 73.063 | 72.745 | Core 4 | 68.5 - 73.5 | 5 | 5 | 100 | 192 | 51 | 849.0 |
| RN7 | 2.16 | 9.875 | 2.00 | 74.333 | 75.156 | 74.745 | Core 5 | 73.5 - 78.5 | 5 | 5 | 100 | 250 | 51 | 1101.2 |
| RN8 | 2.25 | 7.625 | 2.00 | 75.198 | 75.833 | 75.516 | Core 5 | 73.5 - 78.5 | 5 | 5 | 100 | 194 | 51 | 893.5 |
| RN9 | 2.26 | 9.250 | 2.00 | 75.833 | 76.604 | 76.219 | Core 5 | 73.5 - 78.5 | 5 | 5 | 100 | 233.5 | 51 | 1076.3 |
| RN10 | 2.27 | 8.688 | 2.00 | 77.609 | 78.333 | 77.971 | Core 5 | 73.5 - 78.5 | 5 | 5 | 100 | 220 | 51 | 1019.5 |

| **North Standard Picking** | | | | | | | | |
|---|---|---|---|---|---|---|---|---|
| First Arrivals & Elastic Prop. | | | | | | | | |
| | Avg. Dpt. (ft.) | lbf | P-Vel (m/s) | S-Vel (m/s) | Poisson's Ratio | Youngs (MPa) | Bulk (MPa) | Shear (Mpa) |
| RN1 | 65.102 | RN1-30 | 7593 | 1663 | 0.47 | 18102 | 119680 | 6137 |
| | | RN1-205 | 7627 | 1643 | 0.48 | 17665 | 121034 | 5985 |
| | | RN1-410 | 7869 | 1636 | 0.48 | 17540 | 129437 | 5936 |
| RN5 | 71.060 | RN5-30 | 8759 | 2349 | 0.46 | 38685 | 166329 | 13237 |
| | | RN5-220 | 8945 | 2546 | 0.46 | 45275 | 171152 | 15549 |
| | | RN5-440 | 8828 | 2550 | 0.45 | 45348 | 166131 | 15589 |
| RN6 | 72.745 | RN6-30 | 9959 | 2215 | 0.47 | 31321 | 200534 | 10625 |
| | | RN6-230 | 10488 | 2214 | 0.48 | 31336 | 223940 | 10610 |
| | | RN6-460 | 10468 | 2233 | 0.48 | 31873 | 222782 | 10796 |
| RN7 | 74.745 | RN7-30 | 13374 | 2010 | 0.49 | 25922 | 374047 | 8708 |
| | | RN7-235 | 13543 | 2070 | 0.49 | 27495 | 383181 | 9239 |
| | | RN7-470 | 13896 | 2076 | 0.49 | 27660 | 403960 | 9291 |
| RN8 | 75.516 | RN8-30 | 10199 | 1941 | 0.48 | 25164 | 223203 | 8495 |
| | | RN8-240 | 10250 | 2092 | 0.48 | 29185 | 223693 | 9871 |
| | | RN8-480 | 10563 | 2096 | 0.48 | 29299 | 238364 | 9901 |
| RN9 | 76.219 | RN9-30 | 12039 | 1786 | 0.49 | 21435 | 317431 | 7199 |
| | | RN9-240 | 12119 | 1846 | 0.49 | 22894 | 321157 | 7692 |
| | | RN9-480 | 12276 | 1903 | 0.49 | 24324 | 329133 | 8175 |

| **North Altered picking** | | | | | | | | |
|---|---|---|---|---|---|---|---|---|
| Poisson's Point | | | | | | | | |
| | Avg. Dpt. (ft.) | lbf | P-Vel (m/s) | S-Vel (m/s) | Poisson's Ratio | Youngs (MPa) | Bulk (MPa) | Shear (Mpa) |
| RN1 | 65.102 | RN1-30 | 2570 | 1663 | 0.14 | 13988 | 6468 | 6137 |
| | | RN1-205 | 2573 | 1643 | 0.16 | 13837 | 6702 | 5985 |
| | | RN1-410 | 2563 | 1636 | 0.16 | 13729 | 6661 | 5936 |
| RN5 | 71.05989 | RN5-30 | 4215 | 2349 | 0.27 | 33745 | 24957 | 13237 |
| | | RN5-220 | 4252 | 2546 | 0.22 | 37955 | 22635 | 15549 |
| | | RN5-440 | 4269 | 2550 | 0.22 | 38122 | 22916 | 15589 |
| RN6 | 72.74479 | RN6-30 | 3534 | 2215 | 0.18 | 24995 | 12869 | 10625 |
| | | RN6-230 | 3514 | 2214 | 0.17 | 24844 | 12576 | 10610 |
| | | RN6-460 | 3515 | 2233 | 0.16 | 25080 | 12351 | 10796 |
| RN7 | 74.74479 | RN7-30 | 3327 | 2010 | 0.21 | 21120 | 12254 | 8708 |
| | | RN7-235 | 3352 | 2070 | 0.19 | 22021 | 11906 | 9239 |
| | | RN7-470 | 3358 | 2076 | 0.19 | 22128 | 11928 | 9291 |
| RN8 | 75.51563 | RN8-30 | 3106 | 1941 | 0.18 | 20039 | 10423 | 8495 |
| | | RN8-240 | 3135 | 2092 | 0.10 | 21686 | 9000 | 9871 |
| | | RN8-480 | 3159 | 2096 | 0.11 | 21923 | 9299 | 9901 |
| RN9 | 76.21878 | RN9-30 | 3136 | 1786 | 0.26 | 18140 | 12592 | 7199 |
| | | RN9-240 | 3113 | 1846 | 0.23 | 18902 | 11610 | 7692 |
| | | RN9-480 | 3102 | 1903 | 0.20 | 19590 | 10817 | 8175 |

**RN1**

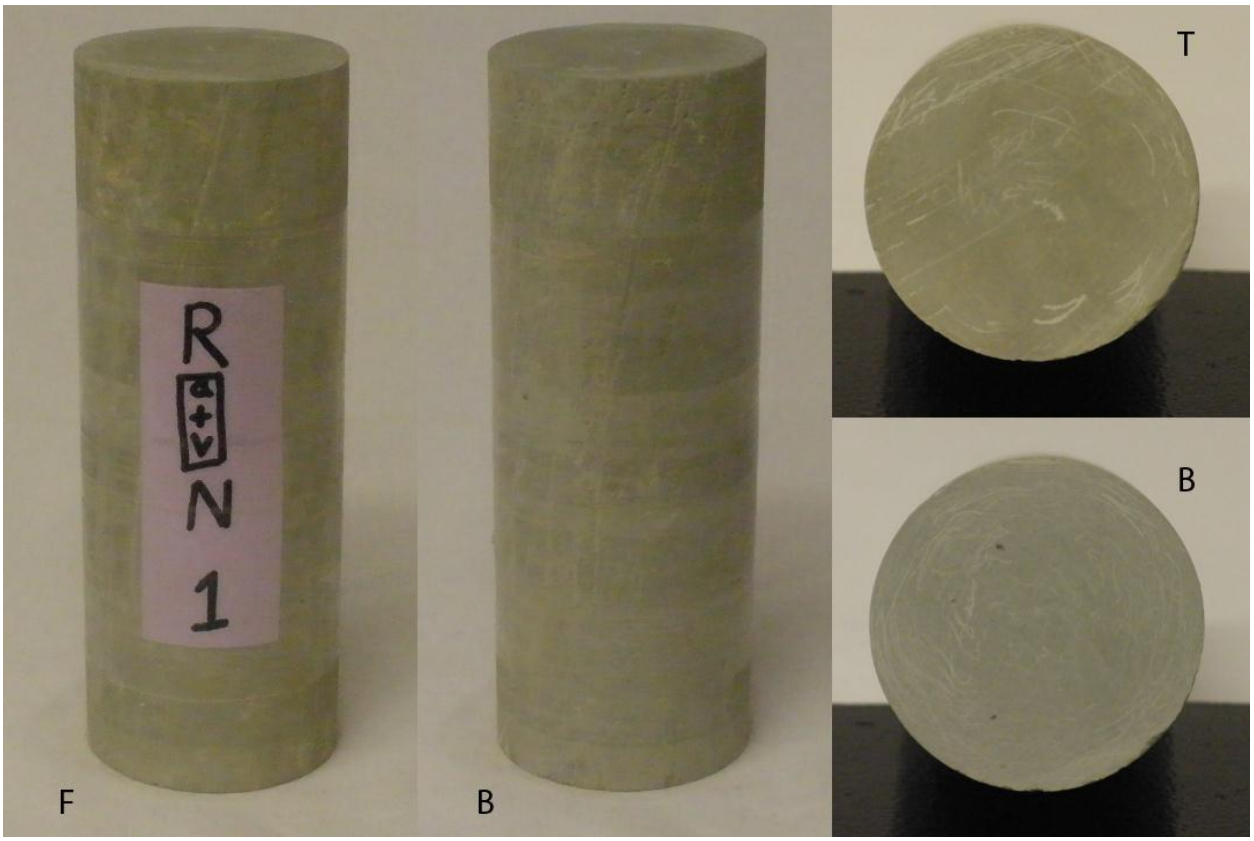


| North (Ogden, Riley CTY) Physical Properties of Cores | | | | | | | | | | | | | | |
|---|---|---|---|---|---|---|---|---|---|---|---|---|---|---|
| ID | Density (g/cm^3) | Lt. (in.) | Dia. (in.) | Top dpt. (ft.) | Bot. dpt. (ft.) | Avg. dpt. (ft) | Core Set | Core set dpt. | C | R | RQD | Lt. (mm) | Dia. (mm) | Mass (g) |
| RN1 | 2.22 | 5.450 | 2.00 | 64.875 | 65.329 | 65.102 | Core 2 | 63.5 - 66.5 | 3 | 2.7 | 2.1/3.0 | 139 | 51 | 629.8 |

| **North Standard Picking** | | | | | | | | |
|---|---|---|---|---|---|---|---|---|
| First Arrivals & Elastic Prop. | | | | | | | | |
| | Avg. Dpt. (ft.) | lbf | P-Vel (m/s) | S-Vel (m/s) | Poisson's Ratio | Youngs (MPa) | Bulk (MPa) | Shear (Mpa) |
| RN1 | 65.102 | RN1-30 | 7593 | 1663 | 0.47 | 18102 | 119680 | 6137 |
| | | RN1-205 | 7627 | 1643 | 0.48 | 17665 | 121034 | 5985 |
| | | RN1-410 | 7869 | 1636 | 0.48 | 17540 | 129437 | 5936 |

| **North Altered picking** | | | | | | | | |
|---|---|---|---|---|---|---|---|---|
| Poisson's Point | | | | | | | | |
| | Avg. Dpt. (ft.) | lbf | P-Vel (m/s) | S-Vel (m/s) | Poisson's Ratio | Young's (MPa) | Bulk (MPa) | Shear (Mpa) |
| RN1 | 65.102 | RN1-30 | 2570 | 1663 | 0.14 | 13988 | 6468 | 6137 |
| | | RN1-205 | 2573 | 1643 | 0.16 | 13837 | 6702 | 5985 |
| | | RN1-410 | 2563 | 1636 | 0.16 | 13729 | 6661 | 5936 |

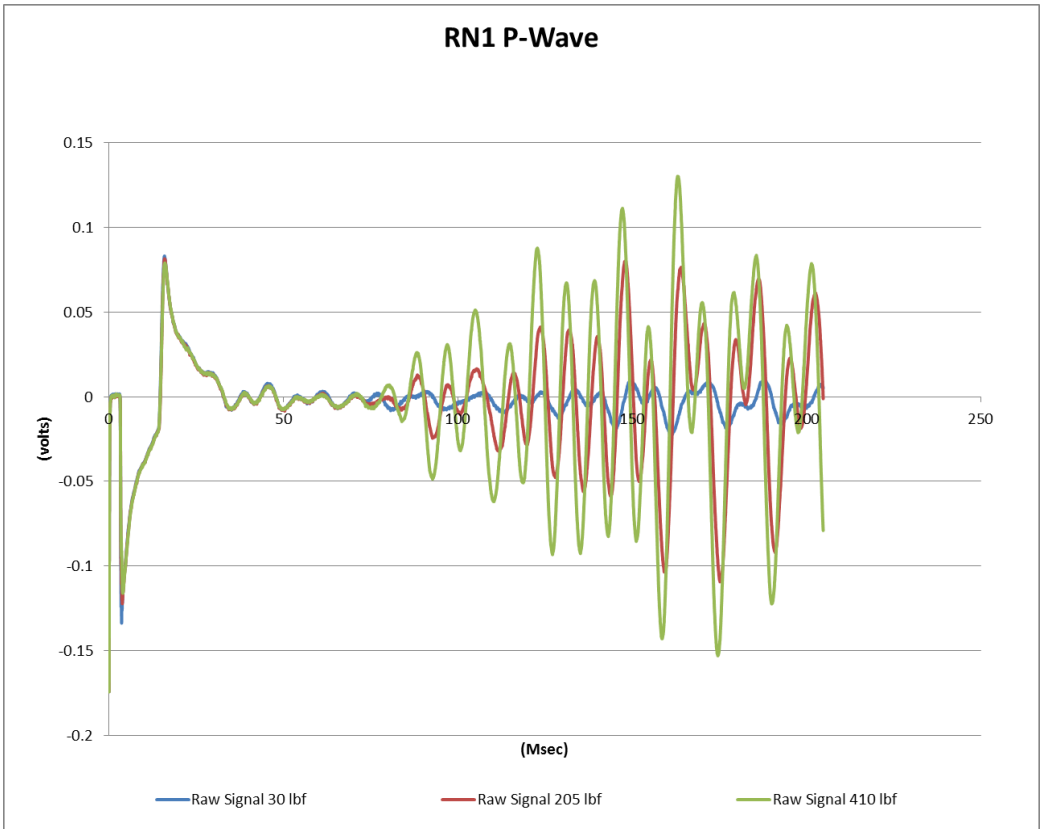
RN1 P-Wave
0.15
0.1
0.05
0
-0.05
-0.1
-0.15
-0.2
(volts)
0
50
100
150
200
250
(Msec)
Raw Signal 30 lbf
Raw Signal 205 lbf
Raw Signal 410 lbf

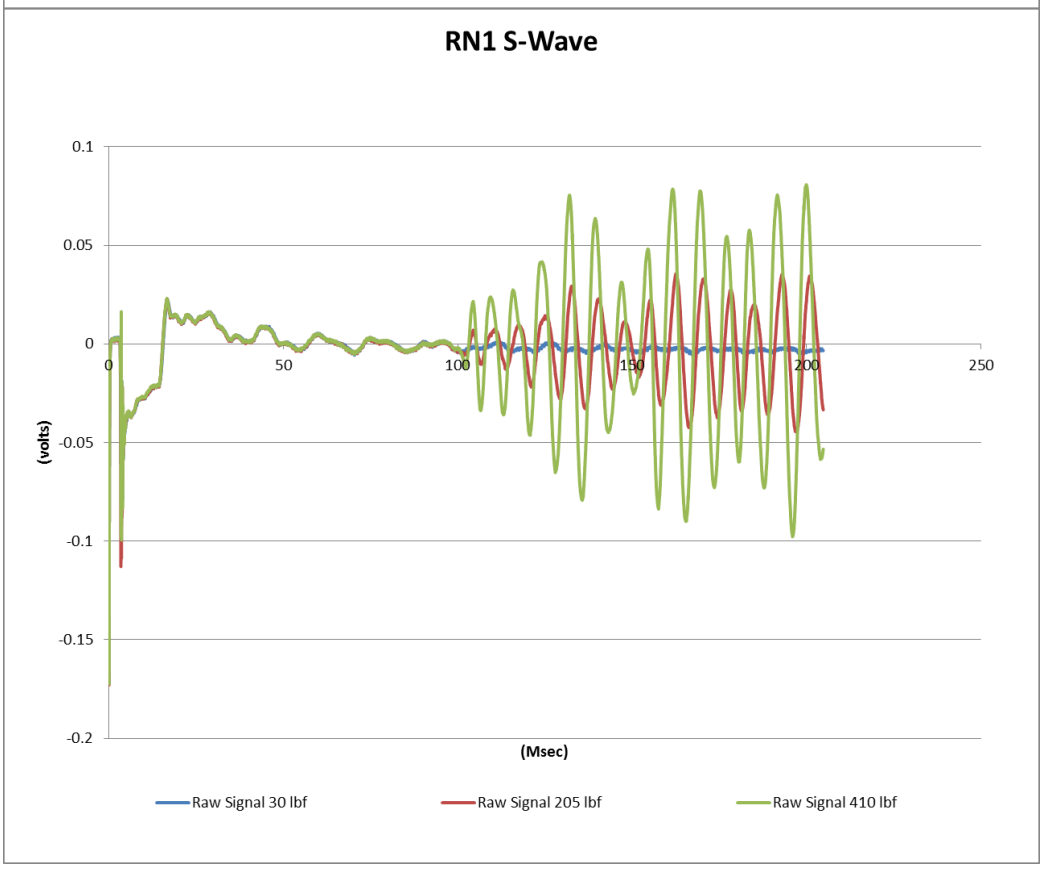
RN1 S-Wave
0.1
0.05
0
-0.05
-0.1
-0.15
-0.2
(volts)
0
50
100
150
200
250
(Msec)
Raw Signal 30 lbf
Raw Signal 205 lbf
Raw Signal 410 lbf

**RN3**

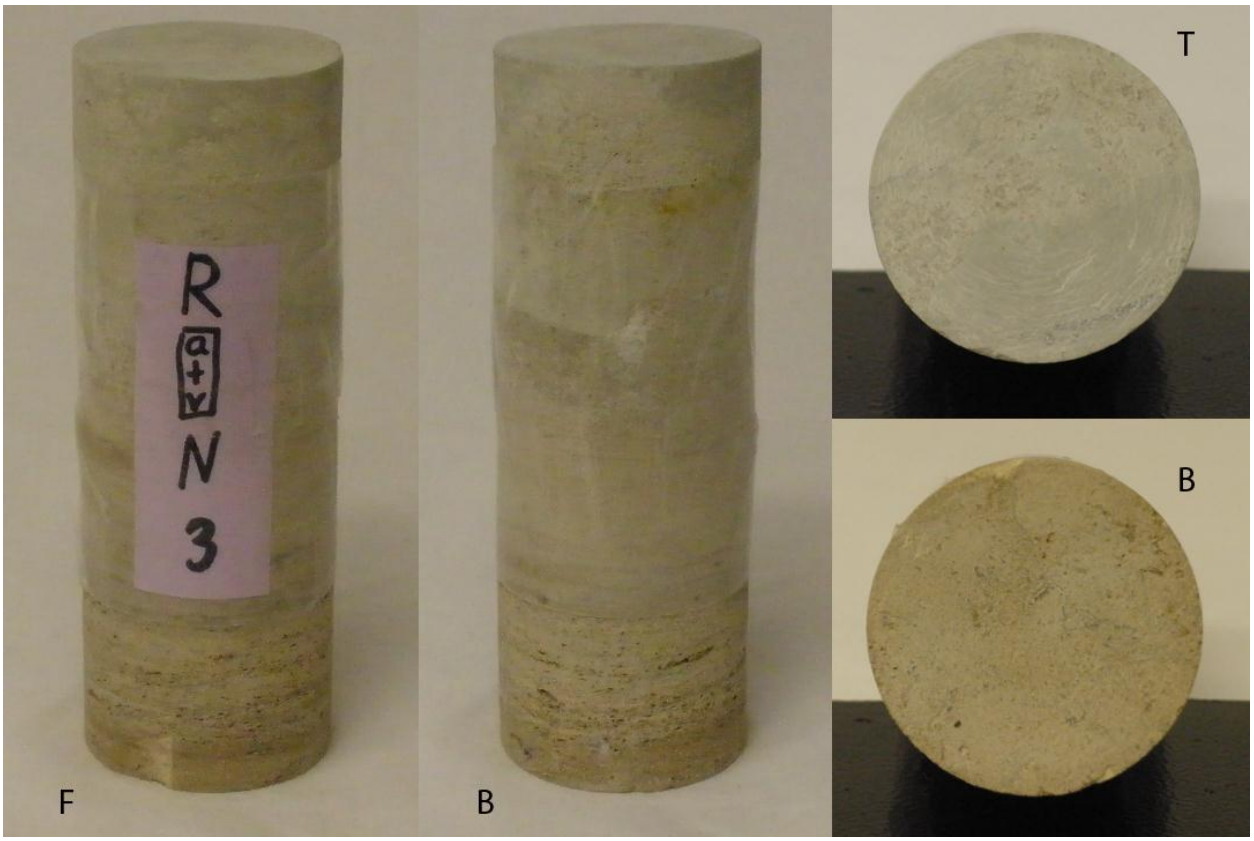


| North (Ogden, Riley CTY) Physical Properties of Cores | | | | | | | | | | | | | | |
|---|---|---|---|---|---|---|---|---|---|---|---|---|---|---|
| ID | Density (g/cm^3) | Lt. (in.) | Dia. (in.) | Top dpt. (ft.) | Bot. dpt. (ft.) | Avg. dpt. (ft) | Core Set | Core set dpt. | C | R | RQD | Lt. (mm) | Dia. (mm) | Mass (g) |
| RN3-S | 2.24 | 5.670 | 2.00 | 67.042 | 67.514 | 67.278 | Core 3 | 66.5 - 68.5 | 2 | 2 | 1.6/2.0 | 144.5 | 51 | 660.4 |
| RN3-R | 2.24 | 5.670 | 2.00 | 67.042 | 67.514 | 67.278 | Core 3 | 66.5 - 68.5 | 2 | 2 | 1.6/2.0 | 144.5 | 51 | 661.5 |

Waveform unsuitable for picking

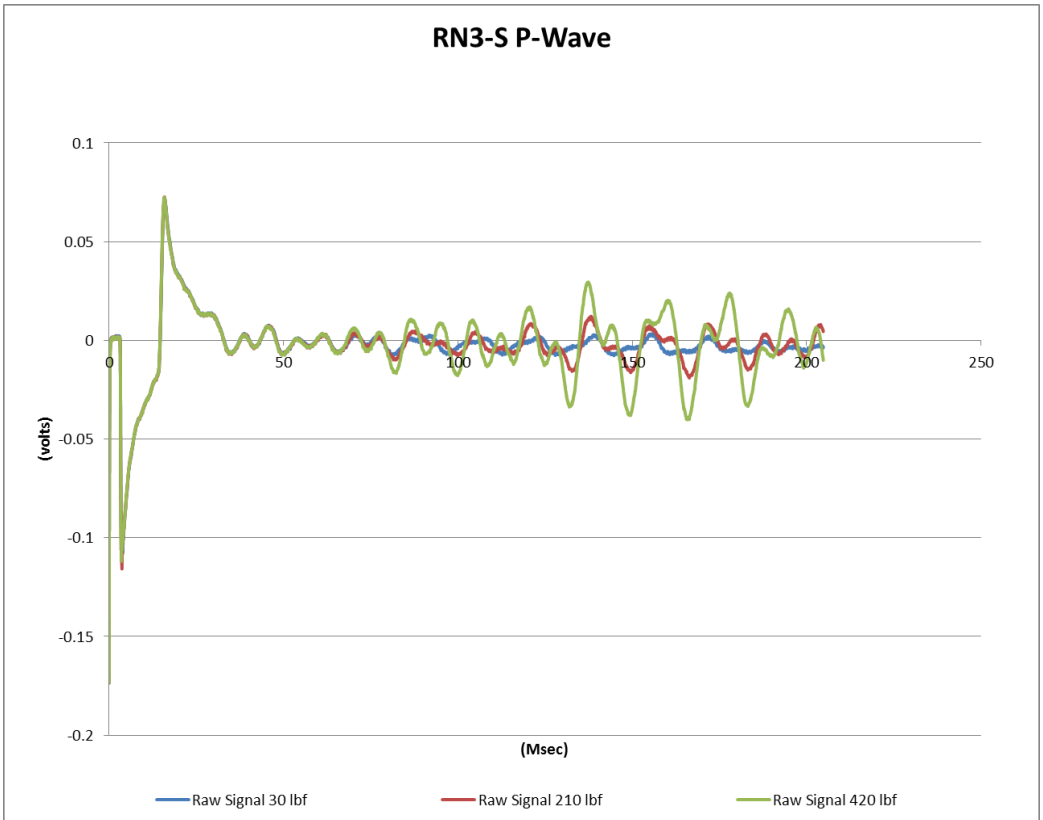
RN3-S P-Wave
0.1
0.05
0
-0.05
-0.1
-0.15
-0.2
(volts)
0
50
100
150
200
250
(Msec)
Raw Signal 30 lbf
Raw Signal 210 lbf
Raw Signal 420 lbf

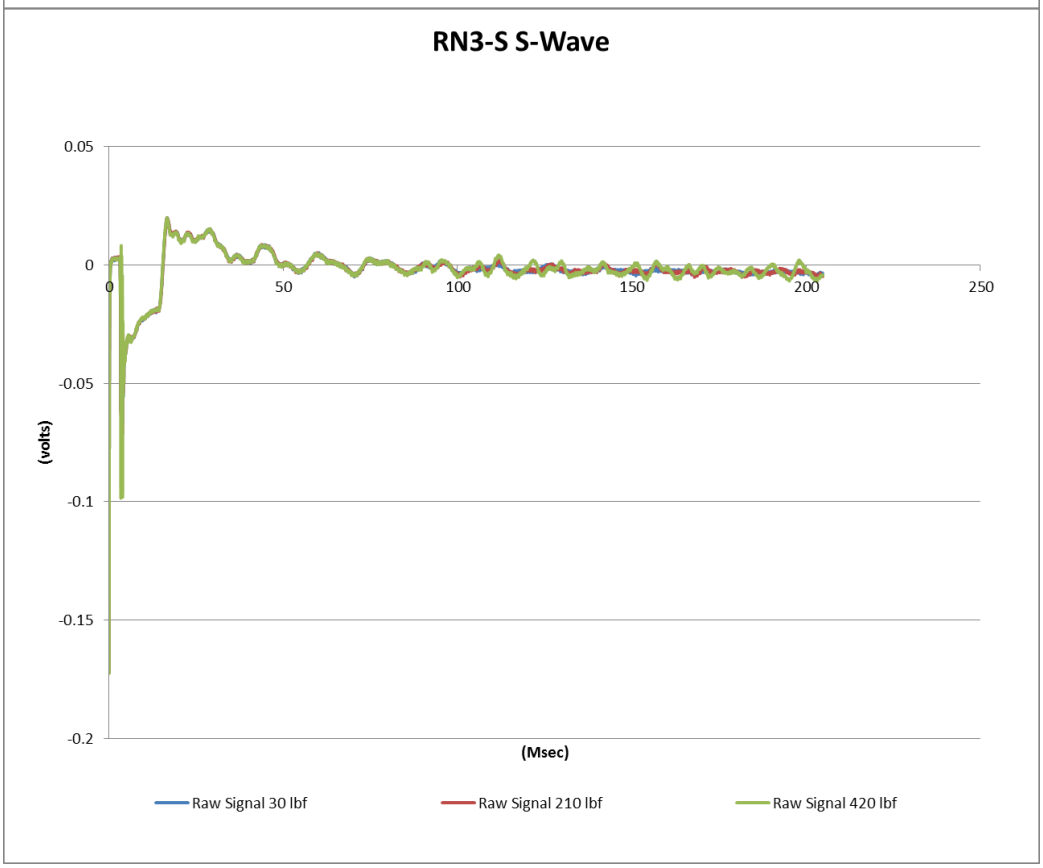
RN3-S S-Wave
0.05
0
-0.05
-0.1
-0.15
-0.2
(volts)
0
50
100
150
200
250
(Msec)
Raw Signal 30 lbf
Raw Signal 210 lbf
Raw Signal 420 lbf

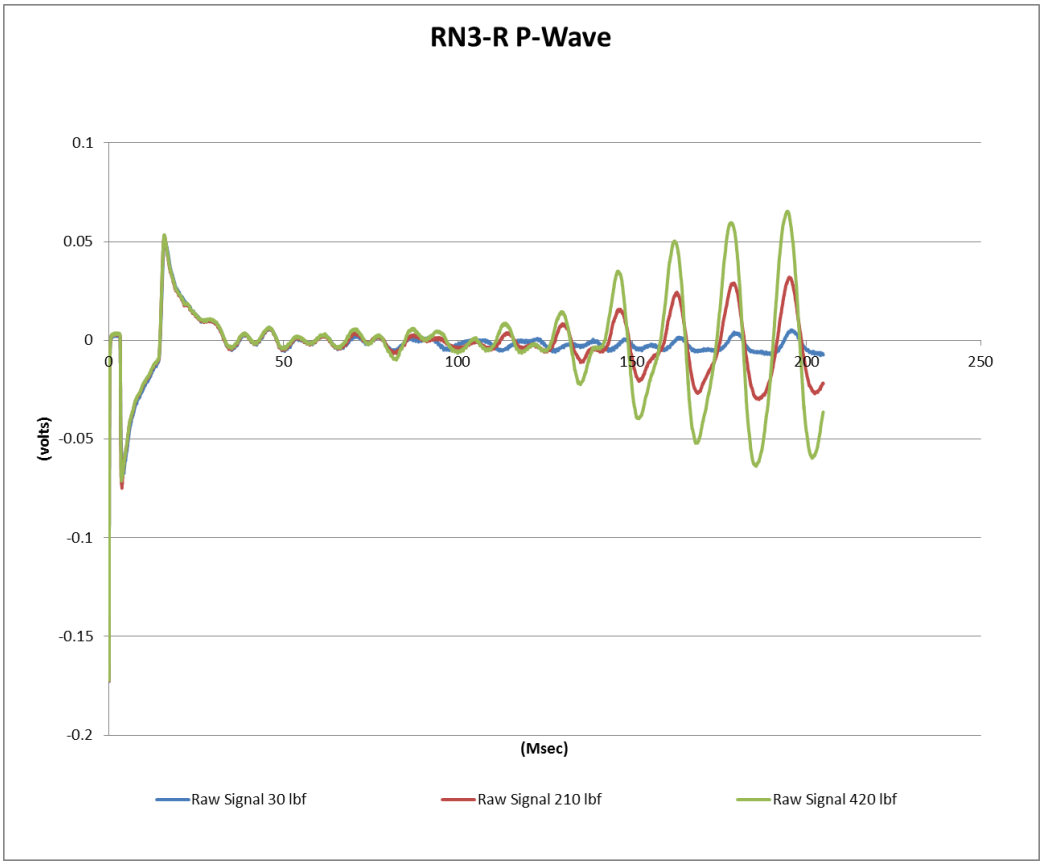
RN3-R P-Wave
0.1
0.05
0
-0.05
-0.1
-0.15
-0.2
0
50
100
150
200
250
(volts)
(Msec)
Raw Signal 30 lbf
Raw Signal 210 lbf
Raw Signal 420 lbf

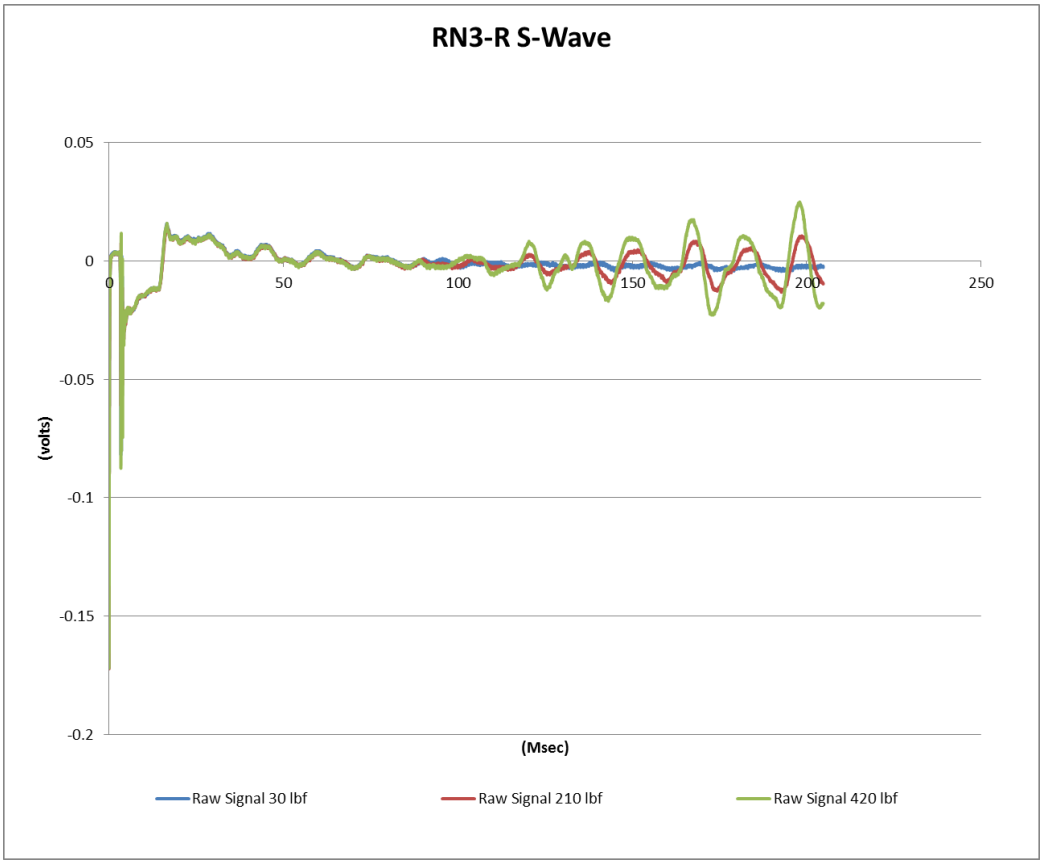
RN3-R S-Wave
0.05
0
-0.05
-0.1
-0.15
-0.2
0
50
100
150
200
250
(volts)
(Msec)
Raw Signal 30 lbf
Raw Signal 210 lbf
Raw Signal 420 lbf

**RN5**

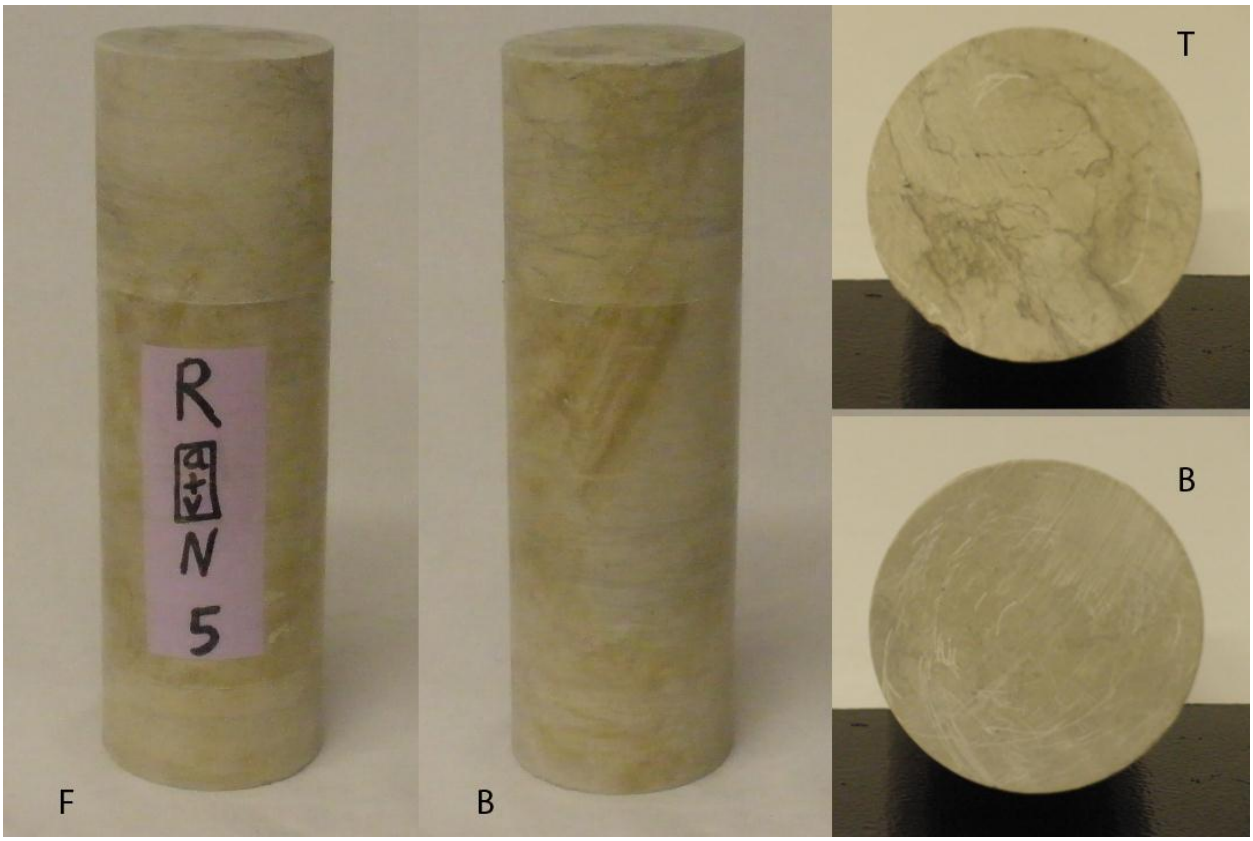


| North (Ogden, Riley CTY) Physical Properties of Cores | | | | | | | | | | | | | | |
|---|---|---|---|---|---|---|---|---|---|---|---|---|---|---|
| ID | Density (g/cm^3) | Lt. (in.) | Dia. (in.) | Top dpt. (ft.) | Bot. dpt. (ft.) | Avg. dpt. (ft) | Core Set | Core set dpt. | C | R | RQD | Lt. (mm) | Dia. (mm) | Mass (g) |
| RN5 | 2.4 | 6.4375 | 2.00 | 70.792 | 71.328 | 71.060 | Core 4 | 68.5 - 73.5 | 5 | 5 | 100 | 162.5 | 51 | 796.1 |

| **North Standard Picking** | | | | | | | | |
|---|---|---|---|---|---|---|---|---|
| First Arrivals & Elastic Prop. | | | | | | | | |
| | Avg. Dpt. (ft.) | lbf | P-Vel (m/s) | S-Vel (m/s) | Poisson's Ratio | Youngs (MPa) | Bulk (MPa) | Shear (Mpa) |
| RN5 | 71.060 | RN5-30 | 8759 | 2349 | 0.46 | 38685 | 166329 | 13237 |
| | | RN5-220 | 8945 | 2546 | 0.46 | 45275 | 171152 | 15549 |
| | | RN5-440 | 8828 | 2550 | 0.45 | 45348 | 166131 | 15589 |

| **North Altered picking** | | | | | | | | |
|---|---|---|---|---|---|---|---|---|
| Poisson's Point | | | | | | | | |
| | Avg. Dpt. (ft.) | lbf | P-Vel (m/s) | S-Vel (m/s) | Poisson's Ratio | Young's (MPa) | Bulk (MPa) | Shear (Mpa) |
| RN5 | 71.05989 | RN5-30 | 4215 | 2349 | 0.27 | 33745 | 24957 | 13237 |
| | | RN5-220 | 4252 | 2546 | 0.22 | 37955 | 22635 | 15549 |
| | | RN5-440 | 4269 | 2550 | 0.22 | 38122 | 22916 | 15589 |

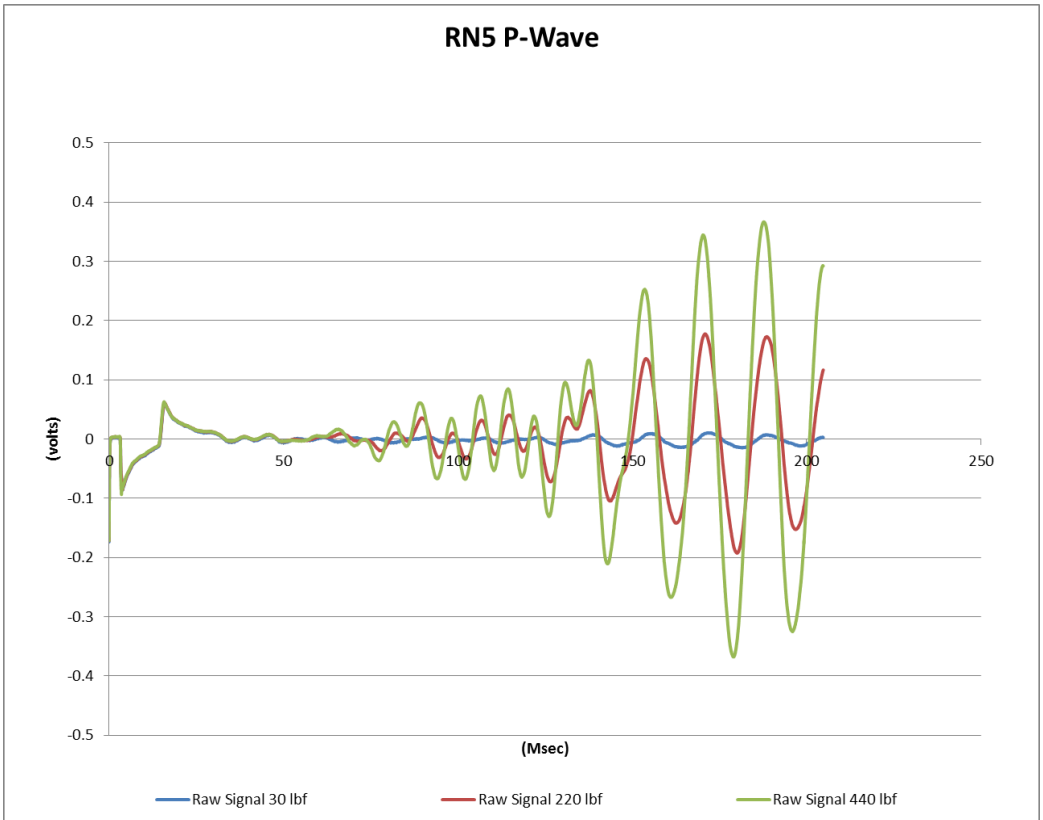
RN5 P-Wave
0.5
0.4
0.3
0.2
0.1
0
-0.1
-0.2
-0.3
-0.4
-0.5
(volts)
0
50
100
150
200
250
(Msec)
Raw Signal 30 lbf
Raw Signal 220 lbf
Raw Signal 440 lbf

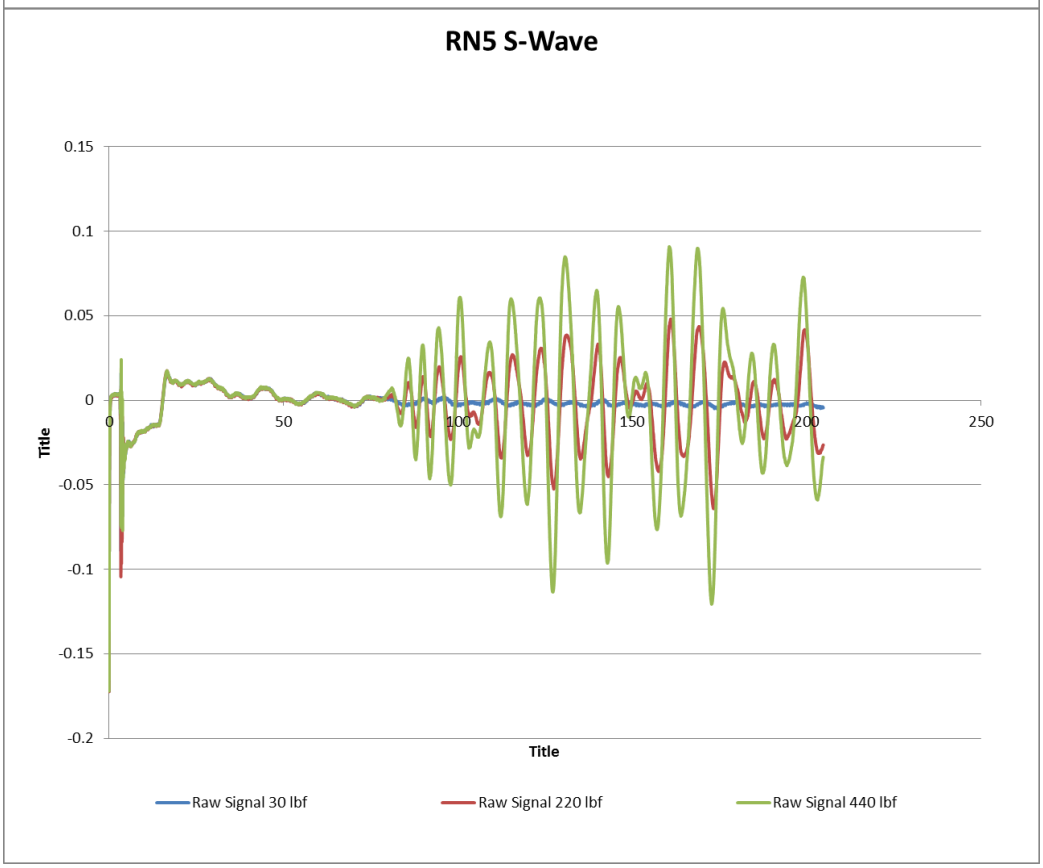
RN5 S-Wave
0.15
0.1
0.05
0
-0.05
-0.1
-0.15
-0.2
Title
0
50
100
150
200
250
Title
Raw Signal 30 lbf
Raw Signal 220 lbf
Raw Signal 440 lbf

## RN6

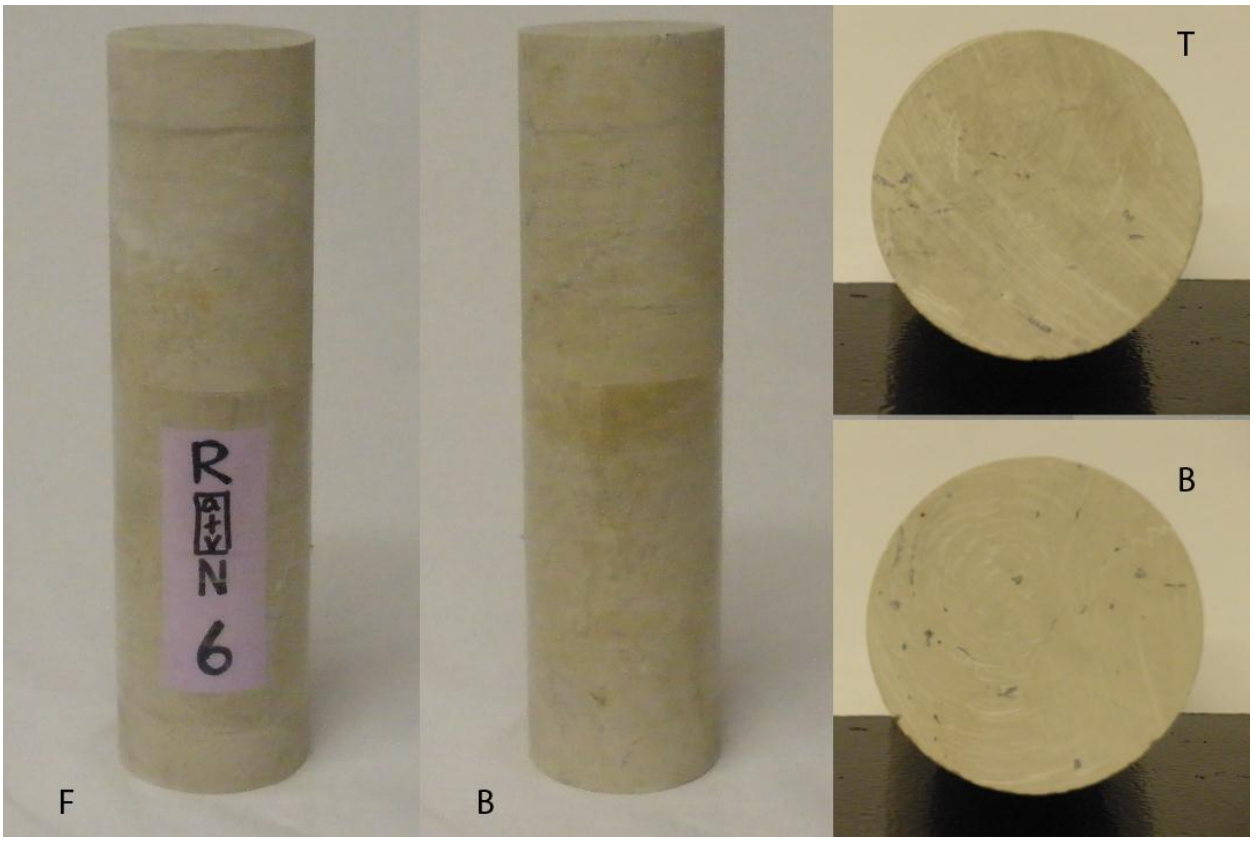


| North (Ogden, Riley CTY) Physical Properties of Cores | | | | | | | | | | | | | | |
|---|---|---|---|---|---|---|---|---|---|---|---|---|---|---|
| ID | Density (g/cm^3) | Lt. (in.) | Dia. (in.) | Top dpt. (ft.) | Bot. dpt. (ft.) | Avg. dpt. (ft) | Core Set | Core set dpt. | C | R | RQD | Lt. (mm) | Dia. (mm) | Mass (g) |
| RN6 | 2.16 | 7.625 | 2.00 | 72.427 | 73.063 | 72.745 | Core 4 | 68.5 - 73.5 | 5 | 5 | 100 | 192 | 51 | 849.0 |

| **North Standard Picking** | | | | | | | | |
|---|---|---|---|---|---|---|---|---|
| First Arrivals & Elastic Prop. | | | | | | | | |
| | Avg. Dpt. (ft.) | lbf | P-Vel (m/s) | S-Vel (m/s) | Poisson's Ratio | Youngs (MPa) | Bulk (MPa) | Shear (Mpa) |
| RN6 | 72.745 | RN6-30 | 9959 | 2215 | 0.47 | 31321 | 200534 | 10625 |
| | | RN6-230 | 10488 | 2214 | 0.48 | 31336 | 223940 | 10610 |
| | | RN6-460 | 10468 | 2233 | 0.48 | 31873 | 222782 | 10796 |

| **North Altered picking** | | | | | | | | |
|---|---|---|---|---|---|---|---|---|
| Poisson's Point | | | | | | | | |
| | Avg. Dpt. (ft.) | lbf | P-Vel (m/s) | S-Vel (m/s) | Poisson's Ratio | Youngs (MPa) | Bulk (MPa) | Shear (Mpa) |
| RN6 | 72.74479 | RN6-30 | 3534 | 2215 | 0.18 | 24995 | 12869 | 10625 |
| | | RN6-230 | 3514 | 2214 | 0.17 | 24844 | 12576 | 10610 |
| | | RN6-460 | 3515 | 2233 | 0.16 | 25080 | 12351 | 10796 |


RN6 P-Wave
0.2
0.15
0.1
0.05
0
-0.05
-0.1
-0.15
-0.2
-0.25
-0.3
(volts)
0
50
100
150
200
250
(Msec)
Raw Signal 30 lbf
Raw Signal 230 lbf
Raw Signal 460 lbf

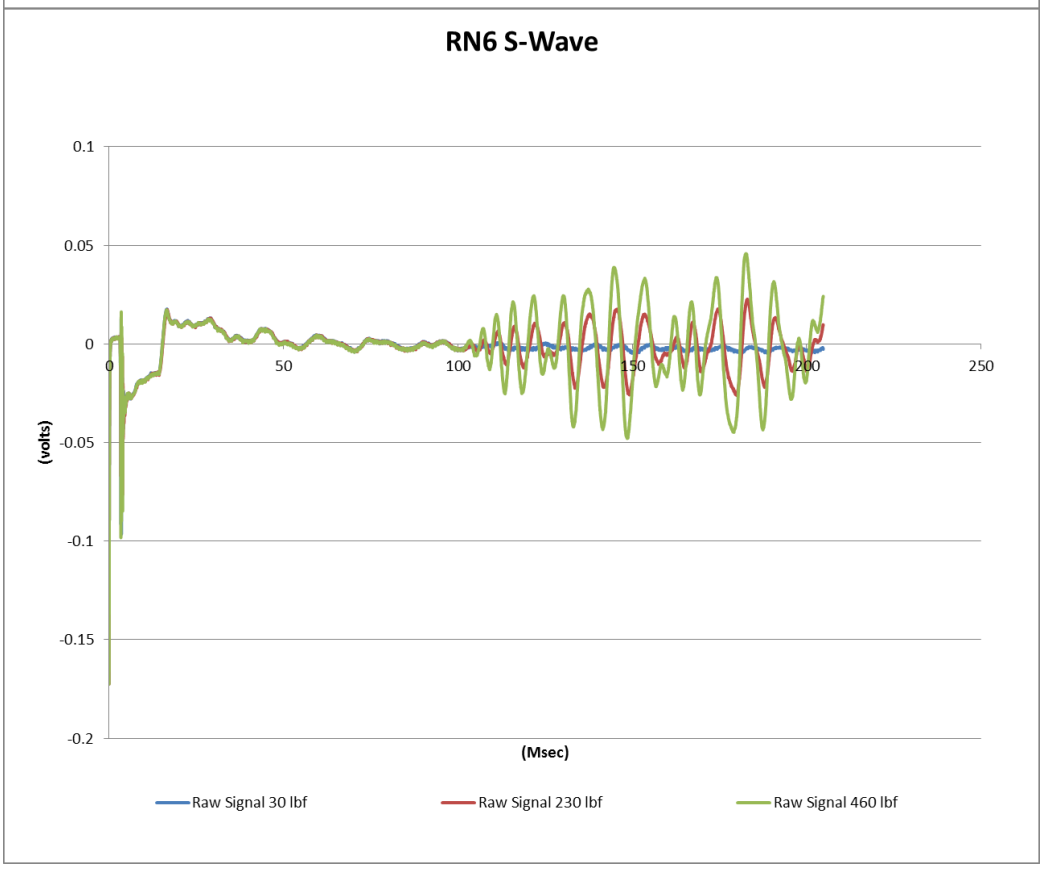
RN6 S-Wave
0.1
0.05
0
-0.05
-0.1
-0.15
-0.2
(volts)
0
50
100
150
200
250
(Msec)
Raw Signal 30 lbf
Raw Signal 230 lbf
Raw Signal 460 lbf

**RN7**

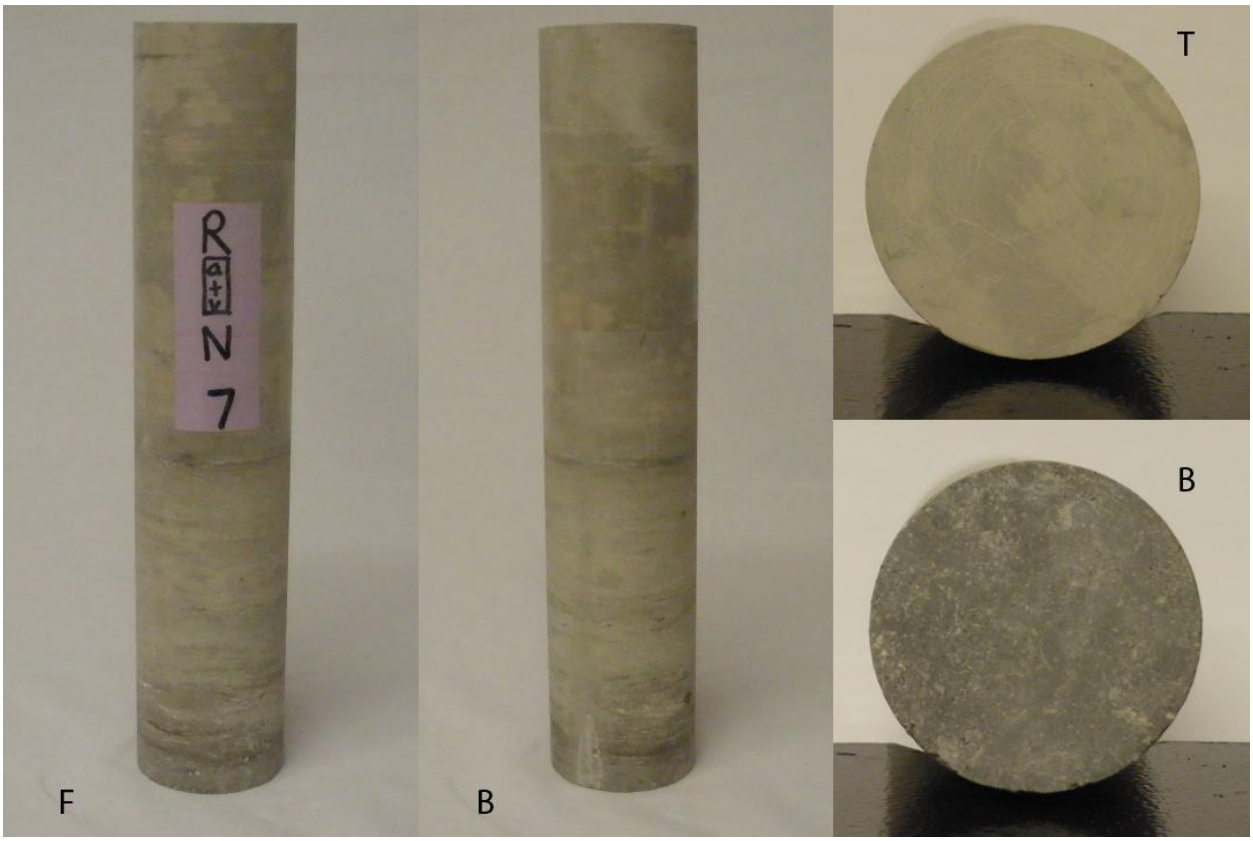


| North (Ogden, Riley CTY) Physical Properties of Cores | | | | | | | | | | | | | | |
|---|---|---|---|---|---|---|---|---|---|---|---|---|---|---|
| ID | Density (g/cm^3) | Lt. (in.) | Dia. (in.) | Top dpt. (ft.) | Bot. dpt. (ft.) | Avg. dpt. (ft) | Core Set | Core set dpt. | C | R | RQD | Lt. (mm) | Dia. (mm) | Mass (g) |
| RN7 | 2.16 | 9.875 | 2.00 | 74.333 | 75.156 | 74.745 | Core 5 | 73.5 - 78.5 | 5 | 5 | 100 | 250 | 51 | 1101.2 |

| **North Standard Picking** | | | | | | | | |
|---|---|---|---|---|---|---|---|---|
| First Arrivals & Elastic Prop. | | | | | | | | |
| | Avg. Dpt. (ft.) | lbf | P-Vel (m/s) | S-Vel (m/s) | Poisson's Ratio | Youngs (MPa) | Bulk (MPa) | Shear (Mpa) |
| RN7 | 74.745 | RN7-30 | 13374 | 2010 | 0.49 | 25922 | 374047 | 8708 |
| | | RN7-235 | 13543 | 2070 | 0.49 | 27495 | 383181 | 9239 |
| | | RN7-470 | 13896 | 2076 | 0.49 | 27660 | 403960 | 9291 |

| **North Altered picking** | | | | | | | | |
|---|---|---|---|---|---|---|---|---|
| Poisson's Point | | | | | | | | |
| | Avg. Dpt. (ft.) | lbf | P-Vel (m/s) | S-Vel (m/s) | Poisson's Ratio | Youngs (MPa) | Bulk (MPa) | Shear (Mpa) |
| RN7 | 74.74479 | RN7-30 | 3327 | 2010 | 0.21 | 21120 | 12254 | 8708 |
| | | RN7-235 | 3352 | 2070 | 0.19 | 22021 | 11906 | 9239 |
| | | RN7-470 | 3358 | 2076 | 0.19 | 22128 | 11928 | 9291 |

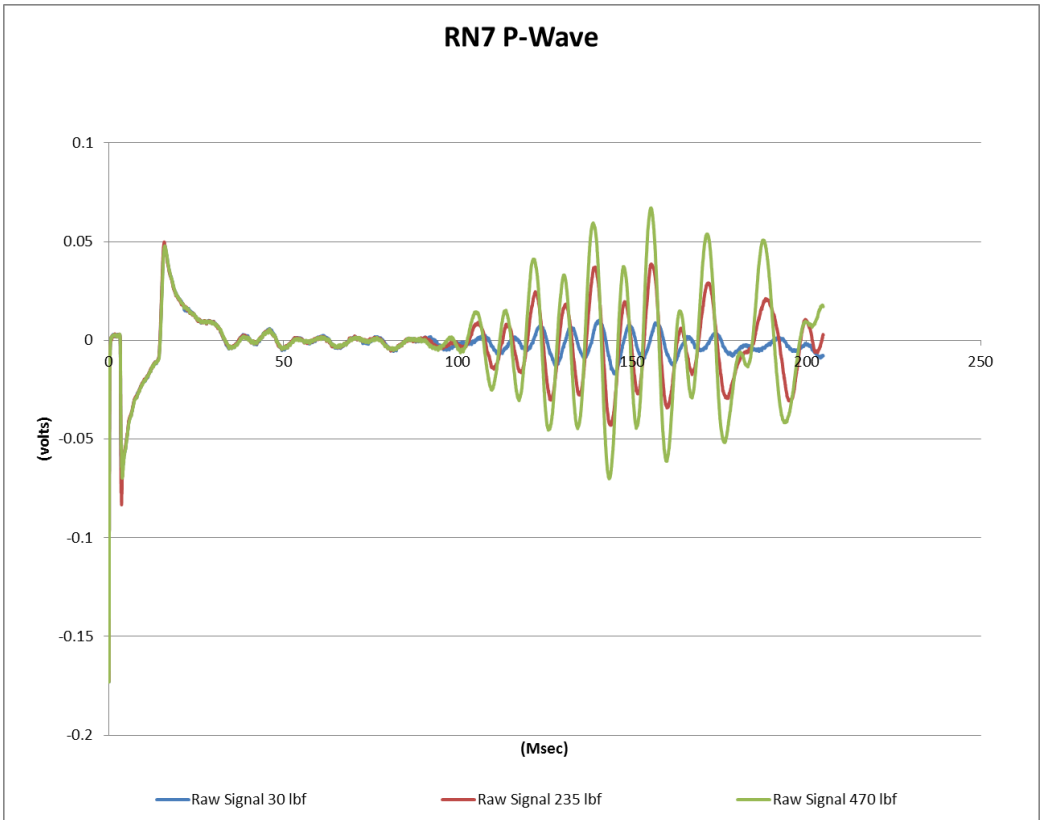
RN7 P-Wave
0.1
0.05
0
-0.05
-0.1
-0.15
-0.2
(volts)
0
50
100
150
200
250
(Msec)
Raw Signal 30 lbf
Raw Signal 235 lbf
Raw Signal 470 lbf

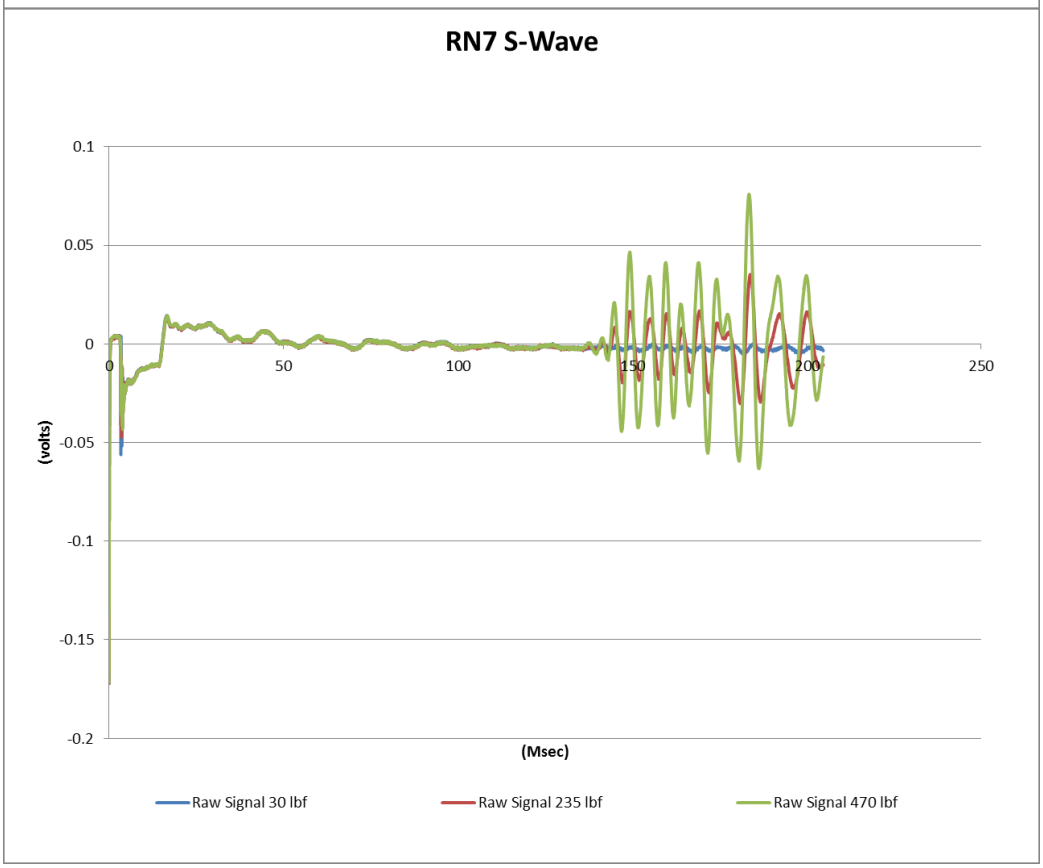
RN7 S-Wave
0.1
0.05
0
-0.05
-0.1
-0.15
-0.2
(volts)
0
50
100
150
200
250
(Msec)
Raw Signal 30 lbf
Raw Signal 235 lbf
Raw Signal 470 lbf

**RN8**

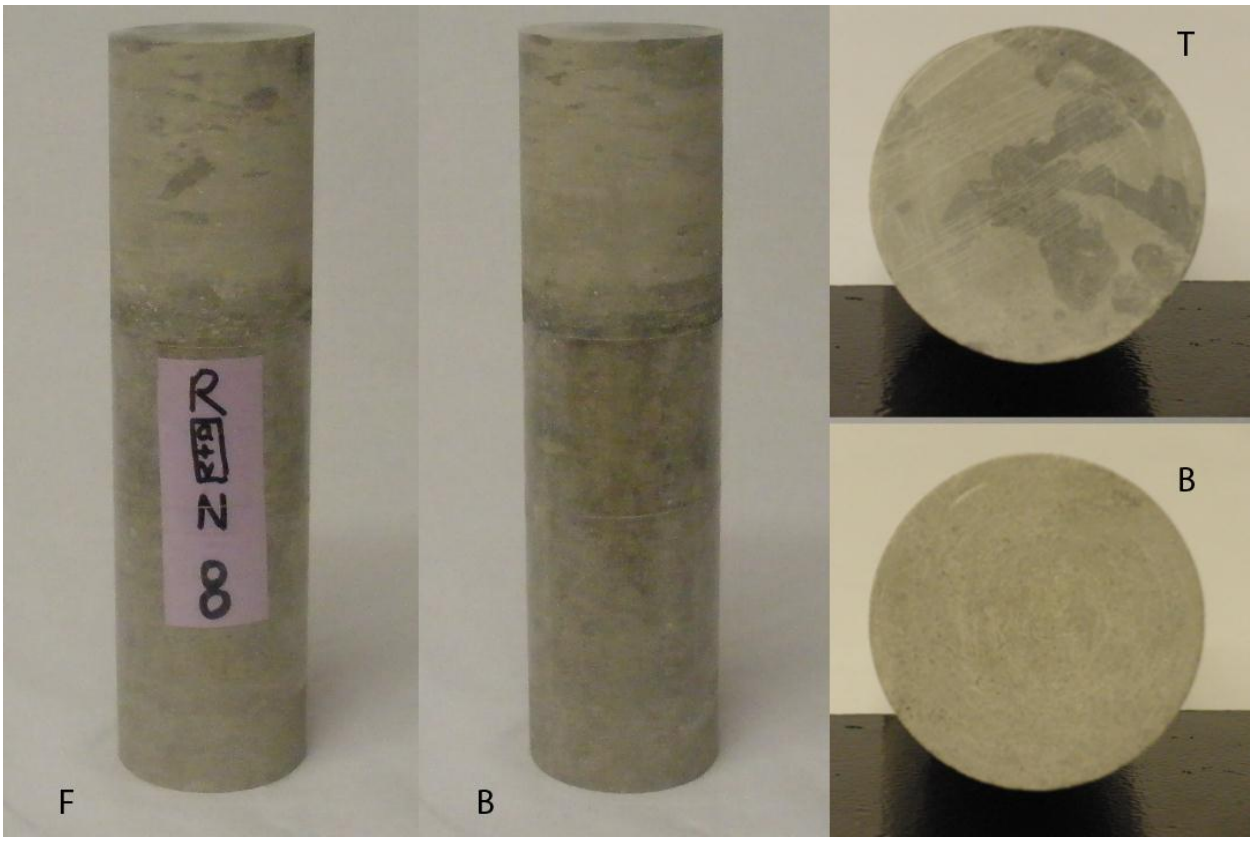


| North (Ogden, Riley CTY) Physical Properties of Cores | | | | | | | | | | | | | | |
|---|---|---|---|---|---|---|---|---|---|---|---|---|---|---|
| ID | Density (g/cm^3) | Lt. (in.) | Dia. (in.) | Top dpt. (ft.) | Bot. dpt. (ft.) | Avg. dpt. (ft) | Core Set | Core set dpt. | C | R | RQD | Lt. (mm) | Dia. (mm) | Mass (g) |
| RN8 | 2.25 | 7.625 | 2.00 | 75.198 | 75.833 | 75.516 | Core 5 | 73.5 - 78.5 | 5 | 5 | 100 | 194 | 51 | 893.5 |

| **North Standard Picking** | | | | | | | | |
|---|---|---|---|---|---|---|---|---|
| First Arrivals & Elastic Prop. | | | | | | | | |
| | Avg. Dpt. (ft.) | lbf | P-Vel (m/s) | S-Vel (m/s) | Poisson's Ratio | Youngs (MPa) | Bulk (MPa) | Shear (Mpa) |
| RN8 | 75.516 | RN8-30 | 10199 | 1941 | 0.48 | 25164 | 223203 | 8495 |
| | | RN8-240 | 10250 | 2092 | 0.48 | 29185 | 223693 | 9871 |
| | | RN8-480 | 10563 | 2096 | 0.48 | 29299 | 238364 | 9901 |

| **North Altered picking** | | | | | | | | |
|---|---|---|---|---|---|---|---|---|
| Poisson's Point | | | | | | | | |
| | Avg. Dpt. (ft.) | lbf | P-Vel (m/s) | S-Vel (m/s) | Poisson's Ratio | Youngs (MPa) | Bulk (MPa) | Shear (Mpa) |
| RN8 | 75.51563 | RN8-30 | 3106 | 1941 | 0.18 | 20039 | 10423 | 8495 |
| | | RN8-240 | 3135 | 2092 | 0.10 | 21686 | 9000 | 9871 |
| | | RN8-480 | 3159 | 2096 | 0.11 | 21923 | 9299 | 9901 |

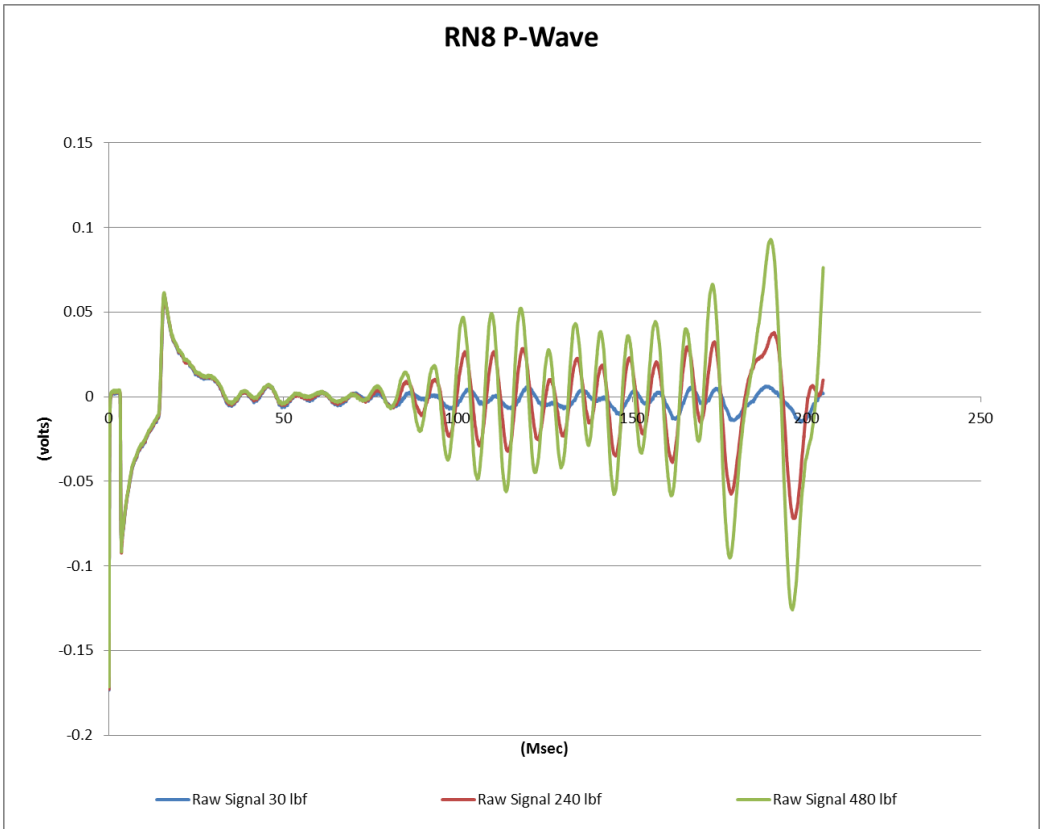
RN8 P-Wave
0.15
0.1
0.05
0
-0.05
-0.1
-0.15
-0.2
(volts)
0
50
100
150
200
250
(Msec)
Raw Signal 30 lbf
Raw Signal 240 lbf
Raw Signal 480 lbf

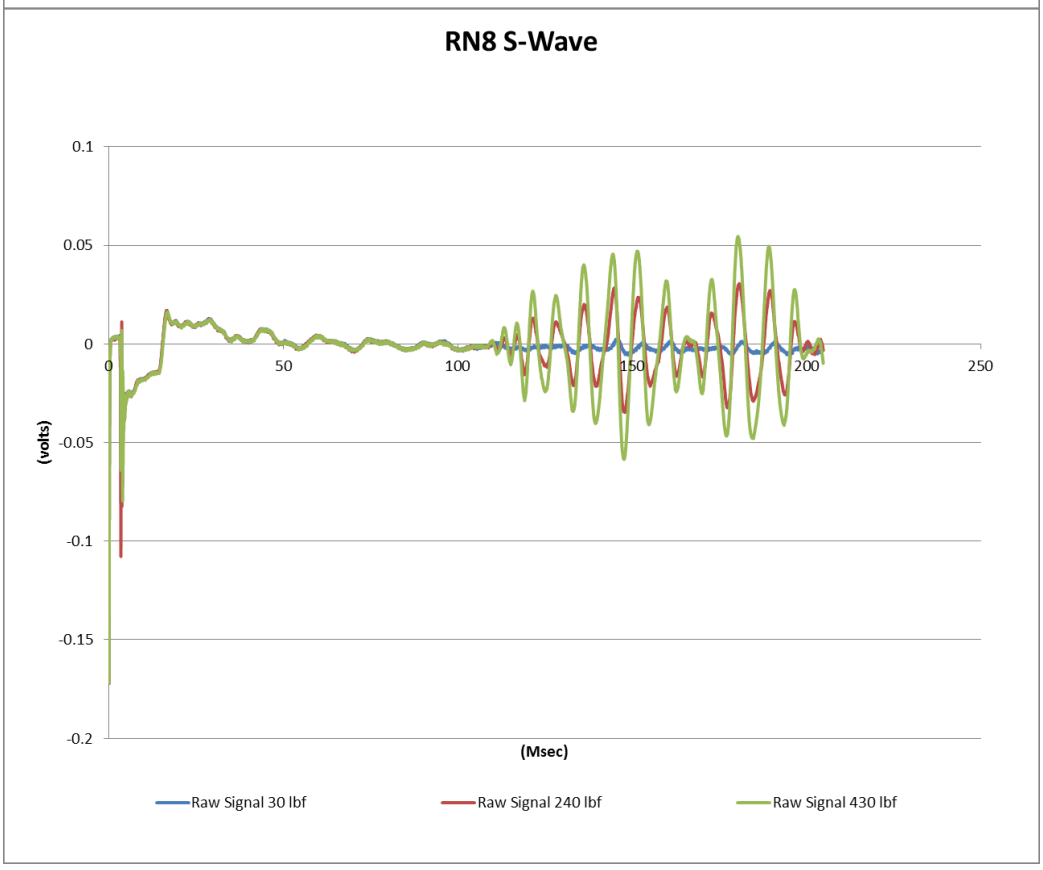
RN8 S-Wave
0.1
0.05
0
-0.05
-0.1
-0.15
-0.2
(volts)
0
50
100
150
200
250
(Msec)
Raw Signal 30 lbf
Raw Signal 240 lbf
Raw Signal 430 lbf

**RN9**

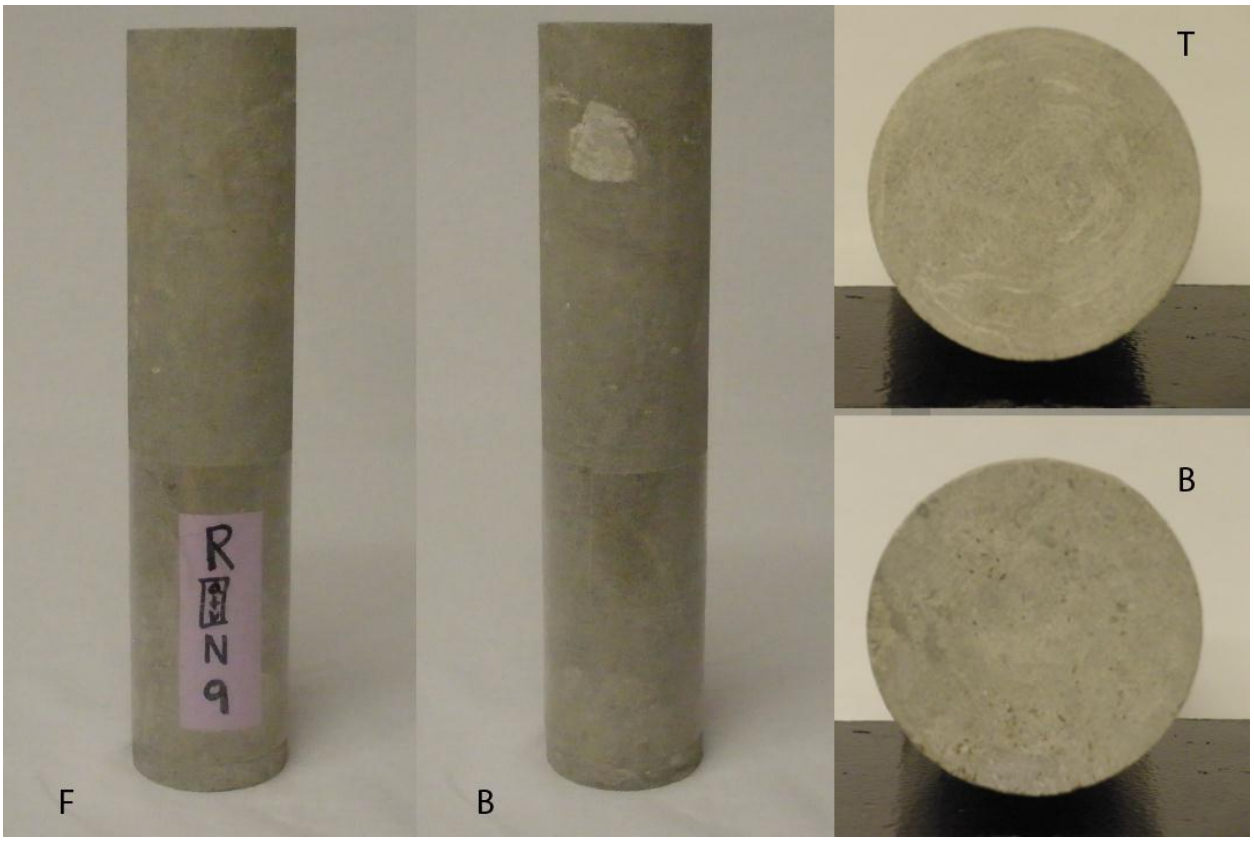


| North (Ogden, Riley CTY) Physical Properties of Cores | | | | | | | | | | | | | | |
|---|---|---|---|---|---|---|---|---|---|---|---|---|---|---|
| ID | Density (g/cm^3) | Lt. (in.) | Dia. (in.) | Top dpt. (ft.) | Bot. dpt. (ft.) | Avg. dpt. (ft) | Core Set | Core set dpt. | C | R | RQD | Lt. (mm) | Dia. (mm) | Mass (g) |
| RN9 | 2.26 | 9.250 | 2.00 | 75.833 | 76.604 | 76.219 | Core 5 | 73.5 - 78.5 | 5 | 5 | 100 | 233.5 | 51 | 1076.3 |

| **North Standard Picking** | | | | | | | | |
|---|---|---|---|---|---|---|---|---|
| First Arrivals & Elastic Prop. | | | | | | | | |
| | Avg. Dpt. (ft.) | lbf | P-Vel (m/s) | S-Vel (m/s) | Poisson's Ratio | Youngs (MPa) | Bulk (MPa) | Shear (Mpa) |
| RN9 | 76.219 | RN9-30 | 12039 | 1786 | 0.49 | 21435 | 317431 | 7199 |
| | | RN9-240 | 12119 | 1846 | 0.49 | 22894 | 321157 | 7692 |
| | | RN9-480 | 12276 | 1903 | 0.49 | 24324 | 329133 | 8175 |

| **North Altered picking** | | | | | | | | |
|---|---|---|---|---|---|---|---|---|
| Poisson's Point | | | | | | | | |
| | Avg. Dpt. (ft.) | lbf | P-Vel (m/s) | S-Vel (m/s) | Poisson's Ratio | Youngs (MPa) | Bulk (MPa) | Shear (Mpa) |
| RN9 | 76.21878 | RN9-30 | 3136 | 1786 | 0.26 | 18140 | 12592 | 7199 |
| | | RN9-240 | 3113 | 1846 | 0.23 | 18902 | 11610 | 7692 |
| | | RN9-480 | 3102 | 1903 | 0.20 | 19590 | 10817 | 8175 |

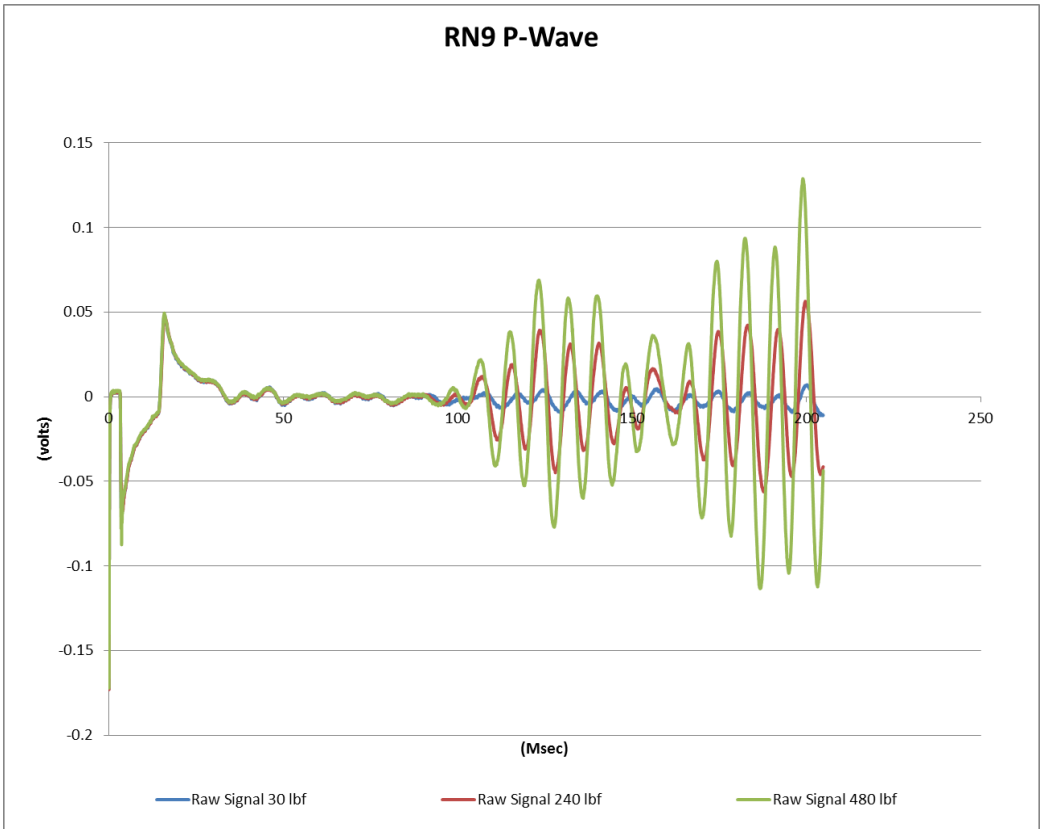
RN9 P-Wave
0.15
0.1
0.05
0
-0.05
-0.1
-0.15
-0.2
(volts)
0
50
100
150
200
250
(Msec)
Raw Signal 30 lbf
Raw Signal 240 lbf
Raw Signal 480 lbf

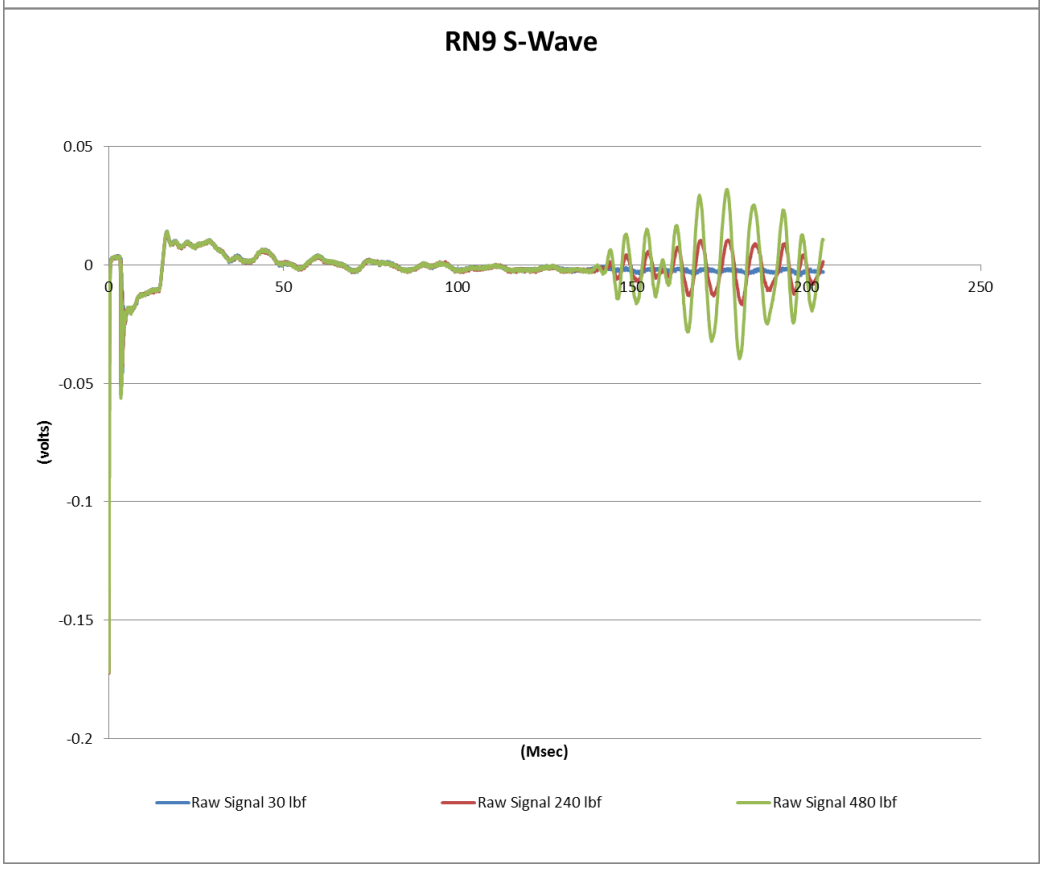
RN9 S-Wave
0.05
0
-0.05
-0.1
-0.15
-0.2
(volts)
0
50
100
150
200
250
(Msec)
Raw Signal 30 lbf
Raw Signal 240 lbf
Raw Signal 480 lbf

**RN10**

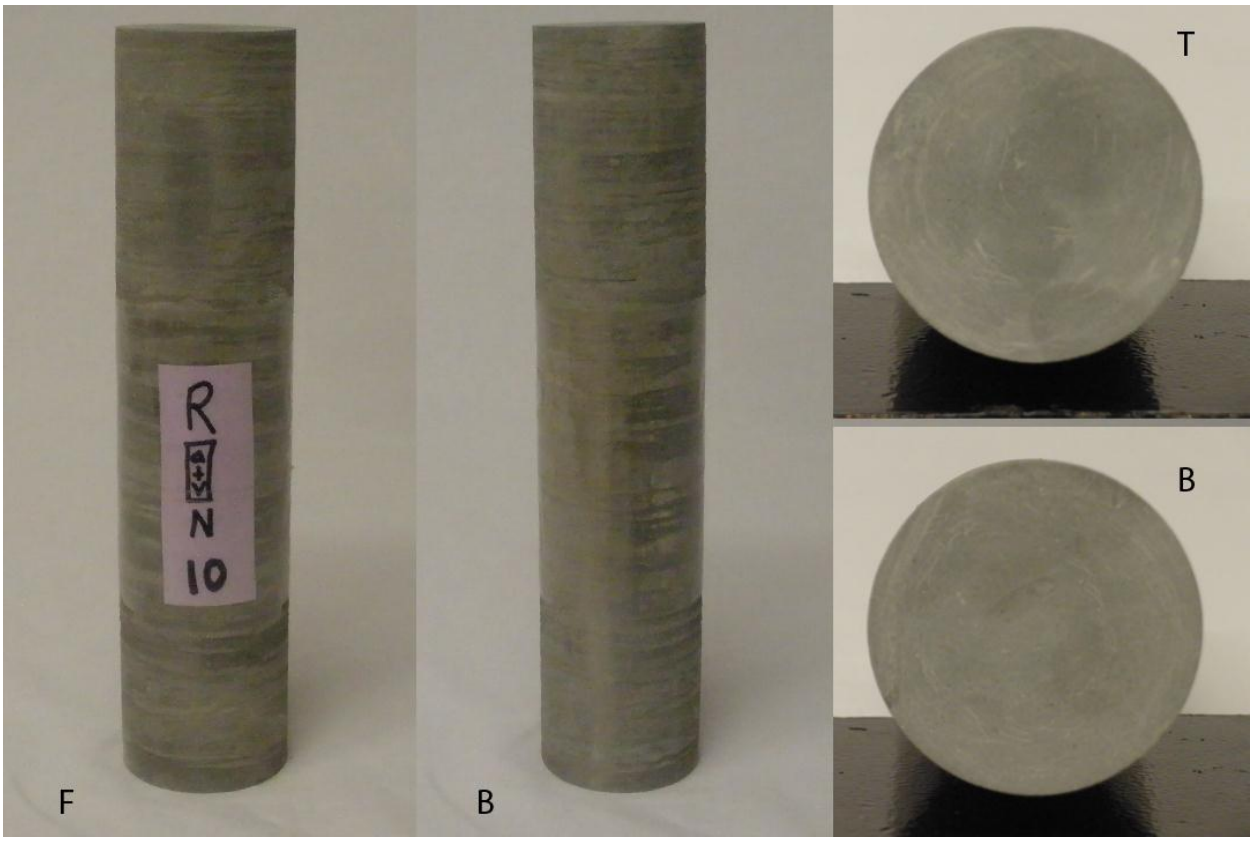


| North (Ogden, Riley CTY) Physical Properties of Cores | | | | | | | | | | | | | | |
|---|---|---|---|---|---|---|---|---|---|---|---|---|---|---|
| ID | Density (g/cm^3) | Lt. (in.) | Dia. (in.) | Top dpt. (ft.) | Bot. dpt. (ft.) | Avg. dpt. (ft) | Core Set | Core set dpt. | C | R | RQD | Lt. (mm) | Dia. (mm) | Mass (g) |
| RN10 | 2.27 | 8.688 | 2.00 | 77.609 | 78.333 | 77.971 | Core 5 | 73.5 - 78.5 | 5 | 5 | 100 | 220 | 51 | 1019.5 |

Waveform unsuitable for picking

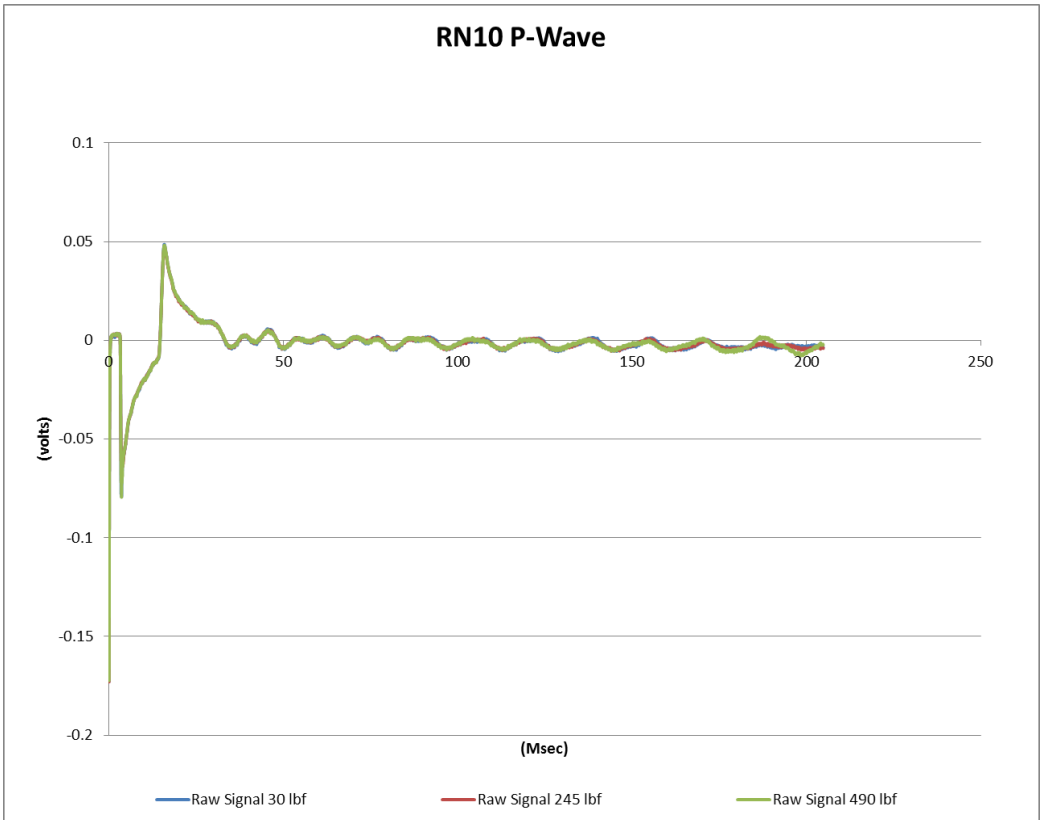
RN10 P-Wave
0.1
0.05
0
-0.05
-0.1
-0.15
-0.2
0
50
100
150
200
250
(volts)
(Msec)
Raw Signal 30 lbf
Raw Signal 245 lbf
Raw Signal 490 lbf

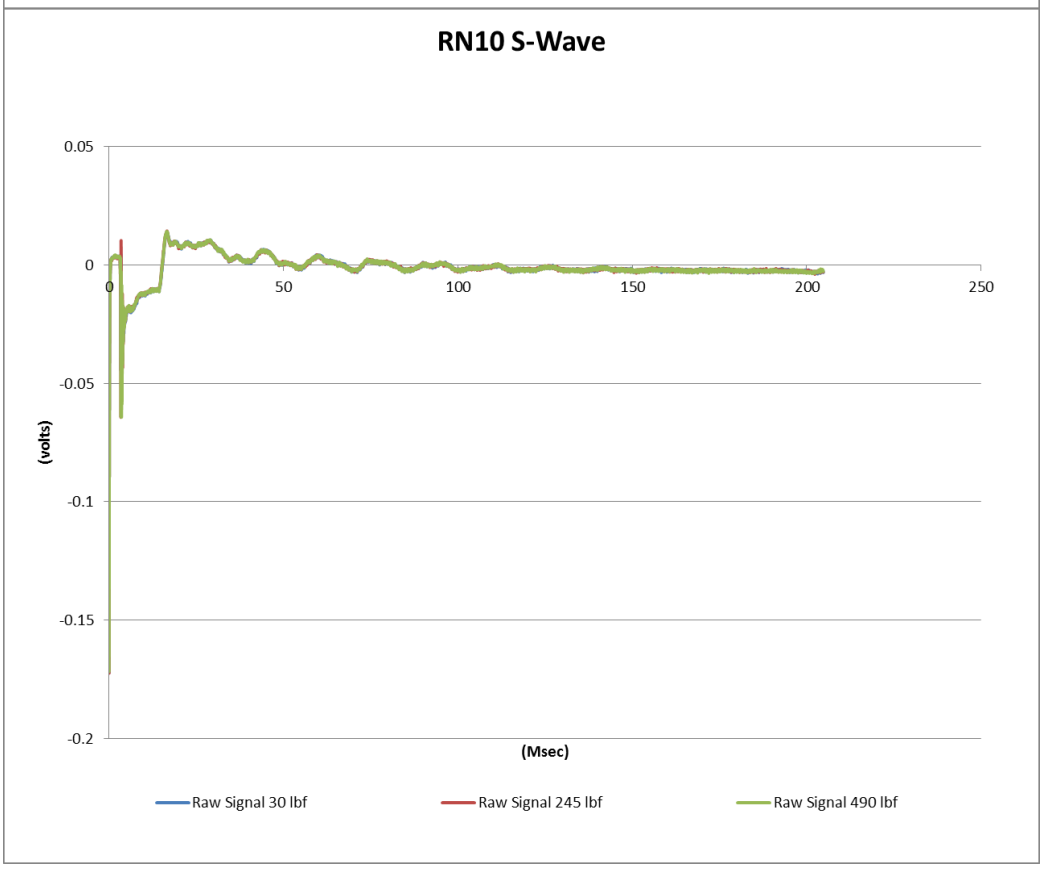
RN10 S-Wave
0.05
0
-0.05
-0.1
-0.15
-0.2
0
50
100
150
200
250
(volts)
(Msec)
Raw Signal 30 lbf
Raw Signal 245 lbf
Raw Signal 490 lbf

## NORTH {KDOT South Borehole} (Ogden, Riley Country)

| South (Ogden, Riley CTY)Physical Properties of Cores | | | | | | | | | | | | | | |
|---|---|---|---|---|---|---|---|---|---|---|---|---|---|---|
| ID | Density ($g/cm^3$) | Lt. (in.) | Dia. (in.) | Top dpt. (ft.) | Bot. dpt. (ft.) | Avg. dpt. (ft) | Core Set | Core set dpt. | C | R | RQD | Lt. (mm) | Dia. (mm) | Mass (g) |
| RS1 | 1.59 | 5.875 | 2.00 | 63.150 | 63.640 | 63.395 | Core 2 | 63.4 - 68.4 | 5 | 5 | 4.2/5.0 | 148 | 51 | 482.0 |
| RS2 | 2.19 | 9.375 | 2.00 | 65.817 | 66.598 | 66.207 | Core 2 | 63.4 - 68.4 | 5 | 5 | 4.2/5.0 | 238.5 | 51 | 1066.5 |
| RS3 | 2.19 | 11.218 | 2.00 | 67.465 | 68.400 | 67.936 | Core 2 | 63.4 - 68.4 | 5 | 5 | 4.2/5.0 | 284 | 51 | 1273.2 |
| RS4 | 2.37 | 4.3125 | 2.00 | 70.067 | 70.420 | 70.246 | Core 3 | 68.4 - 73.4 | 5 | 5 | 3.6/5.0 | 109.5 | 51 | 530.0 |
| RS5 | 2.34 | 4.75 | 2.00 | 71.650 | 72.046 | 71.848 | Core 3 | 68.4 - 73.4 | 5 | 5 | 3.6/5.0 | 120 | 51 | 573.4 |
| RS7 | 2.05 | 5.6875 | 2.00 | 75.192 | 75.666 | 75.429 | Core 4 | 73.4 - 78.4 | 5 | 5 | 100% | 144 | 51 | 602.8 |
| RS8 | 2.24 | 8.1875 | 2.00 | 77.509 | 78.192 | 77.851 | Core 4 | 73.4 - 78.4 | 5 | 5 | 100% | 207 | 51 | 947.4 |

| **South Standard Picking** | | | | | | | | |
|---|---|---|---|---|---|---|---|---|
| First Arrivals & Elastic Prop. | | | | | | | | |
| | Avg. Dpt. (ft.) | lbf | P-Vel (m/s) | S-Vel (m/s) | Poisson's Ratio | Young's (MPa) | Bulk (MPa) | Shear (Mpa) |
| RS2 | 66.2072917 | RS2 30 | 11979 | 1609 | 0.49 | 16904 | 306533 | 5669 |
| | | RS2 210 | 12035 | 1623 | 0.49 | 17187 | 309380 | 5765 |
| | | RS2 420 | 12057 | 1626 | 0.49 | 17245 | 310481 | 5784 |
| RS4 | 70.2463542 | RS4 30 | 5757 | 2544 | 0.38 | 42275 | 58080 | 15332 |
| | | RS4 220 | 5814 | 2552 | 0.38 | 42613 | 59515 | 15432 |
| | | RS4 440 | 5850 | 2559 | 0.38 | 42878 | 60395 | 15517 |
| RS5 | 71.8479167 | RS5 30 | 6278 | 2396 | 0.41 | 37984 | 74290 | 13424 |
| | | RS5 225 | 6336 | 2407 | 0.42 | 38366 | 75838 | 13550 |
| | | RS5 450 | 6640 | 2436 | 0.42 | 39483 | 84626 | 13881 |
| RS7 | 75.4286458 | RS7 30 | 7424 | 1971 | 0.46 | 23268 | 102345 | 7957 |
| | | RS7 235 | 7506 | 1988 | 0.46 | 23694 | 104646 | 8102 |
| | | RS7 470 | 7679 | 1993 | 0.46 | 23823 | 109990 | 8139 |
| RS8 | 77.8505208 | RS8 30 | 10705 | 1746 | 0.49 | 20305 | 247634 | 6830 |
| | | RS8 245 | 10803 | 1892 | 0.48 | 23799 | 250776 | 8018 |
| | | RS8 490 | 10816 | 1905 | 0.48 | 24135 | 251263 | 8132 |

| **South Altered picking** | | | | | | | | |
|---|---|---|---|---|---|---|---|---|
| Poisson's Point | | | | | | | | |
| | Avg. Dpt. (ft.) | lbf | P-Vel (m/s) | S-Velo (m/s) | Poisson's Ratio | Young's (MPa) | Bulk (MPa) | Shear (Mpa) |
| RS2 | 66.20729 | RS2 30 | 2968 | 1609 | 0.29 | 14646 | 11718 | 5669 |
| | | RS2 210 | 2972 | 1623 | 0.29 | 14845 | 11647 | 5764 |
| | | RS2 420 | 2984 | 1626 | 0.29 | 14911 | 11780 | 5784 |
| RS4 | 70.24635 | RS4 30 | 4638 | 2544 | 0.29 | 39399 | 30528 | 15331 |
| | | RS4 220 | 4685 | 2552 | 0.29 | 39783 | 31420 | 15432 |
| | | RS4 440 | 4704 | 2559 | 0.29 | 40029 | 31750 | 15516 |
| RS5 | 71.84792 | RS5 30 | 4404 | 2396 | 0.29 | 34620 | 27467 | 13424 |
| | | RS5 225 | 4425 | 2407 | 0.29 | 34957 | 27731 | 13550 |
| | | RS5 450 | 4420 | 2436 | 0.28 | 35584 | 27179 | 13880 |
| RS7 | 75.42865 | RS7 30 | 3759 | 1971 | 0.31 | 20856 | 18346 | 7957 |
| | | RS7 235 | 3765 | 1988 | 0.31 | 21171 | 18242 | 8101 |
| | | RS7 470 | 3789 | 1993 | 0.31 | 21303 | 18570 | 8138 |
| RS8 | 77.85052 | RS8 30 | 3517 | 1746 | 0.31 | 17919 | 15862 | 6830 |
| | | RS8 245 | 3325 | 1892 | 0.26 | 20214 | 14073 | 8017 |
| | | RS8 490 | 3319 | 1905 | 0.25 | 20399 | 13837 | 8131 |

**RS1**

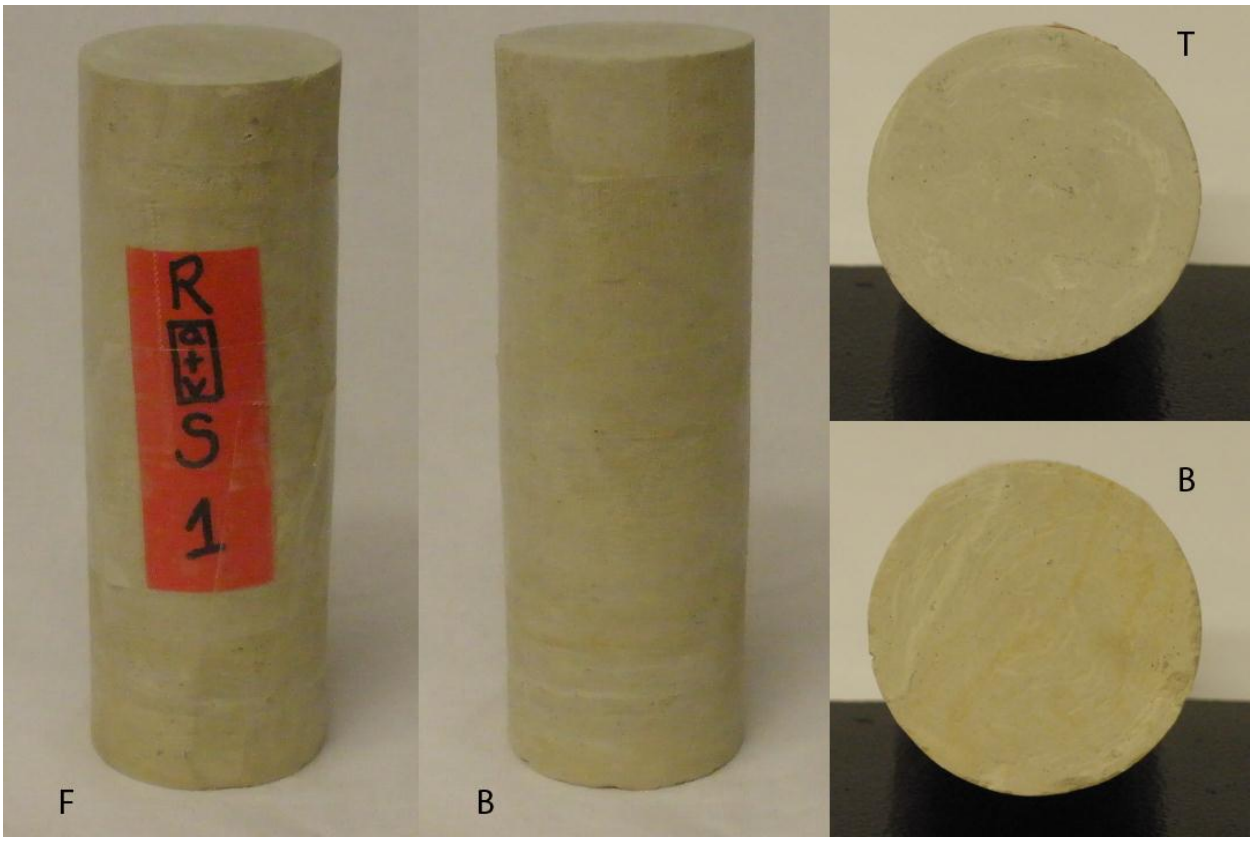


| South (Ogden, Riley CTY)Physical Properties of Cores | | | | | | | | | | | | | | |
|---|---|---|---|---|---|---|---|---|---|---|---|---|---|---|
| ID | Density ($g/cm^3$) | Lt. (in.) | Dia. (in.) | Top dpt. (ft.) | Bot. dpt. (ft.) | Avg. dpt. (ft) | Core Set | Core set dpt. | C | R | RQD | Lt. (mm) | Dia. (mm) | Mass (g) |
| RS1 | 1.59 | 5.875 | 2.00 | 63.150 | 63.640 | 63.395 | Core 2 | 63.4 - 68.4 | 5 | 5 | 4.2/5.0 | 148 | 51 | 482.0 |

Waveform unsuitable for picking

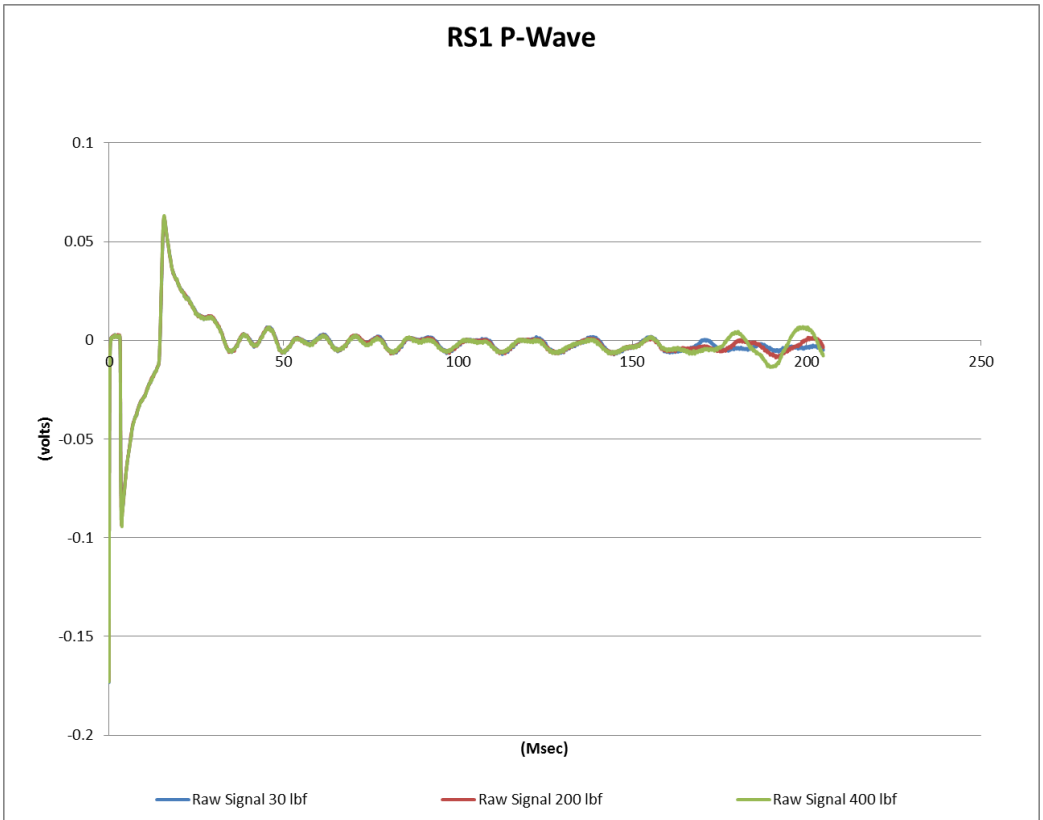
RS1 P-Wave
0.1
0.05
0
-0.05
-0.1
-0.15
-0.2
(volts)
0
50
100
150
200
250
(Msec)
Raw Signal 30 lbf
Raw Signal 200 lbf
Raw Signal 400 lbf

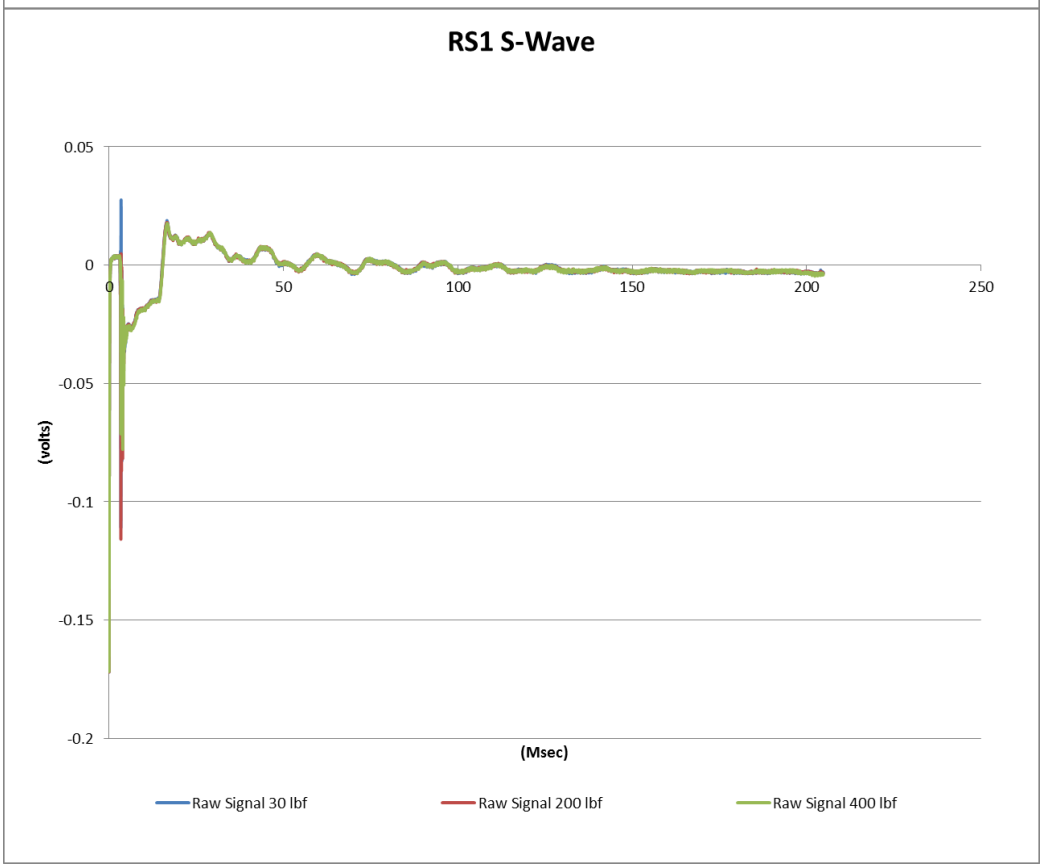
RS1 S-Wave
0.05
0
-0.05
-0.1
-0.15
-0.2
(volts)
0
50
100
150
200
250
(Msec)
Raw Signal 30 lbf
Raw Signal 200 lbf
Raw Signal 400 lbf

## RS2

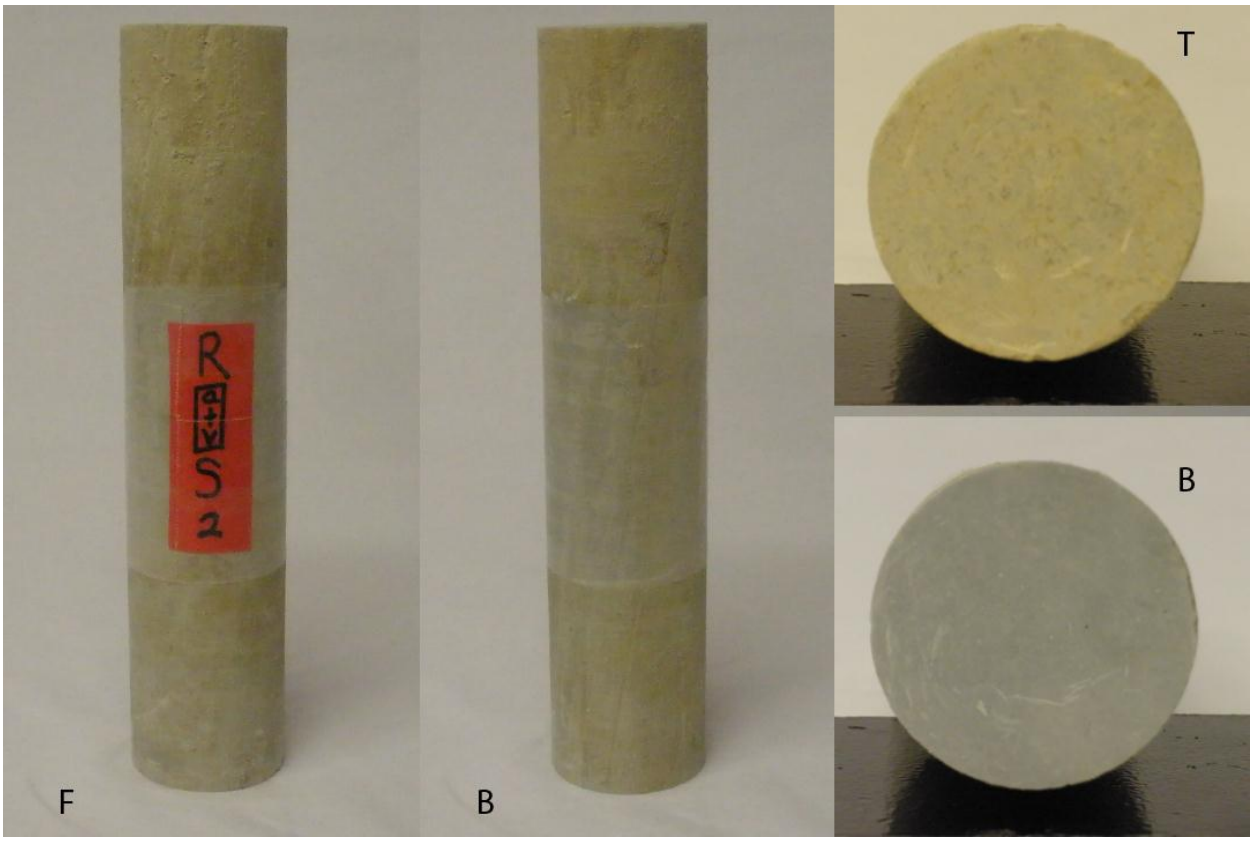


| South (Ogden, Riley CTY)Physical Properties of Cores | | | | | | | | | | | | | | |
|---|---|---|---|---|---|---|---|---|---|---|---|---|---|---|
| ID | Density ($g/cm^3$) | Lt. (in.) | Dia. (in.) | Top dpt. (ft.) | Bot. dpt. (ft.) | Avg. dpt. (ft) | Core Set | Core set dpt. | C | R | RQD | Lt. (mm) | Dia. (mm) | Mass (g) |
| RS2 | 2.19 | 9.375 | 2.00 | 65.817 | 66.598 | 66.207 | Core 2 | 63.4 - 68.4 | 5 | 5 | 4.2/5.0 | 238.5 | 51 | 1066.5 |

| **South Standard Picking** | | | | | | | | |
|---|---|---|---|---|---|---|---|---|
| First Arrivals & Elastic Prop. | | | | | | | | |
| | Avg. Dpt. (ft.) | lbf | P-Vel (m/s) | S-Vel (m/s) | Poisson's Ratio | Young's (MPa) | Bulk (MPa) | Shear (Mpa) |
| RS2 | 66.2072917 | RS2 30 | 11979 | 1609 | 0.49 | 16904 | 306533 | 5669 |
| | | RS2 210 | 12035 | 1623 | 0.49 | 17187 | 309380 | 5765 |
| | | RS2 420 | 12057 | 1626 | 0.49 | 17245 | 310481 | 5784 |

| **South Altered picking** | | | | | | | | |
|---|---|---|---|---|---|---|---|---|
| Poisson's Point | | | | | | | | |
| | Avg. Dpt. (ft.) | lbf | P-Vel (m/s) | S-Vel (m/s) | Poisson's Ratio | Young's (MPa) | Bulk (MPa) | Shear (Mpa) |
| RS2 | 66.20729 | RS2 30 | 2968 | 1609 | 0.29 | 14646 | 11718 | 5669 |
| | | RS2 210 | 2972 | 1623 | 0.29 | 14845 | 11647 | 5765 |
| | | RS2 420 | 2984 | 1626 | 0.29 | 14911 | 11780 | 5784 |

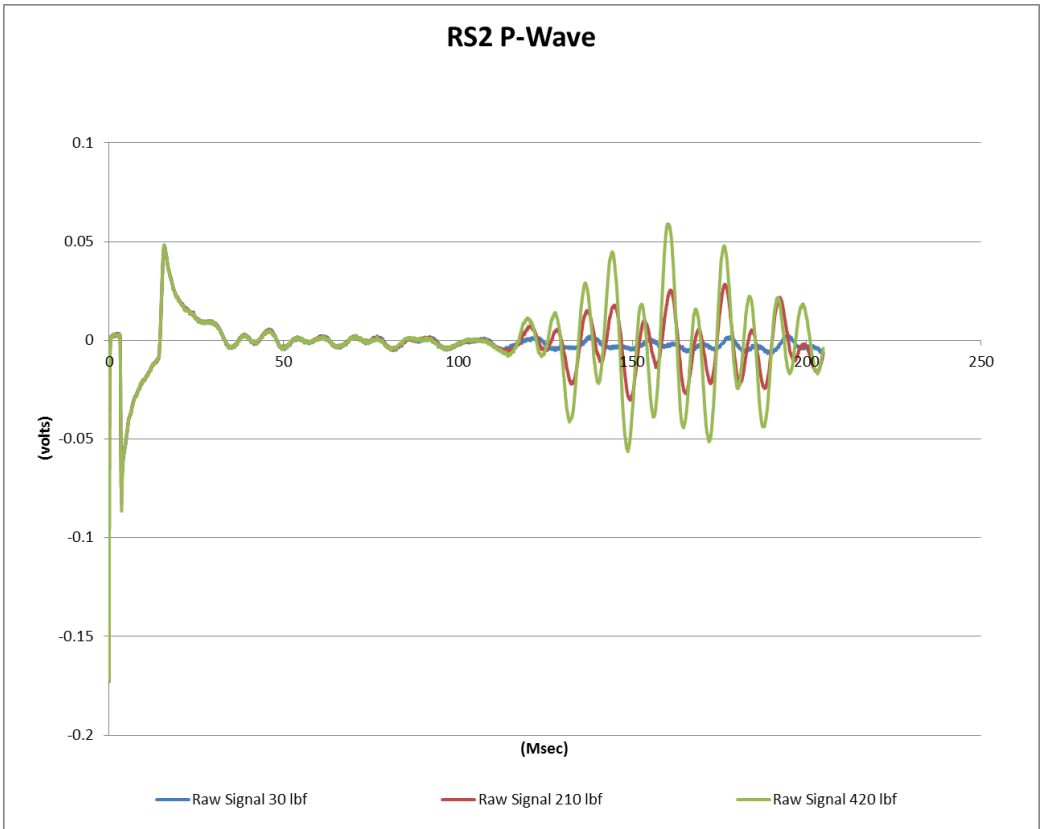
RS2 P-Wave
0.1
0.05
0
-0.05
-0.1
-0.15
-0.2
(volts)
0
50
100
150
200
250
(Msec)
Raw Signal 30 lbf
Raw Signal 210 lbf
Raw Signal 420 lbf

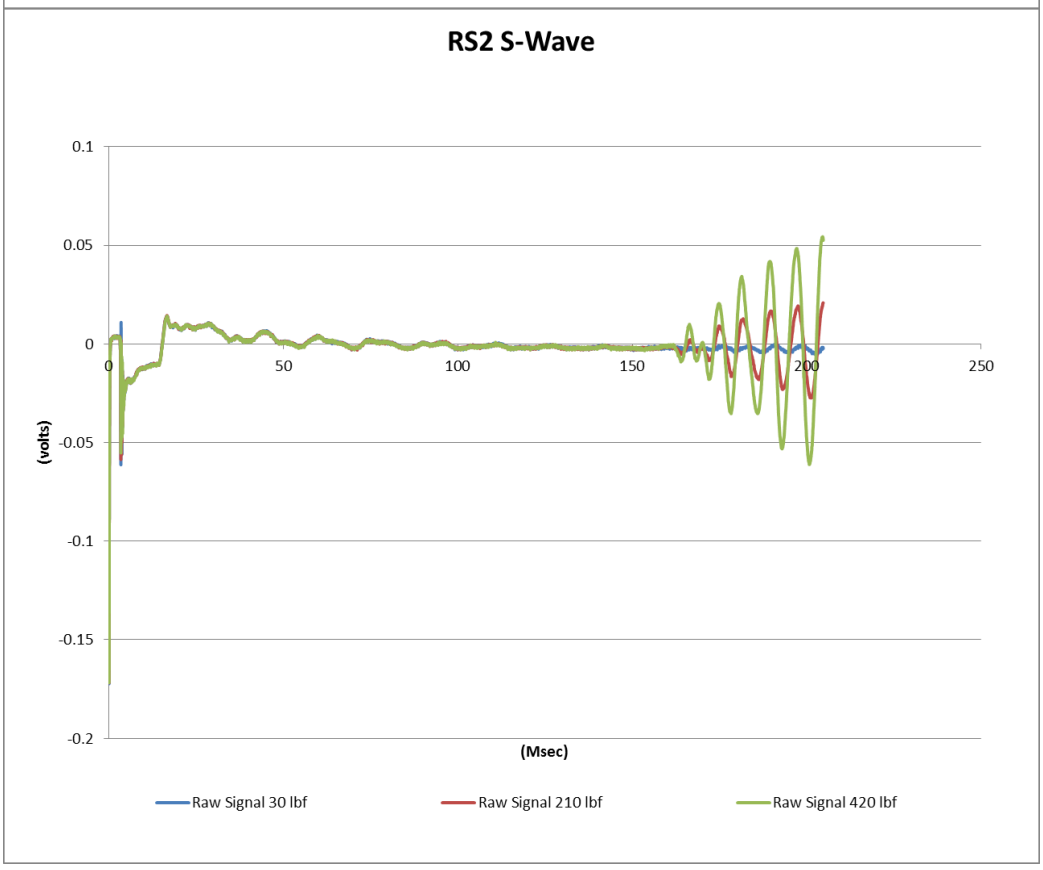
RS2 S-Wave
0.1
0.05
0
-0.05
-0.1
-0.15
-0.2
(volts)
0
50
100
150
200
250
(Msec)
Raw Signal 30 lbf
Raw Signal 210 lbf
Raw Signal 420 lbf

**RS3**

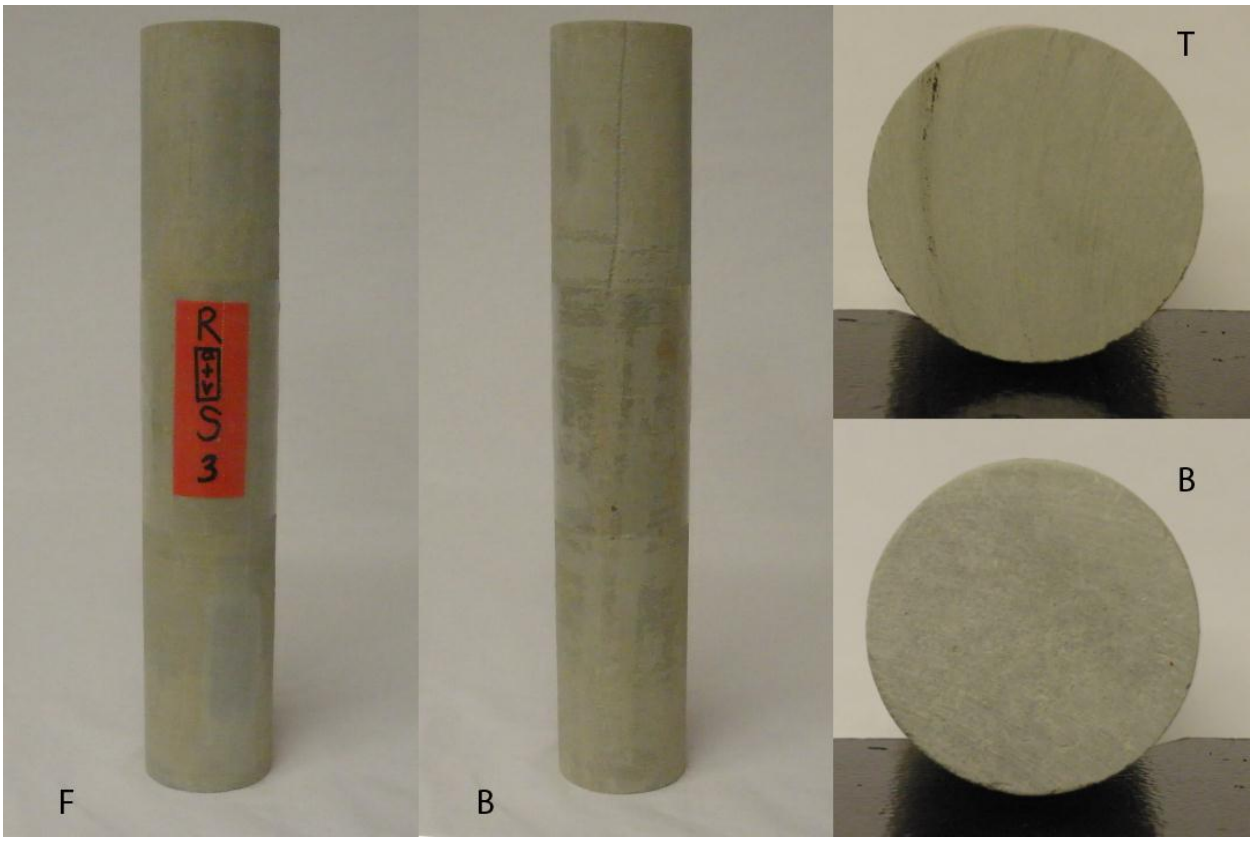


| South (Ogden, Riley CTY)Physical Properties of Cores | | | | | | | | | | | | | | |
|---|---|---|---|---|---|---|---|---|---|---|---|---|---|---|
| ID | Density ($g/cm^3$) | Lt. (in.) | Dia. (in.) | Top dpt. (ft.) | Bot. dpt. (ft.) | Avg. dpt. (ft) | Core Set | Core set dpt. | C | R | RQD | Lt. (mm) | Dia. (mm) | Mass (g) |
| RS3 | 2.19 | 11.21 | 2.00 | 67.465 | 68.400 | 67.936 | Core 2 | 63.4 - 68.4 | 5 | 5 | 4.2/5.0 | 284 | 51 | 1273.2 |

Waveform unsuitable for picking

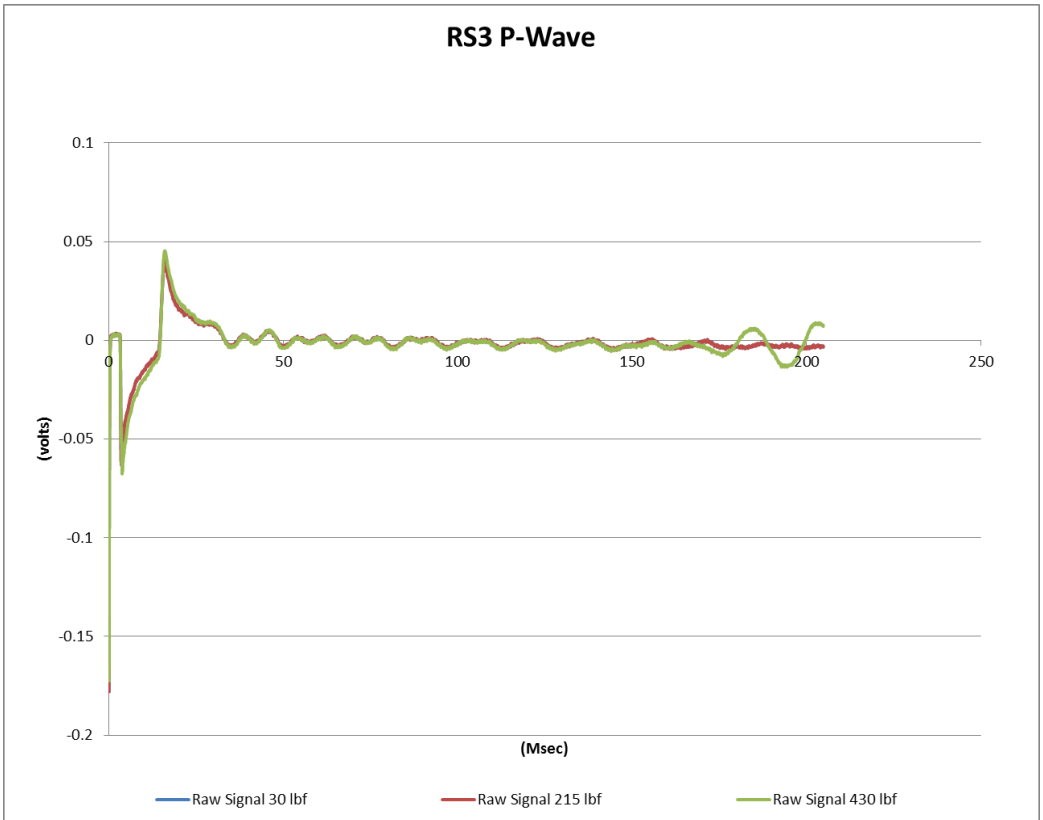
RS3 P-Wave
0.1
0.05
0
-0.05
-0.1
-0.15
-0.2
0
50
100
150
200
250
(volts)
(Msec)
Raw Signal 30 lbf
Raw Signal 215 lbf
Raw Signal 430 lbf

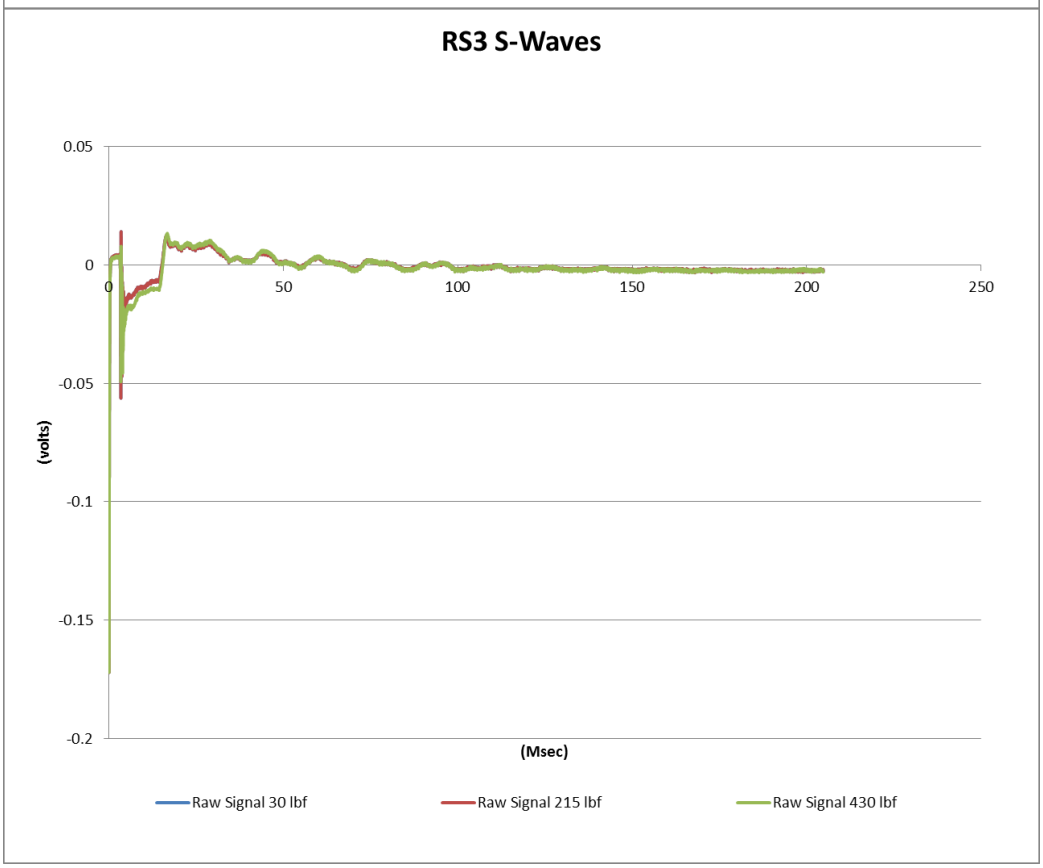
RS3 S-Waves
0.05
0
-0.05
-0.1
-0.15
-0.2
0
50
100
150
200
250
(volts)
(Msec)
Raw Signal 30 lbf
Raw Signal 215 lbf
Raw Signal 430 lbf

**RS4**

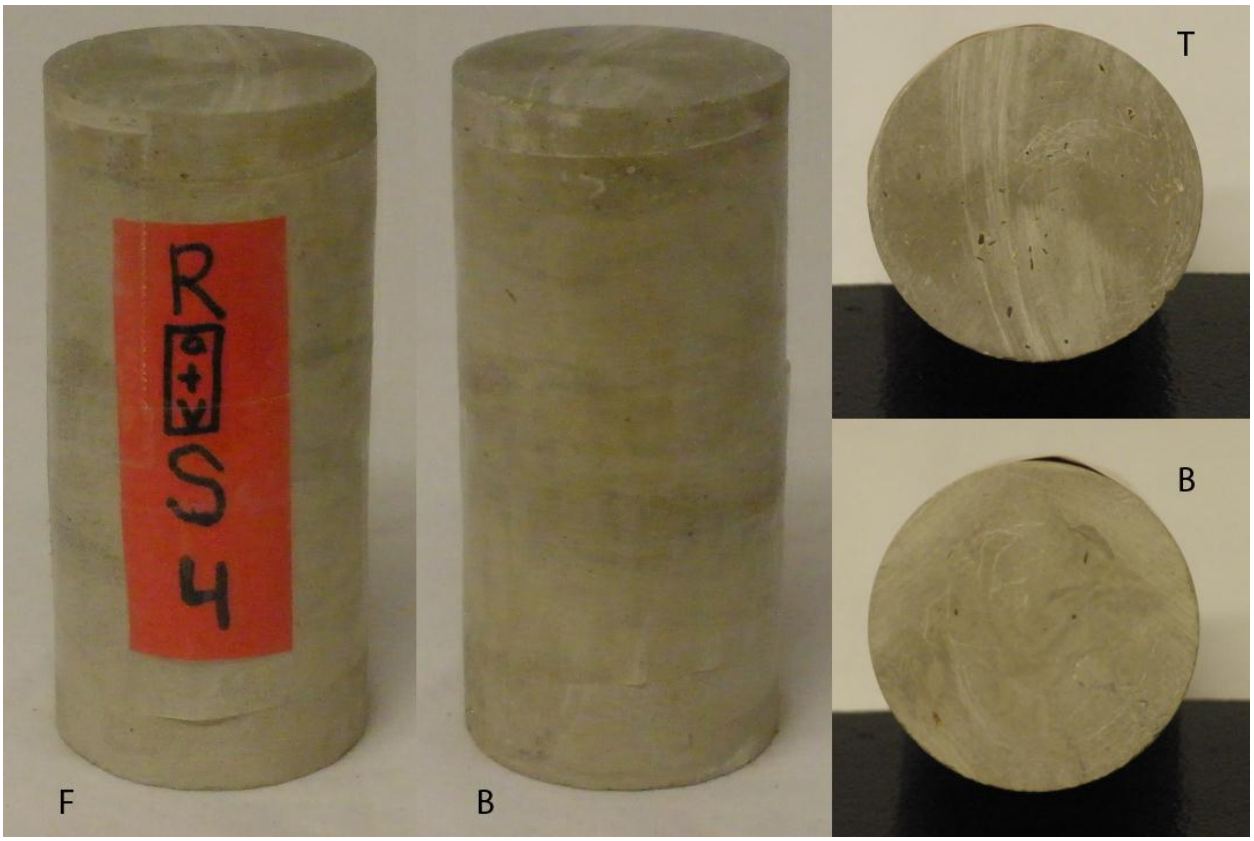


| South (Ogden, Riley CTY)Physical Properties of Cores | | | | | | | | | | | | | | |
|---|---|---|---|---|---|---|---|---|---|---|---|---|---|---|
| ID | Density ($g/cm^3$) | Lt. (in.) | Dia. (in.) | Top dpt. (ft.) | Bot. dpt. (ft.) | Avg. dpt. (ft) | Core Set | Core set dpt. | C | R | RQD | Lt. (mm) | Dia. (mm) | Mass (g) |
| RS4 | 2.37 | 4.3125 | 2.00 | 70.067 | 70.420 | 70.246 | Core 3 | 68.4 - 73.4 | 5 | 5 | 3.6/5.0 | 109.5 | 51 | 530.0 |

| **South Standard Picking** | | | | | | | | |
|---|---|---|---|---|---|---|---|---|
| First Arrivals & Elastic Prop. | | | | | | | | |
| | Avg. Dpt. (ft.) | lbf | P-Vel (m/s) | S-Vel (m/s) | Poisson's Ratio | Young's (MPa) | Bulk (MPa) | Shear (Mpa) |
| RS4 | 70.2463542 | RS4 30 | 5757 | 2544 | 0.38 | 42275 | 58080 | 15332 |
| | | RS4 220 | 5814 | 2552 | 0.38 | 42613 | 59515 | 15432 |
| | | RS4 440 | 5850 | 2559 | 0.38 | 42878 | 60395 | 15517 |

| **South Altered picking** | | | | | | | | |
|---|---|---|---|---|---|---|---|---|
| Poisson's Point | | | | | | | | |
| | Avg. Dpt. (ft.) | lbf | P-Vel (m/s) | S-Vel (m/s) | Poisson's Ratio | Young's (MPa) | Bulk (MPa) | Shear (Mpa) |
| RS4 | 70.24635 | RS4 30 | 4638 | 2544 | 0.29 | 39399 | 30528 | 15331 |
| | | RS4 220 | 4685 | 2552 | 0.29 | 39783 | 31420 | 15432 |
| | | RS4 440 | 4704 | 2559 | 0.29 | 40029 | 31750 | 15516 |

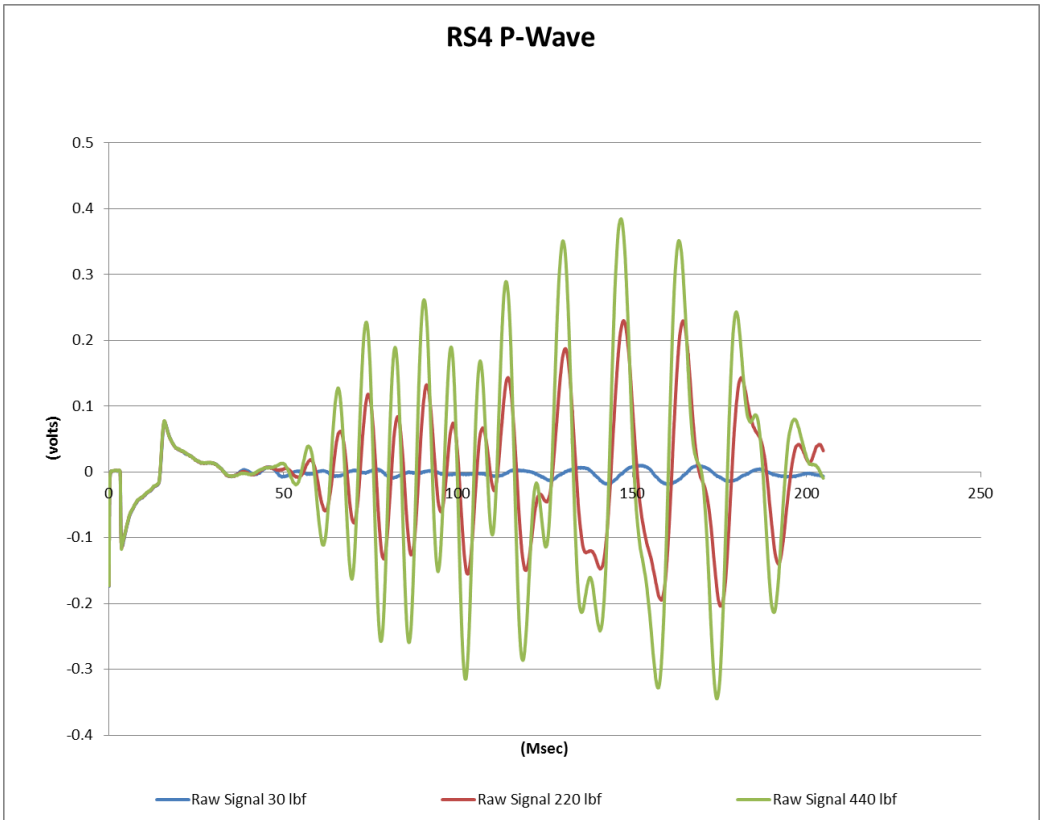
RS4 P-Wave
0.5
0.4
0.3
0.2
0.1
0
-0.1
-0.2
-0.3
-0.4
(volts)
0
50
100
150
200
250
(Msec)
Raw Signal 30 lbf
Raw Signal 220 lbf
Raw Signal 440 lbf

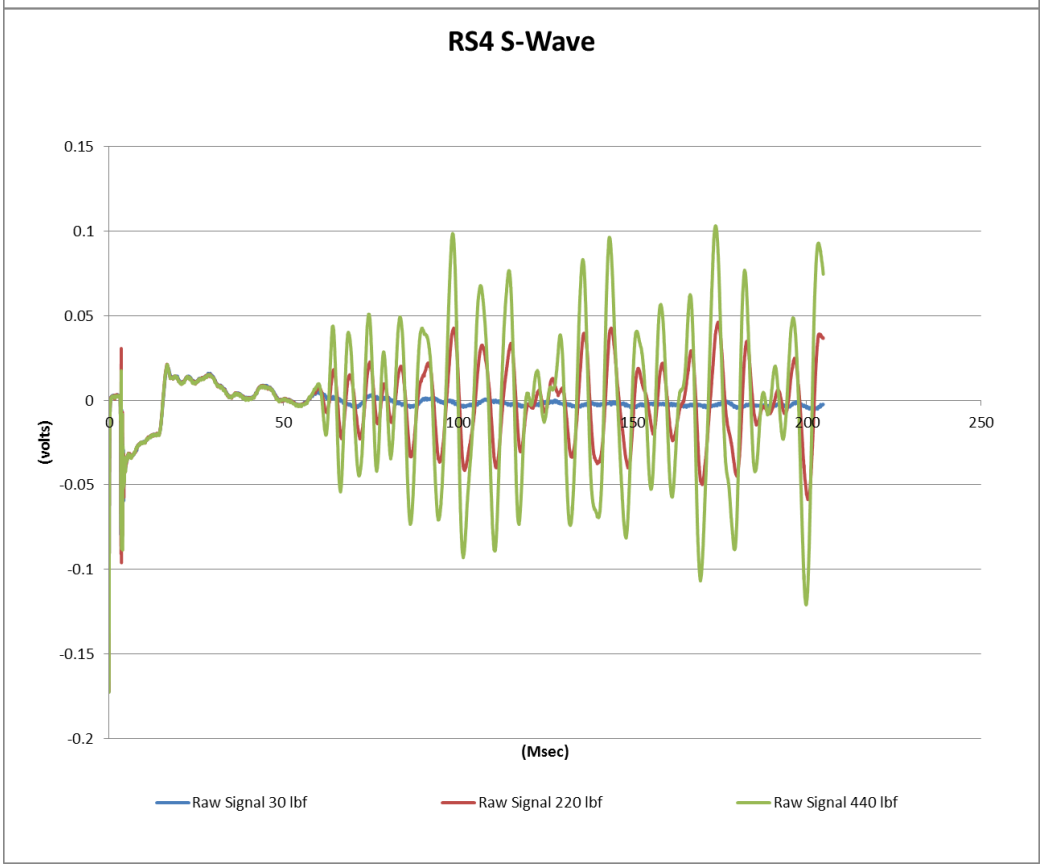
RS4 S-Wave
0.15
0.1
0.05
0
-0.05
-0.1
-0.15
-0.2
(volts)
0
50
100
150
200
250
(Msec)
Raw Signal 30 lbf
Raw Signal 220 lbf
Raw Signal 440 lbf

## RS5

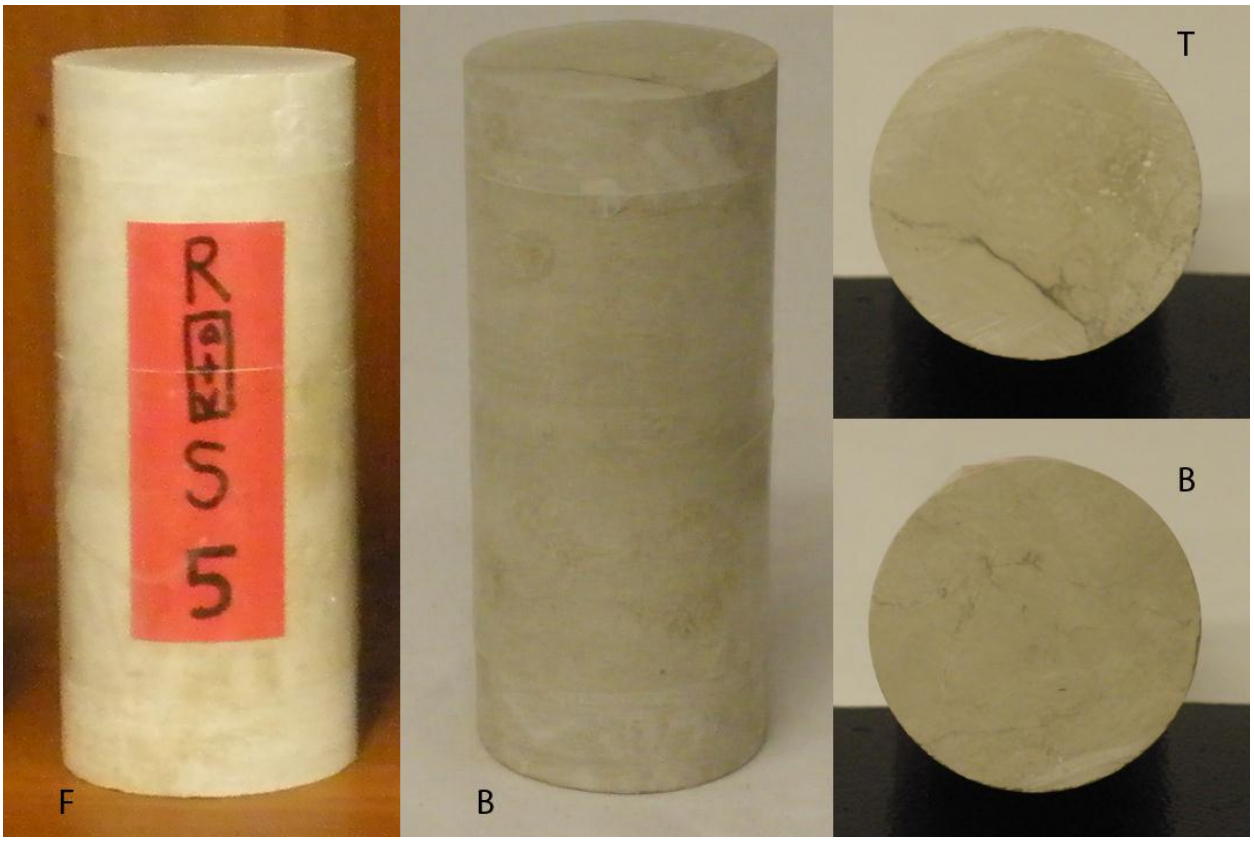


| South (Ogden, Riley CTY)Physical Properties of Cores | | | | | | | | | | | | | | |
|---|---|---|---|---|---|---|---|---|---|---|---|---|---|---|
| ID | Density ($g/cm^3$) | Lt. (in.) | Dia. (in.) | Top dpt. (ft.) | Bot. dpt. (ft.) | Avg. dpt. (ft) | Core Set | Core set dpt. | C | R | RQD | Lt. (mm) | Dia. (mm) | Mass (g) |
| RS5 | 2.34 | 4.75 | 2.00 | 71.650 | 72.046 | 71.848 | Core 3 | 68.4 - 73.4 | 5 | 5 | 3.6/5.0 | 120 | 51 | 573.4 |

| **South Standard Picking** | | | | | | | | |
|---|---|---|---|---|---|---|---|---|
| First Arrivals & Elastic Prop. | | | | | | | | |
| | Avg. Dpt. (ft.) | lbf | P-Vel (m/s) | S-Vel (m/s) | Poisson's Ratio | Young's (MPa) | Bulk (MPa) | Shear (Mpa) |
| RS5 | 71.8479167 | RS5 30 | 6278 | 2396 | 0.41 | 37984 | 74290 | 13424 |
| | | RS5 225 | 6336 | 2407 | 0.42 | 38366 | 75838 | 13550 |
| | | RS5 450 | 6640 | 2436 | 0.42 | 39483 | 84626 | 13881 |

| **South Altered picking** | | | | | | | | |
|---|---|---|---|---|---|---|---|---|
| Poisson's Point | | | | | | | | |
| | Avg. Dpt. (ft.) | lbf | P-Vel (m/s) | S-Vel (m/s) | Poisson's Ratio | Young's (MPa) | Bulk (MPa) | Shear (Mpa) |
| RS5 | 71.84792 | RS5 30 | 4404 | 2396 | 0.29 | 34620 | 27467 | 13424 |
| | | RS5 225 | 4425 | 2407 | 0.29 | 34957 | 27731 | 13550 |
| | | RS5 450 | 4420 | 2436 | 0.28 | 35584 | 27179 | 13880 |

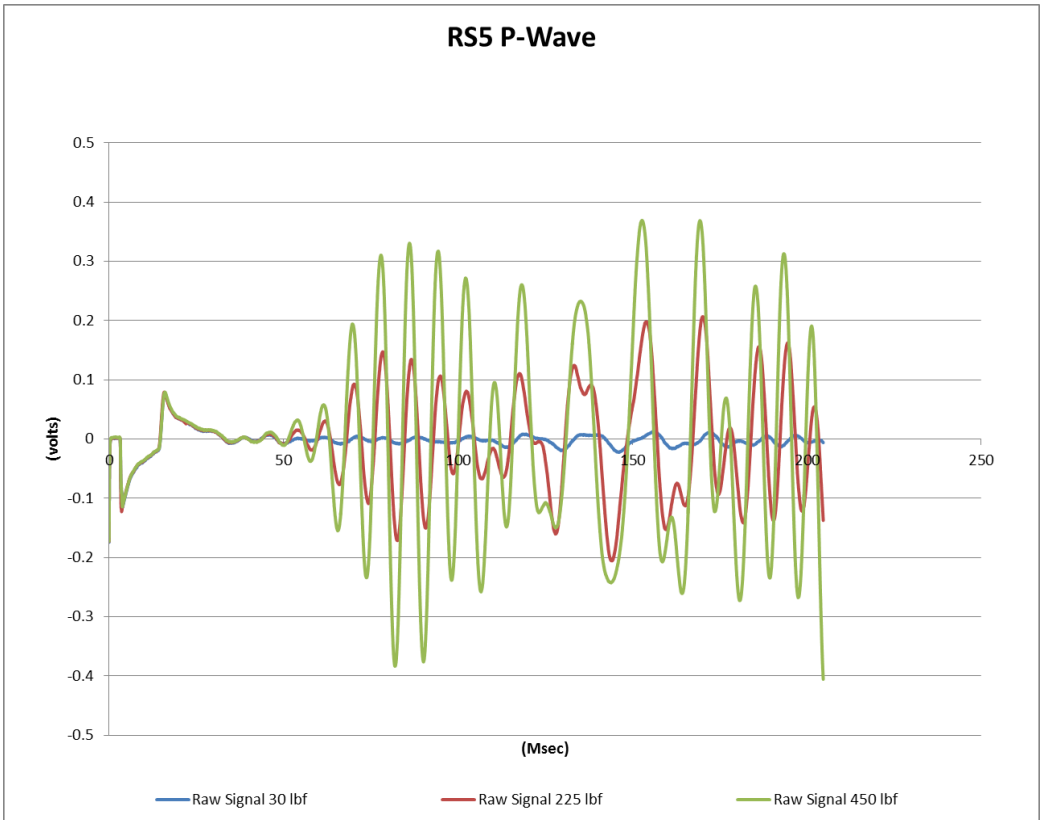
RS5 P-Wave
0.5
0.4
0.3
0.2
0.1
0
-0.1
-0.2
-0.3
-0.4
-0.5
(volts)
0
50
100
150
200
250
(Msec)
Raw Signal 30 lbf
Raw Signal 225 lbf
Raw Signal 450 lbf

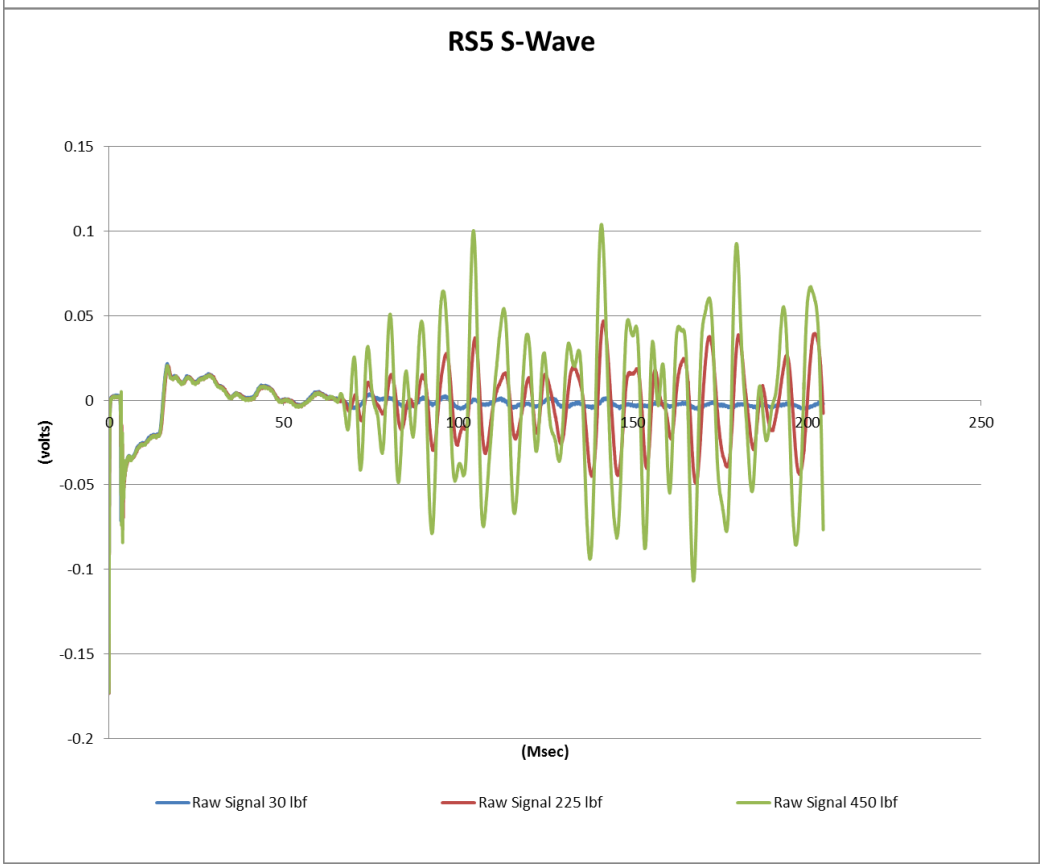
RS5 S-Wave
0.15
0.1
0.05
0
-0.05
-0.1
-0.15
-0.2
(volts)
0
50
100
150
200
250
(Msec)
Raw Signal 30 lbf
Raw Signal 225 lbf
Raw Signal 450 lbf

**RS7**

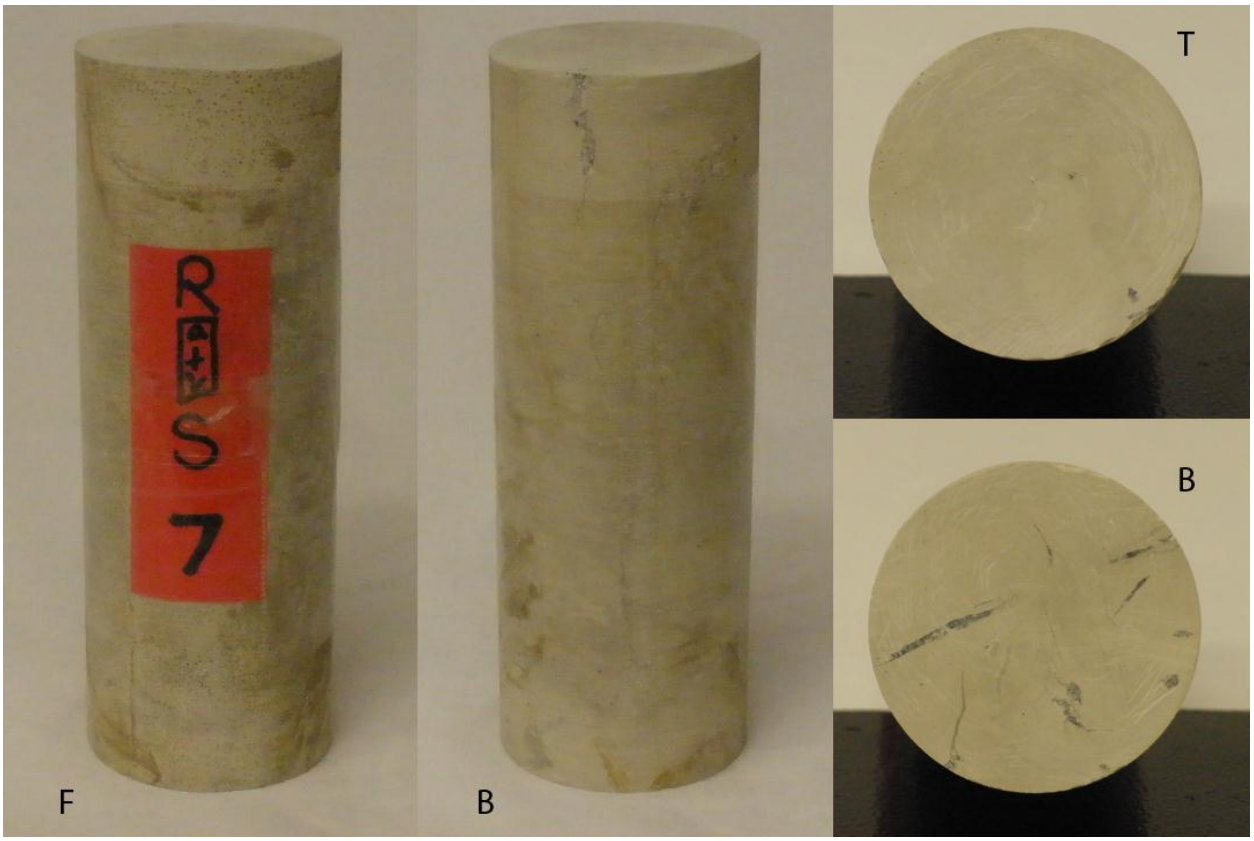


| South (Ogden, Riley CTY)Physical Properties of Cores | | | | | | | | | | | | | | |
|---|---|---|---|---|---|---|---|---|---|---|---|---|---|---|
| ID | Density ($g/cm^3$) | Lt. (in.) | Dia. (in.) | Top dpt. (ft.) | Bot. dpt. (ft.) | Avg. dpt. (ft) | Core Set | Core set dpt. | C | R | RQD | Lt. (mm) | Dia. (mm) | Mass (g) |
| RS7 | 2.05 | 5.6875 | 2.00 | 75.192 | 75.666 | 75.429 | Core 4 | 73.4 - 78.4 | 5 | 5 | 100% | 144 | 51 | 602.8 |

| **South Standard Picking** | | | | | | | | |
|---|---|---|---|---|---|---|---|---|
| First Arrivals & Elastic Prop. | | | | | | | | |
| | Avg. Dpt. (ft.) | lbf | P-Vel (m/s) | S-Vel (m/s) | Poisson's Ratio | Young's (MPa) | Bulk (MPa) | Shear (Mpa) |
| RS7 | 75.4286458 | RS7 30 | 7424 | 1971 | 0.46 | 23268 | 102345 | 7957 |
| | | RS7 235 | 7506 | 1988 | 0.46 | 23694 | 104646 | 8102 |
| | | RS7 470 | 7679 | 1993 | 0.46 | 23823 | 109990 | 8139 |

| **South Altered picking** | | | | | | | | |
|---|---|---|---|---|---|---|---|---|
| Poisson's Point | | | | | | | | |
| | Avg. Dpt. (ft.) | lbf | P-Vel (m/s) | S-Vel (m/s) | Poisson's Ratio | Young's (MPa) | Bulk (MPa) | Shear (Mpa) |
| RS7 | 75.42865 | RS7 30 | 3759 | 1971 | 0.31 | 20856 | 18346 | 7957 |
| | | RS7 235 | 3765 | 1988 | 0.31 | 21171 | 18242 | 8101 |
| | | RS7 470 | 3789 | 1993 | 0.31 | 21303 | 18570 | 8138 |

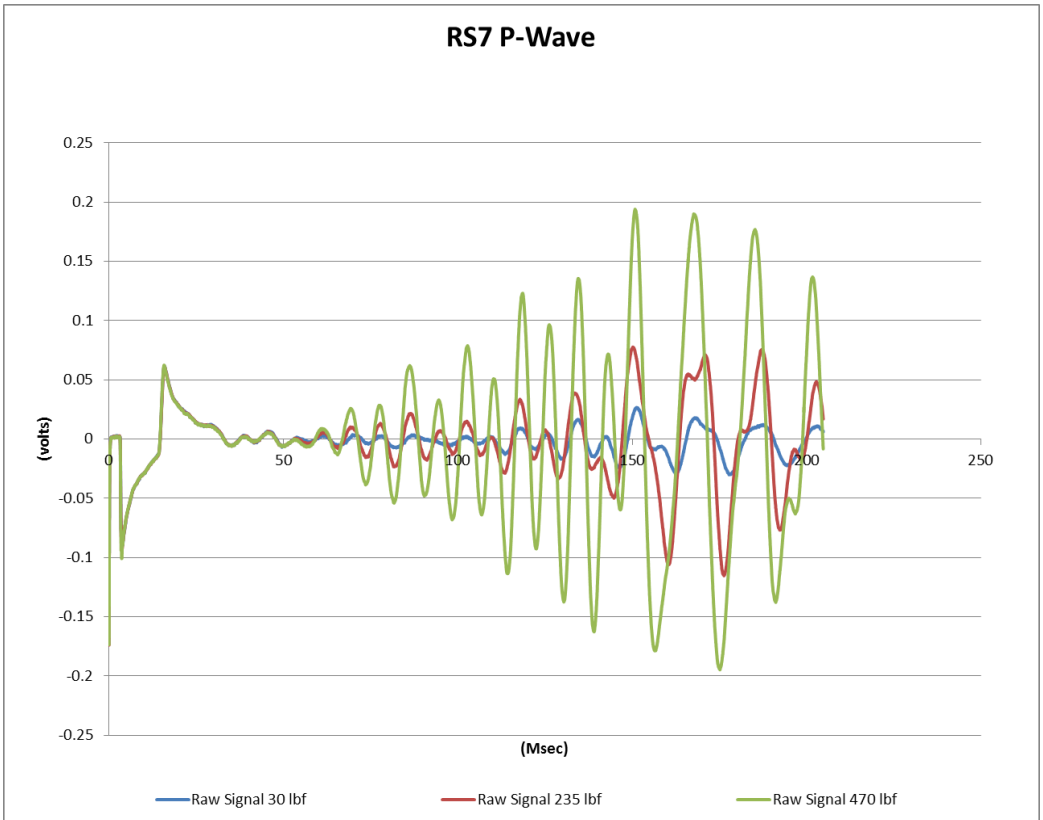
RS7 P-Wave
0.25
0.2
0.15
0.1
0.05
0
-0.05
-0.1
-0.15
-0.2
-0.25
(volts)
0
50
100
150
200
250
(Msec)
Raw Signal 30 lbf
Raw Signal 235 lbf
Raw Signal 470 lbf

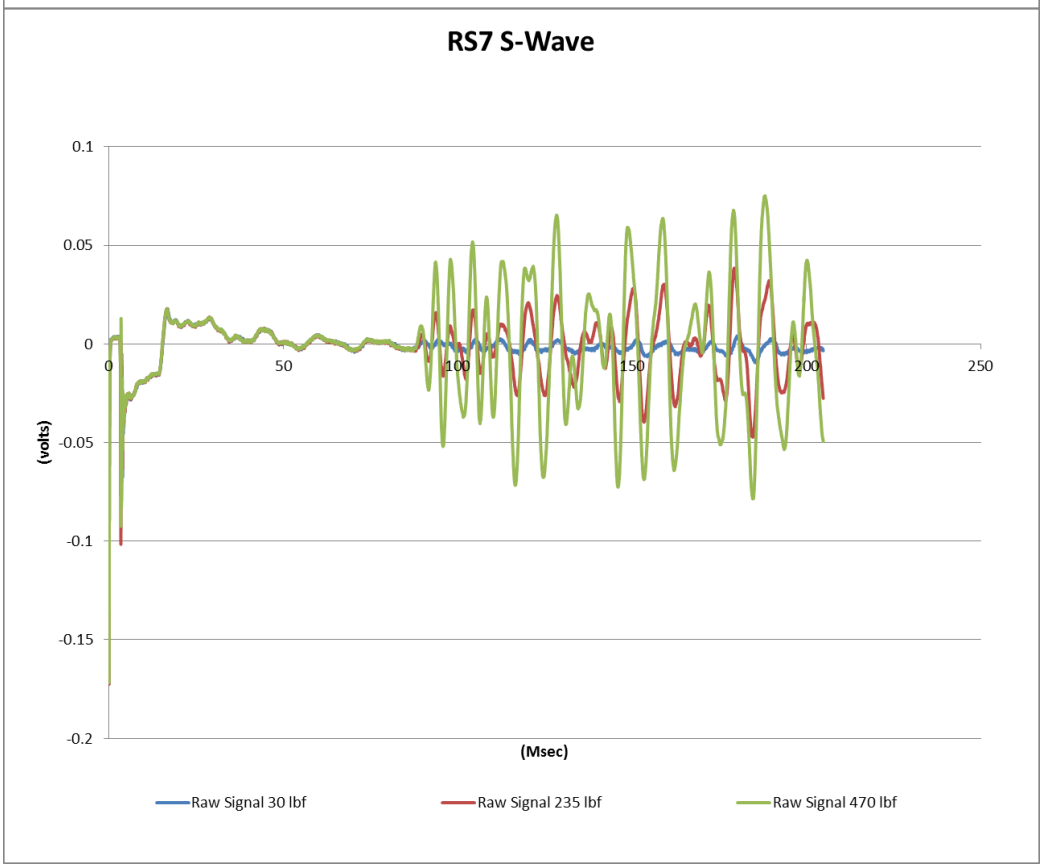
RS7 S-Wave
0.1
0.05
0
-0.05
-0.1
-0.15
-0.2
(volts)
0
50
100
150
200
250
(Msec)
Raw Signal 30 lbf
Raw Signal 235 lbf
Raw Signal 470 lbf

**RS8**

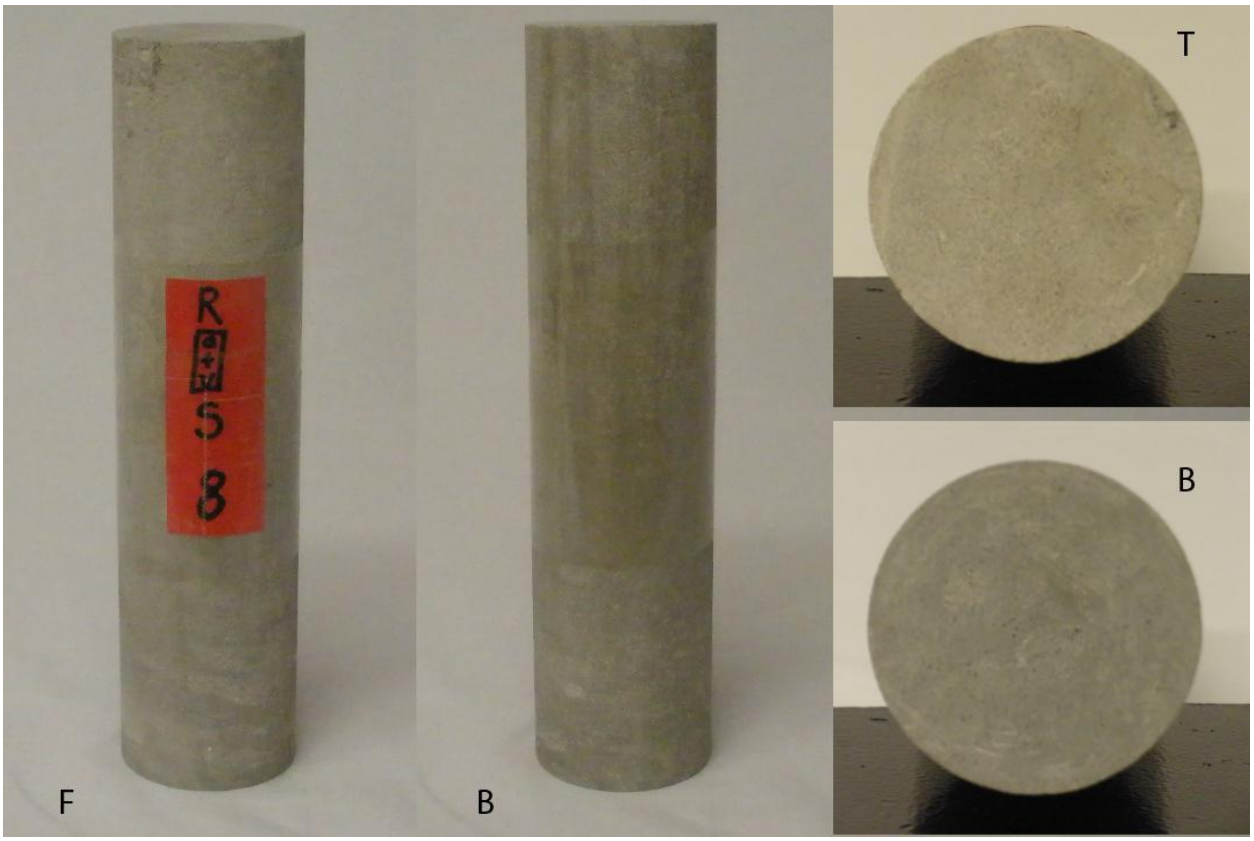


| South (Ogden, Riley CTY)Physical Properties of Cores | | | | | | | | | | | | | | |
|---|---|---|---|---|---|---|---|---|---|---|---|---|---|---|
| ID | Density ($g/cm^3$) | Lt. (in.) | Dia. (in.) | Top dpt. (ft.) | Bot. dpt. (ft.) | Avg. dpt. (ft) | Core Set | Core set dpt. | C | R | RQD | Lt. (mm) | Dia. (mm) | Mass (g) |
| RS8 | 2.24 | 8.1875 | 2.00 | 77.509 | 78.192 | 77.851 | Core 4 | 73.4 - 78.4 | 5 | 5 | 100% | 207 | 51 | 947.4 |

| **South Standard Picking** | | | | | | | | |
|---|---|---|---|---|---|---|---|---|
| First Arrivals & Elastic Prop. | | | | | | | | |
| | Avg. Dpt. (ft.) | lbf | P-Vel (m/s) | S-Vel (m/s) | Poisson's Ratio | Young's (MPa) | Bulk (MPa) | Shear (Mpa) |
| RS8 | 77.8505208 | RS8 30 | 10705 | 1746 | 0.49 | 20305 | 247634 | 6830 |
| | | RS8 245 | 10803 | 1892 | 0.48 | 23799 | 250776 | 8018 |
| | | RS8 490 | 10816 | 1905 | 0.48 | 24135 | 251263 | 8132 |

| **South Altered picking** | | | | | | | | |
|---|---|---|---|---|---|---|---|---|
| Poisson's Point | | | | | | | | |
| | Avg. Dpt. (ft.) | lbf | P-Vel (m/s) | S-Vel (m/s) | Poisson's Ratio | Young's (MPa) | Bulk (MPa) | Shear (Mpa) |
| RS8 | 77.85052 | RS8 30 | 3517 | 1746 | 0.31 | 17919 | 15862 | 6830 |
| | | RS8 245 | 3325 | 1892 | 0.26 | 20214 | 14073 | 8017 |
| | | RS8 490 | 3319 | 1905 | 0.25 | 20399 | 13837 | 8131 |

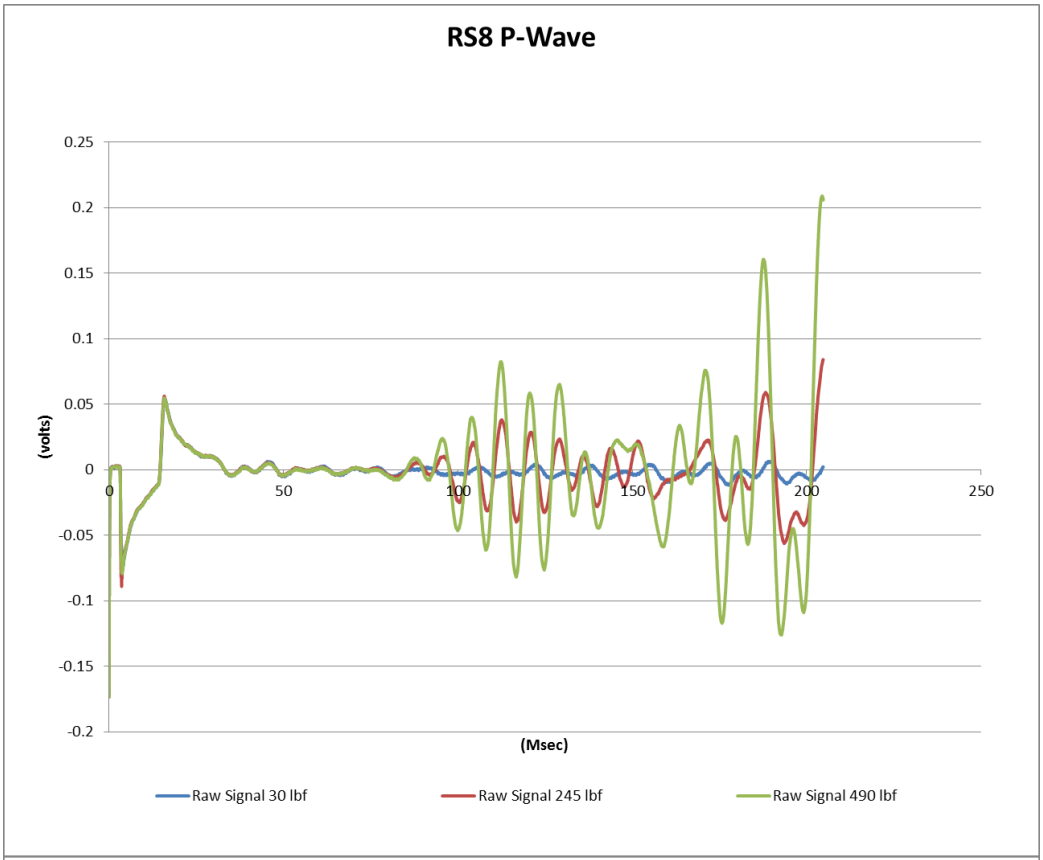
RS8 P-Wave
0.25
0.2
0.15
0.1
0.05
0
-0.05
-0.1
-0.15
-0.2
(volts)
0
50
100
150
200
250
(Msec)
Raw Signal 30 lbf
Raw Signal 245 lbf
Raw Signal 490 lbf

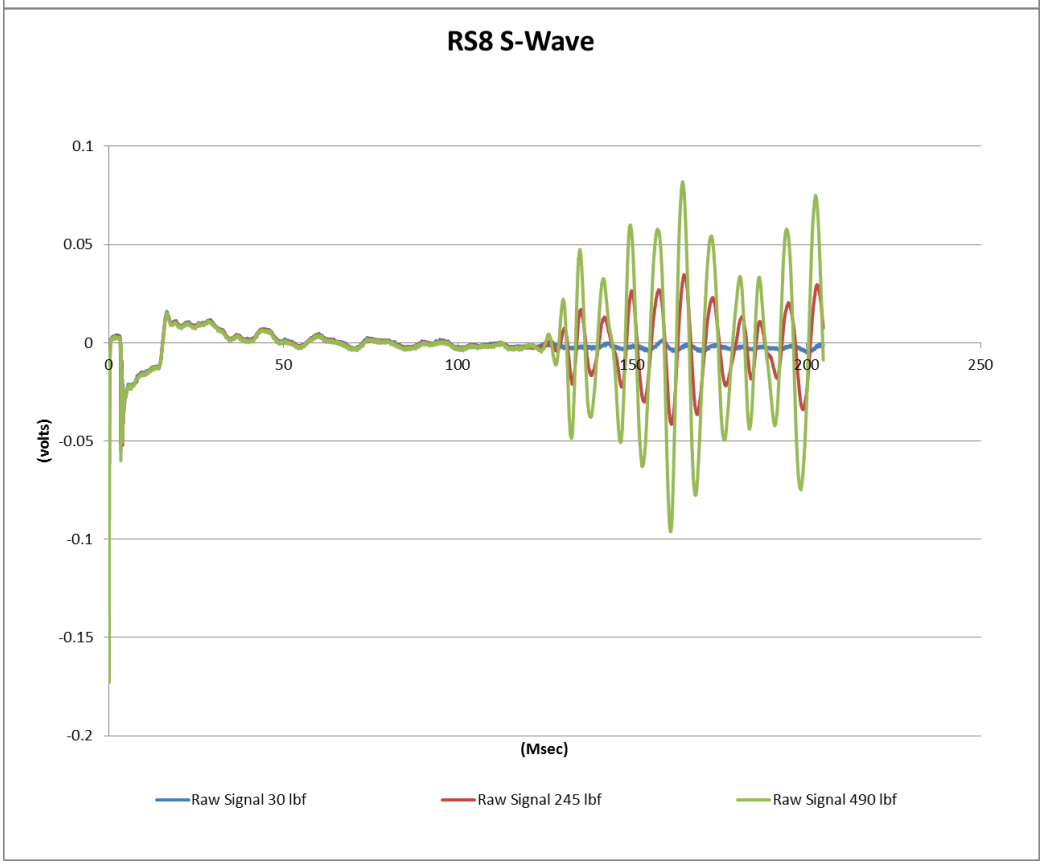
RS8 S-Wave
0.1
0.05
0
-0.05
-0.1
-0.15
-0.2
(volts)
0
50
100
150
200
250
(Msec)
Raw Signal 30 lbf
Raw Signal 245 lbf
Raw Signal 490 lbf

# Chapter 10 - Appendix B – Records & Dispersion Curves (All Lines)

## Maps

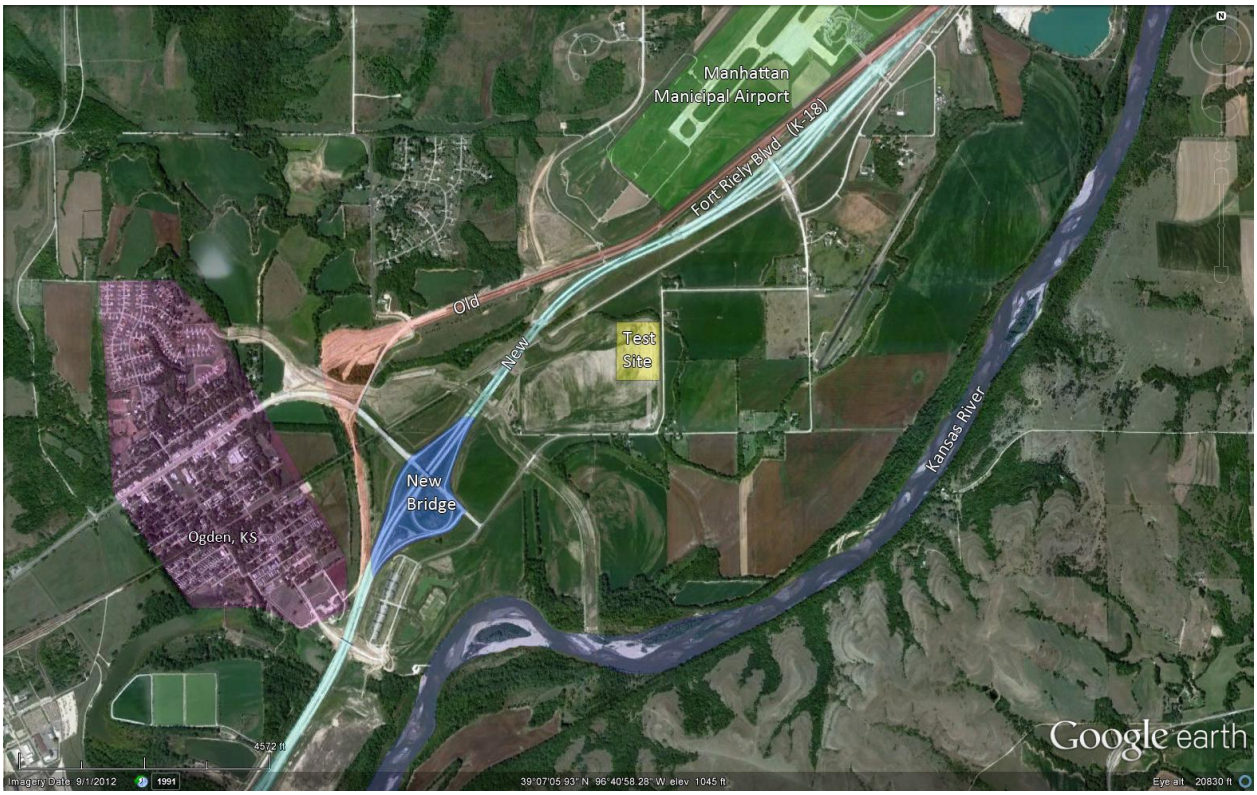


Overview Map


Acquisition map

## Line 10

### Raw

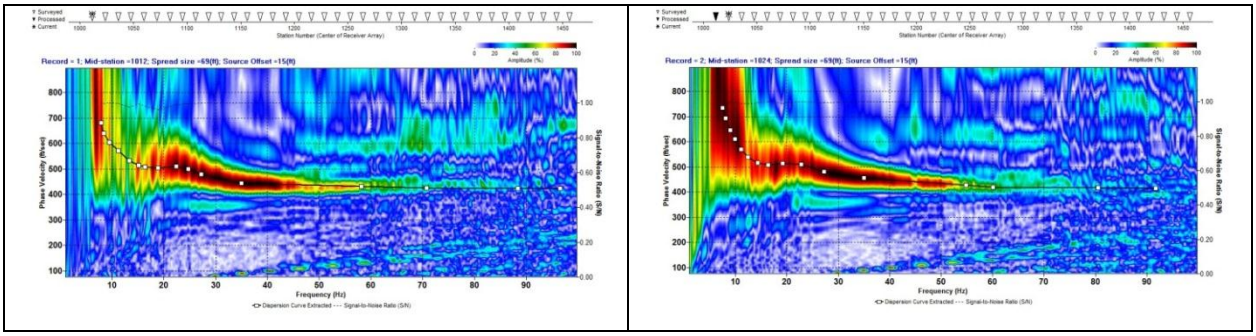

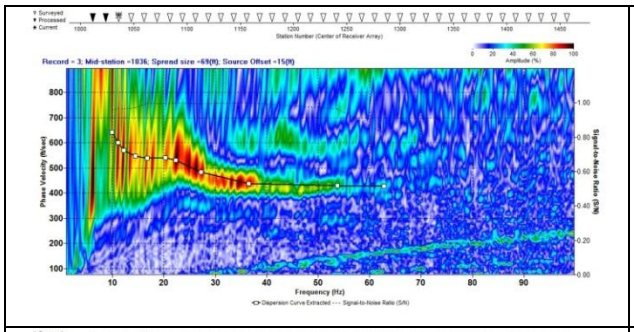
Record = 3; Mid-station =1036; Spread size =69(ft); Source Offset =15(ft)
Phase Velocity (ft/sec)
Frequency (Hz)
Signal-to-Noise Ratio (S/N)

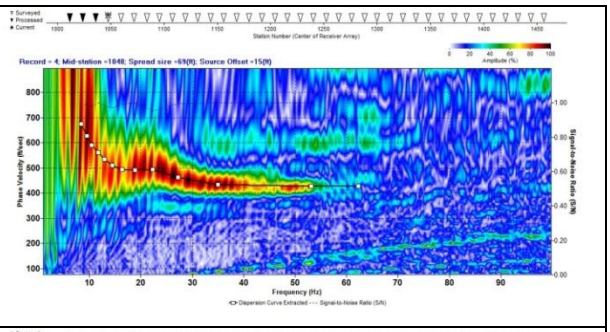
Record = 4; Mid-station =1048; Spread size =69(ft); Source Offset =15(ft)
Phase Velocity (ft/sec)
Frequency (Hz)
Signal-to-Noise Ratio (S/N)

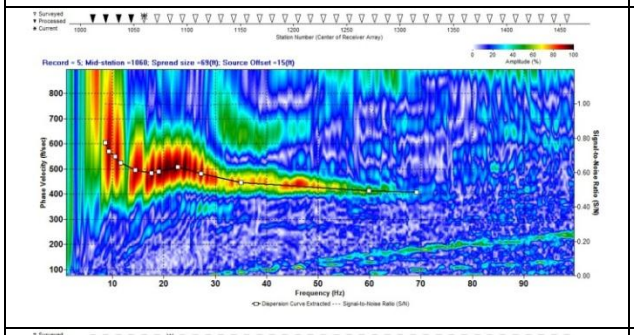
Record = 5; Mid-station =1060; Spread size =69(ft); Source Offset =15(ft)
Phase Velocity (ft/sec)
Frequency (Hz)
Signal-to-Noise Ratio (S/N)

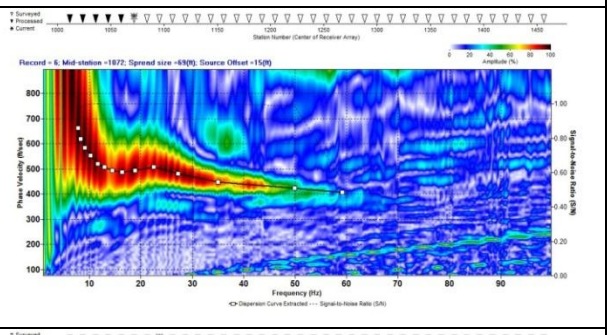
Record = 6; Mid-station =1072; Spread size =69(ft); Source Offset =15(ft)
Phase Velocity (ft/sec)
Frequency (Hz)
Signal-to-Noise Ratio (S/N)

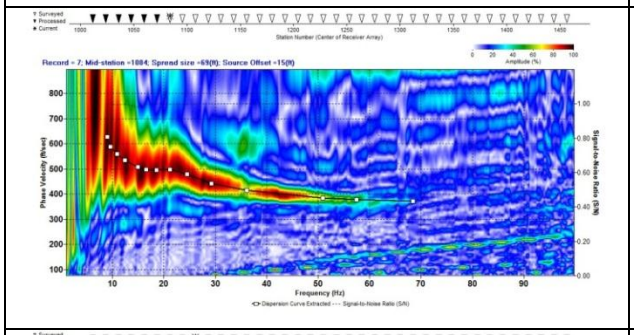
Record = 7; Mid-station =1084; Spread size =69(ft); Source Offset =15(ft)
Phase Velocity (ft/sec)
Frequency (Hz)
Signal-to-Noise Ratio (S/N)

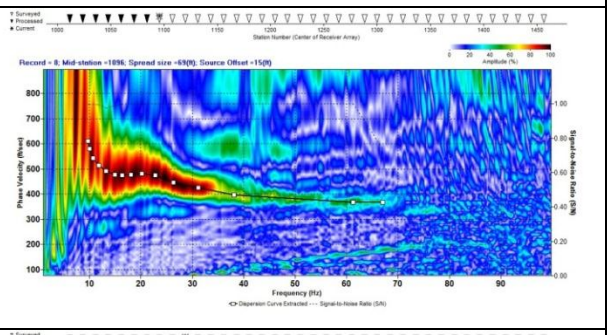
Record = 8; Mid-station =1096; Spread size =69(ft); Source Offset =15(ft)
Phase Velocity (ft/sec)
Frequency (Hz)
Signal-to-Noise Ratio (S/N)

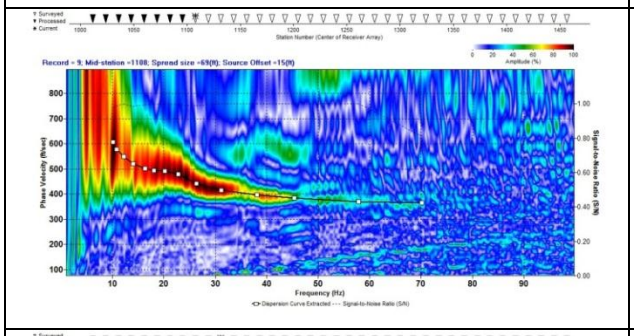
Record = 9; Mid-station =1108; Spread size =69(ft); Source Offset =15(ft)
Phase Velocity (ft/sec)
Frequency (Hz)
Signal-to-Noise Ratio (S/N)

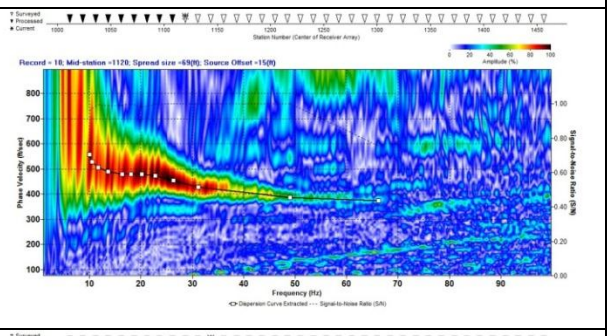
Record = 10; Mid-station =1120; Spread size =69(ft); Source Offset =15(ft)
Phase Velocity (ft/sec)
Frequency (Hz)
Signal-to-Noise Ratio (S/N)

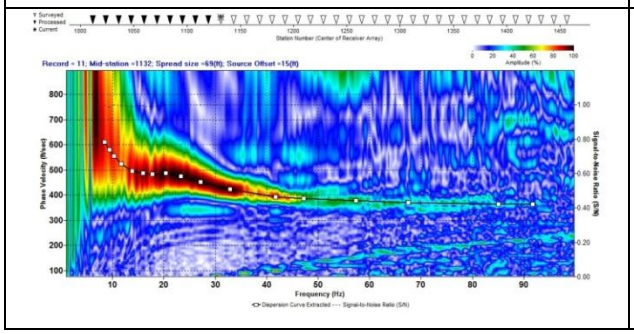
Record = 11; Mid-station =1132; Spread size =69(ft); Source Offset =15(ft)
Phase Velocity (ft/sec)
Frequency (Hz)
Signal-to-Noise Ratio (S/N)

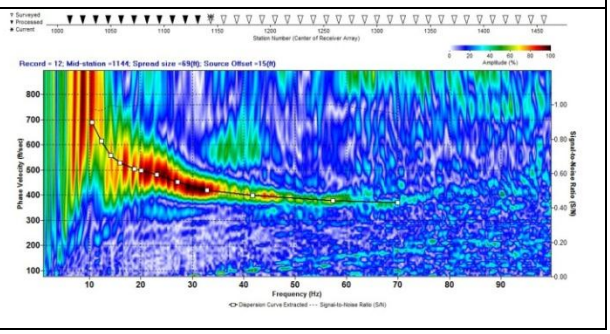
Record = 12; Mid-station =1144; Spread size =69(ft); Source Offset =15(ft)
Phase Velocity (ft/sec)
Frequency (Hz)
Signal-to-Noise Ratio (S/N)

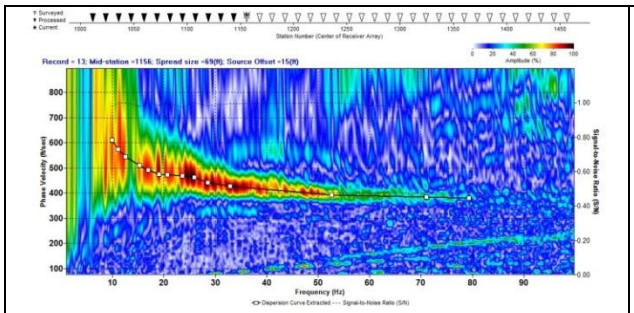
Record = 13; Mid-station =1156; Spread size =69(ft); Source Offset =15(ft)
Phase Velocity (ft/sec)
Frequency (Hz)
Signal-to-Noise Ratio (S/N)

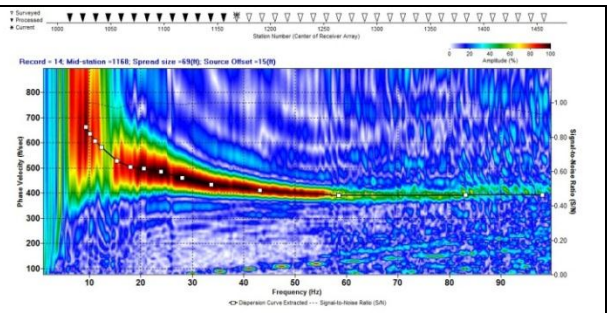
Record = 14; Mid-station =1168; Spread size =69(ft); Source Offset =15(ft)
Phase Velocity (ft/sec)
Frequency (Hz)
Signal-to-Noise Ratio (S/N)

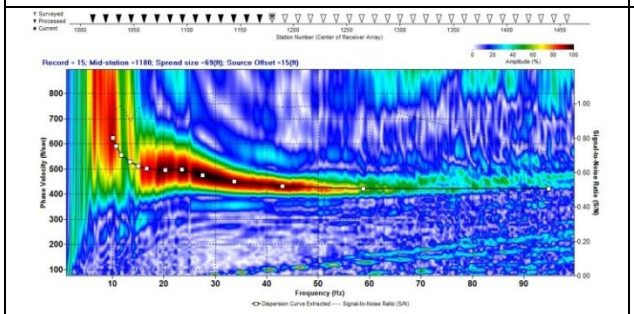
Record = 15; Mid-station =1180; Spread size =69(ft); Source Offset =15(ft)
Phase Velocity (ft/sec)
Frequency (Hz)
Signal-to-Noise Ratio (S/N)

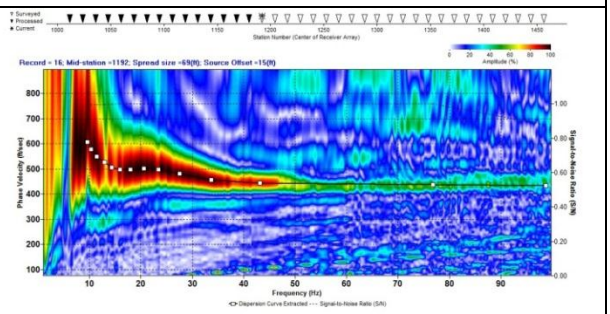
Record = 16; Mid-station =1192; Spread size =69(ft); Source Offset =15(ft)
Phase Velocity (ft/sec)
Frequency (Hz)
Signal-to-Noise Ratio (S/N)

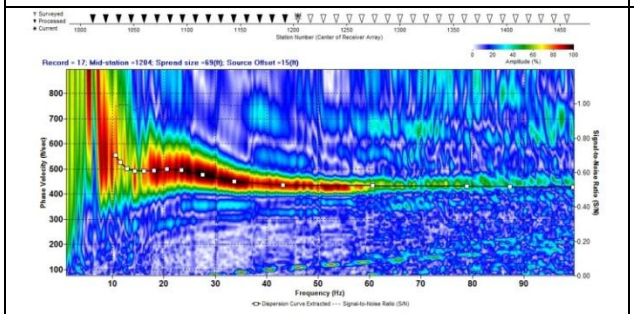
Record = 17; Mid-station =1204; Spread size =69(ft); Source Offset =15(ft)
Phase Velocity (ft/sec)
Frequency (Hz)
Signal-to-Noise Ratio (S/N)

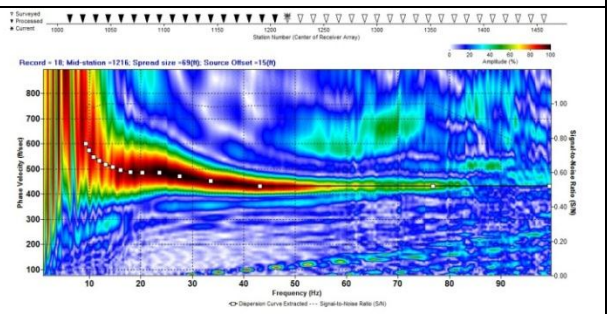
Record = 18; Mid-station =1216; Spread size =69(ft); Source Offset =15(ft)
Phase Velocity (ft/sec)
Frequency (Hz)
Signal-to-Noise Ratio (S/N)

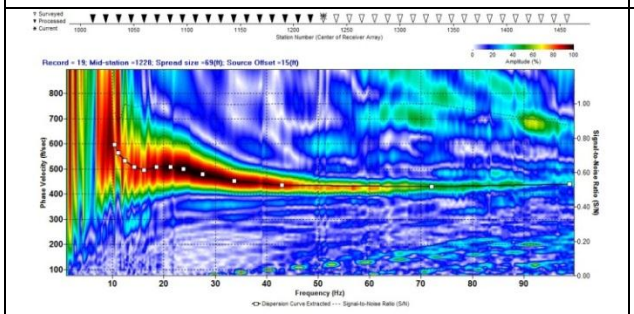
Record = 19; Mid-station =1228; Spread size =69(ft); Source Offset =15(ft)
Phase Velocity (ft/sec)
Frequency (Hz)
Signal-to-Noise Ratio (S/N)

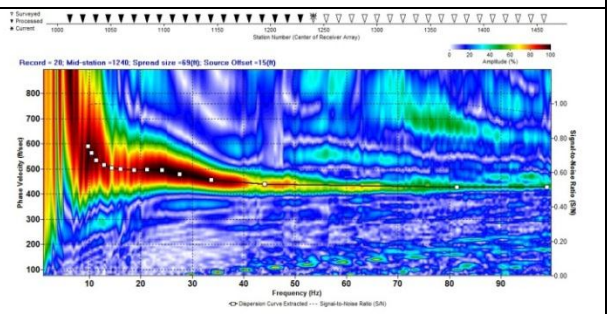
Record = 20; Mid-station =1240; Spread size =69(ft); Source Offset =15(ft)
Phase Velocity (ft/sec)
Frequency (Hz)
Signal-to-Noise Ratio (S/N)

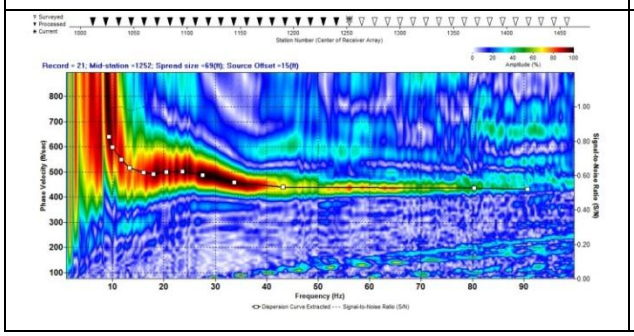
Record = 21; Mid-station =1252; Spread size =69(ft); Source Offset =15(ft)
Phase Velocity (ft/sec)
Frequency (Hz)
Signal-to-Noise Ratio (S/N)

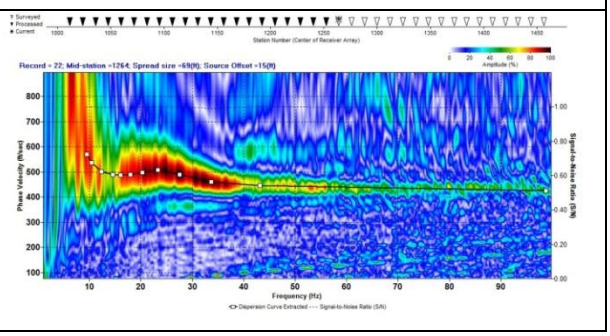
Record = 22; Mid-station =1264; Spread size =69(ft); Source Offset =15(ft)
Phase Velocity (ft/sec)
Frequency (Hz)
Signal-to-Noise Ratio (S/N)

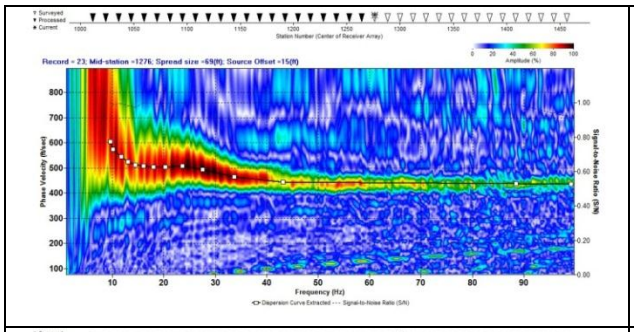
Record = 23; Mid-station =1276; Spread size =69(ft); Source Offset =15(ft)
Phase Velocity (ft/sec)
Frequency (Hz)
Signal-to-Noise Ratio (S/N)

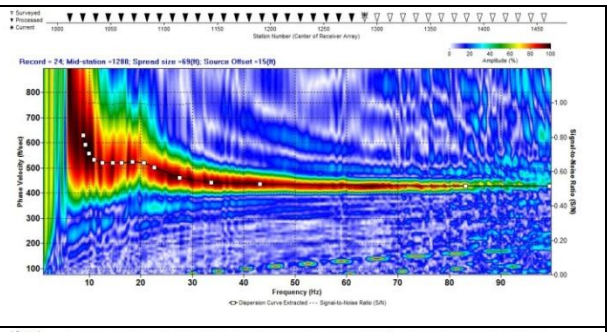
Record = 24; Mid-station =1288; Spread size =69(ft); Source Offset =15(ft)
Phase Velocity (ft/sec)
Frequency (Hz)
Signal-to-Noise Ratio (S/N)

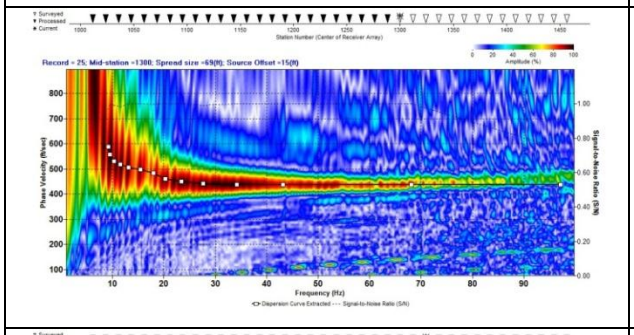
Record = 25; Mid-station =1300; Spread size =69(ft); Source Offset =15(ft)
Phase Velocity (ft/sec)
Frequency (Hz)
Signal-to-Noise Ratio (S/N)

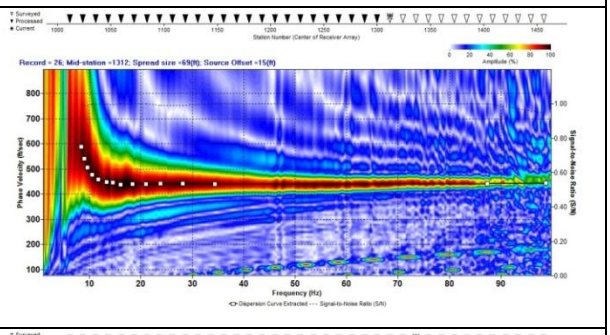
Record = 26; Mid-station =1312; Spread size =69(ft); Source Offset =15(ft)
Phase Velocity (ft/sec)
Frequency (Hz)
Signal-to-Noise Ratio (S/N)

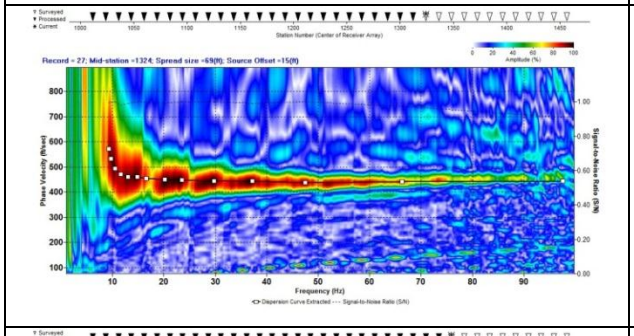
Record = 27; Mid-station =1324; Spread size =69(ft); Source Offset =15(ft)
Phase Velocity (ft/sec)
Frequency (Hz)
Signal-to-Noise Ratio (S/N)

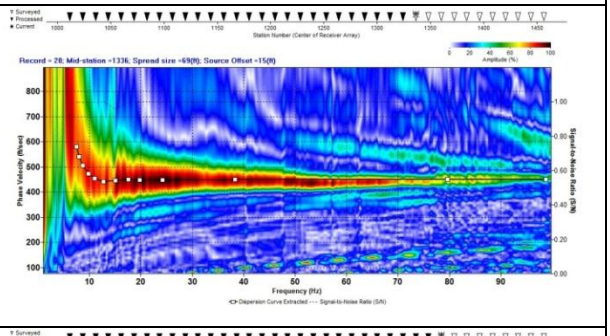
Record = 28; Mid-station =1336; Spread size =69(ft); Source Offset =15(ft)
Phase Velocity (ft/sec)
Frequency (Hz)
Signal-to-Noise Ratio (S/N)

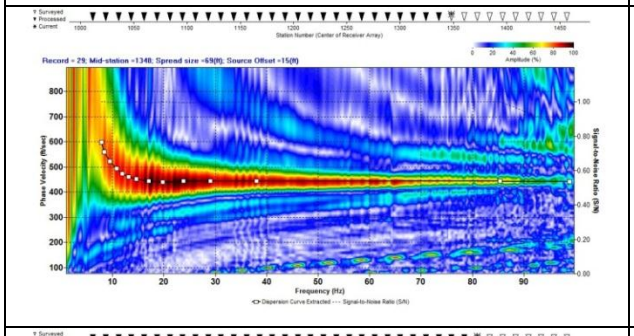
Record = 29; Mid-station =1348; Spread size =69(ft); Source Offset =15(ft)
Phase Velocity (ft/sec)
Frequency (Hz)
Signal-to-Noise Ratio (S/N)

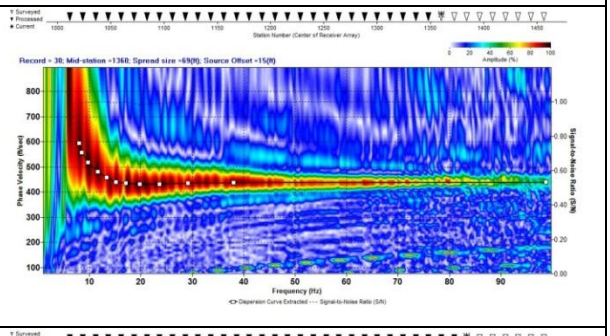
Record = 30; Mid-station =1360; Spread size =69(ft); Source Offset =15(ft)
Phase Velocity (ft/sec)
Frequency (Hz)
Signal-to-Noise Ratio (S/N)

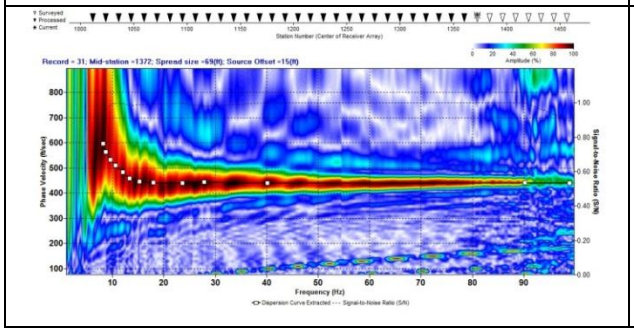
Record = 31; Mid-station =1372; Spread size =69(ft); Source Offset =15(ft)
Phase Velocity (ft/sec)
Frequency (Hz)
Signal-to-Noise Ratio (S/N)

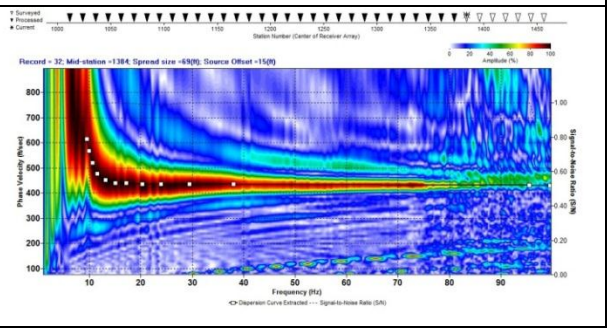
Record = 32; Mid-station =1384; Spread size =69(ft); Source Offset =15(ft)
Phase Velocity (ft/sec)
Frequency (Hz)
Signal-to-Noise Ratio (S/N)

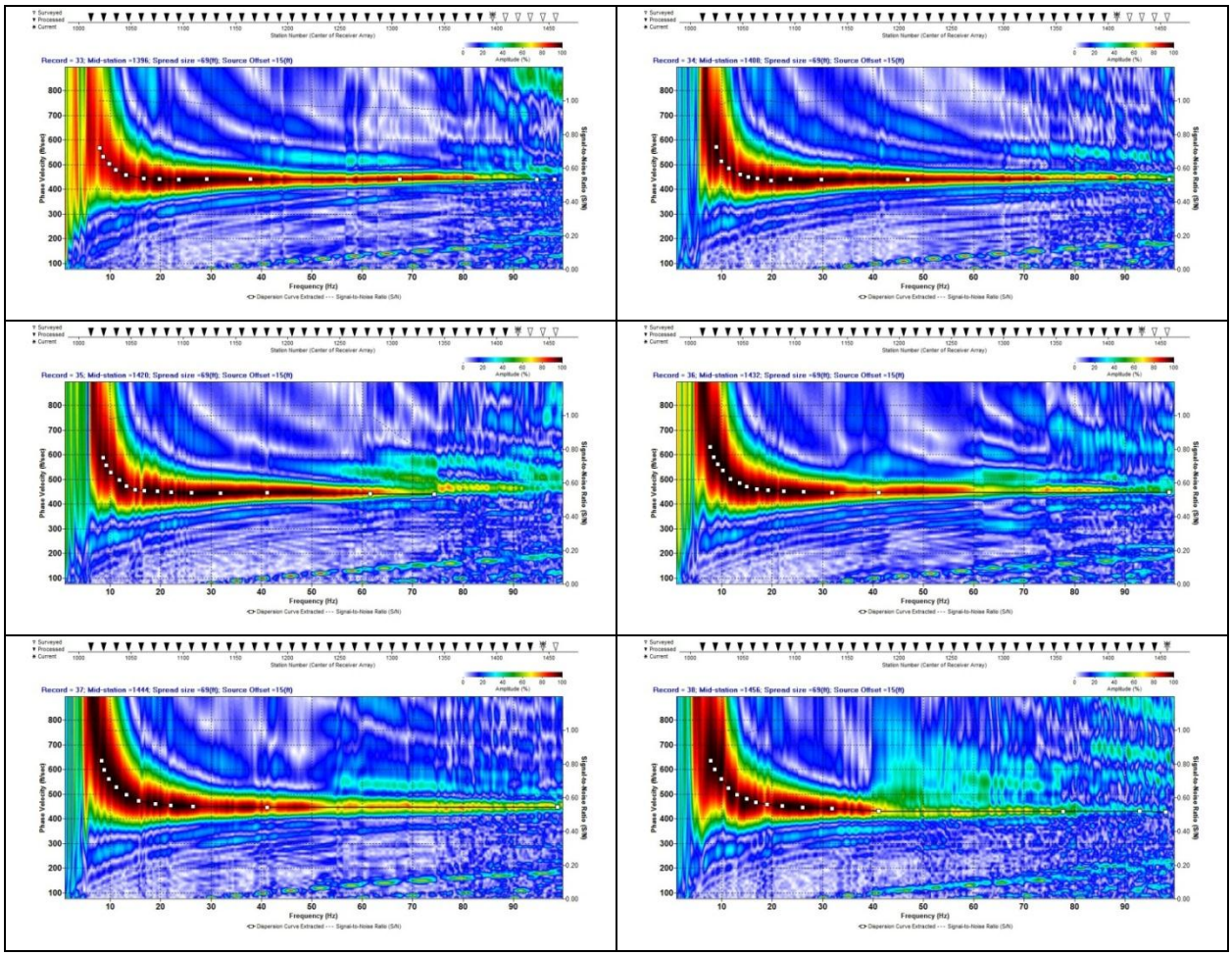
Record = 33; Mid-station =1396; Spread size =69(ft); Source Offset =15(ft)
Record = 34; Mid-station =1408; Spread size =69(ft); Source Offset =15(ft)
Record = 35; Mid-station =1420; Spread size =69(ft); Source Offset =15(ft)
Record = 36; Mid-station =1432; Spread size =69(ft); Source Offset =15(ft)
Record = 37; Mid-station =1444; Spread size =69(ft); Source Offset =15(ft)
Record = 38; Mid-station =1456; Spread size =69(ft); Source Offset =15(ft)
Phase Velocity (ft/sec)
Frequency (Hz)
Signal-to-Noise Ratio (S/N)
Station Number (Center of Receiver Array)
Amplitude (%)

## *Raw Inversion Results*

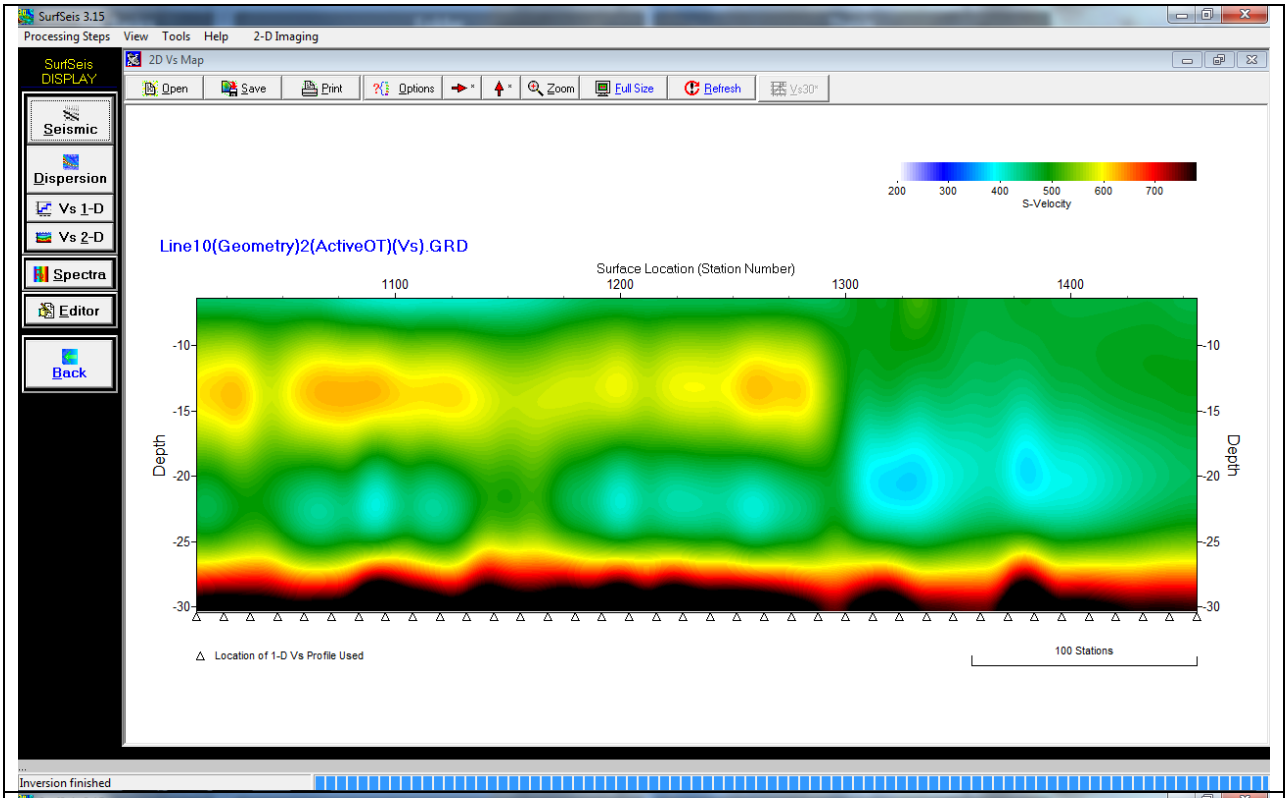


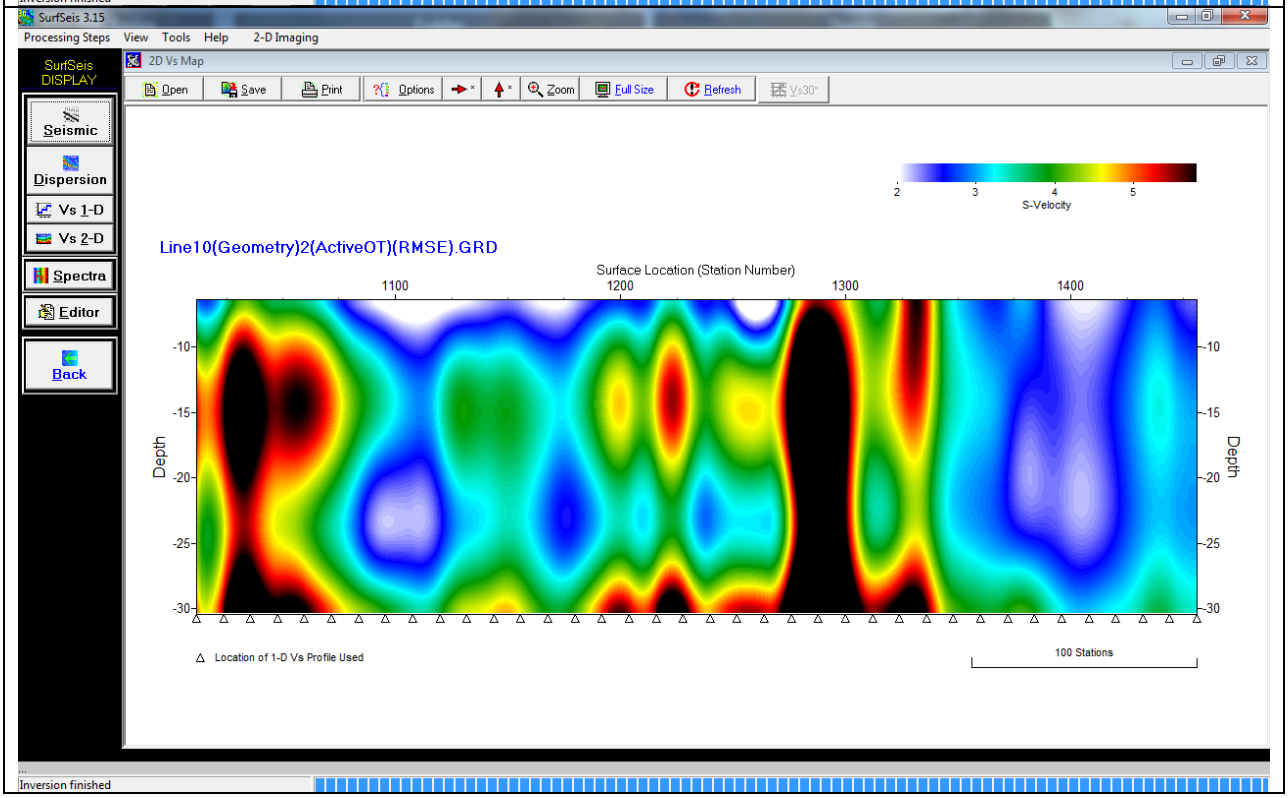

## Loose Bottom Mute

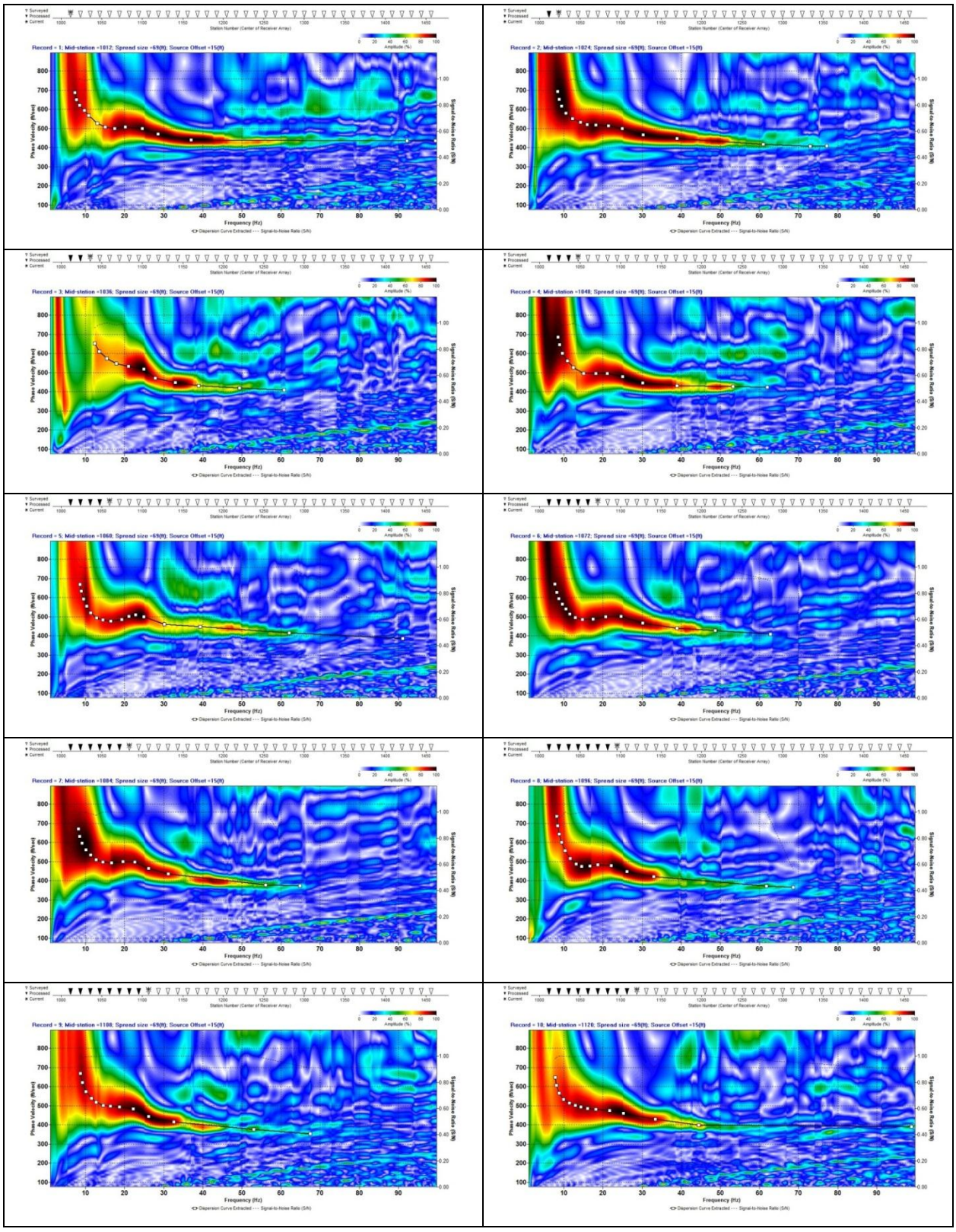

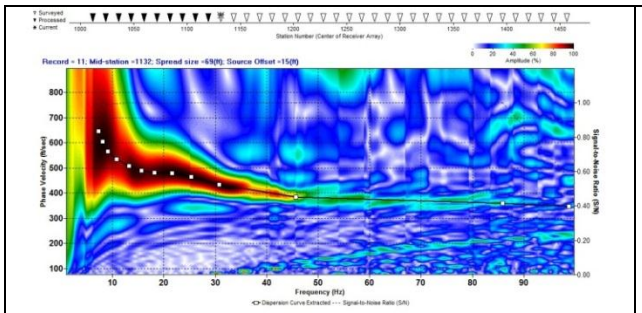
Record = 11; Mid-station =1132; Spread size =69(ft); Source Offset =15(ft)
Phase Velocity (ft/sec)
Frequency (Hz)
Signal-to-Noise Ratio (S/N)

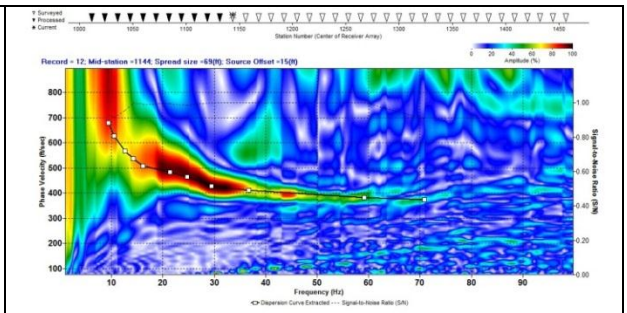
Record = 12; Mid-station =1144; Spread size =69(ft); Source Offset =15(ft)
Phase Velocity (ft/sec)
Frequency (Hz)
Signal-to-Noise Ratio (S/N)

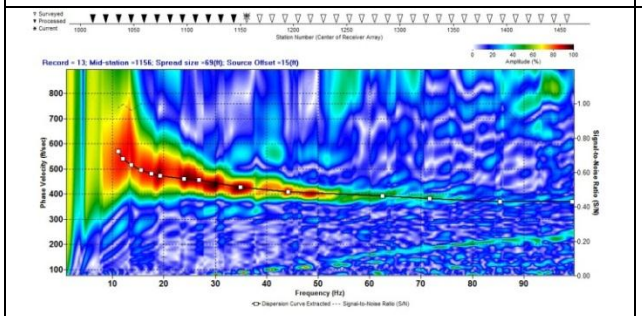
Record = 13; Mid-station =1156; Spread size =69(ft); Source Offset =15(ft)
Phase Velocity (ft/sec)
Frequency (Hz)
Signal-to-Noise Ratio (S/N)

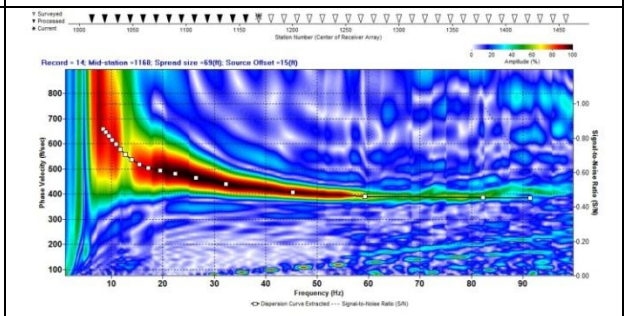
Record = 14; Mid-station =1168; Spread size =69(ft); Source Offset =15(ft)
Phase Velocity (ft/sec)
Frequency (Hz)
Signal-to-Noise Ratio (S/N)

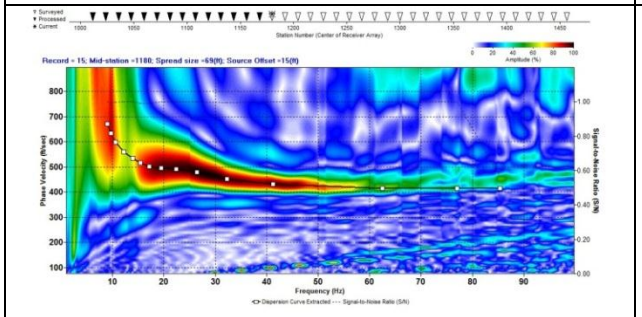
Record = 15; Mid-station =1180; Spread size =69(ft); Source Offset =15(ft)
Phase Velocity (ft/sec)
Frequency (Hz)
Signal-to-Noise Ratio (S/N)

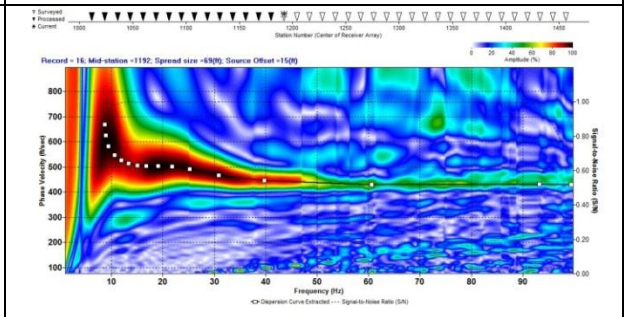
Record = 16; Mid-station =1192; Spread size =69(ft); Source Offset =15(ft)
Phase Velocity (ft/sec)
Frequency (Hz)
Signal-to-Noise Ratio (S/N)

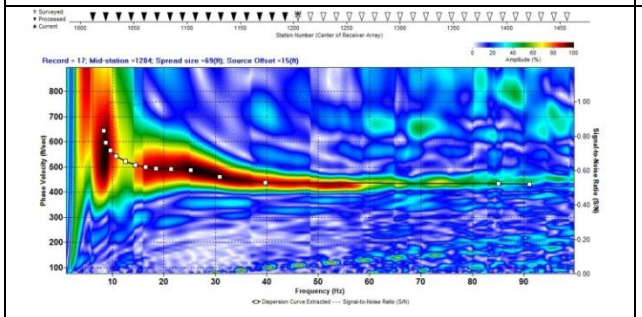
Record = 17; Mid-station =1284; Spread size =69(ft); Source Offset =15(ft)
Phase Velocity (ft/sec)
Frequency (Hz)
Signal-to-Noise Ratio (S/N)

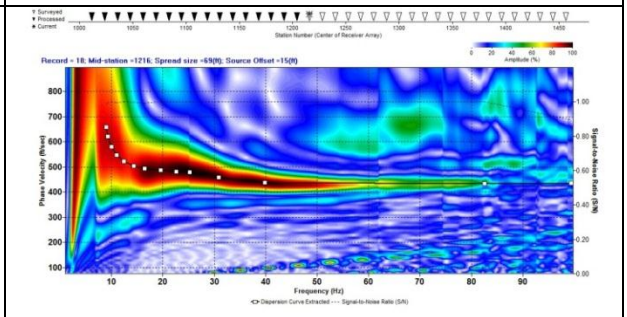
Record = 18; Mid-station =1216; Spread size =69(ft); Source Offset =15(ft)
Phase Velocity (ft/sec)
Frequency (Hz)
Signal-to-Noise Ratio (S/N)

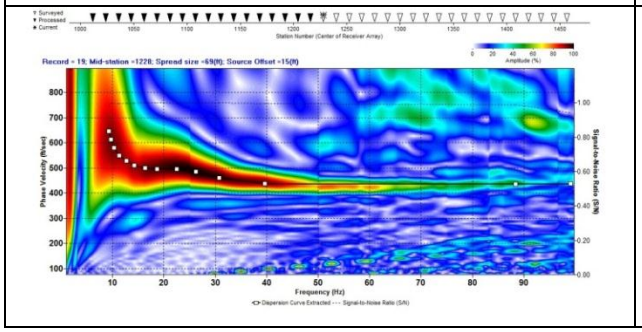
Record = 19; Mid-station =1228; Spread size =69(ft); Source Offset =15(ft)
Phase Velocity (ft/sec)
Frequency (Hz)
Signal-to-Noise Ratio (S/N)

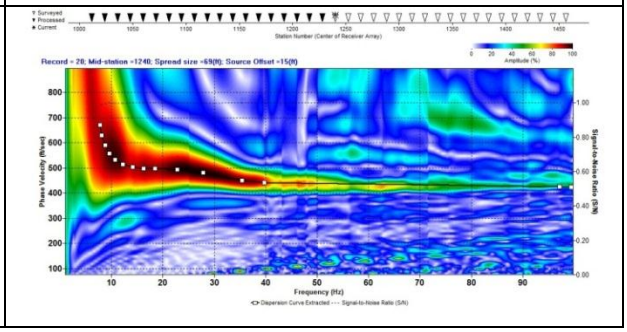
Record = 20; Mid-station =1240; Spread size =69(ft); Source Offset =15(ft)
Phase Velocity (ft/sec)
Frequency (Hz)
Signal-to-Noise Ratio (S/N)

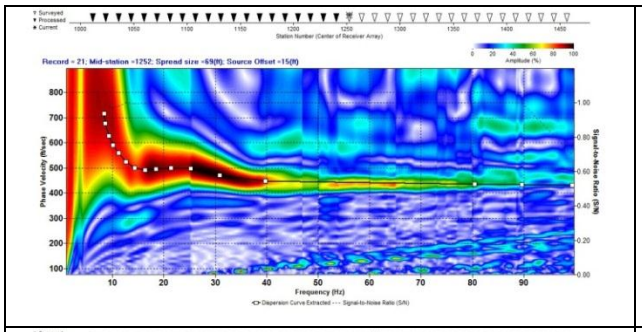
Record = 21; Mid-station =1252; Spread size =69(ft); Source Offset =15(ft)
Phase Velocity (ft/sec)
Frequency (Hz)
Signal-to-Noise Ratio (S/N)

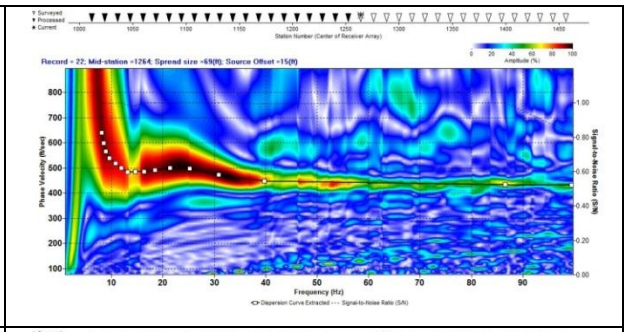
Record = 22; Mid-station =1264; Spread size =69(ft); Source Offset =15(ft)
Phase Velocity (ft/sec)
Frequency (Hz)
Signal-to-Noise Ratio (S/N)

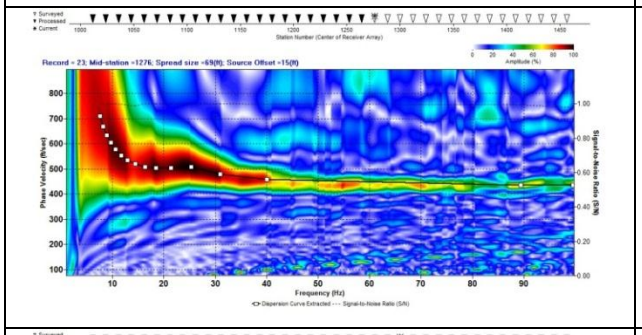
Record = 23; Mid-station =1276; Spread size =69(ft); Source Offset =15(ft)
Phase Velocity (ft/sec)
Frequency (Hz)
Signal-to-Noise Ratio (S/N)

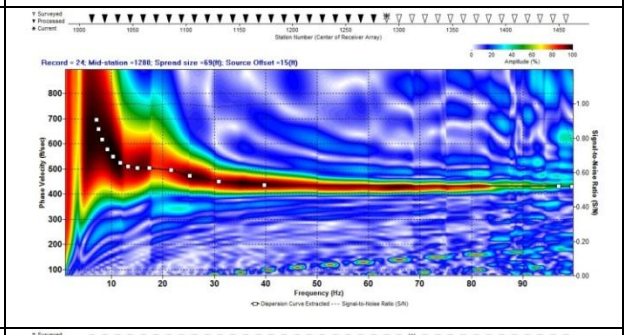
Record = 24; Mid-station =1288; Spread size =69(ft); Source Offset =15(ft)
Phase Velocity (ft/sec)
Frequency (Hz)
Signal-to-Noise Ratio (S/N)

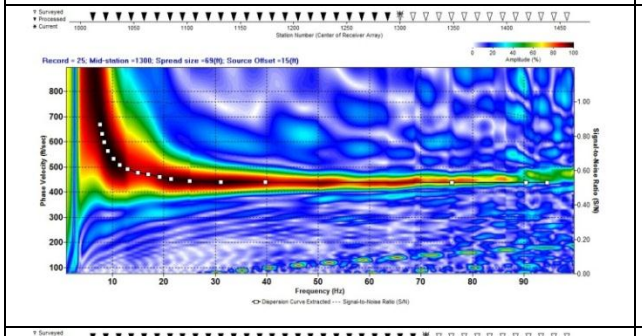
Record = 25; Mid-station =1300; Spread size =69(ft); Source Offset =15(ft)
Phase Velocity (ft/sec)
Frequency (Hz)
Signal-to-Noise Ratio (S/N)

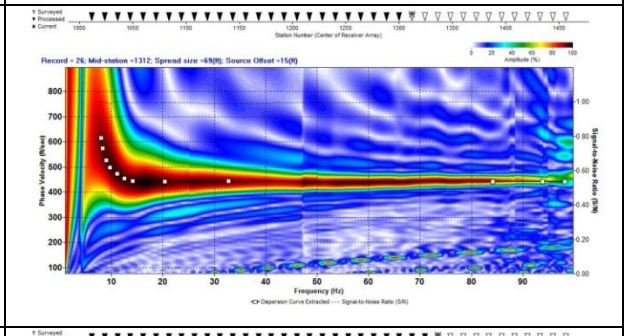
Record = 26; Mid-station =1312; Spread size =69(ft); Source Offset =15(ft)
Phase Velocity (ft/sec)
Frequency (Hz)
Signal-to-Noise Ratio (S/N)

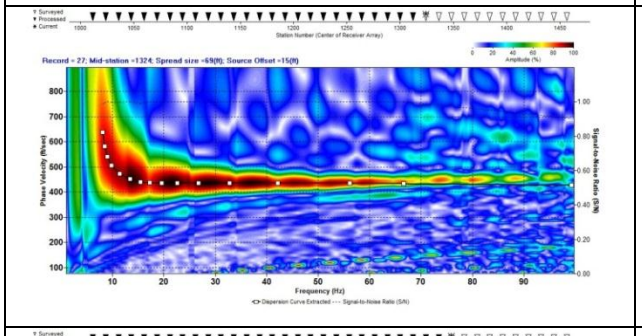
Record = 27; Mid-station =1324; Spread size =69(ft); Source Offset =15(ft)
Phase Velocity (ft/sec)
Frequency (Hz)
Signal-to-Noise Ratio (S/N)

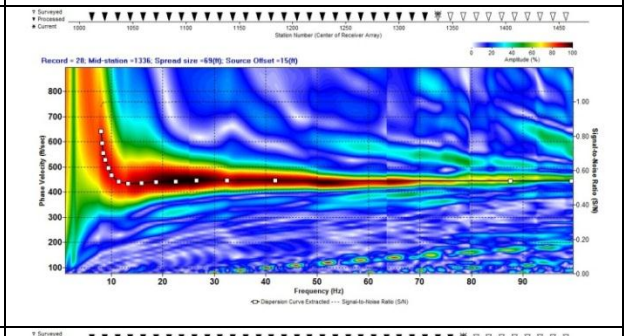
Record = 28; Mid-station =1336; Spread size =69(ft); Source Offset =15(ft)
Phase Velocity (ft/sec)
Frequency (Hz)
Signal-to-Noise Ratio (S/N)

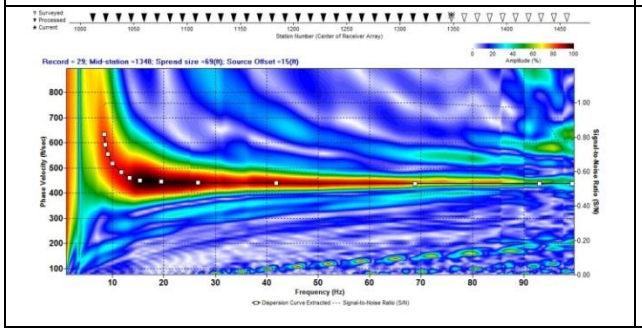
Record = 29; Mid-station =1348; Spread size =69(ft); Source Offset =15(ft)
Phase Velocity (ft/sec)
Frequency (Hz)
Signal-to-Noise Ratio (S/N)

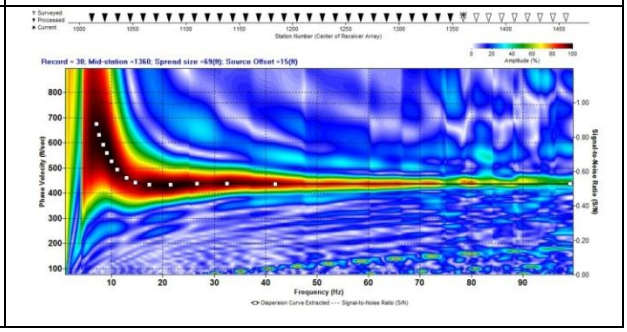
Record = 30; Mid-station =1360; Spread size =69(ft); Source Offset =15(ft)
Phase Velocity (ft/sec)
Frequency (Hz)
Signal-to-Noise Ratio (S/N)

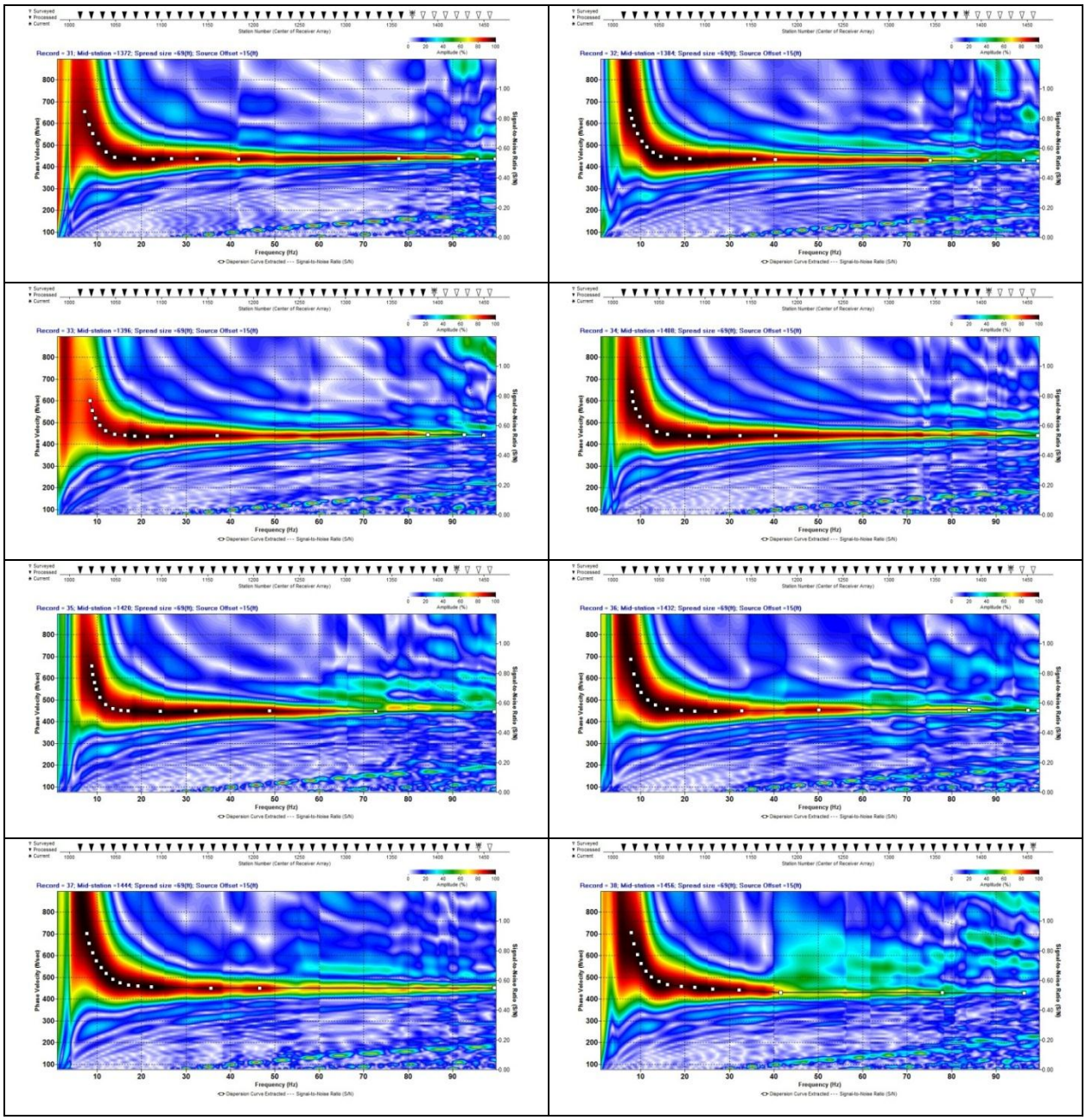
Record = 31; Mid-station =1372; Spread size =69(ft); Source Offset =15(ft)
Record = 32; Mid-station =1384; Spread size =69(ft); Source Offset =15(ft)
Record = 33; Mid-station =1396; Spread size =69(ft); Source Offset =15(ft)
Record = 34; Mid-station =1408; Spread size =69(ft); Source Offset =15(ft)
Record = 35; Mid-station =1420; Spread size =69(ft); Source Offset =15(ft)
Record = 36; Mid-station =1432; Spread size =69(ft); Source Offset =15(ft)
Record = 37; Mid-station =1444; Spread size =69(ft); Source Offset =15(ft)
Record = 38; Mid-station =1456; Spread size =69(ft); Source Offset =15(ft)
Phase Velocity (ft/sec)
Frequency (Hz)
Signal-to-Noise Ratio (S/N)
Amplitude (%)
Station Number (Center of Receiver Array)
Dispersion Curve Extracted --- Signal-to-Noise Ratio (S/N)

## *(LossBot) Inversion Results*

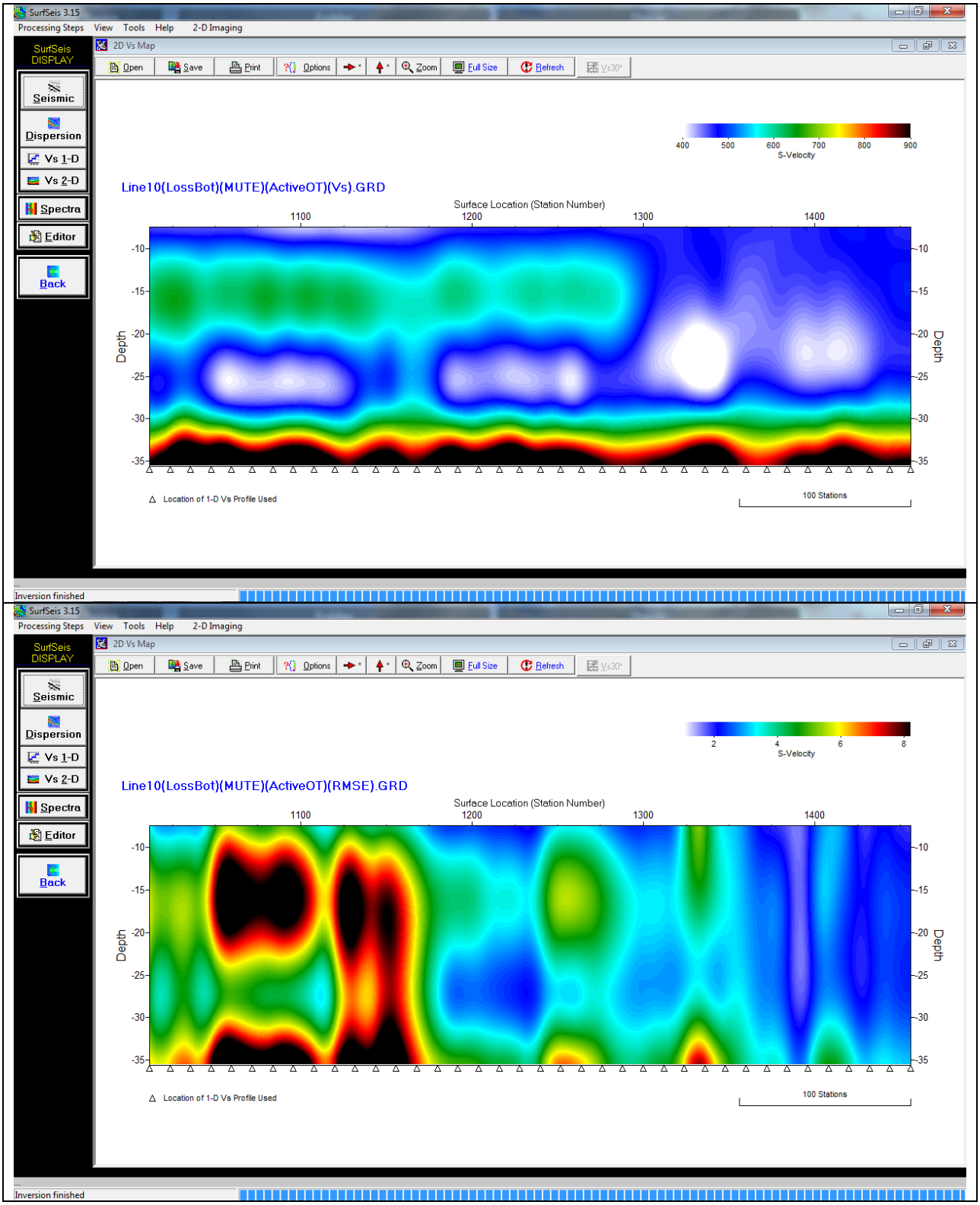

## Aggressive picking on Loose Bottom Mute

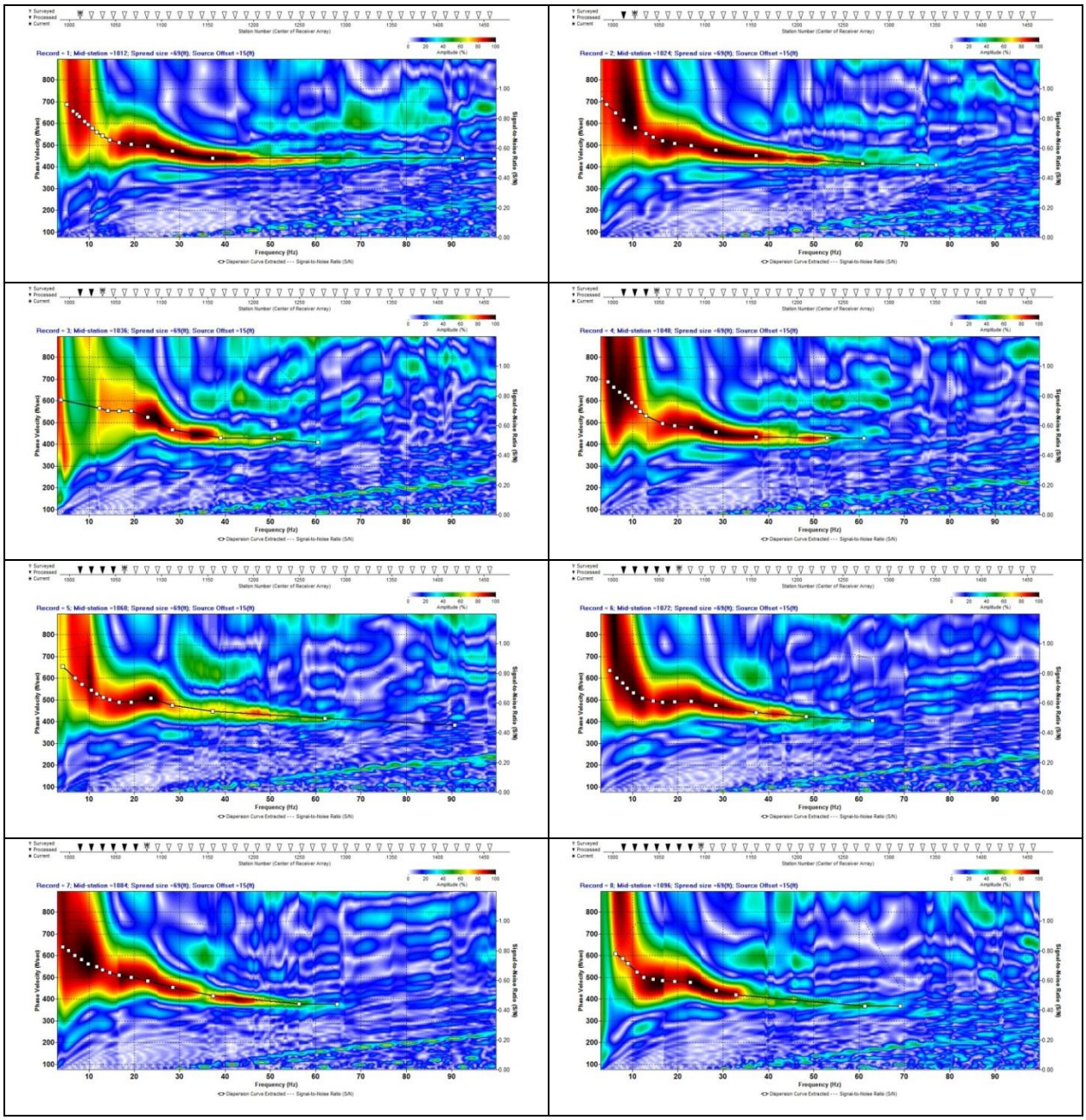

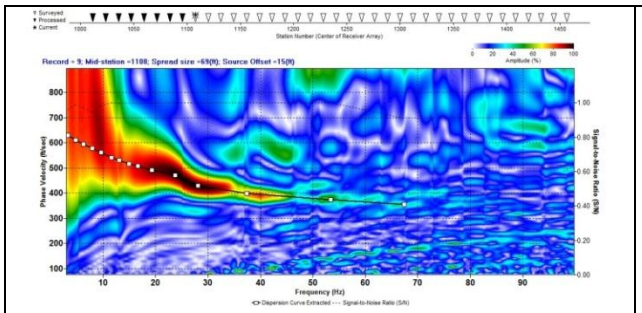
Record = 9; Mid-station =1108; Spread size =69(ft); Source Offset =15(ft)
Phase Velocity (ft/sec)
Frequency (Hz)
Signal-to-Noise Ratio (S/N)

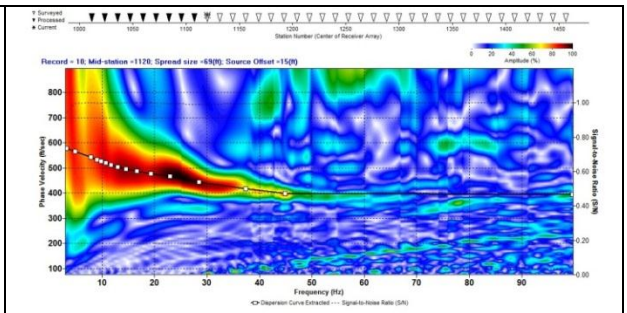
Record = 10; Mid-station =1120; Spread size =69(ft); Source Offset =15(ft)
Phase Velocity (ft/sec)
Frequency (Hz)
Signal-to-Noise Ratio (S/N)

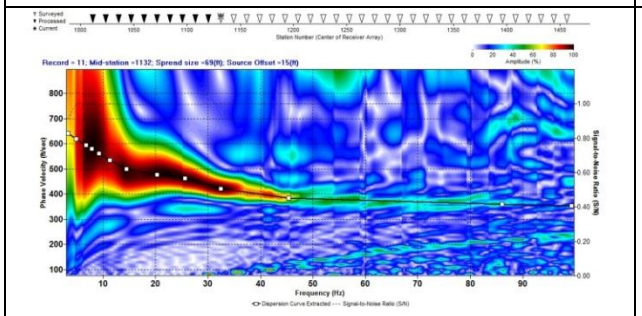
Record = 11; Mid-station =1132; Spread size =69(ft); Source Offset =15(ft)
Phase Velocity (ft/sec)
Frequency (Hz)
Signal-to-Noise Ratio (S/N)

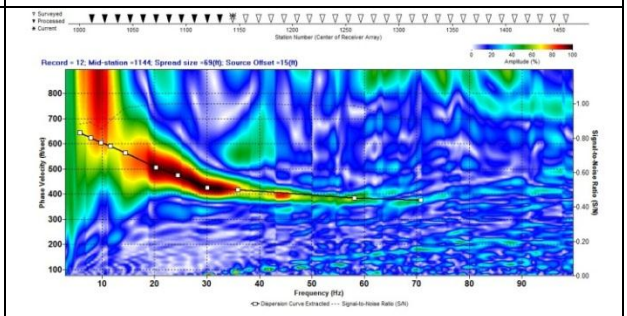
Record = 12; Mid-station =1144; Spread size =69(ft); Source Offset =15(ft)
Phase Velocity (ft/sec)
Frequency (Hz)
Signal-to-Noise Ratio (S/N)

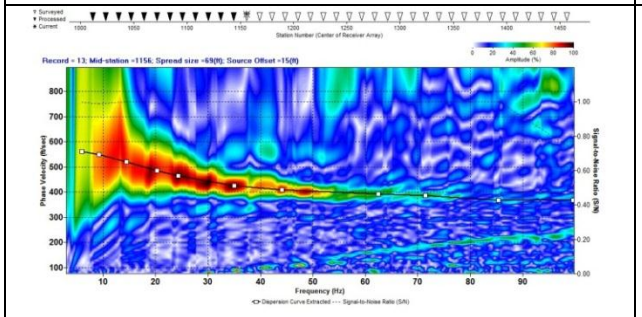
Record = 13; Mid-station =1156; Spread size =69(ft); Source Offset =15(ft)
Phase Velocity (ft/sec)
Frequency (Hz)
Signal-to-Noise Ratio (S/N)

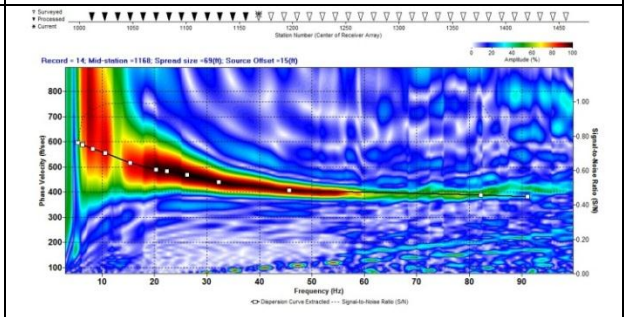
Record = 14; Mid-station =1168; Spread size =69(ft); Source Offset =15(ft)
Phase Velocity (ft/sec)
Frequency (Hz)
Signal-to-Noise Ratio (S/N)

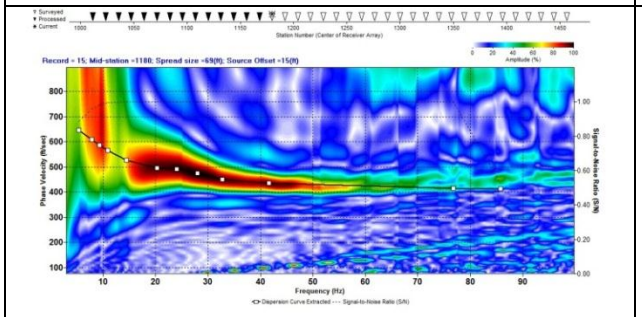
Record = 15; Mid-station =1180; Spread size =69(ft); Source Offset =15(ft)
Phase Velocity (ft/sec)
Frequency (Hz)
Signal-to-Noise Ratio (S/N)

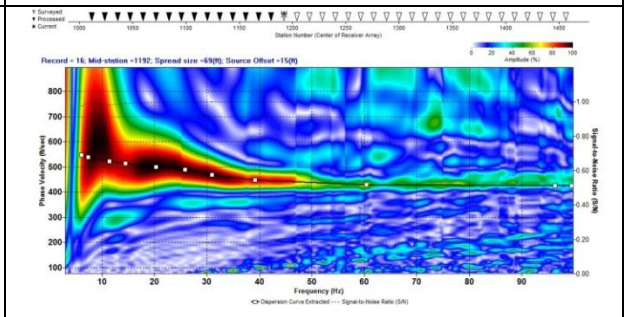
Record = 16; Mid-station =1192; Spread size =69(ft); Source Offset =15(ft)
Phase Velocity (ft/sec)
Frequency (Hz)
Signal-to-Noise Ratio (S/N)

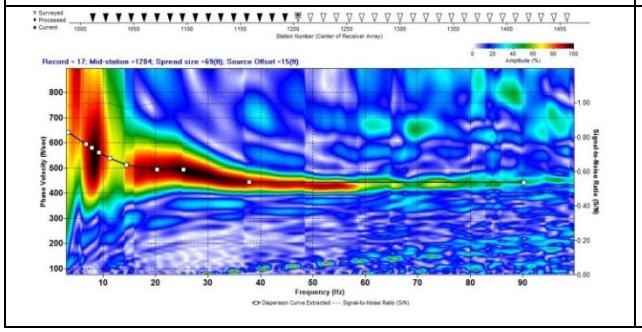
Record = 17; Mid-station =1204; Spread size =69(ft); Source Offset =15(ft)
Phase Velocity (ft/sec)
Frequency (Hz)
Signal-to-Noise Ratio (S/N)

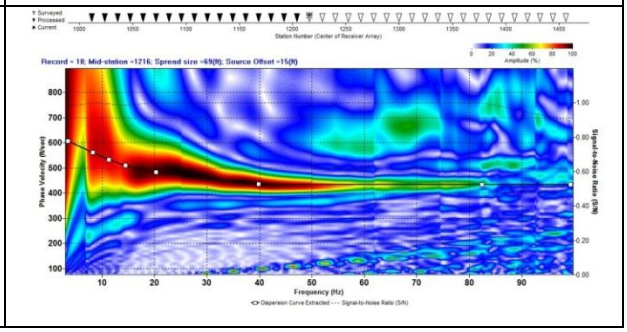
Record = 18; Mid-station =1216; Spread size =69(ft); Source Offset =15(ft)
Phase Velocity (ft/sec)
Frequency (Hz)
Signal-to-Noise Ratio (S/N)

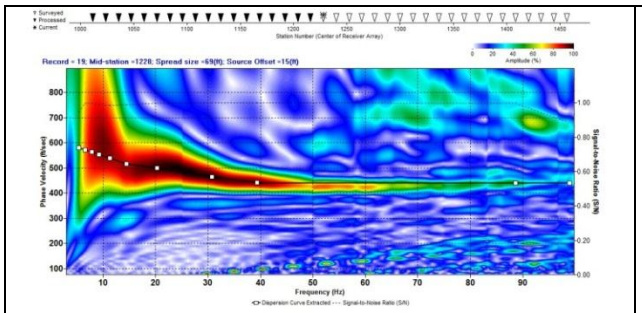
Record = 19; Mid-station =1228; Spread size =69(ft); Source Offset =15(ft)
Phase Velocity (ft/sec)
Frequency (Hz)
Signal-to-Noise Ratio (S/N)

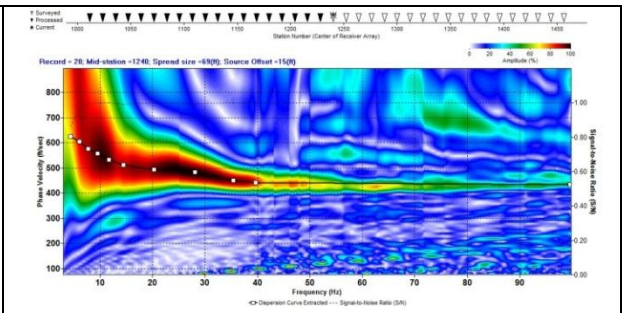
Record = 20; Mid-station =1240; Spread size =69(ft); Source Offset =15(ft)
Phase Velocity (ft/sec)
Frequency (Hz)
Signal-to-Noise Ratio (S/N)

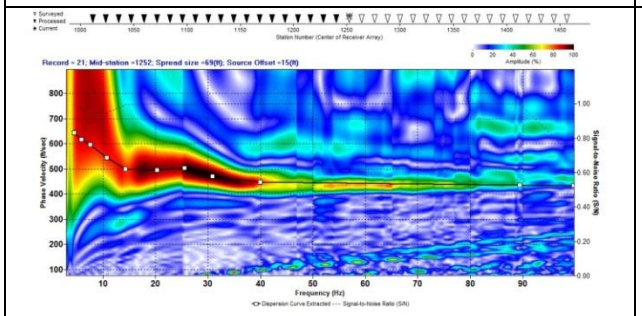
Record = 21; Mid-station =1252; Spread size =69(ft); Source Offset =15(ft)
Phase Velocity (ft/sec)
Frequency (Hz)
Signal-to-Noise Ratio (S/N)

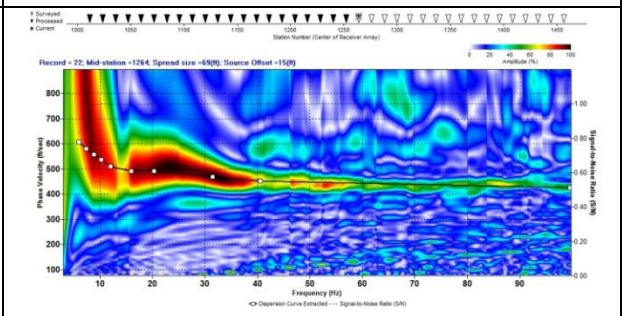
Record = 22; Mid-station =1264; Spread size =69(ft); Source Offset =15(ft)
Phase Velocity (ft/sec)
Frequency (Hz)
Signal-to-Noise Ratio (S/N)

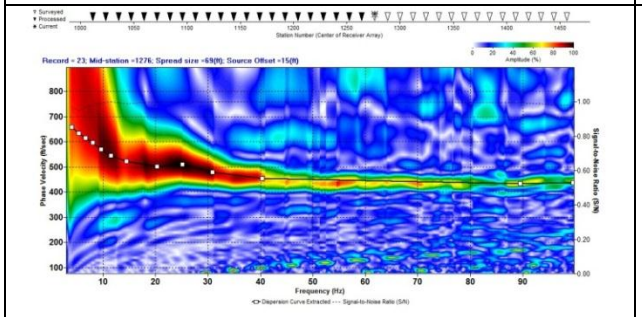
Record = 23; Mid-station =1276; Spread size =69(ft); Source Offset =15(ft)
Phase Velocity (ft/sec)
Frequency (Hz)
Signal-to-Noise Ratio (S/N)

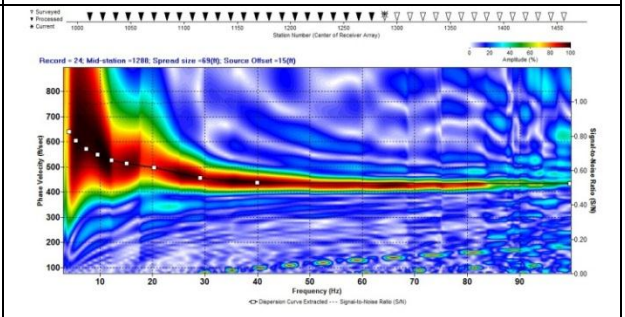
Record = 24; Mid-station =1288; Spread size =69(ft); Source Offset =15(ft)
Phase Velocity (ft/sec)
Frequency (Hz)
Signal-to-Noise Ratio (S/N)

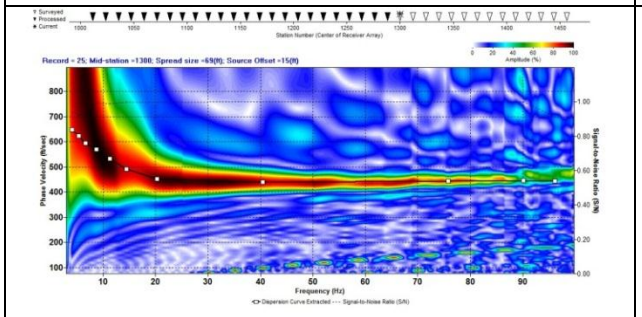
Record = 25; Mid-station =1300; Spread size =69(ft); Source Offset =15(ft)
Phase Velocity (ft/sec)
Frequency (Hz)
Signal-to-Noise Ratio (S/N)

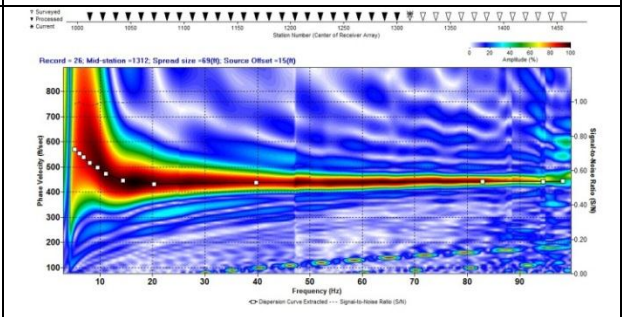
Record = 26; Mid-station =1312; Spread size =69(ft); Source Offset =15(ft)
Phase Velocity (ft/sec)
Frequency (Hz)
Signal-to-Noise Ratio (S/N)

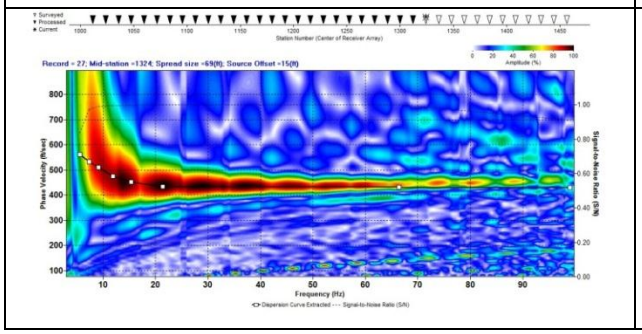
Record = 27; Mid-station =1324; Spread size =69(ft); Source Offset =15(ft)
Phase Velocity (ft/sec)
Frequency (Hz)
Signal-to-Noise Ratio (S/N)

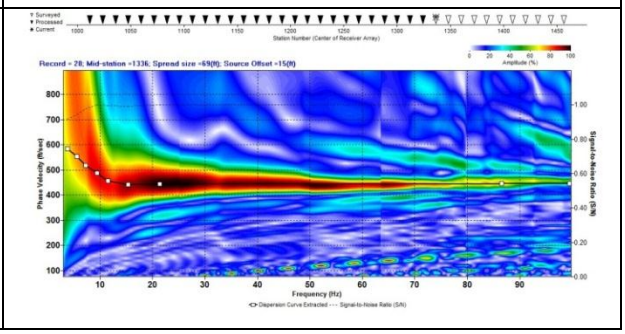
Record = 28; Mid-station =1336; Spread size =69(ft); Source Offset =15(ft)
Phase Velocity (ft/sec)
Frequency (Hz)
Signal-to-Noise Ratio (S/N)

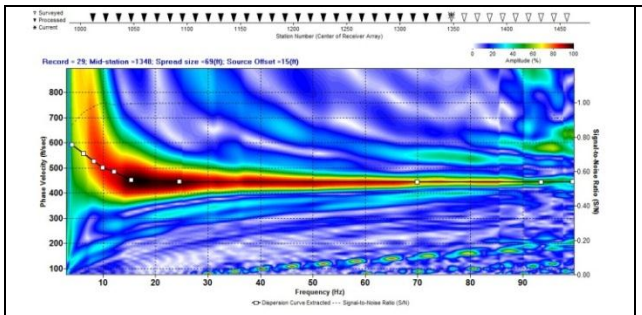
Record = 29; Mid-station =1348; Spread size =69(ft); Source Offset =15(ft)
Phase Velocity (ft/sec)
Frequency (Hz)
Signal-to-Noise Ratio (S/N)

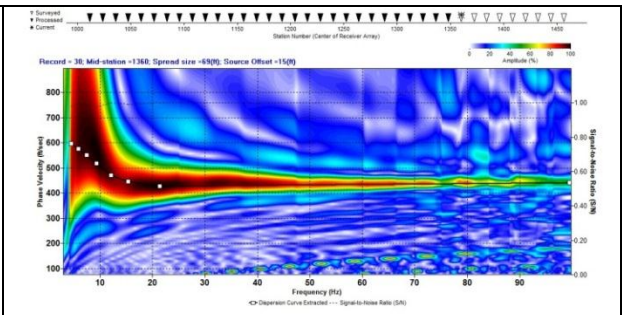
Record = 30; Mid-station =1360; Spread size =69(ft); Source Offset =15(ft)
Phase Velocity (ft/sec)
Frequency (Hz)
Signal-to-Noise Ratio (S/N)

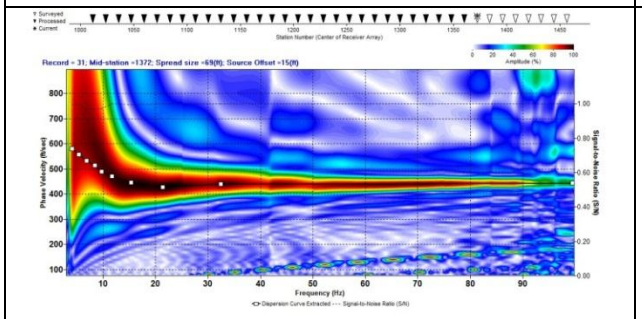
Record = 31; Mid-station =1372; Spread size =69(ft); Source Offset =15(ft)
Phase Velocity (ft/sec)
Frequency (Hz)
Signal-to-Noise Ratio (S/N)

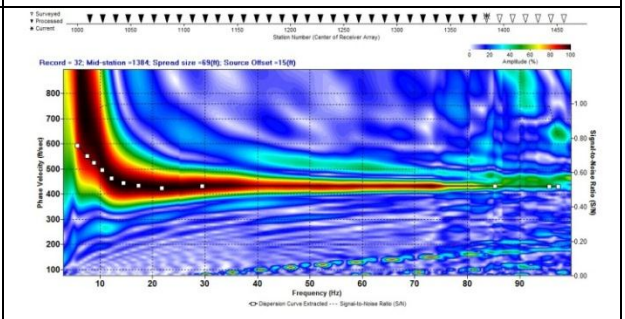
Record = 32; Mid-station =1384; Spread size =69(ft); Source Offset =15(ft)
Phase Velocity (ft/sec)
Frequency (Hz)
Signal-to-Noise Ratio (S/N)

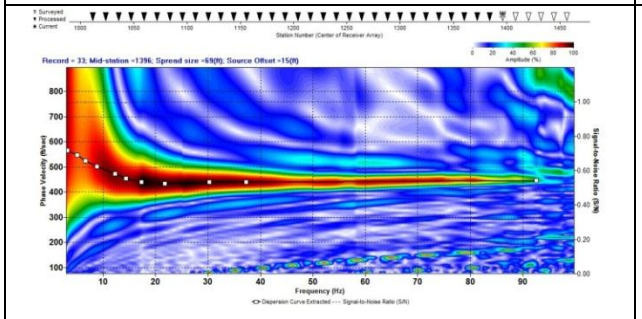
Record = 33; Mid-station =1396; Spread size =69(ft); Source Offset =15(ft)
Phase Velocity (ft/sec)
Frequency (Hz)
Signal-to-Noise Ratio (S/N)

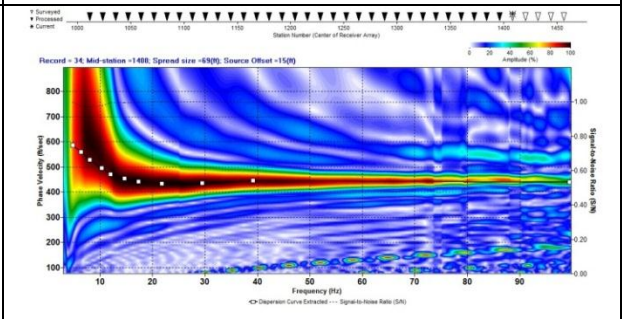
Record = 34; Mid-station =1408; Spread size =69(ft); Source Offset =15(ft)
Phase Velocity (ft/sec)
Frequency (Hz)
Signal-to-Noise Ratio (S/N)

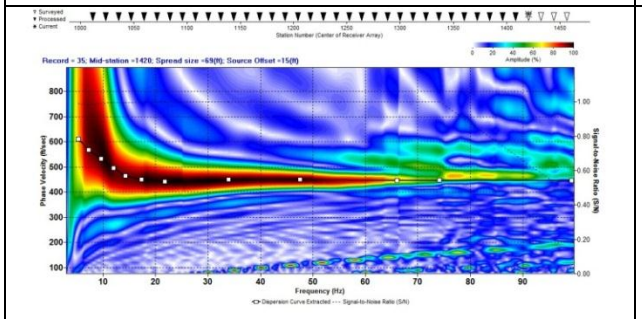
Record = 35; Mid-station =1420; Spread size =69(ft); Source Offset =15(ft)
Phase Velocity (ft/sec)
Frequency (Hz)
Signal-to-Noise Ratio (S/N)

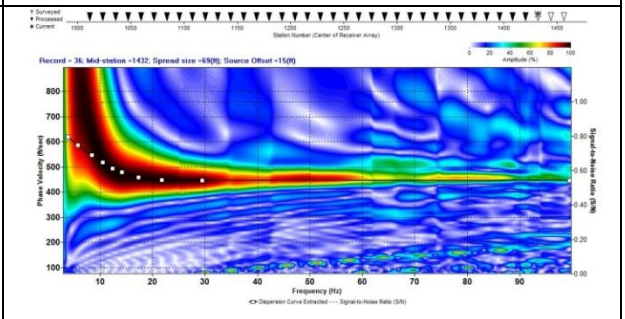
Record = 36; Mid-station =1432; Spread size =69(ft); Source Offset =15(ft)
Phase Velocity (ft/sec)
Frequency (Hz)
Signal-to-Noise Ratio (S/N)

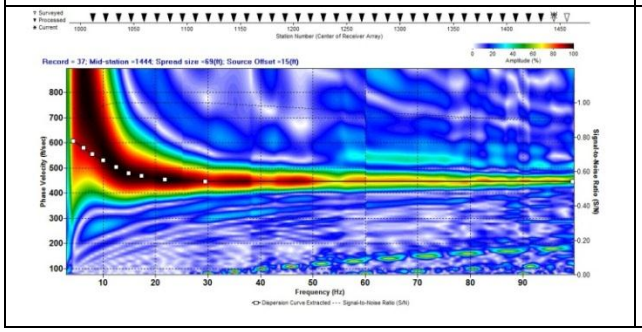
Record = 37; Mid-station =1444; Spread size =69(ft); Source Offset =15(ft)
Phase Velocity (ft/sec)
Frequency (Hz)
Signal-to-Noise Ratio (S/N)

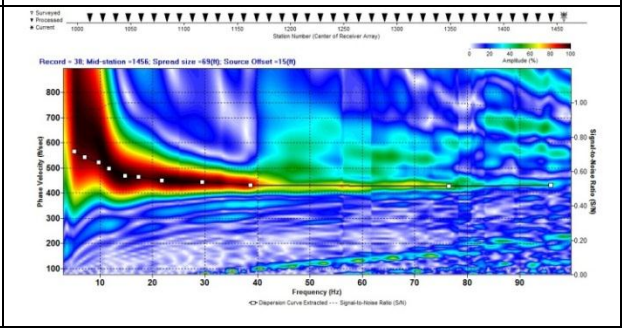
Record = 38; Mid-station =1456; Spread size =69(ft); Source Offset =15(ft)
Phase Velocity (ft/sec)
Frequency (Hz)
Signal-to-Noise Ratio (S/N)

## *(LossBot)Mob Inversion Results*

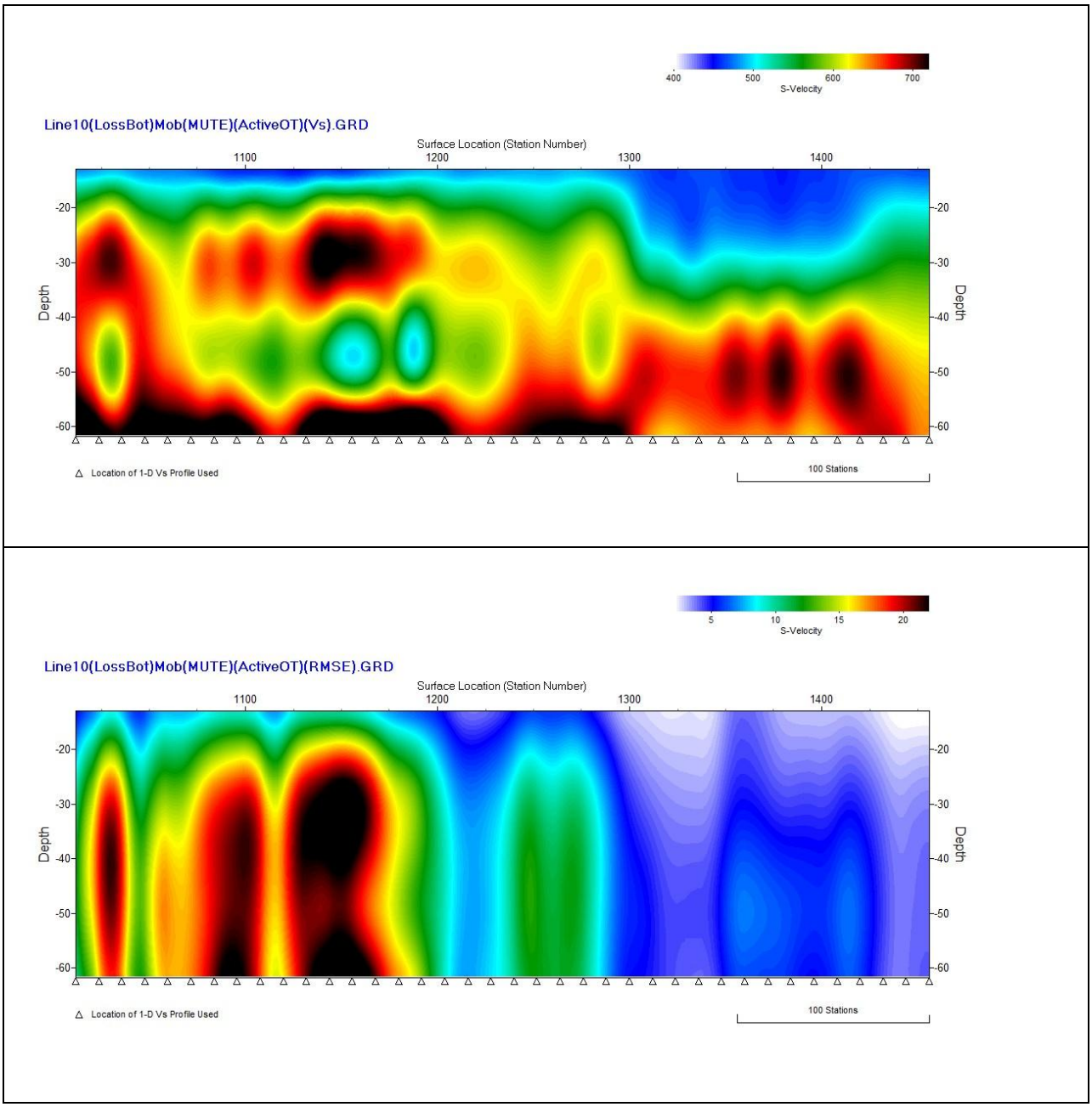

## Line 11

### Raw

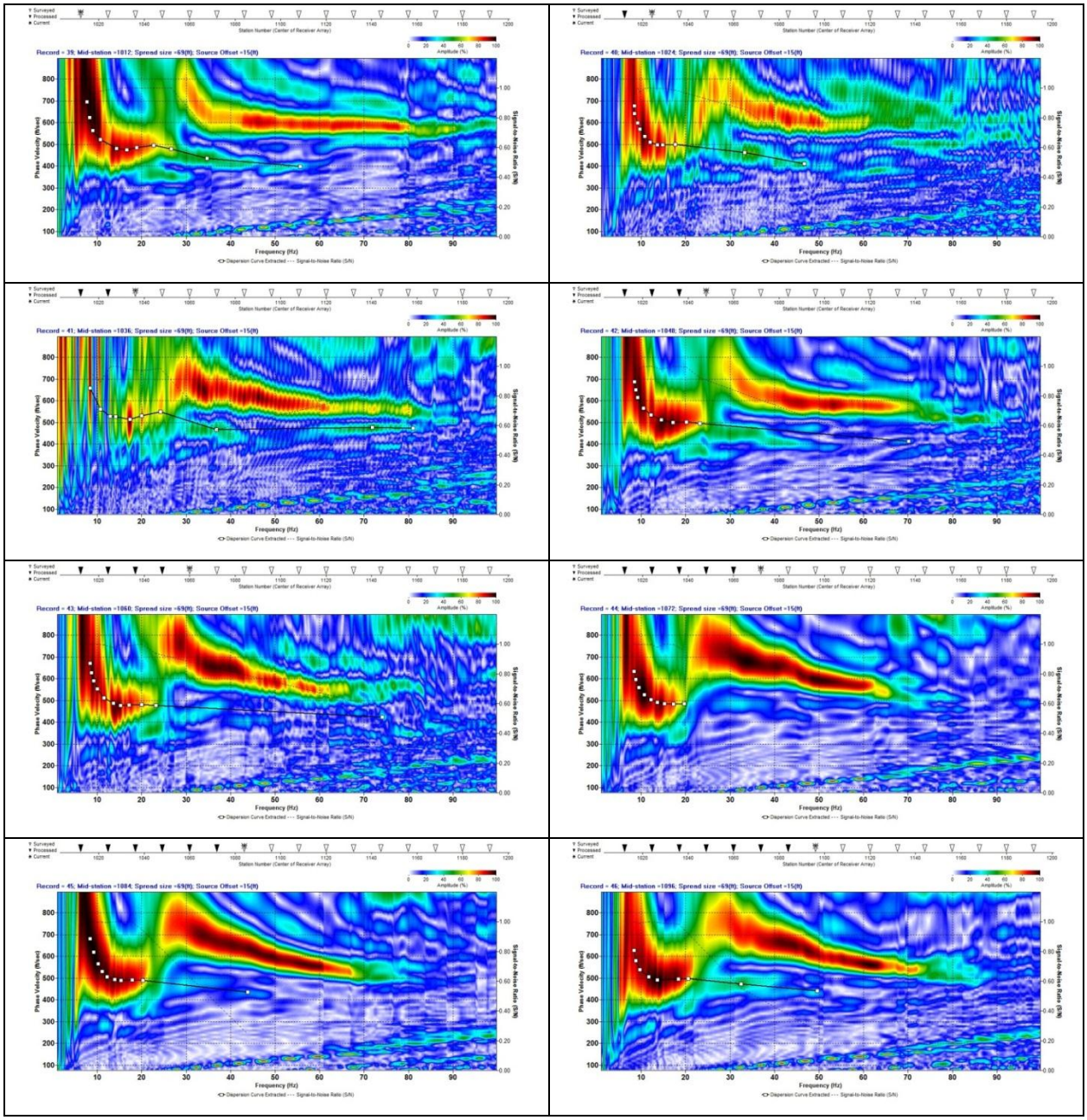
Record = 39; Mid-station =1012; Spread size =69(ft); Source Offset =15(ft)
Record = 40; Mid-station =1024; Spread size =69(ft); Source Offset =15(ft)
Record = 41; Mid-station =1036; Spread size =69(ft); Source Offset =15(ft)
Record = 42; Mid-station =1048; Spread size =69(ft); Source Offset =15(ft)
Record = 43; Mid-station =1060; Spread size =69(ft); Source Offset =15(ft)
Record = 44; Mid-station =1072; Spread size =69(ft); Source Offset =15(ft)
Record = 45; Mid-station =1084; Spread size =69(ft); Source Offset =15(ft)
Record = 46; Mid-station =1096; Spread size =69(ft); Source Offset =15(ft)
Phase Velocity (ft/sec)
Frequency (Hz)
Signal-to-Noise Ratio (S/N)
Station Number (Center of Receiver Array)
Amplitude (%)
Dispersion Curve Extracted --- Signal-to-Noise Ratio (S/N)

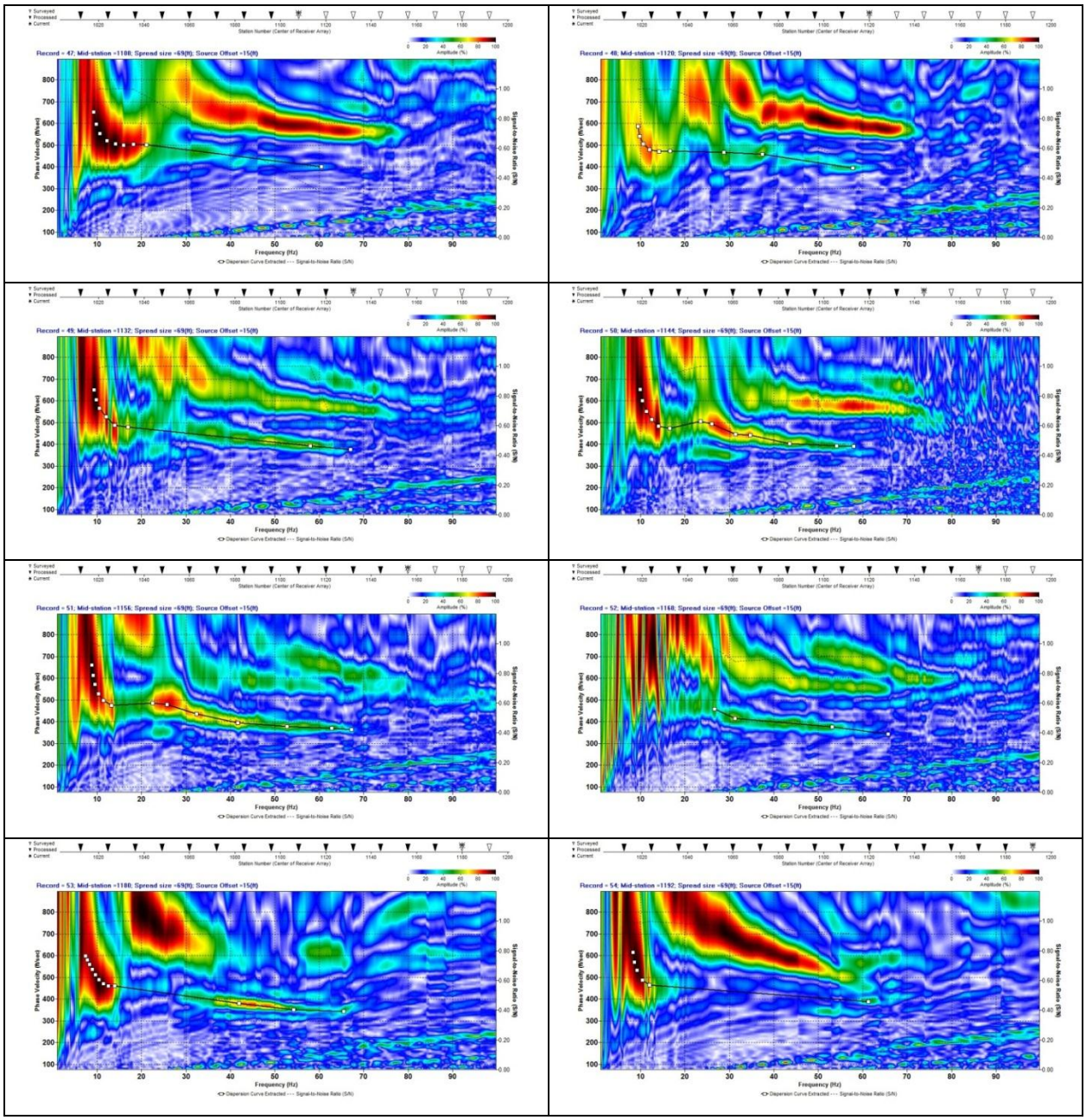
Record = 47; Mid-station =1188; Spread size =69(ft); Source Offset =15(ft)
Record = 48; Mid-station =1120; Spread size =69(ft); Source Offset =15(ft)
Record = 49; Mid-station =1132; Spread size =69(ft); Source Offset =15(ft)
Record = 50; Mid-station =1144; Spread size =69(ft); Source Offset =15(ft)
Record = 51; Mid-station =1156; Spread size =69(ft); Source Offset =15(ft)
Record = 52; Mid-station =1168; Spread size =69(ft); Source Offset =15(ft)
Record = 53; Mid-station =1180; Spread size =69(ft); Source Offset =15(ft)
Record = 54; Mid-station =1192; Spread size =69(ft); Source Offset =15(ft)
Phase Velocity (ft/sec)
Frequency (Hz)
Signal-to-Noise Ratio (S/N)
Station Number (Center of Receiver Array)
Amplitude (%)
Dispersion Curve Extracted --- Signal-to-Noise Ratio (S/N)

## *Raw Inversion Results*

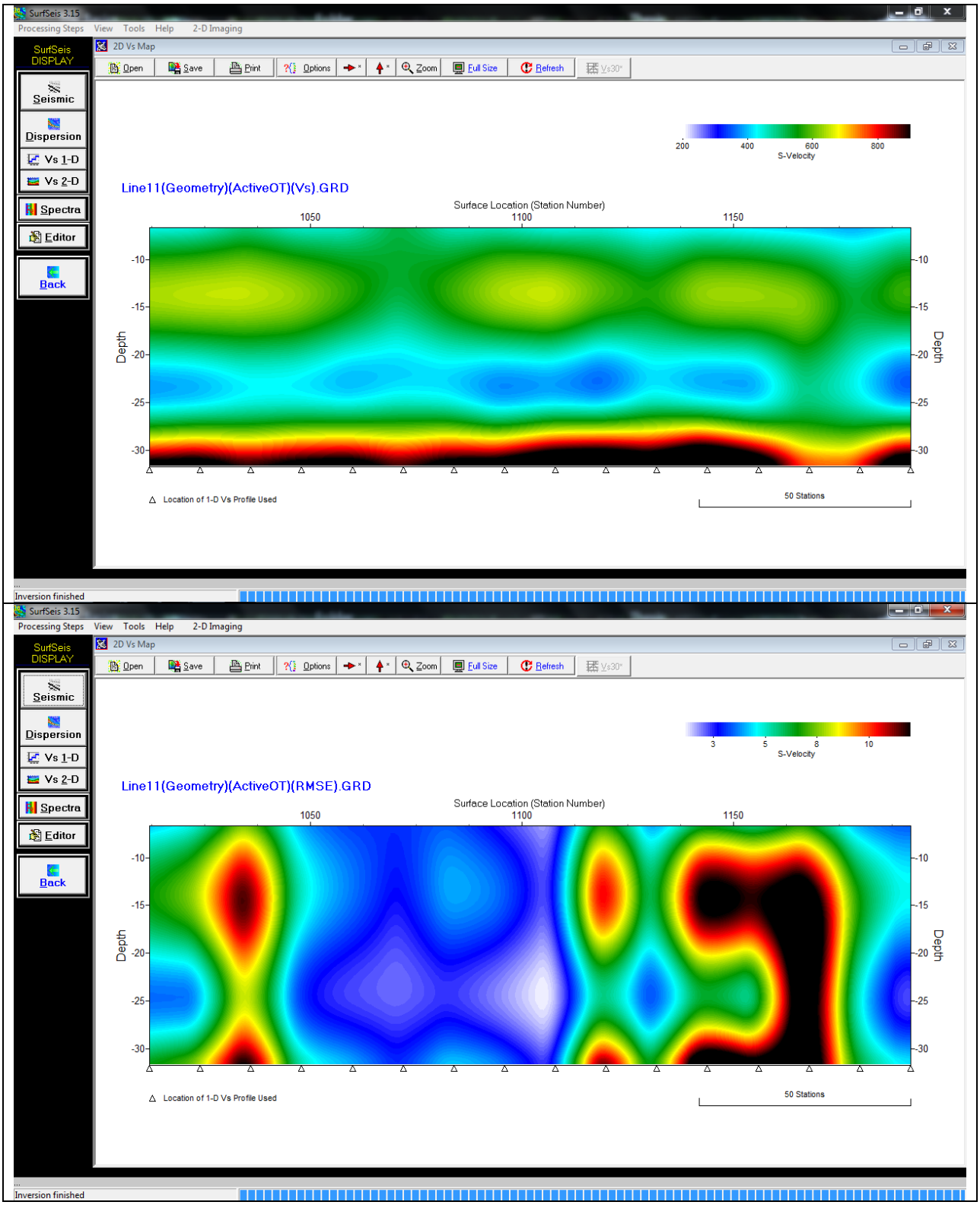

## Loose Bottom Mute

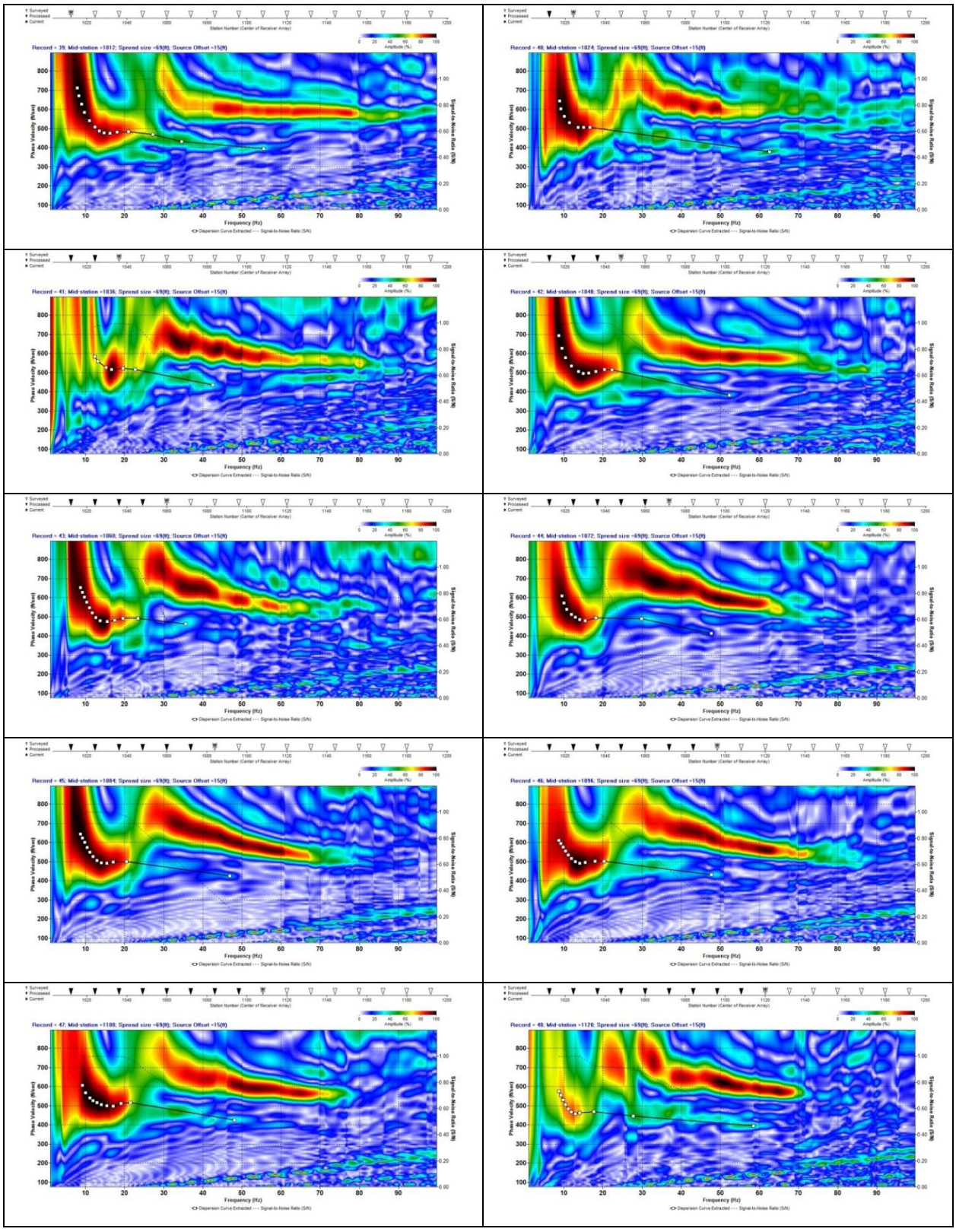

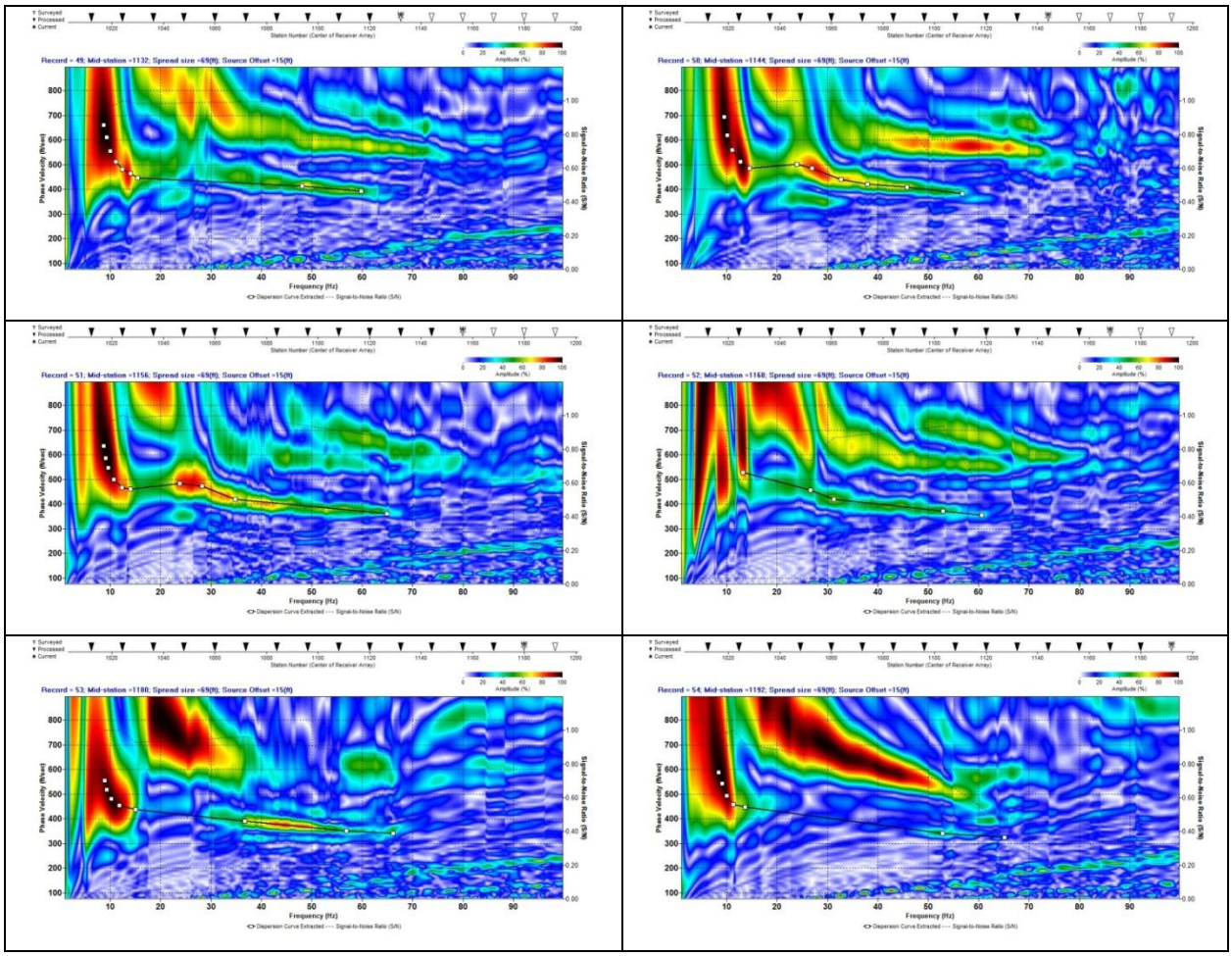
Record = 49; Mid-station =1132; Spread size =69(ft); Source Offset =15(ft)
Record = 50; Mid-station =1144; Spread size =69(ft); Source Offset =15(ft)
Record = 51; Mid-station =1156; Spread size =69(ft); Source Offset =15(ft)
Record = 52; Mid-station =1168; Spread size =69(ft); Source Offset =15(ft)
Record = 53; Mid-station =1180; Spread size =69(ft); Source Offset =15(ft)
Record = 54; Mid-station =1192; Spread size =69(ft); Source Offset =15(ft)
Phase Velocity (ft/sec)
Frequency (Hz)
Signal-to-Noise Ratio (S/N)
Station Number (Center of Receiver Array)
Amplitude (%)
Dispersion Curve Extracted --- Signal-to-Noise Ratio (S/N)

## *(LossBot) Inversion Results*

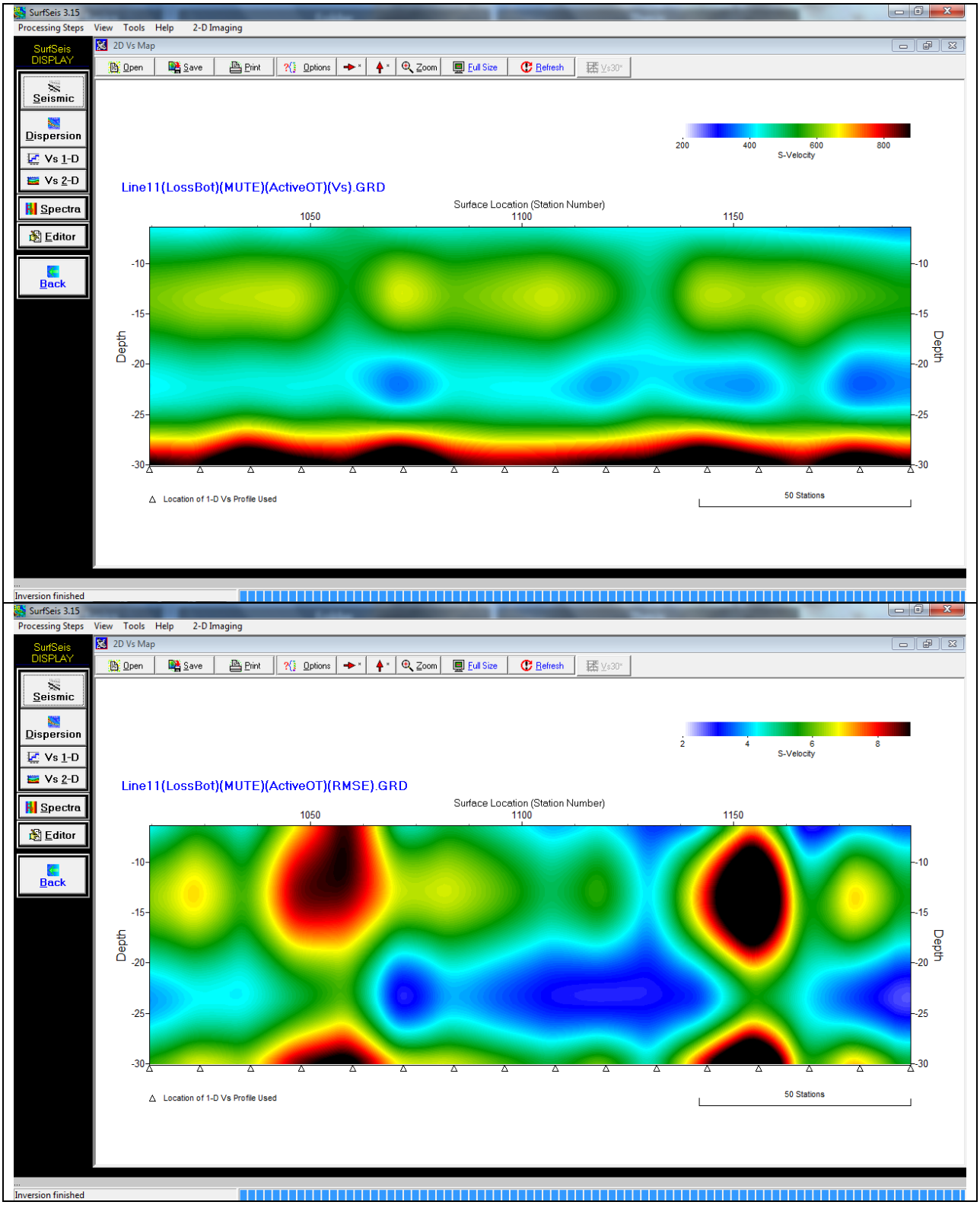

## Aggressive picking on Loose Bottom Mute

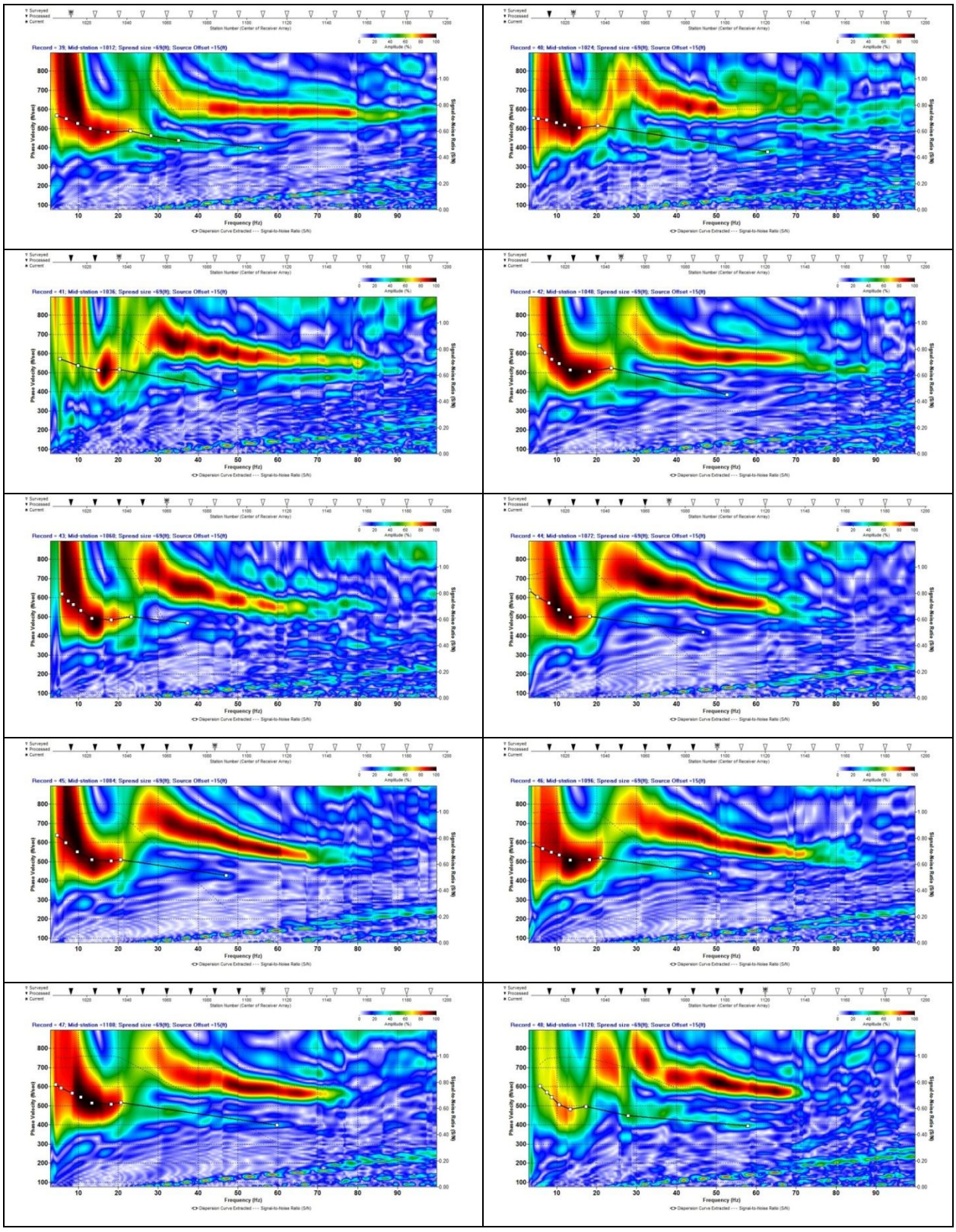

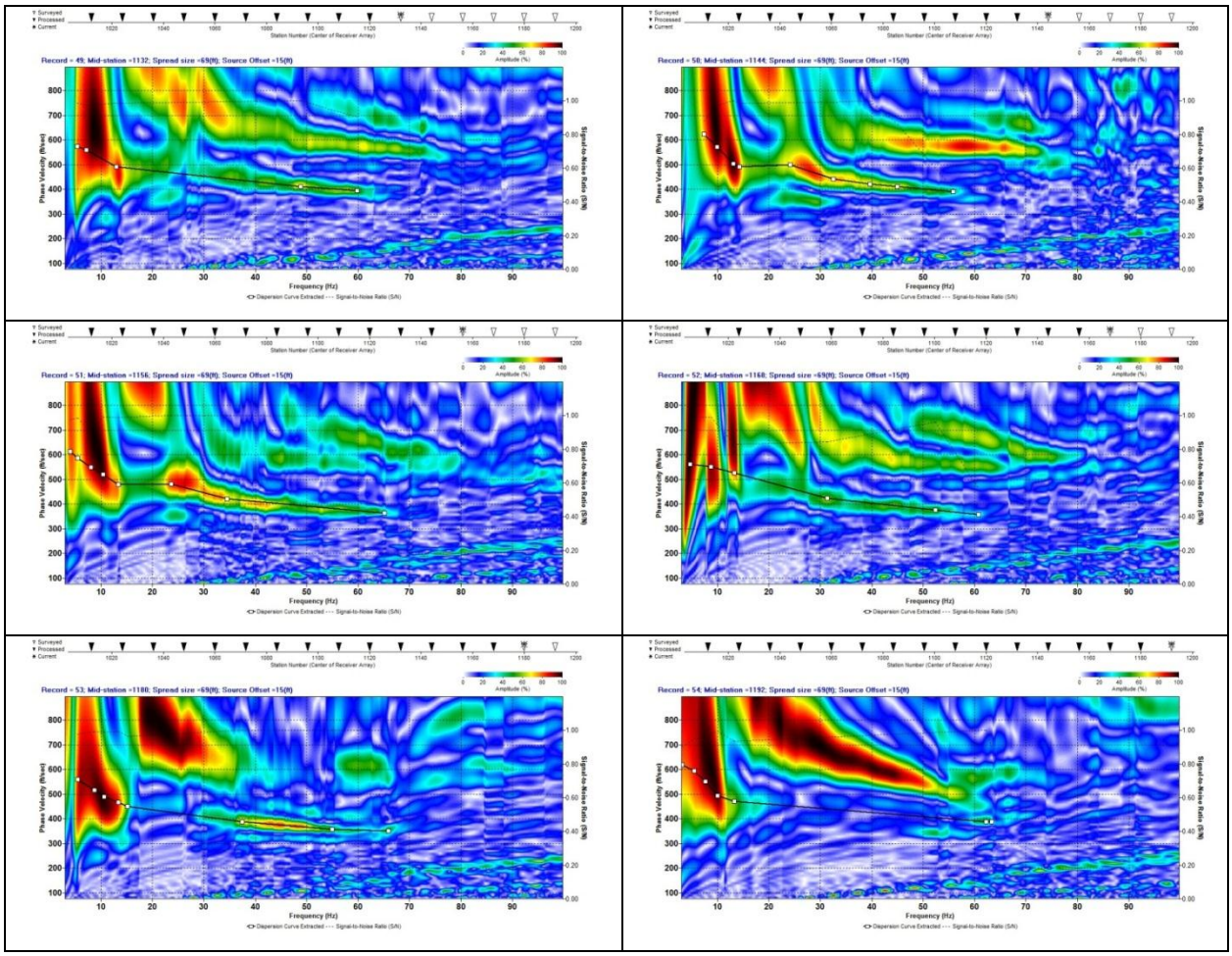
Record = 49; Mid-station =1132; Spread size =69(ft); Source Offset =15(ft)
Record = 50; Mid-station =1144; Spread size =69(ft); Source Offset =15(ft)
Record = 51; Mid-station =1156; Spread size =69(ft); Source Offset =15(ft)
Record = 52; Mid-station =1168; Spread size =69(ft); Source Offset =15(ft)
Record = 53; Mid-station =1180; Spread size =69(ft); Source Offset =15(ft)
Record = 54; Mid-station =1192; Spread size =69(ft); Source Offset =15(ft)
Phase Velocity (ft/sec)
Frequency (Hz)
Signal-to-Noise Ratio (S/N)
Amplitude (%)
Station Number (Center of Receiver Array)
Dispersion Curve Extracted --- Signal-to-Noise Ratio (S/N)

## *(LossBot)Mob Inversion Results*

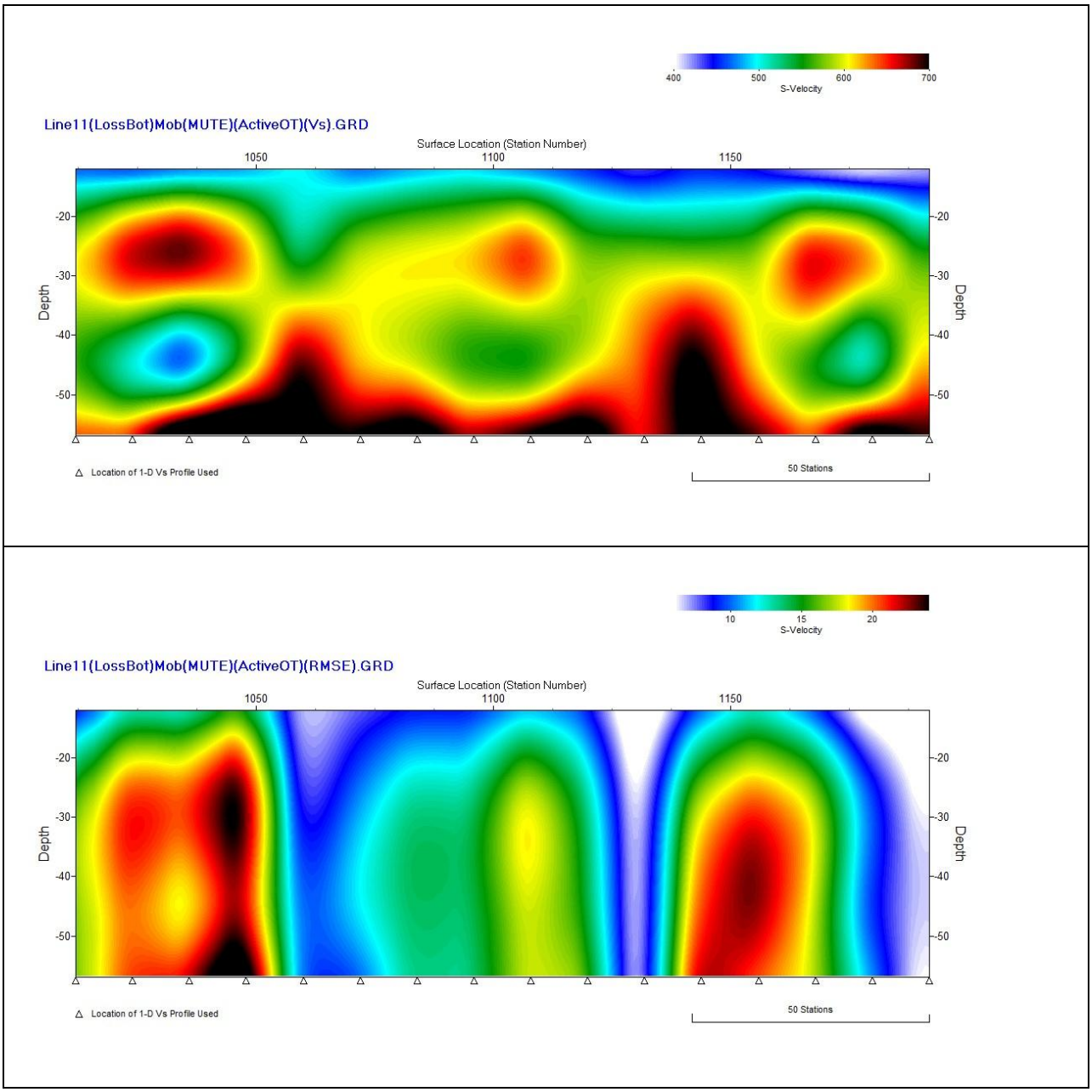

## Line 12

### Raw

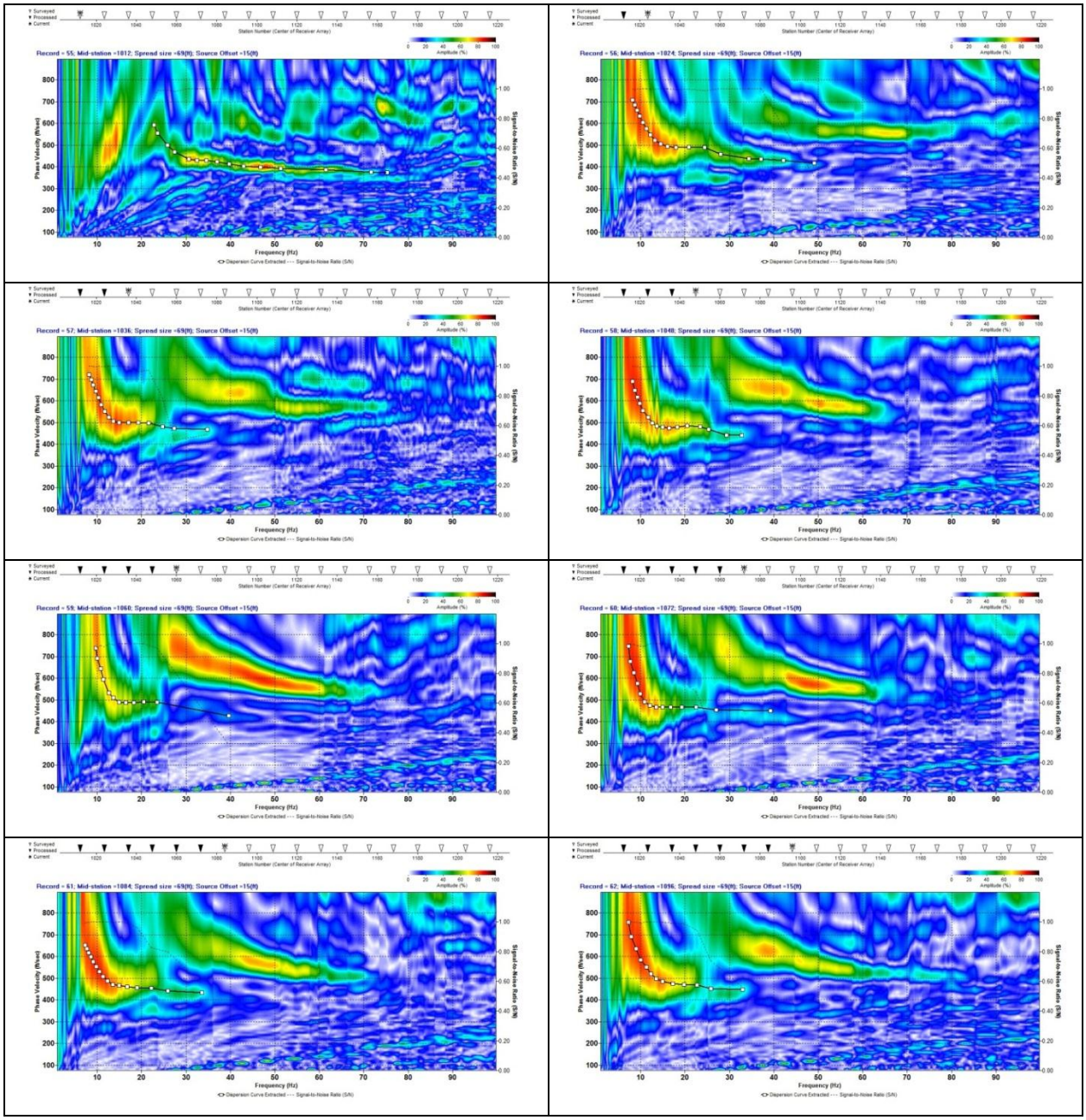
Record = 55; Mid-station =1012; Spread size =69(ft); Source Offset =15(ft)
Record = 56; Mid-station =1024; Spread size =69(ft); Source Offset =15(ft)
Record = 57; Mid-station =1036; Spread size =69(ft); Source Offset =15(ft)
Record = 58; Mid-station =1048; Spread size =69(ft); Source Offset =15(ft)
Record = 59; Mid-station =1060; Spread size =69(ft); Source Offset =15(ft)
Record = 60; Mid-station =1072; Spread size =69(ft); Source Offset =15(ft)
Record = 61; Mid-station =1084; Spread size =69(ft); Source Offset =15(ft)
Record = 62; Mid-station =1096; Spread size =69(ft); Source Offset =15(ft)
Phase Velocity (ft/sec)
Frequency (Hz)
Signal-to-Noise Ratio (S/N)

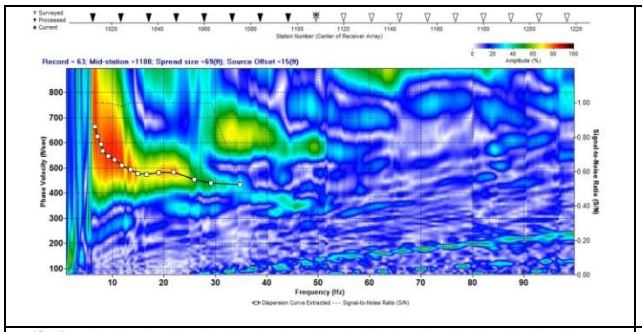
Record = 63; Mid-station =1188; Spread size =69(ft); Source Offset =15(ft)
Phase Velocity (ft/sec)
Frequency (Hz)
Signal-to-Noise Ratio (S/N)

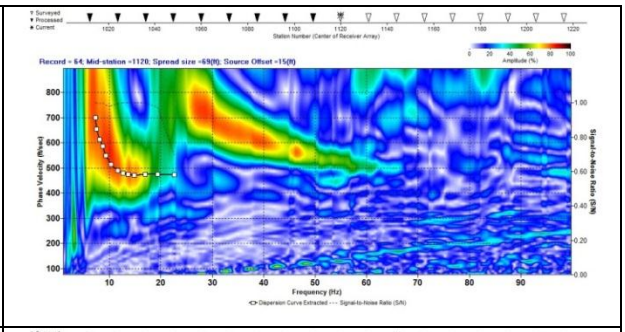
Record = 64; Mid-station =1120; Spread size =69(ft); Source Offset =15(ft)
Phase Velocity (ft/sec)
Frequency (Hz)
Signal-to-Noise Ratio (S/N)

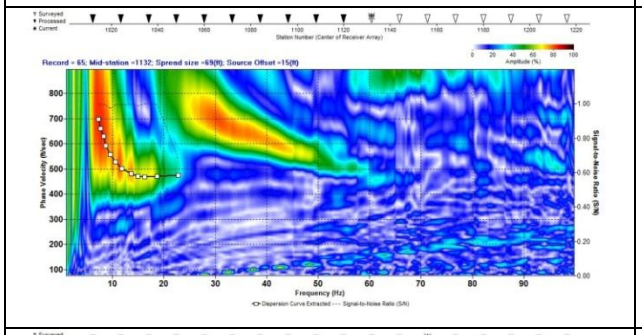
Record = 65; Mid-station =1132; Spread size =69(ft); Source Offset =15(ft)
Phase Velocity (ft/sec)
Frequency (Hz)
Signal-to-Noise Ratio (S/N)

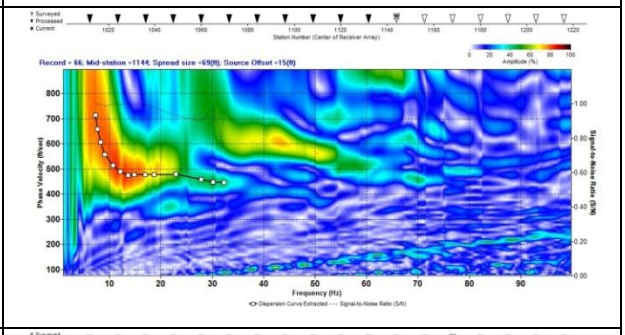
Record = 66; Mid-station =1144; Spread size =69(ft); Source Offset =15(ft)
Phase Velocity (ft/sec)
Frequency (Hz)
Signal-to-Noise Ratio (S/N)

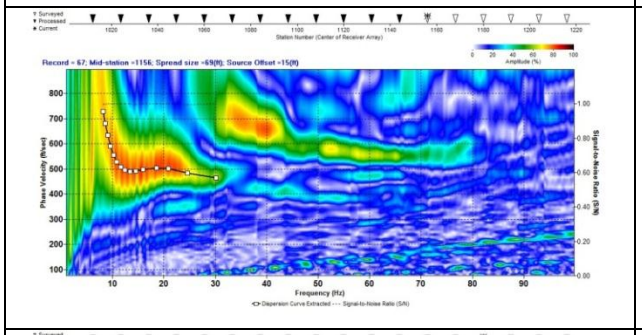
Record = 67; Mid-station =1156; Spread size =69(ft); Source Offset =15(ft)
Phase Velocity (ft/sec)
Frequency (Hz)
Signal-to-Noise Ratio (S/N)

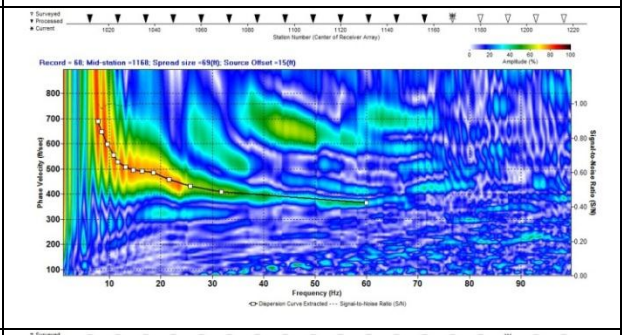
Record = 68; Mid-station =1168; Spread size =69(ft); Source Offset =15(ft)
Phase Velocity (ft/sec)
Frequency (Hz)
Signal-to-Noise Ratio (S/N)

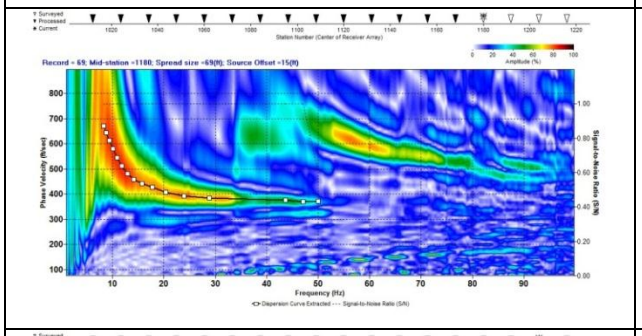
Record = 69; Mid-station =1180; Spread size =69(ft); Source Offset =15(ft)
Phase Velocity (ft/sec)
Frequency (Hz)
Signal-to-Noise Ratio (S/N)

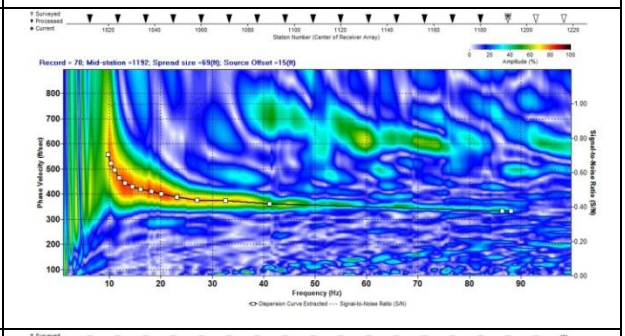
Record = 70; Mid-station =1192; Spread size =69(ft); Source Offset =15(ft)
Phase Velocity (ft/sec)
Frequency (Hz)
Signal-to-Noise Ratio (S/N)

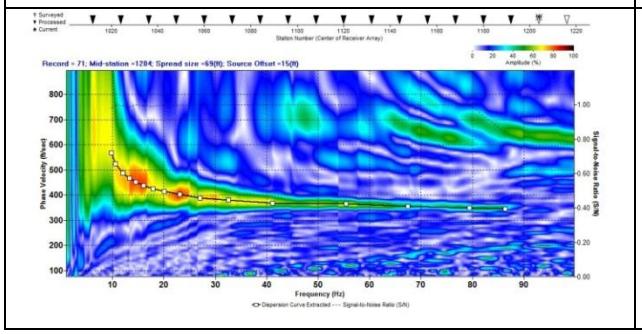
Record = 71; Mid-station =1204; Spread size =69(ft); Source Offset =15(ft)
Phase Velocity (ft/sec)
Frequency (Hz)
Signal-to-Noise Ratio (S/N)

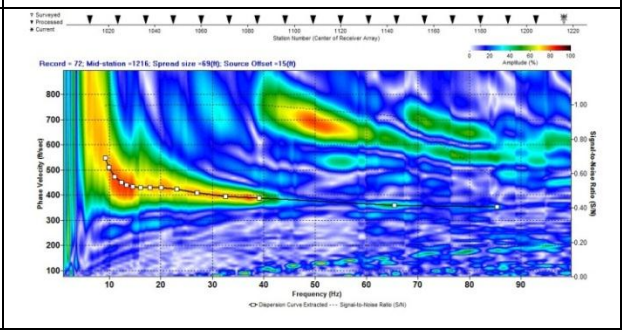
Record = 72; Mid-station =1216; Spread size =69(ft); Source Offset =15(ft)
Phase Velocity (ft/sec)
Frequency (Hz)
Signal-to-Noise Ratio (S/N)

## *Raw Inversion Results*

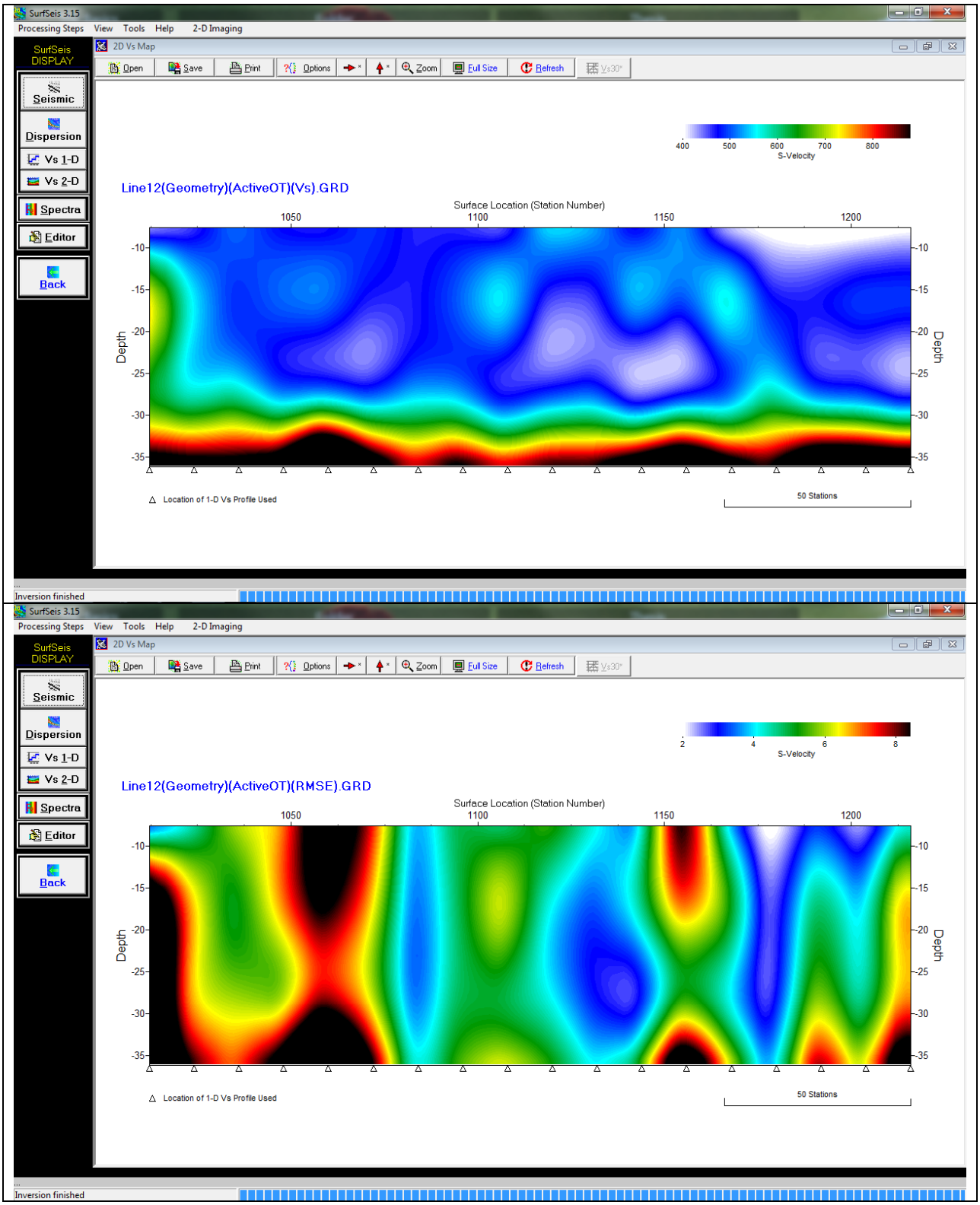

## Loose Bottom Mute

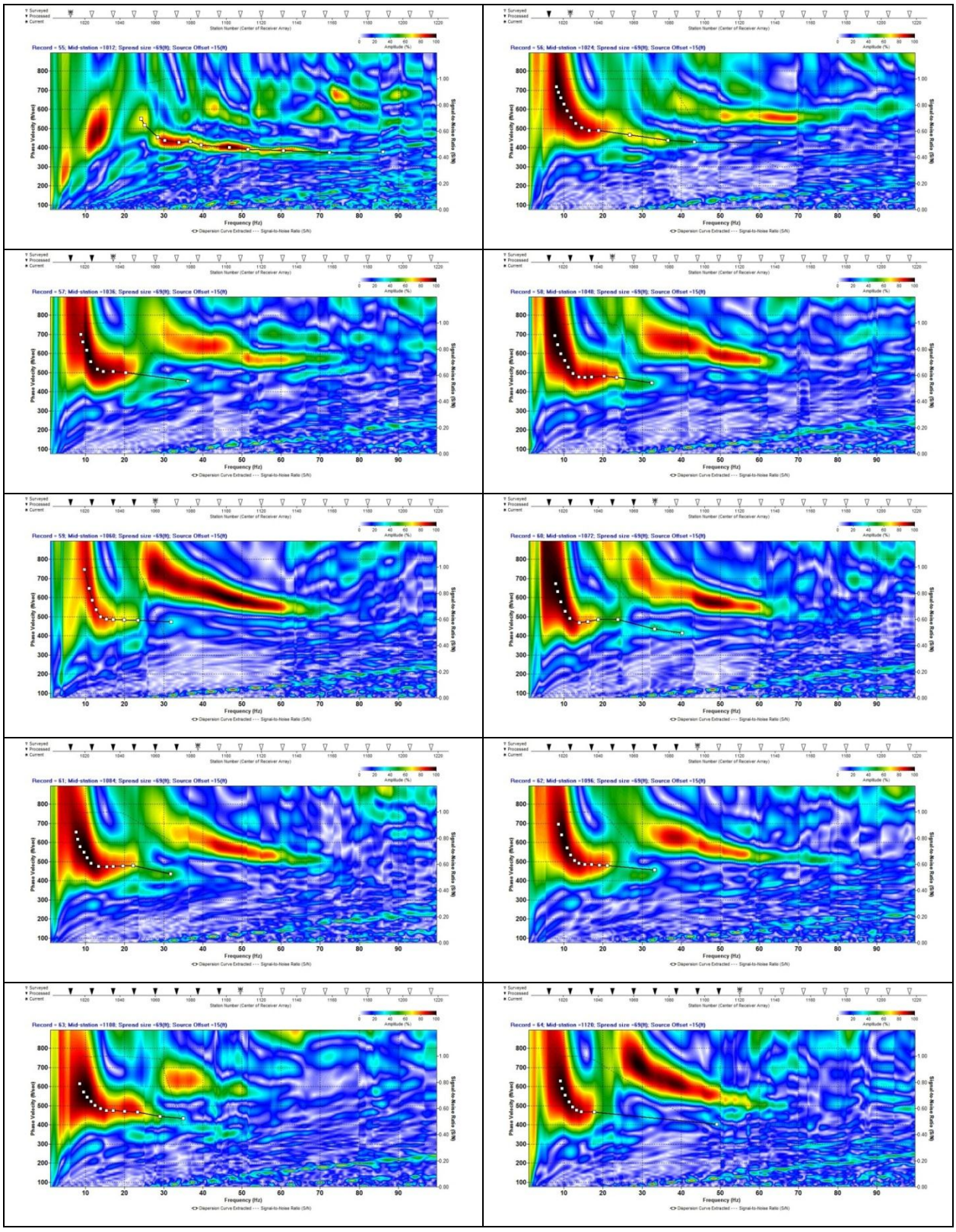

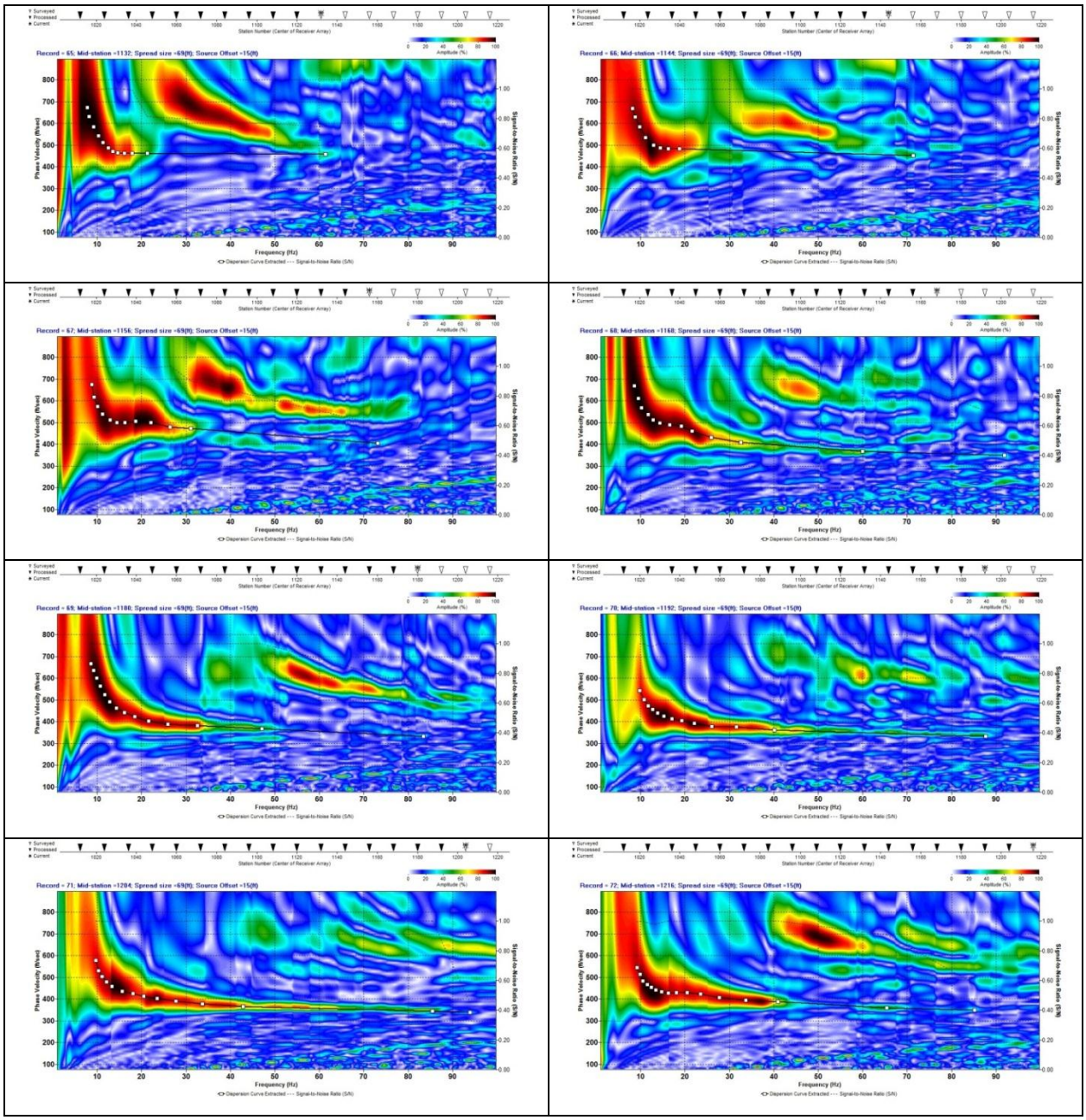
Record = 65; Mid-station =1132; Spread size =69(ft); Source Offset =15(ft)
Record = 66; Mid-station =1144; Spread size =69(ft); Source Offset =15(ft)
Record = 67; Mid-station =1156; Spread size =69(ft); Source Offset =15(ft)
Record = 68; Mid-station =1168; Spread size =69(ft); Source Offset =15(ft)
Record = 69; Mid-station =1180; Spread size =69(ft); Source Offset =15(ft)
Record = 70; Mid-station =1192; Spread size =69(ft); Source Offset =15(ft)
Record = 71; Mid-station =1204; Spread size =69(ft); Source Offset =15(ft)
Record = 72; Mid-station =1216; Spread size =69(ft); Source Offset =15(ft)
Phase Velocity (ft/sec)
Frequency (Hz)
Signal-to-Noise Ratio (S/N)
Station Number (Center of Receiver Array)
Amplitude (%)
Dispersion Curve Extracted --- Signal-to-Noise Ratio (S/N)

## *(LossBot) Inversion Results*

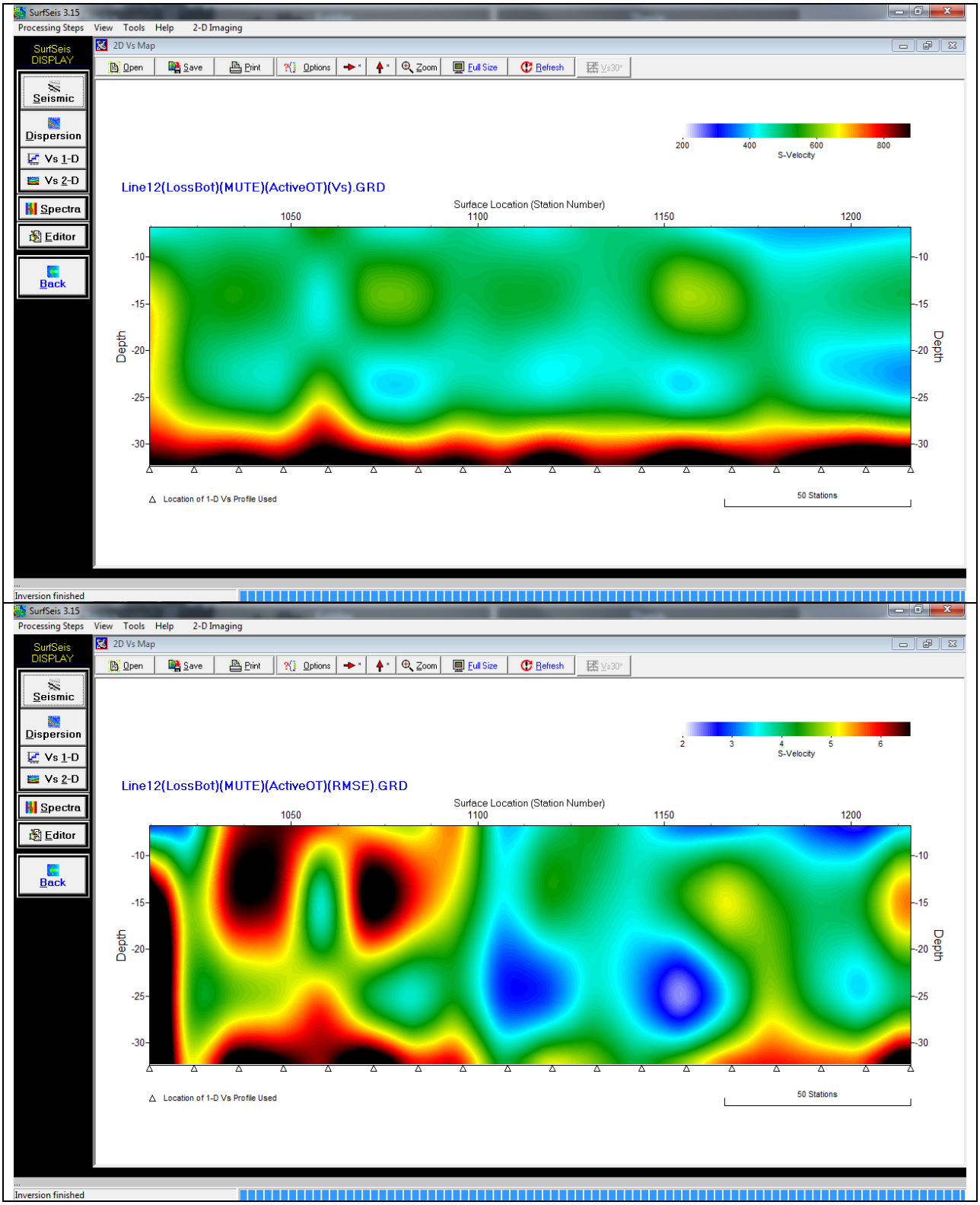

## Aggressive picking on Loose Bottom Mute

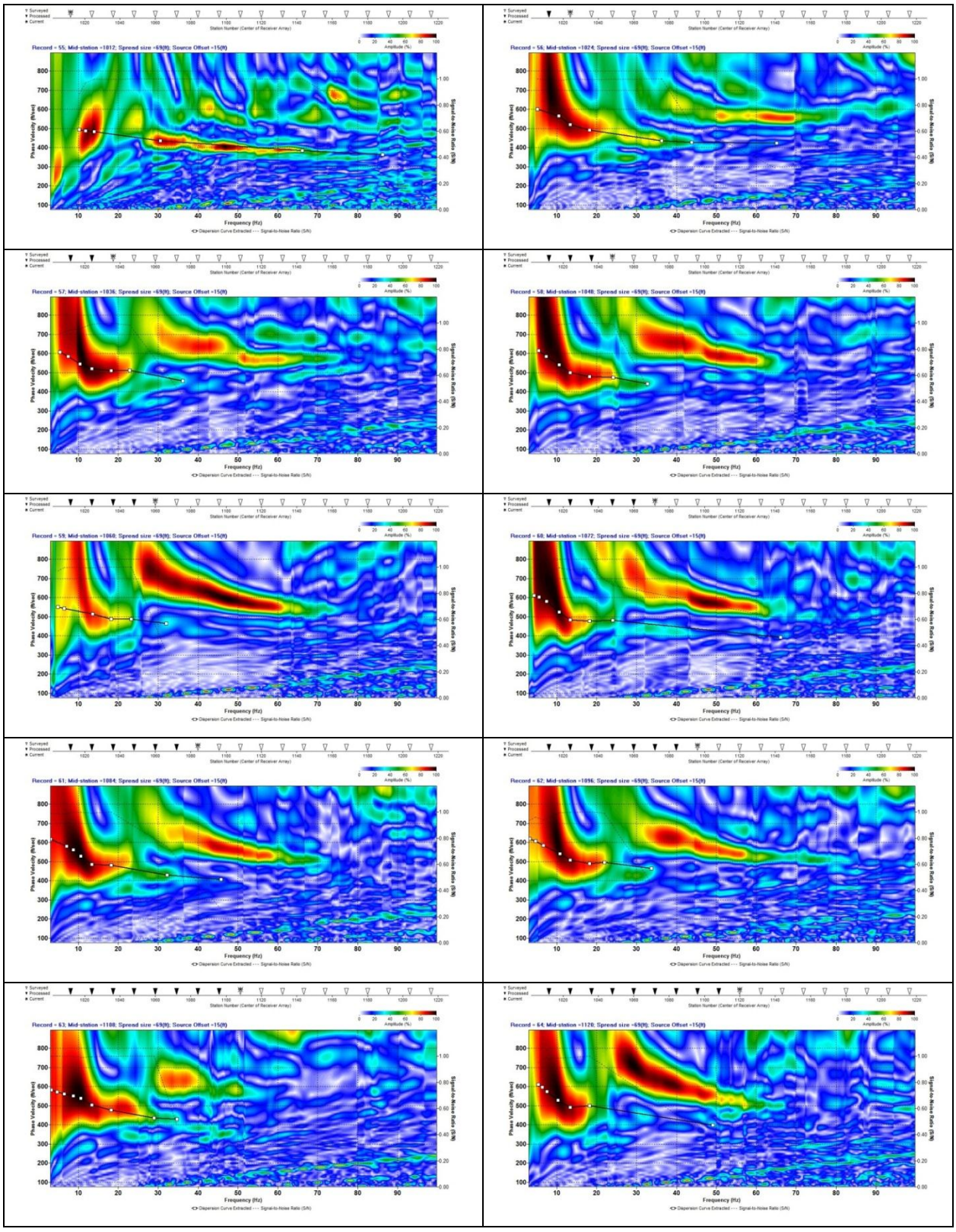

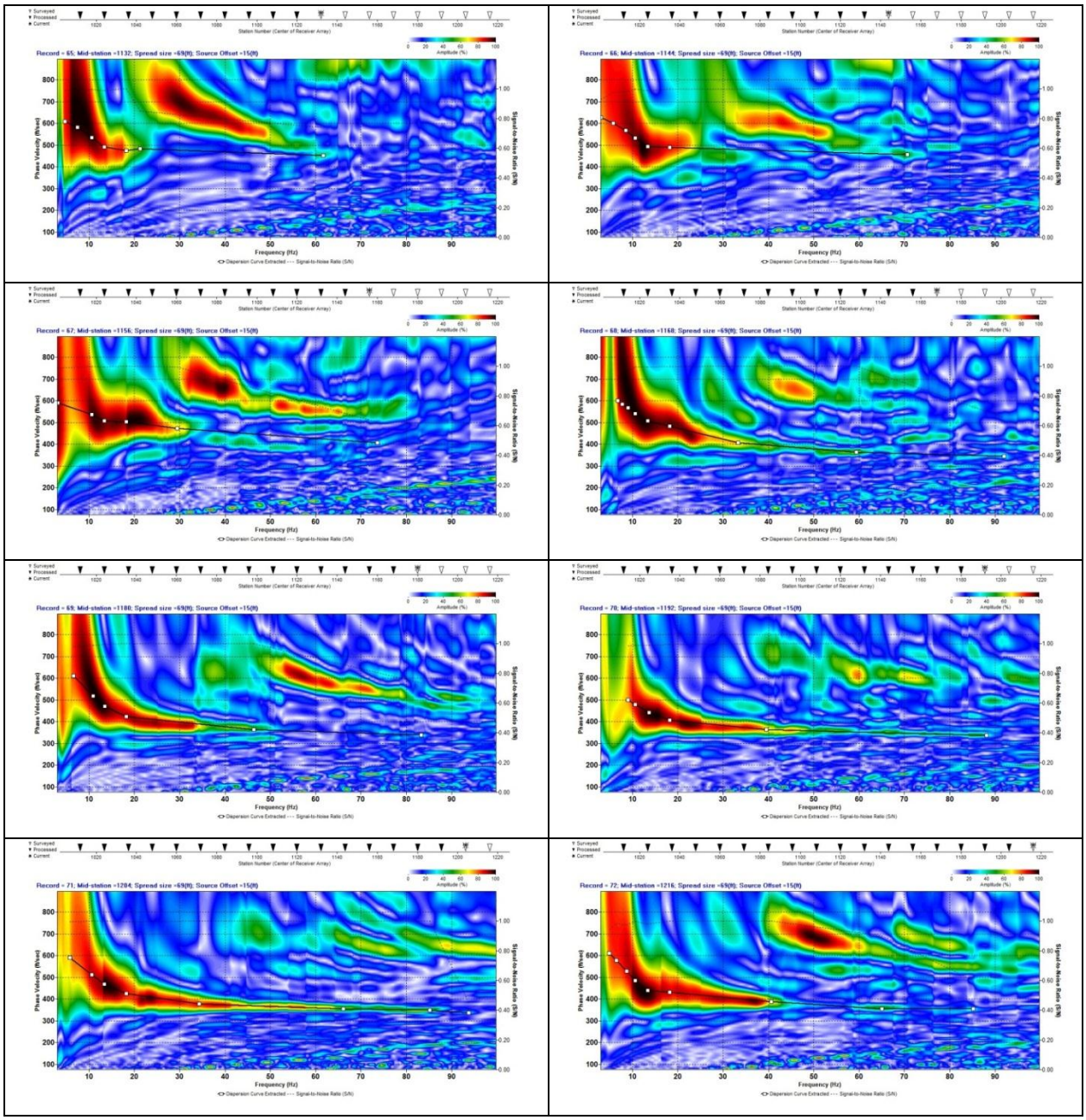
Record = 65; Mid-station =1132; Spread size =69(ft); Source Offset =15(ft)
Record = 66; Mid-station =1144; Spread size =69(ft); Source Offset =15(ft)
Record = 67; Mid-station =1156; Spread size =69(ft); Source Offset =15(ft)
Record = 68; Mid-station =1168; Spread size =69(ft); Source Offset =15(ft)
Record = 69; Mid-station =1180; Spread size =69(ft); Source Offset =15(ft)
Record = 70; Mid-station =1192; Spread size =69(ft); Source Offset =15(ft)
Record = 71; Mid-station =1204; Spread size =69(ft); Source Offset =15(ft)
Record = 72; Mid-station =1216; Spread size =69(ft); Source Offset =15(ft)
Phase Velocity (ft/sec)
Frequency (Hz)
Signal-to-Noise Ratio (S/N)
Station Number (Center of Receiver Array)
Amplitude (%)
Dispersion Curve Extracted --- Signal-to-Noise Ratio (S/N)

## *(LossBot)Mob Inversion Results*

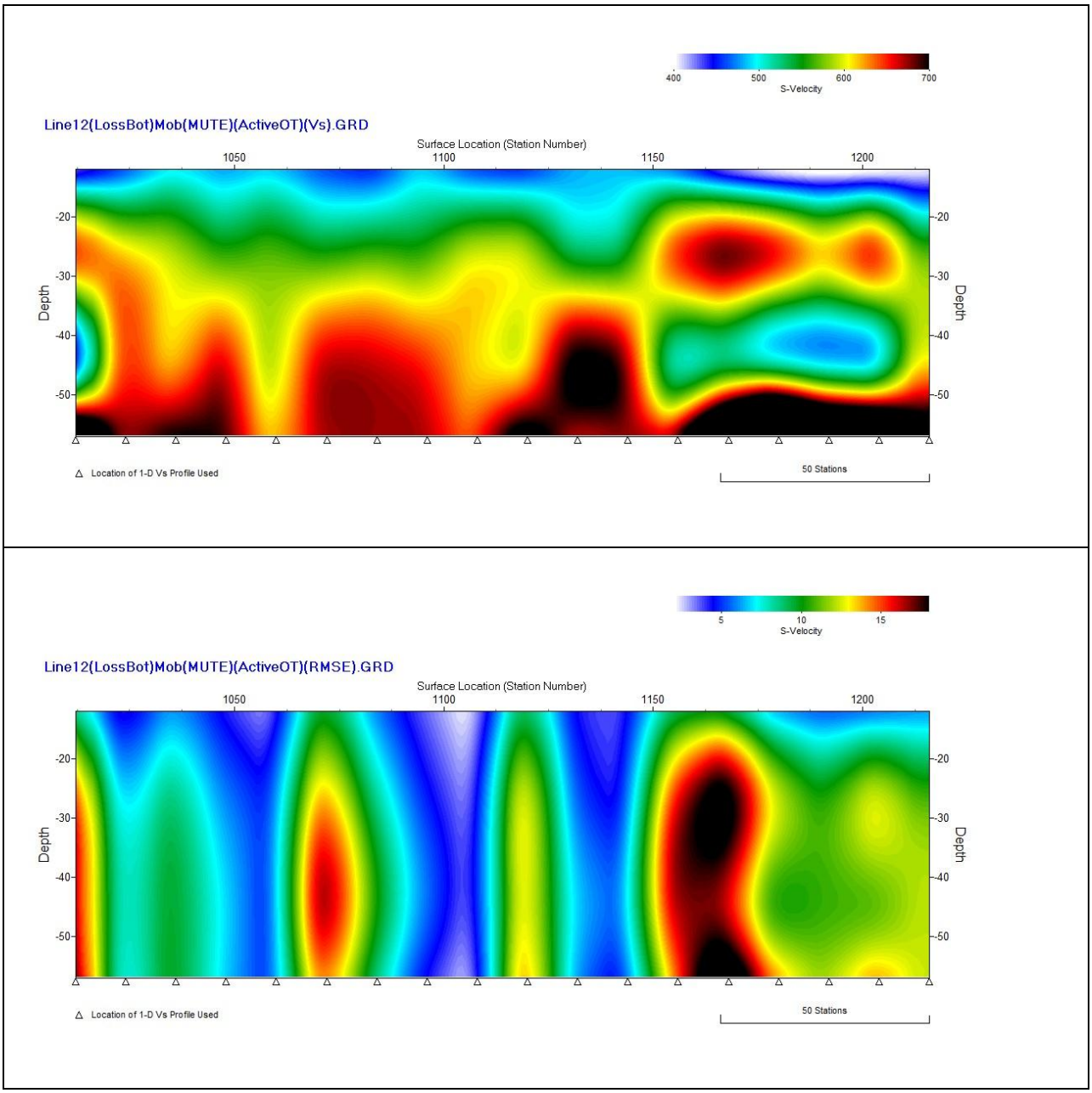

## Line 13

### Raw

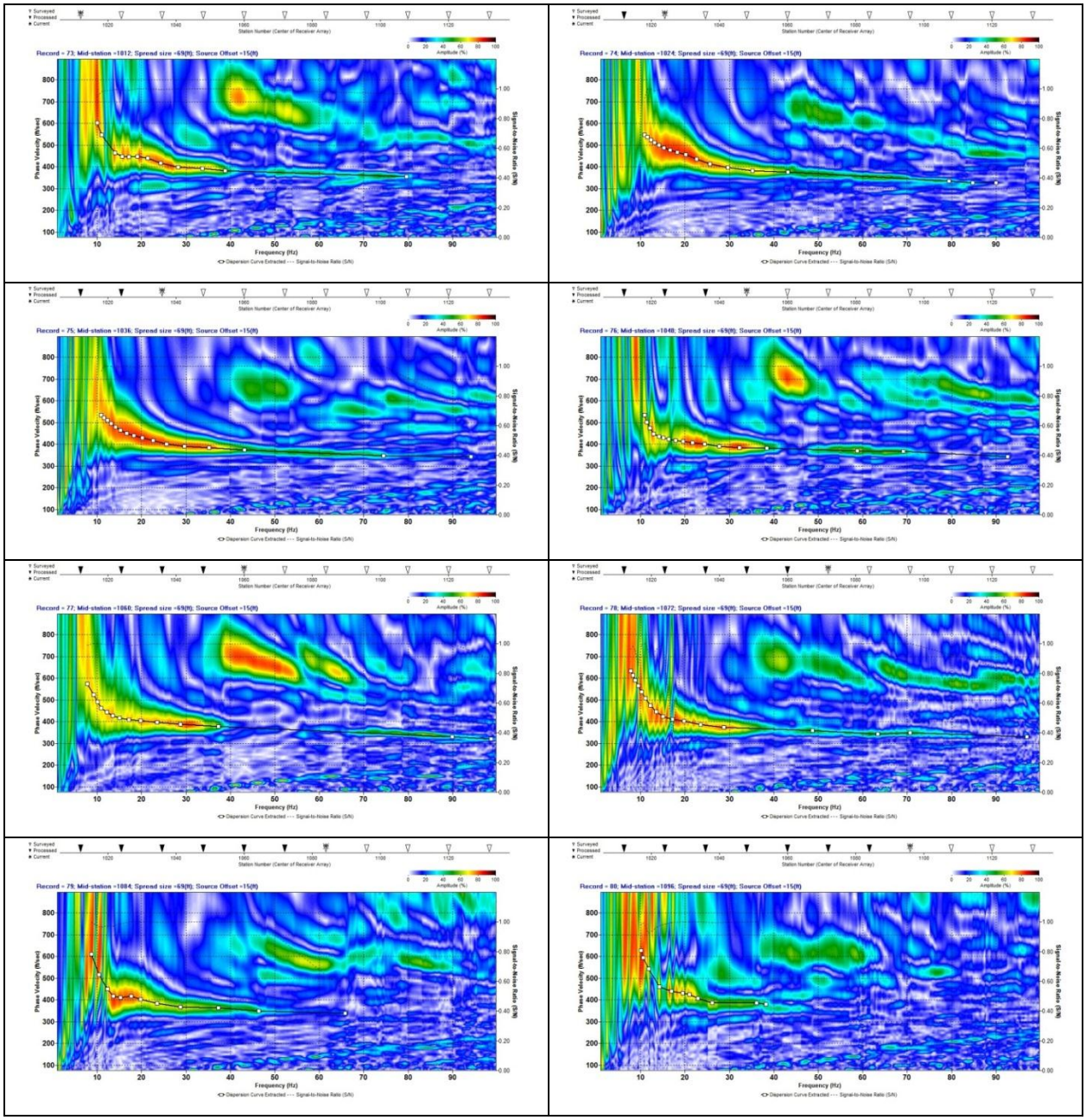
Record = 73; Mid-station =1012; Spread size =69(ft); Source Offset =15(ft)
Record = 74; Mid-station =1024; Spread size =69(ft); Source Offset =15(ft)
Record = 75; Mid-station =1036; Spread size =69(ft); Source Offset =15(ft)
Record = 76; Mid-station =1048; Spread size =69(ft); Source Offset =15(ft)
Record = 77; Mid-station =1060; Spread size =69(ft); Source Offset =15(ft)
Record = 78; Mid-station =1072; Spread size =69(ft); Source Offset =15(ft)
Record = 79; Mid-station =1084; Spread size =69(ft); Source Offset =15(ft)
Record = 80; Mid-station =1096; Spread size =69(ft); Source Offset =15(ft)
Phase Velocity (ft/sec)
Frequency (Hz)
Signal-to-Noise Ratio (S/N)

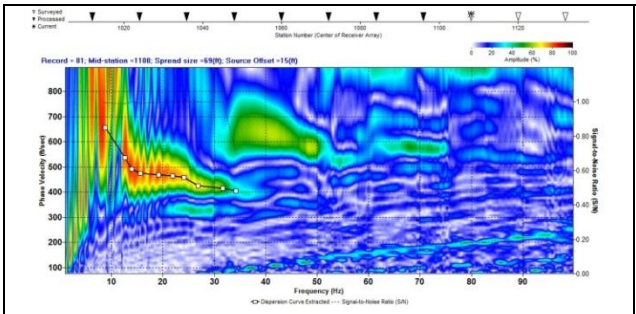
Record = 81; Mid-station =1180; Spread size =69(9); Source Offset =15(9)
Phase Velocity (ft/sec)
Frequency (Hz)
Signal-to-Noise Ratio (S/N)
Amplitude (%)
Station Number (Center of Receiver Array)

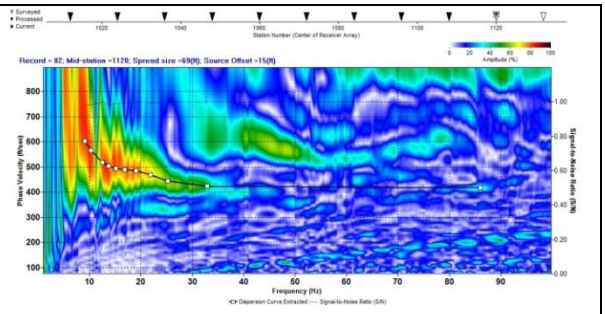
Record = 82; Mid-station =1120; Spread size =69(9); Source Offset =15(9)
Phase Velocity (ft/sec)
Frequency (Hz)
Signal-to-Noise Ratio (S/N)
Amplitude (%)
Station Number (Center of Receiver Array)

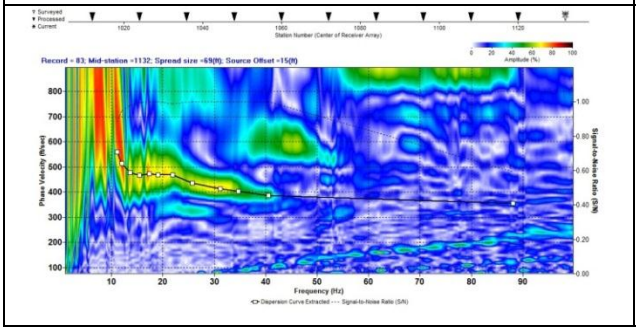
Record = 83; Mid-station =1132; Spread size =69(9); Source Offset =15(9)
Phase Velocity (ft/sec)
Frequency (Hz)
Signal-to-Noise Ratio (S/N)
Amplitude (%)
Station Number (Center of Receiver Array)

## *Raw Inversion Results*

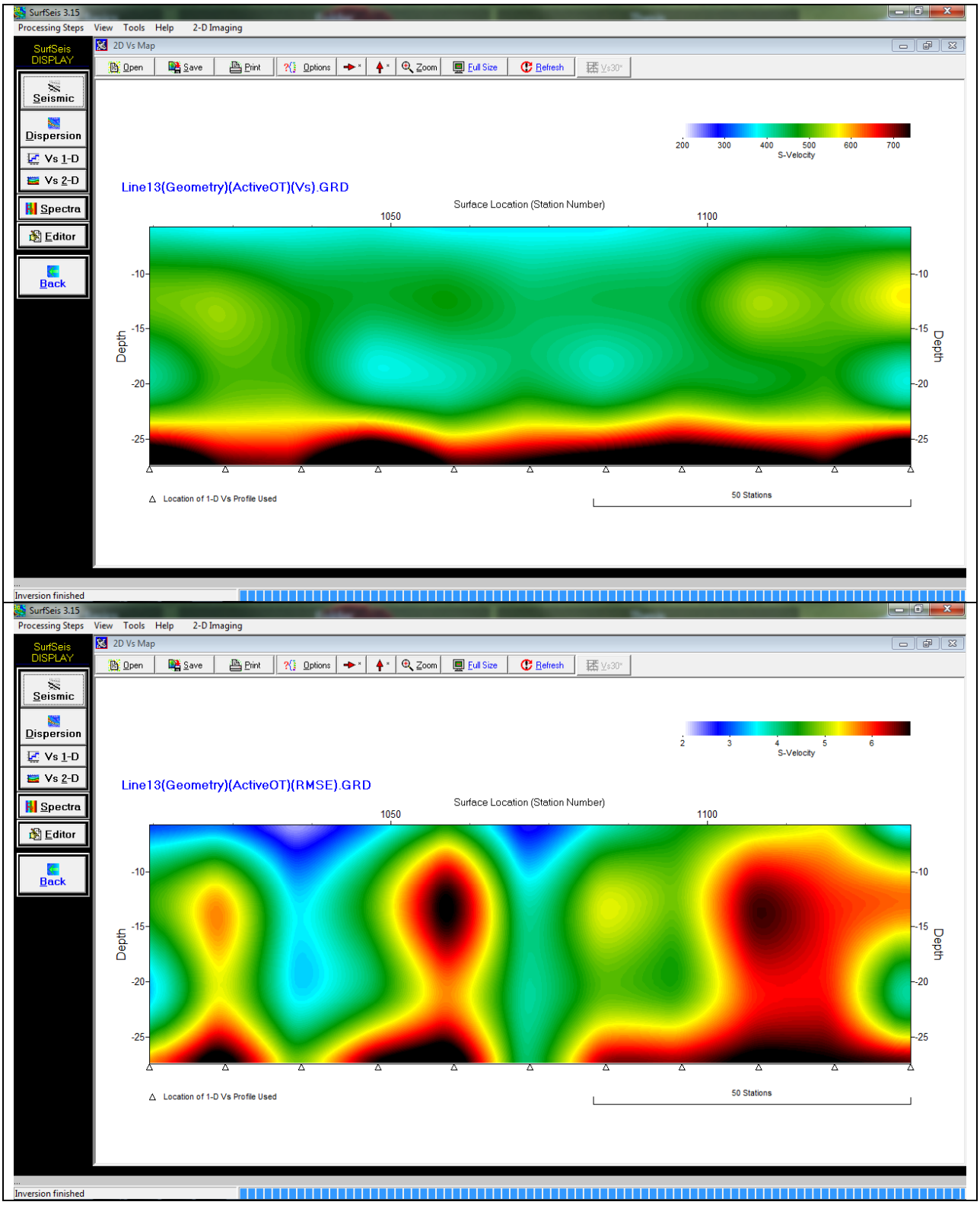

## Loose Bottom Mute

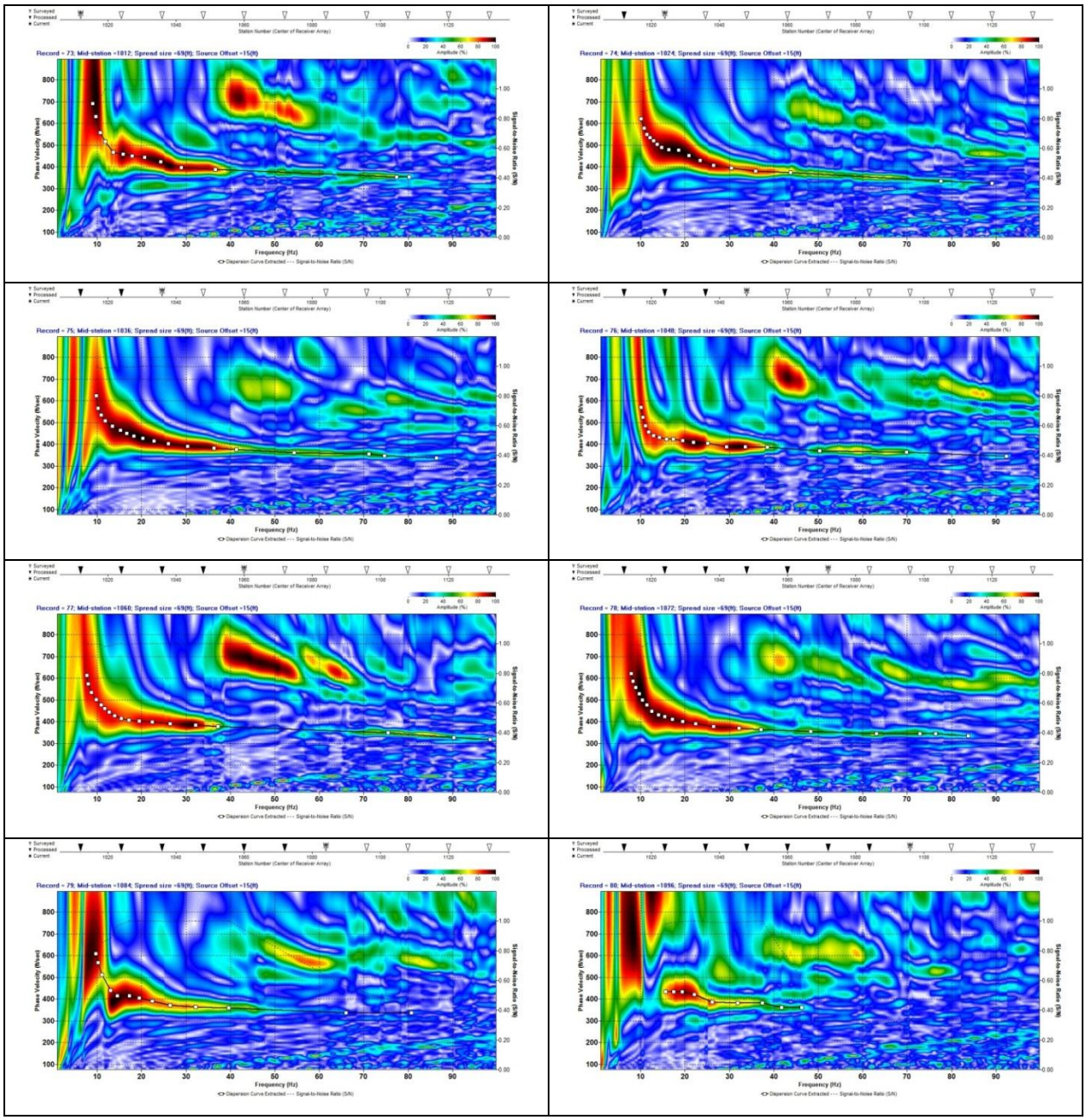

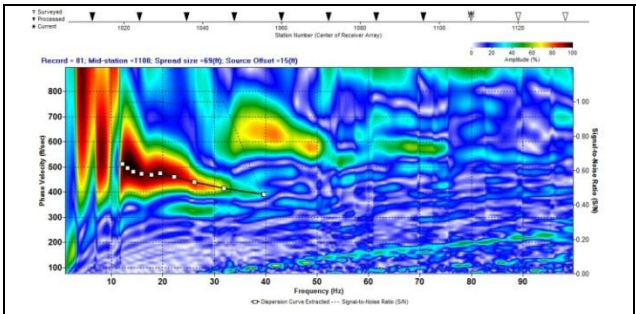
Record = 81; Mid-station =1188; Spread size =69(ft); Source Offset =15(ft)
Phase Velocity (ft/sec)
Frequency (Hz)
Signal-to-Noise Ratio (S/N)

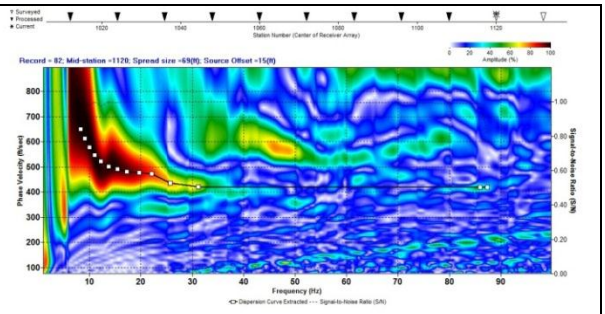
Record = 82; Mid-station =1120; Spread size =69(ft); Source Offset =15(ft)
Phase Velocity (ft/sec)
Frequency (Hz)
Signal-to-Noise Ratio (S/N)

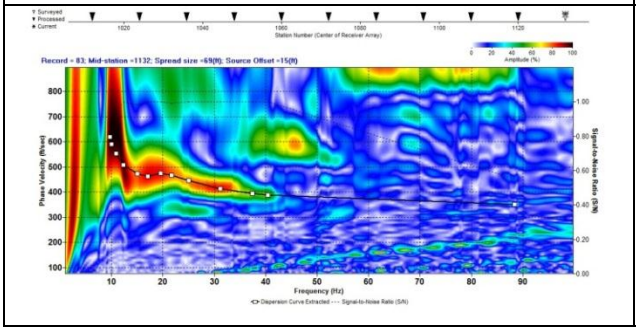
Record = 83; Mid-station =1132; Spread size =69(ft); Source Offset =15(ft)
Phase Velocity (ft/sec)
Frequency (Hz)
Signal-to-Noise Ratio (S/N)

## *(LossBot) Inversion Results*

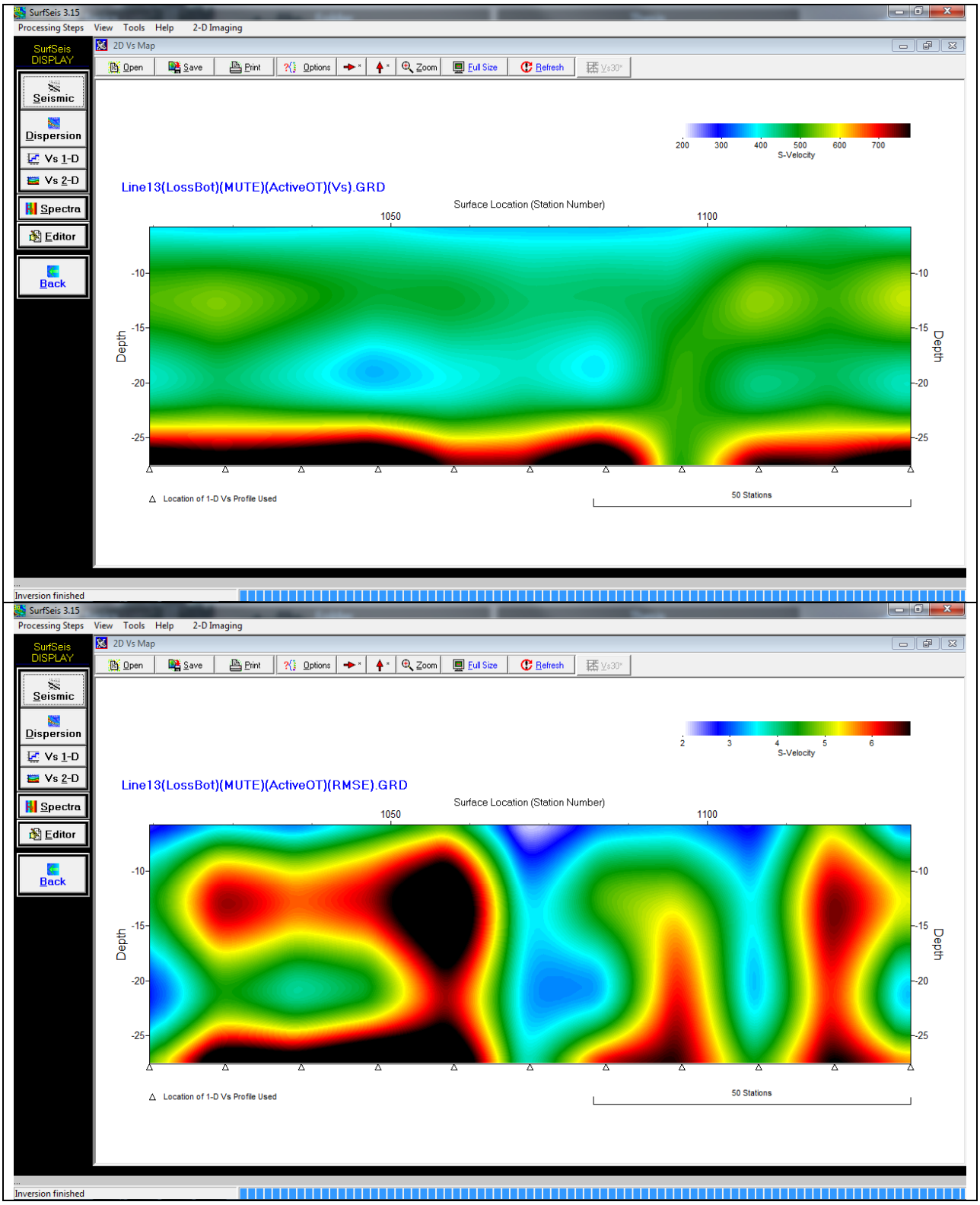

## Aggressive picking on Loose Bottom Mute

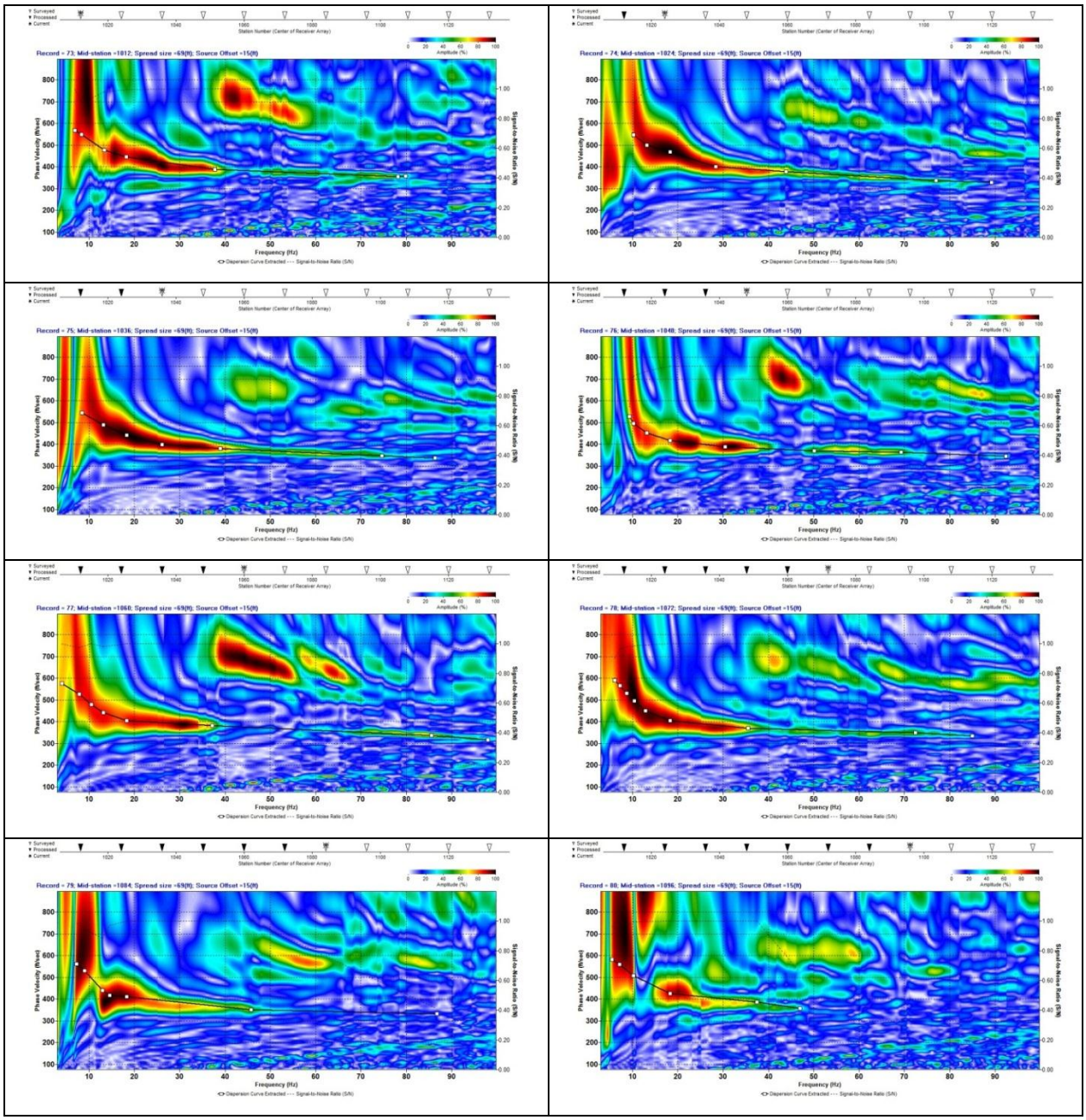

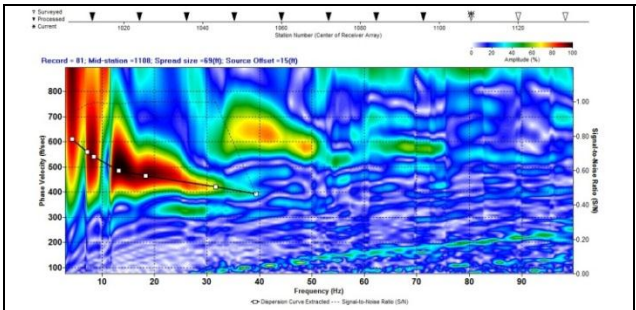
Record = 81; Mid-station =1188; Spread size =69(ft); Source Offset =15(ft)
Phase Velocity (ft/sec)
Frequency (Hz)
Signal-to-Noise Ratio (S/N)
Amplitude (%)
Station Number (Center of Receiver Array)

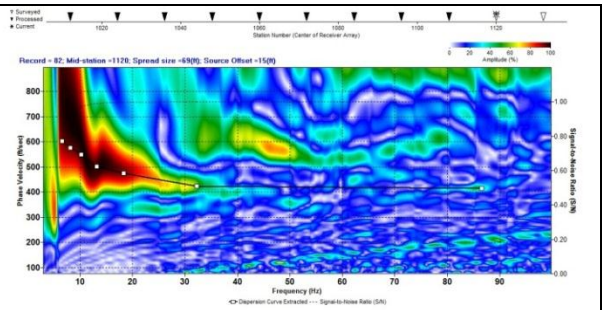
Record = 82; Mid-station =1120; Spread size =69(ft); Source Offset =15(ft)
Phase Velocity (ft/sec)
Frequency (Hz)
Signal-to-Noise Ratio (S/N)
Amplitude (%)
Station Number (Center of Receiver Array)

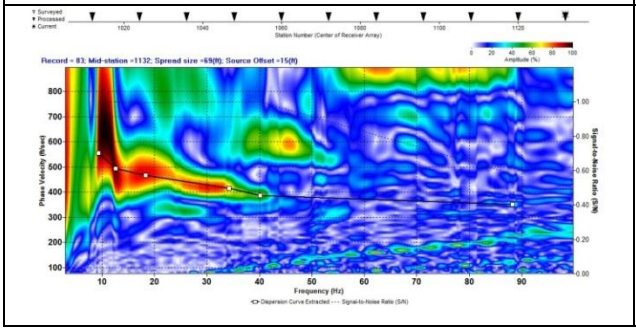
Record = 83; Mid-station =1132; Spread size =69(ft); Source Offset =15(ft)
Phase Velocity (ft/sec)
Frequency (Hz)
Signal-to-Noise Ratio (S/N)
Amplitude (%)
Station Number (Center of Receiver Array)

## *(LossBot)Mob Inversion Results*

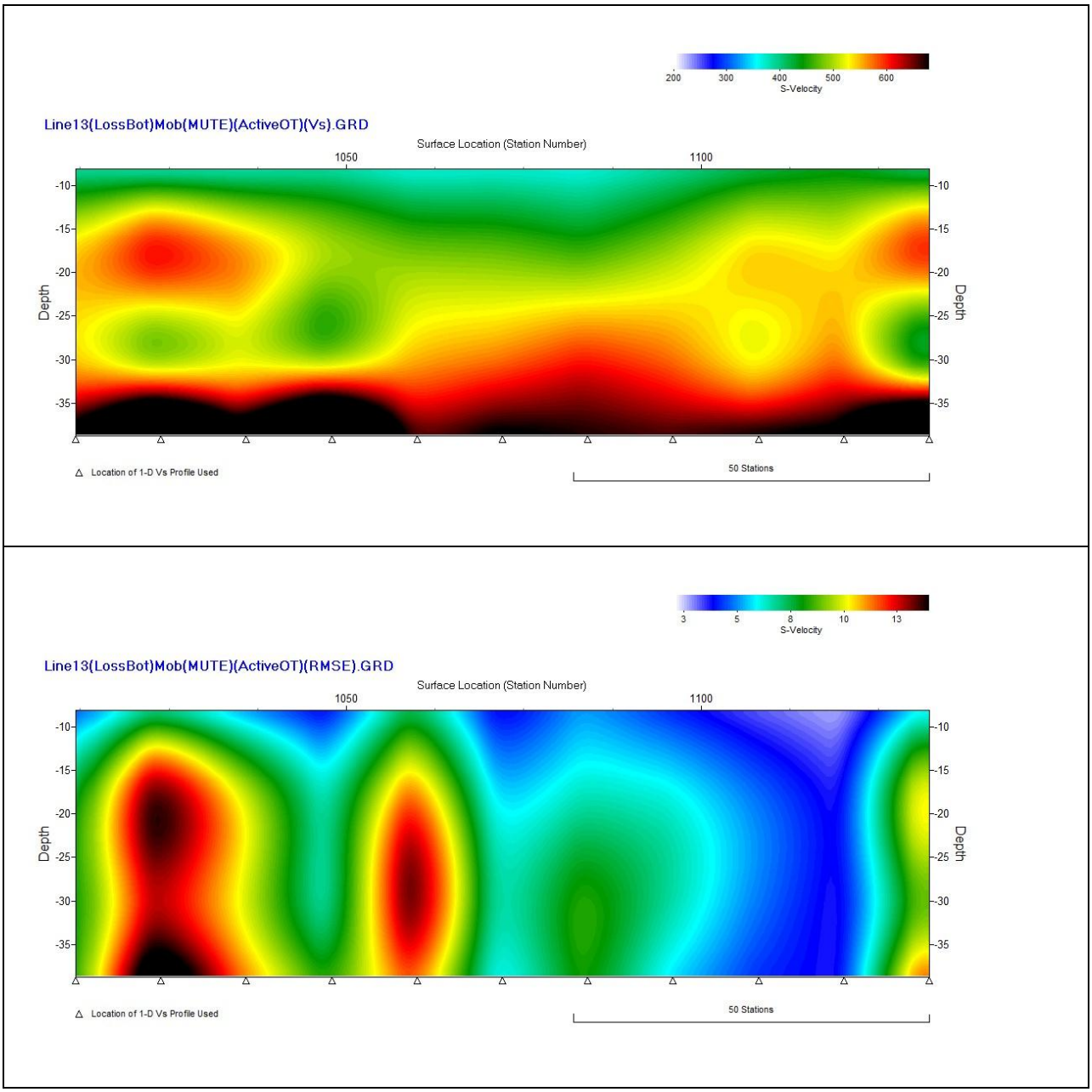

## Line 14

### Raw

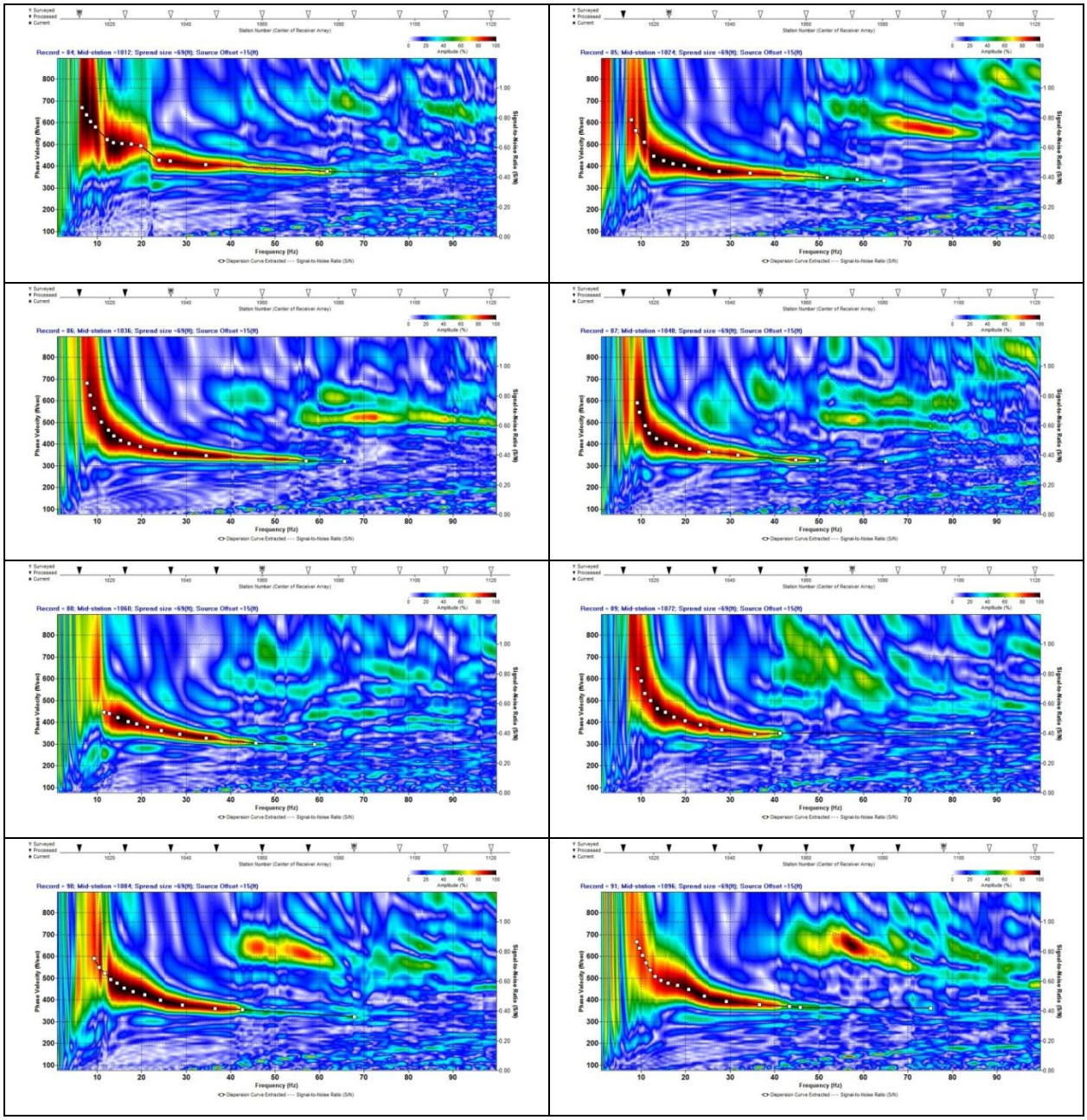
Record = 84; Mid-station =1012; Spread size =69(ft); Source Offset =15(ft)
Record = 85; Mid-station =1024; Spread size =69(ft); Source Offset =15(ft)
Record = 86; Mid-station =1036; Spread size =69(ft); Source Offset =15(ft)
Record = 87; Mid-station =1048; Spread size =69(ft); Source Offset =15(ft)
Record = 88; Mid-station =1060; Spread size =69(ft); Source Offset =15(ft)
Record = 89; Mid-station =1072; Spread size =69(ft); Source Offset =15(ft)
Record = 90; Mid-station =1084; Spread size =69(ft); Source Offset =15(ft)
Record = 91; Mid-station =1096; Spread size =69(ft); Source Offset =15(ft)
Station Number (Center of Receiver Array)
Amplitude (%)
Phase Velocity (ft/sec)
Signal-to-Noise Ratio (S/N)
Frequency (Hz)
Dispersion Curve Extracted --- Signal-to-Noise Ratio (S/N)

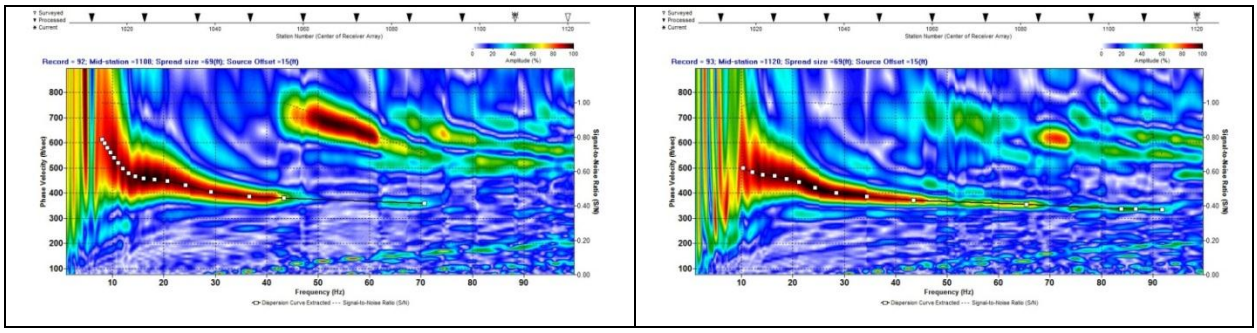

***Raw Inversion Results***

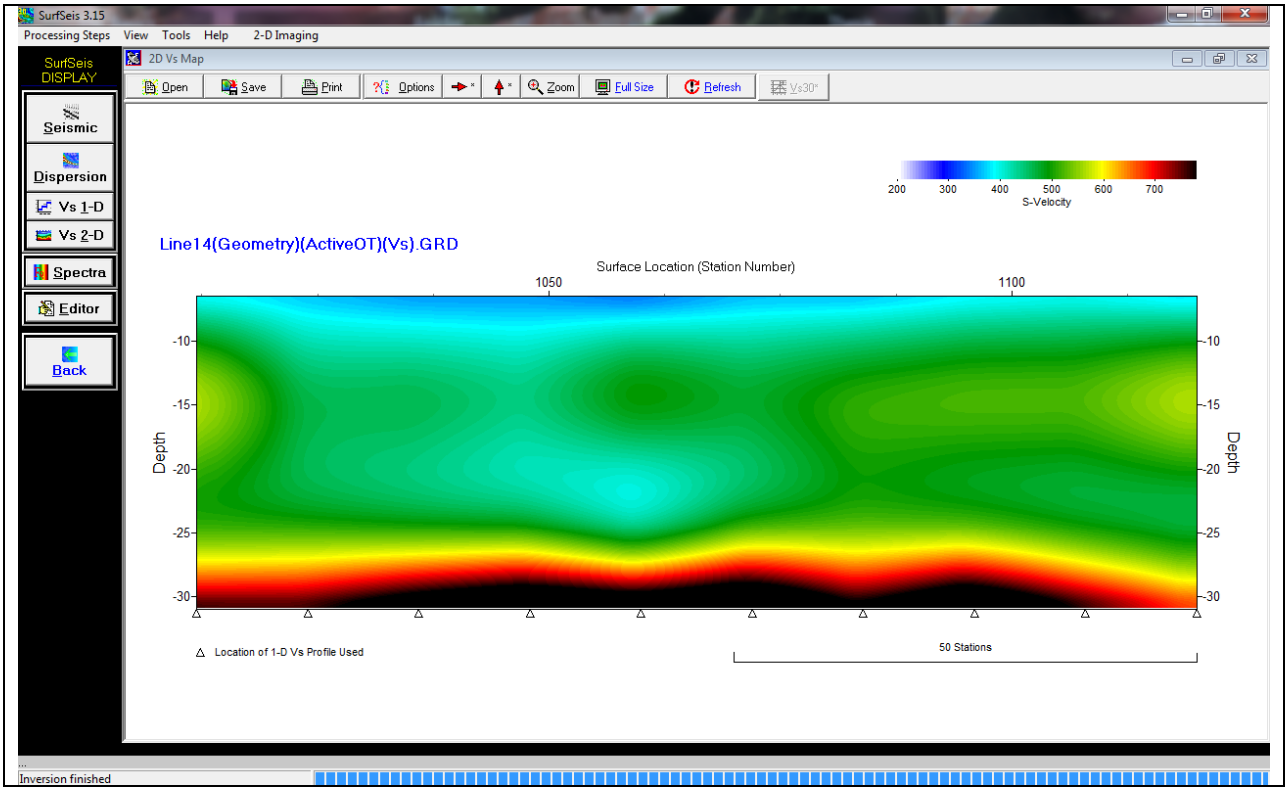

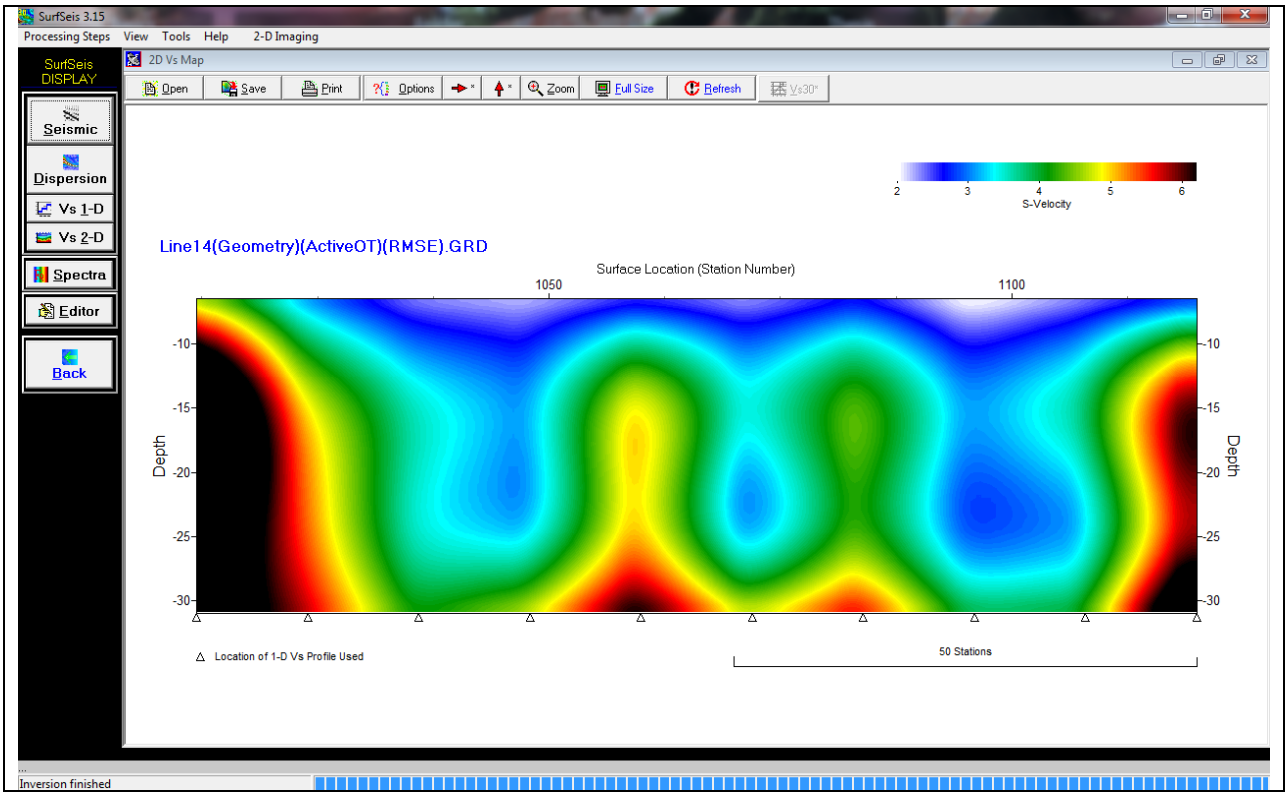


## Loose Bottom Mute

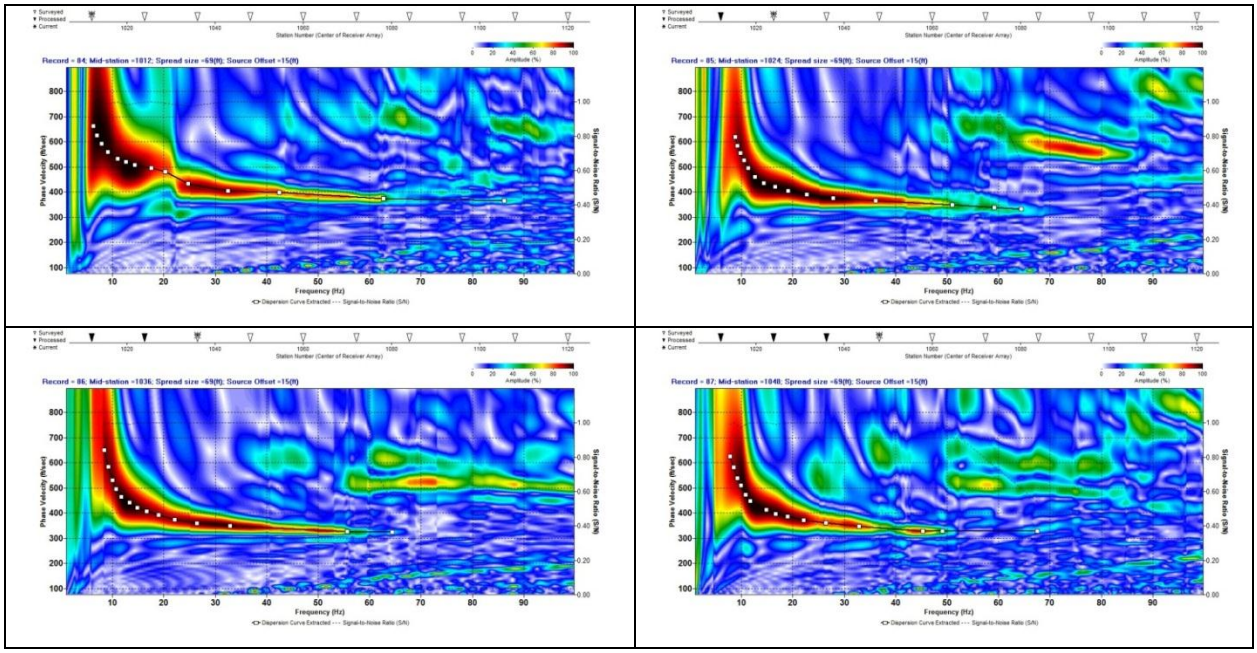

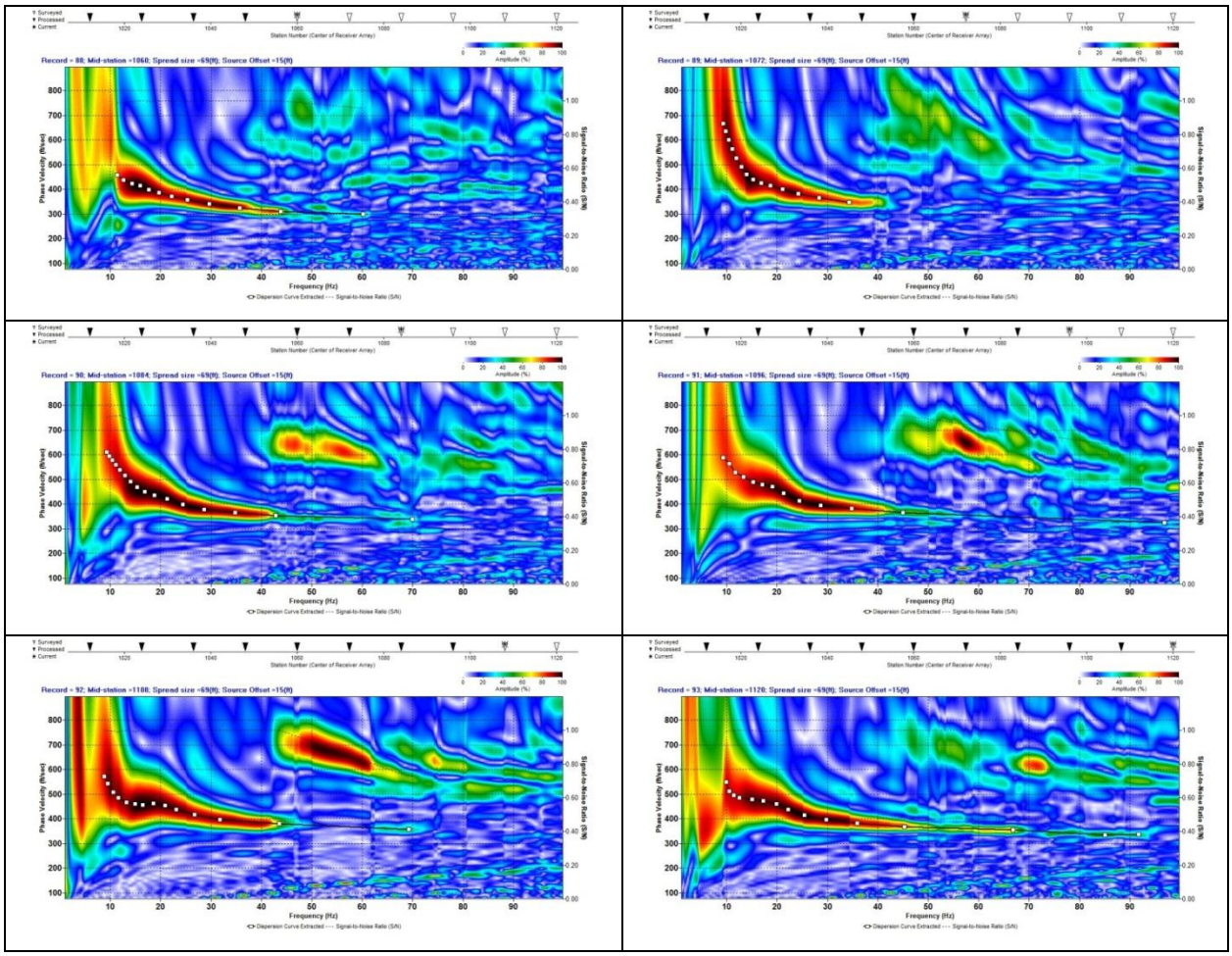
Record = 88; Mid-station =1060; Spread size =69(ft); Source Offset =15(ft)
Record = 89; Mid-station =1072; Spread size =69(ft); Source Offset =15(ft)
Record = 90; Mid-station =1084; Spread size =69(ft); Source Offset =15(ft)
Record = 91; Mid-station =1096; Spread size =69(ft); Source Offset =15(ft)
Record = 92; Mid-station =1108; Spread size =69(ft); Source Offset =15(ft)
Record = 93; Mid-station =1120; Spread size =69(ft); Source Offset =15(ft)
Station Number (Center of Receiver Array)
Amplitude (%)
Phase Velocity (ft/sec)
Signal-to-Noise Ratio (S/N)
Frequency (Hz)
Dispersion Curve Extracted --- Signal-to-Noise Ratio (S/N)

## *(LossBot) Inversion Results*

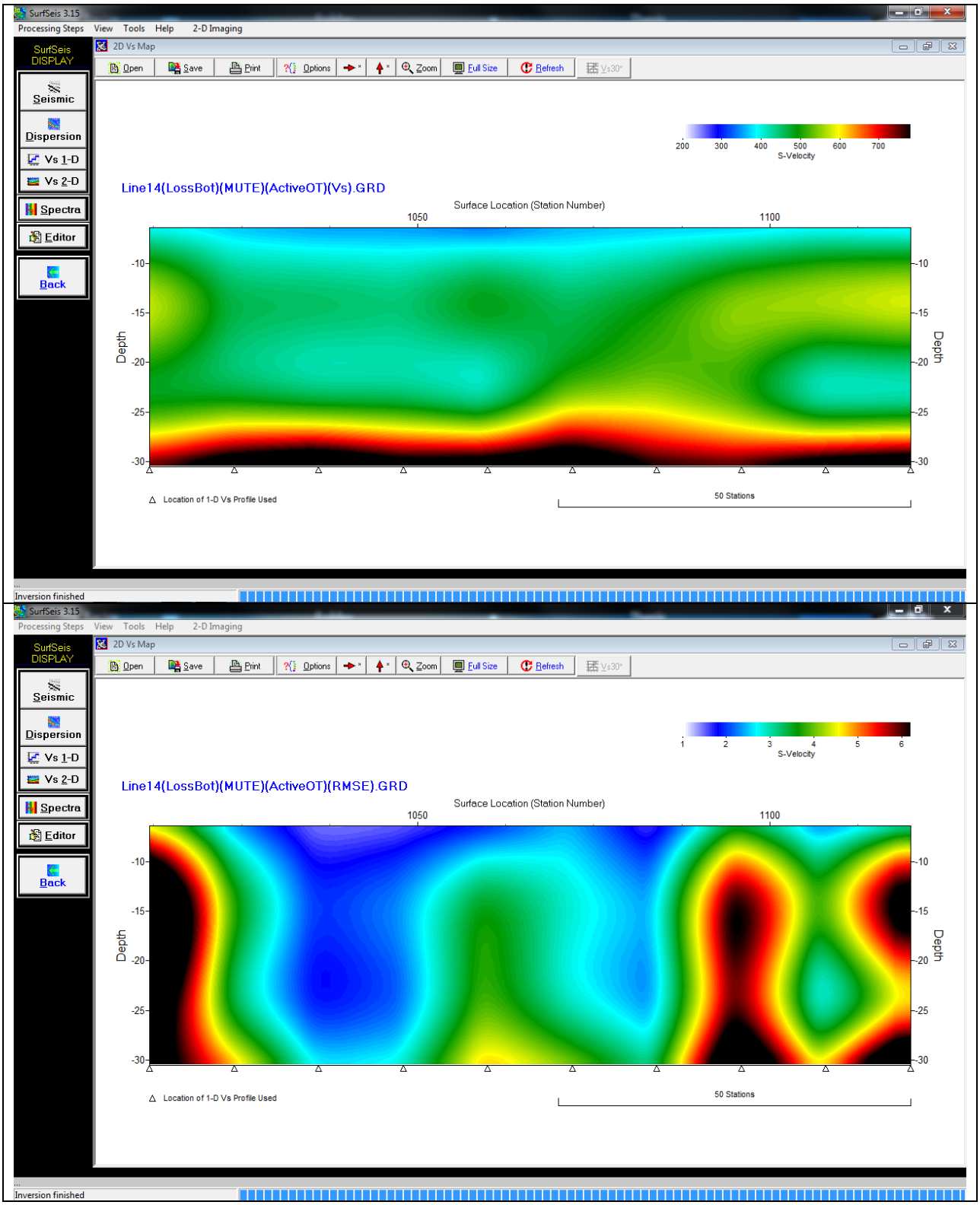

## Aggressive picking on Loose Bottom Mute

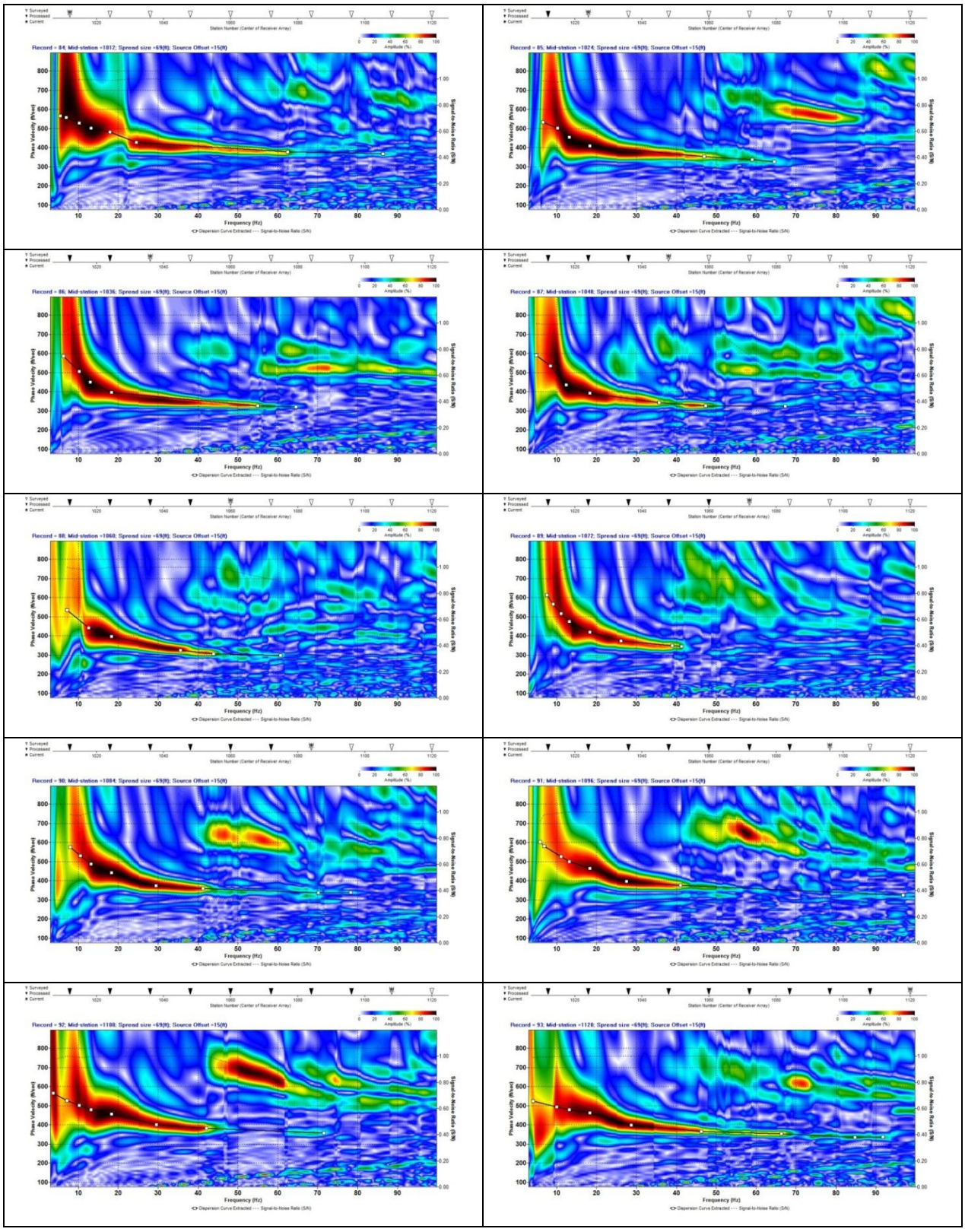

## *(LossBot)Mob Inversion Results*

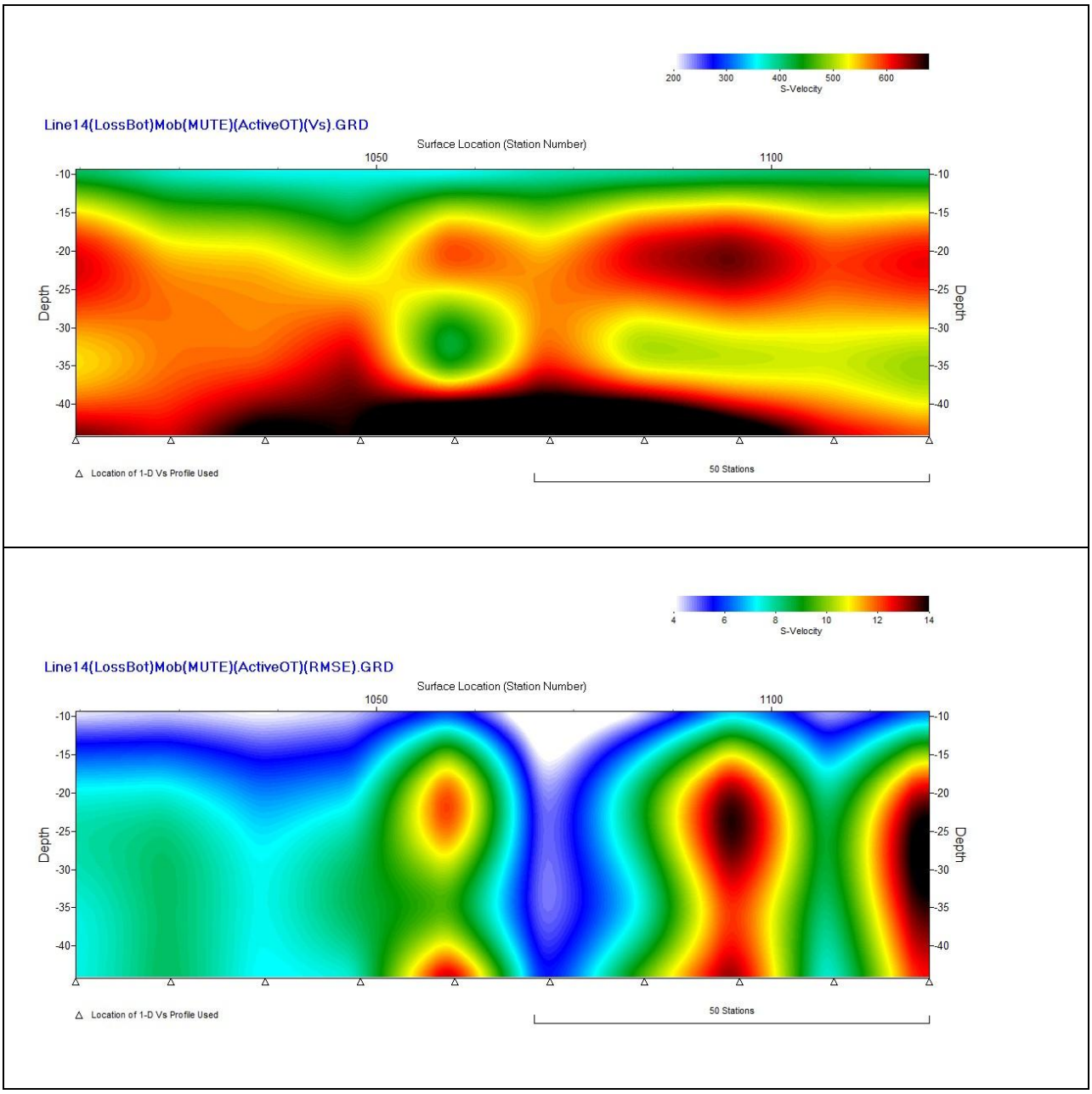

## Line 15

### Raw

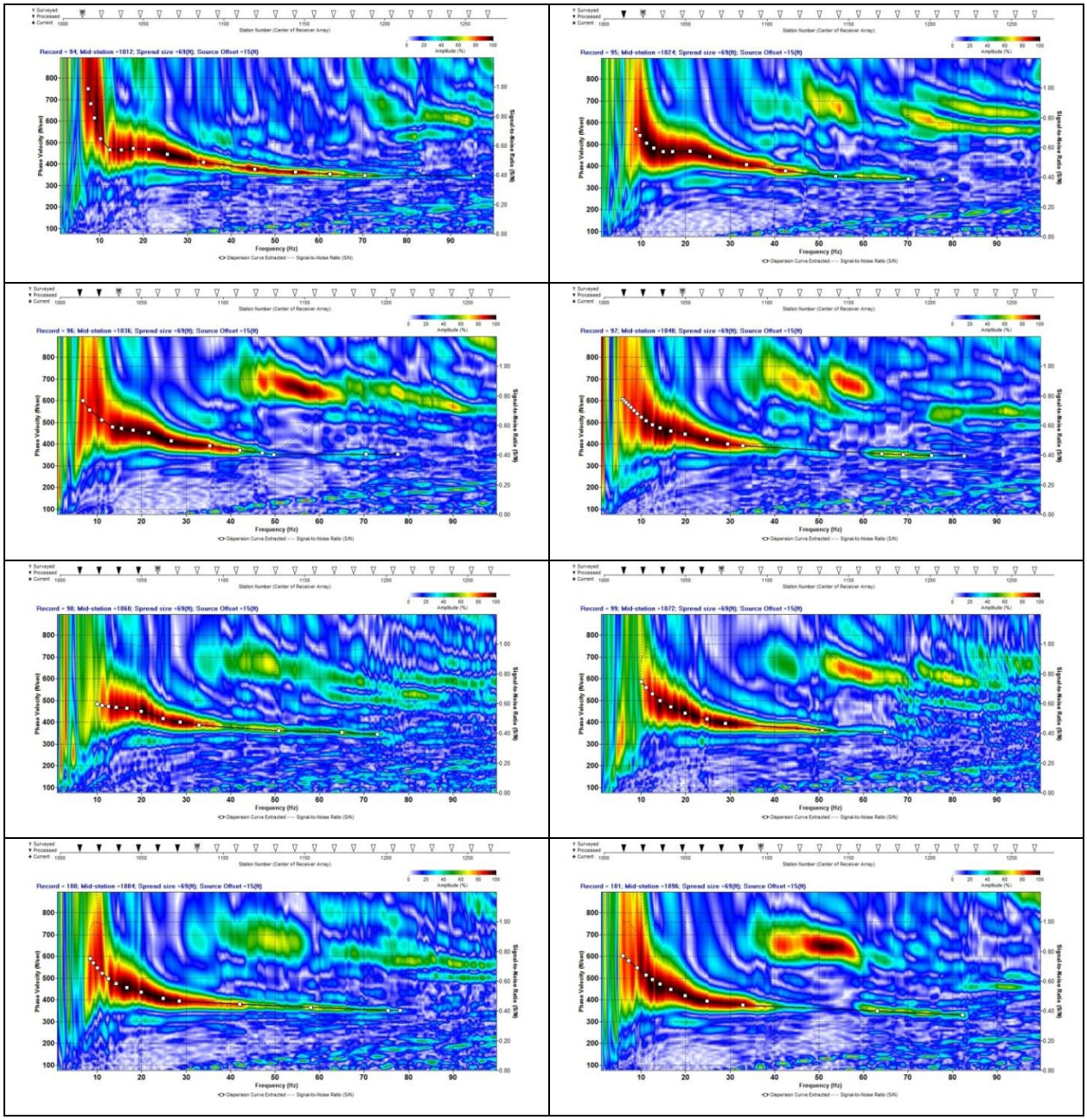
Record = 94; Mid-station =1012; Spread size =69(ft); Source Offset =15(ft)
Record = 95; Mid-station =1024; Spread size =69(ft); Source Offset =15(ft)
Record = 96; Mid-station =1036; Spread size =69(ft); Source Offset =15(ft)
Record = 97; Mid-station =1048; Spread size =69(ft); Source Offset =15(ft)
Record = 98; Mid-station =1060; Spread size =69(ft); Source Offset =15(ft)
Record = 99; Mid-station =1072; Spread size =69(ft); Source Offset =15(ft)
Record = 100; Mid-station =1084; Spread size =69(ft); Source Offset =15(ft)
Record = 101; Mid-station =1096; Spread size =69(ft); Source Offset =15(ft)
Station Number (Center of Receiver Array)
Frequency (Hz)
Phase Velocity (ft/sec)
Signal-to-Noise Ratio (S/N)
Amplitude (%)
Dispersion Curve Extracted --- Signal-to-Noise Ratio (S/N)

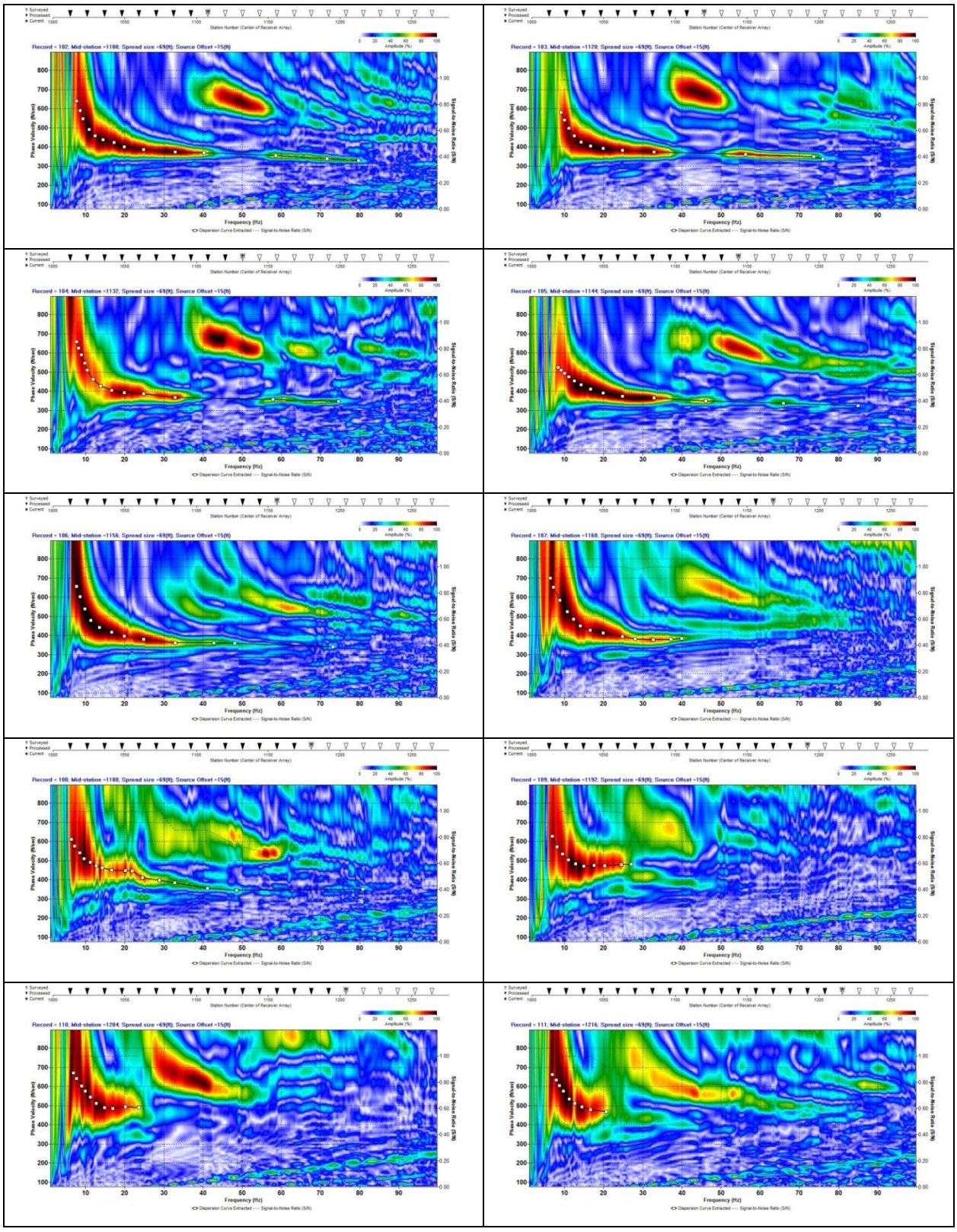
Record = 102; Mid-station =1108; Spread size =69(ft); Source Offset =15(ft)
Record = 103; Mid-station =1128; Spread size =69(ft); Source Offset =15(ft)
Record = 104; Mid-station =1132; Spread size =69(ft); Source Offset =15(ft)
Record = 105; Mid-station =1144; Spread size =69(ft); Source Offset =15(ft)
Record = 106; Mid-station =1156; Spread size =69(ft); Source Offset =15(ft)
Record = 107; Mid-station =1168; Spread size =69(ft); Source Offset =15(ft)
Record = 108; Mid-station =1180; Spread size =69(ft); Source Offset =15(ft)
Record = 109; Mid-station =1192; Spread size =69(ft); Source Offset =15(ft)
Record = 110; Mid-station =1204; Spread size =69(ft); Source Offset =15(ft)
Record = 111; Mid-station =1216; Spread size =69(ft); Source Offset =15(ft)
Station Number (Center of Receiver Array)
Frequency (Hz)
Phase Velocity (ft/sec)
Signal-to-Noise Ratio (S/N)
Amplitude (%)
Dispersion Curve Extracted --- Signal-to-Noise Ratio (S/N)

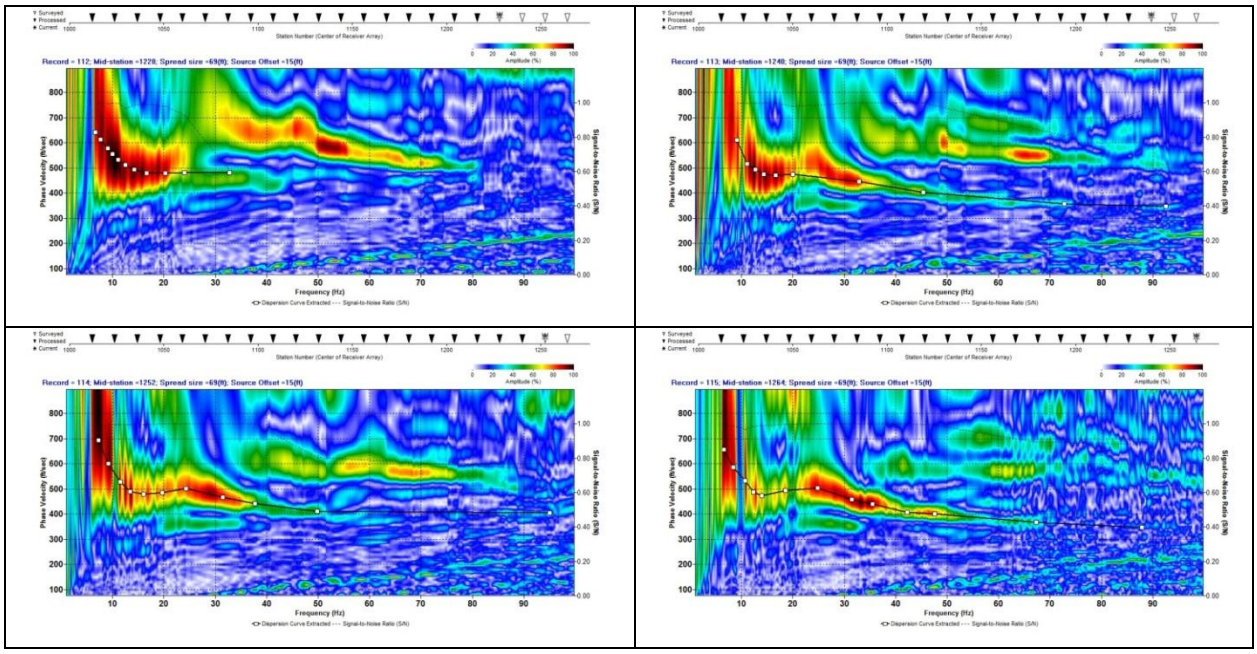
Record = 112; Mid-station =1228; Spread size =69(ft); Source Offset =15(ft)
Record = 113; Mid-station =1240; Spread size =69(ft); Source Offset =15(ft)
Record = 114; Mid-station =1252; Spread size =69(ft); Source Offset =15(ft)
Record = 115; Mid-station =1264; Spread size =69(ft); Source Offset =15(ft)
Station Number (Center of Receiver Array)
Amplitude (%)
Phase Velocity (ft/sec)
Signal-to-Noise Ratio (S/N)
Frequency (Hz)
Dispersion Curve Extracted --- Signal-to-Noise Ratio (S/N)

## *Raw Inversion Results*

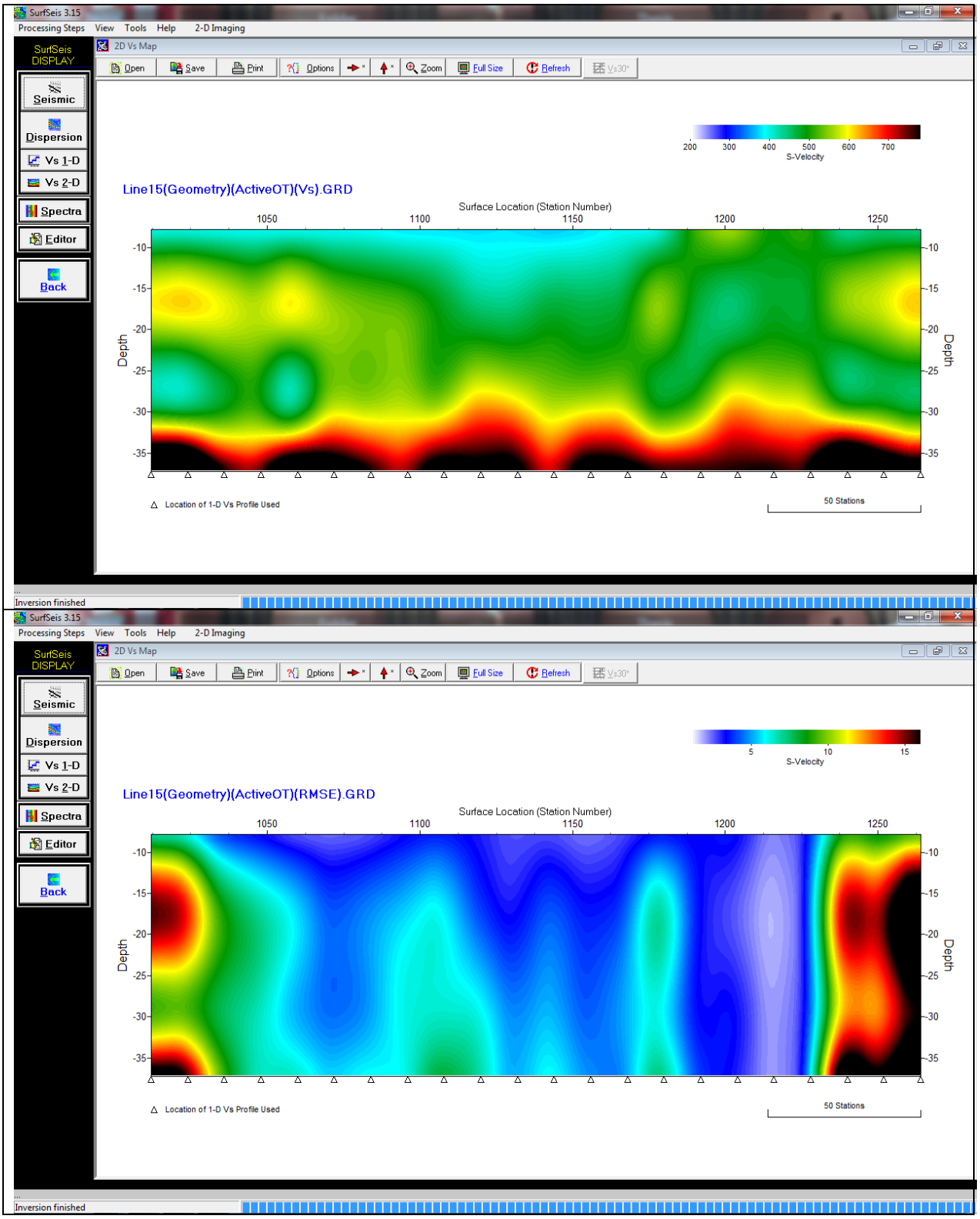

**Loose Bottom Mute**

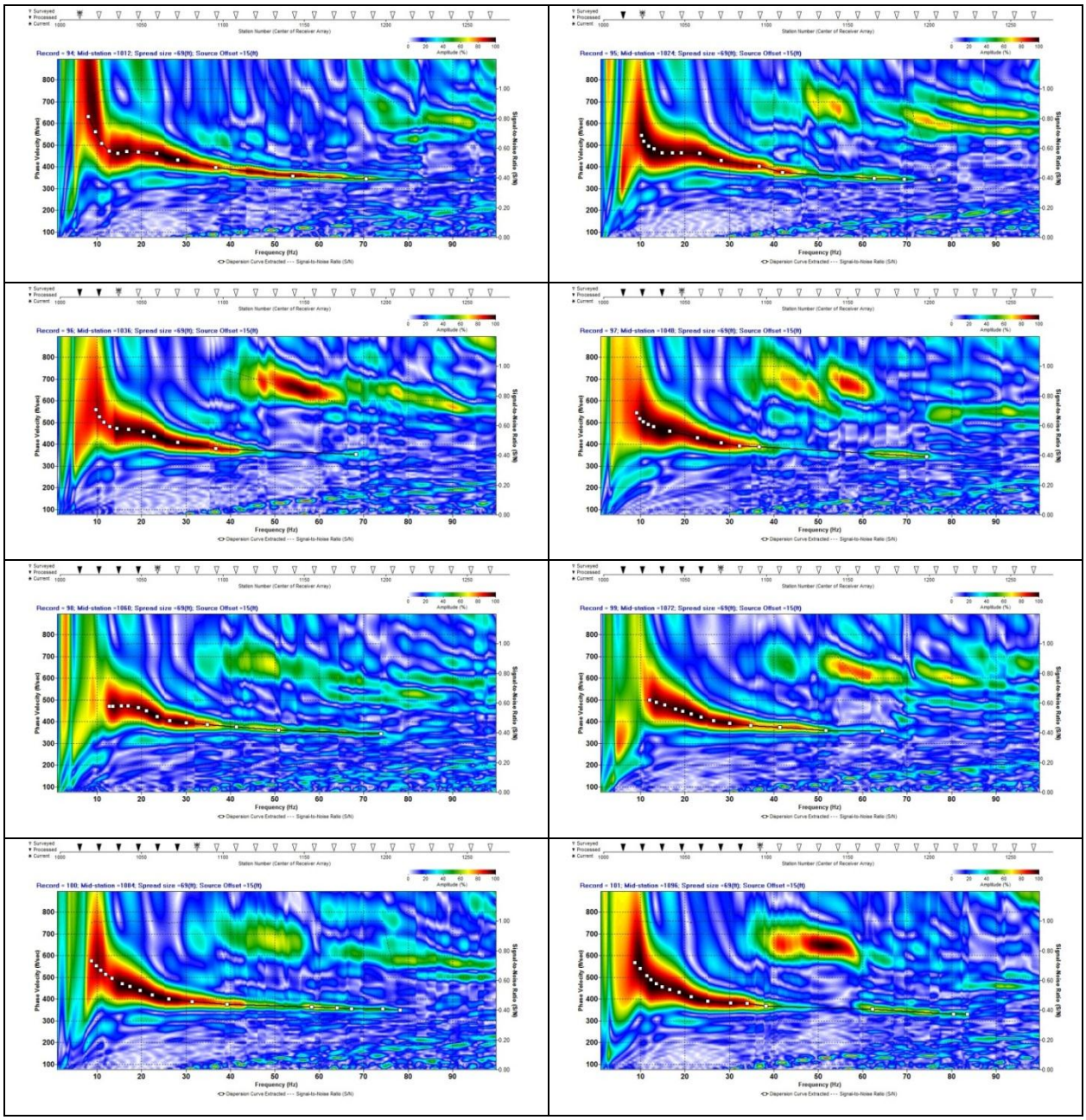

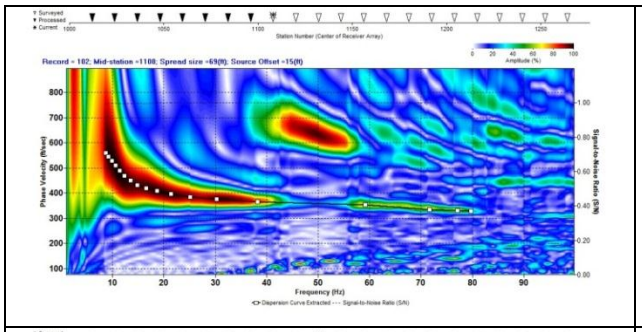
Record = 102; Mid-station =1108; Spread size =69(ft); Source Offset =15(ft)
Phase Velocity (ft/sec)
Frequency (Hz)
Signal-to-Noise Ratio (S/N)

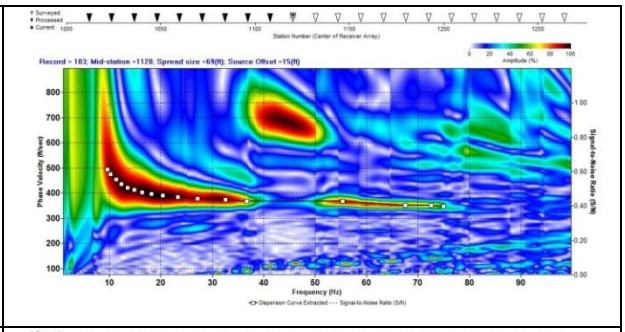
Record = 103; Mid-station =1128; Spread size =69(ft); Source Offset =15(ft)
Phase Velocity (ft/sec)
Frequency (Hz)
Signal-to-Noise Ratio (S/N)

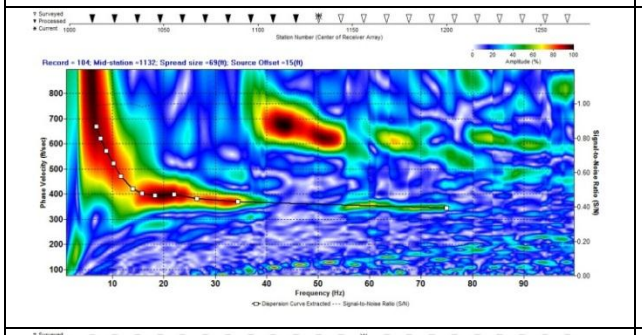
Record = 104; Mid-station =1132; Spread size =69(ft); Source Offset =15(ft)
Phase Velocity (ft/sec)
Frequency (Hz)
Signal-to-Noise Ratio (S/N)

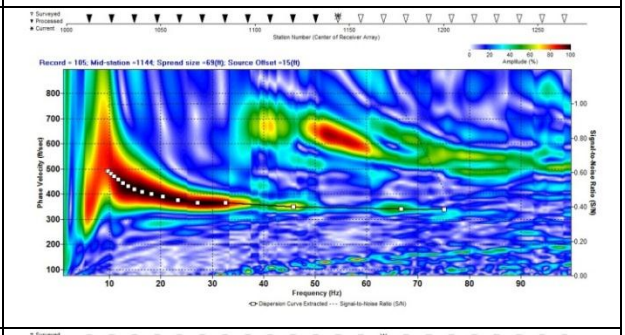
Record = 105; Mid-station =1144; Spread size =69(ft); Source Offset =15(ft)
Phase Velocity (ft/sec)
Frequency (Hz)
Signal-to-Noise Ratio (S/N)

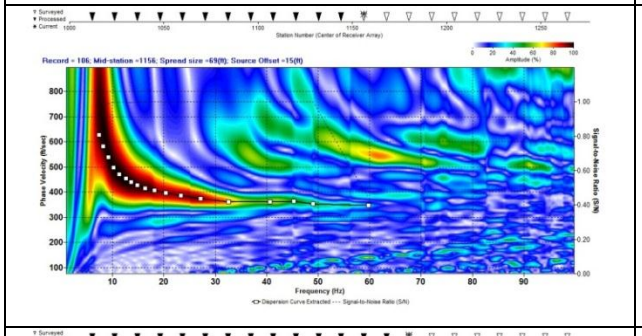
Record = 106; Mid-station =1156; Spread size =69(ft); Source Offset =15(ft)
Phase Velocity (ft/sec)
Frequency (Hz)
Signal-to-Noise Ratio (S/N)

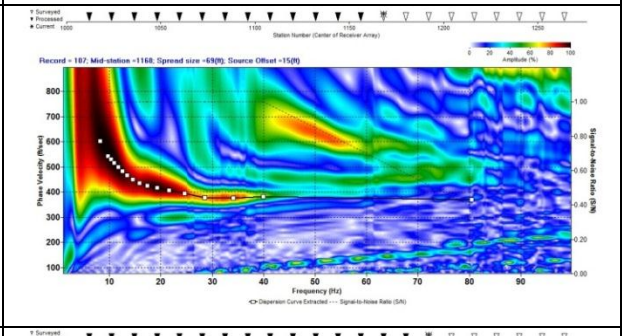
Record = 107; Mid-station =1168; Spread size =69(ft); Source Offset =15(ft)
Phase Velocity (ft/sec)
Frequency (Hz)
Signal-to-Noise Ratio (S/N)

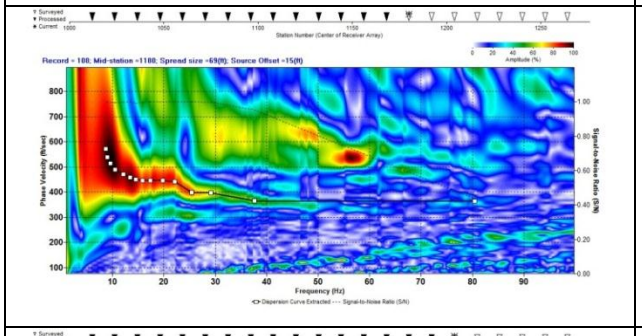
Record = 108; Mid-station =1180; Spread size =69(ft); Source Offset =15(ft)
Phase Velocity (ft/sec)
Frequency (Hz)
Signal-to-Noise Ratio (S/N)

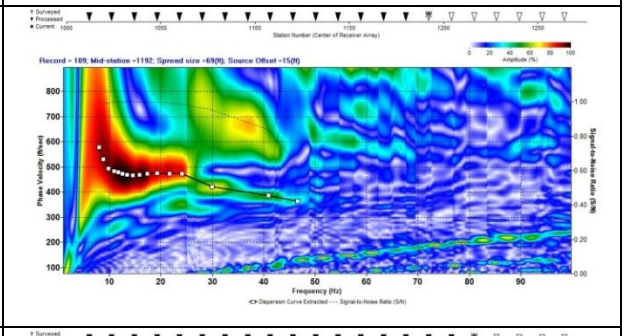
Record = 109; Mid-station =1192; Spread size =69(ft); Source Offset =15(ft)
Phase Velocity (ft/sec)
Frequency (Hz)
Signal-to-Noise Ratio (S/N)

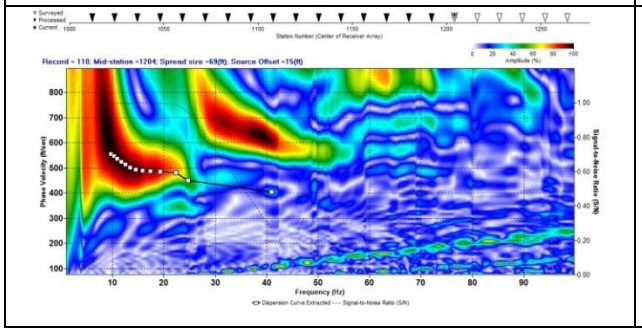
Record = 110; Mid-station =1204; Spread size =69(ft); Source Offset =15(ft)
Phase Velocity (ft/sec)
Frequency (Hz)
Signal-to-Noise Ratio (S/N)

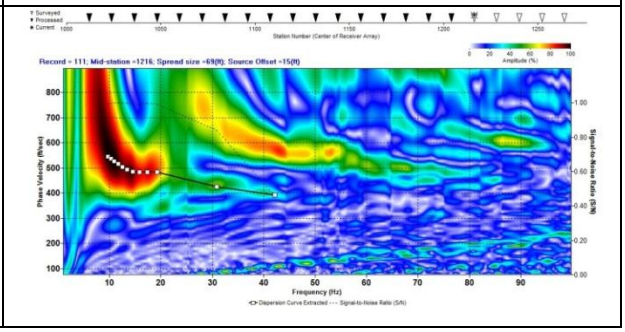
Record = 111; Mid-station =1216; Spread size =69(ft); Source Offset =15(ft)
Phase Velocity (ft/sec)
Frequency (Hz)
Signal-to-Noise Ratio (S/N)

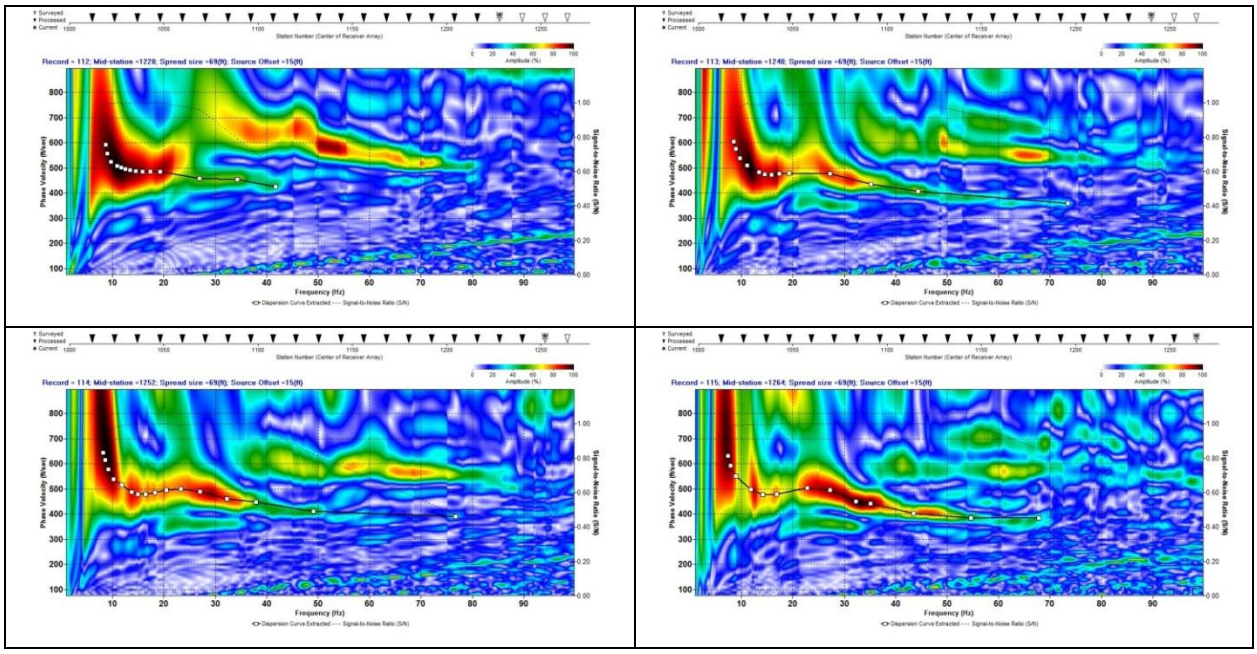
Record = 112; Mid-station =1228; Spread size =69(ft); Source Offset =15(ft)
Record = 113; Mid-station =1248; Spread size =69(ft); Source Offset =15(ft)
Record = 114; Mid-station =1252; Spread size =69(ft); Source Offset =15(ft)
Record = 115; Mid-station =1264; Spread size =69(ft); Source Offset =15(ft)
Station Number (Center of Receiver Array)
Amplitude (%)
Phase Velocity (ft/sec)
Signal-to-Noise Ratio (S/N)
Frequency (Hz)
Dispersion Curve Extracted --- Signal-to-Noise Ratio (S/N)

## *(LossBot) Inversion Results*

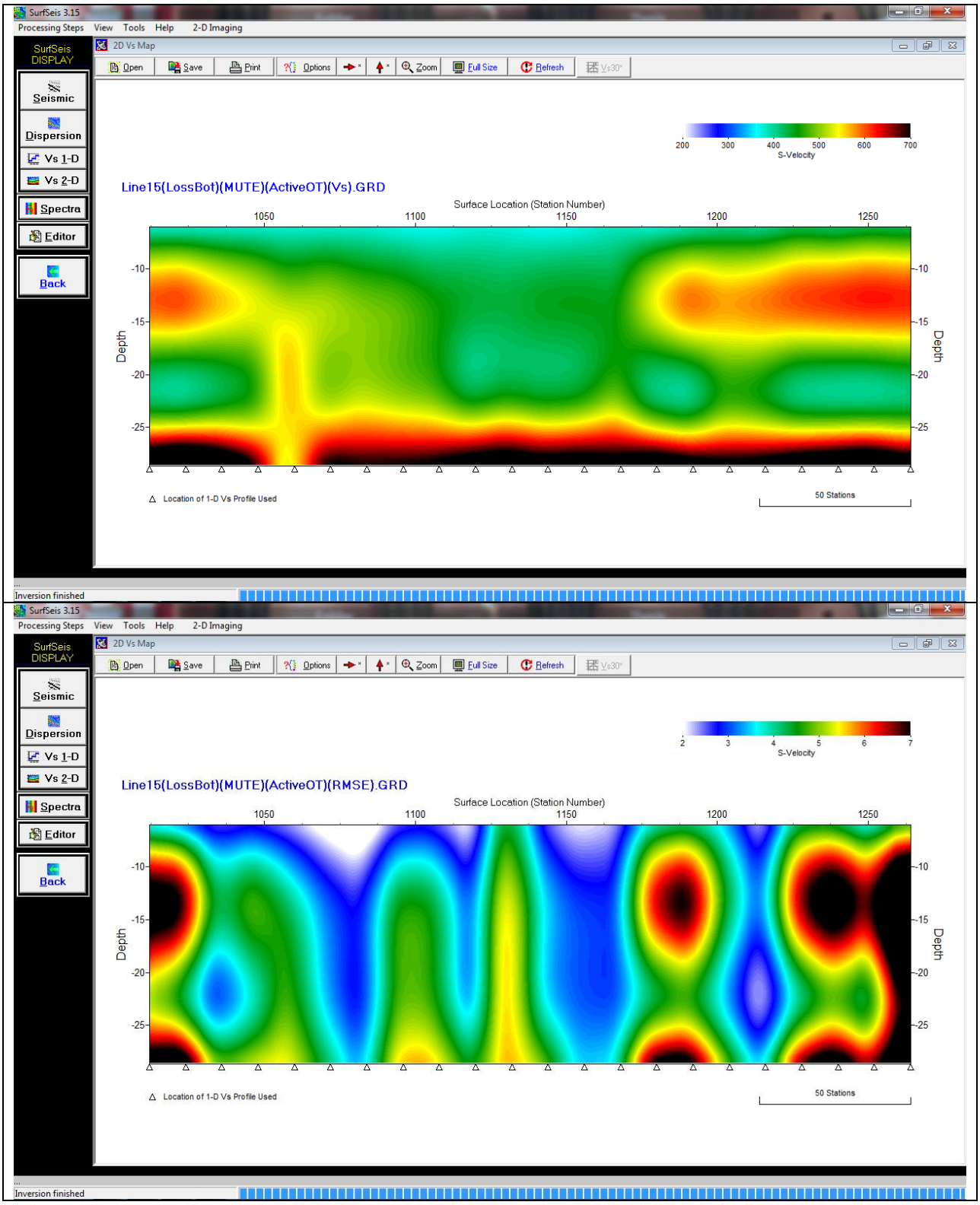

## Aggressive picking on Loose Bottom Mute

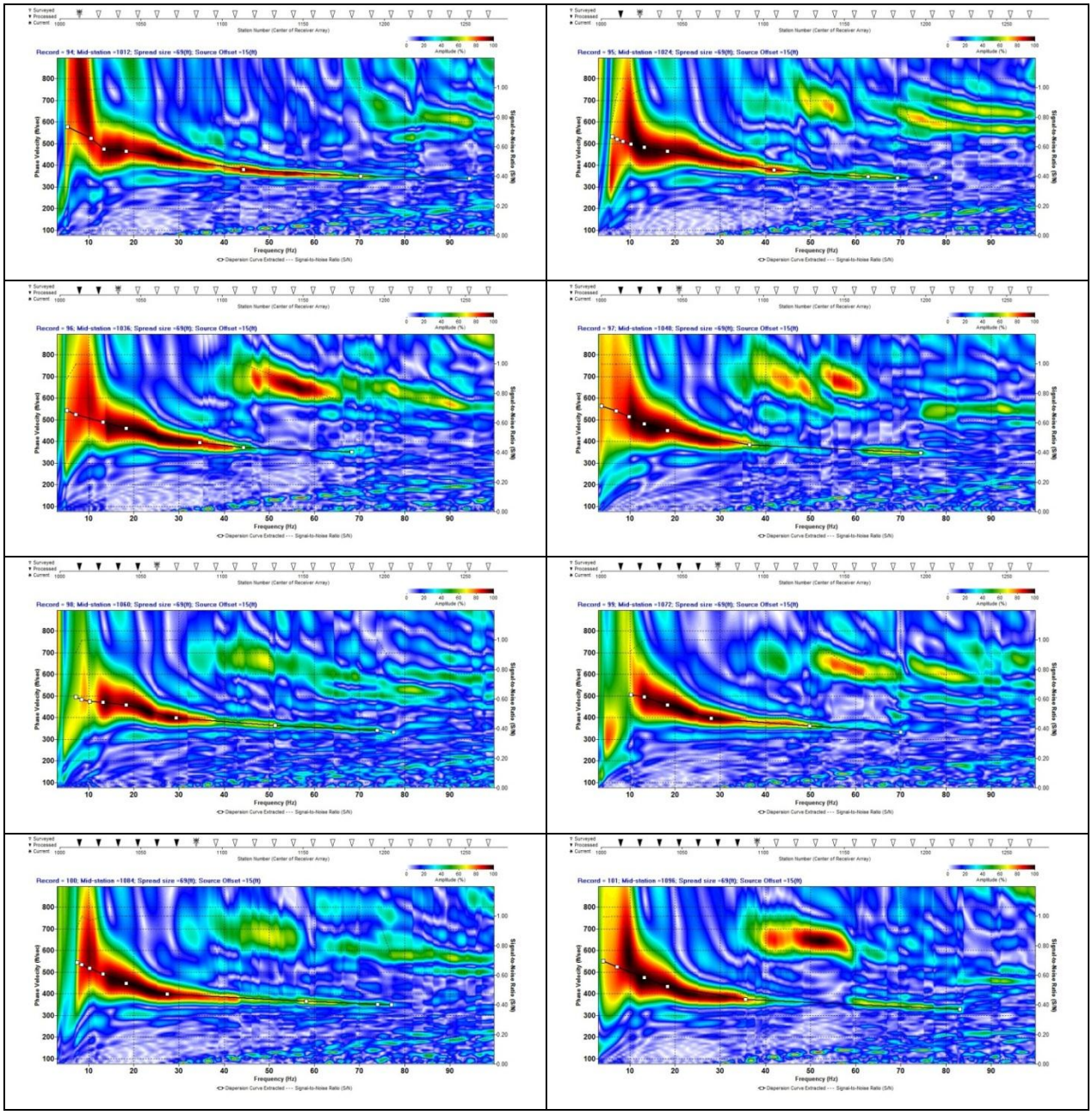

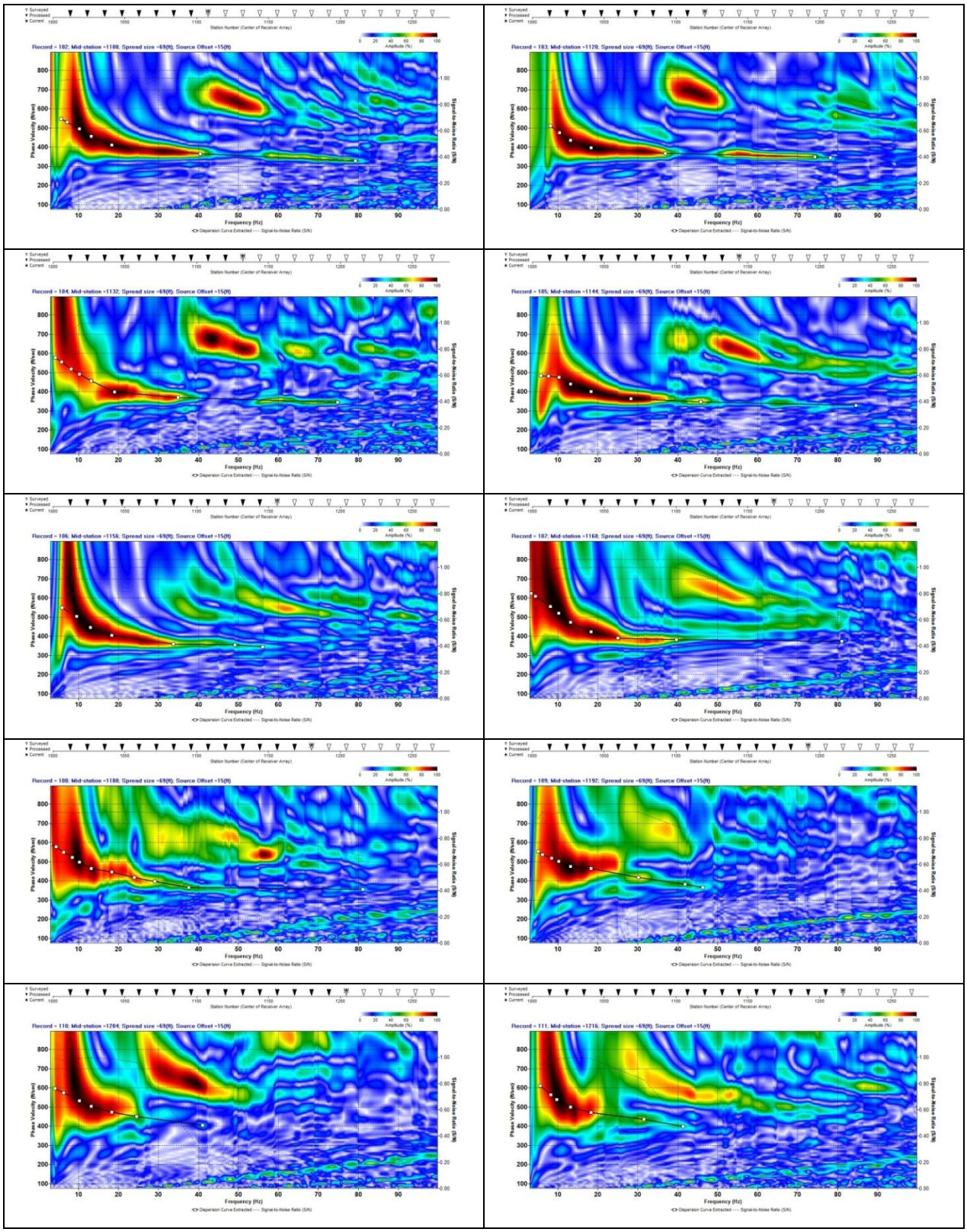
Record = 102; Mid-station =1108; Spread size =69(ft); Source Offset =15(ft)
Record = 103; Mid-station =1128; Spread size =69(ft); Source Offset =15(ft)
Record = 104; Mid-station =1132; Spread size =69(ft); Source Offset =15(ft)
Record = 105; Mid-station =1144; Spread size =69(ft); Source Offset =15(ft)
Record = 106; Mid-station =1156; Spread size =69(ft); Source Offset =15(ft)
Record = 107; Mid-station =1168; Spread size =69(ft); Source Offset =15(ft)
Record = 108; Mid-station =1180; Spread size =69(ft); Source Offset =15(ft)
Record = 109; Mid-station =1192; Spread size =69(ft); Source Offset =15(ft)
Record = 110; Mid-station =1204; Spread size =69(ft); Source Offset =15(ft)
Record = 111; Mid-station =1216; Spread size =69(ft); Source Offset =15(ft)
Station Number (Center of Receiver Array)
Amplitude (%)
Phase Velocity (ft/sec)
Signal-to-Noise Ratio (S/N)
Frequency (Hz)
Dispersion Curve Extracted --- Signal-to-Noise Ratio (S/N)

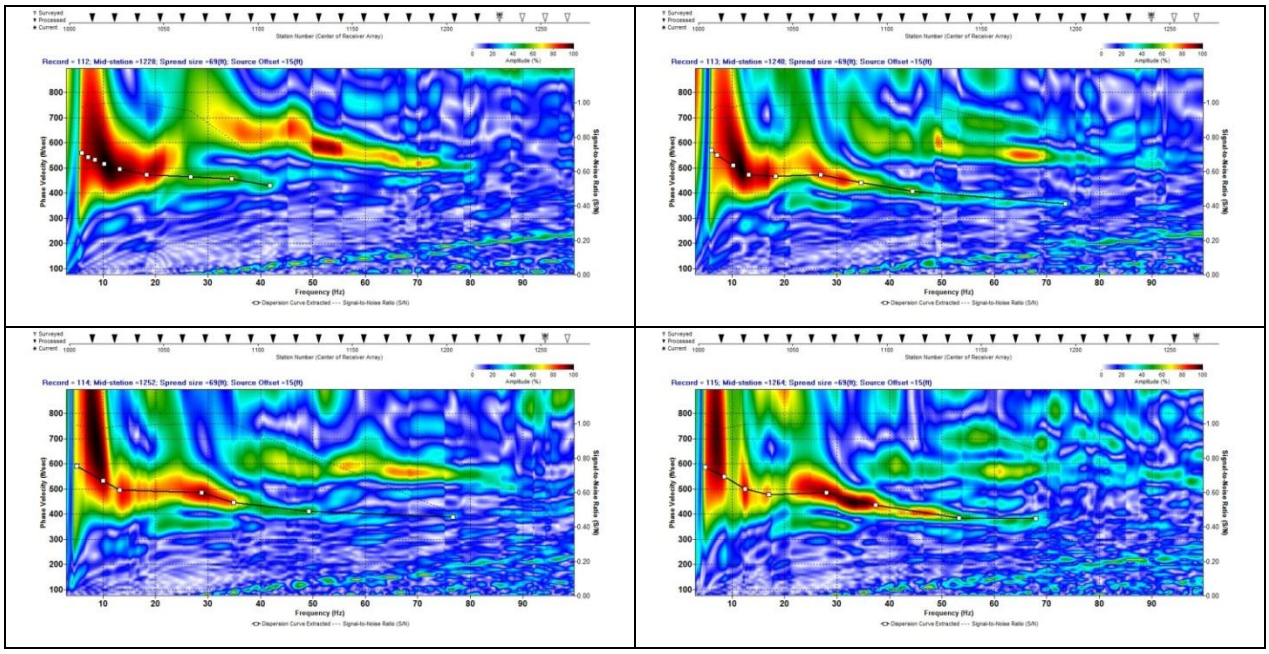
Record = 112; Mid-station =1228; Spread size =69(ft); Source Offset =15(ft)
Record = 113; Mid-station =1240; Spread size =69(ft); Source Offset =15(ft)
Record = 114; Mid-station =1252; Spread size =69(ft); Source Offset =15(ft)
Record = 115; Mid-station =1264; Spread size =69(ft); Source Offset =15(ft)
Station Number (Center of Receiver Array)
Amplitude (%)
Phase Velocity (ft/sec)
Signal-to-Noise Ratio (S/N)
Frequency (Hz)
Dispersion Curve Extracted --- Signal-to-Noise Ratio (S/N)

## *(LossBot)Mob Inversion Results*